frontiers | Research Topics

Coastal and marine environmental quality assessments

Edited by
Dilip Kumar Jha, Ganesh Thiruchitrambalam, Meilin Wu and Prashanthi Devi Marimuthu

Published in
Frontiers in Marine Science



FRONTIERS EBOOK COPYRIGHT STATEMENT

The copyright in the text of individual articles in this ebook is the property of their respective authors or their respective institutions or funders. The copyright in graphics and images within each article may be subject to copyright of other parties. In both cases this is subject to a license granted to Frontiers.

The compilation of articles constituting this ebook is the property of Frontiers.

Each article within this ebook, and the ebook itself, are published under the most recent version of the Creative Commons CC-BY licence. The version current at the date of publication of this ebook is CC-BY 4.0. If the CC-BY licence is updated, the licence granted by Frontiers is automatically updated to the new version.

When exercising any right under the CC-BY licence, Frontiers must be attributed as the original publisher of the article or ebook, as applicable.

Authors have the responsibility of ensuring that any graphics or other materials which are the property of others may be included in the CC-BY licence, but this should be checked before relying on the CC-BY licence to reproduce those materials. Any copyright notices relating to those materials must be complied with.

Copyright and source acknowledgement notices may not be removed and must be displayed in any copy, derivative work or partial copy which includes the elements in question.

All copyright, and all rights therein, are protected by national and international copyright laws. The above represents a summary only. For further information please read Frontiers' Conditions for Website Use and Copyright Statement, and the applicable CC-BY licence.

ISSN 1664-8714
ISBN 978-2-83251-726-0
DOI 10.3389/978-2-83251-726-0

About Frontiers

Frontiers is more than just an open access publisher of scholarly articles: it is a pioneering approach to the world of academia, radically improving the way scholarly research is managed. The grand vision of Frontiers is a world where all people have an equal opportunity to seek, share and generate knowledge. Frontiers provides immediate and permanent online open access to all its publications, but this alone is not enough to realize our grand goals.

Frontiers journal series

The Frontiers journal series is a multi-tier and interdisciplinary set of open-access, online journals, promising a paradigm shift from the current review, selection and dissemination processes in academic publishing. All Frontiers journals are driven by researchers for researchers; therefore, they constitute a service to the scholarly community. At the same time, the *Frontiers journal series* operates on a revolutionary invention, the tiered publishing system, initially addressing specific communities of scholars, and gradually climbing up to broader public understanding, thus serving the interests of the lay society, too.

Dedication to quality

Each Frontiers article is a landmark of the highest quality, thanks to genuinely collaborative interactions between authors and review editors, who include some of the world's best academicians. Research must be certified by peers before entering a stream of knowledge that may eventually reach the public - and shape society; therefore, Frontiers only applies the most rigorous and unbiased reviews. Frontiers revolutionizes research publishing by freely delivering the most outstanding research, evaluated with no bias from both the academic and social point of view. By applying the most advanced information technologies, Frontiers is catapulting scholarly publishing into a new generation.

What are Frontiers Research Topics?

Frontiers Research Topics are very popular trademarks of the *Frontiers journals series*: they are collections of at least ten articles, all centered on a particular subject. With their unique mix of varied contributions from Original Research to Review Articles, Frontiers Research Topics unify the most influential researchers, the latest key findings and historical advances in a hot research area.

Find out more on how to host your own Frontiers Research Topic or contribute to one as an author by contacting the Frontiers editorial office: frontiersin.org/about/contact

Coastal and marine environmental quality assessments

Topic editors

Dilip Kumar Jha — National Institute of Ocean Technology, India

Ganesh Thiruchitrambalam — Pondicherry University, Port Blair Campus, India

Meilin Wu — South China Sea Institute of Oceanology, Chinese Academy of Sciences (CAS), China

Prashanthi Devi Marimuthu — Bharathidasan University, India

Citation

Jha, D. K., Thiruchitrambalam, G., Wu, M., Marimuthu, P. D., eds. (2023). *Coastal and marine environmental quality assessments*. Lausanne: Frontiers Media SA.

doi: 10.3389/978-2-83251-726-0

Table of contents

06 Editorial: Coastal and marine environmental quality assessments
Dilip Kumar Jha, Meilin Wu, Ganesh Thiruchitrambalam and Prashanthi Devi Marimuthu

10 Environmental Quality and Ecological Risk Assessment of Heavy Metals in the Zhuhai Coast, China
Jin Wu, Shaowei Rong, Miaowei Wang, Rong Lu and Jingchao Liu

26 Microplastics in Demersal Sharks From the Southeast Indian Coastal Region
Madhuvandhi Janardhanam, Priya Sivakumar, Gomathi Srinivasan, Rekha Sivakumar, Priscilla Niranjani Marcus, Sujatha Balasubramaniam, Krishnamurthy Rajamanickam, Thiagarajan Raman, Gopalakrishnan Singaram and Thilagam Harikrishnan

33 Ocean Acidification Impact on Haematological and Serum Biochemical Parameters in *Lates calcarifer*
Gomathi Srinivasan, Priscilla Niranjani Marcus, Priya Sivakumar, Pandi Paramasivam, Rekha Sivakumar, Thilagam Harikrishnan and Sujatha Balasubramaniam

40 Coral Reef Health Status *versus* Muricid Bioindicator in the Lakshadweep Archipelago – A Multivariate Approach
Nithyanandam Marimuthu, James Jerald Wilson, Abdulmohsin Abdullah Al-Sofyani and Arumugam Kuppuswamy Kumaraguru

46 Modelling the Role of Temperature-Induced Environmental Noise on Phytoplankton Niche Dynamics
Subrata Sarker, Deen Mohammad, Siam Ahmed Nabil and Md. Alamgir Kabir

57 Diurnal fluctuations in seawater pCO_2 amplify the negative effects of ocean acidification on the biotic performance of the calcifying macroalga *Halimeda opuntia*
Zhangliang Wei, Yating Zhang, Fangfang Yang and Lijuan Long

71 Influence of rainfall events on zooplankton community characteristics and feeding habits in estuarine–coastal environments
Young Seok Jeong, Seohwi Choo and Ho Young Soh

85 Variations in nutrients and microbes during the occurrence and extinction of algal blooms: A mesocosm experiment with the addition of marine aquaculture sediment
Yuanmin Sun, Kunxian Tang, Yong Ma, Xuan Zhu, Heyang Li, Fei Zhang, Shan Chen and Haiping Huang

95 Evaluating the effect of various environmental factors on the growth of the marine microalgae, *Chlorella vulgaris*
Anthony Josephine, Thalavai Shivasankarasubbiah Kumar, Baskaran Surendran, Sundaram Rajakumar, Ramalingam Kirubagaran and Gopal Dharani

100 Modulation of biotransformation enzymes leads to oxidative stress and DNA damage in naphthalene exposed marine bivalve *Perna viridis*
Sathikumaran Ravi, Revathi Thillainayagam, Gopi Janakiraman, Punitha Subramanyam, Rekha Sivakumar, Thiagarajan Raman, Gopalakrishnan Singaram, Thilagam Harikrishnan and Krishnamurthy Rajamanickam

107 Modelling the influence of submesoscale processes on phytoplankton dynamics in the northern South China Sea
Peng Xiu, Lin Guo and Wentao Ma

121 Weathered polyethylene microplastics exposure leads to modulations in glutathione-S-transferase activity in fish
P. Pandi, J. Madhuvandhi, KK. Priya, R. Thiagarajan, S. Gopalakrishnan, S. Elumalai and H. Thilagam

128 The removal of atmospheric aerosols in a heavy industrial coastal city in China with frequent rainfall
Xin Zhou, Zhiyang Li, Chunqing Chen, Huijie Luo, Qingmei Zhu, Zhen Zeng and Qibin Lao

143 Spatial variability in the abundance and prey selection of the corallivorous snail *Drupella* spp. in the southeastern Hainan Island, China
Xinming Lei, Chengyue Liu, Yuyang Zhang, Xiaolei Yu, Jianhui Yang, Yong Luo, Guowei Zhou and Hui Huang

156 Coupled hydrodynamic and water quality modeling in the coastal waters off Chennai, East Coast of India
Umakanta Pradhan, Uma Sankar Panda, Subrat Naik, Pravakar Mishra, D. Satish Kumar, Mehmuna Begum and M. V. Raman Murthy

164 Using dual water isotopes to quantify the mixing of water masses in the Pearl River Estuary and the adjacent northern South China Sea
Xiaoyu Jian, Shuwen Zhang, Qibin Lao, Fajin Chen, Peng Huang, Chunqing Chen and Qingmei Zhu

177 Risk assessment of offshore oil spill in the northern South China Sea: A stochastic scenario modeling approach
Bingxu Geng, Wen Zhou, Lingyan Lu, Qian Cao, Man Hong and Ding Wen

187 Immunomodulatory response of Asian seabass *Lates calcarifer* in an *ex situ* environment: Implications for future ocean acidification scenario
Priscilla Niranjani Marcus, Priya Sivakumar, Gomathi Srinivasan, Rekha Sivakumar, Thilagam Harikrishnan, Sujatha Balasubramaniam and Gopalakrishnan Singaram

193 Categorizing numeric nutrients criteria and implications for water quality assessment in the Pearl River Estuary, China
Peng Zhang, Shujun Ou, Junxiao Zhang, Lirong Zhao and Jibiao Zhang

210 Impact of and recovery from seabed trawling in soft-bottom benthic communities under natural disturbance of summer hypoxia: A case study in subtropical Hong Kong
Wenzhe Xu, Anne Lise Fleddum, Paul K. S. Shin and Jun Sun

226 Comparative evaluation of heavy metal concentration in different organs of the asian seabass: A multivariate approach
Manasi Venkat Koduvayur, Shrivarshini Vasudevan, Vikas Pandey, Jayapal Santhanakumar, Dilip Kumar Jha and Gopal Dharani

233 Macrobenthic community of an anthropogenically influenced mangrove associated estuary on the East coast of India: An approach for ecological assessment
Aswini Nayak, Jawed Equbal, Sonali Sanghamitra Rout, Bhagyashree Dash, Ganesh Thiruchitrambalam, Punyasloke Bhadury, Behara Satyanarayana and Dipti Raut

253 Impacts of hypoxia on the mesozooplankton community structure in a semi-enclosed bay
Eun Hye Lee, Seo Yeol Choi, Min Ho Seo and Ho Young Soh

270 Unraveling the potential of bacteria isolated from the equatorial region of Indian Ocean in mercury detoxification
Gajendra Joshi, Pankaj Verma, Balakrishnan Meena, Prasun Goswami, D Magesh Peter, Dilip Kumar Jha, Nambali Valsalan Vinithkumar and Gopal Dharani

287 Seasonal variability and its impact on the sub-tidal macrobenthic fauna of Diu Island, north-eastern Arabian Sea: A multivariate approach
Vikas Pandey, Dilip Kumar Jha, Krupa Ratnam, Srinivas Venkatnarayanan, Ponnusamy Sathish Kumar, Pankaj Verma and Gopal Dharani

295 Spatial distribution and risk assessment of heavy metals in seawater and sediments in Jieshi Bay, Shanwei, China
Wen Zhou, Qian Cao, Man Hong, Yutao Lei, Ding Wen and Dengfeng Zhang

310 Three-dimensional numerical study of cooling water discharge of Daya Bay Nuclear Power Plant in southern coast of China during summer
Bingxu Geng, Lingyan Lu, Qian Cao, Wen Zhou, Shiyu Li, Ding Wen and Man Hong

frontiers | Frontiers in Marine Science

TYPE Editorial
PUBLISHED 07 February 2023
DOI 10.3389/fmars.2023.1141278

Check for updates

OPEN ACCESS

EDITED AND REVIEWED BY
Hans Uwe Dahms,
Kaohsiung Medical University, Taiwan

*CORRESPONDENCE
Dilip Kumar Jha
dilipjhaniot@gmail.com

SPECIALTY SECTION
This article was submitted to Marine Pollution, a section of the journal Frontiers in Marine Science

RECEIVED 10 January 2023
ACCEPTED 30 January 2023
PUBLISHED 07 February 2023

CITATION
Jha DK, Wu M, Thiruchitrambalam G and Marimuthu PD (2023) Editorial: Coastal and marine environmental quality assessments. *Front. Mar. Sci.* 10:1141278. doi: 10.3389/fmars.2023.1141278

COPYRIGHT
© 2023 Jha, Wu, Thiruchitrambalam and Marimuthu. This is an open-access article distributed under the terms of the Creative Commons Attribution License (CC BY). The use, distribution or reproduction in other forums is permitted, provided the original author(s) and the copyright owner(s) are credited and that the original publication in this journal is cited, in accordance with accepted academic practice. No use, distribution or reproduction is permitted which does not comply with these terms.

Editorial: Coastal and marine environmental quality assessments

Dilip Kumar Jha[1]*, Meilin Wu[2], Ganesh Thiruchitrambalam[3] and Prashanthi Devi Marimuthu[4]

[1]National Institute of Ocean Technology (NIOT), Ministry of Earth Sciences, Govt. of India, Chennai, India, [2]State Key Laboratory of Tropical Oceanography, South China Sea Institute of Oceanology, Chinese Academy of Sciences, Guangzhou, China, [3]Department of Ocean Studies and Marine Biology, Pondicherry University, Port Blair, India, [4]Department of Environmental Science and Management, Bharathidasan University, Tiruchirappalli, India

KEYWORDS

seawater quality, marine environment, plankton, benthos, temporal and spatial variation, anthropogenic influences

Editorial on the Research Topic
Coastal and marine environmental quality assessments

Seawater quality has a considerable impact on the biological productivity and ecological viability of coastal and marine environments (Dheenan et al., 2016; Yuvaraj et al., 2018; Ratnam et al.). Anthropogenic pressure has continuously grown due to population expansion and industrialisation in coastal areas, which has led to a decline in seawater quality along the coast. The environment and ecology have been severely damaged owing to the release of large amounts of pollutants through anthropogenic and natural catastrophes into the coastal and marine ecosystems. As a result, coastal pollution has grown to be a global problem that has to be addressed by using monitoring programs and a mitigation management system.

The physical, chemical, and biological components of coastal and marine ecosystems have a significant role in their productivity and sustainability. These ecosystems have been and continue to be significantly impacted by anthropogenic pollutants. More than 80% of all marine pollutants come from land-based sources, the bulk of which are commercial, agricultural, and urban in nature. Coastal and marine pollution is increased by human activities including offshore gas, oil extraction, and transportation.

Preventing and controlling coastal and marine pollution as well as developing better monitoring techniques and systems are essential for a better understanding of the spatial and temporal variations in seawater quality (Jha et al., 2015). Analyzing real-time data and its effects on the marine ecosystem requires the use of data buoys, remote sensing, and other cutting-edge technological advancements in coastal and marine water quality monitoring.

To analyse physicochemical and biological variables and other environmental issues including harmful algal blooms (HABs), heavy metal pollution, bioaccumulation, and eutrophication, it is necessary to create techniques for analysing long-term ecological data from the coastal and marine environments. The surveillance program provides huge datasets that are extremely useful for determining the health of the marine ecosystem. The approach for analysing environmental factors must be improved in light of current technological breakthroughs to meet the scientific demands for large dataset analysis and understanding. The physicochemical properties of water, phytoplankton, zooplankton, nutrients, metal

toxicity, benthos, microorganisms, ocean acidification, micro-plastic, and sediment quality are important variables that need to be monitored (Dheenan et al., 2014; Pandey et al., 2021; Kumar et al., 2022; Pandey et al., 2022). The research is further extended to look at modelling approaches, newly created statistical tools, or a combination of techniques or biotic index in the coastal and marine environment, concentrating on interactions between land and seawater.

Impact of physicochemical and biological variables

The physicochemical and biological variables are very important for ecosystem maintenance and management. Josephine et al. reported that *Chlorella vulgaris* grows better at 25°C (temperature), 8.0 (pH), 30 PSU (salinity), and blue light (499–465 nm) and further revealed that optimized environmental conditions could increase growth rate and biomass. Lee et al. suggested that hypoxia can affect the mesozooplankton abundance and its occurrence in Gamak Bay and revealed that three cladocerans species like *Pleopis polyphemoides, Pseudoevadne tergestina*, and *Penilia avirostris*, as well as the copepod Acartia sinjiensis, were the dominating species during the hypoxic phase. Jeong et al. found that rainfall causes zooplankton distribution to change in temperate estuaries, as well as changes in salinity and suspended particulate matter. Sun et al. experimentally demonstrated, through a mesocosm experiment that the impact of disturbed sediment on ocean water. The findings demonstrated that the levels of dissolved oxygen (DO) decrease significantly and those of nutrients increased gradually after the addition and stirring of the aquaculture sediment; in specific, the levels of ammonia and dissolved inorganic phosphorus increased considerably. Joshi et al. found that among the four mercury-resistant bacteria (MRB) that were isolated from the equatorial region of the Indian Ocean (ERIO), NIOT-EQR J251 was the most effective at removing mercury from culture media. Zhang et al. divided the Pearl River Estuary (PRE) coastal waters into three sub-areas: freshwater (Zone I), mixed (Zone II), and seawater (Zone III) to establish integrated land-ocean unified nutrient criteria and water quality assessment as well as the implementation of effective coastal eutrophication regulation in the future. According to Zhou et al., clean marine emissions and secondary aerosols were the main sources of total suspended particles and water-soluble inorganic ions. Further, heavy industrial activities and excellent air quality in Zhanjiang could be explained by the high precipitation frequency (63%) and the marine dilution effect (27%). According to Jian et al. mixing of various water masses is crucial for regional, physical and biogeochemical mechanisms as well as for the ocean ecosystems. The mixing of water masses in the Pearl River Estuary and the surrounding northern South China Sea was studied quantitatively using a unique dataset of stable water isotopes (δD and δ18O), temperature, and salinity profiles.

The ecological function of benthos

Benthos are very essential for ecosystem functioning as they play important roles in the energy flow, sediment reworking, cycling of organic matter and nutrients and serve as an indicator to assess the integrity of the ecosystem (Pandey and Ganesh, 2019). Nayak et al. found that Mahanadi Estuarine System is subjected to intense human activity and abound three major benthic faunal groups influenced by tolerant/opportunist species proved with hierarchical clustering analysis. Xu et al. reported that the structure and composition of benthic fauna are significantly impacted by bottom trawling. Furthermore, when a region is subject to hypoxia, bottom trawling may help to increase the level of DO, leading to a higher level of diversity in the trawled area compared to the non-trawled area in the summer. Pandey et al. found that the environmental perturbation during the monsoon season brings significant changes in physicochemical and biological characteristics whereas non-monsoon season revealed a healthy benthic environment in Diu Island.

Marimuthu et al. evaluated the Lakshadweep Archipelago's benthic environment for the geographic variability of the negative biological indicator *Drupella cornus* and its preferred coral species *Pocillopora verrucosa* during the research. Lei et al. examined the quantity and distribution of *Drupella* spp. concerning coral-prey availability, selectivity, and nutritional value suggests that the particular reef habitat and environmental factors may change the prey preference of Drupella spp. Benthic fauna is considered an important indicator and hence Ravi et al. found that regular monitoring programs of the coastal and marine environments might make use of biomarkers to evaluate naphthalene exposure and toxicity in marine creatures (*Perna viridis*).

Heavy metal and its ecological impact

The anthropogenic activities and natural events (like dust deposition, volcanic eruptions, and mineral weathering) cause trace metals to enter the coastal and marine environment (such as mining, burning fossil fuels, agriculture, industry, marine traffic, urbanization, and sewage release) (Sundararajan et al., 2016; Jha et al., 2019; Satheeswaran et al., 2019; Jha et al., 2021). Metal bioaccumulation in the marine ecosystem poses a threat to the flora and fauna and ultimately human beings in the food chain. Zhou et al. revealed the distribution patterns of six metals (Zn, Cu, As, Pb, Cd, and Hg) in the seawater, sediments, and living organisms in Jieshi Bay, it is crucial to preserve the quality of the seawater due to bioaccumulation from seafood and associated products. Wu et al. discovered that the fast urbanization and industrialization in the coastal Zhuhai had caused serious metal contamination and demonstrated that Cu, Zn, and Pb exceeded the standards of seawater, confirming the existence of anthropogenic contamination. The findings of the environmental vulnerability assessment also revealed that the environmental hazards for Cd and Cu were high. Manasi et al. estimated heavy metal concentrations of cadmium, lead, and mercury in different organs of Asian Seabass, *Lates calcarifer*, aimed of determining the associated risk from fish consumption. The results suggested that the metal level in the fish muscle was well within the recommended level for seafood in the Rameswaram coastal region, southeast coast of India, and safe for human consumption.

Ocean acidification and its ecological impact

Long-term pH decreases in the ocean are referred to as ocean acidification (OA), and they are mostly because of atmospheric carbon dioxide. Srinivasan et al. found that ocean acidification has an impact on the haematological and biochemical components and also had an impact on physiology such as growth in *L. calcarifer*, with the impact being stage-specific and pH-dependent. Marcus et al. highlighted the difference between two distinct size groups of fish when exposed to an acidic environment and how the immune system in *L. calcarifer* is modulated. Furthermore, it has been established that the CO_2 driven acidification of seawater affects several stressors, with the rising H+ level being just one of them. Wei et al. conducted a forty-two days laboratory experiment to ascertain how *Halimeda opuntia*, a calcifying macroalga, responds to varying pCO_2 under OA conditions in terms of growth, biological performance, and associated carbon and nitrogen metabolic products (1200 ppmv). It is evident through their study that increased pCO_2-related stress, greater free amino acid level, and proline secretion were connected to maintaining the integrity of algal cellular structures.

Micro-plastic and its impact on fauna

A ubiquitous and persistently threatening global environmental problem is the pollution of the oceans with microplastics (MPs). Over the past fifty years, the annual production of plastics has more than doubled, with an estimated 335 MT of production in 2016. (Galgani et al., 2015; Plastics Europe, 2018). Plastics are a significant contributor to marine pollution because they are present in a wide range of terrestrial and aquatic ecosystems. MPs contaminations endanger marine life and have significant consequences on ecosystems. Janardhanam et al. noticed MPs consumption in demersal sharks taken during trawling in marine seawaters beyond 80 m depth along the Southeast coast of India and discovered 4.67 pieces/shark in which the gastrointestinal system revealed more MPs compared to the gills. Pandi et al. discovered that exposure to weathered Polyethylene (wPE) microplastics affected the glutathione-S-transferase enzymes in zebra fish. This study also discovered that wPE microplastic exposure changed the levels of gene expression for the biotransformation enzymes, which raises the possibility that these enzymes might be used as helpful biochemical markers for determining microplastic exposure in coastal and marine environments.

Seawater quality modelling

Planktons are a diverse collection of organisms found in water that are unable to swim against the water current and are categorized as phytoplankton (plants) and zooplankton (animals). Phytoplankton is small plants among the plankton population and is regarded as the main source of energy in the aquatic environment. Zooplankton and fish species that eat plants use phytoplankton as food. Thus, variation in the biomass and composition of the phytoplankton population regulates the zooplankton composition, which eventually has an impact on fisheries productivity (Schroeder, 1983). Any water quality may be estimated with ease and at a low cost using numerical modelling and remote sensing; nevertheless, field data are necessary to validate the model. Geng et al. found that the spilling of oil is a normally unexpected occurrence that is negative to the ecosystem, its flora, and fauna, however, a numerical model demonstrated that wind direction played a dominating role in the direction of the dispersion of oil in the northern South China Sea. Geng et al. also observed the impact of thermal pollution caused by the cooling water discharge of power plant on the surrounding marine ecology and established a high-resolution 3D cooling water discharge model based on the ECOMSED model in Daya Bay and the model were consistent with the observation results on the distribution of time series of tide level and temperature. Xiu et al. discovered that high concentration patches at the edge area between mesoscale eddies, which were high compared to those in the cyclonic eddy core area in the northern South China Sea (NSCS) as per the observation of the satellite chlorophyll data (May 2015). A high-resolution physical-biological model was used to analyze the underlying mechanisms, highlighting the necessity of high-resolution measurements and the significance of sub-mesoscale processes on phytoplankton dynamics in the NSCS. Pradhan et al. discovered that a coupled hydrodynamic-water quality model had been built to simulate and predict coastal water quality parameters and that the model's performance for both hydrodynamics and water quality was within reasonable limits for up to three days of prediction. Sarkar et al. discovered that species may survive in a noise-induced system due to rhythmic fluctuation in biomass, change in carrying capacity, lack of competitive exclusion, and non-equilibrium conditions. Another putative coexistence mechanism was discovered to be high amplitude species biomass fluctuation at greater ambient noise. Additionally, a change in the mean niche conditions of the species was seen along with the change in ambient noise.

Author contributions

DJ and TG: original draft preparation and writing. MW and PD: reviewing and correcting the editorial. All authors contributed to the article and approved the submitted manuscript for publication.

Acknowledgments

Authors are grateful to Rui Fernandes, Charlie Chen, Alice Lickley, and Talitha Gray for their support in organising the Research Topic, the submission process of articles, and completing the review process. We would like to thank the chief editors for the necessary approval and final acceptance of the peer-reviewed articles. We also thank all the reviewers for their excellent contribution for the successful completion of this issue.

Conflict of interest

The authors declare that the research was conducted in the absence of any commercial or financial relationships that could be construed as a potential conflict of interest.

Publisher's note

All claims expressed in this article are solely those of the authors and do not necessarily represent those of their affiliated organizations, or those of the publisher, the editors and the reviewers. Any product that may be evaluated in this article, or claim that may be made by its manufacturer, is not guaranteed or endorsed by the publisher.

References

Dheenan, P. S., Jha, D. K., Das, A. K., Vinithkumar, N. V., Prashanthi Devi, M., Kirubagaran, R., et al. (2016). Geographic information systems and multivariate analysis to evaluate fecal bacterial pollution in coastal waters of Andaman, India. *Environ. pollut.* 214 (7), 45–53. doi: 10.1016/j.envpol.03.065

Dheenan, P. S., Jha, D. K., Vinithkumar, N. V., Ponmalar, A. A., Venkateshwaran, P., and Kirubagaran, R. (2014). Spatial variation of physicochemical and bacteriological parameters elucidation with GIS in rangat bay, middle andaman. *India. J. Sea Res.* 85, 534–541. doi: 10.1016/j.seares.2013.09.001

Galgani, F., Hanke, G., and Maes, T. (2015). "Global distribution, composition and abundance of marine litter," in *Marine anthropogenic litter*. Eds. M. Bergmann, L. Gutow and M. Klages (Berlin: Springer), 29–56.

Jha, D. K., Devi, M. P., Vidyalaxmi, R., Balan, B., Vinithkumar, N. V., and Kirubagaran, R. (2015). Water quality assessment using water quality index and geographical information system methods in the coastal waters of Andaman Sea, India. *Mar. pollut. Bull.* 100 (1), 555–556. doi: 10.1016/j.marpolbul.2015.08.032

Jha, D. K., Dharani, G., Verma., P., Ratnam, K., Senthil Kumar., R., and Rajaguru, S. (2021). Evaluation of factors influencing the trace metals in puducherry and diu coasts of India through multivariate techniques. *Mar. pollut. Bull.* 167 (6), 2021. doi: 10.1016/j.marpolbul.2021.112342

Jha, D. K., Ratnam, K., Rajaguru, S., Dharani, G., Devi, M. P., and Kirubagaran, R. (2019). Evaluation of trace metals in seawater, sediments, and bivalves of nellore, southeast coast of India, by using the multivariate and ecological tool. *Mar. pollut. Bull.* 146, 1–10. doi: 10.1016/J.MARPOLBUL.2019.05.044

Kumar, P. S., Venkatnarayanan, S., Pandey, V., Ratnam, K., Jha, D. K., Rajaguru, S., et al. (2022). Multivariate approach to evaluate the factors controlling the phytoplankton abundance and diversity along the coastal waters of diu, northeastern Arabian Sea. *Oceanologia* 64 (2), 267–275. doi: 10.1016/j.oceano.2021.11.005

Pandey, V., and Ganesh, T. (2019). Spatial and temporal variability of sandy intertidal macrobenthic communities and their relationship with environmental factors in a tropical island. *Estuar. Coast. Shelf Sci.* 224, 73–83. doi: 10.1016/j.ecss.2019.04.045

Pandey, V., Jha, D. K., Sathish Kumar, P., Santhanakumar, J., Venkatnarayanan, S., Jebakumar, J., et al. (2022). Effect of multiple stressors on the functional traits of sub-tidal macrobenthic fauna: A case study of the southeast coast of India. *Mar. pollut. Bull.* 175, 113355. doi: 10.1016/j.marpolbul.2022.113355

Pandey, V., Venkatnarayanan, S., Sathish Kumar, P., Ratnam, K., Jha, D. K., Rajaguru, S., et al. (2021). Assessment of ecological health of swarnamukhi river estuary, southeast coast of India, through AMBI indices and multivariate tools. *Mar. pollut. Bull.* 164, 112031. doi: 10.1016/j.marpolbul.2021.112031

Plastics Europe (2018). *Plastics – the facts 2017, an analysis of European plastics production, demand and waste data* (Belgium: Brussels), 16.

Satheeswaran, T., Purushothaman, Y., Palani, D., Velmurugan, K., Jha, D. K., Dharani, G., et al. (2019). Assessment of trace metal contamination in the marine sediment, seawater, and bivalves of parangipettai, southeast coast of India. *Mar. pollut. Bull.* 1492019, 110499. doi: 10.1016/j.marpolbul.2019.110499

Schroeder, GL. (1983). Sources of fish and prawn growth in poly culture ponds as indicated by delta C analysis. *Aquaculture* 35, 29–42. doi: 10.1016/j.marpolbul.2019.110499

Sundararajan, S., Khadanga, M. K., Prince Prakash Jeba Kumar, J., Raghumaran, S., Vijaya, R., and Jena, B. K. (2016). Ecological risk assessment of trace metal accumulation in sediments of veraval harbor, Gujarat, Arabian Sea. *Mar. pollut. Bull* 114 (1), 592–601. doi: 10.1016/j.marpolbul.2016.09.016

Yuvaraj, P., Satheeswaran, T., Damotharan, P., Karthikeyan, V., Jha, D. K., Dharani, G., et al. (2018). Evaluation of the environmental quality of parangipettai, southeast coast of India, by using multivariate and geospatial tool. *Mar. pollut. Bull.* 131 (6), 239–247. doi: 10.1016/j.marpolbul.2018.04.022

frontiers | Frontiers in Marine Science

ORIGINAL RESEARCH
published: 20 May 2022
doi: 10.3389/fmars.2022.898423

Environmental Quality and Ecological Risk Assessment of Heavy Metals in the Zhuhai Coast, China

Jin Wu[1], *Shaowei Rong*[1], *Miaowei Wang*[1], *Rong Lu*[2*] and *Jingchao Liu*[1]

[1] Faculty of Architecture, Civil and Transportation Engineering, Beijing University of Technology, Beijing, China, [2] South China Sea Marine Survey Technology Center, State Oceanic Administration, Guangzhou, China

The rapid urbanization and industrialization in the coastal Zhuhai have resulted in severe heavy metal contamination. Heavy metals are extensively used as indicators of coastal contamination, but the comparability among different geographic environments needs to be further explored and scrutinized. In this study, heavy metals (i.e., As, Zn, Cd, Cr, Hg, Cu, and Pb) in surface seawater (20 sites), sediments (10 sites), and organisms (13 sites, shellfish, algae, fish, and crustaceans) were analyzed to assess the distribution, enrichment, and ecological risk in the coastal regions of Zhuhai (2017 and 2018). The results showed that Cu, Zn, and Pb exceeded the standards of seawater, indicating the presence of anthropogenic pollution. Meanwhile, the ecological risk results showed that Cd and Cu indicated moderately high environmental risks. The quantity and quality of heavy metals in organisms showed different trends in the sea, which affected marine organisms in the northeastern area. The main factors contributing to the ecological risk of these two heavy metals are the emissions from chemical companies. Therefore, preserving the high biological diversity in this area is important to ensure the health and productivity of the seawater ecosystem in the coastal area. These results may play a key role in promoting decision makers to manage the sustainability of the Zhuhai coast.

Keywords: heavy metals, water quality assessment, ecological risk assessment, species sensitivity distribution, marine

OPEN ACCESS

Edited by:
Dilip Kumar Jha,
National Institute of Ocean Technology, India

Reviewed by:
Satheeswaran Thangaraj,
Incheon National University, South Korea
Thilagam Harikrishnan,
Pachaiyappa's College for Men, India
Biraja Kumar Sahu,
Council of Scientific and Industrial Research (CSIR), India

***Correspondence:**
Rong Lu
lurong@smst.gz.cn

Specialty section:
This article was submitted to Marine Pollution, a section of the journal Frontiers in Marine Science

Received: *18 March 2022*
Accepted: *18 April 2022*
Published: *20 May 2022*

Citation:
Wu J, Rong S, Wang M, Lu R and Liu J (2022) Environmental Quality and Ecological Risk Assessment of Heavy Metals in the Zhuhai Coast, China. Front. Mar. Sci. 9:898423. doi: 10.3389/fmars.2022.898423

1 INTRODUCTION

Heavy metals are one of the most serious pollutants in the environment and have attracted widespread attention worldwide due to their inherent toxicity, persistence, and bioaccumulation properties (Abaya et al., 2018; Huang et al., 2019; Kong et al., 2021). With industrial, agricultural, and urban development, heavy metals discharged into the coastal marine environment through surface runoff are increasing and enriching in marine sediments and aquatic organisms (Sruthi et al., 2018). When the concentration of heavy metals in the coastal ecosystem reaches a certain level, it will pose a great danger to the marine ecosystem and human health (Wang et al., 2018). The coastal ecosystem is a very important link in the ecological protection of coastal areas and plays an important role in the marine environment, social development, and population growth of coastal areas (Majithiya et al., 2018; Rao et al., 2021). Coastal ecosystems can also provide ecological buffers

to the coastal areas and protect them from external intrusion and hazards (Sruthi et al., 2018). Changes in coastal zone ecosystems are partly due to sea-level rise, climate change, and partly human activities, such as changing land properties for coastal development, aquaculture, agricultural, and industrial activities (Wang et al., 2018; Wang L. et al., 2019).

Ecological risk assessment is developed from risk assessment, and in recent decades, its evaluation content, scope, and research scale have been greatly expanded. In general, the assessment tools can be used to qualitatively evaluate the degree to which the seawater- or sediment-associated chemical status might adversely affect aquatic organisms and are designed to assist in the interpretation of water/sediment quality (Kaikkonen et al., 2018; Quyen et al., 2021). The research scale of ecological risk assessment has been extended from single species to ecosystems, and the research objects have been extended from terrestrial to marine ecosystems (Wang Q. et al., 2019). The species sensitivity distribution (SSD) method, on the basis of differences in the sensitivity of different species to contaminations, was employed to develop environmental criteria for the conservation. The SSD calculates the toxicological data of different species for the whole ecosystem so as to understand the hazards of pollutants at the ecosystem level (Xia et al., 2020). The SSD method has become one of the advantageous methods of risk assessment internationally in recent years due to its advantages of conciseness and clear ecological significance (Xu J. et al., 2018; Xu et al., 2021). However, only a few studies on this method have been reported in China and mainly focused on freshwater organisms and assessed the ecological risk of various organisms such as DDT, lindane, polycyclic aromatic hydrocarbons, chlorophenols, and diisooctyl phthalate to freshwater organisms (Li et al., 2018a; Cui et al., 2021; Xu et al., 2022). Ecological risk assessment based on species sensitivity differences has obvious advantages for solving complex ecosystems (Sruthi et al., 2018), such as integrated ecological risk classification in coastal seas (Kumar et al., 2019; Luo et al., 2019).

The Pearl River is the second most important river system in South China, ranking among the seven major rivers in China in terms of annual runoff. The stability and health of the ecological environment of the Zhuhai coast, which is one of the most important sea outlets in the Zhuhai watershed, are related to the healthy development of this special economic zone. In previous studies, large-scale data on the heavy metal concentration and ecological risk of coastal seawater and sediments along the coast of Guangdong province have been collected, especially focusing on the economically developed Pearl River estuary (Birch, 2018; Wang R. et al., 2020). Previous studies found that the characterization of the distribution of heavy metals in these coastal marine areas has certain regularity. From far to near the coast, the concentration of heavy metals is gradually increasing, and the resulting risk is also gradually increasing (**Table S1**). Usually, the coastal special economic zones are experiencing high economic development, which inevitably leads to the discharge of industrial pollution. Analyzed from the environmental-geochemical point of view, the accumulation of heavy metals is gradually weakened with the extension of migration paths, which is the main reason for the serious excess of heavy metals on the coast of this study area. The ecological risk studies based on SSD have been carried out less for the sea area of the Zhuhai coast. Therefore, in this study, the seawater, sediment, biological species, and productivity were mainly sampled and investigated by selecting the sea area of Gaolan on the Pearl River coast as the study area.

In China, the marine areas with the most serious heavy metal pollution are the bays and estuaries where industrial and mining industries are concentrated, some of them are contaminated with Cd, Cu, Pb, and Hg, and some of them are seriously contaminated with Cd and As (Fang et al., 2018; Hu et al., 2021). Heavy metal pollution in the ocean is bound to bring a great threat to the local ecological diversity (Reddy et al., 2016; Satheeswaran et al., 2019; Pandey et al., 2021; Pandey et al., 2022). Therefore, it is urgent to study the ecological risk of heavy metal pollution in China's oceans. Hence, the target of this research is to assess the potential impact of heavy metals on seawater, sediment, and marine organisms and provide ecological risk evaluation and risk management of heavy metal pollution in China's marine environment. Thus the SSD curves of heavy metals, the 5% hazard concentration (HC5) of marine organisms at different trophic levels, and the potential impact ratio (PAF) were calculated to support the completion of the above goals.

2 MATERIAL AND METHODS

2.1 Description of Study Area

Zhuhai (21°45′–22°40′N, 113°03′–113°35′E) is an economic functional area with a total area of 380 km^2 and is the main coastal hub port in South China (**Figure 1**). Zhuhai and its coastal sea areas have a typical subtropical monsoon climate with an obvious winter monsoon. From 1962 to 2010, the linear warming rate of the annual average temperature in Zhuhai was 0.14°C/10a, the average temperature was 22.61°C (Li and Chen, 2014), and the SD was 0.44. The depth of seawater is about −8 to 10 m, which provides excellent conditions for industrial and agricultural production. As a national-level economic and technological development zone in China, Zhuhai is the gateway to the world from the South China Sea, and the Zhuhai coast is one of the most dynamic and potential areas of Guangdong's marine economy, with the largest berths of liquid chemicals and bulk cargo in the Pearl River Delta. The industrial types in Zhuhai are mainly large equipment manufacturing, petrochemical industry, and fine chemical industry, and aquaculture is also an important contributor to economic development.

2.2 Sampling Collection and Analysis

The location of the study area and the layout of the survey stations are shown in **Figure 1**. A total of 20 water quality survey sites, 10 sediment survey sites, and 13 ecological survey sites (partially overlapping, totaling 20 sampling sites) were studied in this survey. Sample collection and survey studies were conducted in November 2017 (Autumn) and March 2018 (Spring). Samples were collected only once per season. On each of the sampling sites, four subsamples were taken by randomly collecting fresh surfaces around the center sampling site (5 m). Combined with the center

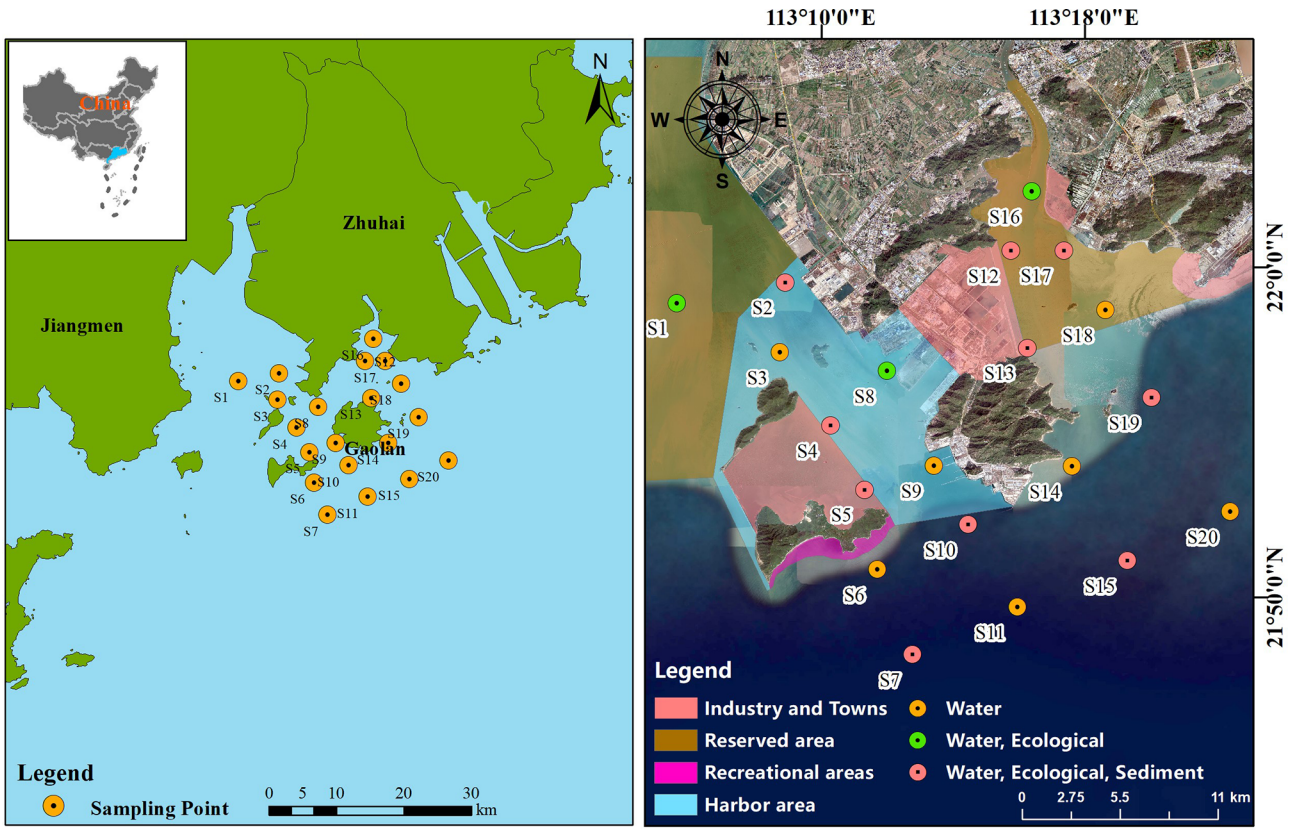


FIGURE 1 | Study area and sampling sites.

sample, five samples are collected and mixed thoroughly into one composite sample for post-processing analysis. Following the collection, all samples were stored in a refrigerator and transported to the laboratory by a professional transporter. The People's Republic of China for Marine Survey Specifications (GB/T 12763-2007) and Marine Monitoring Specifications (GB17378-2007) were chosen as the references for steps and tools in the sample collection process (Li et al., 2018a; Liu et al., 2018; Wang X. et al., 2020). The concentration of heavy metals was determined by inductively coupled plasma mass spectrometry and inductively coupled plasma atomic emission spectrometry. To ensure the quality of analysis, the control methods and laboratory quality assurance were implemented, including the use of standard operating procedures, analysis of reagent blanks, calibration with standards, and analysis of replicates. The relative SD indicating the precision of analytical procedures ranged from 3.5% to 8.5%. The percent recoveries varied between 86% and 95% for all metals.

The seawater depth, transparency, and color were observed on site. Surface and bottom samples were collected at 0.1–1 m from the seawater surface and 2 m from the bottom. Sediment samples were collected using a 0.05-m^2 grab mud collector to collect sediment samples at 0–1 cm from the surface layer of seafloor sediments and were stored in sealed packages. After stones and other debris were removed, samples were air-dried at room temperature (20°C to 23°C). Then the samples were ground with an agate mortar and passed through 160 mesh nylon screens. Four categories of organisms, including locally common and representative shellfish, algae, fish, and crustaceans, were selected among intertidal organisms and benthic organisms for the quality survey, and the samples were collected, preserved, and transported according to the relevant regulations of GB/T 12763.6-2007 for the biological survey (Kim et al., 2018; Wu et al., 2018). A trawling survey was carried out on the sampling site, the net was set at a distance of 2 nautical miles from the station, and the towing speed was controlled at 2–3 knots. A sufficient number (about 1.5 kg) of intact organisms samples were selected and placed in a clean polyethylene bag for sealing and preservation. This bag along with the sample label in another polyethylene bag was sealed and refrigerated. The collected water samples were filtered using a 0.45-μm or 60-mm microporous membrane with HNO_3/H_2SO_4 to pH < 2 for cryogenic refrigeration, the collected sediment samples were sealed and stored away from light, and the samples of various organisms were sorted and stored in polyethylene bags for freezing. As and Hg were determined by atomic fluorescence, while Cu, Cd, Cr, Pb, and Zn were determined by flameless atomic absorption spectrophotometry (Yang et al., 2019; Anusuya et al., 2021).

2.3 Data Analysis

Several statistical tools, mainly including Pearson's correlation analysis, non-metric multidimensional scaling analysis (NMDS), Adonis test, Procrustes analysis, and constrained ordination principal coordinate analysis (CPCOA), were used to investigate the correlations or differences between heavy metals and samples. Network analysis was employed to explore the co-occurrence of heavy metals and organisms in marine based on their strong and significant correlation matrixes (p-value <0.05; Spearman's r > 0.8). Network visualization was performed employing Gephi (v0.9.2). Statistical analyses were conducted in R (v3.4.2) by utilizing several R packages, including gunifrac, car, and vegan. Kriging interpolation method of ArcGIS (v10.8, ESRI, Redlands, CA, USA) was employed for the spatial distribution characteristics of heavy metals in the sediment.

2.4 Partitioning and Bioaccumulation

The distribution coefficient between sediment and water (K_d), biota-sediment accumulation factor (BSAF), and bioaccumulation factor (BAF) were employed to explore the accumulation and adsorption of heavy metals between different phases. The specific formulas were calculated as follows (Ashayeri and Keshavarzi, 2019; Liu et al., 2022):

$$K_d = \frac{C_{sed}}{C_{sea}} \tag{1}$$

$$BSAF = \frac{C_{org}}{C_{sed}} \tag{2}$$

$$BAF = \frac{C_{org}}{C_{sea}} \tag{3}$$

where C_{sed}, C_{sea}, and C_{org} are the concentration of target heavy metal in sediments, seawaters, and marine organisms, respectively. The value of K_d shows the possibilities of heavy metals preferentially retrained through sediments, and a higher K_d value indicates greater liquidity. Both BSAF and BAF are employed to describe the capability of organisms accumulating heavy metals from other mediums in the surrounding. BSAF < 1 or BAF > 100 demonstrates a low accumulation effect between the surrounding environment and organisms (Liu et al., 2022).

2.5 Pollution Assessment

The standard index method (single water quality index (WQI) method) was used to assess the degree of pollution of each heavy metal in seawater, and the characteristic pollution factors were identified based on the ranking of the calculated results (Zhao et al., 2019). In order to assess the regional water quality condition, the WQI method was used for comprehensive water quality assessment (Xiao et al., 2021; Xu Y. et al., 2018). The calculation formula was as follows:

$$A_i = C_a / C_{si} \tag{4}$$

$$\mathrm{WQI} = \frac{1}{\mathrm{n}} \sum_{i=1}^{n} \mathrm{A_i} \tag{5}$$

where A_i is the standard index of i pollutants; C_i is the measured concentration of i pollutants; C_{si} is the evaluation standard of i pollutants. The evaluation is carried out according to the corresponding category standards in the Seawater Quality Standard (GB3097-1997). WQI is a comprehensive index of water quality, A_i is a single factor of the standard index, and n is the number of items of all the water quality parameters involved in the assessment. WQI < 1 means that the water quality is excellent; 1 < WQI < 2, good; 2 < WQI < 3, normal; 3 < WQI < 5, poor; and WQI > 5, very poor (Xu Y. et al., 2018).

2.6 Biological Quality Assessment

In this study, primary productivity and diversity index were used to characterize the biological quality in the study sea, where primary productivity characterizes the richness of the marine environment and diversity index characterizes the dominance of marine organism populations. The primary productivity was estimated by the chlorophyll *a* method according to the simplified formula proposed by Cadée and Hegeman (1974). The diversity index was calculated using the Shannon–Wiener index formula, as follows:

$$P = C_a Q L t / 2 \tag{6}$$

$$H' = -\sum_{i=1}^{S} P_i log_2 P_i \tag{7}$$

where P is the primary productivity, mg·C/m^2·d; C_a is the surface chlorophyll *a* concentration, mg/m^3; Q is the assimilation coefficient, mg·C/(mgChl-a·h), based on the results of the South China Sea survey, which was taken here as 3.70 (Wang X. et al., 2020). H′ is the species diversity index, S is the total number of species in the sample, and P_i is the number of individuals and the total number of species in the *i*th sample. Pi is the ratio of the number of individuals in the *i*th to the total number. Uniformity J is used to characterize the integrity of the marine ecosystem, and Pielou's uniformity formula is J = H′/$\log_2$S, where J represents uniformity, H′ characterizes the species diversity index, and S is the total number of species in the sample.

2.7 Species Sensitivity Distribution Assessment

The SSD method was used to evaluate the ecological effects of heavy metal pollutants in seawater, which is an advanced statistical extrapolation method with high confidence based on the differences in the sensitivity of different species to pollutants, and has the advantages of conciseness and clear ecological significance. The Burr type III distribution was chosen to fit the exposure concentration accumulation curve, and the Burr type III distribution covers a large range in both skewness and kurtosis, which makes it more flexible to fit the parameters (Li et al., 2018b; Liu et al., 2020). The parametric equation of the Burr type III function F(x) is as follows:

$$\mathrm{F(x)} = \frac{1}{\left[1 + \left(\frac{b}{\mathrm{x}}\right)^{\mathrm{c}}\right]^{\mathrm{k}}} \tag{8}$$

$$HC(q) = \frac{b}{\left[\left(\frac{1}{q}\right)^{\frac{1}{k}} - 1\right]^{1/c}} \quad (9)$$

$$PAF(x) = \frac{1}{\left[1 + \left(\frac{b}{x}\right)^{c}\right]^{k}} \quad (10)$$

$$msPAF = 1 - \Pi_{i=1}^{n}(1 - PAF_i) \quad (11)$$

In the equations, b, c, and k are the three parameters of Burr type III distribution; HC5 is the cumulative concentration corresponding to the proportion of hazardous species on the SSD curve when it reaches 5%; and the smaller HC5 means that it represents a more toxic heavy metal. In equation (9), q is the corresponding protection level, and PAF is the proportion of hazardous species corresponding to each measured concentration on the SSD curve. In equation (10), x is the measured concentration of pollutants. In equation (11), msPAF is the proportion of hazardous species produced by the combination of multiple pollutants, which can reflect the joint pollution of multiple pollutants in the water body.

3 RESULTS AND DISCUSSION

3.1 Characteristics of Heavy Metals in Seawater, Sediment, and Marine Organism

3.1.1 Contamination Characteristics of Heavy Metals in the Seawater

The water quality evaluation results of the sea area calculated by using the factor evaluation method are shown in **Table 1** (Liu et al., 2022). It can be seen from **Table 1** that in the autumn of 2017, the main exceedance factors are Cu and Zn, and the exceedance rates are 11.1% and 22.2%, respectively. The exceedance factors in the main discharge areas of industrial towns were inorganic nitrogen and reactive phosphate, with 100% and 50% exceedance rates, respectively. Similarly, it can be seen from **Table 2** that in the spring of 2018, the main exceedance factors of seawater in the agricultural farming area were inorganic nitrogen, Pb, reactive phosphate, and Cu, with exceedance rates of 100%, 66.7%, 33.3%, and 11.1%, respectively. From the overall analysis, the different pollution factors in Autumn 2017 and Spring 2018 are mainly caused by the uneven distribution of seawater caused by seasonal monsoon. On the other hand, the water quality in the lower layer of seawater (B layer) is significantly better than that in the upper layer (A layer), mainly since the upper layer is the main area of influence of farming, industrial discharges, and other activities. The main source of inorganic nitrogen and phosphate, as the main pollutants, is the marine agricultural farming activities near the sea area, and the release of large amounts of inorganic nitrogen and phosphate in this process is the main reason for the exceedance of these two pollutants in the overall sea area.

The analysis results of a heavy metal evaluation in the coastal seawater of Zhuhai are shown in **Figures 2**, **3**. From **Figures 2**, **3**, it can be seen that the concentration of Cu, Zn, Cd, Cr, Hg, and As in the seawater in Autumn 2017 are in line with the first-class standard of seawater quality, and only one site has Pb concentration exceeding the second class standard of seawater quality. The concentration of Cu, Pb, Cd, Cr, Hg, and As in the seawater in spring 2018 is in line with the first-class standard of seawater quality, and only one site has a Zn concentration exceeding the second class standard of seawater quality. Zn concentration at one site exceeded the second standard for seawater quality. At the same time, the concentration of heavy metals in the seawater of the Gaolan Sea has a significant seasonal trend, and the concentrations of As, Cd, and Cr have significant seasonality. The concentrations of As, Cd, and Cr in autumn are higher than those in spring, and this result may be due to the higher rainfall in spring (569.6 mm) than in autumn (288.9 mm) (Cui et al., 2021) and the seasonal variation of river flow in Guangdong Province. This result suggests that dilution leads to lower concentrations of heavy metals in seawater; the seasonal distribution of precipitation in Guangdong is affected by the recession of cold high pressure. The rise and fall of summer winds leading to higher rainfall in spring were also reported in the studies of Zhang et al. (2017) and Liu et al. (2018). As, Cd, Cr, Cu, Hg, and Zn were detected at the highest concentrations at stations closer to the coastline, with a decreasing trend in the direction toward the ocean, while the highest concentrations of Pb were found at 4–5 km south of the coastline. The comparison of the distribution of heavy metal concentration in the sea area with other similar areas is shown in **Table S1**, which shows that the surface heavy metal hazard in the sea area of coastal Zhuhai is not very serious and is at a relatively acceptable level, but the proliferation of heavy metals should still be strictly prevented. The water quality evaluation results of Zhuhai coastal waters are shown in **Figure 4**. It can be found that in 2017, the water quality in the southwestern sea is worse than that in the northeast, while the two are opposite in 2018. This may be due to the seasonal industrial production and agricultural fishing activities. In 2017, there were more factory discharges along the southwestern coast, which led to the accumulation of heavy metals in seawater (Wang R. et al., 2020).

3.1.2 Contamination Characteristics of Heavy Metals in Sediments

The results of the heavy metals in sediments of coastal Zhuhai are shown in **Table 1**. It can be seen from **Table 1** that the main exceedance factors of the marine protected area within the study area are Cu, Cr, and Cd, and the exceedance rates are 80%, 80%, and 40%, respectively. In contrast, the main exceedance factor in the industrial town discharge area is Cd, and the exceedance rate is 50%. The spatial distribution characteristics of heavy metals in the sediment of the Zhuhai coast were simulated by using the Kriging spatial interpolation method. From **Figures 2**, **3**, it can be found that As in this study area is concentrated in the recreational tourism area in the southeast direction; Zn, Pb, Hg, and Cd are mainly concentrated in the discharge area of industrial towns in the east; and Cu and Cr are concentrated in the discharge area of industrial towns in the southwest direction.

TABLE 1 | Results of quality index evaluation.

Area	Carrier	Years	Statistical parameter	Cu	Pb	Zn	Cd	Hg	As	Cr
Agriculture and fisheries	Seawater	2017	Max	1.04	0.66	1.09	0.15	0.66	0.11	0.17
			Min	0.03	<0.015	0.25	0.03	<0.003	0.05	0.01
			CV	11.10%	9.50%	22.20%	0	0	0	0
		2018	Max	1.43	4.24	0.65	0.31	0.66	0.09	0.03
			Min	0.11	<0.03	<0.16	<0.01	<0.02	0.06	<0.01
			CV	11.10%	66.70%	0	0	0	0	0
	Marine organism	2017	Max	10.62	1.5	12.85	2.78	0.2	0.4	0.12
			Min	0.01	0.01	0.001	0.01	0.02	0.02	0.01
			CV	12.50%	12.50%	12.50%	12.50%	0	0	0
		2018	Max	0.33	0.03	0.29	0.461	0.03	0.97	0.06
			Min	0.01	0.01	0.06	0.001	0.02	0.09	0.01
			CV	0	0	0	0	0	0	0
	Sediments	2017	Max	1.02	0.59	0.93	3.33	0.65	1.42	1.48
			Min	0.68	0.33	0.42	0.35	0.28	0.61	0.84
			CV	20.00%	0	0	20.00%	0	60.00%	80.00%
Industry and towns	Seawater	2017	Max	0.1	<0.015	0.14	0.02	0.17	0.04	0.04
			Min	0.03	<0.015	0.06	0.01	0.07	0.03	0.01
			CV	0	0	0	0	0	0	0
		2018	Max	0.06	0	0.08	0.02	0.07	0.03	0.00
			Min	0.03	0	0.06	0	0.07	0.03	0.00
			CV	0	0	0	0	0	0	0
	Marine organism	2017	Max	0.05	0.01	0.03	0.04	0.2	0.04	0.29
			Min	0.03	0.01	0.001	0.02	0.02	0.02	0.13
			CV	0	0	0	0	0	0	0
		2018	Max	0.05	0.01	0.03	0.04	0.2	0.04	0.29
			Min	0.03	0.01	0.001	0.02	0.02	0.02	0.13
			CV	0	0	0	0	0	0	0
	Sediments	2017	Max	0.47	0.21	0.27	0.29	0.40	0.29	0.78
			Min	0.33	0.19	0.21	0.13	0.27	0.28	0.58
			CV	0	0	0	0	0	0	0
Harbor	Seawater	2017	Max	0.05	0	0.35	0.01	0.03	0.04	0.02
			Min	0.03	0	0.1	0.01	<0.003	0.03	0
			CV	0	0	0	0	0	0	0
		2018	Max	0.15	0	0.02	0.02	0.03	0.04	0.00
			Min	0.03	0	<0.01	0	0	0.03	0.00
			CV	0	0	0	0	0	0	0
	Marine organism	2017	Max	0.13	0.05	0.16	0.03	0.05	0.13	0.05
			Min	0.09	0.04	0.12	0.03	0.02	0.05	0.01
			CV	0	0	0	0	0	0	0
		2018	Max	0.13	0.05	0.16	0.03	0.05	0.13	0.05
			Min	0.09	0.04	0.12	0.03	0.02	0.05	0.01
			CV	0	0	0	0	0	0	0
	Sediments	2017	Max	0.24	0.15	0.24	0.12	0.12	0.32	0.37
			Min	0.19	0.12	0.15	0.07	0.09	0.22	0.32
			CV	0	0	0	0	0	0	0
Reserved	Seawater	2017	Max	0.79	0.78	1	0.16	0.3	0.1	0.18
			Min	0.4	<0.03	0.2	<0.03	0.3	0.08	0.06
			CV	0	0	0	0	0	0	0
		2018	Max	0.82	0.4	0.78	0.04	0.3	0.08	0.05
			Min	0.2	<0.03	<0.01	<0.01	<0.02	0.07	0.01
			CV	0	0	0	0	0	0	0
	Marine organism	2017	Max	0.05	0.08	0.07	0.32	0.05	0.08	0.09
			Min	0.04	0.01	0.001	0.03	0.02	0.02	0.03
			CV	0	0	0	0	0	0	0
		2018	Max	0.05	0.03	0.47	0.013	0.03	0.17	0.01
			Min	0.05	0.01	0.08	0.004	0.02	0.09	0.01
			CV	0	0	0	0	0	0	0
	Sediments	2017	-	0.99	0.38	0.38	0.80	0.45	0.51	0.60
			CV	0	0	0	0	0	0	0

The seawater index is judged according to the seawater quality standard (GB3097-1997); the sediment index is judged according to the marine sediment quality standards (GB18668-2002); the marine organism index is judged according to Countrywide Comprehensive Investigations of the Coastal Zone and Tidal land Resources and Technical regulations for the Second National Baseline Survey of Marine Pollution.

TABLE 2 | Partitioning and bioaccumulation index in coastal Zhuhai.

	Year	2017							2018						
	Site	Hg	Cu	Pb	Zn	Cd	As	Cr	Hg	Cu	Pb	Zn	Cd	As	Cr
K_d	2	123.00	30.25	3,630.00	8.25	8.86	17.47	24.24	8.20	23.05	242.00	19.51	4.43	16.50	248.50
	4	5.87	23.50	288.00	7.40	3.67	10.42	24.80	88.00	11.75	2,880.00	16.02	2.54	14.89	173.60
	5	9.13	16.65	2,480.00	12.59	1.82	10.63	10.96	9.13	23.79	15.40	21.23	10.00	13.67	866.00
	7	5.67	14.87	1,166.67	11.11	2.43	12.86	15.52	5.67	26.31	3,500.00	12.84	2.13	13.71	1,071.00
	10	16.67	11.95	1,960.00	9.45	2.64	7.12	8.10	16.67	47.80	14.00	72.80	29.00	8.64	168.00
	12	6.00	10.88	2,300.00	2.90	5.00	5.15	11.93	90.00	26.77	2,300.00	1.48	40.00	6.43	39.43
	13	8.60	12.67	2,690.00	11.64	3.50	13.26	11.75	129.00	14.87	2,690.00	6.65	11.67	18.57	59.53
	15	6.33	7.80	16.21	2.97	18.44	10.42	30.31	95.00	32.00	19.39	63.00	166.00	13.39	1,182.00
	17	13.20	16.10	2,740.00	15.88	2.53	9.69	21.67	198.00	46.70	2,740.00	93.70	43.00	11.51	97.50
	19	6.13	9.62	3,540.00	15.26	4.92	18.90	37.75	92.00	8.90	101.14	9.24	7.38	21.81	1,057.00
BSAF	2	0.08	0.16	0.00	0.12	0.04	0.09	0.00	0.08	0.13	0.00	0.07	0.03	0.02	0.00
	4	0.11	0.88	0.00	0.29	2.26	0.35	0.00	0.11	0.11	0.00	0.09	1.91	0.03	0.00
	5	0.07	0.03	0.00	0.06	0.01	0.23	0.00	0.07	0.03	0.00	0.00	0.15	0.01	0.00
	7	0.12	0.13	0.03	0.25	1.81	0.03	0.00	0.12	0.27	0.00	0.13	0.37	0.02	0.00
	10	0.02	0.23	0.00	0.34	0.02	0.12	0.00	0.02	0.14	0.00	0.06	0.18	0.02	0.00
	12	0.11	0.00	0.18	0.00	25.00	0.00	0.00	0.11	3.05	0.01	4.45	1.39	0.04	0.00
	13	0.08	0.00	0.68	0.00	64.57	0.03	0.00	0.08	0.03	0.00	0.14	0.15	0.01	0.00
	15	0.11	0.00	0.03	0.00	1.99	0.00	0.00	0.11	0.17	0.00	0.39	0.58	0.04	0.00
	17	0.05	0.00	0.32	0.00	100.00	0.00	0.00	0.05	0.02	0.00	0.17	1.39	0.03	0.00
	19	0.11	0.00	0.03	0.00	7.97	0.00	0.00	0.11	0.03	0.00	0.00	0.04	0.00	0.00
BAF	2	10.00	4.94	9.00	1.02	0.37	1.53	0.00	0.67	3.10	0.33	1.28	0.14	0.33	0.03
	4	0.67	20.75	0.10	2.13	8.29	3.60	0.00	10.00	1.34	1.00	1.36	4.85	0.43	0.12
	5	0.67	0.50	1.00	0.73	0.01	2.44	0.00	0.67	0.71	0.01	0.03	1.50	0.07	0.10
	7	0.67	1.91	34.67	2.82	4.40	0.38	0.00	0.67	7.15	8.00	1.61	0.79	0.27	0.70
	10	0.30	2.70	6.00	3.18	0.06	0.82	0.00	0.30	6.60	0.03	4.20	5.10	0.21	0.18
	12	0.67	0.00	410.00	0.00	15.00	0.01	0.00	10.00	81.69	15.00	6.59	55.50	0.25	0.08
	13	0.67	0.00	1,820.00	0.00	26.00	0.44	0.01	10.00	0.43	7.00	0.94	1.73	0.13	0.09
	15	0.67	0.00	0.51	0.00	36.67	0.01	0.00	10.00	5.40	0.04	24.30	57.00	0.50	0.70
	17	0.67	0.00	890.00	0.01	22.94	0.03	0.00	10.00	1.00	1.00	15.60	59.90	0.31	0.04
	19	0.67	0.00	100.00	0.00	39.17	0.01	0.00	10.00	0.25	0.03	0.01	0.29	0.08	4.30

BSAF, biota-sediment accumulation factor; BAF, bioaccumulation factor.

BSAF < 1 or BAF > 100 demonstrates low accumulation effect between surrounding environment and organisms (Liu et al., 2022).

The highly concentrated sediment heavy metal distribution indicates that the main distribution of heavy metals in the sediment of this sea area is still influenced by the discharge of industrial towns under the influence of the oceanic monsoon climate. Although there will be oceanic monsoon currents driving the migration of heavy metals with seawater, in general, sedimentation activities are still dominant (Han et al., 2020). This requires the environmental and ecological management department to focus on the impact of industrial towns on the marine sediment environment in the later planning and management.

3.1.3 Contamination Characteristics of Heavy Metals in Marine Organism

The quality standards of shellfish in marine organisms refer to Marine Biological Quality (GB18421-2001), and the quality evaluation standards of other fish, crustaceans, mollusks, and other marine organisms adopt the standards in the Concise Regulations for the Comprehensive Survey of National Coastal Zone and Sea-coat Resources. The single index method was used to calculate the index of marine biological quality, and the results are shown in **Table 1**. The heavy metal Cu has the greatest impact on marine organisms, especially invertebrates and shellfish, followed by the heavy metal Pb. According to Pandey's study, organisms in the ocean near the coast are mostly affected by external factors (Pandey et al., 2021).

Cu, Pb, Zn, and Cd in shellfish in the fall of 2017 survey area exceeded the first category of biological quality standards, and all other factors met the first category of biological quality standards. In addition, the Cd in the shrimp mayflies exceeded the standards stipulated in the Concise Regulations for the Comprehensive Survey of National Coastal Zone and Sea-coat Resources and the Technical Regulations for the Second National Marine Pollution Baseline Survey (Second Branch), while the quality of fish, shrimp, and other marine organisms in other stations met the Concise Regulations for the Comprehensive Survey of National Coastal Zone and Sea-coat Resources and the Technical Regulations for the Second National Marine Pollution Baseline Survey (Second Branch). The quality of marine organisms in the survey area is good.

In the spring of 2018, there were no shellfish samples in the survey area, and only zinc in the nudibranchs exceeded the standard stipulated in the Concise Regulations for the Comprehensive Survey of National Coastal Zone and Sea-coat Resources, while the quality of other fish, shrimps, and other marine organisms all met the relevant index standards in the Concise Regulations for the Comprehensive Survey of National Coastal Zone and Sea-coat

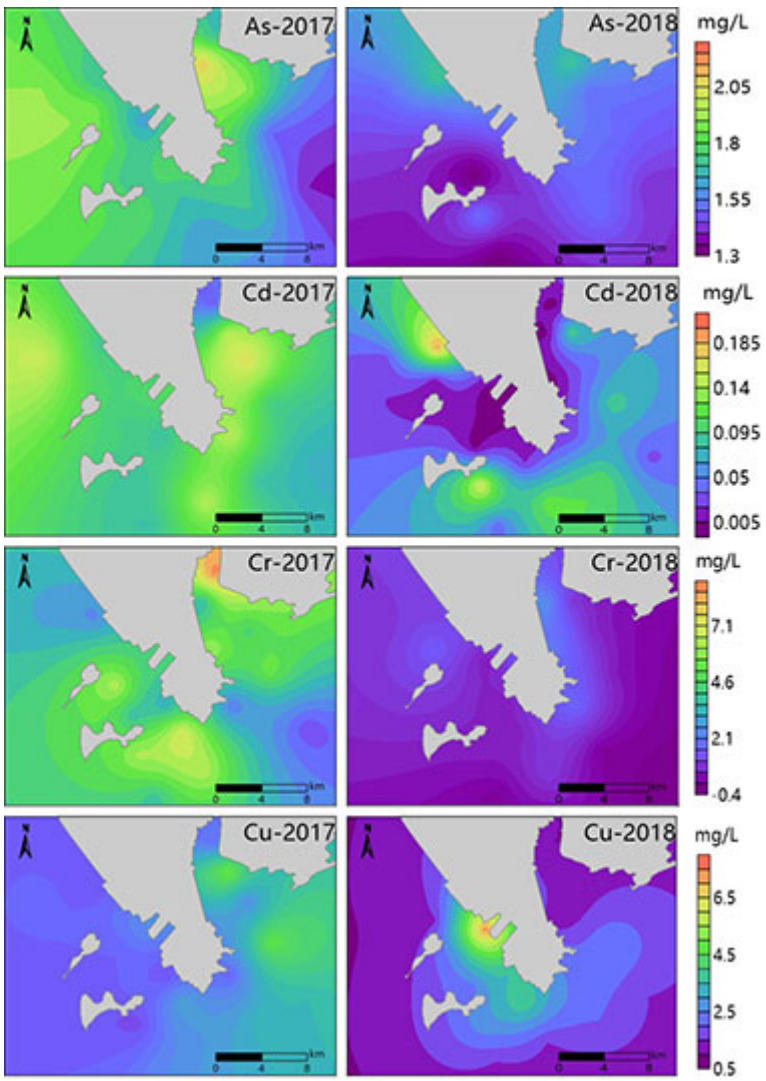


FIGURE 2 | The spatial distribution of As, Cd, Cr and Cu in seawater.

Resources and the Technical Regulations for the Second National Baseline Survey of Marine Pollution (the second volume), indicating that the quality of marine organisms in the survey area was good.

3.2 Marine Organism Quality Assessment

The results of the marine ecological characteristics survey in the sea area of coastal Zhuhai are shown in **Figure 5**. In terms of chlorophyll *a* and primary productivity, the variation of chlorophyll *a* concentration in the surface water column of the sea area surveyed in Autumn 2017 ranged from 0.74 to 5.66 mg/m^3, with a mean value of 1.58 mg/m^3, and the variation of primary productivity ranged from 5.99 to 75.62 mg·C/(m^2·d), with a mean value of 23.55 mg·C/(m^2·d). The variation of chlorophyll *a* concentration in the surface waters of the sea area in Spring 2018 ranged from 1.42 to 11.42 mg/m^3 with a mean value of 4.70 mg/m^3, and the variation of primary productivity ranged from 25.97 to 464.00 mg·C/(m^2·d) with a mean value of 201.89 mg·C/(m^2·d). Overall, the productivity index in the northeast is higher than in other regions, indicating that this region is the priority production fishing area in the study area.

The variation in the number of phytoplankton species at each station in Autumn 2017 ranged from 4 to 22 species, with an average of 12 species (**Figure 6**). The Shannon–Wiener diversity index ranged from 0.009 to 1.486, with an average of 0.366, and the distribution of biomass among species at each station was very heterogeneous. In contrast, the results of Spring 2018 survey showed that the number of phytoplankton species varied from 15 to 35 species at each station, with an average of 23 species. The Shannon–Wiener diversity index ranged from 1.836 to 2.487,

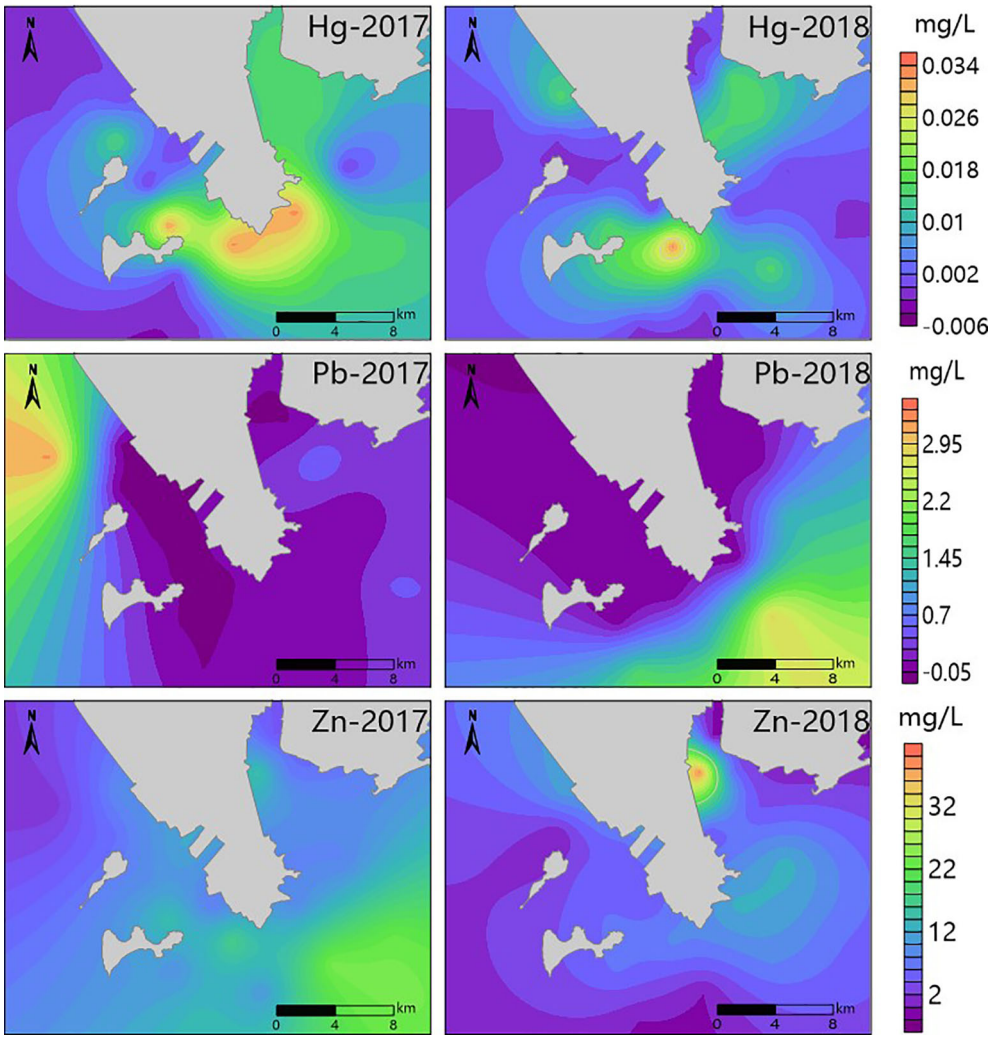


FIGURE 3 | The spatial distribution of Hg, Pb and Zn in seawater.

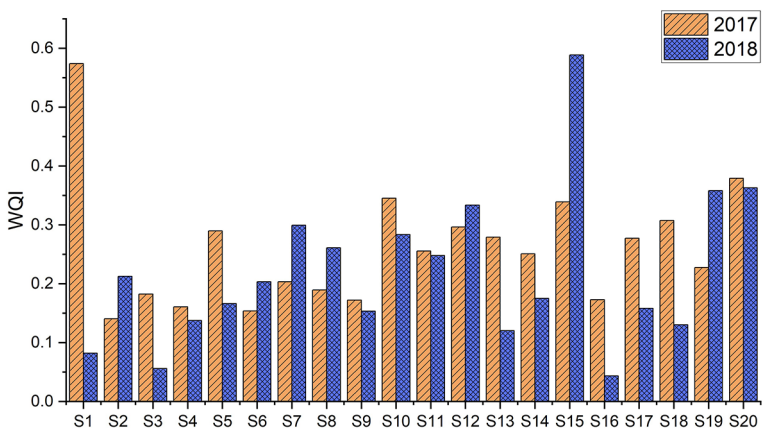


FIGURE 4 | WQI of heavy metals in surface seawater of Zhuhai.

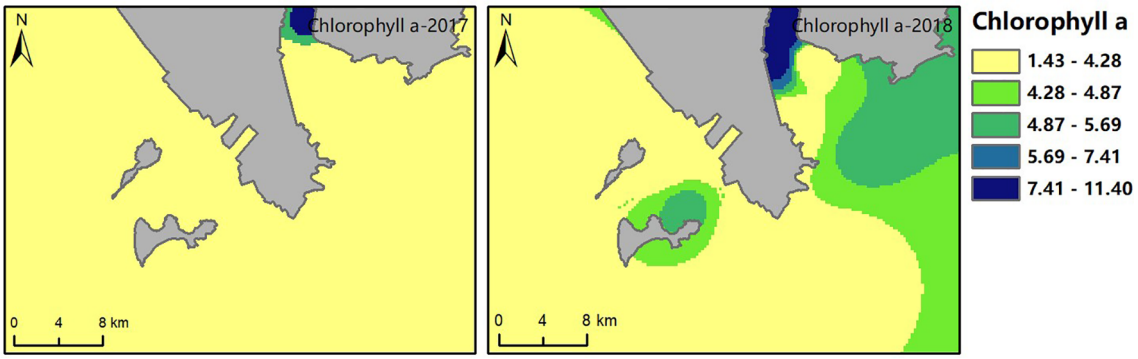


FIGURE 5 | Results of chlorophyll a in coastal of Zhuhai.

with an average of 2.175, and Pielou's evenness index ranged from 0.601 to 0.878, with an average of 0.701. The distribution of biomass among species was relatively uniform, and the planar distribution trends of diversity index and evenness index were basically consistent.

Compared with plankton, benthic organisms showed less variation. The range of species variation of macro-benthic organisms at each quantitative sampling station in the Fall 2017 survey area was from 4 to 14 species/station, with an average of 9 species/station. The variation of the diversity index (H′) ranged from 0.21 to 2.39, with a mean value of 1.56 (**Table S2**), and the benthic biodiversity index in the surveyed sea area was moderately low. The range of uniformity was from 0.15 to 1.00, with an average of 0.72, reflecting the uneven distribution of species, and the variation in the number of macro-benthic species at each quantitative sampling station in the spring of 2018 ranged from 2 to 14 species/s
tation, with an average of 9 species/station. The variation of diversity index (H′) ranged from 0.451 to 2.199, with a mean value of 1.421 (**Table S2**). The benthic biodiversity index of the surveyed sea area was moderately low. The evenness ranged from 0.268 to 0.945, with a mean value of 0.691, reflecting a relatively even distribution of species among the stations.

3.3 Interrelation and Source Analysis of Heavy Metals

The results of heavy metal and other particle correlation analyses in this study area are shown in **Figure 7**. The correlation matrix table shows that salinity was negatively correlated with As and Cr concentrations, indicating that salinity may hinder seawater mixing and maintain higher concentrations of As in surface seawater. Pearson's correlation analysis further showed that the concentration of Cu, Pb, and Zn in coastal sediments of the high bar sea area was significantly and positively correlated with the Gross Domestic Product (GDP) and wastewater discharge of each province ($p = 0.01$), suggesting that these three metals are more influenced by seasonal changes and fishing periods. Pb, Zn, Cd, and As were all significantly and positively correlated with seasons ($p = 0.01$), suggesting that the concentration of these four heavy metals in sediments is more influenced by local seasonal changes. Cu concentration was significantly and positively correlated with the gross industrial product ($p = 0.005$), indicating that Cu concentration was mainly influenced by the discharge of local industrial wastewater.

K_d is the specific coefficient employed to quantify the partition and transport of heavy metals between different phases such as soluble and solid. It can be affected by both the characteristics of heavy metals and the nature of sediment and seawater. The results of heavy metal enrichment in coastal Zhuhai are shown in **Table 2**. In this study, the order of value K_d in both 2017 and 2018 was Pb > Cr > Cu > As > Zn > Hg > Cd, and the value of Pb was much larger than the value of other heavy metals, which suggested that the heavy metal Pb was most easily transported and enriched from seawater to the nearby sediment environment. From the temporal analysis, the overall K_d values of each heavy metal in 2017 were smaller than the K_d

TABLE 3 | Average of heavy metal concentrations in study areas.

Year	Hg	Cu	Pb	Zn	Cd	As	Cr	Reference
2017	0.1092	36.07	28.88	92.31	0.504	20.6	96.8	This study
2016		38.1	44.7	121.77	0.46		79.77	Ye et al., 2020
2015	0.03	29.63	51.3	143.42	0.08	7.31	91.3	Fei et al., 2016
2009			40.51	109.49	0.29	17.42		Ye et al., 2020
2008	0.13	46.76	49.66	143.1	0.46	21.99	78.37	Zhao et al., 2017
2008	0.1	42.89	44.61	135.87	0.84	18.23	55.19	Zhao et al., 2018
2004		46.2	59.3	150.1			89	Zhou et al., 2004

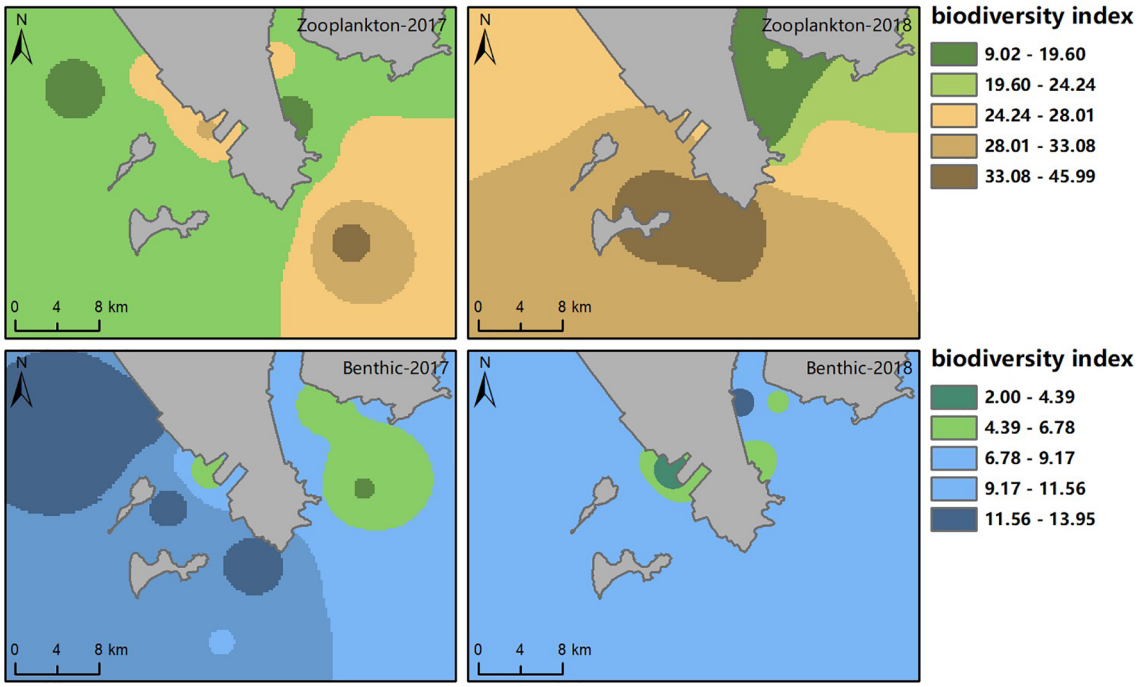


FIGURE 6 | Evaluation results of zooplankton diversity index and benthic biodiversity index in coastal of Zhuhai.

values obtained in 2018, which indicated that the lower seawater temperature was not conducive to the enrichment of heavy metals in the sediment environment. In terms of orientation, the distribution of K_d values of heavy metals was clearly characterized. The K_d values of points near the southwest and southeast coasts are much higher than those in the sea area far from the coast, which indicated that the more submerged the seawater depth was, the easier the heavy metals were enriched.

From **Table 3**, we can see that the pollution of heavy metals in the sediments along the coast of Zhuhai generally showed a decreasing trend; the concentration of Hg, As, and Cr remained unchanged on the whole; and the concentration of Cu, Pb, Cd, and Zn decreased year by year except for the reasons of data errors in individual years. In general, due to the increased national attention to marine heavy metal pollution in recent years, marine heavy metal concentration may decrease in the next few years.

The BSAF values of each heavy metal except Pb in 2017 and 2018 were less than 1, indicating that only the heavy metal Pb is easily enriched in organisms from seawater or sediment environment. Other heavy metals are not easily enriched in organisms due to their metal properties. This required local managers to pay special attention to the management of heavy metal Pb to prevent elevated biological health risks. Geographically, Pb was more likely to be enriched in organisms in the inner bay of the northeastern part of the Zhuhai-Gaolan Peninsula compared to other locations, indicating that the mobility of seawater also had an influence on the bioconcentration of Pb. The highly mobile offshore area was less prone to Pb enrichment and was suitable for mariculture production activities in this area. The above results were also verified by BAF.

From the perspective of heavy metal classification, the main source of As was aquaculture in the sea area of coastal Zhuhai. In the southern sea area, aquaculture was the main source of the local economy, the large area of aquaculture caused the disorderly placement of aquaculture feed, and the discharged seawater will then cause the accumulation of As in the seawater flowing through the sea area (Xu Y. et al., 2018). Pb, Zn, Cu, and other heavy metals were mainly from the local fine processing industries such as precision electronic instruments, chips, electronic product parts processing, and other industries. Coastal Zhuhai is a national industrial park established by the Chinese government in Zhuhai, equipped with a large number of precision electronic processing industries, which inevitably affect the surrounding seawater environment in the process of continuous development and growth, thus causing the accumulation of heavy metals in the sediment.

3.4 Ecological Risk Assessment

The potential biohazard effects of heavy metals in this sea area, calculated according to the species sensitivity analysis function, are shown in **Figure 8** and **Table S3**. It can be seen that the biohazard coefficient of heavy metals in the study area was significantly higher in Autumn 2017 than in Spring 2018, which may be due to the weakened seawater activity and elevated heavy metal concentration due to low temperatures in autumn. From the analysis of heavy metal species, it was found

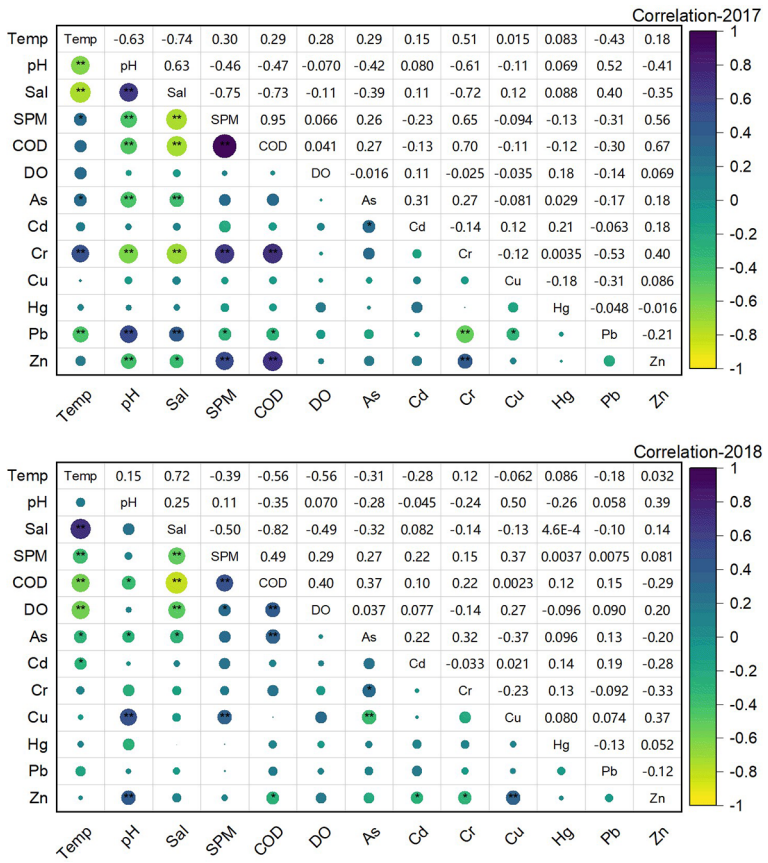


FIGURE 7 | The correlation analysis of heavy metals in the seawater of coastal Zhuhai in 2017 and 2018, respectively (*P < 0.05; **P <0.01).

that Cd, Cu, and Zn were the main heavy metals causing biohazard, while As, Hg, and Pb did not produce heavy metal biohazard. Taken together, the potential biohazard coefficients and ratios (more than 6%) in the northeastern sea area are significantly higher than those in other sea areas. Based on the heavy metal characterization of ocean dynamics, this was caused by seawater currents and coastal topography (Jahan and Strezov, 2018; Khalid et al., 2021). This requires the local ecological and environmental protection department to pay close attention to the protection of marine ecology in the northeast.

In addition, the spatial distribution of bio-sensitivity of heavy metals in the sea area of coastal Zhuhai has obvious directionality. From **Figure 9**, it was found that the bio-sensitivity survey points were all located in the southeast and southwest areas of coastal Zhuhai, and these two areas were also the main precision instrument processing areas in coastal Zhuhai. A large number of metals processing several times the heavy metals discharged from the production of processing industries were accumulated in the sediment, which was the main reason for the significantly higher risk of heavy metal bio-sensitivity in these areas than in other areas. The biological species and biological quality in the sea area were greatly affected by the heavy metal concentration, and the number of biological populations and biological quality that suffer from the risk crisis can also seriously affect the ecological and environmental safety of the sea area in this region (Jawad et al., 2019; Han et al., 2020). So there is a need to carry out wastewater disposal for precision instrument processing enterprises in the southeast and southwest, which can cause the bio-sensitivity crisis collection to reduce the bioecological risk in the region.

3.5 Priority Control and Recommendations

In general terms, few previous studies showed spatial differences in heavy metal contamination on the Zhuhai coast, but while comparing the data with seasonal responses in this study, Cu, Pb, and Zn demonstrated higher values in winter in seawater and sediment, especially near the coast, and this might indicate that organisms near the coast suffered pro-oxidant heavy metal enrichment pressures during the cold season. This explained why organisms, especially invertebrates' biochemical responses, would be higher in winter, which is the beginning of the reserve accumulation period on the Zhuhai coast. From the perspective of aquaculture production, the survey of heavy metals distribution on the Zhuhai coast can further improve the quality of marine products and effectively evade the pollution areas. From the perspective of environmental management, the data of HM

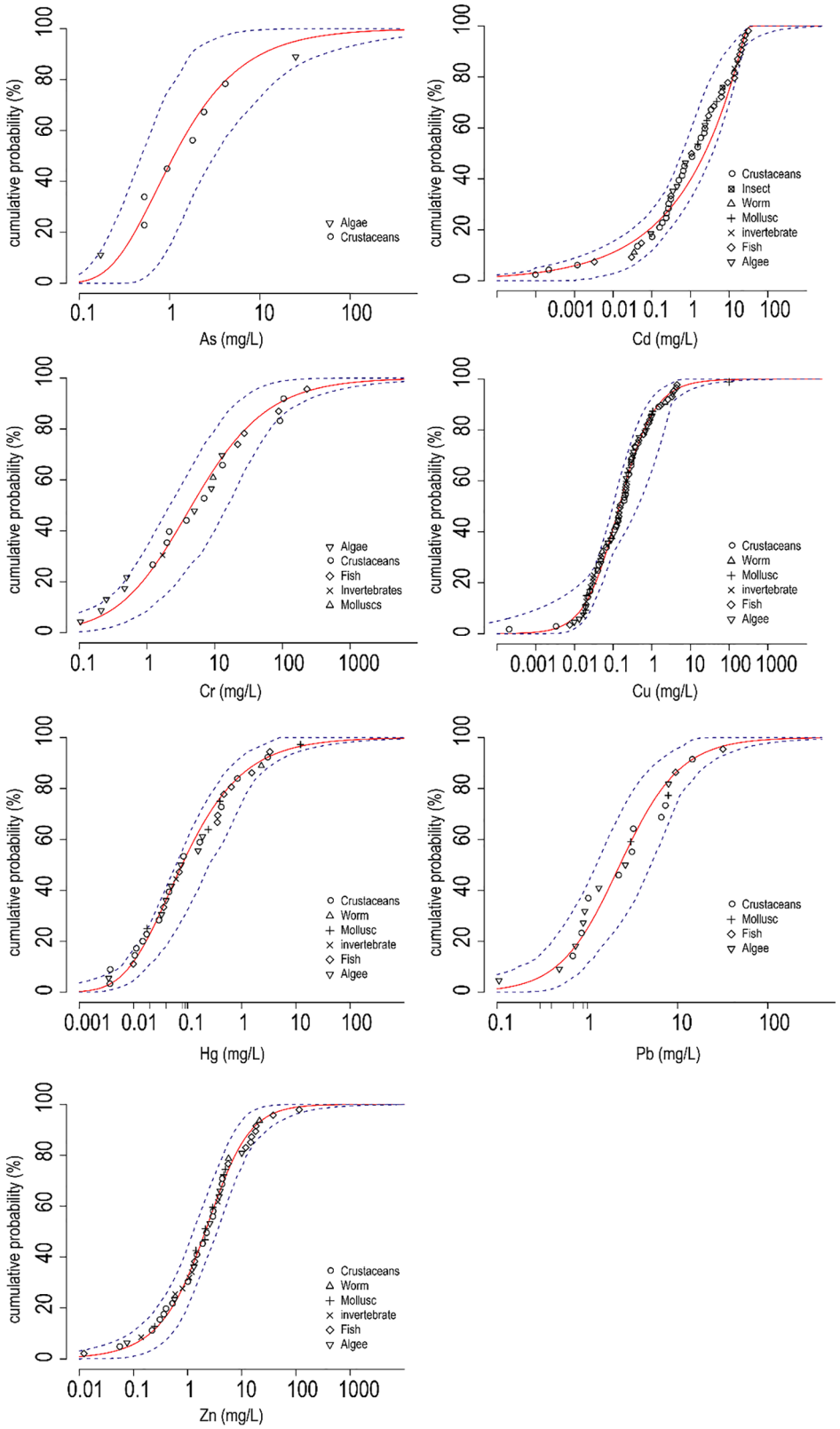


FIGURE 8 | The correlation analysis of heavy metals in the seawater of coastal Zhuhai in 2017 and 2018, respectively.

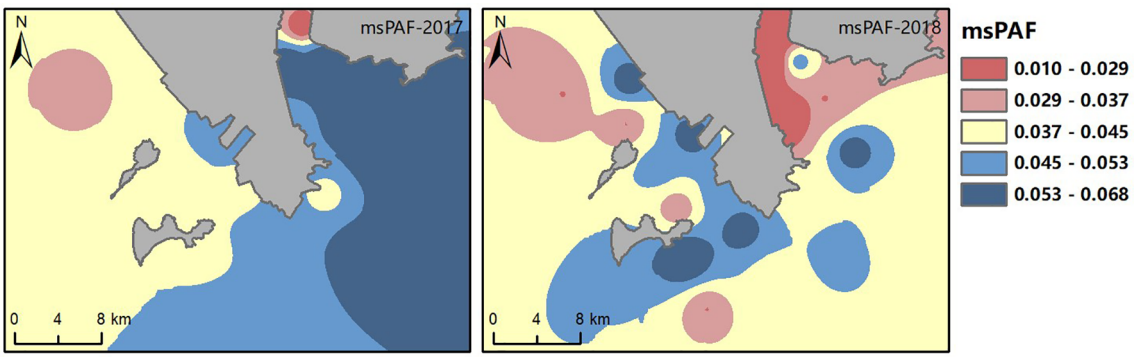


FIGURE 9 | Compound hazard ratio (msPAF) of heavy metals in seawater of Zhuhai.

distribution and risk characteristics can provide accurate information for precise heavy metal pollution control and avoid wasting government resources for ecological protection.

Heavy metals are widespread in aquatic environments on the Zhuhai coast, and understanding their distribution at the local scare is necessary to advise marine environmental protection policymakers. The key issue for heavy metal contamination on the Zhuhai coast is the scarcity of emission control, and it is linked to coastal areas of industrial production, which do not have any option other than polluted rivers as sources for sewage discharge. Industrial wastewater treatment needs massive expenditure and reduces local economic revenue due to the installation of costly treatment installations. For better safeguarding and management of the marine environment including organisms, it is paramount that regional heavy metal polluting enterprises implement the most stringent wastewater treatment and discharge control measures in water bodies. Consequently, provisions and specialized supervision departments and supervisors should be introduced, consisting of GIS online monitoring in order to tap into local contamination information, as well as to recognize pollution sources and information requirements.

Our research exhibited that the cumulative effects of different heavy metals in seawater and sediment were different, indicating that a single evaluation method was not useful to evaluate heavy metal contamination on the Zhuhai coast. The heavy metal distribution characteristics and ecological risk curve evaluation system established in this study can effectively assess the cumulative effects of heavy metals in seawater, sediment, and organisms and can provide scientific and effective information support for the next phase of ecological restoration work. In addition, advance planning is needed based on Zhuhai's special geographical environment and industrial layout. This requires the local government to plan in advance the special disposal institutions and control areas for heavy metal wastewater in order to centralize the management and purification of heavy metal wastewater within the industrial park and to achieve zero pollution discharge. Therefore, the governmental environmental protection department, enterprise regulatory agencies, and local resident representatives need to participate in the development of the regional heavy metal control plan.

4 CONCLUSIONS

In the present study, multi-evaluation methods have been employed to investigate the heavy metal pollution on the Zhuhai coast. The results showed that the study area was heavily polluted by heavy metals, especially on the north coast of Gaolan Island. Comparative studies revealed that the main source of heavy metals was the discharge of local industrial wastewater, especially in offshore waters. The SSD evaluation of organisms showed that the northern part of the Zhuhai coast was in medium risk conditions, with high pollution levels of Cd and Cu.

Overall risk distribution patterns of heavy metals and zonation of SSD obtained from this study could support policymakers to take coherent action based on pollution control measures and marine aquaculture. Our research suggested that chemical fractionation should be considered to provide a more accurate assessment of the ecological risks of heavy metals in marine ecosystems. In addition, marine resources in the northern part of the Zhuhai coast may be more vulnerable to anthropogenic pollution. Our research results provided important information on the ecological response of organisms experiencing heavy metal contamination on the Zhuhai coast. Future studies should focus on integrated prevention and control strategies to ensure better conservation of the coastal and estuarine ecosystem.

DATA AVAILABILITY STATEMENT

The original contributions presented in the study are included in the article/**Supplementary Material**. Further inquiries can be directed to the corresponding author.

AUTHOR CONTRIBUTIONS

JW and SR developed the methodology. JW, SR, and MW wrote the original manuscript. JW and JL revised the manuscript. RL is responsible for contacting the editorial department and

collecting data. All authors contributed to the article and approved the submitted version.

FUNDING

This study was supported by the South China Sea Marine Survey Technology Center, Key Laboratory of Marine Environmental Detection Technology and Application, Ministry of Natural Resources of China, Project Number: MESTA-2020-C002.

SUPPLEMENTARY MATERIAL

The Supplementary Material for this article can be found online at: https://www.frontiersin.org/articles/10.3389/fmars.2022.898423/full#supplementary-material

REFERENCES

Abaya, L. M., Wiegner, T. N., Colbert, S. L., Beets, J. P., Carlson, K. M., Kramer, K. L., et al. (2018). A Multi-Indicator Approach for Identifying Shoreline Sewage Pollution Hotspots Adjacent to Coral Reefs. *Mar. Pollut. Bullet.* 129 (1), 70–80. doi: 10.1016/j.marpolbul.2018.02.005

Anusuya, T., Kumar, V., and Kumar, V. (2021). Hydrophilic Graphene Quantum Dots as Turn-Off Fluorescent Nanoprobes for Toxic Heavy Metal Ions Detection in Aqueous Media. *Chemosphere* 282, 131019. doi: 10.1016/j.chemosphere.2021.131019

Ashayeri, N. Y., and Keshavarzi, B. (2019). Geochemical Characteristics, Partitioning, Quantitative Source Apportionment, and Ecological and Health Risk of Heavy Metals in Sediments and Water: A Case Study in Shadegan Wetland, Iran. *Mar. Pollut. Bullet.* 149, 110495. doi: 10.1016/j.marpolbul.2019.110495

Birch, G. F. A. (2018). Review of Chemical-Based Sediment Quality Assessment Methodologies for the Marine Environment. *Mar. Pollut. Bullet.* 133, 218–232. doi: 10.1016/j.marpolbul.2018.05.039

Cadée, G. C., and Hegeman, J. (1974). Primary Production of Phytoplankton in the Dutch Wadden Sea. *Neth. J. Sea Res.* 8 (2-3), 240–259. doi: 10.1016/0077-7579(74)90019-2

Cui, L., Wang, X., Li, J., Gao, X., Zhang, J., and Liu, Z. (2021). Ecological and Health Risk Assessments and Water Quality Criteria of Heavy Metals in the Haihe River. *Environ. Pollut.* 290, 117971. doi: 10.1016/j.envpol.2021.117971

Fang, L., Li, L., Qu, Z., Xu, H., Xu, J., and Yan, N. (2018). A Novel Method for the Sequential Removal and Separation of Multiple Heavy Metals From Wastewater. *J. Haz. Mat.* 342, 617–624. doi: 10.1016/j.jhazmat.2017.08.072

Fei, Y., Wang, X., Liang, G., Gu, Y., Lin, Q., Ning, J., et al. (2016). Fuzzy Comprehensive Assessment of Heavy Metals and Pb Isotopic Signature in Surface Sediments From a Bay Under Serious Anthropogenic Influences: Daya Bay, China. *Ecotoxicol. Environ. Safe.* 126, 38–44. doi: 10.1016/j.ecoenv.2015.12.011

Han, R., Zhou, B., Huang, Y., Lu, X., and Li, N. (2020). Bibliometric Overview of Research Trends on Heavy Metal Health Risks and Impacts in 1989–2018. *J. Clean. Product.* 276, 123249. doi: 10.1016/j.jclepro.2020.123249

Huang, Y., Zhou, B., Li, N., Li, Y., Han, R., Qi, J., et al. (2019). Spatial-Temporal Analysis of Selected Industrial Aquatic Heavy Metal Pollution in China. *J. Clean. Product.* 238, 117944. doi: 10.1016/j.jclepro.2019.117944

Hu, C., Shui, B., Yang, X., Wang, L., and Zhang, X. (2021). Trophic Transfer of Heavy Metals Through Aquatic Food Web in a Seagrass Ecosystem of Swan Lagoon, China. *Sci. Tot. Environ.* 762, 143139. doi: 10.1016/j.scitotenv.2020.143139

Jahan, S., and Strezov, V. (2018). Comparison of Pollution Indices for the Assessment of Heavy Metals in the Sediments of Seaports of NSW, Australia. *Mar. Pollut. Bullet.* 128, 295–306. doi: 10.1016/j.marpolbul.2018.01.036

Jawad, A., Peng, L., Liao, Z., Zhou, Z., Shahzad, A., Ifthikar, J., et al. (2019). Selective Removal of Heavy Metals by Hydrotalcites as Adsorbents in Diverse Wastewater: Different Intercalated Anions With Different Mechanisms. *J. Clean. Product.* 211, 1112–1126. doi: 10.1016/j.jclepro.2018.11.234

Kaikkonen, L., Venesjärvi, R., Nygård, H., and Kuikka, S. (2018). Assessing the Impacts of Seabed Mineral Extraction in the Deep Sea and Coastal Marine Environments: Current Methods and Recommendations for Environmental Risk Assessment. *Mar. Pollut. Bullet.* 135, 1183–1197. doi: 10.1016/j.marpolbul.2018.08.055

Khalid, N., Aqeel, M., Noman, A., Khan, S. M., and Akhter, N. (2021). Interactions and Effects of Microplastics With Heavy Metals in Aquatic and Terrestrial Environments. *Environ. Pollut.* 290, 118104. doi: 10.1016/j.envpol.2021.118104

Kim, B. S. M., Angeli, J. L. F., Ferreira, P. A. L., Mahiques, M. D., and Figueira, R. L. (2018). Critical Evaluation of Different Methods to Calculate the Geoaccumulation Index for Environmental Studies: A New Approach for Baixada Santista – Southeastern Brazil. *Mar. Pollut. Bullet.* 127, 548–552. doi: 10.1016/j.marpolbul.2017.12.049

Kong, Q., Shi, X., Ma, W., Zhang, F., and Wei, C. (2021). Strategies to Improve the Adsorption Properties of Graphene-Based Adsorbent Towards Heavy Metal Ions and Their Compound Pollutants: A Review. *J. Haz. Mat.* 415, 125690. doi: 10.1016/j.jhazmat.2021.125690

Kumar, V., Parihar, R. D., Sharma, A., Bakshi, P., and Rodrigo-Comino, J. (2019). Global Evaluation of Heavy Metal Content in Surface Water Bodies: A Meta-Analysis Using Heavy Metal Pollution Indices and Multivariate Statistical Analyses. *Chemosphere* 236, 124364. doi: 10.1016/j.chemosphere.2019.124364

Li, S., and Chen, J. (2014). Discussion on Air Temperature Change in Zhuhai in Recent 49 Years and the Effects of Urbanization. *J. Meteorol. Res. Appl.* 35, 02, 40–45.

Li, H., Gao, X., Gu, Y., Wang, R., Xie, P., Liang, M., et al. (2018a). Comprehensive Large-Scale Investigation and Assessment of Trace Metal in the Coastal Sediments of Bohai Sea. *Mar. Pollut. Bullet.* 129 (1), 126–134. doi: 10.1016/j.marpolbul.2018.02.022

Li, H., Sun, Z., Qiu, Y., Yu, X., Han, X., and Ma, Y. (2018b). Integrating Bioavailability and Soil Aging in the Derivation of DDT Criteria for Agricultural Soils Using Crop Species Sensitivity Distributions. *Ecotoxicol. Environ. Safe.* 165, 527–532. doi: 10.1016/j.ecoenv.2018.09.035

Liu, Y., Kuang, W., Xu, J., Chen, J., Sun, X., Lin, C., et al. (2022). Distribution, Source and Risk Assessment of Heavy Metals in the Seawater, Sediments, and Organisms of the Daya Bay, China. *Mar. Pollut. Bullet.* 174, 113297. doi: 10.1016/j.marpolbul.2021.113297

Liu, Q., Wang, F., Meng, F., Jiang, L., Li, G., and Zhou, R. (2018). Assessment of Metal Contamination in Estuarine Surface Sediments From Dongying City, China; Use of a Modified Ecological Risk Index. *Mar. Pollut. Bullet.* 126, 293–303. doi: 10.1016/j.marpolbul.2017.11.017

Liu, J., Wu, J., Feng, W., and Li, X. (2020). Ecological Risk Assessment of Heavy Metals in Water Bodies Around Typical Copper Mines in China. *Int. J. Environ. Res. Public Health* 17 (12), 4315. doi: 10.3390/ijerph17124315

Luo, L., Mei, K., Qu, L., Zhang, C., Chen, H., Wang, S., et al. (2019). Assessment of the Geographical Detector Method for Investigating Heavy Metal Source Apportionment in an Urban Watershed of Eastern China. *Sci. Tot. Environ.* 653, 714–722. doi: 10.1016/j.scitotenv.2018.10.424

Majithiya, D., Yadav, A., and Ram, A. (2018). Behaviour of Trace Metals in the Anoxic Environment of Veraval Harbour, India. *Mar. Pollut. Bullet.* 129 (2), 645–654. doi: 10.1016/j.marpolbul.2017.10.052

Pandey, V., Jha, D. K., Kumar, P. S., Santhanakumar, J., Venkatnarayanan, S., Jebakumar, J., et al. (2022). Effect of Multiple Stressors on the Functional Traits of Sub-Tidal Macrobenthic Fauna: A Case Study of the Southeast Coast of India. *Mar. Pollut. Bullet.* 175, 113355. doi: 10.1016/j.marpolbul.2022.113355

Pandey, V., Venkatnarayanan, S., Kumar, P. S., Ratnam, K., and Dharani, G. (2021). Assessment of Ecological Health of Swarnamukhi River Estuary, Southeast Coast of India, Through AMBI Indices and Multivariate Tools. *Mar. Pollut. Bullet.* 164, 112031. doi: 10.1016/j.marpolbul.2021.112031

Quyen, V. T., Pham, T. H., Kim, J., Dang, M. T., and Kim, T. (2021). Biosorbent Derived From Coffee Husk for Efficient Removal of Toxic Heavy Metals From Wastewater. *Chemosphere* 284, 131312. doi: 10.1016/j.chemosphere.2021.131312

Rao, K., Tang, T., Zhang, X., Mo, W., Ji, E., Bi, W., et al. (2021). Spatial-Temporal Dynamics, Ecological Risk Assessment, Source Identification and Interactions With Internal Nutrients Release of Heavy Metals in Surface Sediments From a Large Chinese Shallow Lake. *Chemosphere* 282, 131041. doi: 10.1016/j.chemosphere.2021.131041

Reddy, B. C., Jayaraju, N., Sreenivasulu, G., Suresh, U., and Reddy, A. N. (2016). Heavy Metal Pollution Monitoring With Foraminifera in the Estuaries of Nellore Coast, East Coast of India. *Mar. Pollut. Bullet.* 113, 542–551. doi: 10.1016/j.marpolbul.2016.08.051

Satheeswaran, A., Yuvaraj, P., Damotharan, P., Karthikeyan, V., Jha, D. K., Dharani, G., et al. (2019). Assessment of Trace Metal Contamination in the Marine Sediment, Seawater, and Bivalves of Parangipettai, Southeast Coast of India. *Mar. Pollut. Bullet.* 149, 110499. doi: 10.1016/j.marpolbul.2019.110499

Sruthi, S. N., Shyleshchandran, M. S., Mohan, M., and Ramasamy, E. V. (2018). Distribution of Priority Pollutants in the Sediment of Vembanad Estuary, Peninsular India. *Mar. Pollut. Bullet.* 133, 294–303. doi: 10.1016/j.marpolbul.2018.05.033

Wang, X., Fu, R., Li, H., Zhang, Y., and Xiong, Y. (2020). Heavy Metal Contamination in Surface Sediments: A Comprehensive, Large-Scale Evaluation for the Bohai Sea, China. *Environ. Pollut.* 260, 113986. doi: 10.1016/j.envpol.2020.113986

Wang, Q., Li, H., Zhang, Y., Wang, X. J., Zhang, C., Xiao, K., et al. (2019). Evaluations of Submarine Groundwater Discharge and Associated Heavy Metal Fluxes in Bohai Bay, China. *Sci. Tot. Environ.* 695, 133873. doi: 10.1016/j.scitotenv.2019.133873

Wang, L., Wang, Y., Ma, F., Tankpa, V., Bai, S., Guo, X., et al. (2019). Mechanisms and Reutilization of Modified Biochar Used for Removal of Heavy Metals From Wastewater: A Review. *Sci. Tot. Environ.* 668, 1298–1309. doi: 10.1016/j.scitotenv.2019.03.011

Wang, R., Zhang, C., Huang, X., Zhao, L., and Yin, D. (2020). Distribution and Source of Heavy Metals in the Sediments of the Coastal East China Sea: Geochemical Controls and Typhoon Impact. *Environ. Pollut.* 260, 113936. doi: 10.1016/j.envpol.2020.113936

Wang, C., Zou, X., Feng, Z., Hao, Z., and Gao, J. (2018). Distribution and Transport of Heavy Metals in Estuarine–Inner Shelf Regions of the East China Sea. *Sci. Tot. Environ.* 644, 298–305. doi: 10.1016/j.scitotenv.2018.06.383

Wu, W., Wu, P., Yang, F., Sun, D., Zhang, D., Zhou, Y., et al. (2018). Assessment of Heavy Metal Pollution and Human Health Risks in Urban Soils Around an Electronics Manufacturing Facility. *Sci. Tot. Environ.* 630, 53–61. doi: 10.1016/j.scitotenv.2018.02.183

Xia, P., Ma, L., Sun, R., Yang, Y., and Yi, Y. (2020). Evaluation of Potential Ecological Risk, Possible Sources and Controlling Factors of Heavy Metals in Surface Sediment of Caohai Wetland, China. *Sci. Tot. Environ.* 740, 140231. doi: 10.1016/j.scitotenv.2020.140231

Xiao, J., Han, X., Sun, S., Wang, L., and Rinklebe, J. (2021). Heavy Metals in Different Moss Species in Alpine Ecosystems of Mountain Gongga, China: Geochemical Characteristics and Controlling Factors. *Environ. Pollut.* 272, 115991. doi: 10.1016/j.envpol.2020.115991

Xu, J., Cao, Z., Zhang, Y., Yuan, Z., Lou, Z., Xu, X., et al. (2018). A Review of Functionalized Carbon Nanotubes and Graphene for Heavy Metal Adsorption From Water: Preparation, Application, and Mechanism. *Chemosphere* 195, 351–364. doi: 10.1016/j.chemosphere.2017.12.061

Xu, X., Hu, X., Wang, T., Sun, M., Wang, L., and Zhang, L. (2021). Non-Inverted U-Shaped Challenges to Regional Sustainability: The Health Risk of Soil Heavy Metals in Coastal China. *J. Clean. Product.* 279, 123746. doi: 10.1016/j.jclepro.2020.123746

Xu, Y., Xie, Y., Zhao, P., Zhang, T., Zhou, Q., and Hu, B. (2018). Heavy Metal Pollution of Seawater in Weizhou Island, Beibu Gulf of Guangxi. *Ecol. Environ. Sci.* 27 (05), 908–915. doi: 10.16258/j.cnki.1674-5906.2018.05.016

Xu, Z., Zhang, Q., Li, X., and Huang, X. (2022). A Critical Review on Chemical Analysis of Heavy Metal Complexes in Water/Wastewater and the Mechanism of Treatment Methods. *Chem. Eng. J.* 429, 131688. doi: 10.1016/j.cej.2021.131688

Yang, T., Cheng, H., Wang, H., Drews, M., Li, S., Huang, W., et al. (2019). Comparative Study of Polycyclic Aromatic Hydrocarbons (PAHs) and Heavy Metals (HMs) in Corals, Surrounding Sediments and Surface Water at the Dazhou Island, China. *Chemosphere* 218, 157–168. doi: 10.1016/j.chemosphere.2018.11.063

Ye, Z., Chen, J., Gao, L., Liang, Z., and Gnanachandrasamy, G. (2020). 210Pb Dating to Investigate the Historical Variations and Identification of Different Sources of Heavy Metal Pollution in Sediments of the Pearl River Estuary, Southern China. *Mar. Pollut. Bull.* 150, 110670. doi: 10.1016/j.marpolbul.2019.110670

Zhang, G., Bai, J., Xiao, R., Zhao, Q., Jia, J., and Cui, B. (2017). Heavy Metal Fractions and Ecological Risk Assessment in Sediments From Urban, Rural and Reclamation-Affected Rivers of The Pearl River Estuary, China. *Chemosphere* 184, 278–288. doi: 10.1016/j.chemosphere.2017.05.155

Zhao, M., Wang, S., Wang, H., Qin, P., Yang, D., Sun, Y., et al. (2019). Application of Sodium Titanate Nanofibers as Constructed Wetland Fillers for Efficient Removal of Heavy Metal Ions From Wastewater. *Environ. Pollut.* 248, 938–946. doi: 10.1016/j.envpol.2019.02.040

Zhao, G., Ye, S., Yuan, H., Ding, X., and Wang, J. (2017). Surface Sediment Properties and Heavy Metal Pollution Assessment in the Pearl River Estuary, China. *Environ. Sci. Pollut.* 24, 2966–2979. doi: 10.1007/s11356-016-8003-4

Zhao, G., Ye, S., Yuan, H., Ding, X., Wan, J., and Laws, E. A. (2018). Surface Sediment Properties and Heavy Metal Contamination Assessment in River Sediments of the Pearl River Delta, China. *Mar. Pollut. Bullet.* 136, 300–308. doi: 10.1016/j.marpolbul.2018.09.035

Zhou, H. Y., Peng, X. T., and Pan, J. M. (2004). Distribution, Source and Enrichment of Some Chemical Elements in Sediments of the Pearl River Estuary, China. *Cont. Shelf. Res.* 24 (16), 0–1875. doi: 10.1016/j.csr.2004.06.012

Conflict of Interest: The authors declare that the research was conducted in the absence of any commercial or financial relationships that could be construed as a potential conflict of interest.

Publisher's Note: All claims expressed in this article are solely those of the authors and do not necessarily represent those of their affiliated organizations, or those of the publisher, the editors and the reviewers. Any product that may be evaluated in this article, or claim that may be made by its manufacturer, is not guaranteed or endorsed by the publisher.

Copyright © 2022 Wu, Rong, Wang, Lu and Liu. This is an open-access article distributed under the terms of the Creative Commons Attribution License (CC BY). The use, distribution or reproduction in other forums is permitted, provided the original author(s) and the copyright owner(s) are credited and that the original publication in this journal is cited, in accordance with accepted academic practice. No use, distribution or reproduction is permitted which does not comply with these terms.

frontiers | Frontiers in Marine Science

BRIEF RESEARCH REPORT
published: 26 May 2022
doi: 10.3389/fmars.2022.914391

Microplastics in Demersal Sharks From the Southeast Indian Coastal Region

Madhuvandhi Janardhanam[1], Priya Sivakumar[1], Gomathi Srinivasan[1], Rekha Sivakumar[1], Priscilla Niranjani Marcus[1], Sujatha Balasubramaniam[1], Krishnamurthy Rajamanickam[2], Thiagarajan Raman[3], Gopalakrishnan Singaram[4] and Thilagam Harikrishnan[1]**

[1] Postgraduate and Research Department of Zoology, Pachaiyappa's College for Men, Chennai, India, [2] Post graduate (PG) and Research Department of Zoology and Aquaculture, Government Arts College for Men (Autonomous), Affiliated to University of Madras, Chennai, India, [3] Department of Zoology, Ramakrishna Mission Vivekananda College (Autonomous), Chennai, India, [4] eProov Assessment Solution Pvt., Limited, Chennai, India

OPEN ACCESS

Edited by:
Dilip Kumar Jha,
National Institute of Ocean Technology, India

Reviewed by:
Nithyanandam Marimuthu,
Zoological Survey of India, India
Mehmuna Begum,
National Centre for Coastal Research, India

***Correspondence:**
Gopalakrishnan Singaram
gopalthilagam@gmail.com
Thilagam Harikrishnan
thilagampachaiyappas@gmail.com

Specialty section:
This article was submitted to Marine Pollution, a section of the journal Frontiers in Marine Science

Received: 06 April 2022
Accepted: 20 April 2022
Published: 26 May 2022

Citation:
Janardhanam M, Sivakumar P, Srinivasan G, Sivakumar R, Marcus PN, Balasubramaniam S, Rajamanickam K, Raman T, Singaram G and Harikrishnan T (2022) Microplastics in Demersal Sharks From the Southeast Indian Coastal Region. Front. Mar. Sci. 9:914391. doi: 10.3389/fmars.2022.914391

Microplastic (MPs) contamination has emerged as a serious worldwide issue. Human activity, commercial enterprises, and fishing are concentrated around the seashore, causing high levels of MPs contamination in coastal and marine organisms. When it comes to their vulnerability to MPs ingestion, sharks are least studied organism. The objective of this study is to investigate MPs accumulation in sharks collected from the Southeast Indian coastal zone (Bay of Bengal). We present evidence of MPs ingestion in demersal sharks caught by the trawlers during trawling operations in marine waters beyond a depth of 80 m in the Southeast India coast. Shark samples were also checked for any gender or size differences in contaminant loading. Gill and gut (digestive tract) were examined in 40 sharks and 82.5% of samples contained at least one MP particle. The average number of MP particles was found to be 4.67 items per individual shark; the gastrointestinal tract showed more MPs than the gills. The majority of the MPs were blue and pale white followed by black and transparent particles with diameters ranging from 0.5 to 2 mm. The fibre fragments were prevalent in the intestines of the shark. Fourier Transform Infrared (FT-IR) spectroscopy revealed that the bulk of polymers were polypropylene (PP), polyacrylamides (PA), and polyethylene (PE). MPs contamination poses an unknown level of harm to shark species. The present study revealed the first scientific data of MPs and associated fibre ingestion in shark species in their habitat in the Bay of Bengal.

Keywords: shark, microplastics, marine pollution, fish, fisheries, aquaculture, bay of bengal

INTRODUCTION

The microplastics (MPs) pollution in oceans is a serious and ongoing global environmental issue. Annual worldwide plastics output has more than quadrupled over the previous half-century, with a 2016 estimate of > 335 Mt. (Galgani et al., 2015; Plastics Europe, 2018; Goswami et al., 2021). Plastics are widespread in both terrestrial and aquatic environments (including freshwater,

estuaries, coastal, and marine), and they are increasingly becoming a major cause of marine pollution in addition to seawater quality (Jha et al., 2015), metal toxicity (Satheeswaran et al., 2019), and microbial contamination (Dheenan et al., 2016). The MPs pollution may threaten the marine life when they are ingested and have far-reaching effects on ecosystems (Nelms et al., 2018). Plastic manufacturing and usage have expanded considerably in recent years due to cost-effectiveness and economy, resulting in greater use of synthetic plastic polymers in terrestrial and aquatic environments (Thompson et al., 2009). Non-biodegradable compounds in the aquatic environment especially in the coastal regions, in particular abandoned fishing gear, carry bags, synthetic packaging materials, and plastic coverings, are harmful to marine life (Kaladharan et al., 2020). The MPs are small pieces of plastic with a diameter of 5 mm or less and are deposited in marine ecosystems (Sharma and Chatterjee, 2017). The MPs may be ingested by a wide range of marine species, including corals, plankton, marine invertebrates, fish, and whales, and are eventually transferred to the food chain (Thompson et al., 2009; Nelms et al., 2018; Kaladharan et al., 2020). These plastic polymers not only endanger marine life directly, but they also have an indirect impact on the environment by adsorbing other marine contaminants including organic and inorganic compounds. Further MPs quickly absorb hydrophobic pollutants from water systems due to their large surface area compare to that of any pollutants (Joo et al., 2021). As a result, MPs contamination is an issue primarily because of its negative impact on the health of the marine environment and biota.

MPs have been demonstrated to be ingested directly by fish and pelagic invertebrates due to their physical resemblance to their food (Phillips and Bonner, 2015). According to global studies on marine MPs, they are more prevalent near the shorelines, and a definite association between the size of terrestrial pollution and the degree of marine pollution has been documented (Harris, 2020). Plastic debris that finds its way to and is dumped in the water is broken by physical, chemical, and biological processes, resulting in the production of MPs in coastal regions (Thompson et al., 2009). Because of the broad dispersion of MPs in aquatic habitats and along the shorelines, MPs pollution has gained relevance as an attractive scientific issue over the last decade (Galgani et al., 2015).

MPs have been discovered in the stomachs of a variety of marine organisms, including invertebrates and vertebrates. We have a better knowledge of the implications of MPs consumption in the preceding group, with evidence revealing dose-dependent detrimental effects on feeding behavior, development, reproduction, and lifespan (Issac and Kandasubramanian, 2021). Despite the fact that elasmobranchs are largely understudied in terms of plastic pollution risks, their susceptibility to MPs ingestion has been documented (Parton et al., 2020). Because of their feeding habits or habitat utilization, some elasmobranch species are thought to be particularly vulnerable to MPs ingestion. Filter-feeding species (such as whale sharks and basking sharks) are considered to be more sensitive to MPs ingestion in habitats that overlap with regions with high amounts of plastic pollution. Many shark species, on the other hand, are non-filter feeders, preying on larger organisms including fish, crabs, marine turtles, and marine mammals, all of which have been proven to ingest MPs (Parton et al., 2020).

The Bay of Bengal is a habitat for a variety of shark and ray species, including tiny to medium-sized demersal sharks. These species may be found at depths ranging from 5 to 900 m and favor benthic settings (Tyabji et al., 2020). They feed on a range of small teleost fishes, crabs, and cephalopods. Because of their habitat preference, they are usually taken as by catch in demersal fisheries; nevertheless, specialist fisheries for these species exist. MPs exposure to demersal shark species is currently understudied, with just a few examples of plastic ingestion, mainly in and around the Mediterranean Sea (Cózar et al., 2015). However, there have been multiple studies of plastic ingestion in bony fish, with ingestion rates varying from 0 to 100% have been reported (Thiele et al., 2021). To the best of our knowledge, there are no studies on MPs accumulation in sharks caught as commercial fish in the southern coastal region of the Bay of Bengal. The findings of the first thorough investigation on MPs ingestion in sharks in the Bay of Bengal are discussed in detail in the present study.

MATERIALS AND METHODS

The samples for this study were collected from the southern coastal region of the Bay of Bengal, India. The shark fish [*Rhizoprionodon acutus* (Rüppell) 1837] was taken as a by catch in a demersal fishery trawling in and around the Bay of Bengal at a depth of 80 m and landed in the fish harbour of Royapuram, Chennai. The samples were collected during the period of November 2020, June-2021 and November, 2021. The number of shark collected during different sampling period is given in **Table 1**. Forty sharks were investigated, comprising 16 males and 24 females. All of the sharks used were subjected to standard morphometric measurements.

The standard dissection method was followed to remove the complete digestive tract from the individual shark samples (Boerger et al., 2010; Davison and Asch, 2011) which were then placed in a watch glass and weighed, the intestines after

TABLE 1 | Microplastics (MPs) in shark collected from Royapuram Fish landing centre, Chennai.

Period of Collection	Species	Total Length(cm)	Wet Weight (g)	Total No. of Shark	No. of MPs	Average Item/per Shark
November- 2020	*Rhizoprionodon acutus*	40.90 ± 5.60	280.9 ± 29.60	16	72	4.50 ± 1.59
June-2021	*Rhizoprionodon acutus*	38.20 ± 4.08	260.8 ± 32.60	11	63	5.72 ± 1.61
November-2021	*Rhizoprionodon acutus*	32.78 ± 1.05	242.8 ± 20.95	13	52	4.00 ± 1.82

weighing were digested with a solution of hydrogen peroxide (30% H_2O_2) at 60°C in a glass beaker (Rochman et al., 2015). MPs were detected by observing the sample under a NIKON stereoscopic microscope fitted with a digital camera. The total number of MPs found in each sample was recorded and classified by type, color, and size (maximum length) (Wessel et al., 2016; Jung et al., 2018). Samples were covered with foil prior to recovery, storage, intestinal digestion, and visual identification.

Non-plastic components of various size classes were manually sorted under a stereomicroscope and removed from each sample using stainless steel forceps prior to segregation (Karthik et al., 2018). Using the method described by Free et al. (2014), MPs and their form were recognized. Granules (spherical, cylindrical particles), film (thin, soft, transparent particles), fragments (small angular, irregular shaped particles), fibre/line (elongated, thin, straight particles), and foam (lightweight particles with spongy texture) were the five categories (Robin et al., 2020). The plastic particles were then divided into seven colour categories: blue, transparent, green, pale white, black, red, and yellow (Young and Elliott, 2016).

SEM AND FTIR ANALYSIS

In most cases, MPs are identified visually before a polymer type is identified. Although smaller particles can be seen with the naked eye, microparticles can be seen clearly with a scanning electron microscope (SEM), and the images were captured using these instruments (Tudor and Williams, 2004). Fourier Transform Infrared Spectroscopy (FT-IR) is a technique used to determine the type of plastic substances present in the observed samples. These methods rely on the energy transmittance of polymer particles' characteristic functional groups. A Bruker ALPHA FT-IR spectrometer with a single reflection diamond Attenuated Total Reflectance (ATR) accessory was used to collect the infrared spectra. A fixed load was applied to a sample of approximately 1 g placed directly on the internal reflection element (IRE) to ensure full contact with the diamond ATR. For each sample, twenty-four scans were averaged at a resolution of 4 cm^{-1} within the wave number range of 400 to 4000 cm^{-1} (default Bruker OPUS 6.5 software settings), and the resulting averaged spectrum was recorded. To confirm the significance of differences in MPs particle numbers between sampling periods, a statistical analysis was performed using the SPSS software (Version 20.0). The T-test was used to differentiate between gender and size groups. A one-way analysis of variance (ANOVA) test was used to determine whether there was a significant difference between the sampling periods. Results from Pearson's correlation co-efficient two-tailed test revealed no correlation between MPs and fish length/weight.

RESULTS

In total, 40 sharks were studied for the presence of MPs, of which 40% were males and 60% were females. The entire sample caught was a mixture of adults and juveniles. Fibres, granules, fragments, films and foams are the different types of MPs identified in sharks (**Figure 1C**). Among 40 sharks analysed in this study, 82.5% of the samples (33/40) contained at least one MP particle. Among the MPs, the number of fibres was about 42%, followed by fragments and granules with 26 and 20%, respectively. Film (5%) and foam (7%) also constituted the total MPs in sharks (**Figures 1A–C**). No significant variations in number of MPs were found between different sampling periods ($p < 0.058$). Similarly, t-test analysis revealed no significant differences in MPs accumulation between male and female sharks over the sample periods ($p < 0.2735$ for November 2020; $p < 0.611$ for June 2021and $p < 0.572$ for November 2021). Additionally, we also analysed microplastic size variations and accumulation and found no significant difference ($p < 0.245$).

Fibres ranged in length from 0.3 to 10.0 mm and had an average length of 3.2 ± 2.2mm. About 75% of the MPs were less than 2 mm in size (**Figures 2A–H**). The vast majority of fibres were blue and pale white (54.0%) in colour, with the remaining colours including transparent, black, red, yellow and other each making up to 13% of maximum [**Supplementary Figure 1A**, (SF 1A)]. Among the organ the gut contained 92% of MPs and gill 8% (**Figure SF1B**). Fibres larger than 5 mm (n = 4) were considered here as macroplastics and were excluded from the analysis. The SEM investigations of MPs of different types are given in **Figures 2I–L**. The surface morphology of fragments, fibre and granules were visible through the SEM investigations. The presence of polyethylene (PE), polyamide (PA) and polypropylene (PP) in the FTIR spectrum was determined by their characteristic wave numbers. **Figure 2M** show representative ATR-FTIR spectra for the three distinct kinds of particles. PE, PP, and PA were identified as the principal categories of MPs based on sample analysis. The existence of PE was determined by the presence of typical wave numbers ranging from 1462 to 1465 cm^{-1}. Similarly, PP was found using characteristic wave numbers in areas of 1737cm^{-1} and 1745 cm^{-1} that showed CH_2 stretching (Veerasingam et al. (2016).

DISCUSSION

MPs pose critical threat to marine species due to the fact that these animals tend to swallow these compounds present in water leading to widespread physiological effects (Barnes, 2002; Dharani et al., 2003). In order to understand the effect of anthropogenic activities on marine ecosystem, more research needs to be focussed on the prevalence, characteristics and residence time of MPs in aquatic food webs. Due to their small size, they are less likely to damage a fish's digestive tract. However, studies of negative physical and biochemical effects of MPs on fish physiology, especially in coastal waters of India, are limited.

Our research is the first to show the presence of MPs in sharks caught in the Bay of Bengal. Despite the fact that there were no significant variations in MPs uptake across the sharks sampled (seasonal, gender and size dependent), the study provides an

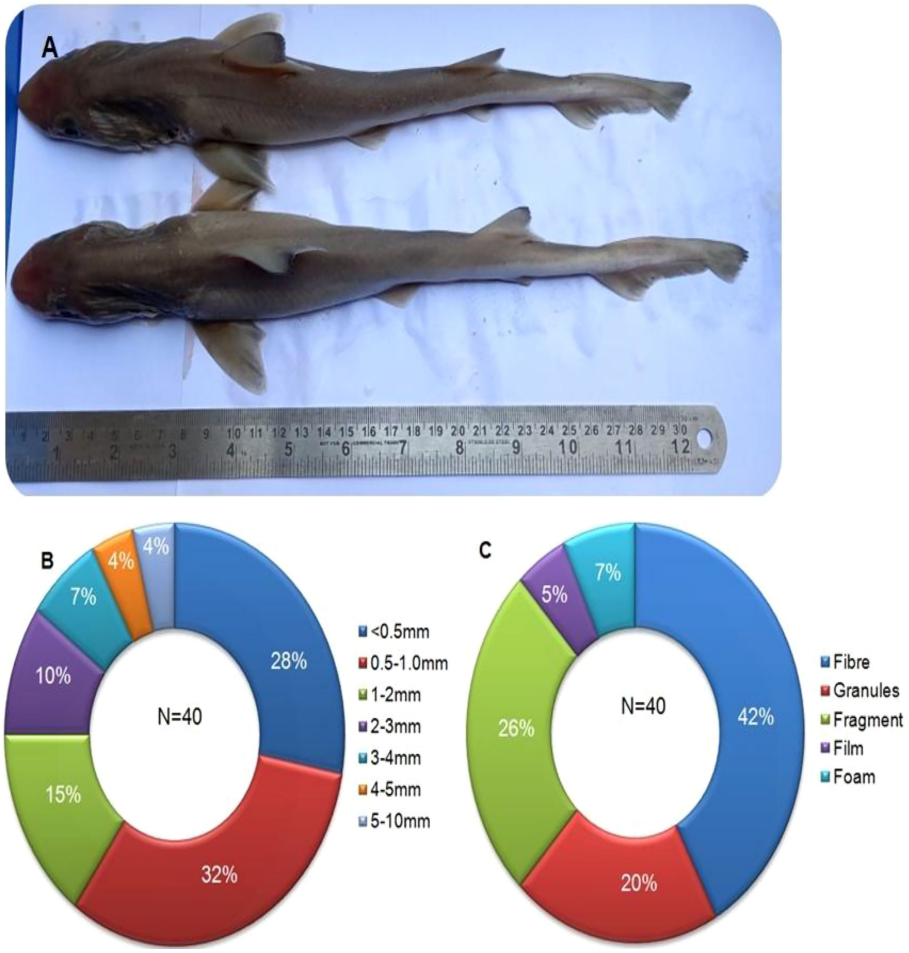


FIGURE 1 | Shark fish samples collected and analyzed for microplastics **(A)** Juvenile male shark **(B)** Pie diagram showing percentage of different size of microplastics **(C)** Pie diagram information showing percentage of different type of microplastics.

essential empirical baseline for future research into contaminant levels in shark fish habitat in Indian coastal and marine regions. From these we could predict that fish habitat in shore regions of South India's coast with poor water quality may be exposed to high amounts of plastic pollution (Veerasingam et al., 2016; Karthik et al., 2018; Robin et al., 2020). Although we haven't investigated its impact on health of sharks, the existence of these particle pollutants suggests their pervasiveness in the marine ecosystem, especially closer to the shores, which can probably cause long term health effects on fishes including sharks number of such marine contaminants is projected to rise as global plastic manufacturing and its ubiquity in everyday items increase (Villarrubia-Gómez et al., 2018).

Very few studies across the world have demonstrated the existence of MPs in shark (Valente et al., 2019; Parton et al., 2020). Patron et al. (2020) reported the presence of MPs in numerous species of shark in the UK's North-East Atlantic coastline area. In our study, over 92% of all sharks examined had at least one MP particle in their digestive system, and 8% showed the presence of MPs in the gills. We also found no gender differences in MPs accumulation during the sampling period, nor any notable changes in MPs accumulation based on shark size. These findings clearly show that MPs accumulation was found in the majority of the samples regardless of size or gender or sampling period. The percentage of sample with MPs was still very high and alarming. The quantity of MP fibres was found to be more in the case of larger sharks compared to smaller ones, indicating the ability of larger sharks to ingest more food and thus indirectly more MP accumulation. For this study, sample collection was done deep in the waters of Bay of Bengal by fishermen and hence we were not able to accurately pinpoint the location or habitat from which these sharks were caught and hence this aspect needs to be looked further. Our results also lead us to hypothesize that nutrition could be an important influencing factor on MPs accumulation in sharks.

The type of MPs in the marine ecosystem could help one to understand the possible sources, and fate of these MPs. The use of FT-IR spectroscopy to analyse environmental materials is a

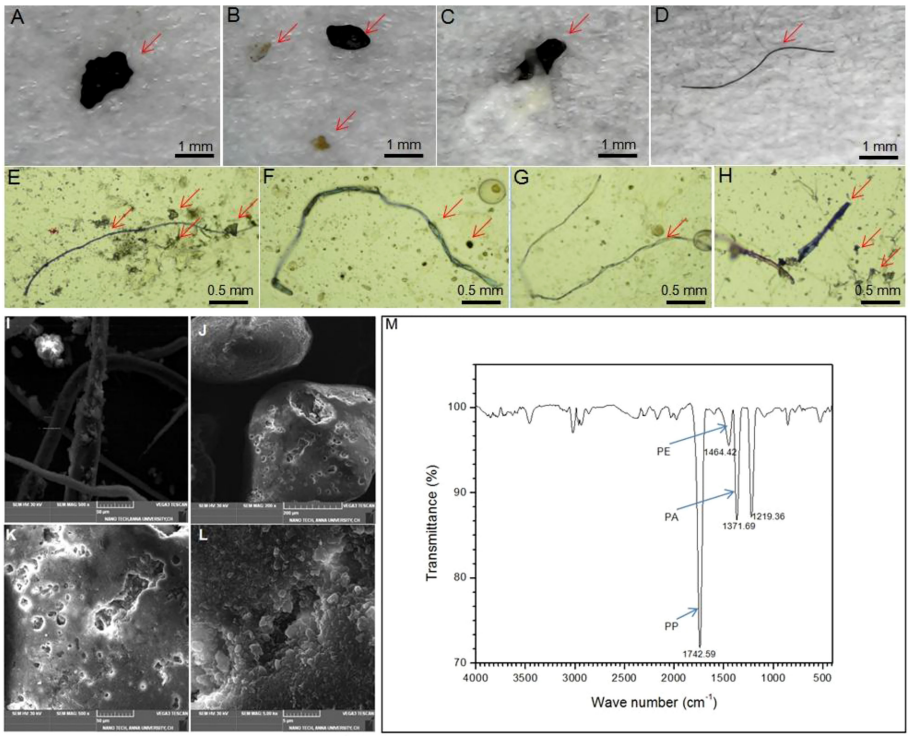


FIGURE 2 | Presence of different types of microplastics in Shark **(A–C)** Fragments and film **(D–H)** Fibre and granules **(I–L)**. SEM images of microplastics **(I)** Fibre **(J**, **K)** Fragment **(L)** Granules **(M)**. FTIR spectra representing PE, PA and PP type.

reliable approach for detecting polymer make-up and should be central to any future research. The polymers we discovered are similar to the polymer variety of MPs found across the world, with polypropylene being one of the most prevalent polymers found. The presence of PE and PP in the fish gut was verified using FT-IR analysis and all three types were found in the gut of the sharks, suggesting that microplastics of all kinds are an environmental problem. Veerasingam et al. (2016) reported similar spectra for microbeads while researching MPs on the Chennai coast. Together these results clearly show the presence of microplastics in the waters of Bay of Bengal which were revealed by their significant presence in the gut of demersal sharks that were collected during routine fishing. However, MPs presence in these sharks was not influenced by animal size, gender or season and hence this particular kind of pollutant could pose a year round problem for marine animals. In addition, presence of MPs of PE, PP and PA types suggests that these pollutants are widespread and their persistence could pose enormous challenges to all marine ecosystems.

CONCLUSION

Our study shows the presence and accumulation of microplastics in the sharks from Bay of Bengal. The size, gender of the animal as well as the season of collection did not have any apparent influence on MPs accumulation in sharks, indicating that MPs could be persistent pollutants in marine ecosystem similar to persistent organic pollutants. Furthermore finding of all the three types of MPs in the sharks indicate that MPs of all kinds are serious marine pollutants. Since MPs in marine waters is a result of anthropogenic activities, this study can be used as a reference for future research on MPs pollution in commercial fish in coastal and estuarine region, as well as for governmental organisations developing management strategies and policies against microplastic pollution.

DATA AVAILABILITY STATEMENT

The original contributions presented in the study are included in the article/**Supplementary Material**. Further inquiries can be directed to the corresponding authors.

ETHICS STATEMENT

Ethical review and approval was not required for the animal study because it's a commercial fish.

AUTHOR CONTRIBUTIONS

MJ, PS, GSrin, RS, PM, sample collection, laboratory analysis, methodology validation, data processing, and writing-original draft. SB and KR, conceptualization, sampling design, data validation, and manuscript review. TR, manuscript corrections

and critical suggestions. GSing and TH, reviewing the manuscript, suggestion, and project administration. All authors contributed to the article and approved the submitted version.

ACKNOWLEDGMENTS

The authors thank Head, Research department of Zoology and also the Principal Pachaiyappa's College for Men, Chennai- 600 030, and Head, Research department of Zoology and also the Principal Government Arts College for men (Autonomous), Chennai-600 035 India for extending their support through the experiment.

SUPPLEMENTARY MATERIAL

The Supplementary Material for this article can be found online at: https://www.frontiersin.org/articles/10.3389/fmars.2022.914391/full#supplementary-material

REFERENCES

Barnes, D. K. A. (2002). Biodiversity: Invasions by Marine Life on Plastic Debris. *Nature* 416, 808–809. doi: 10.1038/416808a

Boerger, C. M., Lattin, G. L., Moore, S. L., and Moore, C. J. (2010). Plastic Ingestion by Planktivorous Fishes in the North Pacific Central Gyre. *Mar. Pollut. Bull.* 60, 2275–2278. doi: 10.1016/j.marpolbul.2010.08.007

Cózar, A., Sanz-Martín, M., Martí, E., González-Gordillo, J. I., Ubeda, B., Gálvez, J. Á., Irigoien, X., and Duarte, C. M.. (2015). Plastic Accumulation in the Mediterranean Sea. *PloS One* 10 (4), e0121762. doi: 10.1371/journal.pone.0121762

Davison, P., and Asch, R. G. (2011). Plastic Ingestion by Mesopelagic Fishes in the North Pacific Subtropical Gyre. *Mar. Ecol. Prog. Ser.* 432, 173–180. doi: 10.3354/meps09142

Dharani, G., Abdul Nazar, A. K., Venkatesan, R., and Ravindran, M. (2003). Marine Debris in Great Nicobar. *Curr. Sci.* 85 (5), 574–575.

Dheenan, P. S., Jha, D. K., Das, A. K., Vinithkumar, N. V., Prashanthi Devi, M., and Kirubagaran, R. (2016). Geographic Information Systems and Multivariate Analysis to Evaluate Fecal Bacterial Pollution in Coastal Waters of Andaman, India. *Environ. Pollut.* 214, 45–53. doi: 10.1016/j.envpol.2016.03.065

Free, C. M., Jensen, O. P., Mason, S. A., Eriksen, M., Williamson, N. J., and Boldgiv, B. (2014). High-Levels of Microplastic Pollution in a Large, Remote, Mountain Lake. *Mar. Pollut. Bull.* 85 (1), 156–163. doi: 10.1016/j.marpolbul.2014.06.001

Galgani, F., Hanke, G., and Maes, T. (2015). "Global Distribution, Composition and Abundance of Marine Litter," in *Marine Anthropogenic Litter*. Eds. M. Bergmann, L. Gutow and M. Klages (Berlin: Springer), 29–56.

Goswami, P., Vinithkumar, N. V., and Dharani, G. (2021). Microplastics Particles in Seafloor Sediments Along the Arabian Sea and the Andaman Sea Continental Shelves: First Insight on the Occurrence, Identification, and Characterization. *Mar. Pollut. Bull.* 167, 112311. doi: 10.1016/j.marpolbul.2021.112311

Harris, P. T. (2020). The Fate of Microplastic in Marine Sedimentary Environments: A Review and Synthesis. *Mar. Pollut. Bull.* 158, 111398. doi: 10.1016/j.marpolbul.2020.111398

Issac, M. N., and Kandasubramanian, B. (2021). Effect of Microplastics in Water and Aquatic Systems. *Environ. Sci. Pollut. Res.* 28, 19544–19562. doi: 10.1007/s11356-021-13184-2

Jha, D. K., Vinithkumar, N. V., Sahu, B. K., Dheenan, P. S., Das, A. K., Begum, M., et al. (2015). Multivariate and Geo-Spatial Approach for Seawater Quality of Chidiyatappu Bay, South Andaman Islands, India. *Mar. Pollut. Bull.* 96 (1–2), 463–470. doi: 10.1016/j.marpolbul.2015.05.004

Joo, S. H., Liang, Y., Kim, M., Byun, J., and Choi, H. (2021). Microplastics With Adsorbed Contaminants: Mechanisms and Treatment. *Environ. Challenges* 3, 100042. doi: 10.1016/j.envc.2021.100042

Jung, M. R., Horgen, F. D., Orski, S. V., Rodriguez, V., Beers, K. L., Balazs, G. H., et al. (2018). Validation of ATR FT-IR to Identify Polymers of Plastic Marine Debris, Including Those Ingested by Marine Organisms. *Mar. Pollut. Bull.* 127, 704–716. doi: 10.1016/j.marpolbul.2017.12.061

Kaladharan, P., Singh, V. V., Asha, P. S., Edward, L., and Sukhadane, K. S. (2020). Marine Plastic Litter in Certain Trawl Grounds Along the Peninsular Coasts of India. *Mar. Pollut. Bull.* 157, 111299. doi: 10.1016/j.marpolbul.2020.111299

Karthik, R., Robin, R. S., Purvaja, R., Ganguly, D., Anandavelu, I., Raghuraman, R., et al. (2018). Microplastics Along the Beaches of Southeast Coast of India. *Sci. Total Environ.* 645, 1388–1399. doi: 10.1016/j.scitotenv.2018.07.242

Nelms, S. E., Galloway, T. S., Godley, B. J., Jarvis, D. S., and Lindeque, P. K. (2018). Investigating Microplastic Trophic Transfer in Marine Top Predators. *Environ. Pollut.* 238, 999–1007. doi: 10.1016/J.ENVPOL.2018.02.016

Parton, K. J., Godley, B. J., Santillo, D., Tausif, M., Omeyer, L. C. M., and Galloway, T. S. (2020). Investigating the Presence of Microplastics in Demersal Sharks of the North-East Atlantic. *Sci. Rep.* 10, 12204. doi: 10.1038/s41598-020-68680-1

Phillips, M. B., and Bonner, T. H. (2015). Occurrence and Amount of Microplastic Ingested by Fishes in Watersheds of the Gulf of Mexico. *Mar. Pollut. Bull.* 100 (1), 264–269. doi: 10.1016/j.marpolbul.2015.08.041

Plastics Europe (2018). *Plastics – The Facts 2017, An Analysis of European Plastics Production, Demand and Waste Data* (Belgium: Brussels), 16.

Robin, R. S., Karthik, R., Purvaja, R., Ganguly, D., Anandavelu, I., Mugilarasan, M., et al. (2020). Holistic Assessment of Microplastics in Various Coastal Environmental Matrices, Southwest Coast of India. *Sci. Total Environ.* 703, 134947. doi: 10.1016/j.scitotenv.2019.134947

Rochman, C. M., Tahir, A., Williams, S. L., Baxa, D. V., Lam, R., Miller, J. T., et al. (2015). Anthropogenic Debris in Seafood: Plastic Debris and Fibers Fromtextiles in Fish and Bivalves Sold for Human Consumption. *Sci. Rep.* 5, 14340. doi: 10.1038/srep14340

Satheeswaran, T., Yuvaraj, P., Damotharan, P., Karthikeyan, V., Jha, D. K., Dharani, G., et al. (2019). Assessment of Trace Metal Contamination in the Marine Sediment, Seawater, and Bivalves of Parangipettai, Southeast Coast of India. *Mar. Pollut. Bull.* 149, 110499. doi: 10.1016/j.marpolbul.2019.110499

Sharma, S., and Chatterjee, S. (2017). Microplastic Pollution, a Threat to Marine Ecosystem and Human Health: A Short Review. *Environ. Sci. Pollut. Res.* 24 21530–21547. doi: 10.1007/s11356-017-9910-8

Thiele, C. J., Hudson, M. D., Russell, A. E., Saluveer, M., Sidaoui-Haddad, G., and Russell, A. E.. (2021). Microplastics in Fish and Fishmeal: An Emerging Environmental Challenge? *Sci. Rep.* 11 (1), 2045. doi: 10.1038/s41598-021-81499-8

Thompson, R. C., Moore, C. J., VomSaal, F. S., and Swan, S. H. (2009). Plastics, the Environment and Human Health: Current Consensus and Future Trends. *Philos. Trans. R. Soc. B* 364 (1526), 2153–2166. doi: 10.1098/rstb.2009.0053

Tudor, D. T., and Williams, A. T. (2004). Development of a 'Matrix Scoring Technique' to Determine Litter Sources at a Bristol Channel Beach. *J. Coast. Conserv.* 9, 119–127. doi: 10.1652/1400-0350(2004)010[0119:DOAMST]2.0.CO;2

Tyabji, Z., Wagh, T., Patankar, V., Jabado, R. W., and Sutaria, D. (2020). Catch Composition and Life History Characteristics of Sharks and Rays (Elasmobranchii) Landed in the Andaman and Nicobar Islands, India. *PloS One* 15 (10), e0231069. doi: 10.1371/journal.pone.0231069

Valente, T., Sbrana, A., Scacco, U., Jacomini, C., Bianchi, J., Palazzo, L., Andrea de Lucia, G., Silvestri, C., and Matiddi, M.. (2019). Exploring Microplastic Ingestion by Three Deep-Water Elasmobranch Species: A Case Study From the Tyrrhenian Sea. *Environ. Pollut.* 253, 342–350. doi: 10.1016/j.envpol.2019.07.001

Veerasingam, S., Mugilarasan, M., Venkatachalapathy, R., and Vethamony, P. (2016). Influence of 2015 Flood on the Distribution and Occurrence of Microplastic Pellets Along the Chennai Coast, India. *Mar. Pollut. Bull.* 109 (1), 196–204. doi: 10.1016/j.marpolbul.2016.05.082

Villarrubia-Gómez, P., Cornell, S. E., and Fabres, S. (2018). Marine Plastic Pollution as a Planetary Boundary Threat – The Drifting Piece in the Sustainability Puzzle. *Mar. Policy* 96, 213–220. doi: 10.1016/j.marpol.2017.11.035

Wessel, C. C., Lockridge, G. R., Battiste, D., and Cebrian, J. (2016). Abundance and Characteristics of Microplastics in Beach Sediments: Insights Into Microplastic Accumulation in Northern Gulf of Mexico Estuaries. *Mar. Pollut. Bull.* 109 (1), 178–183. doi: 10.1016/j.marpolbul.2016.06.002

Young, A. M., and Elliott, J. A. (2016). Characterization of Microplastic and Mesoplastic Debris in Sediments From Kamilo Beach and Kahuku Beach,

Hawaii. *Mar. Pollut. Bull.* 113 (1–2), 477–482. doi: 10.1016/j.marpolbul.2016.11.009

Author Disclaimer: All claims expressed in this article are solely those of the authors and do not necessarily represent those of their affiliated organizations, or those of the publisher, the editors and the reviewers. Any product that may be evaluated in this article, or claim that may be made by its manufacturer, is not guaranteed or endorsed by the publisher.

Conflict of Interest: Author GSing was employed by eProov Assessment Solution Pvt., Limited.

The authors declare that the research was conducted in the absence of any commercial or financial relationships that could be construed as a potential conflict of interest.

Publisher's Note: All claims expressed in this article are solely those of the authors and do not necessarily represent those of their affiliated organizations, or those of the publisher, the editors and the reviewers. Any product that may be evaluated in this article, or claim that may be made by its manufacturer, is not guaranteed or endorsed by the publisher.

Copyright © 2022 Janardhanam, Sivakumar, Srinivasan, Sivakumar, Marcus, Balasubramaniam, Rajamanickam, Raman, Singaram and Harikrishnan. This is an open-access article distributed under the terms of the Creative Commons Attribution License (CC BY). The use, distribution or reproduction in other forums is permitted, provided the original author(s) and the copyright owner(s) are credited and that the original publication in this journal is cited, in accordance with accepted academic practice. No use, distribution or reproduction is permitted which does not comply with these terms.

frontiers | Frontiers in Marine Science

DATA REPORT
published: 23 June 2022
doi: 10.3389/fmars.2022.940573

Ocean Acidification Impact on Haematological and Serum Biochemical Parameters in *Lates calcarifer*

Gomathi Srinivasan†, *Priscilla Niranjani Marcus*†, *Priya Sivakumar*, *Pandi Paramasivam*, *Rekha Sivakumar*, *Thilagam Harikrishnan** and *Sujatha Balasubramaniam**

Postgraduate and Research Department of Zoology, Pachaiyappa's College for Men, Chennai, India

Keywords: Asian seabass, ocean acidification, marine environment, haematology, seawater

OPEN ACCESS

Edited by:
Dilip Kumar Jha,
National Institute of Ocean Technology, India

Reviewed by:
Muthukumar Thangavelu,
Jeonbuk National University, South Korea
Thiagarajan Raman,
Ramakrishna Mission Vivekananda College, India
Vikas Pandey,
National Institute of Ocean Technology, India

****Correspondence:***
Sujatha Balasubramaniam
sujathapachaiyappas@gmail.com
Thilagam Harikrishnan
thilagampachaiyappas@gmail.com

†These authors have contributed equally to this work

Specialty section:
This article was submitted to Marine Pollution, a section of the journal Frontiers in Marine Science

Received: *10 May 2022*
Accepted: *26 May 2022*
Published: *23 June 2022*

Citation:
Srinivasan G, Marcus PN, Sivakumar P, Paramasivam P, Sivakumar R, Harikrishnan T and Balasubramaniam S (2022) Ocean Acidification Impact on Haematological and Serum Biochemical Parameters in Lates calcarifer. Front. Mar. Sci. 9:940573. doi: 10.3389/fmars.2022.940573

INTRODUCTION

Ocean acidification (OA) is a long-term drop in the pH of the ocean caused mostly by atmospheric carbon dioxide (CO_2). It is a consequence of climate change that poses a direct threat to life on earth by affecting the marine ecosystem (Panchang and Ambokar, 2021). The ocean has absorbed around 30% of the carbon dioxide emitted by human activities since the beginning of the industrial revolution (Sabine et al., 2004). The elevated partial pressure of carbondioxide (pCO_2) causes seawater pH and $CaCO_3$ staturation to decrease (Feely et al, 2004). The pCO_2 value is now at 375 atm (Rhein et al., 2013) which is expected to reach 420 to 940 atm by 2100, and pH may decline by 0.13 to 0.42 units scenario (Rhein et al., 2013). The pH of sea water has declined from 8.17 units in pre-industrial periods (Key et al., 2004) to 8.06 units now (Rhein et al., 2013), indicating a decrease of 34.91%. Due to eutrophication and amplification of natural CO_2 some coastal locations may see shifts H^+ that are at least 2–3 times the world average (Melzner et al., 2012). Many marine organisms' physiological activities are predicted to be influenced by such changes in ocean chemistry, potentially having far-reaching effects on marine biodiversity and ecological processes (Murugan et al., 2005; Vijayakumaran et al., 2005; Fabry et al., 2008; Pörtner, 2008; Kumar et al., 2009; Gattuso et al., 2011).

Ocean acidification thought to harm marine fish performance, owing to changes in oxygen availability and delivery capabilities (Pörtner, 2008). Individual survival may be harmed by acidic pH because less energy is allocated to digestion, growth, and reproduction (Munday et al., 2009; Munday et al., 2014). The OA has the ability to change the outcomes of ecologically important processes and the structure of ecological communities (Pörtner, 2008). Given that abiotic variables such as oxygen availability, temperature, and salinity are known to have the greatest influence on aquatic species' early life stages (Bonk, 2005), the possible impact of acidified seawater on their development should be taken into account. Only a few studies on the impact of OA on early life stages of aquatic animals have been conducted, with the majority focusing on invertebrates (Kurihara et al., 2004; Havenhand et al., 2008; Dupont and Thorndyke, 2009; Ellis et al., 2009 Dupont et al., 2010) indicating that the impact of OA on the early life history of vertebrates is scanty.

Because blood is the channel of intercellular transfer and comes into direct contact with multiple organs and tissues of the body, it plays an important part in all physiological systems and hence, an animal's physiological status at any given time is reflected in its blood. Any type of

environmental stress induces oxidative stress in a normal organism, which is reflected in blood proteins and causes haematological changes, and may be used as a method for biological monitoring (Martinez and Souza, 2002). Although organisms are resistant to the harmful effects of oxidative stress caused due to reactive oxygen species, prolonged exposure can cause oxidative damage, including the loss of compensatory mechanisms due to changes in enzyme function (Galloway and Handy, 2003; Dogan and Can, 2011; Narra, 2017). Adverse changes in the haematological and biochemical markers indicate toxicity, and their use in environmental monitoring and aquatic biota health has a wide variety of applications (Thilagam et al., 2009; Narra, 2017).

A few research on the consequences of hypercapnia on various life stages of marine teleosts have been published in recent years (Checkley et al., 2009; Munday et al., 2009; Munday et al., 2014). Increased pCO_2 levels were employed by Kikkawa et al. (2003) to explore the acute lethal effect of pCO_2 on the early life stages of marine fishes. The whole world's seas, especially coastal estuaries and streams, are being affected by OA. Many economies rely on fish and shellfish, and people all over the world use seafood as their major source of protein. Considering the need of the hour and importance of fisheries sector, an experiment was designed to study seawater acidification impacts on the growth rate of Indian seabass at various stages of their lives (Fry and Fingerlings). In both fry and fingerlings, we investigated how acidified medium alter haematological, biochemical markers in blood and consequently affect the growth. Thus, this study will help in designing the long-term effects of ocean acidification on the growth of Indian seabass, which might have implications on coastal and marine ecosystem organisms.

METHODS

For this study, fishes were collected from the Rajiv Gandhi Centre for Aquaculture (RGCA) in Thirumullaivasal, Tamil Nadu, India. Before being utilized in the experiment, fish fry with an average length of 3.58 ± 1.2 cm and a weight of 2.78 ± 0.9 g and fingerling with an average length of 7.42 ± 1.59 cm and a weight of 6.1 ± 1.24 g were acclimatized for a week in a fiberglass tank. During acclimatization, the water temperature, salinity, and pH were all maintained at 28 ± 1°C, 20 PSU, and 8.1, respectively, and the tank received a continuous O_2 supply. The fish were fed finely chopped fresh prawn meat and commercial feed regularly during the conditioning phase. Prior to the start of the exposure, the average individual weight of 180 fries and 180 fingerlings was recorded and randomly distributed into 9 rectangular glass aquaria (3 tanks for each exposure group) with a culture volume of 50 L and a stocking density of 20 fish per tank. However, the total number of fish used per time point per experimental group was 18 (six fish per tank and triplicate maintained for each tank). Similarly, the experimental setup for fingerling was also followed.

The effects of OA were investigated by lowering the pH of seawater and subjecting various size groups of fish to three distinct pH conditions: control pH of 8.1 and two lower pH levels expected under different climate change scenarios (pH 7.7 and pH 7.4). In a brief, lower pH was achieved by bubbling CO_2-enriched air at the proper CO_2 content. Using a dual variable area flow controller, the CO_2 concentration in the bubbled air was regulated and the pH in the experimental tank was monitored regularly. The fish were fed fresh prawn flesh throughout the experiment. To reduce fluctuation, the temperature and salinity were maintained and measured daily with a probe (Hydrolab Quanta Multi-Probe Meter) and the pH of seawater was recorded thrice a day using a well calibrated pH meter (Wensar pH Meter, LMPH-with ± 0.01 pH).

At 20, 40, and 60 d, healthy fish of two different stages (fry and fingerling) were sampled. At each time, 18 fish were dissected per group (6 individuals per tank). Fish were anesthetized for 30 seconds in ice-cold aquarium water, then removed and measured for body length and weight. The fish was kept calm by gently wrapping it in a paper towel soaked in ice-cold aquarium water. The tail was cut 1–2 mm rostral to the caudal fin. To prevent clotting, blood was drawn from the cut end with a micropipette fitted with heparinized tips and immediately diluted with Tris EDTA buffer. Blood samples from three fish in the same tank were pooled as one replicate for fish fry and fingerlings (i.e., total sample number = 6 per group at time point). An aliquot of pooled samples were frozen in liquid nitrogen and kept at -80°C until further processing for biochemical component analysis. The above-mentioned animal handling procedures were approved by the Animal Ethics Committee of the University of Madras.

Using a Neubauer haemocytometer, the red blood cell (RBC) and white blood cell (WBC) counts were measured after dilution with Grower's and Dacie's solutions, respectively (Voigt, 2000). The haemoglobin (Hb) content was measured using the photometrical cyanohaemoglobin technique. Standard formulae given below were used to compute haematocrit (HCT), mean cellular volume (MCV), mean cell haemoglobin (MCH), and mean cellular haemoglobin concentration (MCHC) (Kang et al., 2005).

$$\mathrm{MCV\ (fl)} = \mathrm{HCT\ (\%)/RBC\ \left(million/mm^3\right)} \times 10$$

$$\mathrm{MCH\ (pg)} = \mathrm{Hb\ (g/dl)/RBC} \times 10\ \left(\mathrm{million/mm^3}\right)$$

$$\mathrm{MCHC\ (\%)} = \mathrm{Hb\ (g/dl)/HCT\ (\%)} \times 100$$

The oxygen carrying capacity was estimated by multiplying the haemoglobin concentration by 1.25 oxygen combining the power of Hb/g (Johansen, 1970; Sampath et al., 1998). Total protein content in blood serum was determined using the Bradford (1976) method, which used bovine serum albumin as a reference. The assay Kit measured albumin, globulin, and the albumin: globulin (A/G) ratio (divided albumin content by

globulin content) (Biuret method using dye reagent, Qualigens Fine Chemicals, Mumbai, India).

The average survival, length and weight gain of the fishes during the experiment was estimated by the following formulae:
Survival (%) = Number of fish survived after 60 d/initial number of fish stocked × 100.
Weight gain (%) = Average (Final weight (g) - initial weight (g)/ initial weight (g) × 100.
Length gain (%) = Average (Final length- initial length / initial length) × 100.

The statistical analysis was carried out using SPSS software (version 20). The data was subjected to normality and homogeneity before a two way analysis of variance (ANOVA) to test differences between the groups.Tukey's multiple comparison *post hoc* tests were used to determine the statistical difference between different treatment groups and the p-value of less than 0.05 was considered significant.

DATA DESCRIPTION

Physicochemical parameters of the seawater such as temperature (°C), salinity (PSU), pH, total alkalinity (μmol kg^{-1}), dissolved inogranic carbon (μmol kg^{-1}), turbidity (NTU), specific conductivity (mS), and pressure (pCO_2; μatm) are given in **Supplementary Table 1A**. Physicochemical parameters during the exposure period did not differ significantly ($p > 0.05$) between the exposure groups. **Table 1** shows the changes in haematological parameters such as red blood cell (10^6/μL), white blood cell (10^3/μL) and Hb (g/dl) level, HCT, MCV, MCH, MCHC, O_2 carrying capacity of sea bass fry and fingerling exposed to different pH groups. Between the control and experimental groups, the mean values for most of blood parameters showed significant differences ($p < 0.05$). In both fry and fingerling, WBCs, RBCs, Hb, HCT and O_2 carrying carpacity showed a pH-dependent decline, but MCV and MCHC increased considerably in both fry and fingerlings. However, MCV in fish fry reduced significantly after 60 d of exposure at pH 7.4. MCH values decreased considerably in all the exposure period when the fish fry were exposed to pH 7.4. On the contrary, fish fingerlings exposed to OA do not show any significant differences in MCH values with the respective control groups except after 60 d exposure at pH 7.4, it is clear that extended exposure to OA caused considerable alterations in fingerlings, signalling that fry may be more susceptible than fingerlings to OA.

Fish fry and fingerling exposed to acidified seawater showed decreased oxygen carrying capacity, which could result in poor oxygen transport to organs. The fall in Hb concentration could be reason for a reduction in oxygen transport to the tissues, resulting in a reduction in physical activity (Nussey et al., 1995). Similar findings have been reported earlier, wherein the oxygen carrying capacity of *Heteropneustes fossilis* blood decreased due to a decrease in RBC count and Hb concentration (James and Sampath, 1995).

In the present study the total RBC count in both fry and fingerlings exposed to different pH conditions (8.1, 7.7 and 7.4) reduced considerably and such reduction in RBC count may be due to blood cell disruption, i.e. haemolysis (**Table 1**), which was reflected in changes in red blood indices such as Hb, HCT, PCV, MCV, MCH, and MCHC (**Table 1**) and these variations in RBC could lead to abnormalities in the composition of blood and its functions. Moreover increased MCH and MCHC readings in sea bass blood correspond to fluctuations in erythrocyte count caused by red blood cell breakdown and reduced Hb content in each cell (Sakthivel and Sampath, 1990). The results of RBC indices are also considered and used to differentiate distinct kinds and the cause of anaemia (Whalan, 2015). MCV and MCH levels may rise in response to structural damage to RBC membranes when the acidity level rises and could results in hemolysis, impaired haemoglobin production, and red blood cell enlargement (Fletcher, 1975; Schafhauser-Smith and Benfey, 2003). The elevations in MCV and MCH, together with the lack of change in MCHC, showed that the anaemia was of the macrocytic type (Ates et al., 2008). The MCHC value is used to assess the degree and aetiology of anaemia, as well as to identify differences in erythrocyte size, shape, and Hb concentration (Grant, 2015). The MCHC level in both fry and fingerling seabass subjected to acidified conditions decreased significantly after 60 d of exposure at pH 7.4, while there were no significant changes in the fingerlings exposed to pH 7.7 compared to the control groups. **Figures 1A–D** shows the biochemical characteristics of seabass fry and fingerlings, including total protein (g/ml), albumin (g/ml), globulin (g/ml), and albumin/globulin (A/G) ratio. When seabass fry and fingerlings were exposed to acidified seawater, the total protein, albumin, and globulin concentration in their blood decreased drastically. Albumin content in fish fingerling significantly decreased in both exposure group after 40 d, however in fish fry the same decreased only when the fry were exposed to pH 7.4. On the contrary, globulin content in fish fry reduced significantly in both exposure groups and the same reduced in fish fingerling only when the fish were exposed to pH 7.4. Overall these data suggests that the fry were under stress than the fingerling. Intriguingly, the albumin and globulin ratios in fingerlings and fry did not show any significant decrease throughout the 40-day exposure period.

The total protein level was thought to indicate the health condition of fish, which may directly be related with growth (Gopal et al., 1997). We discovered a decrease in total protein, albumin, globulin, and a change in the albumin to globulin ratio throughout our experimental periods. Marine pollution and/or stress exposure has been shown to cause changes in blood protein levels, which indirectly effect the physiological process of fish (Kroeker et al., 2010; Harvey et al., 2013).

Supplementary Table 1B displays statistics on fish survival and variations in length weight measurement in proportion to the initial values of fish fry and fingerlings, respectively. The percentage increase in length compared to initial values in seabass fry grown in the control treatment (pH 8.1) was 83.51%, however, growth was slowed when the fry were reared in acidified

TABLE 1 | Data of haematological parameters of Asian sea bass *Lates calcarifer* fry and fingerlings exposed to different pH for 60 d.

Parameters		20 d			40 d			60 d	
Fish fry	**Control (pH 8.1)**	**pH 7.7**	**pH 7.4**	**Control (pH 8.1)**	**pH 7.7**	**pH 7.4**	**Control (pH 8.1)**	**pH 7.7**	**pH 7.4**
RBC	2.21±0.047^{a}	1.93±0.061^{b}	1.78±0.047^{b}	2.08±0.060^{a}	1.70±0.051^{b}	1.53±0.061^{b}	2.13±0.049^{a}	1.91±0.047^{b}	1.36±0.055^{c}
HB level (g/dL)	9.28±0.132^{a}	9.30±0.081^{a}	8.73±0.076^{b}	9.31.±0.060^{a}	8.58±0.094^{b}	7.96±0.156^{b}	9.08±0.101^{a}	8.40±0.093^{b}	7.38±0.126^{c}
HCT (%)	31.55±0.482^{a}	29.76±0.555^{a}	26.85±0.788^{b}	31.18.±0.616^{a}	28.15±0.557^{b}	25.30±0.530^{c}	32.10±0.499^{a}	27.45±0.576^{b}	21.68±0.404^{c}
MCV(fL)	140.91±2.40^{a}	149.59±7.41^{a}	153.66±3.30^{b}	154.66.±3.91^{a}	162.36±6.930^{b}	165.28±5.37^{b}	154.43±4.69^{a}	154.96±8.12^{ab}	145.58±4.70^{b}
MCH (Pg)	33.98±0.286^{a}	32.02±0.685^{a}	30.72±0.722^{b}	33.46.±0.596^{a}	32.80±0.672^{a}	30.89±0.537^{b}	35.34±0.508^{a}	32.70±0.825^{b}	29.45±0.484^{c}
MCHC(%)	29.43±0.245^{a}	31.29±0.652^{a}	32.63±0.784^{b}	29.92.±0.537^{a}	30.54±0.633^{a}	32.53±0.738^{b}	28.31±0.400^{a}	30.67±0.778^{b}	34.00±0.544^{c}
O_2 carrying Capacity	11.60±0.165^{a}	11.62±0.102^{a}	10.91±0.095^{a}	11.64.±0.075^{a}	10.72±0.118^{b}	9.95±0.195^{c}	11.35±0.126^{a}	10.50±0.116^{b}	9.20±0.160^{c}
WBC	8.18±0.132^{a}	8.08±0.094^{a}	7.43±0.076^{b}	8.01±0.060^{a}	7.28±0.094^{b}	6.66±0.156^{c}	7.78±0.101^{a}	7.10±0.093^{b}	6.06±0.128^{c}
Fingerlings									
RBC	3.11±0.047^{a}	2.61±0.007^{b}	2.36±0.047^{c}	3.13.±0.060^{a}	2.50±0.051^{b}	2.13±0.061^{c}	3.03±0.049^{a}	2.41±0.047^{b}	1.76±0.055^{c}
HB level (g/dL)	10.18±0.132^{a}	10.36±0.049^{ab}	9.98±0.101^{b}	9.98.±0.094^{a}	9.38±0.094^{b}	8.90±0.093^{c}	9.66±0.186^{a}	8.56±0.156^{b}	7.76±0.128^{c}
HCT (%)	32.43±0.442^{a}	32.21±0.602^{a}	32.96±0.517^{a}	31.95.±0.665^{a}	29.03±0.567^{b}	27.95±0.576^{b}	30.88±0.820^{a}	26.03±0.546^{b}	22.08±0.404^{c}
MCV (fL)	101.68±1.430^{a}	117.52±4.83^{b}	132.23±5.34^{b}	106.10.±3.35^{a}	113.88±3.99^{a}	127.45±6.59^{b}	107.53±3.99^{a}	105.70±3.72^{a}	120.88±5.97^{b}
MCH (Pg)	31.85±0.249^{a}	31.07±0.571^{a}	33.02±0.466^{a}	32.02.±0.749^{a}	30.95±0.620^{a}	31.42±0.771^{a}	31.95±0.726^{a}	30.42±0.716^{a}	28.44±0.453^{b}
MCHC (%)	31.40±0.243^{a}	32.23±0.596^{a}	30.30±0.420^{a}	31.31.±0.731^{a}	32.37±0.659^{a}	31.91±0.788^{a}	31.36±0.685^{a}	32.96±0.785^{a}	35.19±0.546^{b}
O_2 carrying Capacity	12.72±0.165^{a}	12.95±0.618^{a}	12.47±0.126^{a}	12.46.±0.118^{a}	11.72±0.113^{b}	11.12±0.116^{b}	12.08±0.225^{a}	10.70±0.195^{b}	9.70±0.160^{b}
WBC	8.58±0.132^{a}	8.48±0.094^{a}	7.83±0.076^{b}	8.36.±0.055^{a}	7.63±0.080^{b}	7.10±0.134^{c}	8.38±0.101^{a}	7.53±0.098^{b}	6.38±0.119^{c}

Values are expressed as mean± SD of 6 observations. The same letters (a, b, c) indicate no significant difference between exposure groups at different exposure periods, whereas different letters indicate statistically significant differences ($p < 0.05$) between different exposure periods and groups. RBC and WBC expressed ($x10^6$ and10^6 cells/μL respectively) and O_2 carrying Capacity expressed in ($ml O_2\ g^{-1} Hb$).

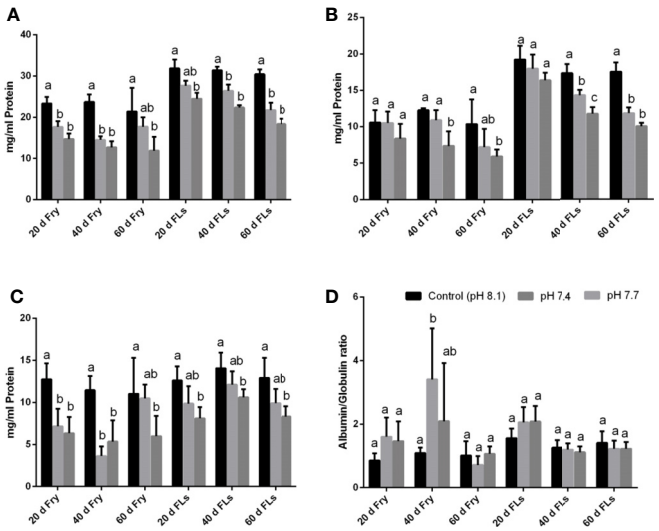


FIGURE 1 | **(A–D)** is the data representing the biochemical components such as **(A)** total protein (mg/ml), **(B)** albumin (mg/ml), **(C)** globulin (mg/ml), **(D)** albumin and globulin (A/G) ratio of seabass fry and fingerling exposed for 60 d under different acidified conditions. Each bar represents mean ± standard deviation of six samples. Two-way analysis of variance followed by Tukey's *post hoc* test was used. The same letters (a, b, c) indicate no significant difference between the exposure groups whereas different letters indicate statistically significant differences ($p < 0.05$) between different groups.

seawater with pH 7.7 and 7.4. In pH 7.7 and 7.4, the increase in length was 62.29% and 41.62%, respectively. Similarly, seabass fingerlings exposed to two acidic seawater environments developed substantially slower than the control groups. The weight of fry after 60 d was 5.91 0.36 g, a rise of 112% over the original weight; however, at pH 7.7 and 7.4, this was reduced to 83.45% and 73.66%, respectively. Fingerlings followed a similar trend. These findings clearly show that acidified seawater has a deleterious impact on fish (fry and fingerlings) growth.

To conclude, this is the first study to our knowledge to look at the impact of OA on the haematological and biochemical parameters in two different size groups of *L. calcarifer*. In both groups, OA causes changes in haematological and biochemical components, according to the findings of this study. The current study also revealed that OA had an effect on physiological processes (growth rate), with the effect being stage-specific and pH dependent. We propose that fish haematological and serum biochemical research have become more important as a result of the increased emphasis on fish farming and rising level of pollution in coastal and marine ecosystems. Its effect on fish growth might aid in the development of a long-term management plan to mitigate ocean acidification.

DATA AVAILABILITY STATEMENT

The datasets presented in this study can be found in online repositories. The names of the repository/repositories and accession number(s) can be found in the article/**Supplementary Material**.

ETHICS STATEMENT

Since culture commercial fish were used, ethical review and approval not required.

AUTHOR CONTRIBUTIONS

GS, PS, PP, RS, and PM: sample collection, laboratory analysis, data processing, TH: data validation and manuscript preparation. SB: Review the manuscript, suggestion, and project administration. All authors contributed to the article and approved the submitted version.

ACKNOWLEDGMENTS

The authors thank the Head, of the Research Department of Zoology and also the Principal Pachaiyappa's College for Men, Chennai- 600 030 for extending their support through the experiment.

SUPPLEMENTARY MATERIAL

The Supplementary Material for this article can be found online at: https://www.frontiersin.org/articles/10.3389/fmars.2022.940573/full#supplementary-material

REFERENCES

Ates, B., Orun, I., Talas, Z. S., Durmaz, G., and Yilmaz, I. (2008). Effects of Sodium Selenite on Some Biochemical and Hematological Parameters of Rainbow Trout (*Oncorhynchus Mykiss* Walbaum 1792) Exposed to Pb2+ and Cu2+. *Fish. Physiol. Biochem.* 34, 53–59. doi: 10.1007/s10695-007-9146-5

Bonk, A. A. (2005). "Influence of the Conditions of Reproduction on the Survival of Herring Embryos in the Western Bering Sea," in *PICES 14th Annual Meeting*, 181 pp.

Bradford, M. M. (1976). A Rapid and Sensitive Method for the Quantitation of Microgram Quantities of Protein Utilizing the Principle of Protein-Dye Binding. *Anal. Biochem.* 72, 248–254. doi: 10.1016/0003-2697(76)90527-3

Checkley, D., Jürgen, A., Oozeki, Y., and Roy, C. (Eds.). (2009). *Climate Change and Small Pelagic Fish*. Cambridge: Cambridge University Press. doi: 10.1017/CBO9780511596681

Dogan, D., and Can, C. (2011). Hematological, Biochemical, and Behavioral Responses of *Oncorhynchus Mykiss* to Dimethoate. *Fish. Physiol. Biochem.* 37 (4), 951–958. doi: 10.1007/s10695-011-9492-1

Dupont, S., Lundve, B., and Thorndyke, M. (2010). Near Future Ocean Acidification Increases Growth Rate of the Lecithotrophic Larvae and Juveniles of the Sea Star Crossaster Papposus. *J. Exp. Zool. (Mol. Dev. Evol.)* 314B, 382–389. doi: 10.1002/jez.b.21342

Dupont, S., and Thorndyke, M. C. (2009). Impact of CO2-Driven Ocean Acidification on Invertebrates Early Life-History What We Know, What We Need to Know and What We can do. *Biogeosciences* 6, 3109–3131. doi: 10.5194/bgd-6-3109-2009

Ellis, R. P., Bersey, J., Rundle, S. D., Hall-Spencer, J. M., and Spicer, J. (2009). I.: Subtle But Significant Effects of CO_2 Acidified Seawater on Embryos of the Intertidal Snail, *Littorina Obtusata*. *Aquat. Biol.* 5, 41–48. doi: 10.3354/ab00118

Fabry, V. J., Seibel, B. A., Feely, R. A., and Orr, J. C. (2008). Impacts of Ocean Acidification on Marine Fauna and Ecosystem Processes. *ICES. J. Mar. Sci.* 65, 414–432. doi: 10.1093/icesjms/fsn048

Feely, R. A., Sabine, C. L., Lee, K., Berelson, W., Kleypas, J., Fabry, V. J., et al (2004). Impact of Anthropogenic CO_2 on the $CaCO_3$ System in the Oceans. *Science* 5682, 362–66. doi: 10.1126/science.1097329

Fletcher, G. (1975). The Effects of Capture," Stress," and Storage of Whole Blood on the Red Blood Cells, Plasma Proteins, Glucose, and Electrolytes of the Winter Flounder (*Pseudopleuronectes Americanus*). *Can. J. Zool.* 53, 197–206. doi: 10.1139/z75-024

Galloway, T., and Handy, R. (2003). Immunotoxicity of Organophosphorous Pesticides. *Ecotoxicology* 12, 345–363. doi: 10.1023/A:1022579416322

Gattuso, J. P., Bijma, J., Gehlen, M., Riebesell, U., and Turley, C. (2011). *Ocean Acidification: Knowns, Unknowns and Perspectives*. doi: 10.1093/oso/9780199591091.003.0020

Gopal, V., Parvathy, S., and Balasubramanian, P. R. (1997). Effect of Heavy Metals on the Blood Protein Biochemistry of the Fish *Cyprinus Carpio* and its Use as a Bio-Indicator of Pollution Stress Environ. *Monit. Ass.* 48, 117–124. doi: 10.1023/A:1005767517819

Grant, K. R. (2015). Fish Hematology and Associated Disorders. *Vet. Clin. North Am. Exot. Anim. Prac.* 18, 83–103. doi: 10.1016/j.cll.2015.05.015

Harvey, B. P., Gwynn-Jones, D., and Moore, P. J. (2013). Meta-Analysis Reveals Complex Marine Biological Responses to the Interactive Effects of Ocean Acidification and Warming. *Ecol. Evol.* 3, 1016–1030. doi: 10.1002/ece3.516

Havenhand, J. N., Buttler, F. R., Thorndyke, M. C., and Williamson, J. E. (2008). Near-Future Levels of Ocean Acidification Reduce Fertilization Success in a Sea Urchin. *Curr. Biol.* 18, R651–R652. doi: 10.1016/j.cub.2008.06.015

James, R., and Sampath, K. (1995). Sublethal Effects of Mixtures of Copper and Ammonia on Selected Biochemical and Physiological Parameters in the Catfish, *Heteropneustes Fossiilis* (Bloch). *Bull. Environ. Contaminat. Toxicol.* 55, 187–194.

Johansen, K. (1970). "Air-Breathing Fishes," in *Fish Physiology*, vol. Vol. IV . Eds. W. S. Hoar and D. J. Randall (New York and London: Academic Press), 361–411.

Kang, J. C., Kim, S. G., and Jang, S. W. (2005). Growth and Hematological Changes of Rockfish, *Sebastes Schlegeli* (Hilgendorf) Exposed to Dietary Cu and Cd. *J. World Aquacul. Soc.* 36, 188–195. doi: 10.1111/j.1749-7345.2005.tb00384.x

Key, R. M., Kozyr, A., Sabine, C. L., Lee, K., Wanninkhof, R., Bullister, J. L., et al. (2004). A Global Ocean Carbon Climatology: Results From Global Data Analysis Project (GLODAP). Global Biogeochem. *Cycles* 18 (4). doi: 10.1029/2004GB002247

Kikkawa, T., Ishimatsu, A., and Kita, J. (2003). Acute CO_2 Tolerance During the Early Developmental Stages of Four Marine Teleosts, Environ. *Toxicol* 18, 375–382.

Kroeker, K. J., Kordas, R. L., Crim, R. N., and Singh, G. G. (2010). Meta-Analysis Reveals Negative Yetvariable Effects of Ocean Acidification on Marine Organisms. *Ecol. Lett.* 13, 1419–1434. doi: 10.1111/j.1461-0248.2010.01518.x

Kumar, T. S., Vijayakumaran, M., Murugan, T. S., Jha, D. K., Sreeraj, G., and Muthukumar, S. (2009). Captive Breeding and Larval Development of the Scyllarine Lobster Petrarctusrugosus. *New Z. J. Mar. Freshw. Res.* 43:1, 101–112. doi: 10.1080/00288330909509985

Kurihara, H., Shimode, S., and Shirayama, Y. (2004). Effects of Raised CO_2 Concentration on the Egg Production Rate and Early Development of Two Marine Copepods (*Acartia Steueri* and *Acartia Erythraea*). *Mar. Poll. Bull.* 49, 721–727. doi: 10.1016/j.marpolbul.2004.05.005

Martinez, C. B. R., and Souza, M. M. (2002). Acute Effects of Nitrite on Ion Regulation in Two Neotropical Fish Species, Comparative Biochemistry and Physiology Part a. *Mol. Integr. Physiol.* 133, 1, 151–160. doi: 10.1016/S1095-6433(02)00144-7

Melzner, F., Thomsen, J., Koeve, W., Oschlies, A., Gutowska, M. A., Bange, H. W., et al. (2012). Future Ocean Acidification Will be Amplified by Hypoxia in Coastal Habitats. *Mar. Biol.* 160, 1875–1888. doi: 10.1007/s00227-012-1954-1

Munday, P. L., Cheal, A. J., Dixson, D. L., Rummer, J. L., and Fabricius, K. E. (2014). Behavioural Impairment in Reef Fishes Caused by Ocean Acidification at CO_2 Seeps. *Nat. Clim. Change* 4, 487–492. doi: 10.1038/nclimate2195

Munday, P. L., Dixson, D. L., Donelson, J. M., Jones, G. P., Pratchett, M. S., Devitsina, G. V., et al. (2009). Ocean Acidification Impairs Olfactory Discrimination and Homing Ability of a Marine Fish. *Proc. Natl. Acad. Sci. U S A* 106, 1848–1852. doi: 10.1073/pnas.0809996106

Murugan, T. S., Remany, M. C., Mary Leema, T., Jha, D. K., Santhanakumar, J., Vijayakumaran, M., et al. (2005). Growth, Repetitive Breeding, and Aquaculture Potential of the Spiny Lobster, *Panulirus Ornatus*. *New Z. J. Mar. Freshw.* 39:2, 311–315. doi: 10.1080/00288330.2005.9517311

Narra, M. R. (2017). Haematological and Immune Upshots in Clarias Batrachus Exposed to Dimethoate and Defying Response of Dietary Ascorbic Acid. *Chemosphere* 168, 988–995. doi: 10.1016/j.chemosphere.2016.10.112

Nussey, G., Van Vuren, J. H. J., and Du Preez, H. H. (1995). Effects of Copper on Haematology and Osmoregulation of the Mozambique Tilapia, *Oreochromis Mossambicus* (Cichlidae). *Comp. Biochem. Physiol.* 111, 369–380. doi: 10.1016/0742-8413(95)00063-1

Panchang, R., and Ambokar, M. (2021). Ocean Acidification in the Northern Indian Ocean : A Review. *J. Asian Earth Sci.* 219, 104904. doi: 10.1016/j.jseaes.2021.104904

Pörtner, H. O. (2008). Ecosystem Effects of Ocean Acidification in Times of Ocean Warming: A Physiologist's View. *Mar. Ecol. Prog. Ser.* 373, 203–217. doi: 10.3354/meps07768

Rhein, M., Rintoul, S. R., Aoki, S., Campos, E., Chambers, D., Feely, R. A., et al. (2013). "Observations: Ocean," in *Climate Change 2013: The Physical Science Basis*. Eds. T. F. Stocker, D. Qin, G.-K. Plattner, M. Tignor, S. K. Allen, J. Boschung, A. Nauels, Y. Xia, V. Bex and P. M. Midgley (Cambridge, United Kingdom and New York, NY, USA: Cambridge University Press).

Sabine, C. L., Feely., R. A., Gruber, N, Key, R. M., Lee, K., Bullister, J. L., et al (2004). The Oceanic Sink for Anthropogenic CO_2. *Science* 305 (5682), 367–71. doi: 10.1126/science.1097403

Sakthivel, M., and Sampath, K. (1990). "Respiration, Blood Cells and Food Conversion Efficiency in Cyprinus Carpio Exposed to Sublethal Concentrations of Tannery Effluents," in *Environment and Experimental Toxicology*. Eds. P. B. Deshmukh, A. T. Mathai, R. C. Dalela and K. S. Pillai (Valvada: Jai Research Foundation), 139–I50.

Sampath, K., James, R., and Akbar Ali, K. M. (1998). Effects of Copper and Zinc on Blood Parameters and Prediction of Their Recovery in *Oreochromis Mossambicus* (Pisces: Cichlidae). *Indian JFisheries* 45 (2), 129–139.

Schafhauser-Smith, D., and Benfey, T. (2003). The Effects of Long-Term Estradiol-17β Treatment on the Growth and Physiology of Female Triploid Brook Trout (Salvelinus Fontinalis). *Gen. Comp. Endocrinol.* 131, 9–20. doi: 10.1016/S0016-6480(02)00626-3

Thilagam, H., Gopalakrishnan, S., Bo, J., and Wang, K. J. (2009). Effect of 17 β-Estradiol on the Immunocompetence of Japanese Sea Bass (*Lateolabrax Japonicus*). *Environ. Toxicol. Chem.* 28, 1722–1731. doi: 10.1897/08-642.1

Vijayakumaran, M., Murugan, T. S., Remany, M. C., Mary Leema, T., Jha, D. K., Santhanakumar, J., et al. (2005). Captive Breeding of the Spiny Lobster, *Panulirus Homarus*. *New Z. J. Mar. Freshw. Res.* 39:2, 325–334. doi: 10.1080/00288330.2005.9517313

Voigt, L. (2000). *Hematology Techniques and Concepts for Veterinary Technicians* (Ames: Iowa State University Press), 139.

Whalan, J. E. (2015). *A Toxicologist's Guide to Clinical Pathology in Animals: Hematology, Clinical Chemistry, Urinalysis* (Cham (CH: Springer International).

Conflict of Interest: The authors declare that the research was conducted in the absence of any commercial or financial relationships that could be construed as a potential conflict of interest.

Publisher's Note: All claims expressed in this article are solely those of the authors and do not necessarily represent those of their affiliated organizations, or those of the publisher, the editors and the reviewers. Any product that may be evaluated in this article, or claim that may be made by its manufacturer, is not guaranteed or endorsed by the publisher.

Copyright © 2022 Srinivasan, Marcus, Sivakumar, Paramasivam, Sivakumar, Harikrishnan and Balasubramaniam. This is an open-access article distributed under the terms of the Creative Commons Attribution License (CC BY). The use, distribution or reproduction in other forums is permitted, provided the original author(s) and the copyright owner(s) are credited and that the original publication in this journal is cited, in accordance with accepted academic practice. No use, distribution or reproduction is permitted which does not comply with these terms.

frontiers | Frontiers in Marine Science

DATA REPORT
published: 13 July 2022
doi: 10.3389/fmars.2022.914240

Coral Reef Health Status *versus* Muricid Bioindicator in the Lakshadweep Archipelago – A Multivariate Approach

Nithyanandam Marimuthu[1*], *James Jerald Wilson*[2], *Abdulmohsin A. Al-Sofyani*[3] *and Arumugam Kuppuswamy Kumaraguru*[4]

[1] Zoological Survey of India, Ministry of Environment, Forest and Climate Change, Government of India, Kolkata, India, [2] Department of Marine and Coastal Studies, Madurai Kamaraj University, Madurai, India, [3] Faculty of Marine Sciences, King Abdulaziz University, Jeddah, Saudi Arabia, [4] Noorul Islam Centre for Higher Education, Kumaracoil, Thuckalay, Kanniyakumari, India

OPEN ACCESS

Edited by:
Dilip Kumar Jha, National Institute of Ocean Technology, India

Reviewed by:
Pankaj Verma, National Institute of Ocean Technology, India
Gopalakrishnan Thilagam, Pachaiyappa's College for Men, India

***Correspondence:**
Nithyanandam Marimuthu
marimuthu@zsi.gov.in

Specialty section:
This article was submitted to Marine Pollution, a section of the journal Frontiers in Marine Science

Received: *06 April 2022*
Accepted: *06 June 2022*
Published: *13 July 2022*

Citation:
Marimuthu N, Wilson JJ, Al-Sofyani AA and Kumaraguru AK (2022) Coral Reef Health Status versus Muricid Bioindicator in the Lakshadweep Archipelago – A Multivariate Approach. Front. Mar. Sci. 9:914240. doi: 10.3389/fmars.2022.914240

Keywords: corals, coral reef, corallivorous snail, *Drupella cornus*, biological indicator, multivariate analyses

INTRODUCTION

Island ecosystems possess pristine environmental characteristics; human influence poses a serious threat to the fragile and susceptible biological processes on the islands (Sahu et al., 2013; Jha et al., 2015). Isolated oceanic islands support a highly sensitive and fragile coral reef ecosystem that offers unique possibilities to study the ecological changes and consequences that come with human settlement (Jha et al., 2011; Connor et al., 2012; Jha et al., 2013). Coral reefs are vital and core economic assets for any country that lies in the tropical and sub-tropical marine environment. Globally, the estimated economic support from this habitat has been calculated to be $375 billion per year (Cesar and Beukering, 2004; Brander et al., 2007). The important ecological services provided by these coral reef habitats have been identified as fish production, control of soil erosion on land, carbon sequestration, breeding grounds, etc. The coral reefs of Lakshadweep Islands are predominantly occupied by Scleractinian corals at various levels of the benthic substrate such as reef flat lagoon, reef crest, and reef slope. They are under great threat due to natural disturbances (Kumaraguru et al., 2005; Wilson et al., 2005) as well as anthropogenic disturbances (Wilson, 2010). The assessment of the biological indicators of benthic reef habitat is a key factor that helps in understanding the health status of any coral reef ecosystem (Al-Sofyani et al., 2014). The Crown-of-thorns Starfish (*Acanthaster planci* Linnaeus, 1758) is a major coral predator reported from various coral reef ecosystems. Their devastating population outbreaks have posed a great threat to coral reefs of the Indo-Pacific coastal region in the last five decades (Birkeland and Lukas, 1990; Fabricius et al., 2010). Besides the Crown-of-thorns Starfish, zooxanthellae-consuming gastropods are also reported as indicators for assessing the health status of corals in the Red Sea reef ecosystem (Mohamed et al., 2012; Al-Sofyani et al., 2014). Various studies on *Drupella cornus* Röding 1798 from its original combination (Röding 1798) to the corallivorous capability on Scleractinian corals of various coastal environments were presented through a timeline series (**Supplementary Figure 1**). The present study aims to interpret the impact of this indicator species and the relationship of physicochemical variables on the coral species cover along the Lakshadweep Archipelago by using the multivariate analytic tool.

MATERIALS AND METHODS

Study Area and Sample Collection

From Minicoy Island in the south to Chetlet Island in the north, 42 locations (**Figure 1**) were chosen to assess the diversity of coral communities and the impact of *Drupella cornus* on these reef habitats in the Lakshadweep group of Islands. Sessile benthic communities were studied using the line intercept transect method (English et al., 1997) during the post-monsoon Season (December-February) between 2015 and 2020. Five replicates of a 50-m long flexible underwater tape were laid on the reefs at a depth of (1) 10m on the reef slope and, (2) 3m on the reef flat, nearly parallel to the shore. Video transects were also taken for further analysis and the benthos present under the transition points were recorded using international codes (English et al., 1997; Al-Sofyani et al., 2014; Ravindran et al., 2014). In the distinct community structure of the reef habitat of Lakshadweep Islands, live coral species cover was recorded in all the selected study sites. The scleractinian fauna was identified up to the generic level from the video transects and verified (Veron, 2000). The abundance of *Drupella cornus* assembled with the coral colonies below the transect line was estimated manually and documented during the monitoring period. Voucher specimens collected from Minicoy Island (latitude 8.317794°N and longitude 73.031218°E), Lakshadweep Island, were deposited (M-29888/7) in the National Zoological Collection of the Zoological Survey of India (ZSI), Kolkata, India. To check the influence of physicochemical variables on the coral species cover, the data on Sea surface temperature (SST), salinity, chlorophyll-*a*, and total suspended matter (TSM) were collected from the Indian National Centre for Ocean Information Services (INCOIS) live access portal. The pH variable was assessed *in-situ* by using Oakton PCS Testr 35 waterproof tester.

Data Analysis

Benthic raw data was sorted and assessed using the Reef Monitoring Data Entry System of AIMS (ARMDES V1.6 Data Entry Program – Long-term reef monitoring project, Australian Institute of Marine Sciences) (ARMDES, 1996). The percentage cover of live coral and Seaweed cover were taken for this study to assess the live coral index, corresponding to the study sites (Murdoch and Murdoch, 2016) by categorizing them into four different classes viz., (1) Excellent (≥40% of live corals), (2) Good (20-39.9%), (3) Fair (10-19.9%) and (4) Poor or Bad (0-9.9%). Principal component analysis (PCA) and Shade plot with Bray-curtis cluster analysis were carried out using PRIMER software (Version 7.0.5) (Clarke and Gorley, 2015) for identifying preferred coral species by *Drupella cornus* and its similarity matrix in different islands. Redundancy analysis (RDA) (Leps and Smilauer, 2003) was also carried out for identifying the correlation between environmental [SST, salinity, chlorophyll-*a*, and TSM] and biological variables using CANOCO 4.5.

RESULTS

The live coral index is presented in **Figure 1**. The coral index of the lagoon portion of Chetlet, Kadamat, and Minicoy Islands was "Excellent". The coral index was between "Fair" and "Poor" in the reef slope region of all the selected Islands. However, in the case of Minicoy Island, three out of five selected study sites of the reef slope region showed an "excellent" coral index. During this extensive reef monitoring of the different Islands of Lakshadweep Archipelago in connection with the health of the reef ecosystem, localized bleaching on the branching form of corals mediated by the corallivorous snail *Drupella cornus* was observed (**Figure 1A**). This impact was significant on the species, *Pocillopora verrucosa*. **Supplementary Figure 2** shows the impact of the assemblage

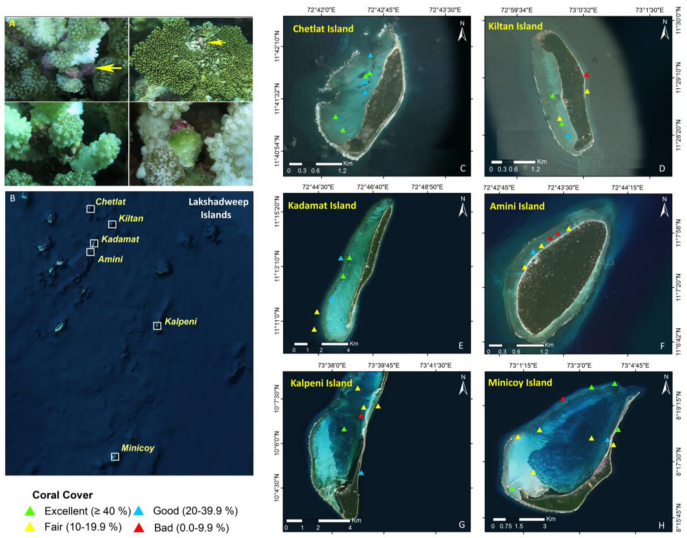


FIGURE 1 | Map showing the study sites. **(A)** *Drupella cornus* on the coral; **(B)** Lakshadweep Archipelago; **(C–H)** Islands of Lakshadweep Archipelago

of corallivorous *Drupella* on *Pocillopora verrucosa* as compared to *Acropora* sp. Based on the coefficient of determination value ($R^2 = 0.844$), it was found that 84% of the variance in the dependant variable (i.e. Abundance of *Drupella cornus*) is explained by the derived regression equation (y = 1.6927x + 1.576). A positive correlation between *Drupella cornus* and *Pocillopora verrucosa* abundance was observed from the collected data (**Supplementary Figure 2C**). Moreover, the assemblage of this species was also high in the offshore environment rather than in the lagoon region. *Drupella cornus* abundance contributed more to the coral *Pocillopora verrucosa* than to other corals, according to the PCA. In this assessment, a strong variability (PC1: 62.9% variance) was observed between a group of Islands based on the assemblage of *Drupella cornus* (**Figure 2A**). The most influencing variable as a negative biological indicator was the impact of *Drupella cornus* on *Pocillopora verrucosa* and *Acropora* sp. in the reef slope region. Chetlet Island is separated from all the other Islands due to the presence of only lagoon sites which resulted in the relatively low occurrence of *Drupella cornus* on *Pocillopora verrucosa*. It was also observed that there was a moderate variance (PC2: 29.6% variance) between the group of Islands, and the most influencing variable was the impact of *Drupella cornus* on *Pocillopora verrucosa* followed by *Acropora* sp.

Bray-curtis cluster analysis under paired linkage (**Figure 2A**) was also done based on the assemblage of *Drupella cornus* on *Pocillopora verrucosa* and *Acropora* sp. Two major mixed clusters were observed with 80% similarity. Among these clusters, a cluster was formed between the sites, Minicoy and Kadamat Islands due to the occurrence of *Drupella cornus* on *Acropora* sp. even though the impact of this snail on *Pocillopora verrucosa* was very high in this site. Hence, the remaining cluster was formed due to the higher contribution and occurrence of the snail on *Pocillopora verrucosa* in the reef slope region. On the other hand, due to the lower effect observed in the lagoon region, Chetlet Island was categorized as an outlier. The intensity of the impact of *Drupella cornus* on *Pocillopora verrucosa* was observed to be higher than that on *Acropora* sp. and it was assessed by merging the cluster on the PCA plot (**Figure 2A**).

The PCA (**Supplementary Figure 3**) of coral species abundance from the reef flat to reef slope regions indicated that there was significant variability (PC1: 32.1% variance) between the lagoon and reef slope regions concerning coral species abundance. The most influencing variable on the reef slope was *Pocillopora verrucosa* whereas *Acropora* spp. and *Montipora* sp. contributed more in the lagoon part. This was interpreted as the reason behind the highest intensity of *Drupella cornus* observed on the reef slope area. Moreover, there was little variation (PC2: 19.7% variance) between the lagoon part of a cluster of Islands (Chetlet Island, Kadamat Island, and Kilthan Island) and the rest of the study sites of Lakshadweep concerning the intensity of *Montipora* sp. followed by *Heliopora* sp. It also indicated their monospecific species occurrence in the lagoon part of Chetlet Island and that there was no impact of *Drupella cornus* in this site. Shade plot merged with Bray-curtis cluster analysis (**Figure 2B**) showed the contribution of coral species richness for Islands and benthic substrate (Reef slope and Lagoon). It perfectly supports PCA that the impacted colony, *Pocillopora verrucosa* on a greater intensity in the reef slope where as *Acropora* spp. and *Montipora* sp. in the lagoonal environment. More over, there were three complete clusters formed based on the coral species diversity. One formed in the Southern region irrespective of benthic substrates with 54.56% similarity; the second formed in the middle region with 56.09% similarity; the third one formed completely on the lagoon portion of the northern and middle region with 47.37% similarity (**Figure 2B**).

In addition to the impact of indicator species, the relationship between the environmental (SST, salinity, chlorophyll-*a*, and TSM) and biological variables were also studied and presented as RDA triplots (**Figure 2C**). Arrows indicating in the same direction represent a high positive correlation between those variables, whereas variables with negative correlation are represented by arrows oriented in opposite direction. SST plays a significant negative role in live coral cover. TSM and Chlorophyll-*a* also slightly influenced the coral cover of the Lakshadweep Archipelago. The impact and assemblage of *Drupella cornus* [Offshore abundance] were positively correlated towards the reef slope region of the southern part of the Lakshadweep Archipelago followed by the middle part (Kadamat Island). Based on the coefficient of determination value, a negative correlation (r = -0.11) of the mean percentage of live coral cover with the abundance of *Drupella cornus* is observed from the collected data. There was no significant variation in pH observed between Southern (7.9 to 8.35), Northern regions (7.9 to 8.4) and central region (7.99 to 8.32) of the Lakshadweep Archipelago.

DISCUSSION

In recent years, *Drupella* has been considered a marine organism that promotes coral reef degradation. This is the first study to report the localized bleaching impact caused by *Drupella cornus* in the Lakshadweep Archipelago. Until 2009, the population of *Drupella (Drupella cornus, Drupella fragum, and Drupella rugosa*) were reported only in three major coastal regions *viz.*, Japan, northern Red Sea, and Ningaloo Reef of Western Australia (Ayling, 2000; Cumming, 2009). In addition, *D. eburnea and D. minuta* have also been recorded on the Japanese coast (Tsuchiya, 1992). Cumming (2009) also reported such assemblages of *Drupella* spp. as a normal population (density of 0-2 per m^2), but recently Koido et al. (2017) recorded its assemblage as an outbreak, by collecting 13.8 kg of *Drupella* spp. off the coast of Cape Toi, Miyazaki, Japan. Al-Sofyani et al. (2014) also reported its impact on the coral reef ecosystem of the Red Sea during their spatial assessment of different growth forms of Scleractinian and non-Scleractinian corals. Recently, the population has considerably declined after a bleaching event (Saponari et al., 2021) that happened near the reef habitat of Maldives. This impact was significant on the species, *Pocillopora verrucosa*. Globally, *Drupella* spp. has expanded its geographical range and posed a serious threat to the coral reef ecosystem worldwide.

During the present large-scale benthic reef monitoring near different Islands of the Lakshadweep Archipelago (Minicoy, Kalpeni, Kilthan, Amini, Kadamat and Chetlet Islands), while studying the health of the reef ecosystem, localized bleaching

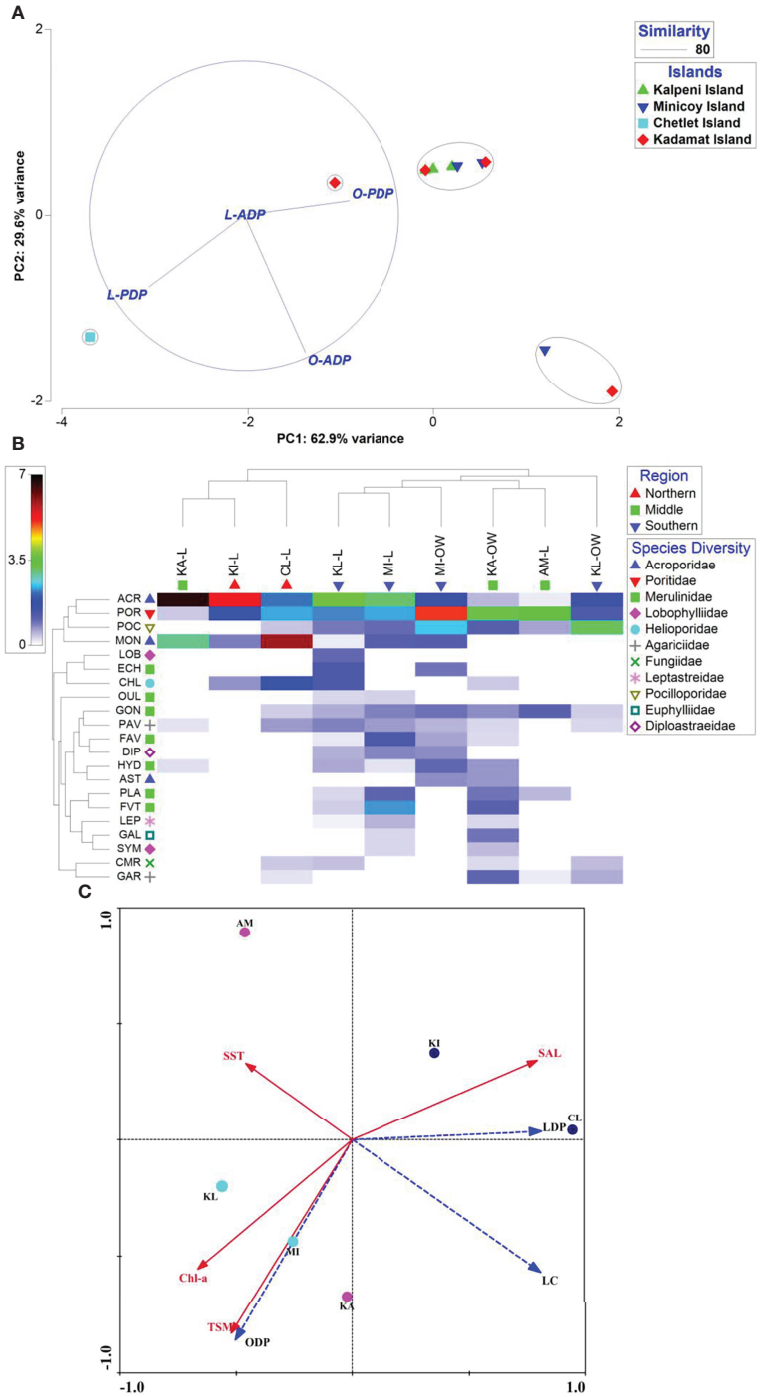


FIGURE 2 | Multivariate analyses. **(A)** PCA and Bray-curtis cluster analysis based on the abundance of *Drupella cornus* on *coral colonies. L Lagoon region; O Openwater Reef slope region; PDP Drupella cornus on Pocillopora verrucosa; ADP Drupella cornus on Acropora sp.;* **(B)** Shade plot combined with Bray-Curtis cluster analysis showing coral species occurrence with respect to the Islands. MI, Minicoy Is.; CL, Chetlet Is.; KA, Kadamat Is.; AM, Amini Is.; KL, Kalpeni Is.; OW, Openwater Reef slope region; L Lagoon region; ACR Acropora sp.; POR, *Porites* sp.; GON, *Goniastrea* sp.; PLA, *Platygyra* sp.; LOB, *Lobophyllia* sp.; OUL, *Oulophyllia* sp.; HYD, *Hydnophora* sp.; CHL, Coral *Heliopora*; PAV, *Pavona* sp.; ECH, *Echinopora* sp.; FAV, *Favia* (*Dipsastraea*) sp.; FVT, *Favites* sp.; CMR, Coral Mushroom; LEP, *Leptastrea* sp.; MON, *Montipora* sp.; DIP, *Diploastrea* sp.; POC, *Pocillopora* sp.; GAR, *Gardineroseris* sp.; GAL, *Galaxea* sp.; SYM, *Symphyllia* (*Lobophyllia*) sp.; AST, *Astreopora* sp; **(C)** Redundancy Analysis Triplot visualizing the distribution of live coral cover and *Drupella cornus* abundance in relation to various environmental variables (SST, salinity, chlorophyll-*a* and TSM). Red arrows indicate the environmental variables and blue coloured arrows represent the biological variables [live coral cover (LC), Offshore *Drupella cornus* abundance (ODP) and Lagoon *Drupella cornus* abundance (LDP)]. The circles indicates respective Islands (MI & KL, Minicoy and Kalpeni Islands of southern part of Lakshadweep; KA & AM, Kadamat and Amini Islands of middle part; CL & KI, Chetlet and Kilthan Islands of Lakshadweep Archipelago).

was observed in some coral colonies that were affected by the corallivorous gastropod, *Drupella cornus*. It was observed only in the coral species *Pocillopora verrucosa*. It is inferred that the bleaching effect (Baird, 1999) in the coral colonies is due to the loss of symbiotic algae, *i.e.*, zooxanthellae, as *Drupella cornus* consume them as food. Information is lacking on the species description and the interaction of *Drupella cornus* on coral species from the Indian coastal region. Marimuthu and Tripathy (2018) reported this species for the first time as a biological indicator of the coral reef habitat of Lakshadweep Archipelago. Antonius and Riegl (1997) reported the outbreak of coral disease caused by this species. In the present study, this outbreak was observed in the reef slope area of the Lakshadweep Archipelago.

Ayling (2000) also correlated the outbreak of this indicator organism on the reef habitat with the result of the impact of various natural and anthropogenic factors. Rosenau et al. (2021) pointed out that commercial vessels are considered a potential vector for coral habitat degradation through coral tissue loss. Drupella assemblage may impact reef resilience in association with SST-induced mortality, coral diseases, pollution, and other corallivores (Saponari et al., 2021). Similarly, a redundancy analysis of the temporal data of physical parameters showed SST mediated less coral cover along the coast of Lakshadweep Islands.

Al-Horani et al. (2011) found that the branching forms such as *Acropora* sp. and *Stylophora* sp. were occupied by *Drupella cornus* during their studies on prey selection and feeding rates on corals in the Gulf of Aquaba, Red Sea. On the other hand, *Pocillopora* sp. was reported in other parts of the Red Sea coast (Al-Sofyani et al., 2014). Similarly, it was observed that *Pocillopora verrucosa* was dominantly chosen as prey by *Drupella cornus* in the Lakshadweep group of Islands. Regression analysis also confirmed that a significant positive correlation exists between the abundance of *Drupella cornus* and *Pocillopora verrucosa*. In the case of the Gulf of Mannar, the corals of Acroporidae, *Acropora muricata, A. cytherea*, and *Montipora* sp. were infested with *Drupella cornus* at Shingle Island and Vaan Island (Raj et al., 2016). Hence, it can be inferred that there is a close relationship of the *Drupella* populations between the Lakshadweep Archipelago and the Red Sea (Al-Sofyani et al., 2014) because of similar prey preferences (*Pocillopora* sp.).

CONCLUSION

The spatial variability of the abundance of negative biological indicator, *Drupella cornus* was assessed to find out their assemblage and preferred coral species in the benthic environment of Lakshadweep Archipelago. *Pocillopora verrucosa* was identified as an impacted/preferred coral species during the study period. The dataset on the coral species diversity, interpretation of the impact of *Drupella cornus*, and physical variables on the coral diversity through multivariate analyses would be helpful for marine managers to study the present status of reef habitats and indicator species of the tropical environments.

AUTHORS CONTRIBUTION

Conceived the study, survey, and multivariate analyses: NM; Ecological interpretation and review: NM, JW, and AAA; Wrote the manuscript: NM and AK. All authors contributed to the article and approved the submitted version.

DATA AVAILABILITY STATEMENT

The datasets presented in this study can be found in online repositories. The names of the repository/repositories and accession number(s) can be found in the article/**Supplementary Material**.

FUNDING

There are no known sources of funding to pay for article processing fees. The payment toward article processing fees is to be borne by the author(s) only.

ACKNOWLEDGMENTS

The authors are thankful to the Directors, Zoological Survey of India; National Centre for Sustainable Coastal Management (all under the Ministry of Environment, Forest and Climate Change, Government of India) for the materials and facilities provided to conduct this study. The authors are also thankful to the ESRI for providing the Digital Globe imagery for map preparation. NM would like to thank the Lakshadweep Administration and Department of Environment and Forests, Union Territory of Lakshadweep for the entry permit and logistic support to carry out the study.

SUPPLEMENTARY MATERIAL

The Supplementary Material for this article can be found online at: https://www.frontiersin.org/articles/10.3389/fmars.2022.914240/full#supplementary-material

REFERENCES

Al-Horani, F. A., Hamdi, M. and Al-Rousan, S. A. (2011). Prey Selection andFeeding Rates of *Drupella Cornus* (Gastropoda: Muricidae) on Corals From the Jordanian Coast of the Gulf of Aqaba, Red Sea. *Jordan. J. Biol. Sci.* 4 (4), 191–198. https://jjbs.hu.edu.jo/FILES/v4n4/Paper%20Number%201.pdf

Al-Sofyani, A. A., Marimuthu, N. and Wilson, J. J. (2014). A Rapid Assessment of Scleractinian and Non-Scleractinian Coral Growth Forms Along the Saudi Arabian Coast, Red Sea. *J. Ocean. Univ. China.* 13 (2), 243–248. doi: 10.1007/s11802-014-2308-z

Antonius, A. and Riegl, B. (1997). A Possible Link Between Coral Diseases and a Corallivorous Snail (*Drupella Cornus*) Outbreak in the Red Sea. *Atoll. Res. Bull.* 443-449, 1–9. doi: 10.5479/si.00775630.447.1

ARMDES (1996). *AIMS Reef Monitoring Data Entry System; Version 1.6 Long Term Reef Monitoring Project* (Townsville: Australian Institute of Marine Science).

Ayling, A. M. (2000). "The Effects of Drupella Spp," in *Grazing on Coral Reefs in Australia*. Available at: http://www.SeareSearch.com.au/reports/drupella/drupella.html.

Baird, A. (1999). A Large Aggregation of *Drupella Rugosa* Following the Mass Bleaching of Corals on the Great Barrier Reef. *Reef. Res.* 9 (2), 6–7.

Birkeland, C. and Lucas, J. S. (1990). *Acanthaster Planci: Major Management Problem of Coral Reefs* (Boca Raton, FL: CRC press),1990 272 p.

Brander, L. M., Beukering, P. J. H. V. and Cesar, H. S. J. (2007). The Recreational Value of Coral Reefs: A Meta-Analysis. *Ecol. Econ.* 63 (1), 209–218. doi: 10.1016/j.ecolecon.2006.11.002

Cesar, H. S. J. and Beukering, P. J. H. V. (2004). Economic Valuation of the Coral Reefs of Hawaii. *Pacific. Sci.* 58 (2), 231–242. doi: 10.1353/psc.2004.0014

Clarke, K. R. and Gorley, R. N. (2015). *PRIMER V7. PRIMER-E*. Ltd., Devon PL21 9RH, UK. http://updates.primer-e.com/primer7/manuals/User_manual_v7a.pdf

Connor, S. E., van Leeuwen, J. F., Rittenour, T. M., van der Knaap, W. O., Ammann, B. and Björck, S. (2012). The Ecological Impact of Oceanic Island Colonization—a Palaeoecological Perspective From the Azores. *J. Biogeogr.* 39, 1007–1023. doi: 10.1111/j.1365-2699.2011.02671.x

Cumming, R. L. (2009). *Population Outbreaks and Large Aggregations of Drupella on the Great Barrier Reef* (Townsville QLD: ReSearch publication No. 96. Great Barrier Reef Marine Park Authority), 26p. Available at: http://elibrary.gbrmpa.gov.au/jspui/bitstream/11017/437/1/Population-outbreaks-large-aggregations-drupella-GBR.pdf.

English, S., Wilkinson, C. and Baker, V. (1997). *Survey Manual for Tropical Marine Resource* (Townsville: Australian Institute of Marine Science), 390 p. Available at: https://www.aims.gov.au/sites/default/files/Survey%20Manual-sm01.pdf.

ESSO-INCOIS (2022) *Live Access Server*. Available at: http://las.incois.gov.in/las/UI.vm# (Accessed 02.05.2022).

Fabricius, K. E., Okaji, K. and De'ath, G. (2010). Three Lines of Evidence to Link Outbreaks of the Crown-of-Thorns Seastar, *Acanthaster Planci* to the Release of Larval Food Limitation. *Coral. Reefs.* 29, 593–605. doi: 10.1007/s00338-010-0628-z

Jha, D. K., Vinithkumar, N. V., Marimuthu, N., Baskar, B., Sahu, B. K., Das, A. K., et al. (2013). Field and GIS Based Post-Tsunami Assessment of Scleractinian Coral Cover in the Aerial Bay Group of Islands, North Andaman, India. *J. Coast. Conserv.* 17, 671–677. doi: 10.1007/s11852-013-0266-z

Jha, D. K., Vinithkumar, N. V., Sahu, B. K., Dheenan, P. S., Das, A. K., Mehmuna, B., et al. (2015). Multivariate and Geo-Spatial Approach for Seawater Quality of Chidiyatappu Bay, South Andaman Islands, India. *Mar. pollut. Bull.* 96 (1–2), 463–470. doi: 10.1016/j.marpolbul.2015.05.004

Jha, D. K., Vinithkumar, N. V., Santhanakumar, J., Nazar, A. and Kirubagaran, R. (2011). Post Tsunami Coral Reef Resource Assessment in Pongi Balu Coast, South Andaman Island. *Curr. Sci.* 100 (4), 530–534. https://www.currentscience.ac.in/Volumes/100/04/0530.pdf

Koido, T., Oku, Y., Fucuda, M., Nakano, A. and Fukami, H. (2017). *Drupella* Outbreak in a Large Coral Community Off the Coast of Cape Toi, Miyazaki, Japan. *Galaxea. J. Coral. Reef. Stud.* 19, 31–32. doi: 10.3755/galaxea.19.1_31

Kumaraguru, A. K., Jeyakumar, K., Wilson, J. J. and Ramakritinan, C. M. (2005). Impact of the Tsunami of 26 December 2004 on the Coral Reef Environment of Gulf of Mannar and Palk Bay in the Southeast Coast of India. *Curr. Sci.* 89 (10), 1729–1741. https://www.currentscience.ac.in/Volumes/89/10/1729.pdf

Leps, J. and Smilauer, P. (2003). *Multivariate Analysis of Ecological Data Using C.A.N.O.C.O.* Cambridge University Press, Cambridge, *CB2 8EA*.

Linnaeus, C. (1758). *Systema Naturae per regna tria naturae, secundum classes, ordines, genera, species, cum characteribus, differentiis, synonymis, locis*. Editio decima, reformata [10th revised edition], vol. 1: 824 pp.

Marimuthu, N. and Tripathy, B. (2018). First Report of *Drupella Cornus* Röding, 1978 (Gastropoda: Muricidae), a Biological Indicator of Coral Reef Habitat of Lakshadweep Archipelago, India. *Rec. zool. Surv. India.* 118 (1), 97–99. doi: 10.26515/rzsi/v118/i1/2018/122305

Mohamed, A. R., Aham, A. and Abdel-Salam, H. A. (2012). "Status of Coral Reef Health in the Northern Red Sea, Egypt," in Proc 12th International Coral Reef Symposium, Cairns, Australia. Available at: (eds.) Yellowlees, D., Hughes, T. P. ARC Centre of Excellence for Coral Reef Studies James Cook University, Townsville, Queensland, Australia.

Murdoch, T. J. T. and Murdoch, J. M. H. (2016). "Baseline Condition of the Coral Reefs and Fishes Across Three Depth Zones of the Fore Reef of Bermuda," in *BREAM: Bermuda Reef Ecosystem Analysis and Monitoring Programme Report* (Flatts Bermuda: Bermuda Zoological Society), BBP–2016-237.

Nelson, N. (2009). Acanthaster planci population dynamics on Nyange Reef, Zanzibar, Tanzania: Implications for resource management and economic sustainability. Independent Study Project, Knox College Department of Biology; University of Dar es Salaam Institute of Marine Science, Mji Mkongwe, Unguja, Tanzania.

Raj, K. D., Aeby, G. S., Mathews, G., Bharath, M. S., Rajesh, S., Laju, R. L., et al. (2016). "Patterns in the abundance of Fish and Snail Corallivores to an Outbreak of Acute Tissue Loss Disease on the Reefs of Vaan Island in the Gulf of Mannar, India," in Proc 13th International Coral Reef symposium, (eds.) Aeby, G. S. Hawaii Institute of Marine Biology, University of Hawaii, HI 96744 USA.

Ravindran, J., Manikandan, B., Venkatesh, M., Murali, R. M., Marimuthu, N. and Wafar, M. V. M. (2014). Repercussions of Embarkation Wharves in Lakshadweep Islands on Coral Communities and Their Ecology. *Ind. J. Geo-Mar. Sci.* 43 (7), 1391–1400. http://nopr.niscair.res.in/bitstream/123456789/34459/1/IJMS%2043%287%29%201391-1400.pdf

Röding, P. F. (1798). *Museum Boltenianum sive Catalogus cimeliorum e tribus regnis naturæ quæ olim collegerat Joa. Fried Bolten*, M. D. p. d. per XL. annos proto physicus Hamburgensis.

Pars secunda continens Conchylia sive Testacea univalvia, bivalvia & multivalvia. Trapp, Hamburg. viii, 199 pp.

Rosenau, N. A., Gignoux-Wolfsohn, S., Everett, R. A., Miller, A. W., Minton, M. S. and Ruiz, G. M. (2021). Considering Commercial Vessels as Potential Vectors of Stony Coral Tissue Loss DiSease. *Front. Mar. Sci.* 8. doi: 10.3389/fmars.2021.709764

Sahu, B. K., Begum, M., Khadanga, M. K., Jha, D. K., Vinithkumar, N. V. and Kirubagaran, R. (2013). Evaluation of Significant Sources Influencing the Variation of Physico-Chemical Parameters in Port Blair Bay, South Andaman, India by Using Multivariate Statistics. *Mar. pollut. Bull.* 66, 246–251. doi: 10.1016/j.marpolbul.2012.09.021

Saponari, L., Dehnert, I., Galli, P. and Montano, S. (2021). Assessing Population Collapse of *Drupella* Spp. (Mollusca: Gastropoda) 2 Years After a Coral Bleaching Event in the Republic of Maldives. *Hydrobiologia.* 848, 2653–2666. doi: 10.1007/s10750-021-04546-5

Tsuchiya, K. (1992). Coral Predation by the Muricid Gastropods, *Drupella* Spp. *Midoriishi.* 3, 14–15.

Veron, J. E. N. (2000). *Corals of the World* (Townsville: Australian Institute of Marine Science).

Wilson, J. J., Marimuthu, N., Kumaraguru, A. K. (2005) Sedimentation of silt in the coral reef environment of southeast coast of India. *J Mar Biol Ass India*. 47 (1), 83-87.

Wilson, J. J. (2010) *Impacts of natural and anthropogenic factors on the corals of Palk Bay, Southeast coast of India.* Ph.D thesis submitted to Madurai Kamaraj University, Tamil Nadu, India. 147 p, http://shodhganga.inflibnet.ac.in:8080/jspui/handle/10603/135366.

Conflict of Interest: The authors declare that the research was conducted in the absence of any commercial or financial relationships that could be construed as a potential conflict of interest.

Publisher's Note: All claims expressed in this article are solely those of the authors and do not necessarily represent those of their affiliated organizations, or those of the publisher, the editors and the reviewers. Any product that may be evaluated in this article, or claim that may be made by its manufacturer, is not guaranteed or endorsed by the publisher.

Copyright © 2022 Marimuthu, Wilson, Al-Sofyani and Kumaraguru. This is an open-access article distributed under the terms of the Creative Commons Attribution License (CC BY). The use, distribution or reproduction in other forums is permitted, provided the original author(s) and the copyright owner(s) are credited and that the original publication in this journal is cited, in accordance with accepted academic practice. No use, distribution or reproduction is permitted which does not comply with these terms.

frontiers | Frontiers in Marine Science

ORIGINAL RESEARCH
published: 25 July 2022
doi: 10.3389/fmars.2022.925796

Modelling the Role of Temperature-Induced Environmental Noise on Phytoplankton Niche Dynamics

Subrata Sarker[1*], *Deen Mohammad*[2], *Siam Ahmed Nabil*[2] *and Md. Alamgir Kabir*[2]

[1] *Department of Oceanography, Shahjalal University of Science and Technology, Sylhet, Bangladesh,* [2] *Department of Mathematics, Shahjalal University of Science and Technology, Sylhet, Bangladesh*

Variability in physical and chemical processes in the marine ecosystem significantly influences the niche ecology of primary producers. However, studies are limited to understand the role of variability in environmental conditions on the niche dynamics of phytoplankton. Therefore, in this study we aimed to understand the role of environmental noise on the niche dynamics of phytoplankton species. This study performed numerical simulations by extending the classic Rosenzweig–MacArthur, predator–prey model for multiple species. We considered the characteristics timescale of seasonal sea surface temperature as environmental noise. Our study found that the oscillatory fluctuation of biomass, variation in carrying capacity, no competitive exclusion, and non-equilibrium state in periodic fluctuation of species biomass enables species to coexist in a noise-induced system. In addition, a high amplitude in species biomass fluctuation at a higher environmental noise was found as another potential coexistence mechanism. Our simulations found that the mean niche and niche width of species are significantly related to environmental noise (R^2 = 0.93 and 0.98, respectively). We observed a shift in mean niche conditions of species with the change in environmental noise. Niche overlapping between species decreased significantly with the increase in environmental noise (R^2 = 0.95). Our study will serve as a baseline to understand the complexity of phytoplankton niche dynamics in a variable environment.

Keywords: temperature, co-existence, fluctuation, ecology, marine

OPEN ACCESS

Edited by:
Dilip Kumar Jha, National Institute of Ocean Technology, India

Reviewed by:
Gopalakrishnan Thilagam, Pachaiyappa's College for Men, India
Subrat Naik, National Centre for Coastal Research, India
Biraja Kumar Sahu, Council of Scientific and Industrial Research (CSIR), India

***Correspondence:**
Subrata Sarker
subratasrk-ocg@sust.edu

Specialty section:
This article was submitted to Marine Pollution, a section of the journal Frontiers in Marine Science

Received: *21 April 2022*
Accepted: *20 June 2022*
Published: *25 July 2022*

Citation:
Sarker S, Mohammad D, Nabil SA and Kabir MA (2022) Modelling the Role of Temperature-Induced Environmental Noise on Phytoplankton Niche Dynamics. Front. Mar. Sci. 9:925796. doi: 10.3389/fmars.2022.925796

INTRODUCTION

Planktons are a group of aquatic organisms which comprise both phytoplankton and zooplankton (Sarker et al., 2020). Among the plankton community, phytoplankton are floating marine organisms and are considered as the primary input of energy for the oceanic ecosystem (Trefault et al., 2021). Phytoplankton serves as food for zooplankton and herbivore fish species. Thus, the variability in phytoplankton community composition and biomass controls the zooplankton composition which ultimately affects the fisheries production (Schroeder, 1983). The diversity of phytoplankton in marine and coastal waters controls the ecosystem functionality through carbon exporting and nutrient cycling (Goebel et al., 2013). In addition, phytoplankton influences the flux of elements, controls the biogeochemical cycles, and fixes the atmospheric CO_2 (Charlson et al., 1987; Andreae and Crutzen, 1997). Therefore, knowledge of the phytoplankton community dynamics is important.

In the coastal ecosystem, variation in interannual and intra-annual environmental conditions characterizes the phytoplankton community dynamics (Winder and Cloern, 2010). Phytoplankton communities are highly sensitive to the fluctuations of environmental conditions. This is due to the capacity of phytoplankton's daily cell division in optimum environmental conditions (Cloern and Jassby, 2008). In marine and coastal habitats, the concentration of micronutrients and the carrying capacity of the ecosystem control the distribution of phytoplankton (Wiltshire et al., 2015; Pitchaikani and Lipton, 2016; Sarker and Wiltshire, 2017). Water temperature controls the metabolic activities of phytoplankton species and thus influences their ecology (Sarker et al., 2020). In addition, pollution controls the occurrence of phytoplankton species in coastal waters (Jakhar, 2013). Hydrodynamic conditions, water current (Dickie and Trites, 1983), diseases, and predation by zooplankton (Wiltshire and Boersma, 2016) also play key roles in determining the phytoplankton community composition.

The health of a marine ecosystem is largely dependent on primary productivity (Pitchaikani and Lipton, 2016). The primary productivity of the ecosystem is largely dependent on the availability of phytoplankton in the ecosystem. Since the phytoplankton community significantly responds to the changes in environmental conditions, they are considered as a vital indicator for global warming and pollution assessment (Heneash et al., 2022). For example, phytoplankton bloom intensity, community composition, and cell size and abundance are widely used to classify the water quality in coastal ecosystems (Facca and Sfriso, 2009; Lugoli et al., 2012). The concentration of chlorophyll-a in combination with nutrients, macrophytes, water column transparency, and dissolved oxygen is used to classify the trophic status in coastal waters (Facca and Sfriso, 2009; Giordani et al., 2009).

The phytoplankton dynamics in a marine ecosystem is linked with the change in environmental conditions which substantially alter their niche ecology (Ajani et al., 2018). Phytoplankton niche is the environmental conditions (i.e., physical and chemical factors) that allow their growth (Hutchinson, 1957). This means that each species operates within a range of environmental conditions, which is favorable for their reproduction and growth (Caracciolo et al., 2020). The niche of species is characterized by their dispersal ability and interspecific and intraspecific competition (Brun et al., 2015). Niche determines the spatial distribution of species, phenology, and temporal fluctuation in abundance. Environmental variability significantly influences the niche dynamics of phytoplankton. For example, warming of the sea surface leads to a niche partitioning of species (Irwin and Oliver, 2009). A shift in temperature can modify the timing of species peak abundance, and this indicates that a change in environmental conditions leads to a shift in the niche dynamics of species (Freund et al., 2006). A change in nutrient levels and pollutants in the ecosystem also leads to a shift in the mean niche condition of species (Brun et al., 2015). The niche partitioning of phytoplankton driven by a change in environmental conditions also influences the functionality of the phytoplankton community (Duerschlag et al., 2022). Thus, the role of environmental change on the niche dynamics of phytoplankton is important to explore. A large number of studies are available on the role of biotic and abiotic conditions on the phytoplankton dynamics. The role of stochastic fluctuations on the phytoplankton community composition is also well studied (Sarker et al., 2020). However, studies on the role of environmental noise on phytoplankton niche dynamics are very rare.

Therefore, this study aimed to understand the role of environmental noise on the niche dynamics of phytoplankton. More specifically, we analyzed the dynamics of phytoplankton in a noise-induced system. In addition, we also examined the role of environmental noise on the mean niche condition and niche overlapping of phytoplankton species.

MATERIALS AND METHODS

Modeling Approach

The prime objective of this study was to understand the role of environmental fluctuations on the phytoplankton niche dynamics. Thus, we performed numerical simulations by utilizing a predator–prey model. We extended the classic Rosenzweig–MacArthur, predator–prey model to generate the dynamics of multiple species of plankton (Rosenzweig and MacArthur, 1963). The extension of the model was performed by formulating species growth (r), mortality (m), carrying capacity (K), and grazing (g) as the function of sea surface temperature (SST). Let N_i and R_k denote the biomass of i phytoplankton and k zooplankton species. Mathematically, the model was then formulated as:

$$\frac{dN_i}{dt} = r_i P N_i \left(1 - \frac{\sum_j \alpha_{ij} P N_j}{K_i}\right) - \sum_k \left(g_k R_k \frac{S_{ik} N_i}{\sum_j \left(S_{jk} N_j\right) + H_k}\right) + u \quad i = 1,2,\ldots,4 \tag{1}$$

$$\frac{dR_k}{dt} = \beta_k g_k R_k \left(\frac{\sum_j \left(S_{jk} N_j\right)}{\sum_j \left(S_{jk} N_j\right) + H_k}\right) - m_k R_k + u \quad k = 1,\ldots,3 \tag{2}$$

Equation (1) defines the phytoplankton dynamics where species grow logistically with specific growth rates (r_i) and carrying capacities (K_i). We assumed that the species are competing with each other and thus defined the competition coefficients between two species i and j as α_{ij}. We described the dynamics of zooplankton in the model by a multispecies Holling type II (Equation 2) functional response. In Equation (2), H_k is the half saturation constant, g_k is the maximum grazing rate of zooplankton, S_{ik} is the selectivity coefficient of zooplankton species k for phytoplankton species i, β_k is the efficiency of zooplankton species k feed on phytoplankton, and m_k is the mortality of zooplankton species k. We assumed that small levels of immigration (u) of species are occurring in the system.

We formulated the growth and carrying capacity of phytoplankton, and the mortality and grazing of zooplankton as the function of SST following the metabolic theory of ecology (MTE). Phytoplankton growth was formulated as the function of body mass and SST by using Equation (3).

$$r_i = r_{0_i} M_i^a e^{-E_r/RT(t)} \tag{3}$$

In Equation (3) T = SST, r_{0i} = normalization constant for phytoplankton species i, M_i = body mass of species i, a = fixed allometric exponent, E_r = activation energy for phytoplankton growth rate r, and R = Boltzmann constant.

We also formulated the carrying capacity of phytoplankton K, mortality of zooplankton m, and zooplankton grazing g_k as the function SST by using Equations (4), (5), and (6), respectively.

$$K_i = K_{0_i} M_i^b e^{-E_K/RT(t)} \tag{4}$$

$$m_k = m_{0_k} M_k^c e^{-E_m/RT(t)} \tag{5}$$

$$g_k = g_{0_k} M_k^q \sum_i M_i^s e^{-E_g/RT(t)} \tag{6}$$

In Equations (4) and (5), K_{0i} = normalization constant for the carrying capacity of phytoplankton, m_{0k} = mortality of zooplankton, M_k = zooplankton species body mass, b = allometric exponents for the carrying capacity of phytoplankton, and c = allometric exponents for mortality of zooplankton. Both E_K and E_m are defined as the activation energy coefficients. In Equation (6), g_{0k} = zooplankton grazing normalization constant, E_g = activation energy of zooplankton grazing, and q = allometric exponent.

For seasonal SST (T) in the model, we relied on SST data using the advanced very-high-resolution radiometer (AVHRR) sensor for the Bay of Bengal (BoB) region. The AVHRR data were downloaded *via* the ERDDAP server (https://coastwatch.pfeg.noaa.gov/erddap/index.html). The BoB is a subtropical marine ecosystem located in the northeastern part of the Indian Ocean. This area is very dynamic and receives a large volume of freshwater discharge from the surrounding river systems. Freshwater discharges from the upstream area carry a large volume of sediments. In addition, BoB is considered thermally stratified and thus less productive compared to the Arabian Sea. This area is under the pressure of both climate and anthropogenic pressure. However, the BoB received very little attention from scientific communities (Hood et al., 2013). Details of the SST data are described in Kilpatrick et al. (2001). For this study, the daily SST data for the time period between 1985 and 2017 were analyzed. The seasonal SST data of BoB usually show two peaks in a year (**Figure 1**). Thus, we used the linear combination of *Sin* and *Cos* to formulate SST function as described in Equation (7).

$$T(t) = T_m + \varnothing_1 Sin\left(\frac{2\pi}{\sigma t}\right) + \varnothing_2 Cos\left(\frac{2\pi}{\sigma t}\right) + \varnothing_3 Sin\left(\frac{4\pi}{\sigma t}\right) + \varnothing_4 Cos\left(\frac{4\pi}{\sigma t}\right) \tag{7}$$

In Equation (7), T_m = mean SST and t = time. We adopted the parameters $\emptyset_1$, $\emptyset_2$, $\emptyset_3$, $\emptyset_4$, and σ through the fitting of daily SST data from AVHRR to Equation (7). Data fitting to estimate the parameters was performed in R (R studio core team, 2005) using a linear function.

Inclusion of Environmental Noise in the Model

Environmental noise is the unpredictable fluctuation in environmental conditions at both spatial and temporal scales (Fujiwara and Takada, 2017). Unpredictability refers to the inability of the precise prediction of the future state of environmental conditions, which is usually a set of abiotic and biotic variables (Adler and Drake, 2008). Fluctuation of

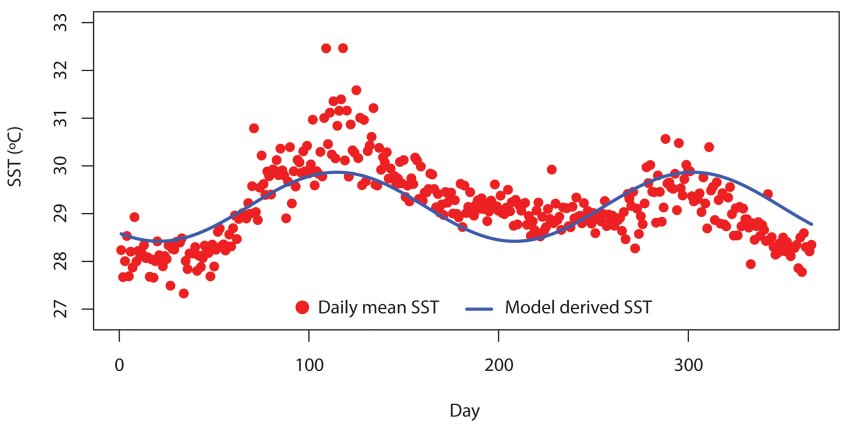


FIGURE 1 | Daily mean variation of sea surface temperature (SST) in the Bay of Bengal (BoB) from 1985 to 2007. Red-filled points indicate the daily SST over BoB derived from a satellite source. Blue solid line indicates the daily SST derived from Equation (7).

temperature in marine ecosystems usually shows persistence in time (Steele, 1985; Roe, 2009; Beninc et al., 2011). We introduced the characteristics time scale of SST fluctuation as red noise in the model. Red noise in the model was introduced by adding a term n_t with seasonal SST as described in Equation (8), which was previously described in Freund et al. (2006) and Sarker et al. (2020).

$$T_n(t) = T(t) + n_t \tag{8}$$

In Equation (8), T_n = SST with red noise.

We used a first-order autoregressive model to define red noise n_t by using Equation (9) as described in Box et al. (2015).

$$n_t = \gamma n_{t-1} + \delta_\epsilon \sqrt{\left(1-\gamma^2\right)}\epsilon_t \tag{9}$$

In Equation (9), = autocorrelation coefficient (the values of γ vary from -1 to 1) and δ_ϵ = magnitude of environmental noise. We defined red noise when γ was found positively auto-correlated. The stochastic term ϵ_t was drawn randomly at each time step which follows a Gaussian distribution. In this study, we considered a time step of 1 day for simulations. The coefficient of autocorrelation γ was formulated as the function of the characteristic timescale of SST fluctuation τ (Equation 10) which was determined by fitting the data to Equation (10).

$$\gamma = exp\left(-\frac{t}{\tau}\right) \tag{10}$$

We performed a number of simulations to achieve the objectives of this study. We first performed a simulation without adding noise in SST function. We then performed simulations to generate the phytoplankton dynamics by varying the environmental noise. For this, we varied the characteristic timescale of SST fluctuation τ. In this study, τ was found 4 days after analyzing the SST data. In this study, we varied τ from 4 to 8 days to generate different noise scenarios.

Parameterization of the Model

To understand the role of environmental noise on phytoplankton niche dynamics, 10 phytoplankton and 7 zooplankton species were considered in this study. Therefore, to perform the numerical simulations we chose the range of parameter values from the literatures. Parameter values related to phytoplankton growth, carrying capacity, zooplankton mortality, grazing rate, assimilation efficiency, half-saturation constant, body mass of phytoplankton, body mass of zooplankton, allometric exponent, and activation energy were derived from field- and experiment-based studies as described in Sarker et al. (2018). However, parameter values related to species competition, selectivity coefficient of zooplankton, and immigration rate were chosen randomly by following Dakos et al. (2009). Coefficients of the intraspecific competition of phytoplankton species α_{ii} were set as 1. Coefficients of the interspecific competition of phytoplankton species α_{ij} were drawn randomly between 0.5 and 1.5. Selectivity coefficients S_{ik} were also drawn randomly between 0 and 1. After selecting the range of all model parameters, a Monte Carlo search was performed to identify an ideal parameter set. We defined a parameter set ideal when all 10 phytoplankton species and 7 zooplankton species can coexist. Details of parameters are given in **Table S1**. For simulations, we did not specify any species; however, the parameter values were within the realistic range.

Model Sensitivity Test

The value of each parameter was changed by ±50% to test the sensitivity of the model. For example, if in an ideal parameter set, a species had the specific growth rate 1, we simulated the dynamics of species by varying the growth rate of that species from 0.5 to 1.5. If the coexistence of all species persists even within this change in parameter values, we considered that the model is not sensitive to large variation in parameter values.

Statistical Analyses of Model Outputs

The prime objective of this study was to understand the role of environmental noise on the niche dynamics of phytoplankton species. Therefore, we simulated the dynamics of 10 phytoplankton species. We then analyzed the dynamics of these phytoplankton species. We analyzed the coexistence mechanism of phytoplankton species in a noise-induced system and the role of noise on species niche dynamics. To understand the coexistence mechanism of phytoplankton species in a noise-induced system, we analyzed species competition, biomass of dominant species, and oscillation and amplitude of species biomass. To understand the role of noise on phytoplankton niche dynamics, we estimated the niche width and niche overlapping of species from each simulation. We used the Levins (1968) measure to estimate the niche width of species by using Equation (11).

$$B = \frac{1}{\sum p_i^2} \tag{11}$$

In Equation (11), B = Levins measure of niche breadth and P_i = proportion of individuals found using resource i. In this case, i is the SST. We used Equation (12) to measure the niche overlapping among the species.

$$NO_N(i,j) = e^{\frac{-\left(\mu_i-\mu_j\right)^2}{\left(2\left(\sigma_i^2+\sigma_j^2\right)\right)}} \tag{12}$$

In Equation (12), μ_i = mean (= mode = median) of the distribution of species i, μ_j = mean of the distribution of species j, σ_i^2 = variance of the distribution of species i, and σ_j^2 = variance of the distribution of species j.

RESULTS

How Do Phytoplankton Species Coexist in a Noise-Induced System?

We examined the dynamics of 10 phytoplankton species under different environmental conditions. We formulated the species growth as a function of temperature. First, we created a system where 10 species of phytoplankton can coexist without any environmental noise in temperature-dependent species growth (**Figure 2**). We then simulated the biomass of phytoplankton species by adding noise in temperature-dependent growth function. Later, we analyzed the drivers of species coexistence in the noise-induced ecosystem (**Figure 3**). Analysis of our model outputs found that an oscillatory state of phytoplankton biomass exists over time in the system without noise (**Figure 4A**). This periodic oscillation also exists in the system with environmental noise (**Figure 4B**). This oscillatory fluctuation of biomass is related to seasonal fluctuation in SST. The interspecific competitions of considered phytoplankton species were identical. This indicates that species shared the same niche when no noise was added to the system. Although species shared the same niche, we did not observe any competitive exclusion. This enabled the species to coexist in both the system with noise and that without noise by preventing competitive exclusion. We observed a non-equilibrium state in periodic fluctuation of phytoplankton species biomass which allowed them to coexist in a noise-induced ecosystem. Analysis of long-term dynamics of simulated phytoplankton biomass found that at a time several species show a peak in their biomass while some species show low biomass. This variation of species biomass at the same time enabled them to coexist in the noise-induced system. The noise-induced seasonal temperature-dependent growth of phytoplankton species results in a periodical fluctuation of biomass. This periodicity repeats every 1 to some year later. This types of succession of species biomass results in the coexistence of 10 phytoplankton species in noise-induced environmental conditions. Phytoplankton species considered in this study had different carrying capacities (3 to 70 mg/m^3).

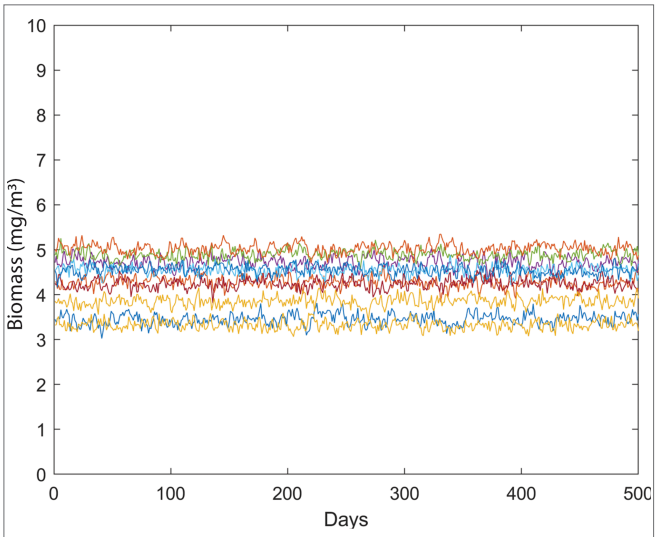


FIGURE 2 | Variability in phytoplankton biomass (mg/m^3) over time in a system without temperature-induced noise.

Diverse carrying capacities also enabled species to coexist in a system where they had an identical niche. We observed variation in amplitude of species biomass over time. This fluctuation in biomass amplitude is correlated with environmental noise. We found that the total amplitude of the simulated plankton biomass increased with the increase in environmental noise ($R^2 = 1$, $p < 0.001$). This fluctuation in amplitude in species biomass is also found as one of the coexistence mechanisms of phytoplankton species.

Role of Noise on Species Niche Dynamics

The daily variation of SST in the BoB after removing the seasonal trend is shown in **Figure 5**. We estimated the characteristic timescale of SST fluctuation by fitting the exponential decay of the autocorrelation function (**Figure 5**). We found that SST

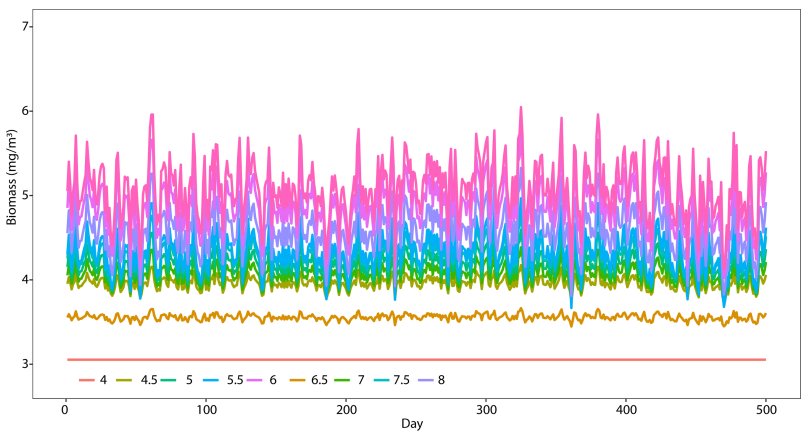


FIGURE 3 | Variability of phytoplankton biomass over time at different noise conditions. Noise conditions were generated by varying the characteristics time scale of temperature fluctuation over the BoB. Solid lines indicate the mean biomass of 10 phytoplankton species from each simulation.

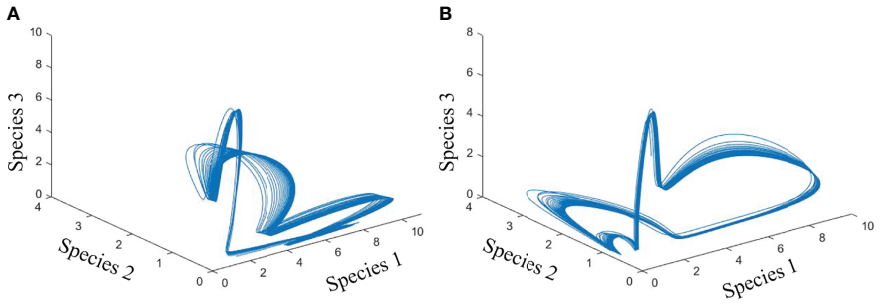


FIGURE 4 | Phase plane diagram showing the cyclic fluctuation of biomass of species 1, 2, and 3 in a system without noise **(A)** and with noise **(B)**.

fluctuations in the BoB can be described by a red-noise process with a characteristic timescale τ of about 8 days. When long-term biomass of phytoplankton species was simulated without adding any noise in the temperature-dependent growth function, we found that niche is identical for all species (**Figure 6**). This suggests that all species shared the same niche (mean niche was found at n_t = 0). However, when we added noise in the growth function, a significant change in niche configuration of species was observed (**Figure 7**). Variation of mean noise conditions changed the mean niche and niche width of species significantly. Mean niche was found at n_t = 0 for species 1. However, the mean niche of the same species shifted at n_t = 0.5 when the characteristic timescale of SST fluctuation τ was considered 15 days (**Figure 7**). Similar shifts were also observed for the other species. When a species showed a narrow niche width at the low environmental noise, the same species showed a very wide niche width at higher environmental noise conditions. For example, at n_t = 0 species 1 had a narrow niche width (-0.5 to 0.5). On the other hand, after adding noise with a characteristic timescale of SST fluctuation τ 15 days, species 1 showed a wider niche width (-1 to 1).

The biomass density of that species was found higher (5 mg/m^3) in mean niche conditions when the noise was low.

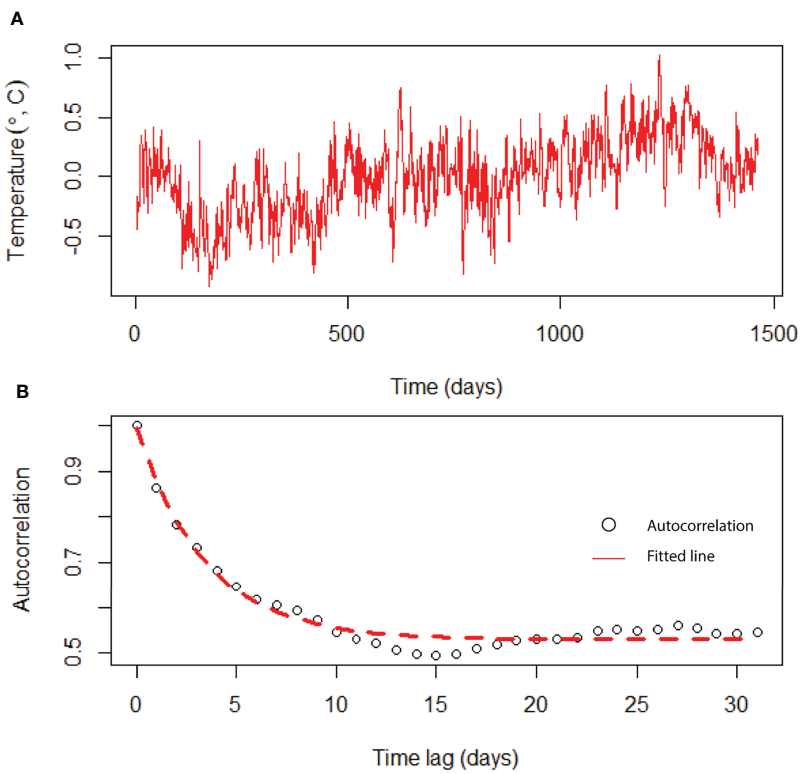


FIGURE 5 | Time-series analysis of temperature fluctuations using data from the BoB. **(A)** Time series of daily surface water temperatures after the seasonal trend was removed from the original data, and **(B)** autocorrelation function of the seasonally detrended temperature data (circles). Red dashed line is an exponential decay fit.

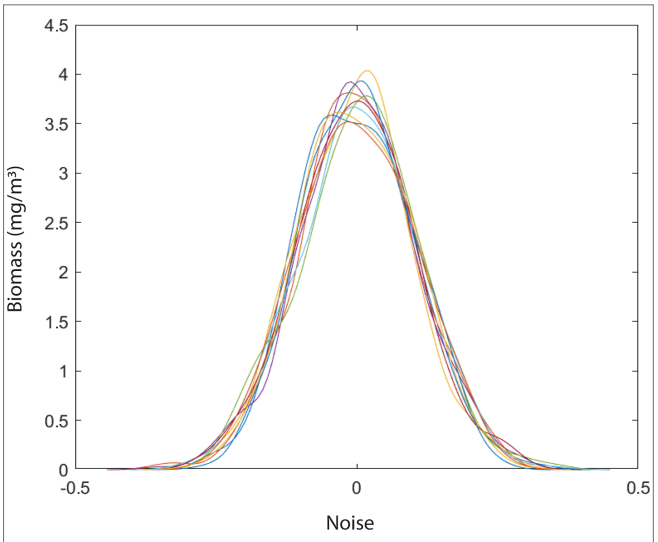


FIGURE 6 | Variation in niche dynamics of phytoplankton species in a system without environmental noise.

However, the density of biomass was comparatively low in mean niche conditions when the noise was higher (3.5 mg/m^3) (**Figure 8**). Environmental noise also significantly influenced the niche overlap between species. We observed high niche overlapping at the low environmental noise conditions. Niche overlapping between species decreased significantly with the increase in environmental noise (**Figure 9**). For example, species 1 had a high level of overlapping with other nine species when the noise was low. On the other hand, species 1 showed low overlapping with other species when the noise was increased gradually (**Figure 9**).

DISCUSSION

The present study aimed to understand the role of environmental noise on phytoplankton niche dynamics. We based our study using a multispecies competition model and formulated the growth, carrying capacity, mortality, and grazing of species as the function of SST. We included red noise in the model by incorporating the characteristics time scale of SST fluctuation of the Bay of Bengal. We first created an ecosystem where 10 phytoplankton species can coexist with the change in environmental forcing and noise. Later, we analyzed the species' biomass and niche dynamics in relation to environmental change.

We found that oscillatory fluctuation of biomass, variation in carrying capacity, no competitive exclusion, non-equilibrium state in periodic fluctuation of species biomass, and periodic fluctuation in biomass enable phytoplankton species to coexist. In addition, a high amplitude in species biomass fluctuation at a higher environmental noise was found to be another potential coexistence mechanism of phytoplankton species. Multiple-species coexistence is considered a long-term puzzle in a community ecology study (Segura et al., 2011). The major

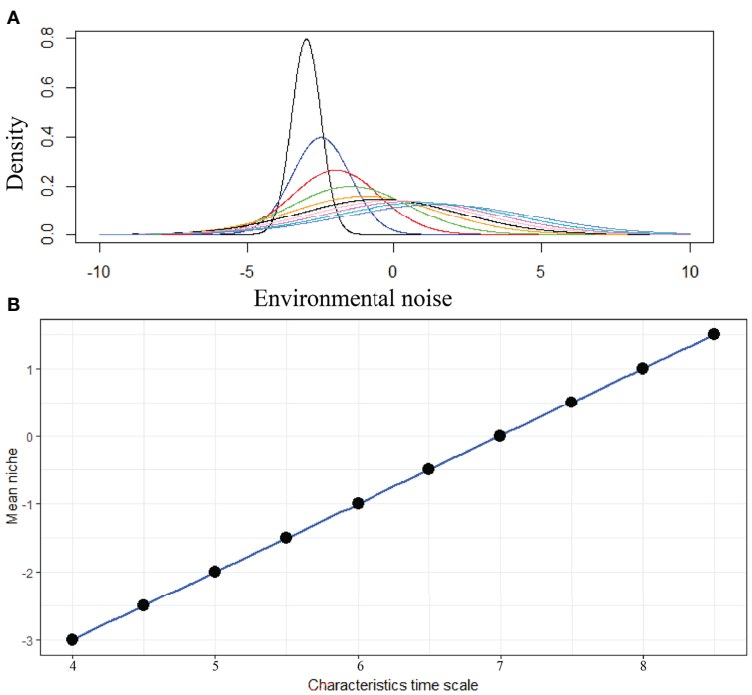


FIGURE 7 | Variation of species niche configuration at different environmental noise. In this figure, niche dynamics in response to environmental variability is shown for species 1. **(A)** Changes in niche configuration of species 1 with environmental variability and **(B)** linear relationship between mean niche condition of species 1 and different characteristics time scales of SST change.

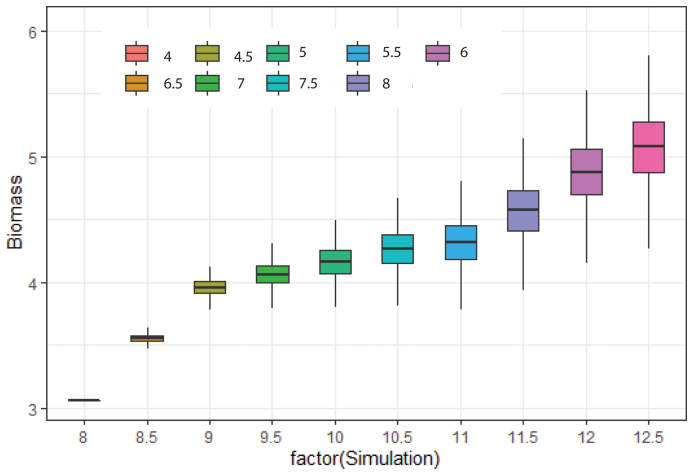


FIGURE 8 | Change in biomass of 10 phytoplankton species considered for simulations at different characteristics time scales of SST change.

challenge to resolve this puzzle lies in the principle of competitive exclusion (Laird and Schamp, 2006). The competitive exclusion principle suggests that identical niches among the species prevent their coexistence in the ecosystem (Hardin, 1960). According to this principle, the competition limits the number of coexisting phytoplankton species in the ecosystem (Benincà et al., 2008). However, Hutchinson (1961) pointed that in nature, thousands of phytoplankton species can coexist while they have identical niches (i.e., they compete for the same resources). Multiple-species coexistence driven by competition is reported by the studies of Huisman and Weissing (1999); Huisman et al. (2001); Baer et al. (2006), and Sarker et al. (2018). In this study, we considered a seasonally driven system with environmental noise. Species competition plays an evolutionary role in speciation and thus increases the diversity (Brännström et al., 2012). In addition, competition governs the interactions among the species through which biodiversity is regulated (Chesson, 2000). The joint influence of competition and seasonality causes a periodical

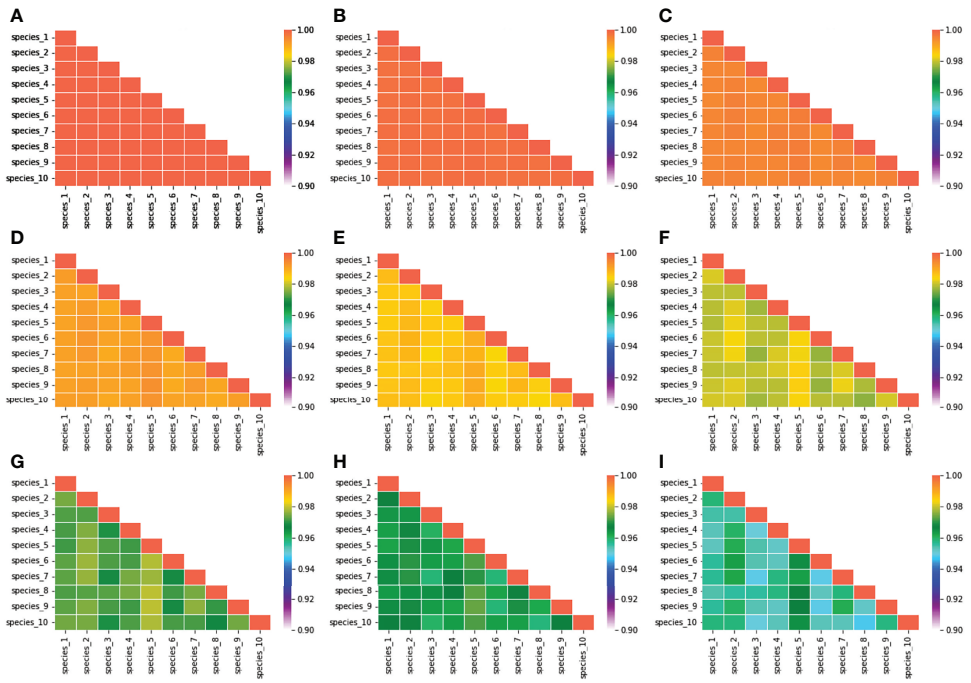


FIGURE 9 | Variation in species niche overlap estimated at different environmental conditions. **(A)** When the characteristics time scale of SST change was considered 4 days, and **(B–I)** when the characteristics time scales of SST change were considered 4.5, 5, 5.5, 6, 6.5, 7, and 7.5 days, respectively.

succession of species one after another. This mechanism causes species coexistence in a noise-induced ecosystem which is also in line with the findings of Sarker et al. (2018) and Sarker et al. (2020) for subtropical and temperate marine ecosystems. Our study also found that the turnover time of species also changes with the change in noise in environmental conditions. This is also found true in the studies conducted by Dutta et al. (2014) and Huisman and Weissing (1999). Field-based studies of Sarker et al. (2018) and Dakos et al. (2009) also found similar results. Carrying capacity is the maximum phytoplankton biomass that can occur in a given environmental condition (Sarker and Wiltshire, 2017). Variation in carrying capacity indicates that each species has a specific biomass limit in the system (Franks, 2001). Therefore, when one species attains the carrying capacity, biomass of other species might be in the condition of undercarrying capacity. This causes the biomass peak of one species and low biomass of another species which enable them to coexist. In our study, we found that at high environmental noise conditions the amplitude of species biomass variation is higher. This is related to periodic succession which is a well-known coexistence mechanism of species (Sarker et al., 2018).

The range of environmental conditions under which a species can persist is known as fundamental niche (Ajani et al., 2018). The ecological niche of phytoplankton is driven by a number of factors, i.e., competition, dispersal ability, disease, and predation (Brun et al., 2015). In addition, changes in environmental conditions are also responsible for the change in the niche configuration of phytoplankton. Addition of noise leads to a change in phenology of species which results in a change in optimal niche conditions (Velthuis et al., 2017). Therefore, species optimal niche conditions may shift from the original. Our study also found the optimal niche of species changes with the change in environmental noise conditions. Several studies also reported similar findings on the species niche and environmental relationship. For example, Adrianet al. (2006), Mazaris et al. (2008), and Stefanescuet al. (2003) found similar findings for zooplankton, turtles, and Mediterranean butterflies, respectively. Our study found that mean niche, niche width, and niche overlapping among the species significantly changed with the variation of noise in the temperature-dependent growth function. These changes are the adaptation options of species in variable environmental conditions (Sarker et al., 2020). There will be an extinction risk if species do not adapt with the changing environment. Field-based studies confirmed such types of adaptation strategies. For example, Edwards and Richardson (2004) found similar adaption strategies of species in the central North Sea. The shift in mean niche condition of species is also related to their nature, i.e., generalists and specialists. In this study, all species were generalist in nature. Therefore, they showed a wider habitat demand and are less sensitive to environmental fluctuations (Preston et al., 2008). For example, temperature rise is less effective for generalist species (Sarker et al., 2020). Thus, this group of species can survive within a wide range of temperature changes (Ranius and Nilsson, 1997).

CONCLUSION

We simulated the phytoplankton dynamics using a competition model. We formulated species growth as a function of the stochastic fluctuation of temperature. Our study found that stochastic fluctuation of temperature changes the species niche configuration. So, how will this study contribute in marine and coastal environmental quality monitoring? Human society is largely dependent on the ocean. For example, the ocean provides half of the global oxygen, food, and means of transportation and livelihood. In addition, the ocean absorbs atmospheric CO_2 significantly and thus plays a vital role in facing the global climate change challenges. However, increasing human dependence on the ocean is making the marine ecosystem vulnerable. Thus, monitoring of the marine ecosystem is important. Globally, the ocean is under the threat of climate change. Temperature rise is a consequence of global climate change. This study will help to monitor the species dynamics under the situation of climate change. Here, we developed a methodology to monitor the ecological niche of species in relation to environmental noise. This methodology can be adopted to explore the impacts of environmental degradation (i.e., pollution) on the phytoplankton niche. This study gives an idea how species will behave if environmental conditions fluctuate randomly. Taking this study as a base, one can formulate the framework to model the role of anthropogenic stressors (i.e., eutrophication and pollution) on phytoplankton ecology which helps to develop coastal monitoring and management systems.

DATA AVAILABILITY STATEMENT

The original contributions presented in the study are included in the article/supplementary material. Further inquiries can be directed to the corresponding author.

AUTHOR CONTRIBUTIONS

SS and MK deigned the study. SS performed the numerical simulations and wrote the manuscript. DM and SN performed the numerical simulations. DM, SN, and MK edited the draft manuscript. All authors contributed to the article and approved the submitted version.

SUPPLEMENTARY MATERIAL

The Supplementary Material for this article can be found online at: https://www.frontiersin.org/articles/10.3389/fmars.2022.925796/full#supplementary-material

REFERENCES

Adler, P. B. and Drake, J. M. (2008). Environmental Variation, Stochastic Extinction, and Competitive Coexistence. *Am. Nat.* 172, E186–E195. doi: 10.1086/591678

Ajani, P. A., McGinty, N., Finkel, Z. V. and Irwin, A. J. (2018). Phytoplankton Realized Niches Track Changing Oceanic Conditions at a Long-Term Coastal Station Off Sydney Australia. *Front. Mar. Sci.* 5. doi: 10.3389/fmars.2018.00285

Andreae, M. O. and Crutzen, P. J. (1997). Atmospheric Aerosols: Biogeochemical Sources and Role in Atmospheric Chemistry. *Science* 276, 1052–1058. doi: 10.1126/science.276.5315.1052

Baer, S. M., Li, B. and Smith, H. L. (2006). Multiple Limit Cycles in the Standard Model of Three Species Competition for Three Essential Resources. *J. Math. Biol.* 52, 745–760. doi: 10.1007/s00285-005-0367-x

Benincà, E., Huisman, J., Heerkloss, R., Jöhnk, K. D., Branco, P., Van Nes, E. H., et al. (2008). Chaos in a Long-Term Experiment With a Plankton Community. *Nature* 451, 822–825. doi: 10.1038/nature06512

Beninc, x. E., Dakos, V., Van Nes, E. H., Huisman, J., et al. (2011). Resonance of Plankton Communities With Temperature Fluctuations. *Am. Nat.* 178, E85–E95. doi: 10.1086/661902

Box, G. E., Jenkins, G. M., Reinsel, G. C. and Ljung, G. M. (2015). *Time Series Analysis: Forecasting and Control* (Hoboken: John Wiley & Sons).

Brännström, Å, Johansson, J., Loeuille, N., Kristensen, N., Troost, T. A., Lambers, R. H. R., et al. (2012). Modelling the Ecology and Evolution of Communities: A Review of Past Achievements, Current Efforts, and Future Promises. *Evolutionary. Ecol. Res.* 14, 601–625.

Brun, P., Vogt, M., Payne, M. R., Gruber, N., O'Brien, C. J., Buitenhuis, E. T., et al. (2015). Ecological Niches of Open Ocean Phytoplankton Taxa. *Limnology. Oceanography.* 60, 1020–1038. doi: 10.1002/lno.10074

Caracciolo, M., Beaugrand, G., Hélaouët, P., Gevaert, F., Edwards, M., Lizon, F., et al. (2020). Annual Phytoplankton Succession Results From Niche-Environment Interaction. *J. Plankton. Res.* 43, 85–102. doi: 10.1093/plankt/fbaa060

Charlson, R. J., Lovelock, J. E., Andreae, M. O. and Warren, S. G. (1987). Oceanic Phytoplankton, Atmospheric Sulphur, Cloud Albedo and Climate. *Nature* 326, 655–661. doi: 10.1038/326655a0

Chesson, P. (2000). Mechanisms of Maintenance of Species Diversity. *Annu. Rev. Ecol. Systematics.* 31, 343–366. doi: 10.1146/annurev.ecolsys.31.1.343

Cloern, J. E. and Jassby, A. D. (2008). Complex Seasonal Patterns of Primary Producers at the Land–Sea Interface. *Ecol. Lett.* 11, 1294–1303. doi: 10.1111/j.1461-0248.2008.01244.x

Dakos, V., Benincà, E., van Nes, E. H., Philippart, C. J. M., Scheffer, M. and Huisman, J. (2009). Interannual Variability in Species Composition Explained as Seasonally Entrained Chaos. *Proc. R. Soc. B.: Biol. Sci.* 276, 2871–2880. doi: 10.1098/rspb.2009.0584

Dickie, L. and Trites, R. (1983). *The Gulf of St. Lawrence.p. 403-425. In Ecosystems of the World, 26: Estuaries and Semi-Enclosed Seas. Elsevier Sci. Pub., Amsterdam.*

Duerschlag, J., Mohr, W., Ferdelman, T. G., LaRoche, J., Desai, D., Croot, P. L., et al. (2022). Niche Partitioning by Photosynthetic Plankton as a Driver of CO2-Fixation Across the Oligotrophic South Pacific Subtropical Ocean. *ISME. J.* 16, 465–476. doi: 10.1038/s41396-021-01072-z

Dutta, P. S., Kooi, B. W. and Feudel, U. (2014). Multiple Resource Limitation: Nonequilibrium Coexistence of Species in a Competition Model Using a Synthesizing Unit. *Theor. Ecol.* 7, 407–421. doi: 10.1007/s12080-014-0228-6

Facca, C. and Sfriso, A. (2009). Phytoplankton in a Transitional Ecosystem of the Northern Adriatic Sea and its Putative Role as an Indicator for Water Quality Assessment. *Mar. Ecol.* 30, 462–479. doi: 10.1111/j.1439-0485.2009.00347.x

Franks, P. J. S. (2001). Phytoplankton Blooms in a Fluctuating Environment: The Roles of Plankton Response Time Scales and Grazing. *J. Plankton. Res.* 23, 1433–1441. doi: 10.1093/plankt/23.12.1433

Freund, J. A., Mieruch, S., Scholze, B., Wiltshire, K. and Feudel, U. (2006). Bloom Dynamics in a Seasonally Forced Phytoplankton–Zooplankton Model: Trigger Mechanisms and Timing Effects. *Ecol. Complexity.* 3, 129–139. doi: 10.1016/j.ecocom.2005.11.001

Fujiwara, M. and Takada, T. (2017). Environmental Stochasticity. *eLS*, John Wiley and Sons, Ltd (Ed.). doi: 10.1002/9780470015902.a0021220.pub2

Giordani, G., Zaldívar, J. M. and Viaroli, P. (2009). Simple Tools for Assessing Water Quality and Trophic Status in Transitional Water Ecosystems. *Ecol. Indic.* 9, 982–991. doi: 10.1016/j.ecolind.2008.11.007

Goebel, N., Edwards, C., Zehr, J., Follows, M. and Morgan, S. (2013). Modeled Phytoplankton Diversity and Productivity in the California Current System. *Ecol. Model.* 264, 37–47. doi: 10.1016/j.ecolmodel.2012.11.008

Hardin, G. (1960). The Competitive Exclusion Principle. *Science* 131, 1292–1297. doi: 10.1126/science.131.3409.1292

Heneash, A. M., Alprol, A. E., El-Naggar, H. A., Gharib, S. M., Hosny, S., El-Alfy, M. A., et al. (2022). Multivariate Analysis of Plankton Variability and Water Pollution in Two Highly Dynamic Sites, Southeastern Mediterranean (Egyptian Coast). *Arabian. J. Geosciences.* 15, 330. doi: 10.1007/s12517-022-09595-1

Huisman, J., Johansson, A. M., Folmer, E. O. and Weissing, F. J. (2001). Towards a Solution of the Plankton Paradox: The Importance of Physiology and Life History. *Ecol. Lett.* 4, 408–411. doi: 10.1046/j.1461-0248.2001.00256.x

Huisman, J. and Weissing, F. J. (1999). Biodiversity of Plankton by Species Oscillations and Chaos. *Nature* 402, 407–410. doi: 10.1038/46540

Hutchinson, G. (1957). Concluding Remarks-Cold Spring Harbor Symposia on Quantitative Biology. Reprinted in 1991: Classics in Theoretical Biology. *Bull. Math. Biol.* 53, 193–213. doi: 10.1007/BF02464429

Hutchinson, G. E. (1961). The Paradox of the Plankton. *Am. Nat.* 95, 137–145. doi: 10.1086/282171

Irwin, A. J., and Oliver, M. J. (2009). Are ocean deserts getting larger? *Geophys. Res. Lett.* 36, L18609. doi: 10.1029/2009GL039883

Jakhar, P. (2013). Role of Phytoplankton and Zooplankton as Health Indicators of Aquatic Ecosystem: A Review. *Int. J. Innovation Res. Study.* 2, 489–500.

Kilpatrick, K. A., Podestá, G. P. and Evans, R. (2001). Overview of the NOAA/NASA Advanced Very High Resolution Radiometer Pathfinder Algorithm for Sea Surface Temperature and Associated Matchup Database. *J. Geophysical. Research.: Oceans.* 106, 9179–9197. doi: 10.1029/1999JC000065

Laird Robert, A. and Schamp Brandon, S. (2006). Competitive Intransitivity Promotes Species Coexistence. *Am. Nat.* 168, 182–193. doi: 10.1086/506259

Lugoli, F., Garmendia, M., Lehtinen, S., Kauppila, P., Moncheva, S., Revilla, M., et al. (2012). Application of a New Multi-Metric Phytoplankton Index to the Assessment of Ecological Status in Marine and Transitional Waters. *Ecol. Indic.* 23, 338–355. doi: 10.1016/j.ecolind.2012.03.030

Pitchaikani, J. S. and Lipton, A. P. (2016). Nutrients and Phytoplankton Dynamics in the Fishing Grounds Off Tiruchendur Coastal Waters, Gulf of Mannar, India. *SpringerPlus* 5, 1405. doi: 10.1186/s40064-016-3058-8

Preston, K. L., Rotenberry, J. T., Redak, R. A. and Allen, M. F. (2008). Habitat Shifts of Endangered Species Under Altered Climate Conditions: Importance of Biotic Interactions. *Global Change Biol.* 14, 2501–2515. doi: 10.1111/j.1365-2486.2008.01671.x

Ranius, T. and Nilsson, S. G. (1997). Habitat of Osmoderma Eremita Scop. (Coleoptera: Scarabaeidae), a Beetle Living in Hollow Trees. *J. Insect Conserv.* 1, 193–204. doi: 10.1023/A:1018416000766

Roe, G. (2009). Feedbacks, Timescales, and Seeing Red. *Annu. Rev. Earth Planetary. Sci.* 37, 93–115. doi: 10.1146/annurev.earth.061008.134734

Rosenzweig, M. L. and MacArthur, R. H. (1963). Graphical Representation and Stability Conditions of Predator-Prey Interactions. *Am. Nat.* 97, 209–223. doi: 10.1086/282272

Sarker, S., Feudel, U., Meunier, C. L., Lemke, P., Dutta, P. S. and Wiltshire, K. H. (2018). To Share or Not to Share? Phytoplankton Species Coexistence Puzzle in a Competition Model Incorporating Multiple Resource-Limitation and Synthesizing Unit Concepts. *Ecol. Model.* 383, 150–159. doi: 10.1016/j.ecolmodel.2018.05.021

Sarker, S. and Wiltshire, K. H. (2017). Phytoplankton Carrying Capacity: Is This a Viable Concept for Coastal Seas? *Ocean. Coast. Manage.* 148, 1–8. doi: 10.1016/j.ocecoaman.2017.07.015

Sarker, S., Yadav, A. K., Akter, M., Shahadat Hossain, M., Chowdhury, S. R., Kabir, M. A., et al. (2020). Rising Temperature and Marine Plankton Community Dynamics: Is Warming Bad? *Ecol. Complexity.* 43, 100857. do: 10.1016/j.ecocom.2020.100857

Schroeder, G. L. (1983). Sources of Fish and Prawn Growth in Polyculture Ponds as Indicated by δc Analysis. *Aquaculture* 35, 29–42. doi: 10.1016/0044-8486(83)90068-6

Segura, A. M., Calliari, D., Kruk, C., Conde, D., Bonilla, S. and Fort, H. (2011). Emergent Neutrality Drives Phytoplankton Species Coexistence. *Proc. R. Soc. B.: Biol. Sci.* 278, 2355–2361. doi: 10.1098/rspb.2010.2464

Steele, J. H. A. (1985). Comparison of Terrestrial and Marine Ecological Systems. *Nature* 313, 355–358. doi: 10.1038/313355a0

Trefault, N., de la Iglesia, R., Moreno-Pino, M., Lopes dos Santos, A., Gérikas Ribeiro, C., Parada-Pozo, G., et al. (2021). Annual Phytoplankton Dynamics

in Coastal Waters From Fildes Bay, Western Antarctic Peninsula. *Sci. Rep.* 11, 1368. doi: 10.1038/s41598-020-80568-8

Velthuis, M., de Senerpont Domis, L. N., Frenken, T., Stephan, S., Kazanjian, G., Aben, R., et al. (2017). Warming Advances Top-Down Control and Reduces Producer Biomass in a Freshwater Plankton Community. *Ecosphere* 8, e01651. doi: 10.1002/ecs2.1651

Wiltshire, K. H. and Boersma, M. (2016). "Meeting in the Middle: On the Interactions Between Microalgae and Their Predators or Zooplankton and Their Food," in *Aquatic Microbial Ecology and Biogeochemistry: A Dual Perspective*. Eds. Glibert, P. M. and Kana, T. M. (Cham: Springer International Publishing), 215–223.

Wiltshire, K. H., Boersma, M., Carstens, K., Kraberg, A. C., Peters, S. and Scharfe, M. (2015). Control of Phytoplankton in a Shelf Sea: Determination of the Main Drivers Based on the Helgoland Roads Time Series. *J. Sea. Res.* 105, 42–52. doi: 10.1016/j.seares.2015.06.022

Winder, M. and Cloern, J. E. (2010). The Annual Cycles of Phytoplankton Biomass. *Philos. Trans. R. Soc. B.: Biol. Sci.* 365, 3215–3226. doi: 10.1098/rstb.2010.0125

Conflict of Interest: The authors declare that the research was conducted in the absence of any commercial or financial relationships that could be construed as a potential conflict of interest.

Publisher's Note: All claims expressed in this article are solely those of the authors and do not necessarily represent those of their affiliated organizations, or those of the publisher, the editors and the reviewers. Any product that may be evaluated in this article, or claim that may be made by its manufacturer, is not guaranteed or endorsed by the publisher.

Copyright © 2022 Sarker, Mohammad, Nabil and Kabir. This is an open-access article distributed under the terms of the Creative Commons Attribution License (CC BY). The use, distribution or reproduction in other forums is permitted, provided the original author(s) and the copyright owner(s) are credited and that the original publication in this journal is cited, in accordance with accepted academic practice. No use, distribution or reproduction is permitted which does not comply with these terms.

frontiers | Frontiers in Marine Science

TYPE Original Research
PUBLISHED 26 July 2022
DOI 10.3389/fmars.2022.968740

Check for updates

OPEN ACCESS

EDITED BY
Dilip Kumar Jha,
National Institute of Ocean Technology, India

REVIEWED BY
Du Hong,
Shantou University, China
Ruiping Huang,
Xiamen University, China
Hailong Wu,
Jiangsu Ocean University, China

*CORRESPONDENCE
Fangfang Yang
ycuyang@scsio.ac.cn
Lijuan Long
longlj@scsio.ac.cn

SPECIALTY SECTION
This article was submitted to Marine Pollution, a section of the journal Frontiers in Marine Science

RECEIVED 14 June 2022
ACCEPTED 04 July 2022
PUBLISHED 26 July 2022

CITATION
Wei Z, Zhang Y, Yang F and Long L (2022) Diurnal fluctuations in seawater pCO_2 amplify the negative effects of ocean acidification on the biotic performance of the calcifying macroalga *Halimeda opuntia*. *Front. Mar. Sci.* 9:968740. doi: 10.3389/fmars.2022.968740

COPYRIGHT
© 2022 Wei, Zhang, Yang and Long. This is an open-access article distributed under the terms of the Creative Commons Attribution License (CC BY). The use, distribution or reproduction in other forums is permitted, provided the original author (s) and the copyright owner(s) are credited and that the original publication in this journal is cited, in accordance with accepted academic practice. No use, distribution or reproduction is permitted which does not comply with these terms.

Diurnal fluctuations in seawater pCO_2 amplify the negative effects of ocean acidification on the biotic performance of the calcifying macroalga *Halimeda opuntia*

Zhangliang Wei[1,2,3], Yating Zhang[1,4], Fangfang Yang[1*] and Lijuan Long[1,2,3*]

[1]Chinese Academy of Sciences (CAS) Key Laboratory of Tropical Marine Bio-Resources and Ecology, South China Sea Institute of Oceanology, Chinese Academy of Sciences, Guangzhou, China, [2]Guangdong Provincial Observation and Research Station for Coastal Upwelling Ecosystem, South China Sea Institute of Oceanology (SCSIO), Shantou, China, [3]Key Laboratory of Tropical Marine Biotechnology of Hainan Province, Sanya Institute of Oceanology, South China Sea Institute of Oceanology (SCSIO), Sanya, China, [4]College of Earth and Planetary Sciences, University of Chinese Academy of Sciences, Beijing, China

Although the adverse effects of increasing atmospheric CO_2-induced ocean acidification (OA) on marine calcifying macroalgae have been widely reported, there are limited studies on how daily fluctuations in pCO_2 (pH) within shallow ecosystems influence the growth and physiological performance of these calcifiers. Therefore, a 42-day laboratory mimetic experiment to determine how growth, biological performance and related carbon and nitrogen metabolic products of the calcifying macroalga, *Halimeda opuntia* are generated in response to fluctuating pCO_2 under OA conditions (1200 ppmv) was performed. The results of present study showed that the adverse effects of OA were more determined by the adverse influence of elevated acidity (H^+) on growth rates, calcification, photosynthesis and the related biotic performance of *H. opuntia* compared with the positive effects that higher CO_2 provided. Moreover, diurnal fluctuations in pCO_2 levels [with higher (nearly 8.10) and lower pH (nearly 7.40) values during day and night times, respectively] have amplified these negative influences on *H. opuntia*. To mitigate elevated pCO_2-related stress, higher contents of free amino acids and proline were highly

secreted and likely linked to protecting the integrity of algal cellular structures. The above results contribute to increasing our understanding of the biological consequences of pCO_2 (pH) variability on calcifying *Halimeda* species and their physiological plasticity in response to further oceanic pCO_2 changes.

KEYWORDS

ocean acidification, diurnal pH fluctuations, calcifying macroalgae, biotic performance, soluble organic molecules

Introduction

Atmospheric CO_2 reached up to 412.15 ± 0.1 ppm in 2020, and preliminary data for 2021 suggest a rebound in CO_2 relative to 2020 of + 4.8% (4.2% to 5.4%) globally, which is thought to be initially and primarily caused by fossil fuel emissions and deforestation (Friedlingstein et al., 2022). The absorption of CO_2 has already caused apparent changes in the carbonate chemistry of surface seawater and is predicted to decrease by 0.44 ± 0.005 units from 1870–1899 to 2080–2099 (Masson-Delmotte et al., 2021), thus, resulting in an ongoing process and this trend called ocean acidification (OA) (Caldeira and Wickett, 2003; Gattuso et al., 2015; Masson-Delmotte et al., 2021). To date, there have been considerable studies on the impacts of OA on marine organisms, especially macroalgae, because they are important marine primary producers. Elevated pCO_2 would benefit the growth and photosynthesis of some autotrophic macroalgae, such as the economically important macroalgae, *Gracilaria lemaneiformis* (Chen et al., 2018), and *Pyropia yezoensis* (Bao et al., 2019), as well as the green macroalga *Ulva lactuca* (Olischläger and Wiencke, 2013) and *U.prolifera* (Gao et al., 2017). In addition, no obvious effects of elevated pCO_2 on *Ulva rigida* have been demonstrated (Rautenberger et al., 2015; Gao et al., 2018). However, downward trends in growth rate and pigment accumulation have been observed in *Pyropia yezoensis* (Mercado et al., 1999) and calcifying macroalgae *Halimeda* spp. (Campbell et al., 2016; Wei et al., 2020a). Egilsdottir et al. (2013) investigated the lower *m*Mg/Ca ratio of calcite and fewer structures in new fragments produced by the red calcareous coralline alga *Corallina elongata* under elevated pCO_2 (550, 750, and 1,000 ppmv) conditions. A similar phenomenon was reported by Ragazzola et al. (2012), who demonstrated that under elevated pCO_2 conditions, the *m*Mg/Ca ratio in the skeletal calcite of the coralline macroalga *Lithothamnion glaciale* was too small to maintain the stability of skeletal structures by higher ecological niche predators and additional energy to withstand bioerosion and physical erosion. These species-specific responses of macroalgae to OA (elevated pCO_2) might be attributed to the efficiency of dissolved inorganic carbon (CO_2 utilization and/or elevated acidity) (Egilsdottir et al., 2013; Qu et al., 2017; Chen et al., 2018).

The *Halimeda* genus of green calcareous macroalgae (Chlorophyta, Bryopsidales) is an ecologically important carbonate macroalgae that is widely distributed in tropical and sub-tropical reefs and lagoons (Hofmann et al., 2014; Wei et al., 2020a; Wei et al., 2020b; Wei et al., 2020c). On a global scale, carbonate sediment production by *Halimeda* species accounts for nearly 8% of the carbonate budget, at 0.15–0.4 Gt $CaCO_3$ $year^{-1}$ (Milliman, 1993; Hillis, 2001). Previous studies suggested that $CaCO_3$ biomineralization in some marine organisms, including *Halimeda* spp., is an enzymatic process that mainly uses bicarbonatefmars.2022.968740, such as the action of a Ca^{2+}/H^{+}-ATPase present in the calicoblastic epithelium (Jury et al., 2010; Wizemann et al., 2015). Studies have documented that biotic $CaCO_3$ precipitation is significantly and adversely affected by the elevation of seawater pCO_2, because the $CaCO_3$ saturation (Ω) and pH values are consequently reduced. However, moderate elevations in pCO_2 induce a higher HCO_3^- availability, which contributes to calcification and photosynthesis processes (Hofmann et al., 2014; Vogel et al., 2015; Campbell et al., 2016; Wei et al., 2020a). For instance, Yildiz et al. (2013) found that low pH (7.7) increased the relative electron transport rates (rETR) of calcified rhodophyte *Corallina officinalis*. These wide variety of responses by calcifiers is likely due to either taxonomic distinctions (Kroeker et al., 2010; Peach et al., 2017) or the interactive effects of other environmental factors, such as light intensities (Teichberg et al., 2013; Wei et al., 2020a), seawater temperature (Campbell et al., 2016), nutrient regimes (Teichberg et al., 2013) and/or pH fluctuations (Cornwall et al., 2013).

Compared with pelagic oceans, in coastal waters the magnitude of diurnal pH variation always exceeds 0.6 units owing to the CO_2 uptake by photosynthesis during the day time and CO_2 release *via* respiration and other biological activities during the night time. Moreover, the large-scale nutrient inputs from human industry and agriculture have aggravated diurnal pH variations in coastal waters (Egilsdottir

et al., 2013). Qu et al. (2017) demonstrated that under diurnal pH fluctuation conditions, from approximately 7.83 to approximately 8.44, the adverse effects of acidity (H^+) on the photosynthetic performance of the red macroalga *Gracilaria lemaneiformis* cultivated under high-density conditions that resulted from the CO_2 uptake was relatively small. Therefore, the diurnal variability of pH occurring in marine ecosystems is a non-negligible environmental factor affecting the growth and metabolic processes of marine organisms in current oceans and may have characteristic implications for predicting the responses of marine calcifiers to OA in the future (Cornwall et al., 2013). The capacity of marine calcifiers to resist significant diurnal pH/pCO_2 fluctuations may be a result of short-term acclimation (due to the phenotypic plasticity of the individual) and/or long-term adaptation (genetic endowment by the population) (Egilsdottir et al., 2013). For instance, Martin and Gattuso (2009) reported that the reduced calcification rate of coralline alga *Lithophyllum cabiochae* was observed under elevated pCO_2 conditions after 1 month, but no obvious effects were observed after acclimatization for 1 year. Thus, to accurately predict how climate changes will affect marine organisms, it is essential to preferentially determine the present detailed effects of specific environmental variabilities on marine species at both local and larger regional scales (Cornwall et al., 2013; Reusch and Boyd, 2013).

Halimeda species may be sensitive to highly variable environments. Teichberg et al. (2013) found that photosynthetic pigment concentrations in *Halimeda opuntia* were usually higher in deep than shallow waters to enhance light acquisition in areas having low light conditions, whereas carotenoids play a role in photoprotection for mitigating light stress. These phenomena have also been widely found in macroalgae that grow in tropical shallow waters (Beach et al., 2003). To date, however, there are limited studies on how daily fluctuations in pCO_2 (pH) within shallow ecosystems influence the growth and physiological performance of marine calcifiers, including *Halimeda* species. Therefore, the purpose of the present study was to examine how abiotic responses of *Halimeda* to OA are influenced by diurnal fluctuations in seawater pCO_2 (pH). It has been hypothesized that (1) periods of relatively lower CO_2/higher pH may ameliorate negative influences of OA on marine calcifiers to some degree, by providing short rest intervals that may be beneficial to their calcification (Hurd et al., 2011; Dufault et al., 2012), or (2) amplify the negative effects of OA on biotic performance owing to the extreme mean decreases in pH, especially during the night (Cornwall et al., 2013). These physiological descriptions of accurately mimicked laboratory incubation experiments will provide a better understanding of the responses of marine calcifying organisms to future global climate change-mediated alterations in pH levels.

Materials and methods

Monitoring *in situ* pH fluctuations and sample collection

For a description of the pH fluctuations at the *Halimeda* community sampling site located in the Xisha Islands, South China Sea (9.53°–9.60° N, 115.34°–115.46° E), pH values were monitored at 6:00 and 18:00 daily for 30 days (June 1 to 30, 2021) using a YSI meter (YSI Professional Plus, Yellow Springs, OH, USA). The average pH values within the *Halimeda* community at 6:00 and 18:00 were 8.43 and 7.63, respectively, indicating that the pH variability ranged by 0.80 units during the *in situ* monitoring period (Figure 1) and contributed to our subsequent experiment design (as described in 2.2). Afterwards, thalli of *H. opuntia* were sampled in a fore reef lagoon at depths ranging from 1.5–2.5 m and then transported back to the laboratory. To acclimatize the macroalgae to the experimental conditions, they were gently rinsed with filtered seawater and maintained in a large mesocosm tank (2, 000 L) that received a constant fresh sandy-filtered seawater (~45 L/min) under controlled conditions (approximately 27°C, 32 PSU, pH ~8.1, and 80 μmol photons m^{-2} s^{-1} with a 12-h: 12-h day: night cycle) for 3 weeks (Hofmann et al., 2014). Irradiance intensities were created using a combination of white FMW39TS and blue FMB5AT5 light bulbs (Arcadia, Redhill, UK) (Wei et al., 2020a). During the acclimation period, *H. opuntia* samples turned healthy green, indicating that subsequent experiments could be undertaken.

Experimental design and treatments

After the monitoring *in situ* pH fluctuations and initial acclimation period, *H. opuntia* individuals were randomly subjected to experimental manipulations of two static pCO_2 levels combined with two fluctuating pCO_2 levels within aquaria for 42 days (July 1 to August 11, 2021). For each treatment, there were eight algal thalli [110–120 g fresh weight (FW) in total] in one aquarium (30 L), and three biological replications were prepared per treatment. All the individuals were evenly spaced across the bottom of each aquarium to avoid self-shading, and the 0.45-μm-filtered seawater was replaced every 3 days. The pCO_2 (OA) was elevated by bubbling pure CO_2 mixed with ambient air automatically into the seawater in each aquarium (CE100C, Wuhan Ruihua Instrument and Equipment Ltd., Wuhan, China). The static elevated pCO_2 (OA-ST) was set at 1,200 ppmv, which is the level predicted under extreme conditions by year 2100 (Caldeira and Wickett, 2005). The fluctuations in the elevated pCO_2 concentration treatment (OA-FT) were 450

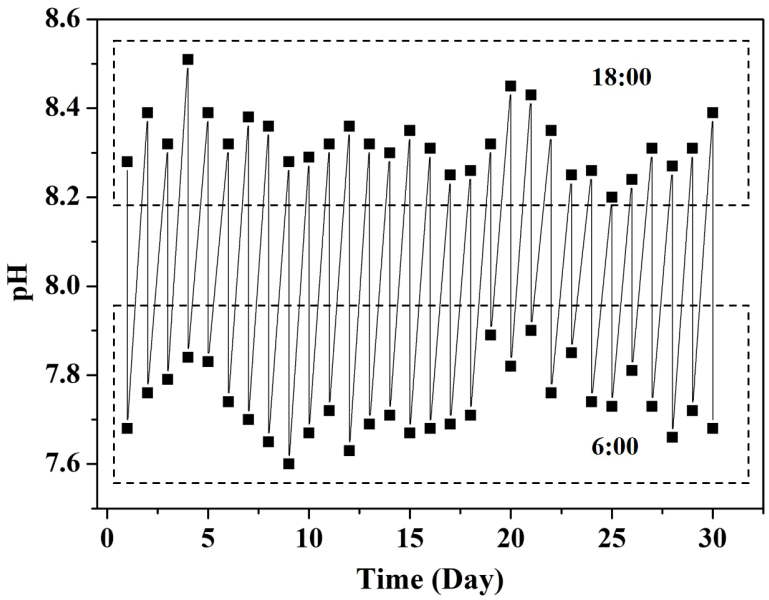


FIGURE 1
The pH measurements at 6:00 and 18:00 daily over 30 days at an average depth of 2.0 m (1.5–2.5 m) from the sampling site located in the South China Sea.

ppmv and 1,800 ppmv during day and night times, respectively. The static ambient pCO_2 concentration (AM-ST) was the current local pCO_2 level (approximately 450 ppmv), whereas the fluctuation in the ambient pCO_2 treatment (AM-FT) during day time was set at 100 ppmv, which was achieved by bubbling post-CO_2 mixed with ambient air, and the pCO_2 during the night time was set at 1,200 ppmv (Table 1).

Monitoring experimental conditions

To ensure the continuity of the culture conditions among treatments, seawater column chemistry monitoring was conducted daily at the end of the light (18:00) and dark (06:00) periods during the 42-day experiment. Seawater temperature (°C) and salinity (PSU) were determined using a handle YSI meter. The pH_{NBS} valves were obtained using an S220 pH electrode (Thermo Scientific Orion, Waltham, MA, USA) and corrected with standard buffer solution (pH 7 and 10). Total alkalinity (TA) in each aquarium was measured daily using the Gran titration method and corrected by alkalinity reference materials (CRM; Andrew Dickson Lab, Scripps Institute of Oceanography) (Metrohm 877 Titrino Plus, Titrando® Metrohm USA, Inc.) (Dickson et al., 2007). Measured seawater parameters (salinity, temperature, pH_{NBS}, and TA) were used to calculate the levels of dissolved inorganic carbon components using the Excel program CO2SYS (Pierrot et al., 2006).

TABLE 1 Experimental design of static (ST) and fluctuated (FT) current ambient pCO_2 (AM), as well as elevated pCO_2 (ocean acidification, OA) levels.

Treatments	pH_{NBS} predicted	pCO_2 set (ppmv)
AM-ST	8.10	Daytime: 450 Night-time: 450
AM-FT	8.10 ± 0.40	Daytime: 100 Night-time: 1200
OA-ST	7.70	Daytime: 1200 Night-time: 1200
OA-FT	7.70 ± 0.40	Daytime: 450 Night-time: 1800

Growth and calcification rates

The relative growth rate (*RGR*, % d^{-1}) of *H. opuntia* was calculated in accordance with the following formula (Wei et al., 2021):

$$RGR = [(lnW_t - lnW_{t-42})/42] \times 100,$$

where W_t and W_{t-42} represent the FWs obtained on the 42nd and 1st days, respectively, and 42 represents the time interval between the two sampling days.

The instantaneous net calcification rates (G_{net}) was estimated using the alkalinity anomaly technique on the 42nd day (Campbell et al., 2016). The algal fragments (5.0 g) were incubated in acrylic transparent bottles (1.0 L) containing filtered seawater under four experimental conditions with an electro-magnetic stirrer. The calculation of G_{net} was based on the changes in TA after an 8-h incubation using the following equation:

$$G_{net} = 0.5p \times (TA_0 - TA_n) \times V/(FW \times t),$$

where G_{net} (μmol $CaCO_3$ g FW^{-1} h^{-1}) represents the net calcification rate of whole thalli *H. opuntia*, *p* represents the seawater density (1.025 kg L^{-1}), TA_0 and TA_n represent the initial TA and TA after *n* hours of culture (8 h), *V* represents the seawater volume (1.0 L), and FW and *t* represent the algal fresh weight (5.0 g) and incubation time (8 h), respectively. When $G_{net} > 0$, calcification occurs, whereas when $G_{net} < 0$, dissolution in $CaCO_3$ mineralogy occurs.

F_v/F_m and pigment contents

The photosystem II (PSII) maximum quantum yield (F_v/F_m) value of *H. opuntia* was measured by a Diving-PAM II fluorometer (Heinz Walz GmbH, Effeltrich, Germany). After 20 min of dark adaptation, F_v/F_m was obtained using red light as the modulated light (5,000 μmol photons m^{-2} s^{-1}, 0.6 s). Together with photosynthetic performance, 200 mg FW of fragment (n = 3) was sampled and immediately frozen in liquid nitrogen for pigment content measurement. Samples were finely ground in 10 ml 90% acetone and extracted at 4°C for 24 h under dark conditions. Afterwards, the homogenate was centrifuged at 4,000 rpm for 10 min (Eppendorf centrifuge 5810 R, Hamburg, Germany). The pigment contents, including chlorophyll (Chl) *a*, *b* and carotenoid concentrations, were measured using the supernatant, as described by Ritchie (2008).

Measurement of total carbon and total nitrogen contents

The total organic carbon (TC_{org}) and total nitrogen (TN) contents (dry weight, % DW) in *Halimeda* tissues subjected to the four treatments were determined at the end of the experiment. The samples (n = 3) were washed five times and then dried to constant weight at 60°C. Afterwards, all the samples were finely ground and determined by a CHN Elemental Analyzer (Flash EA300, Thermo Scientific, Milan, Italy).

Measurement of enzyme activities

Samples (200 mg FW of each, n = 3) used to determine enzymatic activities, external carbonic anhydrase activity (eCAA) and nitrate reductase activity (NRA), were collected at the end of the experiment. The algal fragments were ground in 5.0 mL 20-M veronal buffer (pH 8.3) for eCAA and 0.1 M phosphate buffer (pH 7.5) for NRA. The eCAA and NRA levels in the supernatant were determined using algal enzymatic ELISA Kits (Mlbio, Shanghai, China) following the appropriate manufacturer's instructions. Both enzyme activities were corrected using an optical density (OD) standard curve.

Soluble carbohydrate, malondialdehyde, proline and free amino acids

For the determination of the algal soluble carbohydrate (SC) content, 200 mg FW of each sample was collected and ground in 10 ml filtered seawater. After 10 min of centrifuging (5,000 rpm), the SC level in the supernatant was determined using the phenol–sulfuric acid method (Kochert, 1978). The malondialdehyde (MDA) occurrence was measured because it is a potential indicator of lipid peroxidation encountered after environmental stresses (Wei et al., 2020c). In total, 500 mg FW of algal tissues was sampled and ground in 10 ml of 10% trichloroacetic acid, and then centrifuged at 4, 000 rpm for 10 min. The supernatant was collected and MDA was measured as described by Hodges et al. (1999).

To obtain further insights into the algal physiological regulation after exposure to diurnal fluctuations in seawater pCO_2, the proline and free amino acids (FAAs) were analyzed for maintaining the photosynthetic system functioning and protecting the membranes from various damages (Wei et al., 2020a). At the end of the experiment, 500 mg FW of algal tissue for proline was weighed and finely ground in 5 ml 3% sulfosalicylic acid. The homogenate was shaking for 10 min under 100°C conditions. After 10 min of centrifugation (3,000 rpm), the proline content was measured in the supernatant as described by Shan et al. (2007). To determine FAAs, 200 mg FW of each sample was ground in 5 ml PBS buffer (pH 7.4), and FAAs was measured in the supernatant of the aqueous extract using an algal FAAs ELISA Kit (Mlbio, Shanghai, China), as described in the manufacturer's instructions.

Statistical analyses

All the data in this study were presented as a triplicate mean ± standard deviation (mean ± SD) (n = 3). The figures were created using Origin 8.0 software (Origin Lab Corp., Northampton, MA, USA). All the statistical analyses were conducted using IBM SPSS Statistics 20 software (SPSS Inc., Chicago, IL, USA). A one-way analysis was conducted to determine the differences among the four treatments. Tukey's Honestly Significant Differences was used to make *post hoc* comparisons (95% confidence level). Differences by different uppercase and lowercase letters in Figure 2–7 were considered to be significant at $P < 0.05$ and extremely significant at $P < 0.01$.

Results

Seawater monitoring

The average pH_{NBS} values in static ambient pCO_2 and elevated pCO_2 were 8.10 ± 0.01 and 7.71 ± 0.01, respectively, regardless of day or night time, whereas the average pH_{NBS} values for the two fluctuating pCO_2 levels were 8.43 ± 0.01 and 7.72 ± 0.02 ($P < 0.01$), respectively, in day time and 8.08 ± 0.01 and 7.42 ± 0.02 ($P < 0.01$), respectively, in night time. Nevertheless, the elevated pCO_2 altered the DIC components and aragonite saturation state (Ω_{Arag}) in seawater ($P < 0.01$). In contrast with static ambient (AM-ST) pCO_2 treatments, the mean CO_2 and HCO_3^- concentrations in static elevated (OA-ST) pCO_2 treatments increased from 14.6–15.3 μmol kg^{-1} to 39.9–41.5 μmol kg^{-1} and 1,898.7–1,940.8 μmol kg^{-1} to 2,172.2–2,196.0 μmol kg^{-1}, respectively, whereas CO_3^{2-} concentrations decreased from 184.2–185.9 μmol kg^{-1} to 87.4–88.1 μmol kg^{-1} ($P < 0.01$). The average CO_2, HCO_3^- and CO_3^{2-} concentrations in fluctuated ambient (AM-FT) and elevated (OA-FT) pCO_2 treatments differed significantly among treatments, as well as between day and night times ($P < 0.01$) (Table 2). The Ω_{Arag} values were lower in elevated pCO_2 treatments, ranging from 0.72 to 1.44, and the highest Ω_{Arag} values were obtained in AM-FT during the day time (5.47 ± 0.18).

Growth and calcification rates of *H. opuntia*

After 42-day experimental exposure, the elevated pCO_2 and daily fluctuations in the pCO_2 of seawater had significant effects on the growth rate of *H. opuntia* (Figure 2). The highest *RGR* was recorded in AM-ST, at 0.266% ± 0.012% d^{-1}. The *RGR* under elevated pCO_2 conditions decreased by 22.02%–44.57% in contrast with those in AM-ST. Notably, daily fluctuating pCO_2 amplified the negative effects on growth rates at two pCO_2 concentration levels. In addition, the *RGR* values in AM-FT (0.226% ± 0.009% d^{-1}) and OA-ST (0.218% ± 0.011% d^{-1}) were not significantly different ($P > 0.05$) (Figure 2).

The G_{net} differed significantly among the four treatments under both light and dark conditions ($P < 0.05$) (Figure 3).

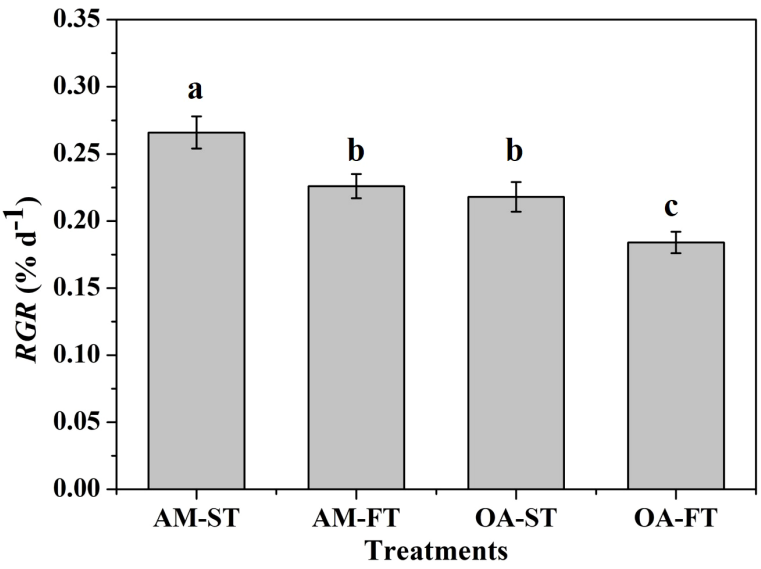


FIGURE 2
The relative growth rates (*RGR*, % d^{-1}) of *Halimeda opuntia* (mean ± SD, n = 3) exposed to the four treatments for 42 days (AM, ambient pCO_2 concentration; OA, ocean acidification; ST, static; FT, fluctuating). Significant differences among the treatments are indicated by different uppercase and lowercase letters, respectively (Tukey's test, P<0.05).

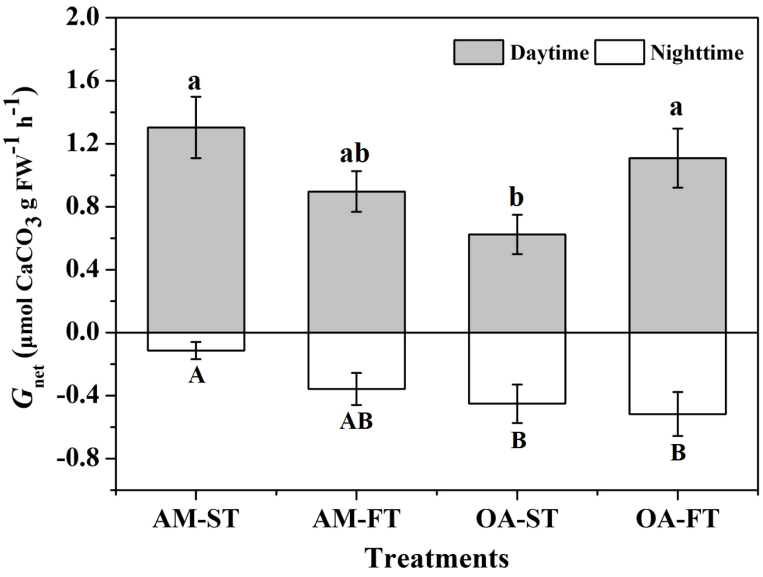


FIGURE 3
The net calcification rates (G_{net}, μmol $CaCO_3$ g FW^{-1} h^{-1}) of *Halimeda opuntia* (mean ± SD, n = 3) under light and dark conditions after exposure to four pCO_2 treatments for 42 days. Significant differences among the treatments are indicated by different uppercase and lowercase letters, respectively (Tukey's test, P<0.05).

Under light conditions, the greatest net calcification levels occurred in the four treatments. The G_{net} of *H. opuntia* in AM-ST, AM-FT and OA-FT did not change significantly, ranging from 0.897 to 1.303 μmol $CaCO_3$ g FW^{-1} h^{-1} (P > 0.05). The lowest G_{net} values were obtained in OA-ST (0.624 ± 0.124 μmol $CaCO_3$ g FW^{-1} h^{-1}) owing to the elevated pCO_2. Under dark conditions, the greatest net dissolution in $CaCO_3$ mineralogy occurred, as shown in Figure 3. The lowest dissolution rate (–0.114 ± 0.054 μmol $CaCO_3$ g FW^{-1} h^{-1}) was measured in AM-ST. However, elevated pCO_2 amplified the negative $CaCO_3$ dissolution rate, and the greatest dissolution rate was –0.517 ± 0.139 μmol $CaCO_3$ g FW^{-1} h^{-1} in OA-FT after dark exposure.

Chlorophyll fluorescence and pigment contents

There were significant direct effects of elevated pCO_2 and daily fluctuating pCO_2 on F_v/F_m and Chl-*a* content (P < 0.05). The lowest F_v/F_m was in AM-FT, with a mean value of 0.562 ± 0.005. Compared with the F_v/F_m (0.630 ± 0.006) in AM-ST, elevated pCO_2 decreased the F_v/F_m to the 0.614–0.618 range (Figure 4A). Similar to the F_v/F_m variations, the lowest Chl-*a* content was in AM-FT, with a mean value of 175.79 ± 12.62 μg g^{-1} FW, and there were no obvious Chl-*a* variations in the other three treatments (194.33–225.61 μg g^{-1} FW) (Figure 4B). Across all the treatments, photosynthetic Chl-*b* and carotenoid contents were not notably influenced, having 134.99–157.49 μg g^{-1} FW and 75.33–87.78 μg g^{-1} FW ranges, respectively (Figures 4C, D).

Tissue total carbon (TC_{org}) and nitrogen (TN) contents

Total organic carbon (TC_{org}) and total nitrogen (TN) in *H. opuntia* tissues were significantly affected by elevated pCO_2 and daily fluctuating pCO_2 (P < 0.05) (Figure 5). There were no notable differences between the ambient pCO_2 treatments, regardless of static or fluctuating pCO_2 concentrations (P > 0.05). However, an elevated pCO_2 significantly stimulated TC_{org} accumulation by 8.93%–24.62% compared with the average TC_{org} in both AM treatments. The highest TC_{org} content occurred in OA-ST (17.79% ± 0.77% DW). The TN contents did not significantly vary among the AM-ST, AM-FT and OA-ST treatments (1.28%–1.39% DW) (P > 0.05), but it significantly decreased in OA-FT to 0.98% ± 0.07% DW (P < 0.01) (Figure 5).

Enzymatic activities (carbonic anhydrase and nitrate reductase)

There were no obvious effects of static and fluctuating pCO_2 on the eCAA among the four treatments (3.280–3.828 IU mg^{-1} FW) (P > 0.05) (Figure 6). Compared with the (NRA in *H. opuntia* tissues incubated under ambient pCO_2 conditions (2.535–2.784 pg

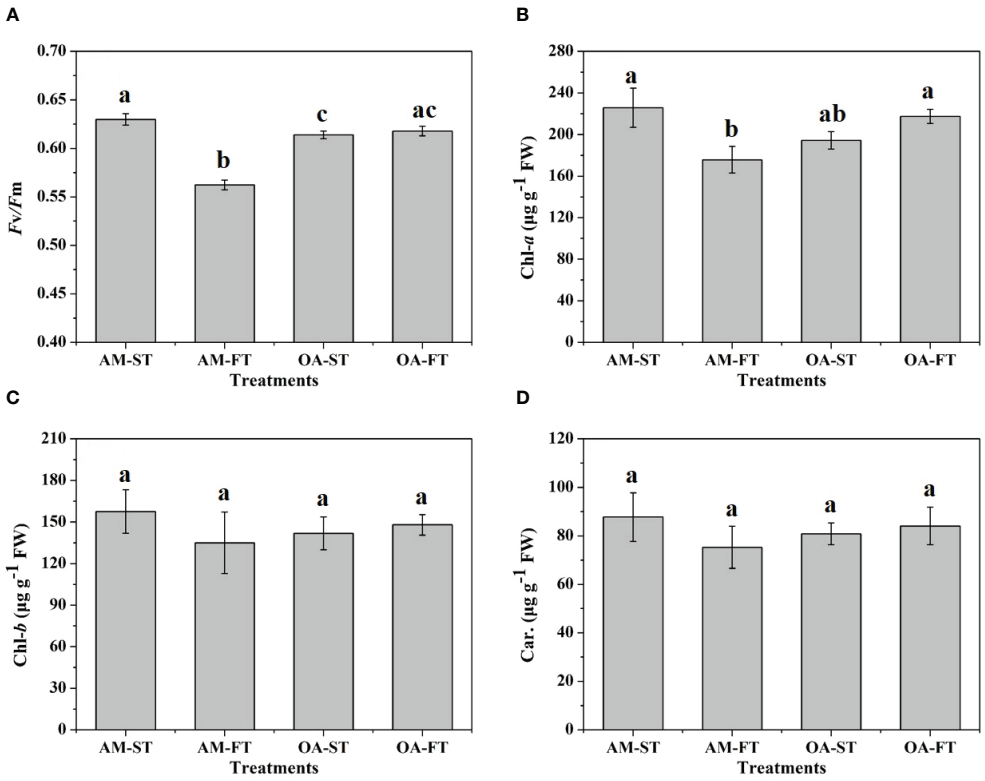


FIGURE 4
Variations in photosynthetic maximum quantum yields (F_v/F_m) **(A)** and in chlorophyll (Chl)*a* **(B)**, *b* **(C)** (μg g^{-1} FW) and carotenoid (Car., μg g^{-1} FW) contents **(D)** of *Halimeda opuntia* (mean ± SD, n = 3) in four pCO_2 treatments. Significant differences among the treatments are indicated by different uppercase and lowercase letters, respectively (Tukey's test, P<0.05).

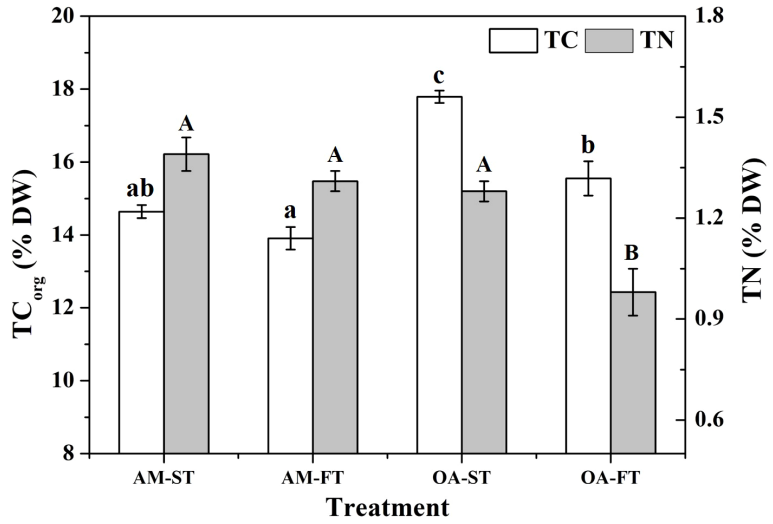


FIGURE 5
Variations in tissue total organic carbon (TC_{org}, % DW) and nitrogen (TN, % DW) from the tissues of *Halimeda opuntia* (mean ± SD, n = 3) in four pCO_2 treatments. Significant differences among the treatments are indicated by different uppercase and lowercase letters, respectively (Tukey's test, P<0.05).

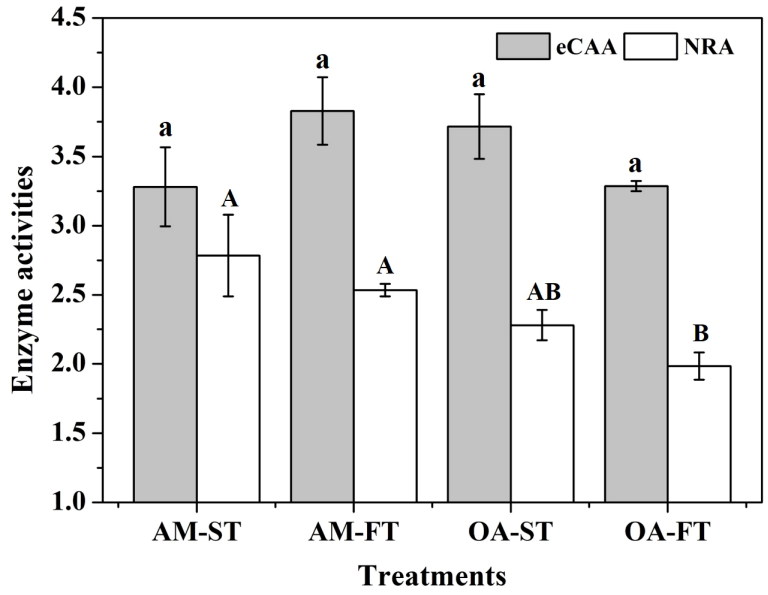


FIGURE 6
Mean (± SD, n = 3) external carbonic anhydrase activity (eCAA, IU mg^{-1} FW) and nitrate reductase activity (NRA, pg mg^{-1} FW) levels in four pCO_2 treatments after a 42-day incubation. Significant differences among the treatments are indicated by different uppercase and lowercase letters, respectively (Tukey's test, P<0.05).

mg^{-1} FW), the NRA decreased under both static and fluctuating elevated pCO_2 conditions by 16.63%–34.01%, and the lowest NRA was obtained in OA-FT, having an average value of 1.984 ± 0.298 pg mg^{-1} FW ($P < 0.05$) (Figure 6).

Soluble carbohydrate, malondialdehyde, proline and free amino acids contents

The soluble cellular compositions were significantly affected by elevated pCO_2 and daily fluctuations ($P < 0.01$) (Figure 7). The SC level decreased by 32.38%–67.65% under elevated and fluctuating pCO_2 conditions, compared with the SC in AM-ST, and the lowest average SC content occurred in AM-FT at 2.12 ± 0.01 μg mg^{-1} FW ($P < 0.01$) (Figure 7A). Under elevated pCO_2 conditions (OA-ST), the MDA content increased to 2.74 ± 0.04 μg mg^{-1} FW ($P < 0.01$). Moreover, fluctuating pCO_2 amplified the effects of abiotic stress on MDA, which increased to 3.98 ± 0.05 μg mg^{-1} FW and 3.69 ± 0.06 μg mg^{-1} FW in AM-FT and OA-FT, respectively (Figure 7B). The proline levels increased notably under elevated and fluctuating pCO_2 conditions ($P < 0.01$). The lowest average proline contents was obtained in AM-ST (2.24 ± 0.06 μg mg^{-1} FW), whereas the highest proline content occurred in OA-FT (4.31 ± 0.08 μg mg^{-1} FW) (Figure 7C). The FAA content significantly increased in the elevated pCO_2 treatment (OA-ST, 3.19 ± 0.09 μg mg^{-1} FW) compared with in AM-ST (2.50 ± 0.06 μg mg^{-1} FW). Furthermore, the effects on FAA were enhanced by the two fluctuating pCO_2 levels ($P < 0.01$), and the highest average FAA content occurred in OA-FT (4.46 ± 0.05 μg mg^{-1} FW) (Figure 7D).

Discussion

The anthropogenic elevation of atmospheric CO_2 induced OA, and a lower aragonite saturation (Ω_{Arag}) has been widely reported to negatively affect the growth and calcification processes of marine calcifiers (Campbell et al., 2016; Wei et al., 2020a). Our results demonstrated that the effects of OA were increased by the adverse influence of elevated acidity (H^+) on growth rates, calcification, photosynthesis and the related biotic performance of *H. opuntia* compared with the positive effects of a higher CO_2 level. Moreover, diurnal fluctuations in pCO_2 levels (with a higher pH during the day time and a lower pH during the night time) amplified these negative influences on *H. opuntia*. Similar with our previous study, the growth rates of *Halimeda cylindracea* and *Halimeda lacunalis* decreased significantly by 6.84%–86.70% under elevated pCO_2 (1,000–1,600 ppmv) conditions (Wei et al., 2020a). In contrast with non-calcifying macroalgae, such as *G. lemaneiformis* (higher pCO_2-grown plants), the increased pCO_2 under OA conditions alleviates dissolved carbon limitations and leads to an enhancement in *RGR* (Zou et al., 2004). In this study, *H. opuntia* exhibited negative growth owing to the extremes in the elevated pCO_2 variations. Because the photosynthetic rate of this alga has been completely saturated at the present seawater pCO_2 (Zou et al.,

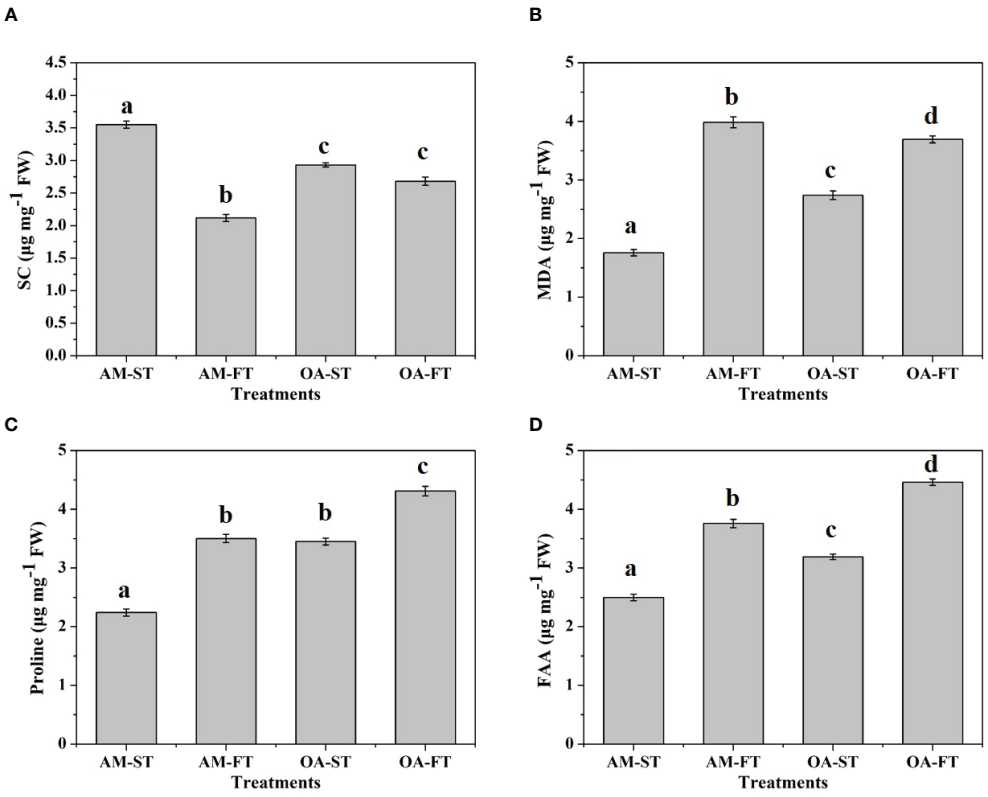


FIGURE 7
Variations in soluble carbohydrate (SC, μg mg^{-1} FW) **(A)**, malondialdehyde (MDA, μg mg^{-1} FW) **(B)**, proline (μg mg^{-1} FW) **(C)** and free amino acids (FAA, μg mg^{-1} FW) **(D)** contents of *Halimeda opuntia* (mean ± SD, n = 3) in four pCO_2 treatments after a 42-day incubation. Significant differences among the treatments are indicated by different uppercase and lowercase letters, respectively (Tukey's test, P<0.05).

2004), the negative effects of elevated pCO_2 were mostly attributed to the decreased pH, which disturbs the acid–base balance on the cell surface (Flynn et al., 2012). Subsequently, more metabolic energy has to be expended to resist this interference, resulting in a reduced growth rate (Xu et al., 2017).

The G_{net} of *H. opuntia* was adversely affected by elevated pCO_2, which was in keeping with the results of previous studies. Wei et al. (2020a) reported that the G_{net} values of *H. cylindracea* and *H. lacunalis* decrease by 51.78%–62.29% owing to high pCO_2 conditions (1,000–1,600 ppmv). Similarly, Campbell et al. (2016)

TABLE 2 Measured seawater parameters of pH (NBS scale), total alkalinity (TA), salinity and temperature, as well as the calculated carbon chemistry of dissolved inorganic carbon (DIC) components (CO_2, HCO_3^- and CO_3^{2-}) using CO2SYS (Pierrot et al., 2006) in each treatment determined at the end of each light (18:00) and dark (06:00) period during the 42-day experiment.

Treatments		pH_{NBS}	Temperature(°C)	TA(μmol kg^{-1})	CO_2(μmol kg^{-1})	HCO_3^-(μmol kg^{-1})	CO_3^{2-}(μmol kg^{-1})	Ω_{Arag}
AM-ST	Day	8.09 ± 0.01	27.1 ± 0.0	2384 ± 16	15.3 ± 0.2	1940.8 ± 3.5	184.2 ± 1.2	3.01 ± 0.19
	Night	8.10 ± 0.01	27.0 ± 0.1	2388 ± 17	14.6 ± 0.1	1898.7 ± 2.5	185.9 ± 0.8	3.03 ± 0.18
AM-FT	Day	8.43 ± 0.01	27.0 ± 0.0	2411 ± 18	5.77 ± 0.3	1601.8 ± 3.1	335.2 ± 0.9	5.47 ± 0.18
	Night	7.72 ± 0.02	27.1 ± 0.1	2384 ± 15	40.2 ± 0.5	2172.2 ± 2.4	88.1 ± 1.3	1.44 ± 0.09
OA-ST	Day	7.71 ± 0.01	27.0 ± 0.1	2406 ± 19	41.5 ± 0.6	2196.0 ± 3.7	87.4 ± 1.1	1.43 ± 0.07
	Night	7.72 ± 0.01	27.0 ± 0.0	2394 ± 17	39.9 ± 0.4	2161.4 ± 2.3	88.3 ± 1.7	1.44 ± 0.06
OA-FT	Day	8.08 ± 0.01	27.0 ± 0.1	2417 ± 10	15.9 ± 0.3	1974.7 ± 1.8	184.0 ± 2.1	3.01 ± 0.14
	Night	7.42 ± 0.02	27.1 ± 0.0	2379 ± 18	86.5 ± 0.7	2243.3 ± 2.7	43.9 ± 0.8	0.72 ± 0.03

Data are the means ± SDs of three measurements.

also demonstrated that the calcification rates of *H. opuntia* and *Halimeda simulans* decline by 15% and 50%, respectively, owing to high pCO_2 concentration (2,400 ppmv). However, other influences were verified for some calcareous organisms, which displayed inconspicuous changes to cope with elevated pCO_2. For instance, Ries et al. (2009) highlighted that the G_{net} of *Halimeda incrassata* only decreases under extremely high pCO_2 (2593 ppmv) conditions, with a Ω_{Arag} value of 0.9. Such differences may be attributed to species-specific acclimation and anti-stress capabilities (Campbell et al., 2016; Wei et al., 2020a, c). The CO_2 enrichment-lowered Ω_{Arag} contributes to the dissolution of micro-anhedral calcareous structures among algal interutricular spaces, especially during dark incubation periods (Andersson et al., 2009). This may cause *Halimeda* to be more susceptible and decomposable than other species (Hofmann et al., 2014). The greatest net dissolution of a calcareous interutricular structure was recorded during a dark period under higher pCO_2 conditions owing to a low Ω_{Arag} and algal respiration (Raven, 2011). This is consistent with previous findings that $CaCO_3$ dissolution occurs in coralline algal species during dark periods, such as in *Corallina pilulifera* incubated at 1,600 ppmv (Gao et al., 1993) and in *Lithothamnion glaciale* grown at 700 ppmv (Budenbender et al., 2011). This addresses the critical influence of Ω_{Arag} status on algal mineralogy (Wei et al., 2020a).

An elevated pCO_2 concentration in surface seawater can promote the photosynthetic processes for some non-calcifying macroalgae, such as *G. lemaneiformis* (Wei et al., 2021), *Pyropia haitanensis* (Chen et al., 2017), *Hizikia fusiformis* (Zou et al., 2011) and *G. chilensis* (Gao et al., 1993), owing to the increased availability of DIC resources. Nevertheless, here, *H. opuntia* showed a negative PSII photochemical efficiency (F_v/F_m) in response to the effects of OA and daily shifts in pCO_2 (pH), which may be caused by the slightly increased the eCAA under high pCO_2 conditions. This suggested that CO_2 concentration may increase in the periplasmic space and lead to enhancement of DIC uptake from environment, although reduced intracellular Ci (DIC) pools (Raven et al., 2012) and poorly passive CO_2 diffusion (Elzenga and Prins, 1989; Miedema and Prins, 1991). Similar conclusions have been made for other *Halimeda* species. Sinutok et al. (2012) found notable declines (50%–70%) of F_v/F_m values in *Halimeda macroloba* and *H. cylindracea* after a 35-day exposure to elevated pCO_2 condition (1,200 ppmv, Ω_{Arag}: 1.97 ± 0.02). Concurrently, a decline in the Chl-*a* contents under static/fluctuating low pH conditions indicated the down-regulation of Chl accumulation or pigment degradation, whereas there were limited effects of elevated pCO_2 on Chl-*b* and carotenoid contents. The lack of changes in photosynthetic performance and pigment contents in *H. opuntia* under fluctuating OA condition was most probably owing to 1) their high tolerance and increased retention of phenotypic plasticity to the dramatic variations in pCO_2 (pH), because they regularly experience daily fluctuations in pH in the coastal regions; and/or 2) a higher daytime pH, which provides a period of suitable conditions for macroalgal photosynthesis (Cornwall et al., 2013).

An elevated/fluctuating pCO_2 is predicted to modulate TC_{org} and TN accumulations in *H. opuntia* tissues. The changes in TC_{org} and TN contents may be due to variations in the characterizations of enzymatic activities (Wei et al., 2021). At static higher pCO_2 levels, the eCAA in chloroplast slightly increased (although there was no statistically significant difference), and this may accelerate the interconversion between CO_2 andHCO_3^-, guaranteeing soluble carbohydrate synthesis at the carboxylation site (Vidal-Dupiol et al., 2013). Meanwhile, the SC synthesis was enhanced by the positive effects of eCAA activity, which played a role in an improvement in the irradiance harvesting capacity and up-regulation of the photosynthetic electron transport chain (Van Oijen et al., 2004). Moreover, a discrepancy in the average NRA was negatively influenced by diurnal fluctuating pCO_2, leading to a noticeable decrease in N accumulations in algal tissues (Figure 6). When NRA decreases, variations in elevated pCO_2 can promote the ammonium to nitrate conversion process, leading to the formation of glutamine and thereby inhibiting NRA (Stitt and Krapp, 1999). Such a response would demand less energy for the formation of ammonium than nitrate and allow this macroalga to allocate more energy for regulating eCAA and C acquisition (Losada and Guerrero, 1979; Syrett, 1981). These findings indicate that the elevated pCO_2 caused modifications in algal C vs. N metabolism, and the increased variability in pCO_2 amplified these influences, which was confirmed by eCAA and NRA driven activities.

The MDA content is used to evaluate lipid peroxidation levels in cell systems (Hodges et al., 1999). Under elevated pCO_2 conditions, *H. opuntia* displayed greater oxidative lipid degradation associated with higher MDA contents, and this adverse physiological performance was amplified in both fluctuating pCO_2 treatments. This was in agreement with the decreased algal growth and lower photosynthetic activity (F_v/F_m) levels. The SC synthesis declined sharply under elevated and fluctuating pCO_2 conditions due to the depression of PSII activities (Wei et al., 2021), which would in turn down-regulate the irradiance harvesting capacity and photosynthetic activities (Van Oijen et al., 2004). Therefore, it is essential for *H. opuntia* to undergo appropriate adjustments to cope with the elevated pCO_2 pressure (Wei et al., 2020a; Wei et al., 2020c; Wei et al., 2021). Our findings indicate that soluble organic molecules (FAAs and proline) are highly secreted and likely linked to protecting the integrity of cellular structures (Sun et al., 2013; Chen et al., 2018; Wei et al., 2020a; Wei et al., 2020c). Thus, as the experiment progressed, greater contents of proline and FAA were obtained in OA, and these effects were strengthened under the two fluctuating pCO_2 conditions, which played a positive role in maintaining the photosynthetic system's function and in protecting membrane integrity (Xiong et al., 2002). This explanation is corroborated by a previous analysis by Wei

et al., (2020a); Wei et al., 2021), who suggested that these modifications give rise to the internal re-partitioning of C and N in *Halimeda* tissues.

In summary, this study attempted to mimic *in situ* pH (pCO_2) changes, and it demonstrated that a static elevated pCO_2 level has adverse effects on the growth, calcification, photosynthesis and other C vs. N metabolic activities of *H. opuntia*. Moreover, diurnal fluctuations in pCO_2 amplified these negative influences of OA, especially during the night time. Under the stress of elevated and/or fluctuating pCO_2, higher MDA contents were obtained, which indicates that the cellular membranes were damaged. This generated a dynamic balance in *H. opuntia* incubated under environmental stress conditions, and it is reasonable to suggest that high contents of proline and FAA, in combination with related-enzymatic activities, play positive roles in protecting cellular structures and mitigating adverse influences. The results of the present study increase our understanding of the biological consequences of pH (pCO_2) variability on specific marine calcifiers and their physiological plasticity under future OA conditions.

Data availability statement

The original contributions presented in the study are included in the article/supplementary material. Further inquiries can be directed to the corresponding authors.

Author contributions

The authors thank all the staff, and particularly LL who conceived and designed the experiments. ZW performed the experiments and wrote the paper. FY analyzed the data, and YZ contributed materials and analysis tools. LL agrees to serve as the author responsible for contact and communication. All authors contributed to the article and approved the submitted version.

Funding

This research was supported by the Science and Technology Program of Guangzhou, China (202102021228), the National Natural Science Foundation of China (42006129), the National Key Research and Development Program of China (2021YFC3100500, 2021YFF0502801), Science and Technology Planning Project of Guangdong Province of China (2021B1212050023), Key Programs of the Chinese Academy of Sciences (E1YD5J01), and the Special Research Assistant Grant Program of the Chinese Academy of Sciences.

Acknowledgments

We thank the staff of the Tropical Marine Biological Research Station in Hainan, Chinese Academy of Sciences for providing logistical support. Thanks are also due to the editors and reviewers for their valuable comments and suggestions.

Conflict of interest

The authors declare that the research was conducted in the absence of any commercial or financial relationships that could be construed as a potential conflict of interest.

Publisher's note

All claims expressed in this article are solely those of the authors and do not necessarily represent those of their affiliated organizations, or those of the publisher, the editors and the reviewers. Any product that may be evaluated in this article, or claim that may be made by its manufacturer, is not guaranteed or endorsed by the publisher.

References

Andersson, A. J., Kuffner, I. B., Mackenzie, F. T., Jokiel, P. L., Rodgers, K. S., and Tan, A. (2009). Net loss of CaCO3 from coral reef communities due to human induced seawater acidification. *Biogeosciences* 6, 2163–2182. doi: 10.5194/bg-6-1811-2009

Bao, M., Wang, J., Xu, T., Wu, H., Li, H., and Xu, J. (2019). Rising CO2 levels alter the responses of the red macroalga pyropia yezoensis under light stress. *Aquaculture* 501, 325–330. doi: 10.1016/j.aquaculture.2018.11.011

Beach, K., Walters, L., Vroom, P., Smith, C., Coyer, J., and Hunter, C. (2003). Variability in the ecophysiology of halimeda spp. (Chlorophyta, bryopsidales) on conch reef, Florida keys, USA. *J. Phycol.* 39 (4), 633–643.

Budenbender, J., Riebesell, U., and Form, A. (2011). Calcification of the Arctic coralline red algae lithothamnion glaciale in response to elevated CO2. *Mar. Ecol.-Prog. Ser.* 441, 79–87. doi: 10.3354/meps09405

Caldeira, K., and Wickett, M. E. (2003). Oceanography: anthropogenic carbon and ocean pH. *Nature.* 425 (6956), 365. doi: 10.1038/425365a

Caldeira, K., and Wickett, M. E. (2005). Ocean model predictions of chemistry changes from carbon dioxide emissions to the atmosphere and ocean. *J. Geophys. Res.-Oceans.* 110 (C9), C09S04. doi: 10.1029/2004JC002671

Campbell, J. E., Fisch, J., Langdon, C., and Paul, V. J. (2016). Increased temperature mitigates the effects of ocean acidification in calcified green algae (Halimeda spp.). *Coral Reefs.* 35, 357–368. doi: 10.1007/s00338-015-1377-9

Chen, B., Zou, D., Du, H., and Ji, W. (2018). Carbon and nitrogen accumulation in the economic seaweed gracilaria lemaneiformis affected by ocean acidification and increasing temperature. *Aquaculture.* 482, 176–182. doi: 10.1016/j.aquaculture.2017.09.042

Chen, B., Zou, D., and Yang, Y. (2017). Increased iron availability resulting from increased CO2 enhances carbon and nitrogen metabolism in the economical marine red macroalga pyropia haitanensis (Rhodophyta). *Chemosphere* 173, 444–451. doi: 10.1016/j.chemosphere.2017.01.073

Cornwall, C. E., Hepburn, C. D., McGraw, C. M., Currie, K. I., Pilditch, C. A., Hunter, K. A., et al. (2013). Diurnal fluctuations in seawater pH influence the response of a calcifying macroalga to ocean acidification. *Proc. R. Soc B-Biol. Sci.* 280 (1772), 20132201. doi: 10.1098/rspb.2013.2201

Dickson, A. G., Sabine, C. L., and Christian, J. R. (2007). *Guide to best practices for ocean CO2 measurements, in PICES special publication* (Sidney, Canada: North Pacific Marine Science Organization), 67–81.

Dufault, A. M., Cumbo, V. R., Fan, T. Y., and Edmunds, P. J. (2012). Effects of diurnally oscillating pCO2 on the calcification and survival of coral recruits. *Proc. R. Soc B-Biol. Sci.* 279, 2951–2958. doi: 10.1098/rspb.2011.2545

Egilsdottir, H., Noisette, F., Noël, L. M. L. J., Olafsson, J., and Martin, S. (2013). Effects of pCO2 on physiology and skeletal mineralogy in a tidal pool coralline alga corallina elongata. *Mar. Biol.* 160, 2103–2112. doi: 10.1007/s00227-012-2090-7

Elzenga, J. T. M., and Prins, H. B. A. (1989). Light-induced polar pH changes in leaves of elodea canadensis. i. effects of carbon concentration and light intensity. *Plant Physiol.* 91, 62–67. doi: 10.1104/pp.91.1.62

Flynn, K. J., Blackford, J. C., Baird, M. E., Raven, J. A., Clark, D. R., Beardall, J., et al. (2012). Changes in pH at the exterior surface of plankton with ocean acidification. *Nat. Clim. Change* 2, 510–513. doi: 10.1038/nclimate1489

Friedlingstein, P., Jones, M., O'Sullivan, M. W., Andrew, R. M., Bakker, D. C. E., Hauck, J., et al. (2022). Global carbon budget 2021. *Earth Syst. Sci. Data* 14, 1917–2005. doi: 10.5194/essd-14-1917-2022

Gao, K., Aruga, Y., Asada, K., and Kiyohara, M. (1993). Influence of enhanced CO2 on growth and photosynthesis of the red algae gracilaria sp. and g. chilensis. *J. Appl. Phycol.* 5, 563–571. doi: 10.1007/BF02184635

Gao, G., Clare, A. S., Rose, C., and Caldwell, G. S. (2018). Ulva rigida in the future ocean: potential for carbon capture, bioremediation, and biomethane production. *GCB. Bioenergy.* 10, 39–51. doi: 10.1111/gcbb.12465

Gao, G., Liu, Y., Li, X., Feng, Z., Xu, Z., Wu, H., et al. (2017). Expected CO2-induced ocean acidification modulates copper toxicity in the green tide alga ulva prolifera. *Environ. Exp. Bot.* 135, 63–72. doi: 10.1016/j.envexpbot.2016.12.007

Gattuso, J. P., Magnan, A., Billé, R., Cheung, W. W. L., Howes, E. L., Joos, F., et al. (2015). Contrasting futures for ocean and society from different anthropogenic CO2 emissions scenarios. *Science.* 349 (6243), 45–55.

Hillis, L. W. (2001). The calcareous reef alga halimeda (Chlorophyta, byropsidales): a cretaceous genus that diversified in the Cenozoic. *Paleogeogr. Paleoclimatol. Paleoecol.* 166 (1–2), 89–100. doi: 10.1016/S0031-0182(00)00203-0

Hodges, D. M., DeLong, J. M., Forney, C. F., and Prange, R. K. (1999). Improving the thiobarbituric acid-reactive-substances assay for estimating lipid peroxidation in plant tissues containing anthocyanin and other interfering compounds. *Planta.* 207, 604–611. doi: 10.1007/s004250050524

Hofmann, L. C., Heiden, J., Bischof, K., and Teichberg, M. (2014). Nutrient availability affects the response of the calcifying chlorophyte halimeda opuntia (L.) J.V. lamouroux to low pH. *Planta.* 239 (1), 231–242.

Hurd, C. L., Cornwall, C. E., Currie, K. I., Hepburn, C. D., McGraw, C. M., Hunter, K. A., et al. (2011). Metabolically-induced pH fluctuations by some coastal calcifiers exceed projected 22nd century ocean acidification: a mechanism for differential susceptibility? *Glob. Change Biol.* 17 (10), 3254–3262. doi: 10.1111/j.1365-2486.2011.02473.x

Jury, C. P., Whitehead, R. F., and Szmant, A. M. (2010). Effects of variations in carbonate chemistry on the calcification rates of madracis auretenra (= madracis mirabilis sensu well: bicarbonate concentrations best predict calcification rates). *Glob. Change Biol.* 16 (5), 1632–1644. doi: 10.1111/j.1365-2486.2009.02057.x

Kochert, G. (1978). "Protein determination by dye binding," in *Handbook of phycological methods: Physiological and biochemical methods*. Eds. J. A. Hellebust and J. S. Craigie (Cambridge, UK: Cambridge University Press), 92–93.

Kroeker, K. J., Kordas, R. L., Crim, R. N., and Singh, G. G. (2010). Meta-analysis reveals negative yet variable effects of ocean acidification on marine organisms. *Ecol. Lett.* 13, 1419–1434. doi: 10.1111/j.1461-0248.2010.01518.x

Losada, M., and Guerrero, M. G. (1979). "The photosynthetic reduction of nitrate and its regulation," in *Photosynthesis in relation to model systems* (Amsterdam: Elsevier), 365–408.

Martin, S., and Gattuso, J. P. (2009). Response of Mediterranean coralline algae to ocean acidification and elevated temperature. *Glob. Change Biol.* 15 (8), 2089–2100. doi: 10.1111/j.1365-2486.2009.01874.x

Masson-Delmotte, V., Zhai, P., Pirani, A., Connors, S. L., Péan, C., Berger, S., et al., eds. (2021). IPCC, 2021: Climate Change 2021: The physical science basis. Contribution of working group I to the sixth assessment report of the intergovernmental panel on climate change. Cambridge University Press.

Mercado, J. M., Javier, F., Gordillo, L., Niell, F. X., and Figueroa, F. L. (1999). Effects of different levels of CO2 on photosynthesis and cell components of the red alga porphyra leucosticta. *J. Appl. Phycol.* 11 (5), 455–461. doi: 10.1023/A:1008194223558

Miedema, H., and Prins, H. B. A. (1991). pH-dependent proton permeability of the plasma membrane is a regulating mechanism of polar transport through the submerged leaves of potamogeton lucens. *Can. J. Bot.-Rev. Can. Bot.* 69, 1116–1122. doi: 10.1139/b91-143

Milliman, J. D. (1993). Production and accumulation of calcium carbonate in the ocean: budget of a nonsteady state. *Glob. Biogeochem Cycle* 7 (4), 927–957. doi: 10.1029/93GB02524

Olischläger, M., and Wiencke, C. (2013). Ocean acidification alleviates low-temperature effects on growth and photosynthesis of the red alga neosiphonia harveyi (Rhodophyta). *J. Exp. Bot.* 64, 5587–5597. doi: 10.1093/jxb/ert329

Peach, K. E., Koch, M. S., Blackwelder, P. L., and Manfrino, C. (2017). Calcification and photophysiology responses to elevated pCO2 in six halimeda species from contrasting irradiance environments on little Cayman island reefs. *J. Exp. Mar. Biol. Ecol.* 486, 114–126. doi: 10.1016/j.jembe.2016.09.008

Pierrot, D., Lewis, E., and Wallace, D. W. R. (2006). "MS excel program developed for CO2 systems calculations: ORNL/CDIAC-105a," in *Carbon dioxide information analysis center oak ridge national laboratory* (Tennessee: U.S. Department of Energy, Oak Ridge).

Poole, L. J., and Raven, J. A. (1997). The biology of enteromorpha. *Prog. Phycol. Res.* 12, 1–148.

Qu, L., Xu, J., Sun, J., Li, X., and Gao, K. (2017). Diurnal pH fluctuations of seawater influence the responses of an economic red macroalga gracilaria lemaneiformis to future CO2-induced seawater acidification. *Aquaculture.* 473, 383–388. doi: 10.1016/j.aquaculture.2017.03.001

Ragazzola, F., Foster, L. C., Form, A., Anderson, P. S. L., Hansteen, T. H., and Fietzke, J. (2012). Ocean acidification weakens the structural integrity of coralline algae. *Glob. Change Biol.* 18, 2804–2812. doi: 10.1111/j.1365-2486.2012.02756.x

Rautenberger, R., Fernández, P. A., Strittmatter, M., Heesch, S., Cornwall, C. E., Hurd, C. L., et al. (2015). Saturating light and not increased carbon dioxide under ocean acidification drives photosynthesis and growth in ulva rigida (Chlorophyta). *Ecol. Evol.* 5 (4), 874–888. doi: 10.1002/ece3.1382

Raven, J. A. (2011). Effects on marine algae of changed seawater chemistry with increasing atmospheric CO2. *Biol. Environ.-Proc. R. Irish Acad.* 111B, 1–17. doi: 10.3318/bioe.2011.01

Raven, J. A., Giordano, M., Beardall, J., and Maberly, S. C. (2012). Algal evolution in relation to atmospheric CO2: carboxylases, carbon concentrating mechanisms and carbon oxidation cycles. *Philos. Trans. R. Soc B-Biol. Sci.* 367, 493–507. doi: 10.1098/rstb.2011.0212

Reusch, T. B. H., and Boyd, P. W. (2013). Experimental evolution meets marine phytoplankton. *Evolution.* 67 (7), 1849–1859. doi: 10.1111/evo.12035

Ries, J. B., Cohen, A. L., and McCorkle, D. C. (2009). Marine calcifiers exhibit mixed responses to CO2-induced ocean acidification. *Geology* 37, 1131–1134. doi: 10.1130/G30210A.1

Ritchie, R. J. (2008). Universal chlorophyll equations for estimating chlorophylls a, b, c, and d and total chlorophylls in natural assemblages of photosynthetic organisms using acetone, methanol, or ethanol solvents. *Photosynthetica.* 46, 115–126. doi: 10.1007/s11099-008-0019-7

Shan, D., Huang, J., Yang, Y., Guo, Y., Wu, C., Yang, G., et al. (2007). Cotton GhDREB1 increases plant tolerance to low temperature and is negatively regulated by gibberellic acid. *New Phytol.* 176, 70–81. doi: 10.1111/j.1469-8137.2007.02160.x

Sinutok, S., Hill, R., Doblin, M. A., Kuhl, M., and Ralph, P. J. (2012). Microenvironmental changes support evidence of photosynthesis and calcification inhibition in halimeda under ocean acidification and warming. *Coral Reefs.* 31, 1201–1213. doi: 10.1007/s00338-012-0952-6

Stitt, M., and Krapp, A. (1999). The interaction between elevated carbon dioxide and nitrogen nutrition: the physiological and molecular background. *Plant Cell Environ.* 22, 583–621. doi: 10.1046/j.1365-3040.1999.00386.x

Sun, Y., Wang, B., Jin, S., Qu, X., Li, Y., and Hou, B. (2013). Ectopic expression of arabidopsis glycosyltransferase UGT85A5 enhances salt stress tolerance in tobacco. *PloS One* 8 (3), e59924. doi: 10.1371/journal.pone.0059924

Syrett, P. J. (1981). Nitrogen metabolism of microalgae. *Can. J. Fish Aquat Sci.* 210, 182–210. doi: 10.1016/0044-8486(81)90166-6

Teichberg, M., Fricke, A., and Bischol, K. (2013). Increased physiological performance of the calcifying green macroalga halimeda opuntia in response to experimental nutrient enrichment on a Caribbean coral reef. *Aquat. Bot.* 104, 25–33. doi: 10.1016/j.aquabot.2012.09.010

Van Oijen, T., Van Leeuwe, M. A., Gieskes, W. W. C., and De Baar, H. J. W. (2004). Effects of iron limitation on photosynthesis and carbohydrate metabolism in the Antarctic diatom. *Eur. J. Phycol.* 39, 161–171. doi: 10.1080/0967026042000202127

Vidal-Dupiol, J., Zoccola, D., Tambutte, E., Grunau, C., Cosseau, C., Smith, K. M., et al. (2013). Genes related to ion-transport and energy production are unregulated in response to CO2-driven pH decrease in corals: new insights from transcriptome analysis. *PloS One* 8 (3), e58652. doi: 10.1371/journal.pone.0058652

Vogel, N., Fabricius, K. E., Strahl, J., Noonan, S. H. C., Wild, C., and Uthicke, S. (2015). Calcareous green alga halimeda tolerates ocean acidification conditions at tropical carbon dioxide seeps. *Limnol. Oceanogr.* 60, 263–275. doi: 10.1002/lno.10021

Wei, Z., Long, C., Yang, F., Long, L., Huo, Y., Ding, D., et al. (2020a). Increased irradiance availability mitigates the physiological performance of species of the

calcifying green macroalga halimeda in response to ocean acidification. *Algal Res.* 48, 101906. doi: 10.1016/j.algal.2020.101906

Wei, Z., Long, C., Yang, F., Long, L., Mo, J., Hu, Q., et al. (2020b). Effects of plant growth regulators on physiological performances of three calcifying green macroalgae halimeda species (Bryopsidales, chlorophyta). *Aquat. Bot.* 161, 103186. doi: 10.1016/j.aquabot.2019.103186

Wei, Z., Mo, J., Huang, R., Hu, Q., Long, C., Ding, D., et al. (2020c). Physiological performance of three calcifying green macroalgae halimeda species in response to altered seawater temperatures. *Acta Oceanol. Sin.* 39 (02), 89–100. doi: 10.1007/s13131-019-1471-3

Wei, Z., Zhang, Y., Yang, F., Liang, J., and Long, L. (2021). Increased light availability modulates carbon and nitrogen accumulation in the macroalga gracilariopsis lemaneiformis (Rhodophyta) in response to ocean acidification. *Environ. Exp. Bot.* 187, 104492. doi: 10.1016/j.envexpbot.2021.104492

Wizemann, A., Meyer, F. W., Hofmann, L. C., Wild, C., and Westphal, H. (2015). Ocean acidification alters the calcareous microstructure of the green macro-alga halimeda opuntia. *Coral Reefs.* 34, 941–954. doi: 10.1007/s00338-015-1288-9

Xiong, L., Schumaker, K. S., and Zhu, J. (2002). Cell signaling during cold, drought, and salt stress. *Plant Cell.* 14, S165–S183. doi: 10.1105/tpc.000596

Xu, Z., Gao, G., Xu, J., and Wu, H. (2017). Physiological response of a golden tide alga (Sargassum muticum) to the interaction of ocean acidification and phosphorus enrichment. *Biogeosciences.* 14, 671–681. doi: 10.5194/bg-14-671-2017

Yildiz, G., Hofmann, L. C., Bischof, K., and Dere, S. (2013). Ultraviolet radiation modulates the physiological responses of the calcified rhodophyte corallina officinalis to elevated CO2. *Bot. Mar.* 56, 161–168. doi: 10.1515/bot-2012-0216

Zou, D., Gao, K., and Luo, H. (2011). Short- and long term effects of elevated CO2 on photosynthesis and respiration in the marine macroalga hizikia fusiformis (Sargassaceae, phaeophyta) grown at low and high n supplies. *J. Phycol.* 47, 87–97. doi: 10.1111/j.1529-8817.2010.00929.x

Zou, D., Xia, J., and Yang, Y. (2004). Photosynthetic use of exogenous inorganic carbon in the agarophyte gracilaria lemaneiformis (Rhodophyta). *Aquaculture.* 237, 421–431. doi: 10.1016/j.aquaculture.2004.04.020

frontiers | Frontiers in Marine Science

TYPE Original Research
PUBLISHED 28 July 2022
DOI 10.3389/fmars.2022.950695

Check for updates

OPEN ACCESS

EDITED BY
Ganesh Thiruchitrambalam,
Pondicherry University, Port Blair Campus, India

REVIEWED BY
Gopalakrishnan Thilagam,
Pachaiyappa's College for Men Rajamanickam Krishnamurthy,
Arignar Anna Government Arts and Science College Chennai, India
Vikas Pandey,
National Institute of Ocean Technology, India

*CORRESPONDENCE
Ho Young Soh
hysoh@chonnam.ac.kr

†These authors have contributed equally to this work and share first authorship

SPECIALTY SECTION
This article was submitted to Marine Pollution, a section of the journal Frontiers in Marine Science

RECEIVED 23 May 2022
ACCEPTED 27 June 2022
PUBLISHED 28 July 2022

CITATION
Jeong YS, Choo S and Soh HY (2022) Influence of rainfall events on zooplankton community characteristics and feeding habits in estuarine–coastal environments. *Front. Mar. Sci.* 9:950695. doi: 10.3389/fmars.2022.950695

COPYRIGHT
© 2022 Jeong, Choo and Soh. This is an open-access article distributed under the terms of the Creative Commons Attribution License (CC BY). The use, distribution or reproduction in other forums is permitted, provided the original author(s) and the copyright owner(s) are credited and that the original publication in this journal is cited, in accordance with accepted academic practice. No use, distribution or reproduction is permitted which does not comply with these terms.

Influence of rainfall events on zooplankton community characteristics and feeding habits in estuarine–coastal environments

Young Seok Jeong[1†], Seohwi Choo[2†] and Ho Young Soh[1,2,3*]

[1]Department of Environmental Oceanography, Chonnam National University, Yeosu, South Korea, [2]Big Data Fishery Resource Management Interdisciplinary Program, Chonnam National University, Yeosu, South Korea, [3]Department of Ocean Integrated Science, Chonnam National University, Yeosu, South Korea

In temperate estuaries, rainfall causes environmental fluctuations, such as salinity and suspended particulate matter (SPM), and can affect zooplankton distribution patterns. This study focused on the effect of temporary freshwater inflow on the composition of major zooplankton species and changes in their ecological status in the Seomjin River estuary before (June) and after (August) rainfall in 2018. Environmental data were collected from 14 and 15 stations before and after rainfall, respectively. All factors except for chlorophyll-*a* (Chl-*a*) concentration differed significantly before and after rainfall ($p<0.05$), and a salinity gradient extended to Yeosu Bay from Gwangyang Bay. Zooplankton abundance decreased significantly after rainfall. There was a high correlation between indicator species abundance and environmental factors after rainfall (correlation coefficient: 0.7521); however, the indicator species and environmental factors did not exhibit a significant correlation with salinity before rainfall. In terms of feeding habit composition, the carnivore proportion showed a significant decrease after rainfall compared to before rainfall ($p<0.001$), while the particle feeder proportion showed a significant increase after rainfall compared to before ($p<0.001$). In particular, *Corycaeus* spp. contributed significantly to the decrease in carnivore abundance after rainfall. Among the particle feeders, Copepodites significantly increased in abundance after rainfall. Carnivore abundance was negatively correlated with salinity, and particle feeder abundance was positively correlated with potential prey sources (SPM and Chl-*a* concentration), suggesting that particle feeders respond to the food-rich environment after rainfall.

KEYWORDS

environmental factor, suspended particulate matter, statistical analysis, zooplankton community, feeding habit structure, Yeosu Bay

Introduction

Estuaries are gradual transition zones between rivers and coasts (Elliott and McLusky, 2002). Estuarine biogeochemical processes, including water mixing, transportation, and salinity gradients, affect the abundance and composition of organisms (Primo et al., 2009; Jones et al., 2016; Gutierrez et al., 2018; Ciszewski et al., 2022). As multiple interactions (e.g., biotic and abiotic, interspecific, and intraspecific) occur simultaneously in an estuarine ecosystem, analyzing the effects of various environmental parameters is challenging (David et al., 2005). In addition, a temporary influx of freshwater can drastically alter the ecosystem in temperate regions during summer (D'Avanzo et al., 1996; Murrell et al., 2018; Shen et al., 2022).

In estuarine environments, zooplankton species diversity and abundance can be affected by many physicochemical conditions and food availability (Froneman, 2004; Modéran et al., 2010; Nandy and Mandal, 2020; Shropshire et al., 2020; Telesh, 2004). In particular, the impact of suspended particulate matter (SPM) on plankton food availability in estuarine–coastal environments may be slightly controversial. Although many studies have shown that SPM has a negative effect on zooplankton in estuarine ecosystems (Alcaraz et al., 1980; White and Dagg, 1989; Arendt et al., 2011; Kang, 2012), several studies have suggested that increases in SPM can have a positive effect on the population maintenance of zooplankton because of the possible nutritional benefits from organic or potential food matter adhered to the SPM (Poulet, 1978; Arruda et al., 1983; Kwon et al., 2002; Cloern et al., 2017). Therefore, SPM can be used as an alternative food source (Poulet, 1978; Roman, 1984; David et al., 2005; David et al., 2006; Lee et al., 2019; Menéndez et al., 2019). Zooplankton have also been recognized as an indicator because they can sensitively respond to environmental changes (Dufrêne and Legendre, 1997; Beaugrand, 2004; Bonnet and Frid, 2004). Copepods, in particular, constitute approximately 70%–90% of the zooplankton abundance in the ocean; thus, it is necessary to understand how they respond to rainfall events and contribute to biogeochemical fluctuations (Kiørboe, 1997; Madhupratap, 1999; Thompson et al., 2013).

In the study area, many studies were focused on zooplankton distribution by the salinity gradient or their seasonal variation (Park et al., 2002; Jang et al., 2004; Lee et al., 2017). However, few studies have evaluated the increase in SPM as a potential food source after rainfall, as well as the changes in the feeding habits of zooplankton caused by the increase in SPM. In this study, we aimed to find and evaluate the factors influenced by a rainfall event in temperate estuarine–coastal environments on changes in the zooplankton community structure and feeding habit composition. To achieve these purposes, we analyzed the following items: (1) the relationship between the indicator species and various environmental variables and (2) changes in the feeding habit composition of the dominant species.

Materials and methods

Study region

Yeosu Bay is located in the south-central region of the Korean Peninsula (Figure 1) and is connected to Gwangyang Bay through the Yeosu Channel. Gwangyang Bay is generally shallow, with a water depth of 2.4–8.0 m compared with the water depth of 30 m in Yeosu Bay (Kim et al., 2014; Choo, 2020). The Seomjin River and Gwangyang Bay are major introducers of nutrients and SPM to the study area (Kwon et al., 2001). However, Kang et al. (2019; 2020a; 2020b) reported that the main component of SPM is a phytoplankton-based autochthonic source, although SPM is gradually increasing, owing to artificial activities such as dredging and reclamation in Gwangyang Bay. The southern part of Yeosu Bay is connected to the South Sea of Korea and is seasonally affected by the Tsushima Warm Current. The tidal cycle is semidiurnal, with a maximum tidal range of 3.40 m during spring tide and 1.10 m during neap tide (Shaha and Cho, 2009). In summer, 300–400 $m^3 s^{-1}$ of the Seomjin River water is continuously discharged into Gwangyang Bay and the Yeosu Channel, with 81.5% outflowing to the outside of Yeosu Bay through the Yeosu Channel (Kim et al., 2014). In this study, 15 stations were chosen in Gwangyang Bay in the Seomjin River Estuary (Stations 1–4) and Yeosu Bay (Stations 5–15).

Environmental factors

Data were collected in June and August 2018, before and after rainfall. We considered the salinity gradient from the downstream entrance of the Seomjin River to the southern end of Geumo Island using the shipping vessel R/V Cheong-Gyeong-Ho from the Chonnam National University (Figure 1). Sea surface temperature (SST) and salinity data were collected using a multiparameter water quality measurement device (Water quality multi-parameter Pro DSS; YSI, Ohio, USA) in June, and a conductivity, temperature, and depth profiler (CTD) (SBE 19plus V2; Sea-bird Electronic, Washington, USA) in August. Although salinity measurements are unitless as indicated by recent studies (Williams et al., 2015; Gustafson et al., 2022; Wang et al., 2022), we used "psu" for distinguishing from classical unit (‰). Chlorophyll-a (Chl-*a*) concentration was obtained at each station by collecting 500 ml of surface seawater using a plastic bucket and filtering it through Whatman glass fiber filters {GF/F 47 mm; Whatman, Birmingham, UK). The filtered glass fibers were frozen until measurement. After

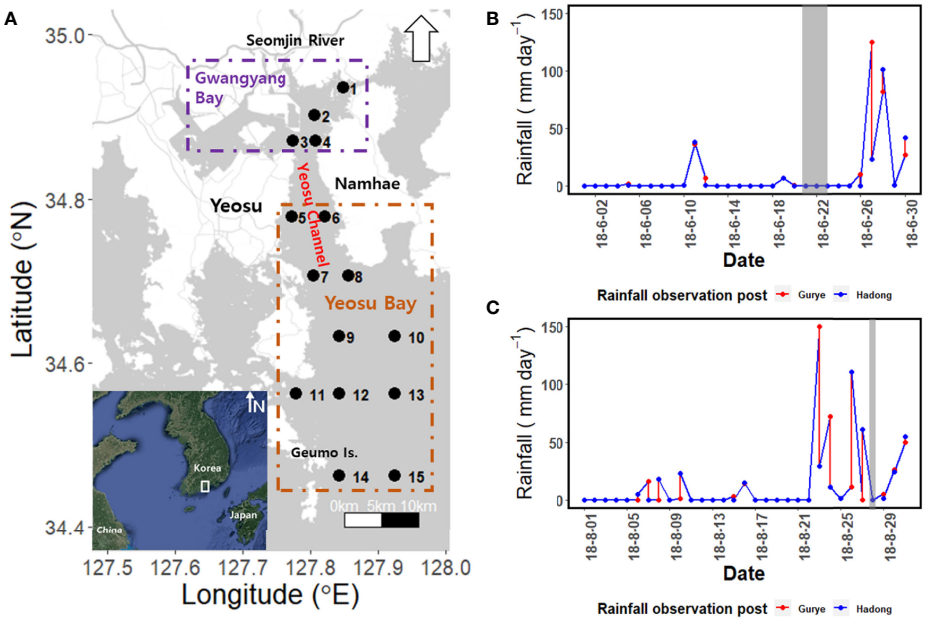


FIGURE 1
(A) Map of the study region, including the Yeosu Channel. Rainfall data for Seomjin River **(B)** upstream (Gurye) and **(C)** downstream (Hadong). Shaded dates indicate the survey period.

adding 90% acetone to the frozen glass fiber filter, the pigment was extracted for 24 h.

Chl-*a* concentrations were measured using a spectrophotometer (Mega-800; Scinco Co., Seoul, Korea), according to the method described by Parsons et al. (1984). For SPM measurements, a glass fiber filter {GF/F 47 mm; Whatman, Birmingham, UK) was washed with distilled water in the laboratory and predried at 60°C for 24 h in a drying oven. The dried filter paper was weighed using an analytical balance (PR124/E; OHAUS Corp., New Jersey, USA) prior to sampling. *In situ*, 500 ml of surface seawater was collected in a plastic bucket, filtered through GF/F, frozen at −20°C, and transported to the laboratory. The dry weight of SPM was measured by drying the transported filter at 60°C for 24 h in a drying oven and weighing it (Korea's Ministry of Environment, 2018). Owing to the possible effects of rainfall in the upper (Gurye) and lower (Hadong) reaches of the Seomjin River on the zooplankton community in Yeosu Bay, relevant data from these two locations were extracted from the Water Resources Management Information System (Figures 1B, C).

Zooplankton sample collection

Owing to the large variation in zooplankton abundance, we performed sampling when the sea level was the highest during the spring tide period. Zooplankton were collected vertically using a conical net (net mouse diameter: 45 cm; mesh size: 200 μm). To calculate the filtered seawater volume, a flowmeter (Model 488115; Hydro-Bios Co., Altenholz, Germany) was attached to the entrance of the net. The collected zooplankton were immediately fixed in the field with a sodium tetraborate–buffered formaldehyde solution at a final concentration of 5%. Zooplankton samples were subsampled using a Folsom-type splitter of 1/8–1/128. Species identification of the zooplankton samples was performed where possible using a stereo microscope (SMZ645; Nikon, Tokyo, Japan), and the microstructure of appendages was observed using a high-magnification optical microscope (Eclipse E200; Nikon, Tokyo, Japan). Zooplankton samples were converted into individuals per cubic meter (inds. m^{-3}). Species were identified according to Chihara and Murano (1997); Soh (2010); Soh et al. (2013), and Soh and Moon (2014), and taxonomic systematics followed the WoRMS Editorial Board (2022).

Data and statistical analyses

Data converted to the log (x+1) index were used to normalize the total zooplankton abundance. For environmental factors (water temperature, salinity, Chl-*a* concentration, and SPM), Z-score standardization was performed to remove the units. Hierarchical cluster analysis was performed according to the Ward link method based on the Bray–Curtis dissimilarity index to measure similarities in zooplankton communities between

stations (Legendre and Legendre, 1998). In addition, cluster analysis was performed using the nMDS (non-metric multidimensional scaling) ordination method (Clarke, 1993).

Using the cluster analysis results, an indicator value analysis was performed to identify the indicator species that affected each classified group (Dufrêne and Legendre, 1997). Subsequently, canonical correspondence analysis (CCA) and correlation analysis were performed by converting the indicator species abundance data to log (x+1) + 1 because of the exclusive species abundance by the assemblage group.

Bio-ENV analysis was performed to detect significant correlations between indicator species abundance and environmental variables (de Carvalho et al., 2015). A *t*-test was performed to identify the differences in environmental factors between the non-rainy period (June) and immediately after rainfall (August), and then, the differences in total zooplankton abundance were confirmed using the Mann–Whitney U test. In addition, the feeding habits of the zooplankton observed in Yeosu Bay in June and August were obtained from previous studies (Table 1). A chi-square test was

TABLE 1 Observed zooplankton occurrence in Yeosu Bay in June and August according to the feeding habits.

Feeding Habits	Species	Occurrence		Reference
		June	August	
Carnivore	*Aidanosagitta crassa* (Tokioka, 1938)	•	•	Amano et al. (2019)
	Flaccisagitta enflata (Grassi, 1881)		•	
	Calanopia thompsoni Scott A., 1909		•	Ohtsuka and Onbé (1991)
	Labidocera rotunda Mori, 1929	•		
	Tortanus forcipatus (Giesbrecht, 1889)	•	•	Anraku and Omori (1963)
	Oncaea spp.		•	Go et al. (1998)
	Oithona spp.	•	•	Nakamura and Turner (1997)
	Corycaeus spp.	•	•	Gophen and Harris (1981)
Particle feeder	*Evadne nordmanni* Lovén, 1836	•		Katechakis and Stibor (2004)
	Pseudevadne tergestina Claus, 1877	•		
	Podon leuckartii (Sars G.O., 1862)	•		
	Oikopleura spp.	•	•	Lombard et al. (2011)
	Acartia erythraea Giesbrecht, 1889	•		Saiz and Kiørboe (1995)
	Acartia hongi Soh and Suh, 2000	•	•	
	Acartia omorii Bradford, 1976	•		
	Acartia ohtsukai Ueda and Bucklin, 2006		•	
	Acartia pacifica Steuer, 1915		•	
	Acartia sinjiensis Mori, 1940		•	
	Acarocalanus spp.		•	McKinnon (1996)
	Bestiolina coreana Moon, Lee, and Soh, 2010		•	Jungbluth et al. (2017)
	Calanus sinicus Brodsky, 1962	•	•	Chen et al. (2010)
	Canthocalanus pauper (Giesbrecht, 1888)		•	Hu et al. (2014)
	Clausocalanus minor Sewell, 1929		•	
	Centropages tenuiremis Thompson I.C. and Scott A., 1903	•	•	Ohtsuka et al. (1996)
	Centropages dorsispinatus Thompson I.C. and Scott A., 1903	•	•	
	Centropages furcatus (Dana, 1849)		•	
	Paracalanus parvus s. l.	•	•	Tiselius et al. (2013)
	Paracalanus aculeatus Giesbrecht, 1888		•	
	Paracalanus gracilis Chen and Zhang, 1965		•	
	Parvocalanus crassirostris (Dahi F., 1894)		•	Jungbluth et al. (2017)
	Pseudodiaptomus marinus Sato, 1913	•	•	Pagano et al. (2003)
	Temora discaudata Giesbrecht, 1889		•	Acros and Fleminger (1986)
	Temora sp.		•	
	Undinula vulgaris (Dana, 1849)		•	Gerber and Gerber (1979)
	Copepodites and Nauplii	•	•	Finlay and Roff (2004)

It was assumed that the feeding habits of species without reference are the same as that of the genus. However, the feeding habits of Sagittidae followed those of Chaetognatha.

performed to confirm the differences in the zooplankton feeding habit composition according to period. All data analyses were performed using the R program (version 4.1.0, R Core Team, 2020), whereas another graphing was performed using the "ggplot2" package; indicator species analysis using the "indicspecies" package; and CCA, correlation analysis, and Bio-ENV analysis using the "vegan" package.

Results

Environmental factors

The SST ranged from 22.5°C to 26.0°C before the rainfall and from 26.3°C to 28.0°C after rainfall (Table 2). Both before and after rainfall, the mean SST was higher in Gwangyang Bay than in Yeosu Bay. In Yeosu Bay, the SST was relatively low in the southwest regions (Figures 2A, B). Surface salinity ranged from 28.3 to 30.7 psu before the rainfall and from 20.8 to 32.8 psu after rainfall (Table 2). There were few differences in the salinity gradient between Gwangyang Bay and Yeosu Bay before the rainfall, but after rainfall, the salinity gradient extended to Yeosu Bay (Figures 2C, D).

SPM ranged from 0.4 to 18.1 mg L^{-1} before the rainfall and from 1.6 to 68.8 mg L^{-1} after rainfall (Table 2). There were no significant spatial differences, except in Station 2, before the rainfall. After rainfall, the SPM gradually decreased with increasing distance from the entrance of the Seomjin River estuary, and its tendency was similar to the distribution of the surface salinity gradient (Figures 2E, F). The Chl-*a* concentration ranged from 1.7 to 7.4 μg L^{-1} before the rainfall and from 0.5 to 8.5 μg L^{-1} after rainfall (Table 2). The Chl-*a* concentration was higher in the northeast of Yeosu Bay and lower in the center of Yeosu Bay before the rainfall, whereas it was higher in the central part of Yeosu Bay and was uniformly distributed after rainfall (Figures 2G, H).

The *t*-test analysis revealed that the average salinity before rainfall was significantly higher than that after rainfall ($p<0.001$). Water temperatures and the SPM were higher after rainfall than before rainfall ($p<0.05$ and $p<0.001$, respectively). The Chl-*a* concentration was not significantly different before and after rainfall ($p>0.05$). The *t*-test analysis revealed that the average salinity before rainfall was significantly higher than that after rainfall ($p<0.001$). SST and SPM were higher after rainfall than before rainfall ($p<0.05$ and $p<0.001$, respectively).

Zooplankton abundance pattern before and after rainfall

Four taxonomic groups (Appendicularians, Branchiopods, Copepods, Chaetognaths) were present before rainfall, and among these, only branchiopods were absent after rainfall (Figure 3). Appendicularian abundance ranged from 2.6% to 17.1%, except for Station 7 (no occurrence), before the rainfall, and in some transition zones (Stations 6–9) ranged from 0.4% to 2.8% after rainfall (Figure 3B). The proportion of appendicularians was higher in Yeosu Bay than in Gwangyang Bay before rainfall (Figure 3B). Branchiopod abundance ranged from 0.3% to 15.9% before rainfall and did not occur after rainfall (Figure 3). Branchiopods occupy a higher proportion in Yeosu Bay than in Gwangyang Bay. Copepod abundance ranged from 58.7% to 96.6% before rainfall and from 79.7% to 98.0 % after rainfall (Figure 3). Copepods were the most dominant among the zooplankton taxa, accounting for more than 58% of the total zooplankton abundance both before and after rainfall. Chaetognath abundance ranged from 0.3% to 29.8% before the rainfall and from 2.0% to 20.3% after rainfall (Figure 3). The

TABLE 2 Environmental variables in Yeosu Bay (each station) during June and August 2018.

	Before rainfall (June 2018)														
Stations	**1**	**2**	**3**	**4**	**5**	**6**	**7**	**8**	**9**	**10**	**11**	**12**	**13**	**14**	**15**
SST (°C)	–	25.9	26	25.5	24.4	25.5	23	23.6	22.8	23.6	22.8	22.5	23.2	22.7	23.2
Surf. Sal. (psu)	–	28.4	29.4	28.3	30.5	29.8	30.2	30.2	30.5	30.7	30.0	30.6	30.4	30.3	30.4
SPM (mg/L)	–	18.1	4.6	4.1	3.0	3.3	2.2	9.2	10.0	4.8	5.8	6.0	0.4	3.5	1.0
Chl-*a* concentration (μg/L)	–	3.8	5.2	4.0	5.1	7.4	3.7	6.4	1.7	3.7	4.8	4.2	4.6	2.4	1.9
	After rainfall (August 2018)														
Stations	**1**	**2**	**3**	**4**	**5**	**6**	**7**	**8**	**9**	**10**	**11**	**12**	**13**	**14**	**15**
SST (°C)	27.6	27.7	28.2	27.6	27.8	27.5	28.0	27.6	27.3	28.6	26.3	26.3	27.1	27.2	27.2
Surf. Sal. (psu)	17.4	18.6	21.4	18.4	22.7	20.8	21.3	27.9	32.4	28.2	32.8	32.7	30.9	32.6	32.6
SPM (mg/L)	65.2	48.8	51.0	42.2	21.0	68.8	60.8	18.4	8.2	53.0	5.0	4.2	26.4	28.6	1.6
Chl-*a* concentration (μg/L)	5.7	5.2	2.1	1.2	8.5	4.9	4.7	2.5	4.3	6.0	0.5	4.2	1.0	6.3	1.0

SST, sea surface temperature; Surf. Sal., surface salinity.

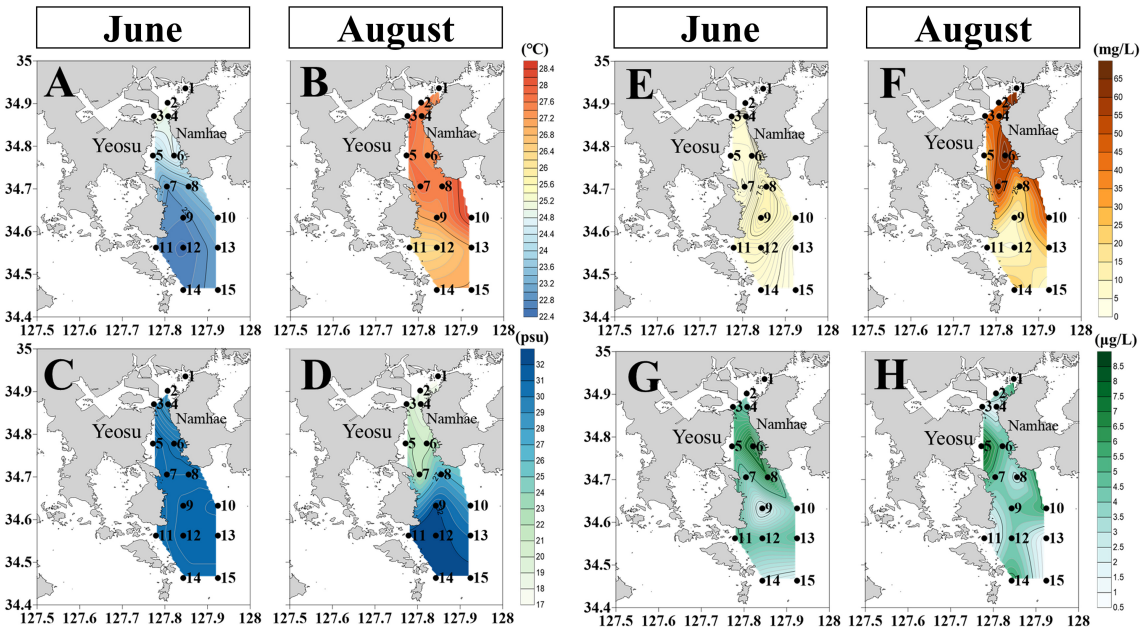


FIGURE 2
Horizontal distribution of environmental variables in June and August 2018. Sea surface temperature during June **(A)** and August **(B)**. Surface salinity during June **(C)** and August **(D)**. SPM during June **(E)** and August **(F)**. Chlorophyll–*a* concentration during June **(G)** and August **(H)**.

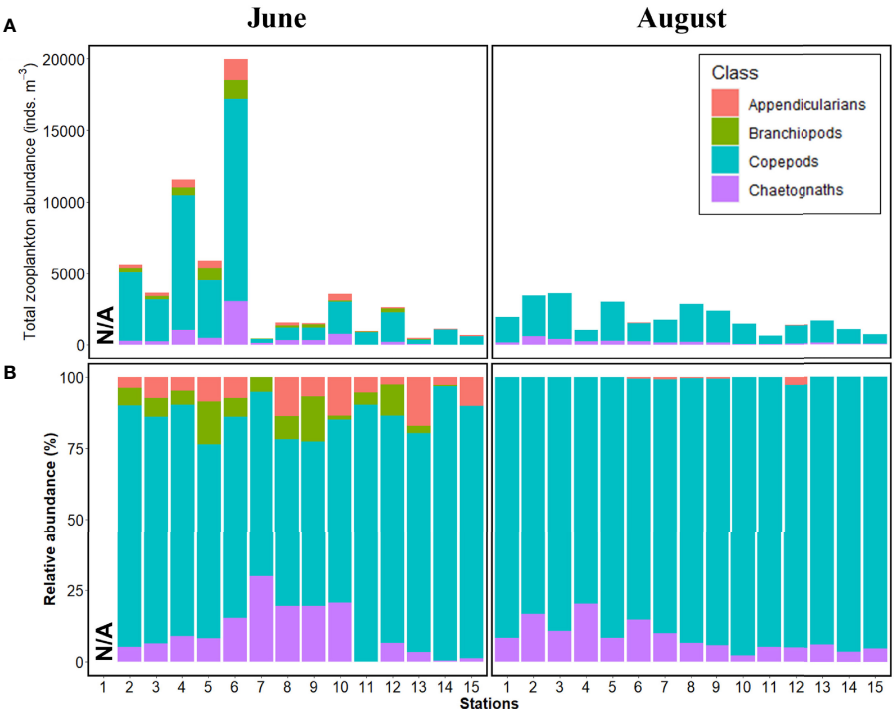


FIGURE 3
Zooplankton abundance patterns in Yeosu Bay in June (left) and August (right). **(A)** Total zooplankton abundance (inds. m^{-3}). **(B)** Stacked percentage (%) of zooplankton abundance. N/A represents non-sampled stations.

proportion of chaetognaths before rainfall was higher in Yeosu Bay than in Gwangyang Bay, whereas it tended to be higher in Gwangyang Bay than in Yeosu Bay (Figure 3B).

The zooplankton abundance ranged from 416 to 19,975 inds. m^{-3} before rainfall, and 617–3,582 inds. m^{-3} after rainfall (Figure 3A). A significant decrease was observed in the total zooplankton abundance after rainfall (mean: 405±833 inds. m^{-3}) than that before rainfall (mean: 141±331 inds. m^{-3}) (Figure 3A, $p<0.001$, Mann–Whitney U test). Copepod abundance significantly contributed to the decrease in the total zooplankton abundance.

Feeding habit composition of the dominant species before and after rainfall

Acartia omorii, Paracalanus parvus s. l., *Corycaeus* spp., and copepodites were predominant before rainfall, and *Bestiolina coreana, Centropages dorsispinatus, P. parvus* s. l., and copepodites after rainfall (Figure 4). Copepodites were the most dominant taxa both before and after rainfall. The proportions of *A. omorii* and *P. parvus* s. l. tended to decrease from Gwangyang Bay to Yeosu Bay before rainfall, whereas the proportions of copepodites and *P. parvus* s. l. tended to increase from Gwangyang Bay to Yeosu Bay after rainfall (Figure 4). Zooplankton were distinguished by their two feeding habits (particle feeders, PFs; carnivores) before and after rainfall (Figure 4B). Before the rainfall, PFs ranged from 59.4% to 87.0%, and the carnivore proportion ranged from 13.0% to 40.6% (Figure 4B). After rainfall, the proportion of PFs increased by 70.3–94.9% and that of carnivores decreased by 5.1–29.7% (Figure 4B). PF accounted for more than 50% of the total zooplankton abundance both before and after rainfall. In addition, a significant increase in the PF proportion (Table 3, $p<0.001$) and a significant decrease in the carnivore proportion before and after rainfall were confirmed (Table 3, $p<0.001$).

Before rainfall, the carnivore abundance was positively correlated with SST, salinity, SPM, and Chl-*a* concentration. PF abundance also showed a positive correlation with all environmental variables, and the relationship with SPM was highly significant (Table 4, $p<0.001$). After rainfall, the carnivore abundance was positively correlated with SST, SPM, and Chl-*a* concentration but negatively correlated with salinity. However, water temperature and Chl-*a* concentrations were the only significant factors (Table 4; $p<0.01$ and $p<0.05$, respectively). Except for the relationship with salinity, which was not statistically significant (Table 4, $p>0.05$), the other factors exhibited a positive correlation ($p<0.05$). This correlation result suggests that salinity caused a reduction in the carnivore

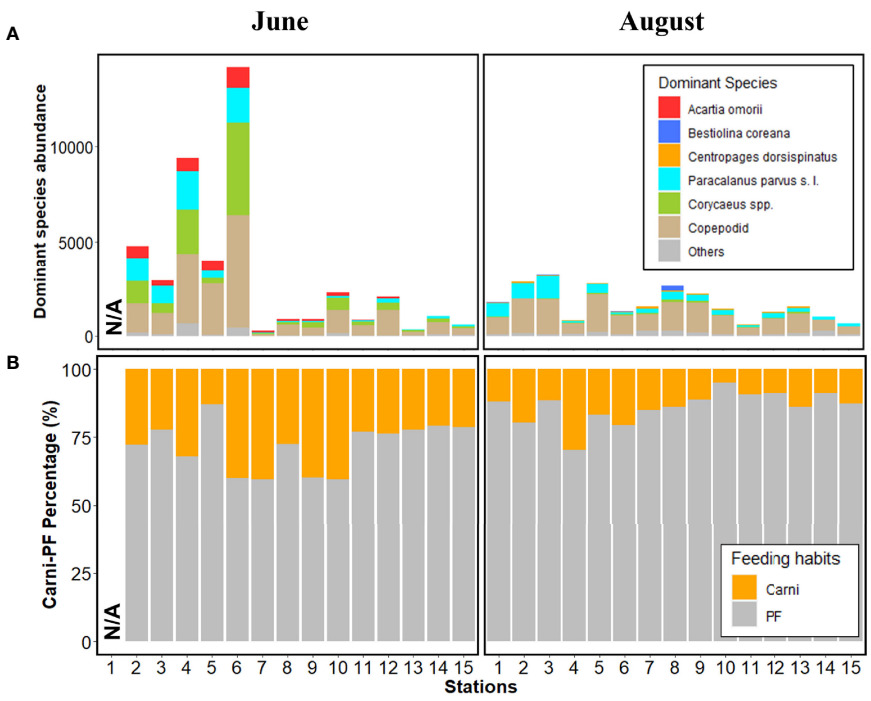


FIGURE 4
(A) Copepod abundance (inds. m^{-3}) in June (left) and August (right). **(B)** Carnivore-particle feeder percentage (%). N/A represents non-sampled stations. Carni, carnivores; PF, particle feeder.

TABLE 3 Results of chi-square test (feeding habits between before and after rainfall).

Test	*df*	X-square	*p*
Carnivore proportion (June > August)	1	1,941.5	< 2.2e-16 ***
Particle feeder proportion (June < August)	1	1,941.5	< 2.2e-16 ***

Asterisks indicate that the correlation is statistically significant (***p<0.001).

abundance, and prey factors (SPM and Chl-*a* concentration) were affected by an increase in PF abundance.

Factors controlling variations in indicator species before and after rainfall

Based on Bray–Curtis dissimilarity–based cluster analysis, the study area was divided into three groups by zooplankton assemblages before rainfall (A, B, and C) and two groups after rainfall (A and B). IndVal analysis was performed only in Groups A and C before rainfall and Groups A and B after rainfall (Figure 5; Table 5). Although Group B included several stations before rainfall event, there were no species with an indicator power index greater than 25. Neritic species (*A. erythraea, A. hongi, Evadne nordmanni, Labidocera rotunda*, and *Tortanus forcipatus*) were extracted from both Groups A and C before rainfall, and they were statistically insignificant (Table 5). After rainfall, Group A comprised neritic and brackish species (*A. erythraea, A. ohtuskai, A. sinjiensis, B. coreana, Parvocalanus crassirostris*, and *Pseudodiaptomus marinus*), whereas Group B mainly comprised offshore warm-current species (*A. pacifica, Canthocalanus pauper, C. furcatus*, and *Temora discaudata*) in Yeosu Bay (Table 5).

The accumulated contribution of the two axes dividing Groups A and C was 83.86% before rainfall. The factors that had a significant correlation with neritic indicator species (*E. nordmanni, A. hongi, A. erythraea*, and *T. forcipatus*) before rainfall were surface water temperature and surface salinity (p<0.05) (Figures 6A, C). However, they did not significantly correlate with other environmental factors (Figures 6A, C). Indicator species showed a positive correlation with water temperature and a negative correlation with salinity (p<0.05) (Figure 6C). After rainfall, the accumulated contribution of the two axes, dividing groups A and B, was 86.62% (Figure 6B). Indicator species were consisted of *A. erythraea, B. coreana, A. ohtsukai, Parvocalanus crassirostris, Pseudocalanus marinus*, and *A. sinjiensis* for Group A and *Calanus sinicus, Canthocalanus pauper, Temora discaudata, C. furcatus*, and *A. pacifica* for Group B. The indicator species of Group A showed a positive correlation with SST and SPM and a negative correlation with salinity (p<0.05) (Figure 6D). The indicator species of Group B showed a positive correlation with salinity and a negative correlation with SST, Chl-*a* concentration, and SPM (p<0.05) (Figure 6D). Moreover, after rainfall, there was a high correlation between the indicator species and the environmental factors (Figure 6D, p<0.05).

Bio-ENV was used to analyze the combination of environmental factors that exerted the greatest effects on indicator species abundance, and the results indicated the highest correlation between surface water temperature and surface salinity before rainfall (correlation coefficient: 0.7576, Table 6). However, the highest correlation was observed for a single combination of surface salinity after rainfall (correlation coefficient: 0.7521, Table 6).

Discussion

SST increased overall, owing to the time difference before and after rainfall (Figures 2A, B). Salinity gradually increased with increasing distance from the Seomjin River after rainfall, whereas there was no spatial difference before rainfall (Figures 2C, D). Although salinity has been recognized as an

TABLE 4 Pearson correlation between the abundance of feeding habit groups on zooplankton and environment factors.

	Before rainfall (June 2018)		After rainfall (August 2018)	
	Carni	PF	Carni	PF
SST	0.8738 **	0.9195 *	0.4193 **	0.5228 *
Salinity	0.7725 ***	0.8325 *	-0.6884	-0.3887
SPM	0.2918 **	0.2596 ***	0.3759	0.2949 *
Chl-*a* concentration	0.6707 *	0.6906 *	0.2288 *	0.4531 *

Asterisks indicate that the correlation is significant (*p<0.05; **p<0.01; ***p<0.001). SST, sea surface temperature; PF, particle feeders; Carni, carnivores.

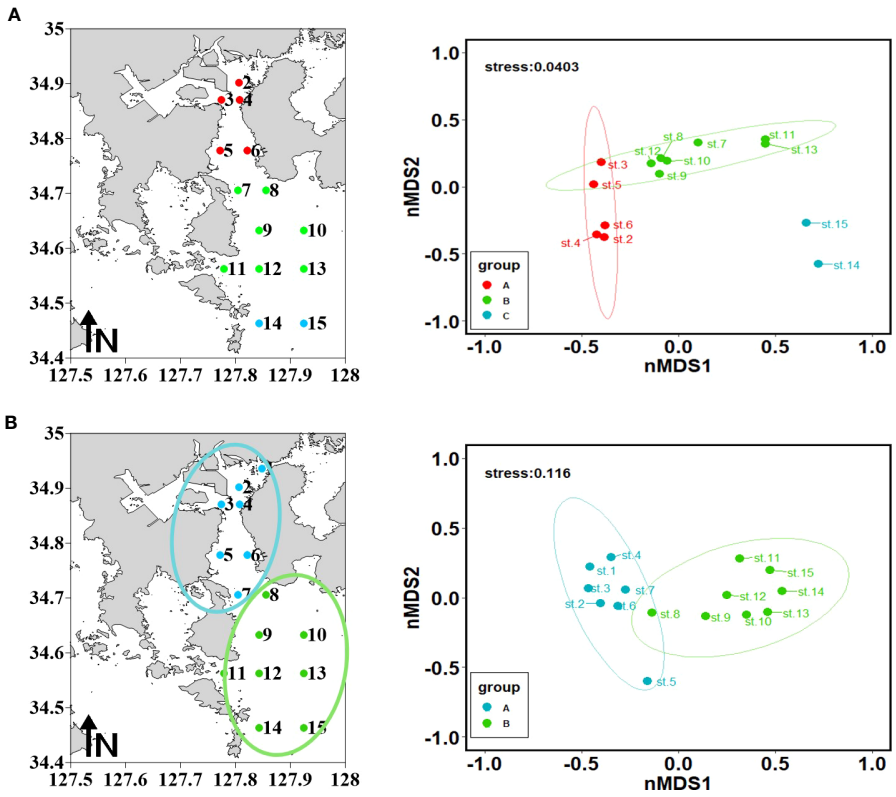


FIGURE 5
Results of Bray–Curtis dissimilarities–based cluster analysis and non-metric multidimensional scaling (nMDS) ordination plots for June **(A)** and August **(B)**.

TABLE 5 Indicator power index (IndVal) of zooplankton communities in Yeosu Bay.

Month	Group	Indicator Species	IndVal (%)
June	A	*Acartia erythraea*	40
		Acartia hongi	40
		Evadne nordmanni	60
		Labidocera rotunda	60
	C	*Tortanus forcipatus*	50
August	A	*Acartia erythraea* *	74.5
		Acartia ohtuskai *	57.1
		Acartia sinjiensis	28.6
		Bestiolina coreana *	59.4
		Parvocalanus crassirostris	42.9
		Pseudodiaptomus marinus	33.9
	B	*Acartia pacifica* ***	75
		Calanus sinicus ***	75
		Canthocalanus pauper ***	87.5
		Centropages furcatus	25
		Temora discaudata ***	77.7

Asterisks indicate that the correlation is statistically significant (*p<0.05; **p<0.01; ***p<0.001).

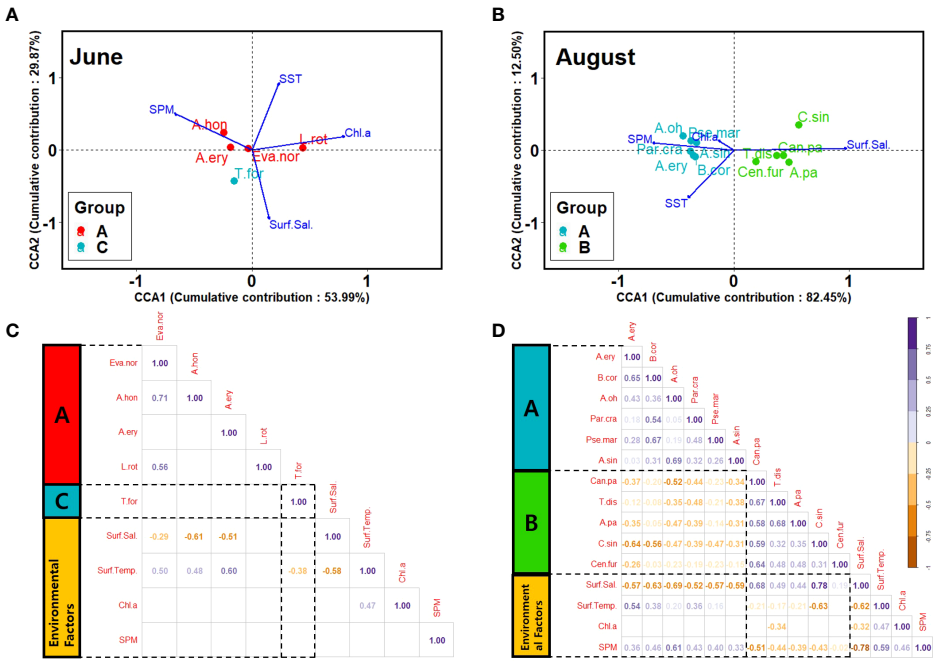


FIGURE 6
Results of canonical correspondence analysis (CCA) and correlation analysis. The correlation analysis between indicator species and environmental factors in this study ($p<0.05$). **(A, C)** June; **(B, D)** August. SST, Sea surface temperature; Eva. nor, *Evadne nordmanni*; A. hon, *Acartia hongi*; A. ery, *A. erythraea*; L. rot, *Labidocera rotunda*; T. for, *Tortanus forcipatus*; A. pa, *A. pacifica*; A. oh, *A. ohtsukai*; C. sin, *Calanus sinicus*; Can. pa, *Canthocalanus pauper*; B. cor, *Bestiolina coreana*; Par. cra, *Parvocalanus crassirostris*; T. dis, *Temora discaudata*.

important factor in the distribution of zooplankton in the Seomjin River Estuary, the salinity gradient can vary greatly depending on rainfall conditions, even within the same season (Figures 2C, D). Large amounts of freshwater are introduced from the surrounding areas into the temperate estuaries during summer (Jha et al., 2013; Parab et al., 2013; Sahu et al., 2013). The inflow of freshwater can transport nutrients to increase the phytoplankton biomass (Zhao and Guo, 2011). However, Chl-*a* concentration was not significantly different before and after rainfall in this study ($p>0.05$, *t*-test), indicating that there was no difference in the phytoplankton biomass used as a food source for zooplankton before and after rainfall (Figures 2G, H). In contrast, SPM increased significantly after rainfall compared to before rainfall ($p<0.05$, *t*-test). It has been found that SPM in the study area is mainly dead or aggregated phytoplankton rather than inorganic matter (Kang et al., 2019; Kang et al., 2020a). SPM inflow from the Seomjin River can be recognized as an increase in the nutritional opportunities for PFs. The PF group increased in abundance, and the carnivore group abundance significantly decreased after rainfall (Table 3). SPM can play a pivotal role as a food source for zooplankton (e.g., copepods and cladocerans) if organic matter-based or nutrient substances are attached to inorganic substances (Poulet, 1978; Arruda et al., 1983). Therefore, these results and the origin of SPM in the study area show that SPM acts as a potential food source for PFs. To understand the fluctuating characteristics of estuaries, it is

TABLE 6 Correlation between environmental factors and log (x+1) + 1-transformed zooplankton abundance data using Bio-ENV analysis (Spearman rank correlation).

	Before rainfall (June 2018)		After rainfall (August 2018)	
Rank	**Factor Combinations**	**Correlation Coefficient**	**Factor Combinations**	**Correlation Coefficient**
1	Surf. Sal., SST	0.7576	Surf. Sal.	0.7521
2	Surf. Sal., SST, SPM	0.6554	Surf. Sal., SPM	0.6191
3	Surf. Sal.	0.6147	Surf. Sal., Chl-*a* concentration, SPM	0.5592
4	Surf. Sal., SST, Chl-*a* concentration, SPM	0.5987	Surf. Sal., SST, Chl-*a* concentration, SPM	0.5320

Surf., surface; SST, sea surface temperature; Sal.,: salinity; Chl-a, chlorophyll-a; SPM, suspended particulate matter.

necessary to periodically monitor the zooplankton population and distribution according to their feeding habits.

According to the zooplankton monitoring data of over 21 years in the study area, PFs were the dominant group in most studies (Table 7). Since the study region is constantly affected by the Seomjin River water, the continuous inflow of SPM seems to consist of an environment in which PF, in particular immature copepods (copepodites), can prosper. However, in previous studies, copepodites have been significantly underestimated in the proportion of PF in feeding habit composition. Therefore, we suggest that the feeding habit composition and the ratio of copepodites can be used as an index that can well express the variability of the environmental condition after rainfall.

Feeding habits after rainfall compared to before rainfall indicated a significant decrease in carnivore proportion and an increase in PF proportion ($p<0.001$, Table 3). The reduction in the carnivore proportion after rainfall was largely attributed to *Corycaeus* spp. (Figure 4). Copepodites contributed greatly to the increase in PF proportion after rainfall, which can be explained as follows: first, copepodites and *P. parvus* s. l., which appeared dominant both before and after rainfall in the study region, would have survived rapid salinity changes because most of them have a euryhaline habitat range (Suh et al., 1991; Moon et al., 2012); second, copepodites and *P. parvus* s. l. would have increased in environments rich in phytoplankton-based particulate prey transported from the Seomjin River (Kwon et al., 2002; Kang et al., 2019; Kang et al., 2020a). This was supported by the correlation analysis results between zooplankton abundance, feeding habits, and environmental factors. In addition, although the particulate organic matter content was not measured separately in this study, previous studies have confirmed that SPM can be used as a food source by copepods (Poulet, 1978; Roman, 1984; David et al., 2005; Lee et al., 2019; Menéndez et al., 2019).

The abundance of branchiopods and appendicularians, a representative taxonomic group belonging to PF, decreased significantly after rainfall (Figure 3). They had population maintenance strategies such as parthenogenesis or with short generation times under environmental conditions suitable for reproduction and growth (Paffenhöfer, 1973; Hopcroft and Roff, 1995; Hopcroft et al., 1998; Korhola and Rautio, 2001). On the other hand, their populations are reduced by various factors, and many studies have been revealed to be determined by biological and chemical factors rather than physical factors (Brett, 1989; Marmorek and Korman, 1993; Tomita et al., 2003). The inflow of freshwater owing to rainfall can cause rapid changes in the estuarine environment and affect their distribution.

Most copepods are salinity-resistant species, such as neritic or brackish species. In particular, *P. parvus* s. l. suitably dominate in summer when environmental fluctuations are severe because of their fast reproduction cycle and short egg hatching time (Ianora, 1998). *A. omorii* occurred only before rainfall, while the species that occurred only after rainfall were *B. coreana* and *C. dorsispinatus* (Figure 4A). *A. omorii* is known to favor water temperatures less

TABLE 7 Dominant copepods in Yeosu Bay from 2001 to 2018.

	2001–2003 Jang et al. (2004)	2005–2010 Lee (2012)	2014–2015 Soh et al. (unpublished)	2015–2016 Lee et al. (2017)	2018.06 Current study	2018.08 Current study
Acartia omorii	●	●	●	●	●	
A. erythraea	●		●			●
A. ohtsukai			●	●		●
A. pacifica						●
Bestiolina coreana						●
Centropages abdominalis	●		●	●		
C. dorsispinatus			●			●
Canthocalanus pauper						●
Clausocalanus furcatus			●			
Calanus sinicus	●					●
Labidocera rotunda					●	
Paracalanus parvus s. l.	●	●	●	●	●	●
Pseudodiaptomus marinus	●					●
Temora discaudata						●
Tortanus forcipatus						●
Ditrichocorycaeus affinis		●	●			
Corycaeus spp.				●	●	●
Oithona spp.			●	●	●	●
Unidentified Harpacticoids				●		●

Black circles denote the dominant species in each year.

than 25°C and is the dominant species in coastal environments (Shim and Yun, 1990; Soh and Suh, 1993). After rainfall, *B. coreana* and *C. dorsispinatus* inhabit brackish waters and coastal waters, mainly in the summer in Gwangyang Bay (Jang et al., 2004; Moon et al., 2011). Our results included most of the species that have been studied in Gwangyang and Yeosu Bay (Table 7). In particular, the increase of particle feeders such as *B. coreana* and *C. dorsispinatus* seems to be related with the increase of SPM after rainfall. Meanwhile, after rainfall, indicator species analysis clearly distinguished Group A, which was affected by the Seomjin River, from Group B, which was affected offshore, and no statistically significant species were observed in Yeosu Bay, regardless of the sufficiently high indicator power index in the IndVal analysis (Table 5). However, before rainfall, the study area was composed of a single ecological community because of the low correlation with physical factors, such as water temperature and salinity.

Conclusions

This study confirmed that the salinity gradient owing to rainfall is extended to the coast with a large difference, even within the same season. SPM, which rapidly increases with rainfall, can provide nutritional benefits to PFs as a potential food source in estuarine–coastal environments. This suggests that it could contribute to restore the decreased zooplankton populations after rainfall in estuarine–coastal environments. Contrary to previous studies, our study is valuable for evaluating SPM as a potential source of zooplankton and supports its importance as a potential source in temporary, highly turbid estuarine–coastal environments. In future studies, periodic monitoring of the process of restoring zooplankton populations will be required through short-term sampling after rainfall.

Data availability statement

The raw data supporting the conclusions of this article will be made available by the authors, without undue reservation.

Author contributions

YSJ contributed to manuscript writing, data analysis and interpretation, discussion, and statistical analysis; authored and reviewed drafts of the manuscript; and approved the final draft. SC contributed to field sampling, zooplankton identification, manuscript writing, data analysis and interpretation, discussion, and statistical analysis; authored and reviewed the drafts of the manuscript; and approved the final draft. HYS contributed to funding acquisition, conceptualization, data interpretation, and discussion; authored and reviewed drafts of the manuscript; and approved the final draft. All authors have contributed to the manuscript and approved the submitted version.

Funding

This research was a part of the project titled “Research center for fishery resource management based on the information and communication technology” (2022, grant number 20180384) and supported by Korea Institute of Marine Science & Technology Promotion (KIMST, 20220558) funded funded by the Ministry of Oceans and Fisheries.

Acknowledgments

We are grateful to the crew of the R/V Cheong-Gyeong-Ho, and Zooplankton Species Diversity Laboratory members at the Chonnam National University for their support in the field. We would also like to thank Editage (www.editage.co.kr) for the English language editing.

Conflict of interest

The authors declare that the research was conducted in the absence of any commercial or financial relationships that could be construed as a potential conflict of interest.

Publisher’s note

All claims expressed in this article are solely those of the authors and do not necessarily represent those of their affiliated organizations, or those of the publisher, the editors and the reviewers. Any product that may be evaluated in this article, or claim that may be made by its manufacturer, is not guaranteed or endorsed by the publisher.

References

Acros, F., and Fleminger, M. (1986). Distribution of filter-feeding calanoid copepods in the eastern equatorial pacific, *CalCOFI rep., vol. 27* (California: California cooperative oceanic fisheries).

Alcaraz, M. T., Paffenhoffer, G., and Strickler, R. (1980). 22. catching the algae: a first account of visual observations on filter–feeding calanoids. *Evol. Ecol.* 3, 241–248.

Amano, K., Abe, Y., Matsuno, K., and Yamaguchi, A. (2019). Yearly comparison of the planktonic chaetognath community in the chukchi Sea in the summers of 1991 and 2007. *Polar. Sci.* 19, 112–119. doi: 10.1016/j.polar.2018.11.011

Anraku, M., and Omori, M. (1963). Preliminary survey of the relationship between the feeding habit and the structure of the mouth-parts of marine copepods 1. *Limnol. Oceanogr.* 8 (1), 116–126. doi: 10.4319/lo.1963.8.1.0116

Arendt, K. E., Dutz, J., Jónasdóttir, S. H., Jung–Madsen, S., Mortensen, J., Møller, E. F., et al. (2011). Effects of suspended sediments on copepods feeding in a glacial influenced sub–Arctic fjord. *J. Plankton. Res.* 33 (10), 1526–1537. doi: 10.1093/plankt/fbr054

Arruda, J. A., Marzolf, G. R., and Faulk, R. T. (1983). The role of suspended sediments in the nutrition of zooplankton in turbid reservoirs. *Ecology* 64 (5), 1225–1235. doi: 10.2307/1937831

Beaugrand, G. (2004). The north Sea regime shift: evidence, causes, mechanisms and consequences. *Prog. Oceanogr.* 60 (2–4), 245–262. doi: 10.1016/j.pocean.2004.02.018

Bonnet, D., and Frid, C. (2004). Seven copepod species considered as indicators of water-mass influence and changes: results from a Northumberland coastal station. *ICES J. Mar. Sci.* 61 (4), 485–491. doi: 10.1016/j.icesjms.2004.03.005

Brett, M. T. (1989). Zooplankton communities and acidification processes (a review). *Wat. Air Soil pollut.* 44, 387–414. doi: 10.1007/BF00279267

Chen, M. R., Kâ, K., and Hwang, J. S. (2010). Diet of the copepod calanus sinicus brodsky 1962 (Copepoda, calanoida, calanidae) in northern coastal waters of Taiwan during the northeast monsoon period. *Crustaceana*, 83(7):851–864. doi: 10.1163/001121610x504360

Chihara, M., and Murano, M. (1997). *An illustrated guide to marine plankton in Japan* (Tokyo, Japan: Tokai University Press), 1–260.

Choo, H. S. (2020). Temporal and spatial fluctuation characteristics of sea surface temperature in yeosu bay, Korea. *J. Korean Soc Fish. Ocean. Technol.* 56 (4), 322–339. doi: 10.3796/KSFOT.2020.56.4.322

Ciszewski, K., Wawrzyniak, W., and Czerniejewski, P. (2022). Effect of artificial regime shifts and biotic factors on the intensity of foraging of planktivorous fish. *Animals* 12 (1), 17. doi: 10.3390/ani12010017

Clarke, K. R. (1993). Non-parametric multivariate analyses of changes in community structure. *Austral. Ecol.* 18 (1), 117–143. doi: 10.1111/j.1442–9993.1993.tb00438.x

Cloern, J. E., Jassby, A. D., Schraga, T. S., Nejad, E., and Martin, C. (2017). Ecosystem variability along the estuarine salinity gradient: Examples from long-term study of San Francisco bay. *Limnol. Oceanogr.* 62 (S1), S272–S291. doi: 10.1002/lno.10537

D'Avanzo, C., Kremer, J. N., and Wainright, S. C. (1996). Ecosystem production and respiration in response to eutrophication in shallow temperate estuaries. *Mar. Ecol. Prog. Ser.* 141, 263–274. doi: 10.3354/meps141263

David, V., Sautour, B., Chardy, P., and Leconte, M. (2005). Long-term changes of the zooplankton variability in a turbid environment: the gironde estuary (France). *Estuar. Coast. Shelf. Sci.* 64 (2-3), 171–184. doi: 10.1016/j.ecss.2005.01.014

David, V., Sautour, B., Galois, R., and Chardy, P. (2006). The paradox high zooplankton biomass–low vegetal particulate organic matter in high turbidity zones: what way for energy transfer? *J. Exp. Mar. Biol. Ecol.* 333 (2), 202–218. doi: 10.1016/j.jembe.2005.12.045

de Carvalho, G. C., de Sá–Neto, R. J., and Barros, F. (2015). Thirty years of use of multivariate quantitative methods in benthic community ecology of marine and coastal habitats: looking to the past to planning the future. *Scientometrics* 105 (1), 593–610. doi: 10.1007/s11192–015–1667–6

Dufrêne, M., and Legendre, P. (1997). Species assemblages and indicator species: the need for a flexible asymmetrical approach. *Ecol. Monogr.* 67 (3), 345–366. doi: 10.1890/0012–9615(1997)067[0345:SAAIST]2.0.CO;2

Elliott, M., and McLusky, D. S. (2002). The need for definitions in understanding estuaries. *Estuar. Coast. Shelf. Sci.* 55 (6), 815–827. doi: 10.1006/ecss.2002.1031

Finlay, K., and Roff, J. C. (2004). Radiotracer determination of the diet of calanoid copepod nauplii and copepodites in a temperate estuary. *ICES. J. Mar. Sci.* 61 (4), 552–562. doi: 10.1016/j.icesjms.2004.03.010

Froneman, P. W. (2004). Zooplankton community structure and biomass in a southern African temporarily open/closed estuary. *Estuar. Coast. Shelf. Sci.* 60 (1), 125–132. doi: 10.1016/j.ecss.2003.12.002

Gerber, R. P., and Gerber, M. B. (1979). Ingestion of natural particulate organic matter and subsequent assimilation, respiration and growth by tropical lagoon zooplankton. *Mar. Biol.* 52 (1), 33–43. doi: 10.1007/bf00386855

Go, Y. B., Oh, B. C., and Terazaki, M. (1998). Feeding behavior of the poecilostomatoid copepods oncaea spp. on chaetognaths. *J. Mar. Syst.* 15 (1–4), 475–482. doi: 10.1016/S0924–7963(97)00038–9

Gophen, M., and Harris, R. P. (1981). Visual predation by a marine cyclopoid copepod, corycaeus anglicus. *J. Mar. Biol. Assoc. UK.* 61 (2), 391–399. doi: 10.1017/S0025315400047020

Gustafson, C. D., Key, K., Siegfried, M. R., Winberry, J. P., Fricker, H. A., Venturelli, R. A., et al. (2022). A dynamic saline groundwater system mapped beneath an Antarctic ice stream. *Science* 376 (6593), 640–644. doi: 10.1126/science.abm3301

Gutierrez, M. F., Tavşanoğlu, Ü.N., Vidal, N., Yu, J., Teixeira–de Mello, F., Çakiroglu, A. I., et al. (2018). Salinity shapes zooplankton communities and functional diversity and has complex effects on size structure in lakes. *Hydrobiologia* 813 (1), 237–255. doi: 10.1007/s10750–018–3529–8

Hopcroft, R. R., and Roff, J. C. (1995). Zooplankton growth rates: extraordinary production by the larvacean oikopleura dioica in tropical waters. *J. Plankton Res.* 17 (2), 205–220. doi: 10.1093/plankt/17.2.205

Hopcroft, R. R., Roff, J. C., and Bouman, H. A. (1998). Zooplankton growth rates: the larvaceans appendicularia, fritillaria and oikopleura in tropical waters. *J. Plankton Res.* 20 (3), 539–555. doi: 10.1093/plankt/20.3.539

Hu, S., Guo, Z., Li, T., Carpenter, E. J., Liu, S., and Lin, S. (2014). Detecting *in situ* copepod diet diversity using molecular technique: development of a copepod/symbiotic ciliate–excluding eukaryote–inclusive PCR protocol. *PloS One* 9 (7), e103528. doi: 10.1371/journal.pone.0103528

Ianora, A. (1998). Copepod life history traits in subtemperate regions. *J. Mar. Syst.* 15 (1-4), 337–349. doi: 10.1016/S0924-7963(97)00085-7Acros

Jang, M. C., Jang, P. G., Shin, K. S., Park, D. W., and Jang, M. (2004). Seasonal variation of zooplankton community in gwangyang bay. *Korean J. Environ. Biol.* 22, 11–29.

Jha, D. K., Prashanthi Devi, M., Vinithkumar, N. V., Das, A. K., Dheenan, P. S., Venkateshwaran, P., et al. (2013). Comparative investigation of water quality parameters of aerial & rangat bay, Andaman islands using in-situ measurements and spatial modelling techniques. *Water Qual. Expo. Health* 5 (2), 57–67. doi: 10.1007/s12403-013-0086-2

Jones, S., Perissinotto, R., Carrasco, N. K., and Vosloo, A. (2016). Impact of a flood event on the zooplankton of an estuarine lake. *Mar. Biol. Res.* 12 (2), 158–167. doi: 10.1080/17451000.2015.1104417

Jungbluth, M. J., Selph, K. E., Lenz, P. H., and Goetze, E. (2017). Species–specific grazing and significant trophic impacts by two species of copepod nauplii, parvocalanus crassirostris and bestiolina similis. *Mar. Ecol. Prog. Ser.* 572, 57–76. doi: 10.3354/meps12139

Kang, H. K. (2012). Effects of suspended sediments on reproductive responses of paracalanus sp. (Copepoda: Calanoida) in the laboratory. *J. Plankton. Res.* 34 (7), 626–635. doi: 10.1093/plankt/fbs033

Kang, Y., Kang, Y. H., Kim, J. K., Kang, H. Y., and Kang, C. K. (2020b). Year–to–year variation in phytoplankton biomass in an anthropogenically polluted and complex estuary: A novel paradigm for river discharge influence. *Mar. Pollut. Bull.* 161, 111756. doi: 10.1016/j.marpolbul.2020.111756

Kang, S., Kim, J. H., Hwang, J. H., Bong, Y. S., Ryu, J. S., and Shin, K. H. (2020a). Seasonal contrast of particulate organic carbon (POC) characteristics in the geum and seomjin estuary systems (South Korea) revealed by carbon isotope (δ13C and Δ14C) analyses. *Water Res.* 187, 116442. doi: 10.1016/j.watres.2020.116442

Kang, S., Kim, J. H., Kim, D., Song, H., Ryu, J. S., Ock, G., et al. (2019). Temporal variation in riverine organic carbon concentrations and fluxes in two contrasting estuary systems: Geum and seomjin, south Korea. *Environ. Int.* 133, 105126. doi: 10.1016/j.envint.2019.105126

Katechakis, A., and Stibor, H. (2004). Feeding selectivities of the marine cladocerans penilia avirostris, podon intermedius and evadne nordmanni. *Mar. Biol.* 145 (3), 529–539. doi: 10.1007/s00227–004–1347–1

Kiørboe, T. (1997). Population regulation and role of mesozooplankton in shaping marine pelagic food webs. *Hydrobiologia* 363 (1), 13–27. doi: 10.1023/A:1003173721751

Kim, B. J., Ro, Y. J., Jung, K. Y., and Park, K. S. (2014). Numerical modeling of circulation characteristics in the kwangyang estuarine system. *J. Korean. Soc Coast. Ocean. Eng.* 26 (4), 253–266. doi: 10.9765/KSCOE.2014.26.4.253

Korea's Ministry of Environment (2018). *Standard methods for the examination of seawater*. 46–49pp. (Korea: NIBR and Ministry of Environment).

Korhola, A., and Rautio, M. (2001). "Cladocera and other branchiopod crustaceans," in *Tracking environmental change using lake sediments* (Dordrecht: Springer), 5–41. doi: 10.1007/0-306-47671-1_2

Kwon, K. Y., Moon, C. H., Kang, C. K., and Kim, Y. N. (2002). Distribution of particulate organic matters along the salinity gradients in the seomjin river estuary. *Korean. J. Fish. Aquat. Sci.* 35 (1), 86–96. doi: 10.5657/kfas.2002.35.1.086

Kwon, K. Y., Moon, C. H., and Yang, H. S. (2001). Behavior of nutrients along the salinity gradients in the seomjin river estuary. *Korean. J. Fish. Aquat. Sci.* 34 (3), 199–206.

Lee, S. J. (2012). "Long term variation of zooplankton community in the northern channel of Gwangyang bay. M. S. Thesis," (Yeosu, Korea: Chonnam National Univ.).

Lee, S. W., Park, G., and Choi, K. H. (2019). Biomass of plankton and macrobenthos and benthic species diversity in relation to environmental gradients in a nationwide coastal survey. *Reg. Stud. Mar. Sci.* 26, 100502. doi: 10.1016/j.rsma.2019.100502

Lee, E. H., Seo, M. H., Yoon, Y. H., Choi, S. D., and Soh, H. Y. (2017). Environmental factors affecting zooplankton community in gwangyang bay. *Korean J. Environ. Biol.* 35 (4), 631–639. doi: 10.11626/kjeb.2017.35.4.631

Legendre, P., and Legendre, L. (1998). "Developments in environmental modelling," in *Numerical ecology* (Kidlington, UK: Elsevier).

Lombard, F., Selander, E., and Kiørboe, T. (2011). Active prey rejection in the filter-feeding appendicularian oikopleura dioica. *Limnol. Oceanogr.* 56 (4), 1504–1512. doi: 10.4319/lo.2011.56.4.1504

Madhupratap, M. (1999). Free-living copepods of the Arabian Sea: Distributions and research perspectives. *Indian. J. Mar. Sci.* 28, 146–149.

Marmorek, D. R., and Korman, J. (1993). The use of zooplankton in a biomonitoring program to detect lake acidification and recovery. *Wat. Air Soil pollut.* 69, 223–241. doi: 10.1007/BF00478160

McKinnon, A. D. (1996). Growth and development in the subtropical copepod acrocalanus gibber. *Limnol. Oceanogr.* 41 (7), 1438–1447. doi: 10.4319/lo.1996.41.7.1438

Menéndez, M. C., Baleani, C. A., Amodeo, M. R., Acha, E. M., and Piccolo, M. C. (2019). Assessment of surf zone zooplankton dynamics in a southwestern Atlantic sandy beach: Seasonal cycle and tidal height influence. *Estuar. Coast. Shelf. Sci.* 227, 106307. doi: 10.1016/j.ecss.2019.106307

Modéran, J., Bouvais, P., David, V., Le Noc, S., Simon–Bouhet, B., Niquil, N., et al. (2010). Zooplankton community structure in a highly turbid environment (Charente estuary, france): Spatio–temporal patterns and environmental control. *Estuar. Coast. Shelf. Sci.* 88 (2), 219–232. doi: 10.1016/j.ecss.2010.04.002

Moon, S. Y., Seo, M. H., Shin, Y. S., and Soh, H. Y. (2012). Seasonal variation of mesozooplankton communities in the semi-enclosed muan bay, Korea. *Ocean. Polar. Res.* 34 (1), 1–18. doi: 10.4217/OPR.2012.34.1.001

Moon, S. Y., Seo, M. H., and Soh, H. Y. (2011). Distribution characteristics of two dominant paracalanids on temperature and salinity in the brackish and coastal waters from the west and south coasts of Korea. *Korean J. Environ. Biol.* 29 (1), 11–16.

Murrell, M. C., Caffrey, J. M., Marcovich, D. T., Beck, M. W., Jarvis, B. M., and Hagy, J. D. (2018). Seasonal oxygen dynamics in a warm temperate estuary: effects of hydrologic variability on measurements of primary production, respiration, and net metabolism. *Estuaries Coasts* 41 (3), 690–707. doi: 10.1007/s12237-017-0328-9

Nakamura, Y., and Turner, J. T. (1997). Predation and respiration by the small cyclopoid copepod oithona similis: How important is feeding on ciliates and heterotrophic flagellates? *J. Plankton. Res.* 19 (9), 1275–1288. doi: 10.1093/plankt/19.9.1275

Nandy, T., and Mandal, S. (2020). Unravelling the spatio-temporal variation of zooplankton community from the river matla in the sundarbans estuarine system, India. *Oceanologia* 62 (3), 326–346. doi: 10.1016/j.oceano.2020.03.005

Ohtsuka, S., and Onbé, T. (1991). Relationship between mouthpart structures and *in situ* feeding habits of species of the family pontellidae (Copepoda: Calanoida). *Mar. Biol.* 111 (2), 213–225. doi: 10.1007/BF01319703

Ohtsuka, S., Shimozu, M., Tranmura, A., Fukuchi, M., Hattori, H., Sasaki, H., et al. (1996). Relationships between mouthpart structures and *in situ* feeding habits of five neritic calanoid copepods in the chukchi and northern Bering seas in October 1988 *Proceedings of the NIPR Symposium on Polar Biology*, (17th symposium on polar biology) (9), 153–168. doi: 10.15094/00005312

Paffenhöfer, G. A. (1973). The cultivation of an appendicularian through numerous generations. *Mar. Biol.* 22 (2), 183–185. doi: 10.1007/BF00391782

Pagano, M., Kouassi, E., Saint–Jean, L., Arfi, R., and Bouvy, M. (2003). Feeding of acartia clausi and pseudodiaptomus hessei (Copepoda: Calanoida) on natural particles in a tropical lagoon (Ebrié, côte d'Ivoire). *Estuar. Coast. Shelf. Sci.* 56 (3–4), 433–445. doi: 10.1016/S0272–7714(02)00193–2

Parab, S. G., Matondkar, S. P., Gomes, H. D. R., and Goes, J. I. (2013). Effect of freshwater influx on phytoplankton in the mandovi estuary (Goa, India) during monsoon season: Chemotaxonomy. *J. Water Resour. Prot.* 5, 349–361. doi: 10.4236/jwarp.2013.53A036

Park, C., Lee, P. G., and Yang, S. R. (2002). Variation of zooplankton distribution in the seomjin river estuary with respect to season and salinity gradients. *Sea.* 7 (2), 51–59.

Parsons, T. R., Maita, Y., and Lalli, C. M. (1984). *A manual of chemical and biological methods for seawater analysis* (Oxford: Pergamon Press), 173.

Poulet, S. A. (1978). Comparison between five coexisting species of marine copepods feeding on naturally occurring particulate matter. *Limnol. Oceanogr.* 23 (6), 1126–1143. doi: 10.4319/lo.1978.23.6.1126

Primo, A. L., Azeiteiro, U. M., Marques, S. C., Martinho, F., and Pardal, M.Â. (2009). Changes in zooplankton diversity and distribution pattern under varying precipitation regimes in a southern temperate estuary. *Estuar. Coast. Shelf. Sci.* 82 (2), 341–347. doi: 10.1016/j.ecss.2009.01.019

R Core Team (2020). *R: A language and environment for statistical computing* (Vienna, Austria: R Foundation for Statistical Computing). Available at: https://www.R-project.org/.

Roman, M. R. (1984). Utilization of detritus by the copepod, acartia tonsa 1. *Limnol. Oceanogr.* 29 (5), 949–959. doi: 10.4319/lo.1984.29.5.0949

Sahu, B. K., Begum, M., Khadanga, M. K., Jha, D. K., Vinithkumar, N. V., and Kirubagaran, R. (2013). Evaluation of significant sources influencing the variation of physico-chemical parameters in port Blair bay, south Andaman, India by using multivariate statistics. *Mar. Pollut. Bull.* 66 (1-2), 246–251. doi: 10.1016/j.marpolbul.2012.09.021

Saiz, E., and Kiørboe, T. (1995). Predatory and suspension feeding of the copepod acartia tonsa in turbulent environments. *Mar. Ecol. Prog. Ser.* 122, 147–158. doi: 10.3354/meps122147

Shaha, D. C., and Cho, Y. K. (2009). Comparison of empirical models with intensively observed data for prediction of salt intrusion in the Sumjin River estuary, *Korea. Hydrol. Earth Syst. Sci.*, 13 (6), 923–933. doi: 10.5194/hess-13-923-2009

Shen, X., Cai, Y., Su, M., Wan, H., Shen, Y., and Yang, Z. (2022). High discharge intensified low net ecosystem productivity, hypoxia, and acidification at three outlets of the pearl river estuary, China. *Water Res.* 214, 118171. doi: 10.1016/j.watres.2022.118171

Shim, J. H., and Yun, K. H. (1990). Seasonal variation and production of zooplankton in chonsu bay, Korea. *Korea. J. Oceanol. Soc* 25 (4), 229–239.

Shropshire, T. A., Morey, S. L., Chassignet, E. P., Bozec, A., Coles, V. J., Landry, M. R., et al. (2020). Quantifying spatiotemporal variability in zooplankton dynamics in the gulf of Mexico with a physical–biogeochemical model. *Biogeosciences* 17 (13), 3385–3407. doi: 10.5194/bg-17-3385-2020

Soh, H. Y. (2010). *Invertebrate fauna of Korea: Volume 21, number 3, marine planktonic copepods* (Korea: National Institute of Biological Resources), 1–197 pp.

Soh, H. Y., and Moon, S. Y. (2014). *Invertebrate fauna of Korea: Volume 34, number 28, marine planktonic copepods* (Korea: National Institute of Biological Resources), 1–138 pp.

Soh, H. Y., Moon, S. Y., and Wi, J. H. (2013). *Invertebrate fauna of Korea: Volume 21, number 28, marine planktonic copepods* (Korea: National Institute of Biological Resources), 1–157 pp.

Soh, H. Y., and Suh, H. L. (1993). Seasonal fluctuation of the abundance of the planktonic copepods in kwangyang bay. *Korean J. Environ. Biol.* 11 (1), 26–34.

Suh, H. L., Soh, H. Y., and Cha, S. S. (1991). Salinity and distribution of zooplankton in the estuarine system of mankyong river and dongjin river. *Korean J. Environ. Biol.* 26, 181–192.

Telesh, I. V. (2004). Plankton of the Baltic estuarine ecosystems with emphasis on Neva estuary: a review of present knowledge and research perspectives. *Mar. pollut. Bull.* 49 (3), 206–219. doi: 10.1016/j.marpolbul.2004.02.009

Thompson, G. A., Dinofrio, E. O., and Alder, V. A. (2013). Structure, abundance and biomass size spectra of copepods and other zooplankton communities in upper waters of the southwestern Atlantic ocean during summer. *J. Plankton. Res.* 35 (3), 610–629. doi: 10.1093/plankt/fbt014

Tiselius, P., Saiz, E., and Kiørboe, T. (2013). Sensory capabilities and food capture of two small copepods, paracalanus parvus and pseudocalanus sp. *Limnol. Oceanogr.* 58 (5), 1657–1666. doi: 10.4319/lo.2013.58.5.1657

Tomita, M., Shiga, N., and Ikeda, T. (2003). Seasonal occurrence and vertical distribution of appendicularians in toyama bay, southern Japan Sea. *J. Plankton Res.* 25 (6), 579–589. doi: 10.1093/plankt/25.6.579

Wang, W., Yu, Z., Song, X., Chi, L., Zhou, P., Wu, Z., et al. (2022). Hypoxia formation in the East China Sea by decomposed organic matter in the kuroshio subsurface water. *Mar. Pollut. Bull.* 177, 113486. doi: 10.1016/j.marpolbul.2022.113486

White, J. R., and Dagg, M. J. (1989). Effects of suspended sediments on egg production of the calanoid copepod acartia tonsa. *Mar. Biol.* 102 (3), 315–319. doi: 10.1007/BF00428483

Williams, A. K., McInnes, A. S., Rooker, J. R., and Quigg, A. (2015). Changes in microbial plankton assemblages induced by mesoscale oceanographic features in the northern gulf of Mexico. *PloS One* 10 (9), e0138230. doi: 10.1371/journal.pone.0138230

WoRMS Editorial Board (2022) *World register of marine species* (VLIZ). Available at: https://www.marinespecies.org (Accessed 2022-03-30).

Zhao, L., and Guo, X. (2011). Influence of cross-shelf water transport on nutrients and phytoplankton in the East China Sea: a model study, *Ocean Sci.*, 7(1), 27–43. doi: 10.5194/os-7-27-2011

frontiers | Frontiers in Marine Science

TYPE Original Research
PUBLISHED 01 August 2022
DOI 10.3389/fmars.2022.959161

Check for updates

OPEN ACCESS

EDITED BY
Meilin Wu,
South China Sea Institute of Oceanology, Chinese Academy of Sciences (CAS), China

REVIEWED BY
Xianmin Wang,
Guangdong Ocean University, China
Yalan Peng,
State Oceanic Administration, China

*CORRESPONDENCE
Kunxian Tang
tangkunxian@tio.org.cn

SPECIALTY SECTION
This article was submitted to Marine Pollution, a section of the journal Frontiers in Marine Science

RECEIVED 01 June 2022
ACCEPTED 08 July 2022
PUBLISHED 01 August 2022

CITATION
Sun Y, Tang K, Ma Y, Zhu X, Li H, Zhang F, Chen S and Huang H (2022) Variations in nutrients and microbes during the occurrence and extinction of algal blooms: A mesocosm experiment with the addition of marine aquaculture sediment. *Front. Mar. Sci.* 9:959161. doi: 10.3389/fmars.2022.959161

COPYRIGHT
© 2022 Sun, Tang, Ma, Zhu, Li, Zhang, Chen and Huang. This is an open-access article distributed under the terms of the Creative Commons Attribution License (CC BY). The use, distribution or reproduction in other forums is permitted, provided the original author(s) and the copyright owner(s) are credited and that the original publication in this journal is cited, in accordance with accepted academic practice. No use, distribution or reproduction is permitted which does not comply with these terms.

Variations in nutrients and microbes during the occurrence and extinction of algal blooms: A mesocosm experiment with the addition of marine aquaculture sediment

Yuanmin Sun[1,2,3], Kunxian Tang[1,2,3]*, Yong Ma[1,2,3], Xuan Zhu[1,4], Heyang Li[1,2,3], Fei Zhang[1,2,3], Shan Chen[1] and Haiping Huang[1]

[1]Third Institute of Oceanography, Ministry of Natural Resources, Xiamen, China, [2]Key Laboratory of Marine Ecological Conservation and Restoration, Ministry of Natural Resources, Xiamen, China, [3]Fujian Provincial Key Laboratory of Marine Ecological Conservation and Restoration, Xiamen, China, [4]College of Fisheries, Jimei University, Xiamen, China

The release of pollutants in sediment often causes secondary pollution of seawater. In this paper, marine aquaculture sediment was added to seawater in a coastal land–based mesocosm, and the changes in microbial and physicochemical parameters were measured to study the influence of sediment disturbance on seawater. The results showed that sediment disturbance had adverse effects on seawater. After adding and stirring the aquaculture sediment, the concentration of dissolved oxygen (DO) gradually decreased, and those of nutrients gradually increased; in particular, the concentrations of ammonia and dissolved inorganic phosphorus (DIP) increased most sharply. After day 9, a bloom dominated by *Chaetoceros* occurred. Concentrations of chlorophyll a (Chl-a) increased, and two obvious Chl-a peaks were observed; the trends of DO and pH were similar to that of Chl-a during the bloom period; and DIP and ammonia were exhausted during periods of Chl-a peaks. During the extinction of algal blooms, the concentrations of Chl-a and DO decreased, whereas those of DIP and ammonia increased. The variation trends of bacteria and viruses were similar to that of Chl-a, with two obvious peaks, which were later than those of Chl-a. There were close connections between Chl-a and nutrients, bacteria and viruses and they showed a trend of changes in turn from nutrients to phytoplankton to bacteria to viruses during the experiment. We concluded that bloom formation was mainly affected by nutrients and weather, and the main reason for bloom decline was the depletion of nutrients. The increase in zooplankton, bacteria, and virus abundance was the ecological effect after the occurrence of algal blooms, and they affected the development of algal blooms.

KEYWORDS

algal bloom, nutrient, bacterium, virus, mesocosm experiment, marine aquaculture sediment

Introduction

There are large amounts of nutrients in aquaculture sediment, which can be released into water under certain conditions (De Casabianca et al., 1997), causing secondary pollution that may also lead to algal blooms (Rasmussen et al., 2003; Robb et al., 2003; Gao et al., 2014; Lei et al., 2022). The algal blooms may also have other severe influences on marine aquaculture and the marine environment (Anderson et al., 2002; Alonso-Rodriguez and Paez-Osuna, 2003; Gary DiLeone and Ainsworth, 2019; Brown et al., 2020). Therefore, research on the mechanisms of algal bloom formation is important for protecting the marine environment and biology (Ou et al., 2022).

Many authors have researched the conditions of bloom formation, the main parameters during blooms, and the impacts on the environment during bloom decline through field investigations and mesocosm experiments (Tada et al., 2001; Sellner et al., 2003; Gao and Song, 2005; Li et al., 2015; Chen, 2019). A number of studies have shown that nutrients, light intensity, temperature, and so on are important conditions for forming algal blooms (Berges and Falkowski, 2003; Ornolfsdottir et al., 2004; Zohdi and Abbaspour, 2019; Lin et al., 2019). Nutrient limits, weather, zooplankton grazing, and viral lysis are usually key factors causing bloom decline (Evans et al., 2003; Zhang et al., 2018). In particular, the interactions between microbes and phytoplankton have become a hot topic in recent years. Some authors have proposed that bacteria could affect the growth of algae by directly lysing algae, secreting extracellular substances indirectly lysing algae, competing for nutrients and so on (Wu et al., 2003; Zhao et al., 2005; Gao et al., 2021). There are also reports abroad that bacteria can attack the outer membrane of diatom cell walls by hydrolytic enzymes (Bidle and Azam, 1999), but there has been no report in which bacteria can lead to the disappearance of algal blooms. Viruses can infect algae, and many authors consider them to be one of the main causes of bloom decline. However, reports on the mortality rate of phytoplankton by viruses have been significantly different (Jacquet et al., 2002; Zhang et al., 2018). There have been few reports on the effects of various factors together on the formation and extinction impacts of algal blooms.

To explore the impacts of special factors on algal blooms, especially nutrients, bacteria, and viruses, an experiment enriched with marine aquaculture sediment was conducted in a mesocosm. Diatom red tides occur frequently in the sea area where the project was located due to land-based pollution discharge and nutrient input from the Jiulong River (Chen et al., 2013). The main physicochemical and microbial parameters were measured during the experiment. The relationships between chlorophyll a (Chl-a) and nutrients, dissolved oxygen (DO), bacteria, and viruses during the whole period of an algal bloom were revealed. The mechanisms of algal blooms and the potential harm of marine aquaculture sediment to the environment were examined. The purpose of this study is to provide a reference for preventing blooms and reducing the environmental impacts after algal blooms.

Materials and methods

The experiment site

The coastal land–based mesocosm (24°26.11′N, 118°5.49′E) was located in Xiamen, Fujian Province, southeastern China and the western Taiwan Strait, adjacent to southern Xiamen Bay.

Mesocosm construction

Two mesocosm bags were mounted in a concrete pool with bamboo poles. Each enclosure's length, width, and depth were 5.08, 2.40, and 1.90 m, respectively. The enclosures were composed of 0.15-mm-thick polyethylene film and opened to the air. Two mesocosms were designated A and B. A glass shed was built above the mesocosms.

Methods

Mesocosms A and B were filled with seawater pumped from the adjoining sea and filtered by gunny bags at the same time. Each mesocosm depth was 1.65 m, and the volume was 20.1 m^3. In the first afternoon, Mesocosm B was added to marine aquaculture sediment collected from Dongshan Island, Fujian Province, a typical mariculture area that was approximately 150 km away from Xiamen. The wet weight of mud in Mesocosm B was 1,184.82 kg, and the thickness was 6.2 cm. Mesocosm A acted as a control group without mud. During the experiment, the "T" type agitator made of stainless steel pipes was used to agitate the sediment around Mesocosm B approximately 20 times daily, prompting the nutrients in the sediment to be released into the water.

Parameters and analysis methods

Light intensity and transparency were measured with an illuminometer and transparency disk in the field, respectively. Parameters of temperature, salinity, pH, DO, and DO saturation were measured with probes, P4 multiparameters made by WTW, Germany, in the field. Seawater samples were filtered through a 0.45-μm filter membrane, and then, the concentration of Chl-a was measured by a spectrophotometer after extraction in 90% acetone for 24 h at 4°C in darkness. Concentrations of

dissolved inorganic phosphorus (DIP), NH_4-N, NO_2-N, NO_3-N, and SiO_3-Si were measured with a spectrophotometer within 12 h. Chemical oxygen demand (COD) was measured by the alkaline potassium permanganate method.

Seawater samples were fixed with polyformaldehyde (2% final concentration), filtered onto 0.2-μm pore size, 25-mm-diameter black polycarbonate filters, and stained with di-amidino-phenyl-indole. Then, bacteria were photographed and counted under a fluorescence microscope. Two milliliters of seawater samples were fixed with glutaraldehyde (0.5% final concentration) and frozen at −20°C until laboratory analysis. The samples were stained with SYBR green I, and then, virus abundance was determined by flow cytometry (FCM). Samples were fixed in Lugol's solution (1% final concentration) in the field, the phytoplankton cell number was counted, and the species were identified under a microscope with an algal counting box.

Sampling time and frequency

Samples were sampled or measured at approximately 12:00 every day, usually once a day, and once every 2~3 days in the last 10 days during postbloom. The samples were collected at 0.5 m below the water surface center for each half mesocosm. The average value calculated from two parallel datasets of each mesocosm is expressed as the mean ± SD.

Experiment of nutrient release from sediment

A total of 100 g (wet weight) of sediment was placed into 1 L of ammonia-free water and fully stirred. After precipitation, the supernatant was filtered through filter paper and 0.45-μm pore size filters to determine the concentrations of DIP, NH_4-N, NO_2-N, NO_3-N, and SiO_3-Si.

Data analysis

Linear regression and ANOVA were performed with SPSS software, and the significance level was 0.05.

Results

Nutrient release and water quality before and after sediment addition

The results of the nutrient release experiment from the sediment showed that a large amount of DIP and NH_4-N was released from the sediment after full stirring. Concentrations of nutrients in Mesocosm B could theoretically rise to very high levels if fully released after adding aquaculture sediment (Table 1). However, the concentrations of nutrients in Mesocosm B were much lower than the possible concentrations after mud was mixed. The concentrations of DIP and NH_4-N, which had the largest increase in the addition and stirring of sediment on the second day, were only 8.7% and 5.7% of the results of the experiment of nutrient release, respectively.

Although nutrients were not fully released, there were obvious variations in the main parameters of water quality before (day 1) and after (day 2) adding sediment (Figure 1). In particular, the concentrations of NH_4-N and DIP increased, and the concentration of DO decreased.

Main environmental parameters

The results of the main environmental parameters during the experiment are shown in Table 2. Affected by the canopy, the light intensity in mesocosms was approximately 1/4 of the direct sunlight outside. In mesocosms, the light intensity was mostly less than 10,000 lx on cloudy or rainy days and was generally greater than 10,000 lx on sunny days. Transparency in Mesocosm B usually ranged from 0.7 to 1.1 m, except at approximately 0.5 m during blooms, and the lowest value was 0.2 m after adding sediment. In contrast, the transparency in Mesocosm A was greater than 1.65 m at all times. Water temperature increased in general during the experiment, and the difference was small between the two mesocosms. The range of salinity was only approximately 1 during the experiment. The pH value in Mesocosm B gradually decreased after adding and stirring sediment, reaching the lowest value, 7.90, on day 4. pH increased after bloom formation, reaching the highest value, 8.82, on day 17, and then gradually decreased during bloom decline. Concentrations of COD in Mesocosm B

TABLE 1 Results of the experiment of nutrient release from sediment and nutrient concentrations before and after adding sediment to Mesocosm B.

Parameters	DIP	NH_4-N	NO_2-N	NO_3-N	DIN	SiO_3-Si
Nutrient release rate from sediment (mg kg^{-1})	3.40	41.00	0.04	6.00	47.04	268.41
Concentrations of nutrients before adding sediment in Mesocosm B (mg L^{-1})	0.025	0.001	0.002	0.704	0.707	2.464
Possible concentrations after adding sediment in Mesocosm B (mg L^{-1})	0.225	2.418	0.005	0.356	3.480	18.285

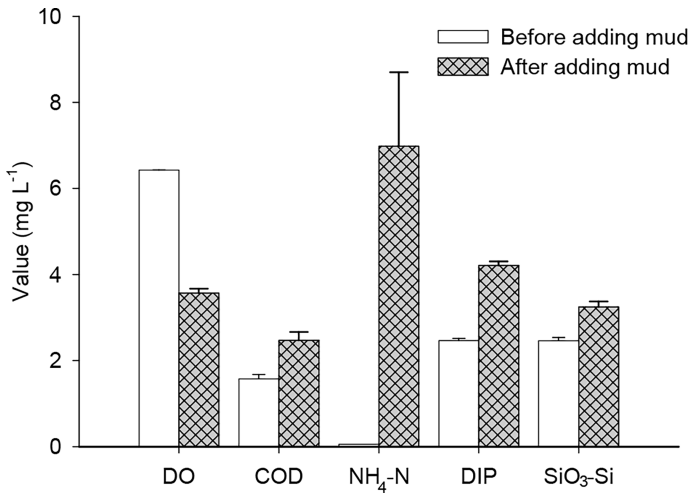


FIGURE 1
DO, COD, NH_4-N, DIP, and SiO_3-Si values before and after adding sediment into Mesocosm B (mean ± SD, NH_4-N × 50, and DIP × 100).

increased obviously after adding sediment, reached the highest value, 2.47 mg L^{-1}, and then gradually decreased. During the algal bloom, it reached another peak value of 2.30 mg L^{-1} on day 16 and then gradually decreased during the bloom decline. Nevertheless, pH and COD values in Mesocosm A were smaller than those in Mesocosm B.

Chl-a and plankton

The concentrations of Chl-a were in a low range during the first 8 days in the two mesocosms. Those in Mesocosm B increased rapidly on day 9 and then reached the first peak on day 11, showing that an algal bloom had formed. The concentrations of Chl-a decreased from days 12 to 14 and reached the second peak from days 15 to 17, with the highest values, 64.00 mg m^{-3}. The dominant genus of the bloom was *Chaetoceros*, whose cell density was 4.44 × 10^7 cells L^{-1} and density was 96.2% of the total density at 12:00 on day 16. The highest density appeared at 18:00 that day, which was 1.29 × 10^8 cells L^{-1}. The diatoms decreased, whereas dinoflagellates increased after day 18. After the formation of blooms, ciliates, fleas, rotifers, and other zooplankton were observed successively. The density of zooplankton was the largest during the bloom decline, and the individual species were small in the early stage and large in the later stage. There were no obvious dominant species of diatoms and dinoflagellates during the third Chl-a peak from days 14 to 18. An algal bloom was observed in Mesocosm A on day 10; however, the concentration and variation range of Chl-a were smaller than those in Mesocosm B, and the highest concentration of Chl-a was only 11.88 mg m^{-3} (Figure 2A).

DO

After adding the sediment, the DO concentration gradually decreased in the early period, reaching the lowest value, 1.50 mg L^{-1}, on day 7, and the lowest DO saturation was 21.3% in Mesocosm B, and then DO concentration gradually increased. The DO concentration increased rapidly after bloom formation, and the trend was similar to that of Chl-a in general, reaching the first peak on day 11 and then decreasing from days 12 to 14. DO concentrations reached the second peak on days 16 and 17, when

TABLE 2 Comparisons of the main environmental parameters during the experiment.

Parameter	Mesocosm B		Mesocosm A	
	Range	Average (Mean ± SD, n = 29)	Range	Average (Mean ± SD, n = 29)
Light intensity (lx)	2,425~29,650	16,600 ± 8,260	2,750~29,300	17,000 ± 7,900 lx
Temperature (°C)	27.0~32.1	29.9 ± 1.9	26.9~31.9	29.6 ± 1.8
Salinity	23.5~24.7	23.9 ± 0.38	23.5~24.4	23.7 ± 0.32
pH	7.90~8.74	8.27 ± 0.27	8.03~8.45	8.30 ± 0.15
COD (mg L^{-1})	0.81~2.47	1.38 ± 0.42	0.56~1.80	0.93 ± 0.28

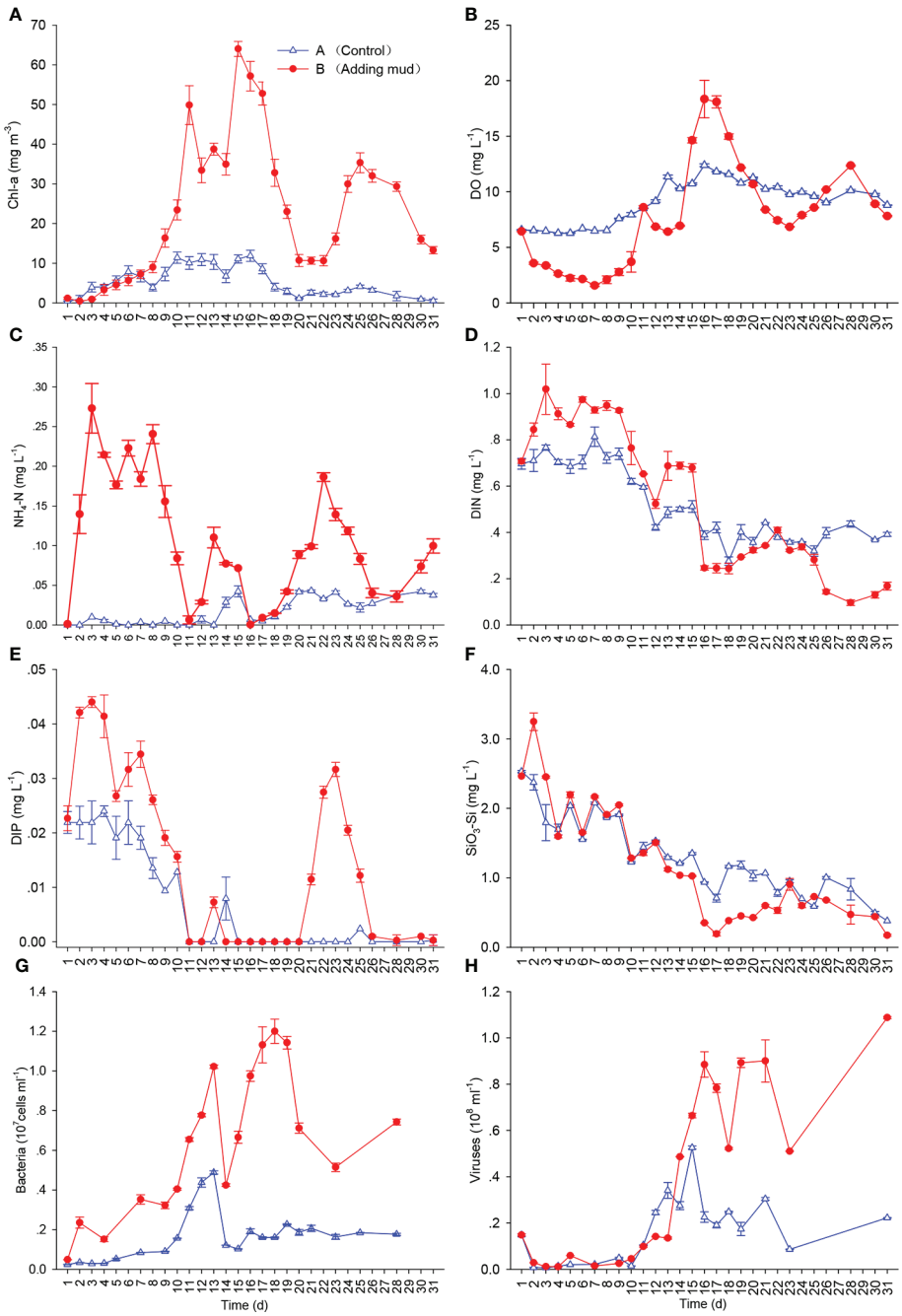


FIGURE 2
Concentrations of Chl-a **(A)**, DO **(B)**, NH4-N **(C)**, DIN **(D)**, DIP **(E)**, and SiO_3-Si **(F)** and abundances of bacteria **(G)** and viruses **(H)** during the experiment (Mean ± SD).

Chl-a concentrations reached the second peak as well, with the highest DO value, 19.53 mg L^{-1}, and the highest DO saturation, 262%, on day 16. DO concentrations gradually decreased during bloom decline and reached another trough on day 23. The variation range of DO concentrations in Mesocosm A was much smaller than that in Mesocosm B (Figure 2B).

Nutrients

As shown in Figures 2C–F, after adding sediment, the concentrations of dissolved inorganic nitrogen (DIN), DIP, and SiO_3-Si increased rapidly in the early days and then decreased gradually. They decreased sharply after bloom

formation and increased during bloom decline, in general. Variations in DIP concentrations were the largest among the three main nutrients, and DIP was even exhausted when Chl-a concentrations peaked. The concentrations of DIN and SiO_3-Si showed downward trends in general during the experiment, but they were never exhausted. The trend of nutrients in Mesocosm A was wholly similar to that in Mesocosm B. The concentration of nutrients in Mesocosm A was relatively stable in the beginning period in cloudy or rainy weather and showed a downward trend under later sunny weather conditions, with a smaller range in Mesocosm A than in Mesocosm B. In contrast, the concentrations of DIN and SiO_3-Si in Mesocosm A were higher than those in Mesocosm B in the late period of the experiment.

Bacteria and viruses

The abundance of bacteria in Mesocosm B increased gradually after bloom formation and reached the first peak on day 13 as Chl-a was at a low concentration. After the second Chl-a peak, the abundance of bacteria decreased sharply and then gradually increased following the bloom, reaching the second peak during bloom decline. Two peaks of bacterial abundance were obviously the same as those of Chl-a in Mesocosm B, but the peaks of bacterial abundance were approximately 2 days later than those of Chl-a. The abundance of bacteria in Mesocosm A was lower than that in Mesocosm B, with only one obvious peak (Figure 2G).

The trend of viral abundance was similar to that of bacteria. The viral abundance in Mesocosm B was very low in the early period, and two obvious peaks were observed, but the occurrence time was approximately 2 days later than that of bacteria. The viral abundance was smaller in Mesocosm A than in Mesocosm B, and only one obvious peak was observed (Figure 2H).

Correlation of Chl-a with NH_4-N, DIP, bacteria, and virus

The correlation analysis results of the main environmental parameters and Chl-a are shown in Table 3. The F-values of DIP, DIN, and SiO_3-Si were all significantly negatively related to Chl-a. The R^2 and F-values of DIP were larger than those of DIN and SiO_3-Si, and the P-value was lower than those of DIN and SiO_3-Si. In the three types of DIN, only NH_4-N was significantly negatively correlated with Chl-a. Significant relationships were also found between DO concentrations, pH values, and Chl-a concentrations. No relationship was found between light intensity and Chl-a during the whole experiment, but the relationship was significant in the early stage of the experiment (days 2 to 17). In addition, the DO concentrations and NH_4-N concentrations were significantly negatively correlated.

There was no significant correlation between Chl-a concentrations and bacterial abundance or viral abundance during blooms. If the time of bacteria and viruses was advanced 2 and 4 days, respectively, then they were significantly correlated (Table 4).

Discussion

Impact of sediment on the environment

Aquaculture sediment contains a large amount of nutrients, which can be effectively released into the water after full stirring (Table 1). The most severe influences on the environment were the sharp increase in the concentrations of DIP and NH_4-N and the gradual decrease in the concentrations of DO, whereas the abundance of bacteria increased slightly and the abundance of viruses did not change obviously (Figures 2B, C, E, G, H). On the other hand, nutrients continuously released from the daily stirring of sediment affected the occurrence and maintenance of algal blooms.

TABLE 3 Correlation analysis between the main environmental parameters and Chl-a.

Parameters	Correlation Equation	R^2	F	P	n
DIP	y = −0.0006x + 0.0286	0.516	28.839 *	0.000 *	29
NH_4-N	y = −0.0028x + 0.169	0.432	20.503 *	0.000 *	29
NO_2-N	y = −0.00005x + 0.0126	0.030	0.832	0.370	29
NO_3-N	y = −0.0039x + 0.519	0.070	2.047	0.164	29
DIN	y = −0.0068x + 0.698	0.161	5.188 *	0.031 *	29
SiO_3-Si	y = −0.0236x + 1.712	0.240	8.506 *	0.007 *	29
DO	y = 0.195x + 3.364	0.551	33.148 *	0.000 *	29
pH	y = 0.0104x + 8.035	0.482	23.224 *	0.000 *	29
Light intensity	y = 150x + 13009	0.100	2.897	0.101	29
Light intensity (days 2~17)	y = 222x + 5858	0.511	14.649 *	0.002 *	16

*Significant at the 0.05 level.

TABLE 4 Correlation analysis between bacteria, viruses, and Chl-a.

Parameters	Correlation Equation	R^2	F	P	n
Bacteria	y = 56730x + 5724718	0.074	0.715	0.420	11
Viruses	y = 1017222x + 3104872	0.203	2.290	0.164	11
Bacteria (2 days later)	y = 142851x + 2900439	0.754	27.649 *	0.001 *	11
Viruses (4 days later)	y = 1575672x + 2455708	0.820	41.002 *	0.000 *	11

*Significant at the 0.05 level.

Relationship between nutrients and algal blooms

The nutrients provide sources for the formation of algal blooms. The higher concentration of nutrients led to the higher concentration of Chl-a during algal blooms; therefore, obvious algal blooms and higher concentrations of Chl-a were observed in Mesocosm B than in Mesocosm A (Figure 2A). The increase and decrease in Chl-a were accompanied by a sharp decline and increase in nutrients, indicating that the formation of algal blooms consumed a large amount of nutrients. After the disappearance of algal blooms, nutrients were remineralized and released into the water.

DIP was the nutrient limitation factor of algal blooms in the experiment. The mole ratio of DIN and DIP released from sediment was 31:1 and that of water pumped from the sea was 63:1 (Table 1). Both were far higher than the ratio of N and P in normal algal cells (16:1). The mole ratio of DIN and DIP of mixed water in Mesocosm B was 53:1; therefore, it could be seen that the seawater of the experiment had a phosphorus limitation status. Other studies have also shown that the sea area where the project was located has potential P limitation characteristics (He et al., 2021). When the two peaks of Chl-a were formed, DIP was exhausted quickly, whereas DIN and SiO_3-Si were never depleted (Figures 2A, D–F). The correlation between DIP concentrations and Chl-a concentrations was the most significant, suggesting that DIP had the closest relationship with Chl-a among the three main nutrients (Table 1). Among the three types of DIN, only NH_4-N concentrations were significantly correlated with Chl-a concentrations (Table 1). Because NH_4-N can be directly absorbed by phytoplankton and synthesized into amino acids (Carpenter and Dunham, 1985), algae absorb NH_4-N during the formation of algal blooms and then absorb NO_2-N and NO_3-N after NH_4-N exhaustion. In addition, NH_4-N was produced foremost during bloom decline (Figure 2C); therefore, NH_4-N values were the most obvious during the formation and decline of algal blooms.

DIP and NH_4-N were exhausted on day 11 during the first Chl-a peak, but DIN concentrations continued to decrease on day 12, indicating that algae could continue to absorb and store nitrogen when phosphorus was depleted. DIP was exhausted again at the beginning of the second Chl-a peak (Figure 2E), but NH_4-N was exhausted after two days (Figure 2C), and DIN also maintained a stable period of 3 days (Figure 2D), indicating that there was still sufficient nitrogen in algal cells when the second peak was just formed, which might have been stored during the period when DIP was depleted. Andersen et al. (1991) pointed out that the phosphorus stored in the body could maintain the growth of microalgae for several hours. In this study, Chl-a reached its maximum value on day 15 after DIP was exhausted on day 14, which may be related to the continuous release of DIP from sediment to seawater. However, phosphorus limitation arrested the growth of microalgae, and the Chl-a concentration and algal cell density decreased gradually (Figures 2A, E). This indicated that phosphorus limitation was one of the main reasons for the disappearance of this bloom.

Relationship between bacteria and algal blooms

The results showed that the abundance of bacteria increased after algal bloom formation and reached peaks during bloom decline. A significant increase in the number of debris in the water during bloom decline was observed by microscopy, and a large number of bacteria were often observed on the surface under a fluorescence microscope. Riemann et al. (2000) pointed out that dead diatoms would be quickly invaded by bacteria with a strong particle hydrolysis function, and the proportion of adherent bacteria during late blooms was much higher than that during early blooms.

Although the abundance of bacteria peaked after the first Chl-a peak decline (days 12~13), the second Chl-a peak formed rapidly as the weather became clear (Figures 2A, G), indicating that bacteria could not effectively control the formation of algal blooms. Riemann et al. (2000) also found that the abundance of bacteria in the early stage of algal blooms was large, but it did not hinder the formation of algal blooms. Therefore, the role of bacteria was to degrade cell detritus and accelerate nutrient cycling.

Relationship between viruses and algal blooms

A large number of viruses can effectively infect a considerable part of the phytoplankton community (Fuhrman, 1999).

Algal dynamics could be controlled by reducing the number of hosts or preventing the number of algae from reaching a high level (Brussaard, 2004). There have also been reports of the isolation of *Trichomonas* viruses in the East China Sea (Wu et al., 2011). In this study, the abundance of viruses did not increase obviously as the Chl-a concentration decreased (days 12~14). The abundance decreased from days 16 to 18 during the bloom decline (Figures 2H), indicating that viruses did not play an important role in the bloom decline, and the reduction in the number of algal cells did not release a large number of viruses. The effects of viruses on algal death have varied greatly in different research studies. Some studies have shown that the mortality of algae caused by viruses is only 2%–10% (Waterbury and Valois, 1993; Cottrell and Suttle, 1995). Nevertheless, Jacquet et al. (2002) estimated that 230–400 viruses could be released from each algal cell after lysis, and the mortality rate of viral infection per day accounted for 40%–100% of the total net mortality of algal cells. Evans et al. (2003) estimated that the virus-induced mortality of *Micromonas* ranged from 10% to 34% every day. Therefore, they considered that viruses played an important role in bloom decline. However, their experiments only measured the density of phytoplankton and the abundance of viruses and did not measure the abundance of bacteria nor did they confirm whether these viruses came from the lysis of algal cells or whether they all had an algal-killing function. They may have also regarded bacterial viruses as alga viruses, and the role of viruses may have been overestimated. In this study, the viruses could be divided into algal viruses and bacterial viruses by flow cytometry, and bacterial viruses accounted for 93.0 ± 3.5% of the total viruses. Moreover, the trend of viruses was similar to that of bacteria, and the peaks of viruses were approximately 2 days later than those of bacteria (Figures 2G, H). These results indicated that viruses were released mainly from lysed cells of bacteria, and algal viruses only accounted for a small fraction of the total viruses. Winter et al. (2005) also pointed out that viruses mainly came from the infection of prokaryotic organisms, and algal viruses did not contribute significantly to the virus pool. Schroeder et al. (2003) considered that although several viral genotypes appeared at the beginning of an *Emiliania huxleyi* bloom, only a small number of viral genotypes eventually continued to show algaecidal function in the late bloom. Therefore, we point out that viruses mainly came from bacterial infection and did not play a key role in the extinction of algal blooms. In addition, the first peak of viruses occurred during the sustained phase of the second Chl-a peak (Figures 2A, H), indicating that viruses could not effectively control the formation of algal blooms.

Relationship between bacteria, viruses, and algal blooms

In this study, there was no significant correlation between bacteria, viruses, and Chl-a during algal blooms (Table 4). The main reason for this was that the peak time of bacteria and viruses lagged behind that of Chl-a (Figures 2A, G, H). If the data of bacteria and viruses were advanced by 2 and 4 days, respectively, there was a significant correlation between bacteria, viruses, and Chl-a (Table 4), indicating that phytoplankton, bacteria, and viruses were closely linked in regard to temporal changes. The death of phytoplankton promoted the mass reproduction of bacteria, and bacterial lysis released a large number of viruses. Marchant et al. (2000) found that the abundance of viruses was not significantly correlated with the abundance of bacteria and the concentration of Chl-a in the Southern Ocean, whereas there were significant correlations between bacteria or viruses and Chl-a in other studies (Culley and Welschmeyer, 2002). Different correlations may be related to the duration of algal blooms. If the duration of algal blooms is longer, then there may be a good correlation between bacteria, viruses, and Chl-a in their spatial distribution.

Other factors affecting the formation and extinction of algal blooms

The algal bloom occurred shortly after seawater was pumped into mesocosms, whereas no bloom was observed in the adjacent sea area during that period, showing that the stable water body was beneficial to the formation of algal blooms.

Sufficient light intensity is one of the conditions for the formation of algal blooms (Kana et al., 2004). The number of algal cells decreases sharply when light is insufficient, and algae can grow again after relighting (Berges and Falkowski, 2003). Therefore, the first 9 days of cloudy and rainy weather conditions prevented the formation of algal blooms. The 10th day after the weather turned clear, algal blooms quickly formed, but due to the subsequent days of cloudy and rainy weather, algal blooms declined. The 14th day turned clear and a second peak of algal blooms formed.

Zooplankton grazing on phytoplankton is usually one of the main reasons for bloom decline (Strom et al., 2001). Zooplankton grazing has little effect on phytoplankton during algal blooms but increases during diatom bloom decline (Tsuda et al., 2006). In this study, the density of zooplankton in the early stage of algal blooms was small, which had little effect on algal blooms and could not control the rapid formation of the second algal bloom peak. However, the density of zooplankton increased sharply during the bloom decline. Therefore, zooplankton grazing was another main reason for the bloom decline.

During the algal bloom, the concentration of DO increased, and the concentration of nutrients decreased. Phytoplankton and zooplankton with large densities are ideal food for cultured

animals. Therefore, maintaining a certain density of phytoplankton in aquaculture ponds is conducive for improving water quality and promoting the growth of aquacultural organisms.

However, it is difficult to control phytoplankton, and some reasons for this include nutrient depletion and weather changes, which usually cause bloom decline. During bloom decline, the concentration of DO decreased, whereas the concentration of ammonia increased, which is harmful to aquatic animals and leads to disease outbreak and spread.

Research prospects

The formation and extinction of algal blooms were affected by nutrient concentrations, light intensity, and water stability. The extinction process was accompanied by an increase in NH_3 concentration and a decrease in DO concentration, which may lead to the deterioration of seawater quality and the outbreak of marine biological diseases. Research on the mechanisms of algal blooms and the early warning and monitoring of algal blooms should be further strengthened to prevent algal blooms and reduce the harm to aquaculture and the ecological environment after algal blooms.

Data availability statement

The original contributions presented in the study are included in the article/supplementary material. Further inquiries can be directed to the corresponding author.

Author contributions

KT and YM conducted the sampling and measurements. HL, SC, and FZ analyzed the results. YS wrote the original manuscript. KT, XZ and HH revised the manuscript. All authors contributed to the article and approved the submitted version.

Funding

This research was supported by National Key R&D Program of China (Grant No. 2020YFA0607603) and Co-construction Program of Xiamen Ocean Research and Development Institute (Grant No. K200701).

Conflict of interest

The authors declare that the research was conducted in the absence of any commercial or financial relationships that could be construed as a potential conflict of interest.

Publisher's note

All claims expressed in this article are solely those of the authors and do not necessarily represent those of their affiliated organizations, or those of the publisher, the editors and the reviewers. Any product that may be evaluated in this article, or claim that may be made by its manufacturer, is not guaranteed or endorsed by the publisher.

References

Alonso-Rodriguez, R., and Paez-Osuna, F. (2003). Nutrients, phytoplankton and harmful algal blooms in shrimp ponds: A review with special reference to the situation in the gulf of California. *Aquaculture* 219, 317–336. doi: 10.1016/S0044-8486(02)00509-4

Andersen, T., Schartau, A. K. L., and Paasche, E. (1991). Quantifying external and internal nitrogen and phosphorus pools, as well as nitrogen and phosphorus supplied through remineralization, in coastal marine plankton by means of a dilution technique. *Mar. Ecol. Prog. Ser.* 69, 67–80. doi: 10.3354/meps069067

Anderson, D. M, Gilbert, P. M., and Burkholder, J. M. (2002). Harmful Algal Blooms and Eutrophication: Nutrient Sources, Composition, and Consequences. *Estuaries* 25(4), 704–726. doi: 10.1007/BF02804901

Berges, J. A., and Falkowski, P. G. (2003). Physiological stress and cell death in marine phytoplankton: Induction of proteases in response to nitrogen or light limitation. *Limnol. Oceanogr.* 43 (1), 129–135. doi: 10.4319/lo.1998.43.1.0129

Bidle, K. D., and Azam, F. (1999). Accelerated dissolution of diatom silica by marine bacterial assemblages. *Nature* 397, 509–512. doi: 10.1038/17351

Brown, A. R., Lilley, M., Shutler, J., Lowe, C., Artioli, Y., Torres, R., et al. (2020). Assessing risks and mitigating impacts of harmful algal blooms on mariculture and marine fisheries. *Rev. Aquacult.* 12 (3), 1663–1688. doi: 10.1111/raq.12403

Brussaard, C. P. D. (2004). Viral control of phytoplankton populations-a review. *J. Eukaryot. Microbiol.* 51 (2), 125–138. doi: 10.1111/j.1550-7408.2004.tb00537.x

Carpenter, E. J., and Dunham, S. (1985). Nitrogenous nutrient uptake, primary production, and species composition of phytoplankton in the carmans river estuary, long island, new York. *Limnol. Oceanogr.* 30 (3), 513–526. doi: 10.4319/lo.1985.30.3.0513

Chen, J. (2019). Effects of sand dust addition and nutrient input on phytoplankton in the offshore waters. [master's thesis] [Xiamen (China)]. *Xiamen University*.

Chen, B., Ji, W., Chen, J., Lin, C., Huang, H., Huo, Y., et al. (2013). Characteristics of nutrients in the jiulong river and its impact on xiamen water, China. *Chin. J. Oceanol. Limn.* 31 (5), 1055–1063. doi: 10.1007/s00343-013-2263-3

Cottrell, M. T., and Suttle, C. A. (1995). Dynamics of a lytic virus infecting the photosynthetic marine picoflagellate *Micromonas pusilla*. *Limnol. Oceanog.* 40 (4), 730–739. doi: 10.4319/lo.1995.40.4.0730

Culley, A. I., and Welschmeyer, N. A. (2002). The abundance, distribution, and correlation of viruses, phytoplankton, and prokaryotes along a pacific ocean transect. *Limnol. Oceanogr.* 47 (5), 1508–1513. doi: 10.4319/lo.2002.47.5.1508

De Casabianca, M. L., Laugier, T., and Marinho-Soriano, E. (1997). Seasonal changes of nutrients in water and sediment in a Mediterranean lagoon with shellfish farming activity (Thau lagoon, France). *Ices. J. Mar. Sci.* 54, 905–916. doi: 10.1006/jmsc.1996.0201

Evans, C., Archer, S. D., Jacquet, S., and Wilson, W. H. (2003). Direct estimates of the contribution of viral lysis and microzooplankton grazing to the decline of a *Micromonas* spp. population. *Aquati. Microb. Ecolo.* 30 (3), 207–219. doi: 10.3354/ame030207

Fuhrman, J. A. (1999). Marine viruses and their biogeochemical and ecological effects. *Nature* 399, 541–548. doi: 10.1038/21119

Gao, Q., Huang, L., Xu, W., Chen, X., Gu, H., and Luo, Z. (2021). Review on the algicidal effect of bacteria on red tide related algae. *J. Fish. Res.* 43 (4), 426–435. doi: 10.14012/j.cnki.fjsc.2021.04.010

Gao, X., and Song, J. (2005). Phytoplankton distributions and their relationship with the environment in the changjiang estuary, China. *Mar. pollut. Bull.* 50 (3), 327–335. doi: 10.1016/j.marpolbul.2004.11.004

Gao, D., Zhang, M., and Hong, B. (2014). The quality control of eutrophic culture sediment by immobilized cells and conditions manipulation. *Appl. Mechanics Mater.* 644-650, 5169–5173. doi: 10.4028/www.scientific.net/AMM.644-650.5169

Gary DiLeone, A. M., and Ainsworth, C. H. (2019). Effects of *Karenia brevis* harmful algal blooms on fish community structure on the West Florida shelf. *Ecol. Model.* 392, 250–267. doi: 10.1016/j.ecolmodel.2018.11.022

He, E., Ji, X., Li, X., Li, X., Wang, D., and Yang, J. (2021). The spatial-temporal distribution and hazard grading of red tides in fujian coast waters during 2001-2020. *Mar. Sci. Bull.* 40 (5), 578–590. doi: 1001-6932(2021)05-0578-13

Jacquet, S., Heldal, M., Iglesias-Rodriguez, D., Larsen, A., Wilson, W., and Bratbak, G. (2002). Flow cytometric analysis of an *Emiliana huxleyi* bloom terminated by viral infection. *Aquat. Microb. Ecol.* 27 (2), 111–124. doi: 10.3354/ame027111

Kana, T. M., Lomas, M. W., MacIntyre, H. L., Cornwell, J. C., and Gobler, C. J. (2004). Stimulation of the brown tide organism, *Aureococcus anophagefferens*, by selective nutrient additions to *in situ* mesocosms. *Harmful Algae.* 3 (4), 377–388. doi: 10.1016/j.hal.2004.06.008

Lei, X., Zhang, Y., Jiang, L., Luo, Y., Zhou, G., Sun, Y., et al. (2022). Zonal macroalgae blooms influenced by different aquaculture discharges in the xuwen fringing reef, southern China. *Sci. Total Environ.* 822. doi: 10.1016/j.scitotenv.2022.153594

Li, B., Lan, W., Li, T., and Li, M. (2015). Variation of environmental factors during *Phaeocystis globosa* blooms and its implications for the bloom decay. *Chin. J. Ecol.* 34 (5), 1351–1358. doi: 1000-4890(2015) 5-1351-08

Lin, S., Ji, N., and Luo, H. (2019). Recent progress in marine harmful algal bloom research. *Chin. J. Oceanol. Limn.* 50 (3), 495–510. doi: 10.11693/hyhz20180800191

Marchant, H., Davidson, A., Wright, S., and Glazebrook, J. (2000). The distribution and abundance of viruses in the southern ocean during spring. *Antarct. Sci.* 12 (4), 414–417. doi: 10.1017/S0954102000000481

Ornolfsdottir, E. B., Lumsden, S. E., and Pinckney, J. L. (2004). Phytoplankton community growth-rate response to nutrient pulses in a shallow turbid estuary, Galveston bay, Texas. *J. Plankton. Res.* 26 (3), 325–339. doi: 10.1093/plankt/fbh035

Ou, L., Li, J., Zhang, X., Wang, Z., Zou, J., and Lu, S. (2022). Dissolved organic matter and activities of extracellular enzymes in two lagoons (South China Sea) affected by aquaculture. *Front. Mar. Sci.* 9. doi: 10.3389/fmars.2022.864579

Rasmussen, B., Gustafsson, B. G., Stockenberg, A., and Ærtebjerg, G. (2003). Nutrient loads, advection and turnover at the entrance to the Baltic Sea. *J. Marine. Syst.* 39, 43–56. doi: 10.1016/S0924-7963(02)00246-4

Riemann, L., Steward, G. F., and Azam, F. (2000). Dynamics of bacterial community composition and activity during a mesocosm diatom bloom. *Appl. Environ. Microbi.* 66 (2), 578–587. doi: 10.1128/AEM.66.2.578-587.2000

Robb, M., Greenop, B., Goss, Z., Douglas, G., and Adeney, J. (2003). Application of Phoslock^{TM}, an innovative phosphorus binding clay, to two Western Australian waterways: Preliminary findings. *Hydrobiologia* 494, 237–243. doi: 10.1023/A:1025478618611

Schroeder, D. C., Oke, J., Hall, M., Malin, G., and Wilson, W. H. (2003). Virus succession observed during an *Emiliania huxleyi* bloom. *Appl. Environ. Microb.* 69 (5), 2484–2490. doi: 10.1128/AEM.69.5.2484-2490.2003

Sellner, K. G., Doucette, G. J., and Kirkpatrick, G. J. (2003). Harmful algal blooms: Causes, impacts and detection. *J. Ind. Microbiol. Biot.* 30 (7), 383–406. doi: 10.1007/s10295-003-0074-9

Strom, S. L., Brainard, M. A., Holmes, J. L., and Olson, M. B. (2001). Phytoplankton blooms are strongly impacted by microzooplankton grazing in coastal north pacific waters. *Mar. Biol.* 138 (2), 355–368. doi: 10.1007/s002270000461

Tada, K., Morishita, M., Hamada, K., Montani, S., and Yamada, M. (2001). Standing stock and production rate of phytoplankton and a red tide outbreak in a heavily eutrophic embayment, dokai bay, Japan. *Mar. pollut. Bull.* 42 (11), 1177–1186. doi: 10.1016/S0025-326X(01)00136-9

Tsuda, A., Saito, H., Nishioka, J., Ono, T., Noiri, Y., and Kudo, I. (2006). Mesozooplankton response to iron enrichment during the diatom bloom and bloom decline in SERIES (NE pacific). *Deep-Sea Res. Pt. II.* 53, 2281–2296. doi: 10.1016/j.dsr2.2006.05.041

Waterbury, J. B., and Valois, F. W. (1993). Resistance to Co-occurring phages enables marine synechococcus communities to coexist with cyanophages abundant in seawater. *Appl. Environ. Microb.* 59 (10), 3393–3399. doi: 10.1128/AEM.59.10.3393-3399.1993

Winter, C., Smit, A., Herndl, G. J., and Weinbauer, M. G. (2005). Linking bacterial richness with viral abundance and prokaryotic activity. *Limnol. Oceanogr.* 50 (3), 968–977. doi: 10.4319/lo.2005.50.3.0968

Wu, W., An, C., Liu, X., Wu, X., Wen, D., and Shi, M. (2003). Preliminary research on alga removal characteristics and efficiency of the algae-lysing bacterium (Strain B_5). *Acta Scientiarum Naturalium Universitatis Pekinensis.* 39 (4), 489–493. doi: 10.13209/j.0479-8023.2003.074

Wu, Q., Cheng, K., Yang, J., Chen, J., Zhao, Y., and Xu, M. (2011). Isolation and characterization of a marine *Chaetoceros muelleri* virus. *Oceanol. Et Limnol. Sinica.* 42 (3), 455–459. doi: 10.11693/hyhz201103019019

Zhang, Z., Tang, L., and Zhang, Y. (2018). Algae-bacteria interactions and their ecological functions in the ocean. *Microbiol. China* 45 (9), 2043–2053. doi: 10.13344/j.microbiol.china.180178

Zhao, C., Pu, Y., Yin, L., Lu, X., and Li, X. (2005). Isolation and algicidal effect of a lytic microcystis bacterium from taihu lake. *J. Southeast Univ. (Natural Sci. Ed.)* 35 (4), 602–606. doi: 1001-0505(2005)04-0602-05

Zohdi, E., and Abbaspour, M. (2019). Harmful algal blooms (Red tide): A review of causes, impacts and approaches to monitoring and prediction. *Int. J. Environ. Sci. Te.* 16 (3), 1789–1806. doi: 10.1007/s13762-018-2108-x

frontiers | Frontiers in Marine Science

TYPE Data Report
PUBLISHED 02 August 2022
DOI 10.3389/fmars.2022.954622

Check for updates

OPEN ACCESS

EDITED BY
Meilin Wu,
South China Sea Institute of Oceanology (CAS), China

REVIEWED BY
Thilagam Harikrishnan,
Pachaiyappa's College for Men, India
Rajamanickam Krishnamurthy,
Arignar Anna Government Arts and Science College Chennai, India
P. Soundarapandian Pandian,
Annamalai University, India

*CORRESPONDENCE
Thalavai Shivasankarasubbiah Kumar
tskumarniot@gmail.com
Gopal Dharani
dhara@niot.res.in
Anthony Josephine
ajosephineanthony@gmail.com

SPECIALTY SECTION
This article was submitted to Marine Pollution, a section of the journal Frontiers in Marine Science

RECEIVED 27 May 2022
ACCEPTED 28 June 2022
PUBLISHED 02 August 2022

CITATION
Josephine A, Kumar TS, Surendran B, Rajakumar S, Kirubagaran R and Dharani G (2022) Evaluating the effect of various environmental factors on the growth of the marine microalgae, *Chlorella vulgaris*. *Front. Mar. Sci.* 9:954622. doi: 10.3389/fmars.2022.954622

COPYRIGHT
© 2022 Josephine, Kumar, Surendran, Rajakumar, Kirubagaran and Dharani. This is an open-access article distributed under the terms of the Creative Commons Attribution License (CC BY). The use, distribution or reproduction in other forums is permitted, provided the original author(s) and the copyright owner(s) are credited and that the original publication in this journal is cited, in accordance with accepted academic practice. No use, distribution or reproduction is permitted which does not comply with these terms.

Evaluating the effect of various environmental factors on the growth of the marine microalgae, *Chlorella vulgaris*

Anthony Josephine[1,2]*, Thalavai Shivasankarasubbiah Kumar[1]*, Baskaran Surendran[3], Sundaram Rajakumar[4], Ramalingam Kirubagaran[1] and Gopal Dharani[1]*

[1]National Institute of Ocean Technology, Ministry of Earth Sciences, Government of India, Chennai, Tamil Nadu, India, [2]Central Research Laboratory, Meenakshi Academy of Higher Education and Research (MAHER-Deemed to be University), Chennai, Tamil Nadu, India, [3]Department of Pharmacology, JSS College (Jagadguru Sri Shivarathreeswara University, Mysuru), Rockland's, Udhagamandalam-643001, Tamil Nadu, India, [4]Department of Marine Biotechnology, Bharathidasan University, Tiruchirapalli, Tamil Nadu, India

KEYWORDS

plankton, microalgae, *Chlorella*, marine environment, long term study

Introduction

Chlorella is a green single-celled alga (Bito et al., 2020) that is easily cultivable, and it consists of 20% lipid content from dry biomass (Scarsella et al., 2010; Al-lwayzy et al., 2014). It is also the most popular microalga in the market and is often selected due to the higher level of carotenoids present and its ability to grow in a wide variety of climatic conditions (Gors et al., 2009). *Chlorella* has a high content of about 51%–58% protein, 12%–17% carbohydrate, and 14%–22% lipid (calculated as % of dry matter). Most importantly, its growth rate and biomass production largely depend on environmental factors (Spolaore et al., 2006).

Microalgae have received a lot of attention due to their potential benefits in many applications, and therefore, enhancing the biomass by regulating environmental factors responsible for the growth becomes necessary for feasible algal culture (Khan et al., 2018). The chemical composition of algae (cellular content) varies according to species and its physiological responses to biotic and abiotic factors such as temperature, illumination, pH, nutrients, and growth phase (Brown et al., 1993; Carvalho and Malcata, 2000). Apart from light intensity, other physicochemical parameters like temperature, pH, and salinity are also the vital environmental factors that influence the photosynthetic activity and behavior of microalgal growth rate (Blinová et al., 2015). Pulz and Gross (2004) stated that successful algal biotechnology mainly depends on selecting the right species with relevant properties for specific culture conditions and products.

Numerous studies have documented that environmental factors such as temperature, pH, salinity, and light have a substantial impact on the growth of microalgae (Mata et al., 2010; Zongo and Boussim, 2015; Chowdury et al., 2020). In general, studies on microalgae

have shown that their growth was significantly enhanced when one or two optimum environmental factors were combined. The compensatory effects of numerous factors are observed to be responsible for this improvement (Cheng and He, 2014; Salama et al., 2018). The current study will explore how *Chlorella vulgaris* would respond to the ideal environmental parameters such as temperature, pH, salinity, and light intensity, both individually and in combination. The present study is an attempt to achieve high growth and biomass production with optimized environmental variables.

Methods

Sample collection and growth determination

The NIOT vessel Sagar Paschimi was used for a scientific cruise to survey the microalgal diversity near the Puducherry coast. The study species *C. vulgaris* was isolated from the coastal waters (11° 54′ 27.54″ N; 79° 49′ 35.70″ E) and identified (JF894249, NCBI GenBank, USA) and deposited in a public repository at National Facility for Marine Cyanobacteria, Bharathidasan University, India (Accession number, BDU GD 003). The micro algae were cultured in 20-L polycarbonate carboys using F/2 medium (Guillard). The cell growth was monitored by cell count with the help of a Neubauer chamber (Santos and Mariano, 2014). The dry biomass was estimated by filtering 5 ml of the sample using 0.22-µm GFC filter paper and dried in a hot air oven for 24 h maintained at 70°C (Zhu and Lee, 1997).

Experiments on temperature, pH, salinity, and light intensities

The effects of physicochemical parameters like temperature, pH, and salinity were examined to identify the optimal growth conditions for *C. vulgaris*. Different temperatures like 20°C, 25°C, 30°C, 35°C, and 40°C were attempted in this experiment using separately controlled incubators (Scigenics Biotech, Orbitek) fitted with fluorescent lamps (42 µmol m^{-2} s^{-1}). Similarly, studies were conducted at different pH, *viz*., 6, 7, 8, 9, and 10. The pH of the culture medium was measured using a pH meter (Metrohm), and the pH level was adjusted using NaOH and HCl to raise or lower the value. In another set of experiments, the effect of salinity on the growth rate was carried out at different salinities (0, 10, 20, 30, and 50 Practical Salinity Unit (PSU)). Salinity was determined using a refractometer (Atago, Japan), and the culture medium was adjusted with distilled water or NaCl to either reduce and/or increase the salinity. Experiments on different light intensities was carried out under phototrophic conditions using fluorescent lamp (Philips 23W) covered with different colored filters such as red (700–625 nm), orange (624–600 nm), blue (499–465 nm), violet (425–400 nm), green (569–500 nm), and yellow (599–670 nm), along with one positive control (+) (white light, 400–700 nm) and negative control (–) (dark).

The experiments were conducted over a 15-day period in triplicate. The biomass was estimated every 5 days, and the cell count was monitored daily. The values are expressed as mean ± S.E. The SPSS software (version 20.0) was used for the statistical analysis. To find out statistical differences, the data were subjected to a two-way analysis of variance (ANOVA) followed by Tukey's multiple comparison *post hoc* test. Differences were statistically significant at $p < 0.05$ and $p < 0.001$.

Results and discussion

In the present investigation, a higher growth rate was observed at 25°C in terms of cell count and biomass. The trend was then followed by 20°C and 30°C compared with 35°C and 40°C on the 15th day (Figure 1A). Higher biomass of around 1.0 g L^{-1} was achieved on the 10th day itself at 25°C (Supplementary Figure 1), and in some cases, maximum cell counts were observed from the 10th to 12th day of the experiment. In line with our observation, a report has documented that the optimum temperature for freshwater *Chlorella* is also 25°C (Singh and Singh, 2015). Another study has revealed that *C. vulgaris* cells were able to tolerate a higher temperature of even 40°C (Sharma et al., 2012). Our findings indicated that *C. vulgaris* can grow in a wide range of temperatures (20°C–35°C), but the best growth rate was noticed at 25°C, followed by 20°C. Importantly, the biomass tends to decrease at higher temperature.

Among the cultures maintained at different pH, pH 8.0 showed higher growth rate followed by pH 9.0 and 7.0 (Figure 1B). Cultures maintained at pH 6.0 and 10.0 are also observed with a considerable growth rate. A report has documented that *C. vulgaris* can grow in a wide range of pH, from 4 to 10 (Khalil et al., 2010). From the results of the present study, it was concluded that higher biomass production was obtained on 15th day, between pH 8 (0.959 g L^{-1}) and 9 (0.924 g L^{-1}) compared with other pH conditions (Supplementary Figure 2). Earlier reports have suggested that microalgal cultures grown at pH 8 to 9 favor high growth and biomass production (Difusa et al., 2015; Bartley et al., 2016; Qiu et al., 2017). Our study results indicated that all pH conditions tested (6–10) supported the growth of the algae, with the best growth rate being at pH 8, followed by pH 9.

The influence of different salinities (0, 10, 20, 30, and 50 PSU) was investigated in the present study on the growth rate of *C. vulgaris*. The better growth rate in terms of cell counts (Figure 1C) and biomass was observed at 30 PSU, followed by 20, 10, 0, and 50 PSU (Supplementary Figure 3). Previous studies have shown that the highest growth rate in terms of cell counts was observed at 30 PSU on the 15th day of the experiment (Jiang and Chen, 1999; Ranga Rao et al., 2007). In the present study, 30

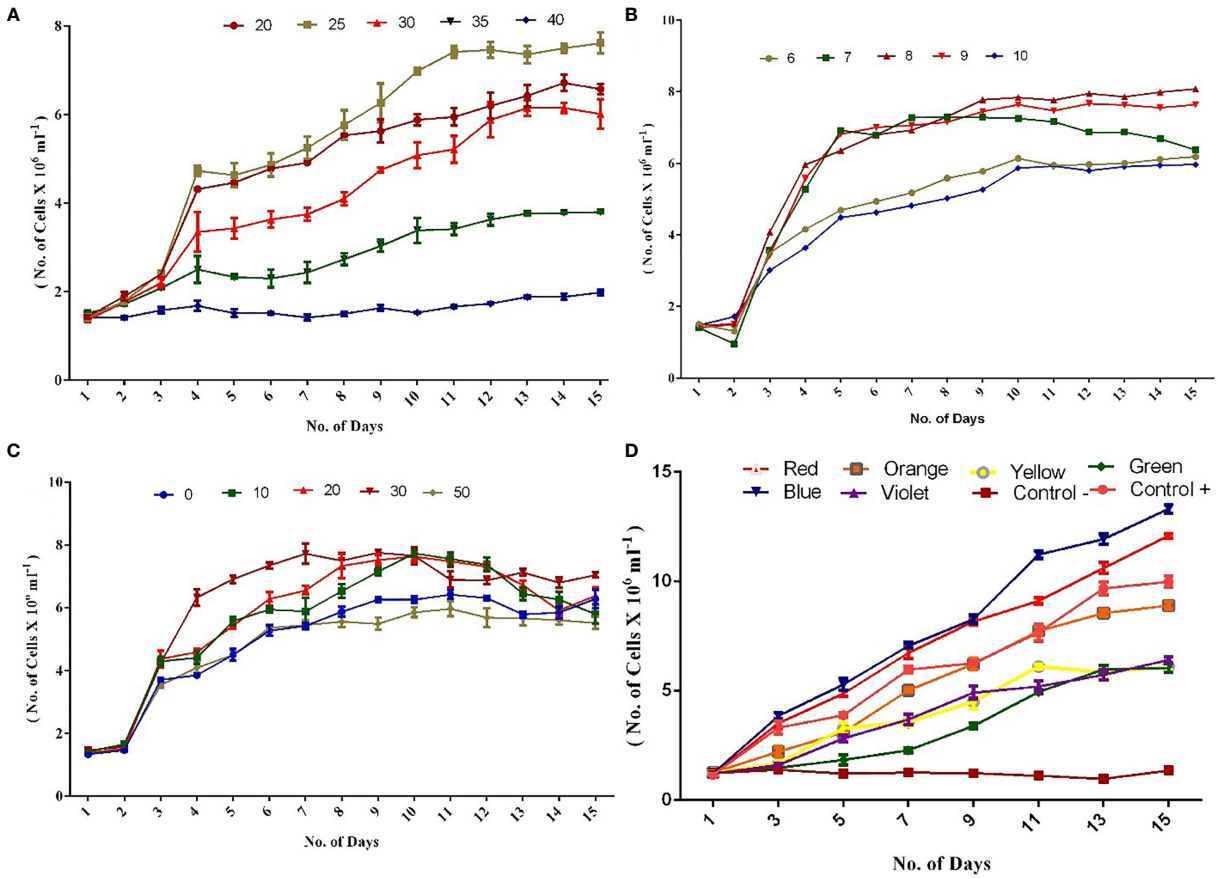


FIGURE 1
(A) Growth of *C. vulgaris* culture at different temperature. **(B)** Growth of *C. vulgaris* culture at different pH. **(C)** Growth of *C. vulgaris* culture at different salinities. **(D)** Growth of *C. vulgaris* culture at different light intensities. (Experiments were conducted in triplicate and the values are expressed as mean ± S.E.).

PSU resulted in higher biomass (1.0 g L^{-1}) on the 10th day compared with other salinity groups, and this observation is supported by a previous study by Fathi and Asem (2013). Interestingly, an important observation was noticed during the experiment, which highlighted that 0 PSU showed a better growth rate and biomass production than 50 PSU.

In the different light intensities experiments conducted under phototrophic conditions, blue light followed by red exhibited a significant increase in cell count (Figure 1D) on 15th day. Asuthkar et al. (2016) demonstrated that *Chlorella pyrenoidosa* cultured under blue light showed a higher growth rate than under red and white lights. In the present study, colored lights such as green and yellow showed fewer cell counts compared with control + (white light). The results of the present study revealed that a higher biomass production was recorded on the 15th day in blue light–exposed cells (1.3 g L^{-1}), followed by red (1.14 g L^{-1}) and other light-exposed cells (Supplementary Figure 4).

On the basis of individual tests performed under various environmental conditions, the ideal environmental factors were combined and evaluated for the growth rate of *C. vulgaris*. The culture was kept at 25°C, pH 8.0, and 30 PSU with light covered with a blue filter. The results were fascinating in that the maximum production of cells and biomass (1.52 g L^{-1}) was recorded under the blue light on the 10th day and was also the highest outcome in comparison with previous trials (Figures 2A, B). A study has also demonstrated that *Pavlova lutheri* grows at its maximum specific growth rate and has the highest lipid content when exposed to 30 to 40 PSU, pH 7.5 to 9.0, and 24 h of light (Shah et al., 2014). The findings of this study show that blue wavelengths, when combined with optimized environmental factors, favored the better growth rate of the algae and also enhanced the biomass production to a significant extent.

Conclusion

It can be concluded that a temperature of 25°C, pH 8.0, salinity of 30 PSU, and blue light (499–465 nm) are the ideal

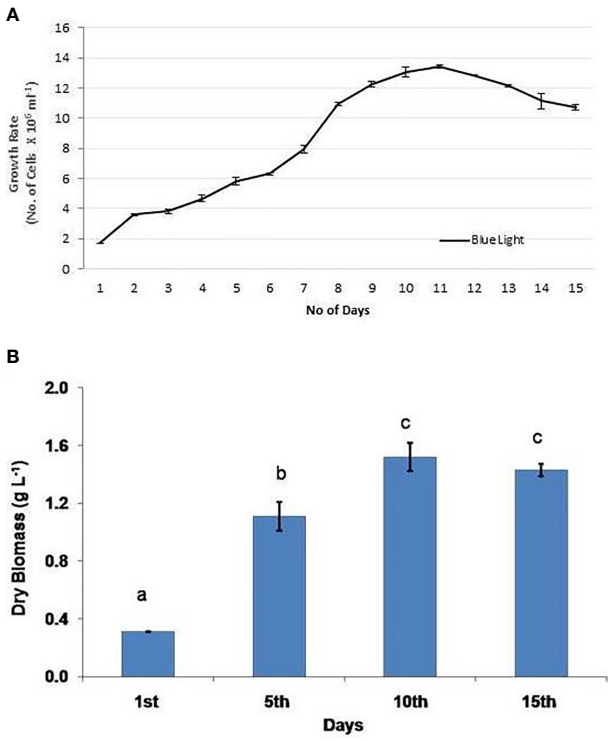


FIGURE 2
Combined experiment with optimized environmental variables: **(A)** cell growth and **(B)** biomass production. Experiments were conducted in triplicate and the values are expressed as mean ± S.E. The same letters (a, b, and c) indicate no significant difference between exposure groups at different exposure periods, whereas different letters indicate statistically significant differences ($p < 0.05$) between different exposure periods and groups.

parameters for the best growth of *C. vulgaris*. A combined experiment with optimized environmental factors showed enhanced growth rate and higher biomass production. Further, experiments are being explored to utilize the chlorella biomass to extract the most vital bioactive compounds and evaluate its pharmacological properties.

Data availability statement

The original contributions presented in the study are included in the article/supplementary material. Further inquiries can be directed to the corresponding author.

Author contributions

AJ: Methodology validation, data processing, and writing—original draft. TK: Conceptualization, sampling design, sample collection, laboratory analysis, and data validation. BS: Laboratory analysis. SR: Manuscript corrections and suggestions. RK: Manuscript review. GD: Manuscript review, suggestion, and project administration. All authors contributed to the article and approved the submitted version.

Acknowledgments

The authors gratefully acknowledge the Ministry of Earth Sciences, Govt. of India, for funding this project. The authors are thankful to Dr. G. A. Ramadass, Director, National Institute of Ocean Technology, for his constant support and encouragement. The authors thank the Management of Meenakshi Academy of Higher Education and Research (MAHER) for the support. We would also like to thank Mr. Krupa Ratnam from National Institute of Ocean Technology for his untiring help in presenting the figures.

Conflict of interest

The authors declare that the research was conducted in the absence of any commercial or financial relationships that could be construed as a potential conflict of interest.

Publisher's note

All claims expressed in this article are solely those of the authors and do not necessarily represent those of their affiliated organizations, or those of the publisher, the editors and the reviewers. Any product that may be evaluated in this article, or claim that may be made by its manufacturer, is not guaranteed or endorsed by the publisher.

Supplementary material

The Supplementary Material for this article can be found online at: https://www.frontiersin.org/articles/10.3389/fmars.2022.954622/full#supplementary-material

References

Al-lwayzy, S. H., Yusaf, T., and Al-Juboori, R. A. (2014). Biofuels from the fresh water microalgae chlorella vulgaris (FWM-CV) for diesel engines. *Energies.* 7, 1829–1851. doi: 10.3390/en7031829

Asuthkar, M., Gunti, Y., Rao, R., Rao, C. S., and Yadavalli, R. (2016). Effect of different wavelengths of light on the growth of chlorella pyrenoidosa. *Int. J. Pharma. Scien. Res.* 7, 847–851. doi: 10.13040/IJPSR.0975-8232

Bartley, M. L., Boeing, W. J., Daniel, D., Dungan, B. N., and Schaub, T. (2016). Optimization of environmental parameters for nannochloropsis salina growth and lipid content using the response surface method and invading organisms. *J. Appl. Phycol.* 28, 15–24. doi: 10.1007/s10811-015-0567-8

Bito, T., Okumura, E., Fujishima, M., and Watanabe, F. (2020). Potential of chlorella as a dietary supplement to promote human health. *Nutrients.* 12, 2524. doi: 10.3390/nu12092524

Blinová, L., Bartošová, A., and Gerulová, K. (2015). Cultivation of microalgae (Chlorella vulgaris) for biodiesel production. *Res. Pap. Fac. Mater. Sci. Technol. Slovak. Univ. Technol.* 23, 87–95. doi: 10.1515/rput-2015-0010

Brown, M. R., Dunstan, G. A., Jeffrey, S. W., Volkman, J. K., Barrett, S. M., and LeRoi, J. M. (1993). The influence of irradiance on the biochemical composition of the prymnesiophyte isochrysis sp. *J. Phycol* 29, 601–612. doi: 10.1111/j.0022-3646.1993.00601.x

Carvalho, A. P., and Malcata, F. X. (2000). Effect of culture media on production of polyunsaturated fatty acids by pavlova lutheri. *Cryptogamie Algol.* 21, 59–71. doi: 10.1016/S0181-1568(00)00101-X

Cheng, D., and He, Q. (2014). Assessment of environmental stresses for enhanced micro algal biofuel production - an overview. *Front. Energy Res.* 2, 1–8. doi: 10.3389/fenrg.2014.00026

Chowdury, K. H., Nahar, N., and Deb, U. K. (2020). The growth factors involved in microalgae cultivation for biofuel production: A review. *Comput. Water Energy Environ. Engin.* 9, 185–215. doi: 10.4236/cweee.2020.94012

Difusa, A., Talukdar, J., Kalita, M. C., Mohanty, K., and Goud, V. V. (2015). Effect of light intensity and pH condition on the growth, biomass and lipid content of microalgae scenedesmus species. *Biofuels* 6, 37–44. doi: 10.1080/17597269.2015.1045274

Fathi, M., and Asem, A. (2013). Investigating the impact of NaCl salinity on growth, β-carotene, and chlorophyll a in the content life of halophytes of algae chlorella sp. *AACL Bioflux.* 6, 241–245. http://www.bioflux.com.ro/docs/2013.20133143677

Gors, M., Schumann, R., Hepperle, D., and Karsten, U. (2009). Quality analysis of commercial chlorella products used as dietary supplement in human nutrition. *J. Appl. Phycol.* 22, 265–276. doi: 10.1007/s10811-009-9455-4

Jiang, Y., and Chen, F. (1999). Effects of salinity on cell growth and docosahexaenoic acid content of the heterotrophic marine microalga crypthecodinium cohnii. *J. Industr. Microbiol. Biotechnol.* 23, 508–513. doi: 10.1038/sj.jim.2900759

Khalil, Z. I., Asker, M. M., El-Sayed, S., and Kobbia, I. A. (2010). Effect of pH on growth and biochemical responses of dunaliella bardawil and chlorella ellipsoidea. *World J. Microbiol. Biotechnol.* 26, 1225–1231. doi: 10.1007/s11274-009-0292-z

Khan, M. I., Shin, J. H., and Kim, J. D. (2018). The promising future of microalgae: current status, challenges, and optimization of a sustainable and renewable industry for biofuels, feed, and other products. *Microb. Cell factor.* 17, 36. doi: 10.1186/s12934-018-0879-x

Mata, T. M., Martins, A. A., and Caetano, N. S. (2010). Microalgae for biodiesel production and other applications: A review. *Renew. Sust. Ener. Rev.* 14, 217–232. doi: 10.1016/j.rser.2009.07.020

Pulz, O., and Gross, W. (2004). Valuable products from biotechnology of microalgae. *Appl. Microbiol. Biotechnol.* 65, 635–648. doi: 10.1007/s00253-004-1647-x

Qiu, R., Gao, S., Lopez, P. A., and Ogden, K. L. (2017). Effects of pH on cell growth, lipid production and CO2 addition of microalgae chlorella sorokiniana. *Algal Res.* 28, 192–199. doi: 10.1016/j.algal.2017.11.004

Ranga Rao, A., Sarada, R., and Ravishankar, G. A. (2007). Influence of CO2 on growth and hydrocarbon production in botryococcus braunii. *J. Microbiol. Biotechnol.* 17, 414–419.

Salama, E. S., Hwang, J. H., El-Dalatony, M. M., Kurade, M. B., Kabra, A. N., Abou-Shanab, R. A., et al. (2018). Enhancement of microalgal growth and biocomponent-based transformations for improved biofuel recovery: A review. *Bioresource Technol.* 258, 365–375. doi: 10.1016/j.biortech.2018.02.006

Santos, K. R., and Mariano, A. B. (2014). Determination of optimal algae concentration for continuous growth of scenedesmus sp. in CHU and modified CHU media. *Therm. Engin.* 13, 52–58. doi: 10.5380/reterm.v13i2.62096

Scarsella, M., Belotti, G., De Filippis, P., and Bravi, M. (2010). Study on the optimal growing conditions of chlorella vulgaris in bubble column photobioreactors. *Chem. Engin. Trans.* 20, 85–90. doi: 10.3303/CET1020015

Shah, S. M.U., Che Radziah, C., Ibrahim, S., Latiff, F., Othman, M. F., and Abdullah, M. A.. (2014). Effects of photoperiod, salinity and pH on cell growth and lipid content of pavlova lutheri. *Ann. Microbiol.* 64, 157–164. doi: 10.1007/s13213-013-0645-6

Sharma, R., Singh, G. P., and Sharma, V. K. (2012). Effects of culture conditions on growth and biochemical profile of chlorella vulgaris. *Plant Pathol. Microbiol.* 3, 2–6. doi: 10.4172/2157-7471.1000131

Singh, S. P., and Singh, P. (2015). Effect of temperature and light on the growth of algae species: A review. *Renew. Sustain. Energy Rev.* 50, 431–444. doi: 10.1016/j.rser.2015.05.024

Spolaore, P., Joannis-Cassan, C., Duran, E., and Isambert, A. (2006). Commercial applications of microalgae. *J. Biosci. Bioeng.* 101, 87–96. doi: 10.1263/jbb.101.87

Zhu, C. J., and Lee, Y. K. (1997). Determination of biomass dry weight of marine microalgae. *J. Appl. Phycol.* 9, 189–194. doi: 10.1023/A:1007914806640

Zongo, B., and Boussim, J. I. (2015). The effects of physicochemical variables and tadpole assemblages on microalgal communities in freshwater temporary ponds through an experimental approach. *Aquat. Biosyst.* 11, 1. doi: 10.1186/s12999-014-0013-4

frontiers | Frontiers in Marine Science

TYPE Data Report
PUBLISHED 04 August 2022
DOI 10.3389/fmars.2022.969589

Check for updates

OPEN ACCESS

EDITED BY
Dilip Kumar Jha,
National Institute of Ocean Technology, India

REVIEWED BY
Sudarshan Singh Rathore,
Central Institute of Mining and Fuel Research, India
Pankaj Verma,
National Institute of Ocean Technology, India

*CORRESPONDENCE
Thilagam Harikrishnan
thilagampachaiyappas@gmail.com
Krishnamurthy Rajamanickam
professorkrishnamurthy@gmail.com

†These authors have contributed equally to this work

SPECIALTY SECTION
This article was submitted to Marine Pollution, a section of the journal Frontiers in Marine Science

RECEIVED 15 June 2022
ACCEPTED 15 July 2022
PUBLISHED 04 August 2022

CITATION
Ravi S, Thillainayagam R, Janakiraman G, Subramanyam P, Sivakumar R, Raman T, Singaram G, Harikrishnan T and Rajamanickam K (2022) Modulation of biotransformation enzymes leads to oxidative stress and DNA damage in naphthalene exposed marine bivalve *Perna viridis*. *Front. Mar. Sci.* 9:969589. doi: 10.3389/fmars.2022.969589

COPYRIGHT
© 2022 Ravi, Thillainayagam, Janakiraman, Subramanyam, Sivakumar, Raman, Singaram, Harikrishnan and Rajamanickam. This is an open-access article distributed under the terms of the Creative Commons Attribution License (CC BY). The use, distribution or reproduction in other forums is permitted, provided the original author(s) and the copyright owner(s) are credited and that the original publication in this journal is cited, in accordance with accepted academic practice. No use, distribution or reproduction is permitted which does not comply with these terms.

Modulation of biotransformation enzymes leads to oxidative stress and DNA damage in naphthalene exposed marine bivalve *Perna viridis*

Sathikumaran Ravi[1†], Revathi Thillainayagam[2†], Gopi Janakiraman[2], Punitha Subramanyam[2], Rekha Sivakumar[1], Thiagarajan Raman[3], Gopalakrishnan Singaram[4], Thilagam Harikrishnan[1*] and Krishnamurthy Rajamanickam[2*]

[1]Postgraduate and Research Department of Zoology, Pachaiyappa's College for Men, Chennai, India, [2]Post Graduate and Research Department of Zoology and Aquaculture, Government Arts College for Men (Autonomous), (Affiliated to University of Madras), Chennai, India, [3]Department of Zoology, Ramakrishna Mission Vivekananda College (Autonomous), Chennai, India, [4]eProov Assessment Solution Pvt., Limited, Chennai, India

KEYWORDS

biotransformation enzymes, DNA damage, oxidative stress, antioxidant, naphthalene, marine, *Perna viridis*

Introduction

Polycyclic aromatic hydrocarbons (PAHs) are organic pollutants having two or more condensed aromatic rings and are considered the ninth most harmful substance to human health (Jia and Batterman, 2010; Ifegwu and Anyakora, 2015). Because of the large and unregulated exploitation of natural resources, PAH contamination has become a global concern. As far as the aquatic environment is concerned PAHs are found in sediments, benthic fauna, fish, sea birds, and mammals (Baali and Yahyaoui, 2019). Naphthalene is a PAH that is widely found in soil, water, air, and aquatic ecosystems, as well as in petroleum-derived fuels and consumer items (Jia and Batterman, 2010). The most prevalent use of naphthalene in consumer goods is the manufacture of mothballs (Sudakin et al., 2011). Ingesting naphthalene can cause both immediate and delayed toxicity (Kundra, et al., 2015).

The main mechanism of PAH toxicity is that they attach to the hydrophobic regions of macromolecules in the cell, causing molecular and cellular damage and disrupting

normal physiology (Honda and Suzuki, 2020). Cytochrome P450 (CYP) enzymes are haeme-containing proteins found in vertebrates, animals, plants, and microbes. These enzymes catalyze the oxidative biotransformation of a wide range of lipophilic xenobiotic and endogenous substances, including steroids, fatty acids, medicines, and organic pollutants (Walker et al., 2001). In addition, CYP enzymes are also well recognized in the detoxification of halogenated and non-halogenated hydrocarbons in the food chain (Shu et al., 2008).

Individual CYP enzyme levels have a crucial role in bioaccumulation and vulnerability to environmental pollutant exposure. The primary hydrocarbon inducible form, CYP1A, has attracted the greatest attention as a potential biomarker of exposure to marine hydrocarbon pollutants (Buhler and Wang-Buhler, 1998). Glutathione S transferase (GST) is a phase II detoxification enzyme that may catalyze the reaction of reduced glutathione (GSH) with xenobiotic or indigenous harmful chemicals, allowing toxins to be expelled quickly from cells (Park et al., 2009). GST has also been used as a sensitive biomarker of exposure to a variety of pollutants, including PAHs and petrochemical compounds, in both field and laboratory research (Gopalakrishnan et al., 2011; Gan et al., 2021). Moreover, the antioxidants play a crucial role in maintaining homeostasis and when antioxidant defenses are compromised, oxidative stress products, particularly reactive oxygen species (ROS), can cause DNA damage, peroxidation of cell components, and enzymatic inactivation. Using the marine green mussel (Perna viridis) as a model species, the current work aims to assess the role of the CYP system in the metabolism of PAHs by marine animals, as well as how these modulations of biotransformation enzymes cause oxidative stress. It is also known that in response to oxidative stresses, marine organisms would be expected to have larger amounts of antioxidant enzymes such as catalase (CAT), glutathione peroxidase (GPx), and superoxide dismutase (SOD). Variations in antioxidant levels can thus be utilized to identify xenobiotic exposure (Gopalakrishnan et al., 2011).

P. viridis is a green-lipped marine mussel that may be found in coastal waters on both the east and west coasts of India. It absorbs pollutants easily and exhibits a variety of physiological and biochemical responses, providing information on the overall state of contamination as well as animal health. P. viridis has been utilized as an environmental bio-indicator in toxicity-related experiments using a range of biomarkers. The majority of bivalves like P. viridis toxicity research has been focused on the animal's metal bio-accumulation mechanism and the organs involved (Jha et al., 2019; Satheeswaran et al., 2019). There has been very little research on the impact of naphthalene on the physiological processes of bivalves like P. viridis (Bagchi et al., 1998). This is the first research to look at how biotransformation enzymes and DNA damage in P. viridis are affected by chronic long-term exposure to sublethal concentrations of naphthalene. The goal of the study was to see if altering these biotransformation enzymes causes oxidative stress in P. viridis and the resulting antioxidant response.

Methods

Green mussels, P. viridis measuring with range of 7.15- 8.95 cm in length and 15.4-22.1 g in weight were collected and transported to the lab from a coastal location near the sea mouth of the Pulicat Lake, Tamil Nadu, India. The acclimatization and toxicity study procedures were adopted from the protocol of EPA/ROC, 1998 and Gopi et al. (2021). Sixty mussels were used in the present study and the mussels were divided into five groups of six specimens in each tank. Duplicate tank for each concentration was maintained. To ensure the solubility of naphthalene in seawater, acetone was used as a solvent. The mussels in Group I was reared in normal seawater (control group). Group II mussels were reared in a solvent control (Vacetone/Vseawater = 1/20 000), group III mussels were exposed to 1 mg L-1 naphthalene in seawater, group IV mussels were exposed to 2 mg L-1 naphthalene in seawater and group V were exposed to seawater with 4 mg L-1 naphthalene. Mussels were fed with fresh phytoplankton (Chlorella autotrophica) cultured during the experimental periods. The water temperature, salinity, and pH were all maintained at 28 ± 1°C, 33 ± 1 PSU, and 8.1 ± 0.1 respectively, and the tank received a continuous O2 supply. After 28 days of exposure, the animals were analyzed by removing their gills and digestive glands and stored at -20°C for subsequent enzyme and biochemical analysis. Protein concentrations in all tissues were determined using the Bradford (1976) technique.

To study the modulation of biotransformation enzymes due to the sublethal effect of naphthalene, activities of cytochrome c reductase, oxidase and glutathione S transferase and oxidative stress related parameters lipid peroxidation (LPO), DNA damage, reactive oxygen species (ROS) measurement and also the antioxidant parameter including catalase (CAT), super oxide dismutase (SOD), reduced glutathione (GSH) content and glutathione peroxidise (GPX) were analyzed. As a sensitive and practical early warning system for biological exposure to organic contaminants, these parameters have been widely employed.

The activities of cytochrome c reductase were determined spectrophotometrically using Williams and Kamin's (1962) modified technique. Berry and Trumpower (1987) spectrophotometric approach was used to assess the activity of cytochrome c oxidase. During variations in its oxidation state, the absorbance of cytochrome c oxidase at 550 nm was measured. Shugart's (1988) alkaline unwinding technique was used to assess DNA strand breakage using an alkaline unwinding assay, in which strand separation is obtained under controlled conditions and the quantities of double and single-stranded DNA after alkaline unwinding were measured using fluorescence at 360 nm excitation and 450 nm emission wavelengths (Ref). Glutathione

S-transferase (GST) activity was determined using the 1-chloro-2, 4-dinitrobenzene (CDNB) substrate after conjugating the acceptor substrate with glutathione, as reported by Habig et al. (1974).

LPO was calculated using the protocol of Devasagayam and Tarachand (1987), the color developed was detected at 532 nm, and Malondialdehyde (MDA) level was represented as nmol of MDA generated/mg protein. ROS was assessed using the methods of Driver et al. (2000). CAT activity was measured according to Sinha (1972). SOD activity was determined by measuring the degree of inhibition of pyrogallol auto-oxidation at an alkaline pH using the Marklund and Marklund technique (1974). GPx was determined by measuring the quantity of GSH consumed in the reaction mixture by following the protocol of Rotruck et al. (1973). GSH was calculated by measuring the optical density of the yellow color generated when 5,5'-dithio-bis-(2-nitrobenzoic acid) (DTNB) is reduced by glutathione at 412 nm, as described by Moron et al. (1979).

SPSS software (version 20) was used to perform the statistical analysis. The data were analyzed for significance and reported as the mean ± standard deviation (SD). One-way analysis of variance (ANOVA) was used to analyze the data, followed by Tukey's multiple-comparison post hoc test. Principal component analysis (PCA) is one of the most effective approaches for decreasing the dimensionality of large datasets while preserving their content (Wunderlin et al., 2001). Strong (> 0.75), moderate (0.75–0.50), and weak (0.50–0.30) factor loadings were classified according to Liu et al. (2003) criteria. To establish sample adequacy, the Kaiser–Meyer–Olkin (KMO) criterion was used. To reduce the impact of discrepancies in measurement units and variance, all parameters were normalized using a Z-scale transformation (mean = 0; variance = 1), which rendered the data dimensionless for PCA. Further, the Pearson correlation coefficient was used to determine the inter-relationship between the parameters. There was no significant difference between the solvent and blank controls, and therefore only the results of the solvent control are shown in the figures.

Data description

The digestive gland of P. viridis showed the maximum activity of cytochrome c reductase at the highest concentration of naphthalene examined, while the mussels subjected to 1mg/L showed the lowest activity, with no significant difference from the control group after 28 d of exposure (Figure 1A). Among the two organs studied, digestive gland exhibited comparatively higher cytochrome c reductase activity than gill samples. However, both the organs showed up to 4-fold increase in cytochrome c reductase activity when compared to the respective control group after 28 d of exposure to 4mg/L of naphthalene, and such increase was statistically significant ($p < 0.001$). Gills exhibited a dose-dependent increase in cytochrome c reductase activity when the mussels were exposed to different concentrations of naphthalene (Figure 1A). Such increase in this marker enzyme in both the organs could be due animal detoxification mechanism and needs to be elucidated further. Harlocker et al. (1991) opined that gill tissue might not be primarily important for carbon flow control but rather for detoxification reactions as evidenced by alterations to these enzymes in the gill. However, because the enzyme activity trend was strongly associated with other tissues like the digestive gland, this study highlights the fact that mussel gill tissue enzyme might be a biomarker for naphthalene exposure. Furthermore, changes in the activity of the cytochrome c reductase enzyme under naphthalene stress possibly indicate physiological changes in the organisms. These results suggest the possible use of cytochrome c reductase as a biomarker for studying the impact of organic pollutants in mussels.

The activity of cytochrome c oxidase was shown to be increased in mussels exposed to various concentrations of naphthalene over 28 d. The highest level of cytochrome c oxidase enzyme activity in both organs was recorded when the mussels were exposed to the highest concentration of naphthalene (4 mg/L), and the digestive gland showed the highest amount of induction of this biotransformation enzyme. When mussels were exposed to naphthalene, the activity of cytochrome c oxidase in their digestive glands increased in a dose-dependent manner (Figure 1B). Gills on the other hand, showed a significant ($p < 0.001$) increase in cytochrome c oxidase only when the mussels were exposed to the highest naphthalene (4 mg/L) concentration.

Furthermore, the current study demonstrated that the cytochrome c oxidase activity in the mussel digestive gland was greater than that in the gills. Fontanesi et al. (2006) found that cytochrome c oxidase biogenesis and activity were controlled by changing environmental or physiological factors in the metabolism of adaptive cells. Increased cytochrome c oxidase activity may indicate increased mitochondrial high energy bond Adenosine triphosphate (ATP) production, which is required for highly synthetic processes including DNA synthesis, mitosis, and cellular proliferation (Zorov et al.,2014). When the mitotic index and proliferation (epithelialization) grow dramatically in regenerated tissues, cytochrome c oxidase activity spikes (Saprunova et al., 2008). This represents changes in mitochondria and other sub-cellular components that occur during tissue breakdown (Li et al., 2006). Similar induction of cytochrome c oxidase due to PAH was reported in mussels (Xavier Michel et al., 1994).

DNA damage in the gill and digestive gland was observed when mussels were exposed to naphthalene (Figure 1C). After 28 d of exposure of mussels to 4 mg/L naphthalene, there was a significant reduction ($p < 0.001$) in the DNA integrity in the gill. A similar trend was observed for DNA integrity in the digestive gland of P. viridis when exposed to naphthalene (Figure 1C). However, the digestive gland had a greater loss in terms of DNA integrity than gill after 28 d exposure and all these changes were statistically significant ($p < 0.001$). The changes observed in DNA integrity were attributed by Brooks et al. (2009) to

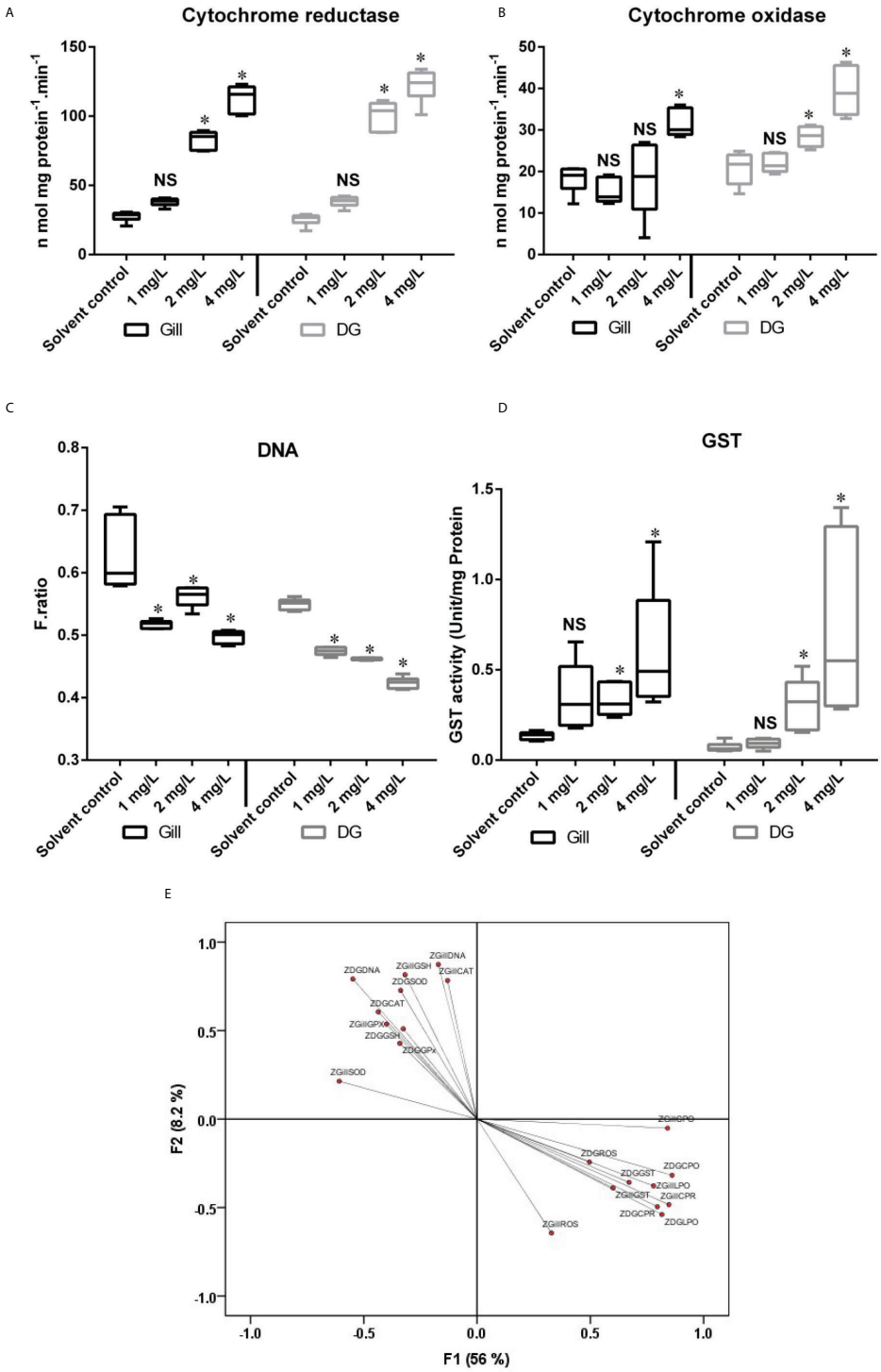


FIGURE 1
Showing the level of **(A)** Cytochrome c reductase, **(B)** Cytochrome c oxidase, **(C)** DNA damage, **(D)** GST activity and **(E)** Factor loading F1 and F2 for different biomarkers analyzed in mussel exposed to different concentration of naphthalene. The line in each box represents median and whiskers represents the upper and lower 95% confidence intervals of the mean of six determinations using samples from different preparations. One-way analysis of variance (ANOVA) followed by Tukey's *post hoc* test was used. The significant difference between control and exposure groups were indicated with asterisks ($P < 0.05$); NS, No significant difference with respective control group. The Z-represent that the data is normalized. DG, Digestive gland.

variations in the concentration and/or activity of xenobiotic metabolizing enzymes such as cytochrome P450, which are known to alter substantially with seasons and environmental conditions. Ching et al. (2001) reported that mussels exposed to benzo (a) pyrene showed a similar increase in DNA damage.

The GST activity was significantly induced in the digestive gland of mussels after 28 d of exposure to all the naphthalene concentrations. However, such induction was not significant when the mussels were exposed to the lowest naphthalene concentration. A similar increase was also observed in the gill after 28 d of exposure to naphthalene (Figure 1D). Phase II of the metabolic process includes GST activity in mussels in response to an organic contaminant as has been previously reported (Fitzpatrick et al., 1997). According to our findings, GST activity was ineffective in preventing DNA damage after 28 d of naphthalene exposure. This could be due to electrophilic intermediates formed by phase I mixed function oxidase being able to bind to nucleophilic sites of DNA during naphthalene metabolism.

Supplementary Figure 1 depicts changes in antioxidant enzymes, ROS, and LPO levels in the digestive gland and gill of mussels subjected to various naphthalene concentrations. SOD activity in both organs dropped considerably after the mussels were exposed to greater (4 mg/L) naphthalene concentrations for 28 d. Similarly, when mussels were exposed to naphthalene concentrations for 28 d, their CAT activity fell significantly, however it was lower in the gills than in the digestive gland. When mussels were exposed to naphthalene, GSH levels in their gills and digestive glands dropped drastically. Similarly, GPx activity also decreased in mussels exposed, and this reduction was statistically significant ($p<0.05$) when the mussels were exposed to a greater naphthalene concentration (4 mg/L).

Antioxidant enzyme activities in marine invertebrates are affected by xenobiotic exposure (Cravo et al., 2012; Gopalakrishnan et al., 2011). When toxicant concentrations are low, the modulation of these enzymes is observed and returns to normal, but when the time or dose of toxicant exposure is increased, the modulation of these enzymes remains permanent, and they respond by decreasing their level or becoming blocked in the majority of cases. According to our results, antioxidant enzyme activity in the digestive gland and gills decreased at all dosages, implying an increase in the oxygen-free radical formation and oxidative stress upon naphthalene toxicity (O2 and H2O2). The Pearson correlation matrix calculated for the digestive gland and gill tissues is given in Table 1. The correlation between individual

TABLE 1 Correlation Matrix for measured parameters in digestive gland and gill of *Perna viridis* exposed to different concentration of Naphthalene.

Digestive gland

	ROS	LPO	CAT	SOD	GPx	GSH	GST	DNA	CPR	CPO
ROS	1	.514*	-.431*	-.396	-.378	-.261	.391	-.460*	.589**	.399
LPO		1	-.689**	-.658**	-.533**	-.487*	.765**	-.866**	.928**	.861**
CAT			1	.778**	.404	.307	-.474*	.768**	-.693**	-.551**
SOD				1	.366	.305	-.416*	.731**	-.666**	-.510*
GPx					1	.215	-.526**	.507*	-.457*	-.483*
GSH						1	-.390	.579**	-.463*	-.418*
GST							1	-.648**	.648**	.591**
DNA								1	-.825**	-.724**
CPR									1	.834**
CPO										1

Gill	ROS	LPO	CAT	SOD	GPx	GSH	GST	DNA	CPR	CPO
ROS	1	.428*	-.433*	-.273	-.468*	-.752**	.380	-.455*	.636**	.327
LPO		1	-.419*	-.478*	-.485*	-.526**	.646**	-.577**	.807**	.743**
CAT			1	.344	.369	.618**	-.419*	.887**	-.464*	-.325
SOD				1	.539**	.320	-.310	.341	-.596**	-.412*
GPx					1	.431*	-.492*	.504*	-.571**	-.315
GSH						1	-.396	.644**	-.716**	-.288
GST							1	-.557**	.636**	.545**
DNA								1	-.527**	-.313
CPR									1	.698**
CPO										1

*Correlation is significant at the $p<0.05$ level (2-tailed), ** correlation is significant at the $p< 0.01$ level (2-tailed). (CPR) - Cytochrome c Reductase and (CPO) Cytochrome c Oxidase.

parameters produced similar results to those of PCA and showed a significant ($P<0.01$; $P<0.05$) association between the parameters in both the digestive gland and gill studied. There were good correlations between LPO and all other parameters in P. viridis. The correlation coefficients in most cases were greater than 0.50. ROS generated in the digestive gland showed a significant relationship with DNA damage and cytochrome c reductase in the mussels exposed to naphthalene. Similarly, cytochrome c reductase and cytochrome c oxidase showed a correlation with both oxidative stress and corresponding antioxidant response. Cytochrome c reductase in gill showed a significant relation with DNA damage, oxidative stress, and antioxidant responses (Table 1).

The KMO criterion values of 0.638 revealed that by factor analysis (FA), a considerable diminution in the dimensionality of the data set has been obtained (Wu et al., 2010). Through FA four significant factors (Eigen value >1) were obtained which elucidating 76.67% of the total variation among the biomarker data in the gill and digestive gland. The factor loadings and communality of the dataset are given in Table S1 (supplemental material). Factor 1 elucidates 56% of the total variance and reveals strong positive loading of DG-LPO (0.815), Gill-LPO (0.779), DG-CPR (0.796), Gill-CPR (0.847), DG-CPO (0.86) and Gill-CPO (0.841) (Figure 1E). It could be attributed to the influence of naphthalene concentrations and the duration of exposure played a major role in modulating the biotransformation enzymes. Factor 2 elucidates 8.2% of the total variance and revealed a strong positive loading of Gill-CAT (0.783), Gill-GSH (0.816), DG-DNA (0.791), and Gill-DNA (0.873). It might be explained by the various metabolites formed from the organic pollutant during biotransformation could impair the physiological system in the mussels. Further based on this finding, we hypothesized that the duration of exposure influenced the antioxidant response and increased oxidative stress, potentially resulting in DNA damage.

In conclusion, cytochrome c reductase and cytochrome c oxidase activities may provide insight into the general health of an organism exposed to PAHs, more specifically to naphthalene as per our study. As indicated by an increase in DNA damage and other oxidative stress indicators, we may deduce that exposing P. viridis to naphthalene elevates reactive oxygen species and oxidative stress in mussels, which may have an inverse influence on antioxidant activity. Together these biomarkers could be vital tools for assessing naphthalene exposure and toxicity in marine animals and can be used in regular coastal and marine environment monitoring programs.

Data availability statement

The original contributions presented in the study are included in the article/Supplementary Material. Further inquiries can be directed to the corresponding authors.

Ethics statement

For the care and use of animals, all applicable international, national, and/or institutional guidelines were followed, since we use the invertebrate and commercial animal ethical approval not necessary.

Author contributions

SR, RT, GJ, PS and RS sample collection, performed experiment and laboratory analysis. KR: conceptualization, experimental design, data validation. TR: manuscript corrections and critical suggestions. GS: statistical analysis of data and manuscript correction. TH and KR: manuscript preparation, reviewing the manuscript and project administration. All authors contributed to the article and approved the submitted version.

Acknowledgments

The authors thank Head, Research department of Zoology and the Principal Government Arts College for men (Autonomous), Chennai-600 035 and Head, Research department of Zoology and also the Principal Pachaiyappa's College for Men, Chennai- 600 030 India for extending their support through the experiment.

Conflict of interest

Author GS was employed by eProov Assessment Solution Pvt., Limited.

The remaining authors declare that the research was conducted in the absence of any commercial or financial relationships that could be construed as a potential conflict of interest.

Publisher's Note

All claims expressed in this article are solely those of the authors and do not necessarily represent those of their affiliated organizations, or those of the publisher, the editors and the reviewers. Any product that may be evaluated in this article, or claim that may be made by its manufacturer, is not guaranteed or endorsed by the publisher.

Supplementary material

The Supplementary Material for this article can be found online at: https://www.frontiersin.org/articles/10.3389/fmars.2022.969589/full#supplementary-material

References

Baali, A., and Yahyaoui, A. (2019). Polycyclic Aromatic Hydrocarbons (PAHs) and Their Influence to Some Aquatic Species., M. Ince, O. K. Ince and G. Ondrasek (Eds.) *IntechOpen* (Biochemical Toxicology - Heavy Metals and Nanomaterials). doi: 10.5772/intechopen.86213

Bagchi, M., Bagchi, D., Balmoori, J., Ye, X., and Stohs, S. J. (1998). Naphthalene-induced oxidative stress and DNA damage in cultured macrophage J774A.1 cells. *Free Radic. Biol. Med.* 25 (2), 137–143. doi: 10.1016/s0891-5849(98)00063-x

Berry, E. A., and Trumpower, B. L. (1987). Simultaneous determination of hemes a, b, and c from pyridine hemochrome spectra. *Anal. Biochem.* 161, 1–15. doi: 10.1016/0003-2697(87)90643-9

Bradford, M. M. (1976). A rapid and sensitive method for the quantitation of microgram quantities of protein utilizing the principle of protein-dye binding. *Anal. Biochem.* 72, 248–254. doi: 10.1006/abio.1976.9999

Brooks, S., Lyons, B., Goodsir, F., Bignell, J., and Thain, J. (2009). Biomarker responses in mussels, an integrated approach to biological effects measurements. *J. Toxicol. Environ. Health Part A* 72 (3), 196–208. doi: 10.1080/15287390802539038

Buhler, D. R., and Wang-Buhler, J. L. (1998). Rainbow trout cytochrome P450's: purification, molecular aspects, metabolic activity, induction and role in environmental monitoring. *Comp. Biochem. Physiol.* 121C, 107–137. doi: 10.1016/S0742-8413(98)10033-6

Ching, E. W., Siu, W. H., Lam, P. K., Xu, L., Zhang, Y., Richardson, B. J., et al. (2001). DNA Adduct formation and DNA strand breaks in green-lipped mussels (Perna viridis) exposed to benzo[a]pyrene: dose- and time-dependent relationships. *Mar. pollut. Bull.* 42 (7), 603–610. doi: 10.1016/s0025-326x(00)00209-5

Cravo, A., Pereira, C., Gomes, T., Cardoso, C., Serafim, A., Almeida, C., et al. (2012). A multibiomarker approach in the clam ruditapes decussatus to assess the impact of pollution in the ria Formosa lagoon, south coast of Portugal. *Mar. Environ. Res.* 75, 23–34. doi: 10.1016/j.marenvres.2011.09.012

Devasagayam, T. P., and Tarachand, U. (1987). Decreased lipid peroxidation in the rat kidney during gestation. *Biochem. Biophys. Res. Commun.* 145, 134–138. doi: 10.1016/0006-291x(87)91297-6

Driver, A. S., Kodavanti, P. R., and Mundy, W. R. (2000). Age-related changes in reactive oxygen species production in rat brain homogenates. *Neurotoxicol Teratol* 22, 175–181. doi: 10.1016/s0892-0362(99)00069-0

EPA/ROC (1998). "Standard guide for conducting acute tests with fishes. static renewal test for common carp," in *NIEA B904.10B, environmental protection administration of the republic of China*(Taipei, Taiwan).

Fitzpatrick, P. J., Halloran, J. O., Sheehan, D., and Walsh, A. R. (1997). Assessment of a glutathione s-transferase and related proteins in the gill and digestive gland of mytilus edulis (L.), as potential organic pollution biomarkers. *Biomarkers* 2:1, 51–56. doi: 10.1080/135475097231977

Fontanesi, F., Soto, I. C., Horn, D., and Barrientos, A. (2006). Assembly of mitochondrial cytochrome coxidase, a complicated and highly regulated cellular process. *Am. J. Physiol. Cell Physiol.* 291, 1129–1147. doi: 10.1152/ajpcell.00233.2006

Gan, N., Martin, L., and Xu, W. (2021). Impact of polycyclic aromatic hydrocarbon accumulation on oyster health. *Front. Physiol.* 12. doi: 10.3389/fphys.2021.734463

Gopalakrishnan, S., Nai, Z., Thilagam, H., Bei, C., Ding, J., Wang, X. H., et al. (2011). Biochemical responses and DNA damage in red sea bream from coastal fujian province, China. *Ecotoxicol Environ. Saf.* 74 (6), 1526–1535. doi: 10.1016/j.ecoenv.2011.05.007

Gopi, J., Nathiya, K. R., Sangeetha, R., and Krishnamurthy, R. (2021). Induction of oxidative stress and modulation of antioxidant defense in the haemolymph of green mussel perna viridis exposed to naphthalene. *Uttar Pradesh J. Zoology* 42 (23), 161–169.

Habig, W. H., Pabst, M. J., and Jakoby, W. B. (1974). Glutathione s-transferases. the first enzymatic step in mercapturic acid formation. *J. Biol. Chem.* 249, 7130–7139. doi: 10.1016/S0021-9258(19)42083-8

Harlocker, S. L., Kapper, M. A., Greenwalt, D. E., and Bishop, S. H. (1991). Phosphoenolpyruvate carboxykinase from ribbed mussel gill tissue: reactivities with metal ions, kinetics, and action of 3-mercaptopicolinic acid. *J. Exp. Zool* 257, 285–298. doi: 10.1002/jez.1402570302

Honda, M., and Suzuki, N. (2020). Toxicities of polycyclic aromatic hydrocarbons for aquatic animals. *Int. J. Environ. Res. Public Health* 17 (4), 1363. doi: 10.3390/ijerph17041363

Ifegwu, O. C., and Anyakora, C. (2015). "Chapter six - polycyclic aromatic hydrocarbons: Part I. exposure," in *Advances in clinical chemistry*, vol. 72 . Eds. S. Gregory and Makowski, (Elsevier), 277–304. doi: 10.1016/bs.acc.2015.08.001

Jha, D. K., Ratnam, K., Rajaguru, S., Dharani, G., Devi, M. P., and Kirubagaran, R. (2019). Evaluation of trace metals in seawater, sediments, and bivalves of nellore, southeast coast of India, by using multivariate and ecological tool. *Mar. pollut. Bull.* 146, 1–10. doi: 10.1016/j.marpolbul.2019.05.044

Jia, C., and Batterman, S. (2010). A critical review of naphthalene sources and exposures relevant to indoor and outdoor air. *Int. J. Environ. Res. Public Health* 7 (7), 2903–2939. doi: 10.3390/ijerph7072903

Kundra, T. S., Bhutatani, V., Gupta, R., and Kaur, P. (2015). Naphthalene poisoning following ingestion of mothballs: A case report. *J. Clin. Diagn. Res. JCDR* 9 (8), UD01–UUD2. doi: 10.7860/JCDR/2015/15503.6274

Li, Y., Park, J. S., Deng, J. H., and Bai, Y. (2006). Cytochrome c oxidase subunit IV is essential for assembly and respiratory function of the enzyme complex. *J. Bioenerg Biomembr.* 38, 283–291. doi: 10.1007/s10863-006-9052-z

Liu, C. W., Lin, K. H., and Kuo, Y. M. (2003). Application of factor analysis in the assessment of groundwater quality in a blackfoot disease area in Taiwan. *Sci. Total Environ.* 313, 77–89. doi: 10.1016/S0048-9697(02)00683-6

Marklund, S., and Marklund, G. (1974). Involvement of the superoxide anion radical in the autoxidation of pyrogallol and a convenient assay for superoxide dismutase. *Eur. J. Biochem.* 47, 469–474. doi: 10.1111/j.1432-1033.1974.tb03714.x

Michel, X., Salaün, J.-P., Galgani, François, and Narbonne, Jean-François (1994). Benzo(a)pyrene hydroxylase activity in the marine mussel mytilus galloprovincialis: a potential marker of contamination by polycyclic aromatic hydrocarbon-type compounds. *Mar. Environ. Res.* 38, 257–273. doi: 10.1016/0141-1136(94)90027-2

Moron, M. S., Depierre, J. W., and Mannervik, B. (1979). Levels of glutathione, glutathione reductase and glutathione s-transferase activities in rat lung and liver. *Biochem. Biophys. Acta* 582, 67–78. doi: 10.1016/0304-4165(79)90289-7

Park, H., In-Y, A., Kim, H., Lee, J., and Chul Shin, S. (2009). Glutathione s-transferase as a biomarker in the Antarctic bivalve laternula elliptica after exposure to the polychlorinated biphenyl mixture aroclor 1254. *Comp. Biochem. Physiol. Part C: Toxicol. Pharmacol.* 150, 4, 528–536. doi: 10.1016/j.cbpc.2009.07.008

Rotruck, J. T., Pope, A. L., Ganther, H. E., Swanson, A. B., Hafeman, D. G., and Hoekstra, W. G. (1973). Selenium: biochemical role as a component of glutathione peroxidase. *Science* 179, 588–590. doi: 10.1126/science.179.4073.588

Saprunova, V. B., Solodovnikova, I. M., and Bakeeva, L. E. (2008). Cytochrome c oxidase activity in mitochondria of cardiomyocytes from isolated cardiac tissue incubated under long-term hypoxic conditions. *Cell Tissue Biol.* 2, 153–157. doi: 10.1134/S1990519X08020089

Satheeswaran, T., Purushothaman, Y., Palani, D., Velmurugan, K., Jha, D. K., Dharani, G., et al. (2019). Assessment of trace metal contamination in the marine sediment, seawater, and bivalves of parangipettai, southeast coast of India. *Mar. pollut. Bull.* 1492019, 110499. doi: 10.1016/j.marpolbul.2019.110499

Shugart, L. R. (1988). Quantitation of chemically induced damage to DNA of aquatic organisms by alkaline unwinding assay. *Aquat Toxicol.* 13, 43–52. doi: 10.1016/0166-445X(88)90071-9

Shu, Y. Z., Johnson, B. M., and Yang, T. J. (2008). Role of biotransformation studies in minimizing metabolism-related liabilities in drug discovery. *AAPS J.* 10, 178–192. doi: 10.1208/s12248-008-9016-9

Sinha, A. K. (1972). Colorimetric assay of catalase. *Anal. Biochem.* 47, 389–394. doi: 10.1016/0003-2697(72)90132-7

Sudakin, D. L., Stone, D. L., and Power, L. (2011). Naphthalene mothballs: Emerging and recurring issues and their relevance to environmental health. *Curr. topics Toxicol.* 7, 13–19.

Walker, C. H., Hopkin, S. P., Sibly, R. M., and Peakall, D. B. (2001). *Principles of ecotoxicology. 2nd ed* (London: Taylor & Francis).

Williams, C. H., and Kamin, H. (1962). Microsomal triphosphopyridine nucleotide-cytochrome c reductase of liver. *J. Biol. Chem.* 237, 587–595. doi: 10.1016/S0021-9258(18)93967-0

Wunderlin, D. A., Diaz, M. P., Ame, M. V., Pesce, S. F., Hued, A. C., and Bistoni, M. (2001). Pattern recognition techniques for the evaluation of spatial and temporal variation in water quality. *A Case study: Suquia river basin (Cordoba Argentina). Water Res.* 35, 2881–2894. doi: 10.1016/S0043-1354(00)00592-3

Wu, M. L., Wang, Y. S., Sun, C. C., Wang, H., Dong, J. D., Yin, J. P., et al. (2010). Identification of coastal water quality by statistical analysis methods in daya bay, south China Sea. *Mar. pollut. Bull.* 60, 852–860. doi: 10.1016/j.marpolbul.2010.01.007

Zorov, D. B., Juhaszova, M., and Sollott, S. J. (2014). Mitochondrial reactive oxygen species (ROS) and ROS-induced ROS release. *Physiol. Rev.* 94 (3), 909–950. doi: 10.1152/physrev.00026.2013

frontiers | Frontiers in Marine Science

TYPE Original Research
PUBLISHED 08 August 2022
DOI 10.3389/fmars.2022.967678

Check for updates

OPEN ACCESS

EDITED BY
Dilip Kumar Jha,
National Institute of Ocean Technology, India

REVIEWED BY
Pankaj Verma,
National Institute of Ocean Technology, India
Nithyanandam Marimuthu,
Zoological Survey of India, India
Mehmuna Begum,
National Centre for Coastal Research, India

*CORRESPONDENCE
Wentao Ma
wtma@sio.org.cn

SPECIALTY SECTION
This article was submitted to Marine Pollution, a section of the journal Frontiers in Marine Science

RECEIVED 13 June 2022
ACCEPTED 20 July 2022
PUBLISHED 08 August 2022

CITATION
Xiu P, Guo L and Ma W (2022) Modelling the influence of submesoscale processes on phytoplankton dynamics in the northern South China Sea. *Front. Mar. Sci.* 9:967678. doi: 10.3389/fmars.2022.967678

COPYRIGHT
© 2022 Xiu, Guo and Ma. This is an open-access article distributed under the terms of the Creative Commons Attribution License (CC BY). The use, distribution or reproduction in other forums is permitted, provided the original author(s) and the copyright owner(s) are credited and that the original publication in this journal is cited, in accordance with accepted academic practice. No use, distribution or reproduction is permitted which does not comply with these terms.

Modelling the influence of submesoscale processes on phytoplankton dynamics in the northern South China Sea

Peng Xiu[1,2], Lin Guo[1,2] and Wentao Ma[3]*

[1]Southern Marine Science and Engineering Guangdong Laboratory (Guangzhou), Guangzhou, China, [2]Guangdong Key Laboratory of Ocean Remote Sensing, State Key Laboratory of Tropical Oceanography, South China Sea Institute of Oceanology, Chinese Academy of Sciences, Guangzhou, China, [3]State Key Laboratory of Satellite Ocean Environment Dynamics, Second Institute of Oceanography, Ministry of Natural Resources, Hangzhou, China

Submesoscale processes in the ocean vary rapidly in both space and time, and are often difficult to capture by field observations. Their dynamical connection with marine biology remains largely unknown because of the intrinsic link between temporal and spatial variations. In May 2015, satellite chlorophyll data demonstrated high concentration patches in the edge region between mesoscale eddies, which were higher than those in the cyclonic eddy core region in the northern South China Sea (NSCS). The underlying mechanisms were examined with a high-resolution physical-biological model. By tracking Lagrangian particles in the model, this study shows that the edge region between eddies is a submesoscale frontal region that is prone to intense upwelling and downwelling motions. We identified two key submesoscale mechanisms that affect nutrient transport flux significantly, submesoscale fontal dynamics and submesoscale coherent eddies. The dynamics associated with these two mechanisms were shown to be able to inject subsurface nutrients into the upper layer, generate the high chlorophyll patch, and alter phytoplankton community structure in the NSCS. This study shows the importance of submesoscale processes on phytoplankton dynamics in the NSCS and highlights the need for high-resolution observations.

KEYWORDS

submesoscale process, mesoscale eddy, phytoplankton chlorophyll, nutrient flux, phytoplankton community

Introduction

Mesoscale eddies are a ubiquitous feature and important in regulating physical and biogeochemical environments in the ocean (e.g., Falkowski et al., 1991; McGillicuddy et al., 1998; McGillicuddy et al., 2007; Chelton et al., 2011; Siegel et al., 2011; Mahadevan et al., 2012; Gaube et al., 2013; Omand et al., 2015). Regions around mesoscale eddies are known to be associated with strong current shear and strain, which can induce intense upward and downward motions at submesoscale (Lapeyre et al., 2006; Mahadevan and Tandon, 2006). These vertical motions can efficiently transport nutrients into the euphotic zone and lead to elevated biological patches (Lévy et al., 2001; Lehahn et al., 2007; Mahadevan, 2016).

In the ocean, vertical velocities are generally orders of magnitude smaller than horizontal ones (Klein and Lapeyre, 2009), and direct measurements of vertical velocities are not currently available. With the Omega equation, one can diagnose the vertical velocity by using measured density and velocity fields (e.g., Martin and Richards, 2001). Legal et al. (2007) reported an anticorrelation between vertical velocity and density gradient in a frontal region, and suggested that the large-scale strain can dynamically change small-scale filaments. The edge region of a mesoscale eddy or between eddies can be treated as a front because of the horizontal density gradient. Klein and Lapeyre (2009) thus suggested that the vertical exchange should be more efficient at the eddy edge than eddy center.

In addition to fronts, submesoscale eddies that are defined as energetic eddies with a radius smaller than the Rossby deformation radius and a localized structure, have also been observed in different parts of the ocean (McWilliams, 1985; Li et al., 2017; Zhang et al., 2022). They can be very long lived and travel far from their origins. As they can retain their core water mass during their life, they can transport waters with anomalous properties over long distances (Lukas and Santiago-Mandujano, 2001). The cumulative effect of these submesoscale eddies can potentially affect the large-scale transport and distribution of heat, nutrients, and other materials (e.g., Frenger et al., 2018; Gula et al., 2019).

The South China Sea (SCS) is an oligotrophic marginal sea adjacent to the western Pacific Ocean. Seasonally changing monsoon winds play an important role in modulating the upper ocean biology (Liu et al., 2002; Gan et al., 2006). Superimposed on the basin-scale variability, significant spatial and temporal variations of phytoplankton dynamics have been found to be related to mesoscale eddies (Ning et al., 2004; Chen et al., 2007; Huang et al., 2010; Xiu and Chai, 2011; Guo et al., 2015; He et al., 2016; Liu et al., 2017; Xiu et al., 2019). Most of the eddies show high chlorophyll concentrations in the cyclonic eddy core and low concentrations in the anticyclonic eddy core, which is likely related to the mesoscale eddy mechanism (McGillicuddy et al., 1998). A lot of studies have been conducted focusing on physical characteristics of submesoscale features in the northern SCS (Liu et al., 2010; Zhang et al., 2016; Dong and Zhong, 2018; Qiu et al., 2019; Ni et al., 2021; Zhang et al., 2022). However, less attention has been given to the biological impact from submesoscale processes at the eddy edge where enhanced shear and strain exist. Observations from Zhou et al. (2013) and Wang et al. (2018) indicated that possible submesoscale structures around an anticyclonic eddy may enhance phytoplankton production and increase carbon export; however, their samplings were too coarse in space (30-50 km) to resolve detailed submesoscale dynamics. With satellite data in the western SCS, Liu et al. (2017) showed high chlorophyll anomaly present at the northwestern periphery of anticyclonic eddies and suggested that it could be induced by the ageostrophic secondary circulation.

The submesoscale process has a typical spatial scale of 1-10 km and a temporal scale of ~1 day that are difficult to observe by coarse-resolution ship measurements or regular-frequency Argo floats. How these submesoscale processes affect phytoplankton and nutrient distributions in the northern SCS (NSCS), however, remains largely unknown. Moreover, the high energy of the submesoscale field also has significant implications for predictive modeling of oceanic pollutant pathways and concentrations. In this study, a high-resolution physical-biological model was built to investigate the influence of submesoscale features around mesoscale eddies on biological processes in the NSCS.

Data and model

To study biological responses to submesoscale structures, a coupled physical-biological model was developed for the NSCS region. The physical model was based on the Regional Ocean Modelling System (ROMS), and the biological model was based on a modified version of the Carbon Silicate Nitrate Ecosystem (CoSiNE; Chai et al., 2002) model. This modified version of CoSiNE model includes two phytoplankton groups (small phytoplankton with S1 for nitrogen based biomass and Chl1 for chlorophyll concentration, diatom with S2 for nitrogen based biomass, and Chl2 for chlorophyll concentration), two zooplankton classes (microzooplankton (Z1), mesozooplankton (Z2)), two size classes of detritus (small (SPON), large (LPON)), biogenic silica (bSi), nitrate (NO_3), ammonium (NH_4), silicate ($SiOH_4$), phosphate (PO_4), dissolved inorganic carbon (DIC), total alkalinity (TALK) and dissolved oxygen (DO). In the model, both small phytoplankton and diatom uptake the NO_3, NH_4, and PO_4 for growth, and diatom needs extra nutrient, $SiOH_4$. The microzooplankton grazes on small phytoplankton, while the mesozooplankton grazes on diatoms, microplankton, and detritus. The mortality and aggregation of phytoplankton and zooplankton are the source terms of detritus. Predation by mesozooplankton and the remineralization are the sink terms of detritus. The detailed model equations and parameters can be found in Ma et al. (2019).

The three-dimensional coupled model was set up for the NSCS (116-120° E, 18-22°N). It has a 1/108° (~ 1 km) resolution horizontally and has 30 vertical levels in terrain-following sigma-coordinates. The coupled model was initialized and one-way nested to the Hybrid Coordinate Ocean Model (HYCOM) dataset that has a spatial resolution of 1/12° and a temporal resolution of 1 day. The HYCOM model uses the Navy Coupled Ocean Data Assimilation system (NCODA) to assimilate available altimeter data, satellite, *in-situ* profiles from XBTs, buoys and Argo floats, which gives a better representation of the state of the ocean. In addition, eight tidal constituents (M2, S2, N2, K2, K1, O1, P1, and Q1) were used to calculate the hourly tidal elevation at the boundary. Here, M2 is the principal lunar semidiurnal constituent, S2 is the principal solar semidiurnal constituent, N2 is the larger lunar elliptic semidiurnal constituent, K2 is the luni-solar semidiurnal constituent, K1 is the luni-solar diurnal constituent, O1 is the principal lunar diurnal constituent, P1 is the principal solar diurnal constituent, and Q1 is the larger lunar elliptic constituent. For the surface forcing, the 6-hourly surface winds were obtained from the Cross-Calibrated Multi-Platform (CCMP) wind dataset with a spatial resolution of 0.25°. The surface heat and freshwater fluxes were calculated by the COARE3.0 bulk formula using both the CCMP wind and 6-hourly NCEP/NCAR reanalysis data. The initial and boundary conditions for biological variables were derived from a coarse-resolution coupled model, which covers the Pacific Ocean and runs continuously from 1993 to present (Xiu and Chai, 2011).

The coupled model was integrated from 1 January 2015 for one year and daily averaged model outputs were used for analysis. Model outputs were further used to drive an offline particle tracking code (TRACMASS; https://www.tracmass.org/) to examine vertical motions. The TRACMASS code was developed by Döös (1995), which computes numerically the trajectory through each grid cell by solving a differential equation that depends on the velocities on the grid box wall. The chosen water trajectories from any location can be followed along the path both forward and backward in time.

Daily sea-level anomaly (SLA) field with a grid of 1/4° by 1/4° was obtained from the Archiving, Validation and Interpretation of Satellite Data in Oceanography (AVISO). The finite-size Lyapunov exponent (FSLE) product was also obtained from AVISO, which is commonly used to diagnose regions of large stretching and straining by advection (d'Ovidio et al., 2004). The FSLE is defined as the inverse time of separation of two particles from their initial distance to final distance. The particles were advected by altimetry velocities and their trajectories are computed by backward-time integrating the altimetry velocities. Thus, regions with large FSLE generally correspond to the regions where surface current divergence are strong. Chlorophyll concentration data was obtained from a multi-sensor (SeaWiFS, MODIS and MERIS) merged product with a spatial resolution of 4 km and a temporal resolution of 1 day, developed by the Ocean Color Climate Change Initiative (OC_CCI) (Lavender et al., 2015). For analysis, the SLA and FSLE were interpolated onto the chlorophyll data grid.

Results

Submesoscale features between eddies

On 28 April 2015, two cyclonic eddies were present to the west of Luzon Strait, with one located on the north (CE1) and the other one on the south (CE2). There was another anticyclonic eddy (AC1) present to the west of the two cyclonic eddies (Figure 1). The water property in AC1 was similar to that of Kuroshio water, suggesting that the AC1 was generated by Kuroshio intrusion (Shu et al., 2016). When tracing back to February 2015, we can see that the two CEs were generated locally in the NSCS (Shu et al., 2016). The locations of the three eddies were relatively stable between late April and early May. The strength of the two CEs gradually reduced after early May, while the AC maintained its strength and propagated to the west.

Satellite-derived surface chlorophyll concentration showed clearly localized high patches with magnitude higher than 0.15 mg m^{-3} in the edge regions between CE1 and CE2, and between AC1 and the CEs (Figures 2A, B). Due to cloud contamination, we can only show four-day-averaged chlorophyll concentration, which is not fine enough to resolve detailed submesoscale dynamics. For the daily chlorophyll data, the mean cloud coverage in the study region in April and May was about 76% and it reduced to about 31% when using the four-day-averaged data. Unlike physical variables, it usually takes days for phytoplankton to show biological changes in response to dynamical forcings. Four-day-averaged chlorophyll is probably able to reflect biological changes to submesoscale dynamics, but locations might not be consistent with physical variables (Mahadevan, 2016; Lévy et al., 2018). The spatial decoupling between upwelling, phytoplankton new production, and export production across a submesoscale front has been reported (Estapa et al., 2015). Large horizontal stretching and straining represented by large FSLE calculated from altimeter data were found in the edge area between these eddies (Figures 2C, D). These regions are very dynamic where unstable and stable manifolds cross each other and are prone to frontogenesis that is accompanied with large vertical velocities (>10 m d^{-1}; Lehahn et al., 2007; d'Ovidio et al., 2009).

A transect through the edge region between CE1 and CE2 also showed that chlorophyll concentration in the CE was generally higher than that in the AC. The highest chlorophyll was present in the edge region with small negative SLAs and large FSLE values (Figure 3). High strain between eddies may create submesoscale upwelling/downwelling motion that facilitates nutrient transport vertically. Because the surface NSCS in May is generally in a nutrient-limited condition, submesoscale nutrient transport is

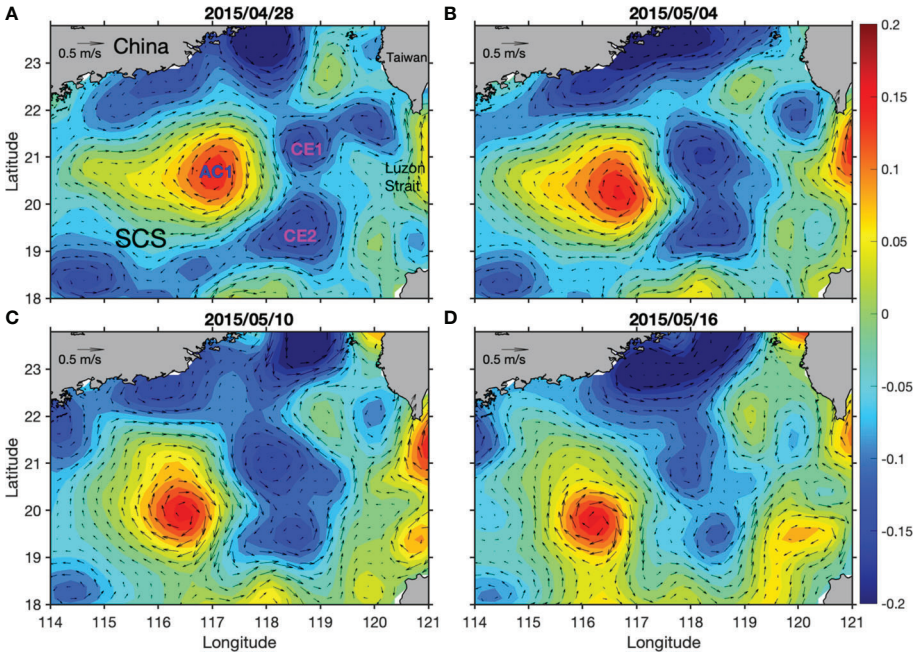


FIGURE 1
Time evolutions of SLA (units: m) overlaid by geostrophic current anomalies on 28 April **(A)**, 04 May **(B)**, 10 May **(C)** and 16 May 2015 **(D)**.

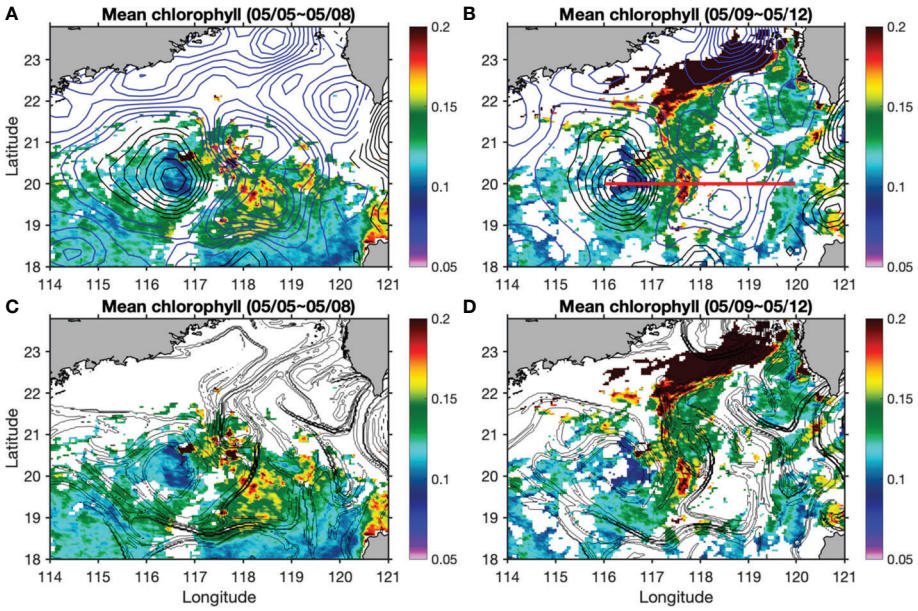


FIGURE 2
Surface chlorophyll concentration (units: mg m^{-3}) overlaid by SLA (units: m; black contours for positive and blue ones for negative values) in **(A, B)**, and overlaid by FSLE contours larger than 0.1 d^{-1} in **(C, D)** during 5-12 May. The red line in **(B)** denotes the position of the transect for further analysis.

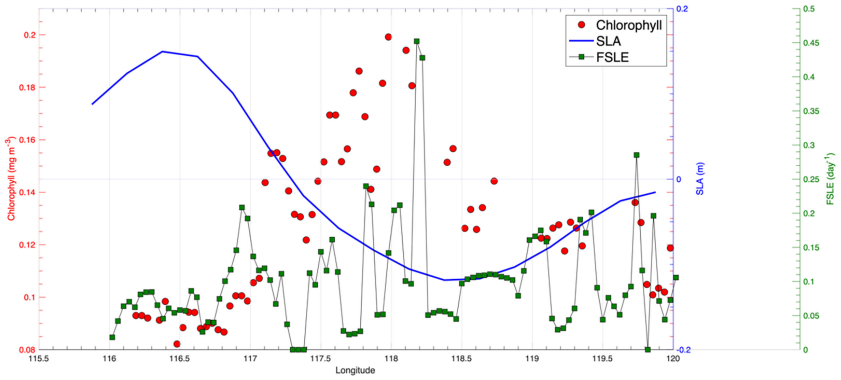


FIGURE 3
Spatial variability of SLA (units: m), surface chlorophyll concentration (units: mg m^{-3}), and FSLE (units: day^{-1}) along the transect shown in Figure 2B.

likely to stimulate phytoplankton growth and generate localized high chlorophyll patches.

To investigate the existence of upwelling, movements of passive particles were tracked in the model. Although the model missed the SLA magnitudes slightly, it reproduced CE1, CE2 and AC1 reasonably well (Figure 4). On 4 May, over 50,000 passive particles were released in the model at 50 m in the area between CE1 and CE2, covering both the core and edge regions (Figure 4). The movements of these particles were tracked over time in the model. These particles were first stretched along the hyperbolic region and then advected away mostly at the eddy edge. Only a relatively small number of particles stayed in the eddy core as it propagated. We tracked those particles that entered the mixed layer after seven days from their release, and found that they were

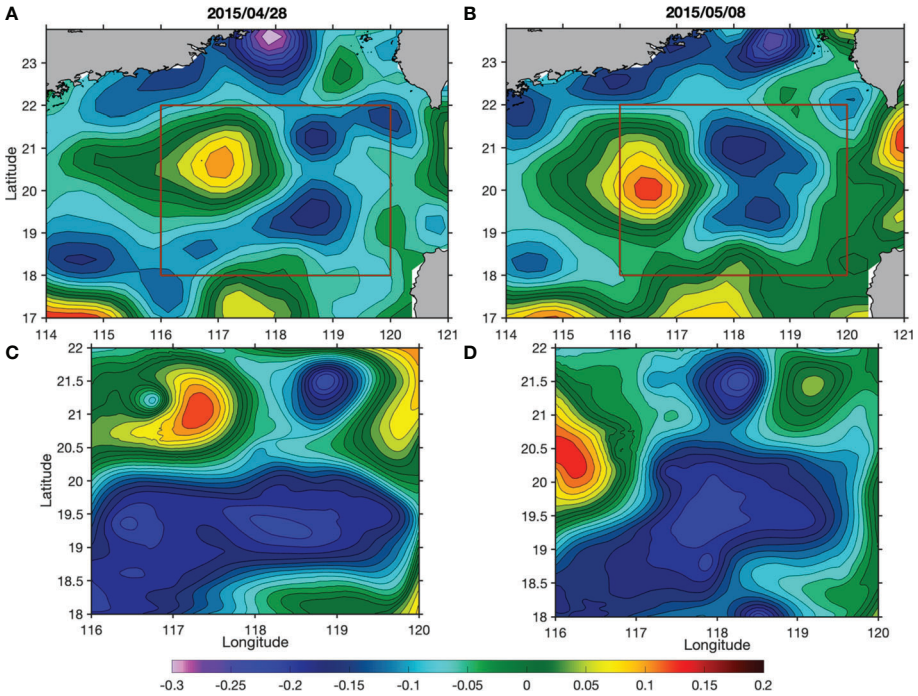


FIGURE 4
Comparisons of spatial distributions of SLA (units: m) from altimeter data **(A, B)** and the model outputs **(C, D)** on 28 April and 8 May. The red rectangles in **(A, B)** depict the domain of the model.

generally the ones released at the eddy edge regions (Figure 5). Consistent with this pattern, the probability of particles staying in the mixed layer during the one-month period is particularly higher at the eddy edge regions (Figure 6).

Driving mechanisms

The submesoscale nutrient transport was further examined in the model. On May 8, the nitrate concentration at 50 m showed localized high patches (Figure 7). These patches were at a submesoscale length scale and present around mesoscale eddies. To examine the physical processes driving these nitrate patches, two cases were chosen. We used two moving boxes (50×50 km) to encompass two nitrate patches and follow their movements (white box for case1, red box for case2).

For case1, the high nitrate patch was associated with a coherent submesoscale eddy that can be captured from surface SLA (Figure 7). This eddy has a radius of ~20 km. It was formed near the Dongsha Island, probably related to the current-topography interactions (Zhang et al., 2022). From 5 May, it was advected to the southwest by the current at the edge of mesoscale eddies. This submesoscale eddy associated with high nitrate concentration eventually merged into the mesoscale cyclonic eddy, CE2, providing a significant contribution of nitrate input flux to CE2. While the submesoscale eddy propagated, the distribution of vertical velocity (w) at 80 m displayed a diapole pattern with positive w at the leading edge and negative w at its trailing edge (Figure 8). The similar distribution pattern of current divergence ($\delta=u_x+v_y$; where u, v are the velocity components in x, y, i.e., east and north, directions) with positive and negative values corresponding to upwelling and downwelling, respectively, suggests that current divergence is the possible mechanism leading to the upwelling and downwelling processes (Figure 8).

Following the propagation of the submesoscale eddy, both positive and negative w decreased with time in a similar manner, probably suggesting a connected circulation cell (Figure 9A). Nevertheless, the box-averaged w stayed positive during the eddy propagation, which also drives the positive nitrate flux vertically Figure. The vorticity ($\zeta=v_x-u_y$) normalized by the Coriolis frequency (f) indicated that the submesoscale eddy experienced both the developing stage before 29 April and the decay stage afterwards (Figure 9B). During its developing stage, nitrate level at 50 m was relatively stable and it started to increase

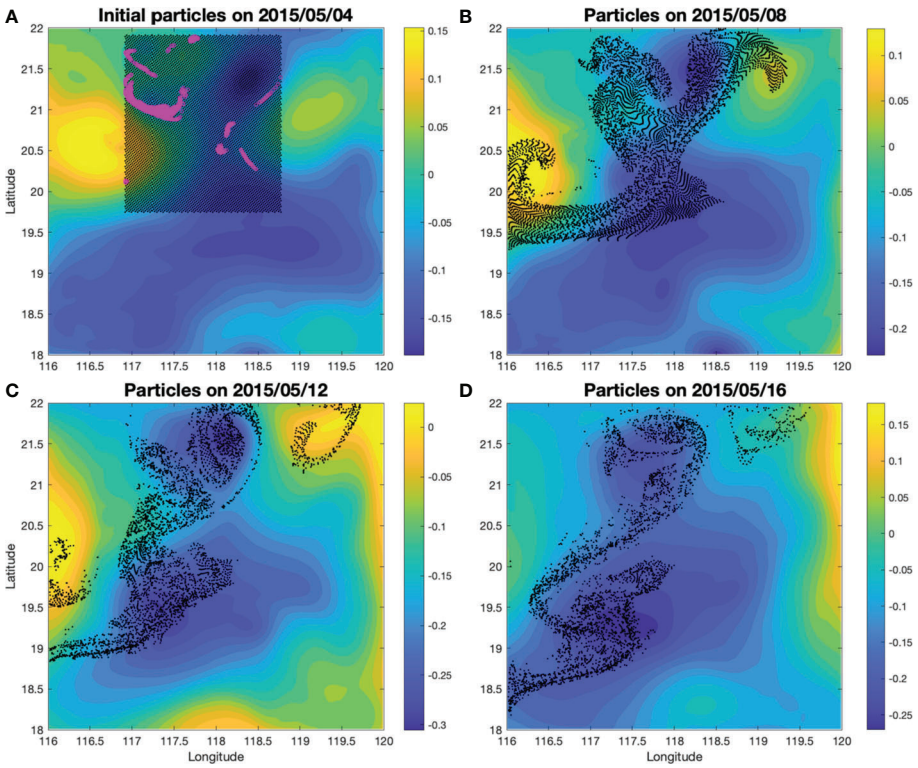


FIGURE 5
Lagrangian particle releasing results on 04 May **(A)**, 08 May **(B)**, 12 May **(C)** and 16 May 2015 **(D)**. The particles were released at the surface of a depth of 50 m. The black dots show the particle locations on different days. The shadings are SLA (units: m). The magenta circles in **(A)** are the particles being brought into the mixed layer 7 days after being released.

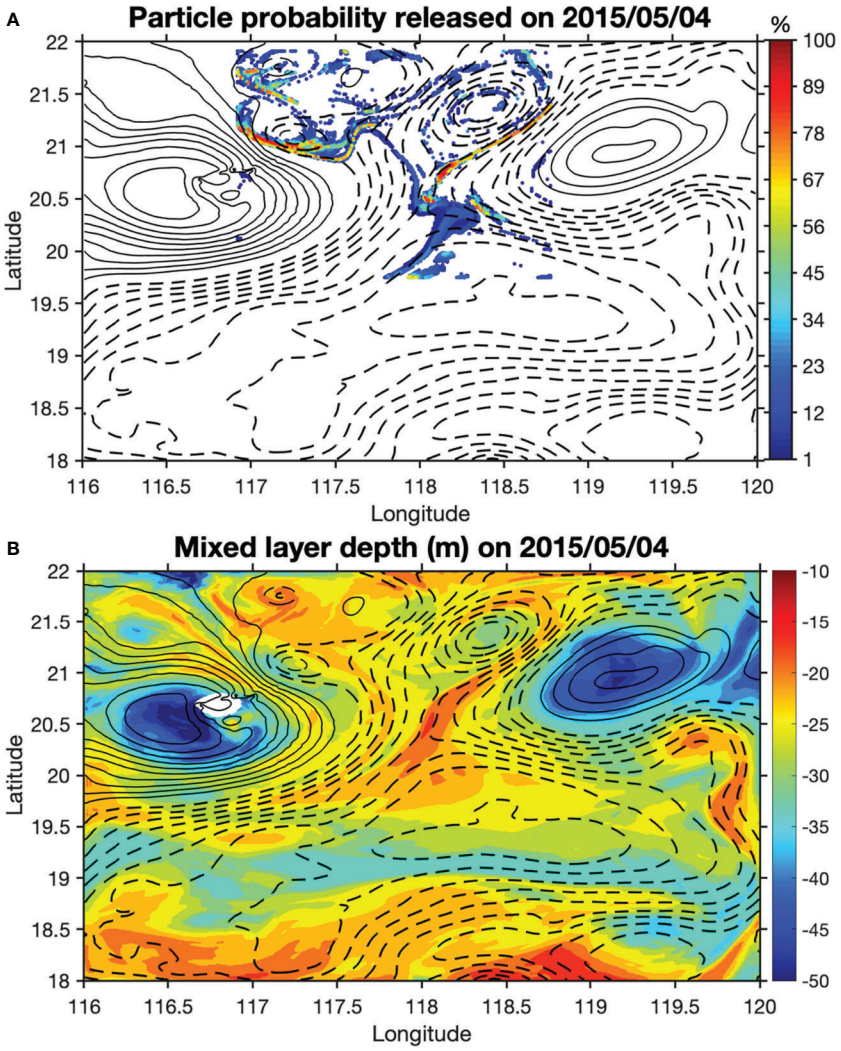


FIGURE 6
The spatial distribution of particle probability of staying in the mixed layer in May 2015 **(A)** and the spatial distribution of modeled mixed layer depth (m) on 4 May 2015 **(B)**. The particles were released at 50-m depth on 4 May. The contours are the SLA isolines with solid and dashed lines denoting positive and negative values, respectively.

during its decay stage while propagating (Figure 9C). During its propagation, the net nitrate flux was generally positive due to the relatively smaller negative horizontal flux, which resulted in the accumulation of nitrate concentration in the upper layer (Figure 9D). Following the movement of the submesoscale eddy, modeled mean chlorophyll concentration in the upper 50 m increased from 0.1 mg m^{-3} to 0.24 mg m^{-3}, which was in a similar magnitude as the satellite data.

For case2, the high nitrate patch that can reach higher than 2.0 mmol m^{-3} was not associated with any coherent circulation structures (red box in Figure 7). It showed up on 5 May and was eventually stretched away by the horizontal current between mesoscale eddies. The box averaged nitrate concentration showed a similar temporal pattern (Figure 10A). The increase of nitrate from 5 May was induced by the positive net nitrate flux (horizontal plus vertical flux) into the box that was largely driven by the increase of positive w (Figures 10B, C). On 4 May, there was an increase of north-south density gradient (Figure 10E), which can consequently lead to enhanced horizontal strain ($St = \sqrt{(u_x - v_y)^2 + (v_x + u_y)^2}$) and further induce secondary circulation with strong upward water motions (Figures 10B, D). This mechanism is consistent with frontal dynamics. We further composited the *w* at 80 m from 6 May to 12 May when the case2 patch moved generally in a zonal direction along the front between a mesoscale anticyclonic eddy in the north and a mesoscale cyclonic eddy in the south. The spatial distribution pattern of composited *w* demonstrated positive values in the

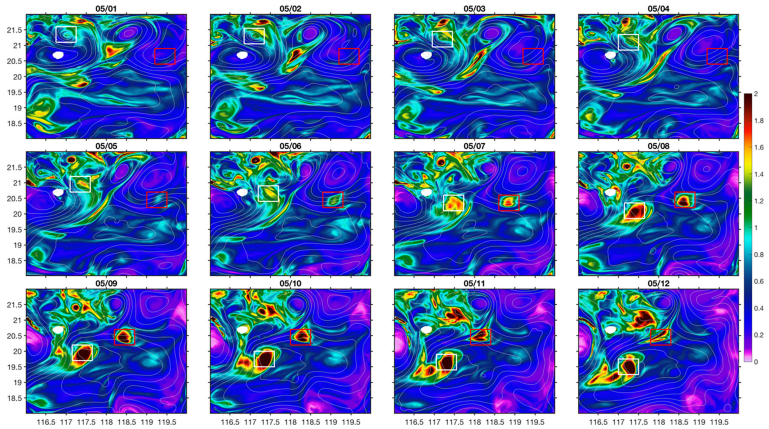


FIGURE 7
Spatial distributions of nitrate concentration (mmol m^{-3}) at 50 m from the model outputs. The white and red rectangles mark the locations of two high nitrate patches for analysis.

north and negative values in the south in correspondence to the low density in the north and high density in the south, respectively (Figure 11). Therefore, the elevated nitrate concentration in case2 was mainly induced by the frontal dynamics. The modeled chlorophyll change in the case2 patch generally followed the change of nitrate concentration over time.

Discussion and conclusions

Mesoscale eddies are known to induce perturbations in biogeochemistry in the eddy core through mesoscale dynamics. In addition to mesoscale responses, high-resolution chlorophyll images often show patchy distribution patterns that vary over a distance of a few kilometers at a temporal scale of

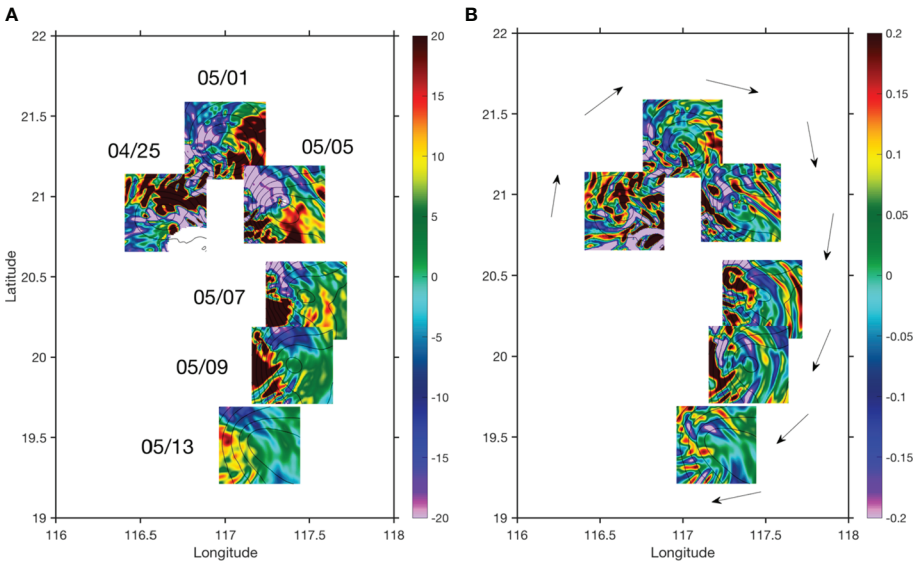


FIGURE 8
Distributions of vertical velocity **(A** units: m d^{-1}**)** at 80 m and normalized current divergence **(A)** at 50 m following the propagation the submesoscale eddy of case1. The arrows in **(B)** illustrates the general moving directions of the box.

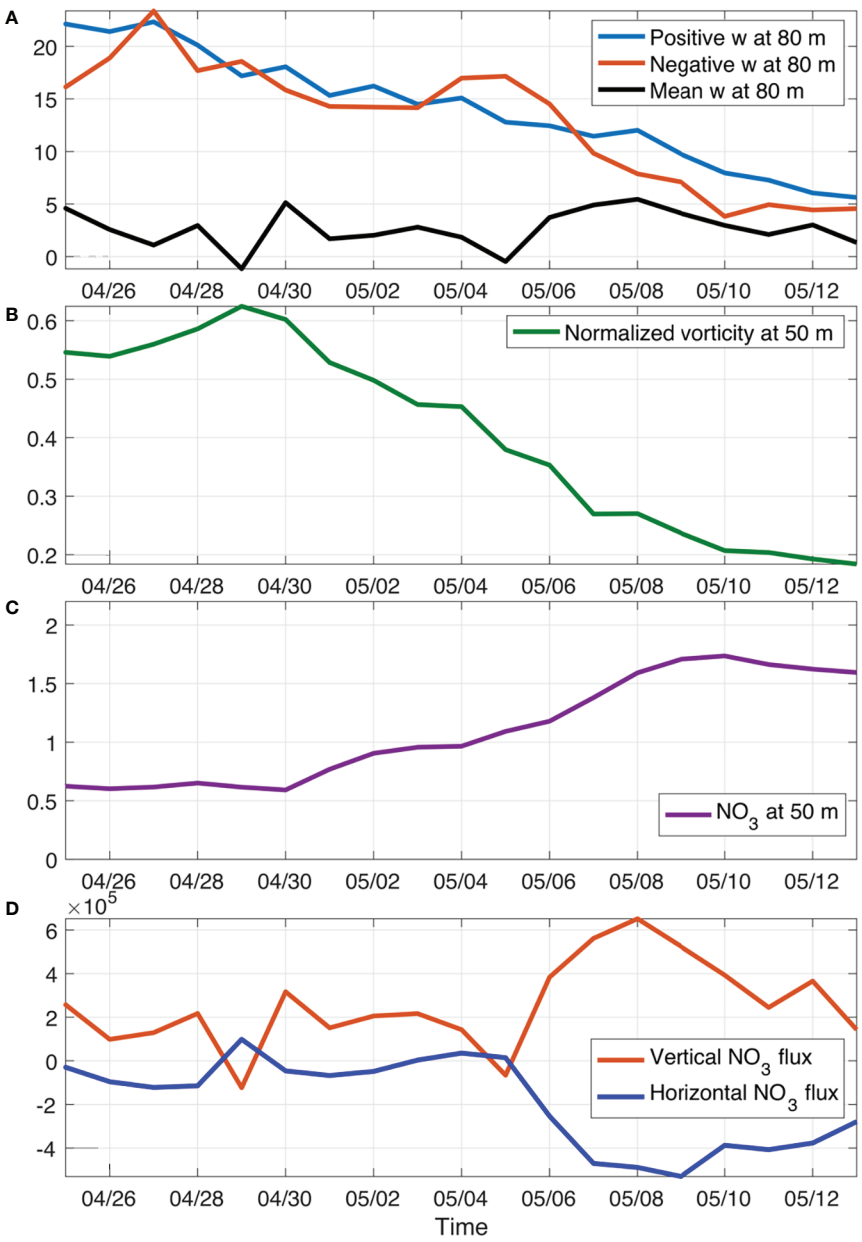


FIGURE 9
Temporal variations of box-averaged vertical velocities **(A**; units: m d^{-1}**)**, normalized vorticity by *f* **(B)**, nitrate concentration **(C**; mmol m^{-3}**)**, and nitrate fluxes **(D**; units: mmol s^{-1}**)** following the movement of case1 patch. Here, the horizontal nitrate flux was calculated from surface to 80 m and the vertical flux was calculated at 80 m.

days, which are suggested to link to submesoscale dynamics. At submesoscale, the spatial and temporal variations of tracers such as phytoplankton chlorophyll is often related (Mahadevan, 2016). Thus, to resolve submesoscale structures, both spatial and temporal resolutions need to be fine enough.

Two mechanisms have been previously suggested to generate submesoscale structures. One is the mesoscale-driven frontogenesis (Lapeyre et al., 2006; Mahadevan and Tandon, 2006), and the other is the mixed-layer instability (MLI; Boccaletti et al., 2007). The vertical scale of MLI is the mixed layer depth. The mixed layer depth during the study period was generally shallower than 40 m, except in the regions where anticyclonic eddies were present (Figure 6B). From the model results, we found strong fluctuations of isopycnals and upwelling/downwelling motions below the mixed layer. These fluctuations of isopycnals were conspicuously observed in the

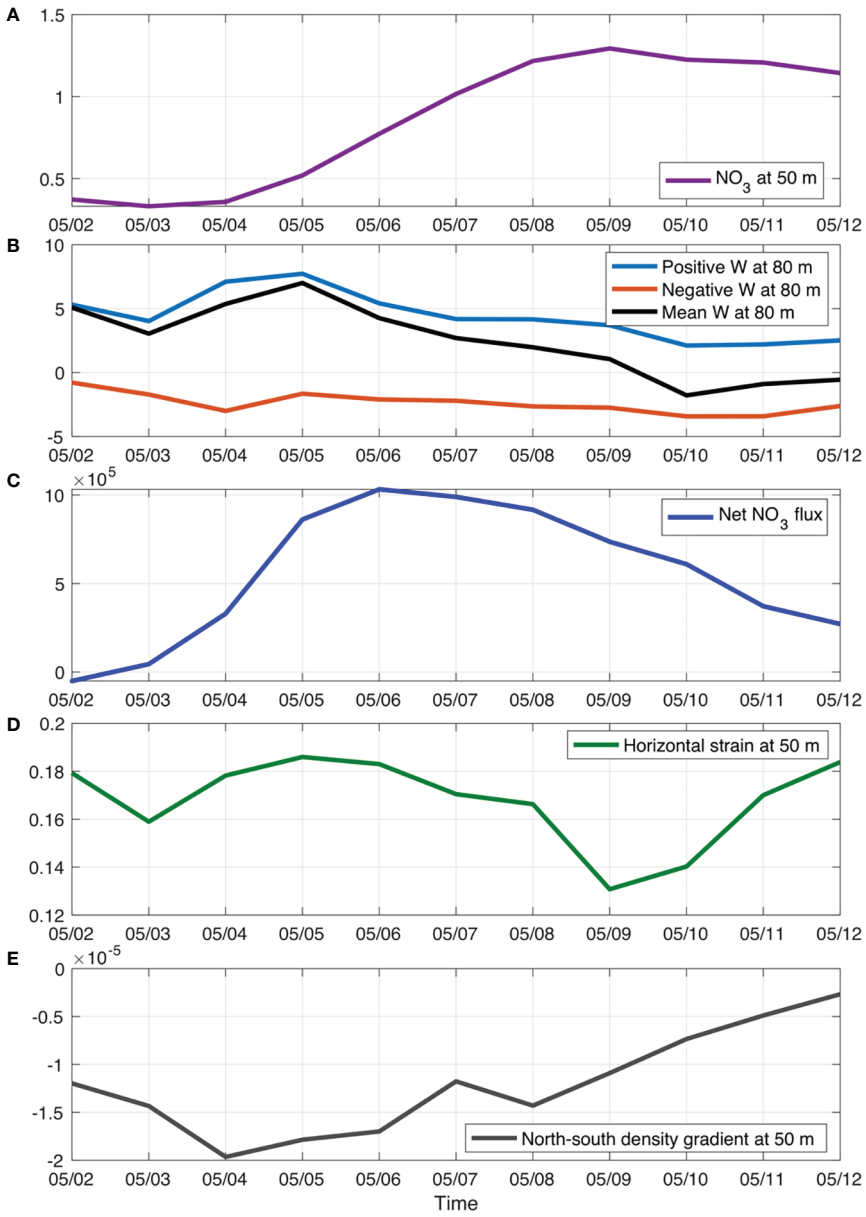


FIGURE 10
Temporal variations of box-averaged nitrate concentration **(A**; unit: mmol m^{-3}**)**, vertical velocities (**B**; units: m d^{-1}), net nitrate advection flux **(C**; unit: mmol s^{-1}**)**, normalized horizontal strain by *f* **(D)**, and north-south density gradient **(E**; unit: kg m^{-4}**)** of case2 patch.

edge region between mesoscale eddies, where enhanced shear and strain can sharpen existing horizontal density gradient and give rise to submesoscale upwelling/downwelling motions. It is thus likely that the submesoscale processes were induced by frontogenesis and baroclinic instabilities (Ramachandran et al., 2014; Zhang et al., 2021). Other studies also indicated that the frontogenesis plays a key role in generating submesoscale processes in the SCS (Zhong et al., 2017).

By simplifying the omega equation in a frontal region, we can obtain its two-dimensional version, that is,

$$\left(N^2 w\right)_{yy} + f^2 w_{zz} = 2\frac{g}{\rho_0}\left(v_y \cdot \rho_y\right)_y \quad (1)$$

This omega equation is derived by assuming that the *x* variation (along the front) in the data is much smaller than its *y* variation (across the front). It states that mesoscale flow can drive the growth of submesoscale density gradient associated with vertical velocity. With further simplification of this equation, Legal et al. (2007) derived an expression indicating the robust correlation between vertical velocity and density anomaly. It is consistent with the findings of this study, in

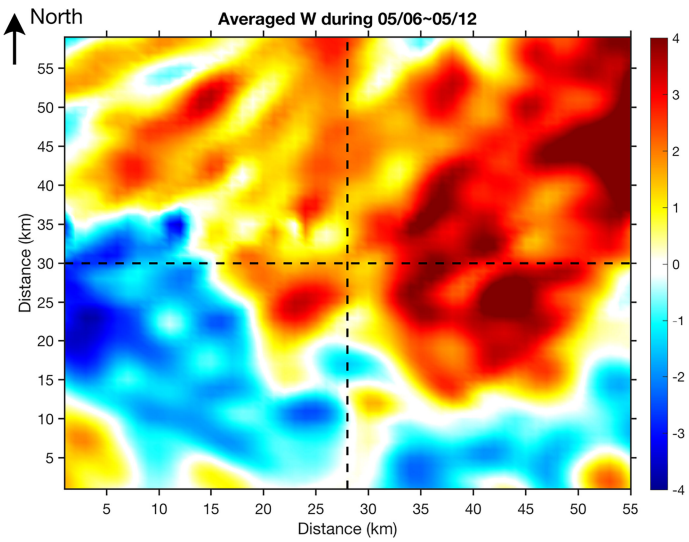


FIGURE 11
Composted mean of modeled vertical velocity (unit: m d^{-1}) at 80 m for case2 during 6 May~12 May, 2015.

which intense vertical velocity was illustrated by particle trajectories between eddies. The modeling results for submesoscale case2 have shown that such vertical motion is often linked with the vertical transport of tracers, such as nutrients, consistent with previous studies (Lévy et al., 2001; Lapeyre and Klein, 2006).

In addition, the modeling results showed that submesoscale eddy could be another mechanism inducing strong vertical nutrient transport at submesoscale. Although case1 was not generated at the eddy edge, it was carried away by the flow around the mesoscale eddy after formation. During its movements, divergence induced upwelling at the leading edge kept injecting nutrient from subsurface to the upper layer. Previous satellite study in the western SCS has observed such small-scale eddies associated with high surface chlorophyll concentrations (Liu et al., 2015). The submesoscale eddy could also be a potential nutrient source to mesoscale eddy once they merge together.

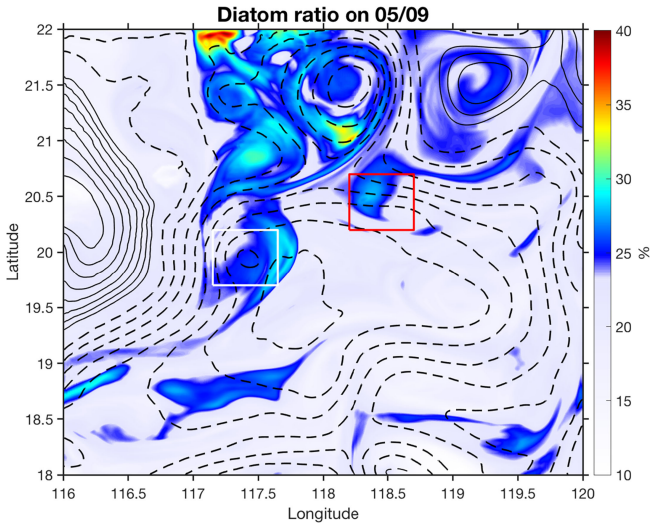


FIGURE 12
Modeled diatom ratio (%) in total phytoplankton averaged in the upper 50 m on 9 May 2015. The red and white rectangles depict two submesoscale nitrate patches. The contours are the SLA isolines with solid and dashed lines denoting positive and negative values, respectively.

Biological responses to submesoscale processes are more complicated than physical tracers. Nutrients upwelled from subsurface can be taken up by different phytoplankton species that are further modulated by ecosystem dynamics and other biogeochemical processes, which are all subject to different temporal scales (Lévy et al., 2018). The short time scales associated with strong submesoscale vertical nutrient injections and the biological response time favour dominance by the large phytoplankton size class (diatoms) of the model (Figure 12; Lévy et al., 2012; Guo et al., 2022). Different physical dynamics between mesoscale and submesoscale processes can thus lead to spatial and temporal heterogeneities in community structure and ecosystem dynamics (d'Ovidio et al., 2010; Lévy et al., 2012; Clayton et al., 2014; Mousing et al., 2016; Clayton et al., 2017). Moreover, the intensity of nutrient injection induced by submesoscale processes is also determined by the background nutricline depths that are set by mesoscale or large-scale processes. Consequently, regions with high physical straining and stretching are not always associated with enhanced total chlorophyll concentration (e.g., Guo et al., 2022).

In conclusion, with a high-resolution coupled model, we examined submesoscale processes between mesoscale eddies in the NSCS. By calculating the FSLE from altimeter data and tracking Lagrangian particles in the three-dimensional model, the submesoscale upwelling motion was revealed between eddies. We found that both frontal dynamics and submesoscale coherent eddies can inject subsurface nutrients into the upper layer, stimulate phytoplankton growth, and alter community structure. As the coupled model didn't include data assimilation, model discrepancies were found in simulating the strength and locations of mesoscale and submesoscale features. This study can serve as a process-orientated study to investigate potential dynamics and impacts of submesoscale features on biology. This study shows the strong physical-biological links at submesoscale in the NSCS, highlighting the importance of submesoscale processes on marine ecosystem and the need for high-resolution observations.

Data availability statement

The raw data supporting the conclusions of this article will be made available by the authors, without undue reservation.

Author contributions

Conceptualization: PX, WM; Methodology: LG, PX. Writing: PX. Review and editing: LG, WM. Funding acquisition: PX. All authors contributed to the article and approved the submitted version.

Funding

This research was supported by the Key Special Project for Introduced Talents Team of Southern Marine Science and Engineering Guangdong Laboratory (Guangzhou) (GML2019ZD0305) and the National Natural Science Foundation of China (41890805, 41730536).

Acknowledgments

The Ocean Color Climate Change Initiative (OC-CCI, Version 3.1) data were obtained from http://www.esa-oceancolour-cci.org/. The Cross-Calibrated Multi-Platform (CCMP) Version-2.0 data were obtained from www.remss.com. Six-hourly NCEP/NCAR Reanalysis surface forcing data were obtained from https://www.esrl.noaa.gov/psd/. The SLA and FSLE data were obtained from https://www.aviso.altimetry.fr/.

Conflict of interest

The authors declare that the research was conducted in the absence of any commercial or financial relationships that could be construed as a potential conflict of interest.

Publisher's note

All claims expressed in this article are solely those of the authors and do not necessarily represent those of their affiliated organizations, or those of the publisher, the editors and the reviewers. Any product that may be evaluated in this article, or claim that may be made by its manufacturer, is not guaranteed or endorsed by the publisher.

References

Boccaletti, G., Ferrari, R., and Fox-Kemper, B. (2007). Mixed layer instabilities and restratification. *J. Phys. Oceanogr.* 37, 2228–2250. doi: 10.1175/JPO3101.1

Chai, F., Dugdale, R. C., Peng, T. H., Wilkerson, F. P., and Barber, R. T. (2002). One dimensional ecosystem model of the equatorial pacific upwelling system, part I: Model development and silicon and nitrogen cycle. *Deep. Sea. Res. II.* 49, 2713–2745. doi: 10.1016/S0967-0645(02)00055-3

Chelton, D. B., Gaube, P., Schlax, M. G., Early, J. J., and Samelson, R. M. (2011). The influence of nonlinear mesoscale eddies on near-surface oceanic chlorophyll. *Science* 334 (6054), 328–332. doi: 10.1126/science.1208897

Chen, Y.-L., Chen, H.-Y., Lin, I.-I., Lee, M.-A., and Chang, J. (2007). Effects of cold eddy on phytoplankton production and assemblages in Luzon strait bordering the south China Sea. *J. Oceanogr.* 671–683, 63. doi: 10.1007/s10872-007-0059-9

Clayton, S., Dutkiewicz, S., Jahn, O., Hill, C., Heimbach, P., and Follows, M. J. (2017). Biogeochemical versus ecological consequences of modeled ocean physics. *Biogeosciences* 14, 2877–2889. doi: 10.5194/bg-14-2877-2017

Clayton, S., Nagai, T., and Follows, M. J. (2014). Fine scale phytoplankton community structure across the kuroshio front. *J. Plankton. Res.* 36 (4), 1017–1030. doi: 10.1093/plankt/fbu020

Dong, J., and Zhong, Y. (2018). The spatiotemporal features of submesoscale processes in the northern south China Sea. *Acta Oceanol. Sin.* 37 (11), 8–18. doi: 10.1007/s13131-018-1277-2

Döös, K. (1995). Interocean exchange of water masses. *J. Geophys. Res.* 100, 13499–13514. doi: 10.1029/95JC00337

d'Ovidio, F., De Monte, S., Alvain, S., Dandonneau, Y., and Lévy, M. (2010). Fluid dynamical niches of phytoplankton types. *Proc. Natl. Acad. Sci.* 107 (43), 18366. doi: 10.1073/pnas.1004620107

d'Ovidio, F., Fernandez, V., Hernandez-Garca, E., and Lopez, C. (2004). Mixing structures in the Mediterranean Sea from finite-size lyapunoov exponent. *Geophys. Res. Lett.* 31, L17203. doi: 10.1029/2004GL020328

d'Ovidio, F., Isern-Fontanet, J., López, C., Hernández-García, E., and García-Ladona, E. (2009). Comparison between eulerian diagnostics and finite-size lyapunov exponents computed from altimetry in the Algerian basin. *Deep-Sea. Res. I.* 56, 15–31. doi: 10.1016/j.dsr.2008.07.014

Estapa, M. L., Siegel, D. A., Buesseler, K. O., Stanley, R. H. R., Lomas, M. W., and Nelson, N. B. (2015). Decoupling of net community and export production on submesoscales in the Sargasso Sea. *Global Biogeochem. Cycles.* 29, 1266–1282. doi: 10.1002/2014GB004913

Falkowski, P. G., Ziemann, D., Kolber, Z., and Bienfang, P. K. (1991). Role of eddy pumping in enhancing primary production in the ocean. *Nature* 352, 55–58. doi: 10.1038/352055a0

Frenger, I., Bianchi, D., Stührenberg, C., Oschlies, A., Dunne, J., Deutsch, C., et al. (2018). Biogeochemical role of subsurface coherent eddies in the ocean: Tracer cannonballs, hypoxic storms, and microbial stewpots? *Global Biogeochem. Cycles.* 32 (2), 226–249. doi: 10.1002/2017GB005743

Gan, J., Li, H., Curchitser, E. N., and Haidvogel, D. B. (2006). Modeling south China Sea circulation. response to seasonal forcing regimes. *J. Geophys. Res.* 111, C06034. doi: 10.1029/2005JC003298

Gaube, P., Chelton, D. B., Strutton, P. G., and Behrenfeld, M. J. (2013). Satellite observations of chlorophyll, phytoplankton biomass, and ekman pumping in nonlinear mesoscale eddies. *J. Geophys. Res.: Oceans* 118, 6349–6370. doi: 10.1002/2013JC009027

Gula, J., Blacic, T. M., and Todd, R. E. (2019). Submesoscale coherent vortices in the gulf stream. *Geophysical. Res. Lett.* 46, 2704–2714. doi: 10.1029/2019GL081919

Guo, M., Chai, F., Xiu, P., Li, S., and Rao, S. (2015). Impacts of mesoscale eddies in the south China Sea on biogeochemical cycles. *Ocean. Dynamics.* 65, 1335–1352. doi: 10.1007/s10236-015-0867-1

Guo, M., Xiu, P., and Xing, X. (2022). Oceanic fronts structure phytoplankton distributions in the central south Indian ocean. *J. Geophys. Res.: Oceans.* 127, e2021JC017594. doi: 10.1029/2021JC017594

He, Q., Zhan, H., Cai, S., and Li, Z. (2016). Eddy effects on surface chlorophyll in the northern south China Sea: Mechanism investigation and temporal variability analysis. *Deep-Sea. Res. I.* 112, 25–36. doi: 10.1016/j.dsr.2016.03.004

Huang, B., Hu, J., Xu, H., Cao, Z., and Wang, D. (2010). Phytoplankton community at warm eddies in the northern south China Sea. *Deep-Sea. Res. II.* 57, 1792–1798. doi: 10.1016/j.dsr2.2010.04.005

Klein, P., and Lapeyre, G. (2009). The ocean vertical pump induced by mesoscale and submesoscale turbulence. *Annu. Rev. Mar. Sci.* 1, 351–375. doi: 10.1146/annurev.marine.010908.163704

Lapeyre, G., and Klein, P. (2006). Impact of the small-scale elongated filaments on the oceanic vertical pump. *J. Mar. Res.* 64, 835–851. doi: 10.1357/002224006779698369

Lapeyre, G., Klein, P., and Hua, B. L. (2006). Oceanic restratification forced by surface frontogenesis. *J. Phys. Oceanogr.* 36, 1577–1590. doi: 10.1175/JPO2923.1

Lavender, S., Jackson, T., and Sathyendranath, S. (2015). The ocean color climate change initiative. *Ocean. Challenge.* 21 (1).

Legal, C., Klein, P., Treguier, A.-M., and Paillet, J. (2007). Diagnosis of the vertical motions in a mesoscale stirring region. *J. Phys. Oceanogr.* 37 (5), 1413–1424. doi: 10.1175/JPO3053.1

Lehahn, Y., d'Ovidio, F., Lévy, M., and Heifetz, E. (2007). Stirring of the northeast Atlantic spring bloom: A Lagrangian analysis based on multisatellite data. *J. Geophys. Res.* 112, C08005. doi: 10.1029/2006JC003927

Lévy, M., Ferrari, R., Franks, P. J., Martin, A. P., and Rivière, P. (2012). Bringing physics to life at the submesoscale. *Geophys. Res. Lett.* 39, L14602. doi: 10.1029/2012GL052756

Lévy, M., Franks, P. J., and Smith, K. S. (2018). The role of submesoscale currents in structuring marine ecosystems. *Nat. Commun.* 9, 4758. doi: 10.1038/s41467-018-07059-3

Lévy, M., Klein, P., and Treguier, A.-M. (2001). Impact of sub-mesoscale physics on production and subduction of phytoplankton in an oligotrophic regime. *J. Mar. Res.* 59, 535–565. doi: 10.1357/002224001762842181

Liu, K. K., Chao, S. Y., Shaw, P. T., Gong, G. C., Chen, C. C., and Tang, T. Y. (2002). Monsoon-forced chlorophyll distribution and primary production in the south China Sea: observations and a numerical study. *Deep. Sea. Res. I.* 49, 1387–1412. doi: 10.1016/S0967-0637(02)00035-3

Liu, G., He, Y., Shen, H., and Qiu, Z. (2010). Submesoscale activity over the shelf of the northern south China Sea in summer: simulation with an embedded model. *Chin. J. Oceanography. Limnology.* 28 (5), 1073–1079. doi: 10.1007/s00343-010-0030-2

Liu, F., Tang, S., and Chen, C. (2015). Satellite observations of the small-scale cyclonic eddies in the western south China Sea. *Biogeosciences* 12, 299–305. doi: 10.5194/bg-12-299-2015

Liu, F., Tang, S., Huang, R., and Yin, K. (2017). The asymmetric distribution of phytoplankton in anticyclonic eddies in the western south China Sea. *Deep-Sea. Res. I.* 120, 29–38. doi: 10.1016/j.dsr.2016.12.010

Li, C., Zhang, Z., Zhao, W., and Tian, J. (2017). A statistical study on the subthermocline submesoscale eddies in the northwestern pacific ocean based on argo data. *J. Geophys. Res.: Oceans.* 122, 3586–3598. doi: 10.1002/2016JC012561

Lukas, R., and Santiago-Mandujano, F. (2001). Extreme water mass anomaly observed in the Hawaii ocean time-series. *Geophys. Res. Lett.* 28, 2931–2934. doi: 10.1029/2001GL013099

Mahadevan, A. (2016). The impact of submesoscale physics on primary productivity of plankton. *Annu. Rev. Mar. Sci.* 8, 17.1–17.24. doi: 10.1146/annurev-marine-010814-015912

Mahadevan, A., D'Asaro, E., Perry, M.-J., and Lee, C. (2012). Eddy-driven stratification initiates north Atlantic spring phytoplankton blooms. *Science* 3376090), 54–58. doi: 10.1126/science.1218740

Mahadevan, A., and Tandon, A. (2006). An analysis of mechanisms for submesoscale vertical motion at ocean fronts. *Ocean. Model.* 14, 241–256. doi: 10.1016/j.ocemod.2006.05.006

Martin, A. P., and Richards, K. J. (2001). Mechanisms for vertical nutrient transport within a north Atlantic mesoscale eddy. *Deep-Sea. Res. II.* 48, 757–773. doi: 10.1016/S0967-0645(00)00096-5

Ma, W., Xiu, P., Chai, F., and Li, H. (2019). Seasonal variability of the carbon export in the central south China Sea. *Ocean. Dynamics.* 69 (8), 955–966. doi: 10.1007/s10236-019-01286-y

McGillicuddy, D. J., Anderson, L. A., Bates, N. R., Bibby, T., Buesseler, K. O., Carlson, C. A., et al. (2007). Eddy/wind interactions stimulate extraordinary mid-ocean plankton blooms. *Science* 316, 1021–1026. doi: 10.1126/science.1136256

McGillicuddy, D. J., Robinson, A. R., Siegel, D. A., Jannasch, H. W., Johnson, R., Dickey, T. D., et al. (1998). Influence of mesoscale eddies on new production in the Sargasso Sea. *Nature* 394, 263–266. doi: 10.1038/28367

McWilliams, J. C. (1985). Submesoscale, coherent vortices in the ocean. *Rev. Geophysics.* 23, 165–182. doi: 10.1029/RG023i002p00165

Mousing, E. A., Richardson, K., Bendtsen, J., Cetinić, I., and Perry, M. J. (2016). Evidence of small-scale spatial structuring of phytoplankton alpha- and beta-diversity in the open ocean. *J. Ecol.* 104 (6), 1682–1695. doi: 10.1111/1365-2745.12634

Ning, X., Chai, F., Xue, H., Cai, Y., Liu, C., Zhu, G., et al. (2004). Physical-biological oceanographic coupling influencing phytoplankton and primary production in the south China Sea. *J. Geophys. Res.* 109, C10005. doi: 10.1029/2004JC002365

Ni, Q., Zhai, X., Wilson, C., Chen, C., and Chen, D. (2021). Submesoscale eddies in the south China. *Geophys. Res. Lett.* 48, e2020GL091555. doi: 10.1029/2020GL091555

Omand, M. M., D'Asaro, E. A., Lee, C. M., Perry, M. J., Briggs, N., Cetinic, I., et al. (2015). Eddy-driven subduction exports particulate organic carbon from the spring bloom. *Science* 348, 222–225. doi: 10.1126/science.1260062

Qiu, C., Mao, H., Liu, H., Xie, Q., Yu, J., Su, D., et al. (2019). Deformation of a warm eddy in the northern south China Sea. *J. Geophys. Res.: Oceans.* 124, 5551–5564. doi: 10.1029/2019JC015288

Ramachandran, S., Tandon, A., and Mahadevan, A. (2014). Enhancement in vertical fluxes at a front by mesoscale- submesoscale coupling. *J. Geophys. Res.: Oceans.* 119, 8495–8511. doi: 10.1002/2014JC010211

Shu, Y., Xiu, P., Xue, H., Yao, J., and Yu, J. (2016). Glider-observed anticyclonic eddy in northern south China Sea. *Aquat. Ecosyst. Health Manage.* 19, 233–241. doi: 10.1080/14634988.2016.1208028

Siegel, D. A., Peterson, P., McGillicuddy, D. J., Maritorena, S., and Nelson, N. B. (2011). Bio-optical footprints created by mesoscale eddies in the Sargasso Sea. *Geophys. Res. Lett.* 38, L13608. doi: 10.1029/2011GL047660

Wang, L., Huang, B., Laws, E. A., Zhou, K., Liu, X., Xie, Y., et al. (2018). Anticyclonic eddy edge effects on phytoplankton communities and particle export in the northern south China Sea. *J. Geophys. Res.* 123 (11), 7632–7650. doi: 10.1029/2017JC013623

Xiu, P., and Chai, F. (2011). Modeled biogeochemical responses to mesoscale eddies in the south China Sea. *J. Geophys. Res. Oceans.* 116, C10006. doi: 10.1029/2010JC006800

Xiu, P., Dai, M., Chai, F., Zhou, K., Zeng, L., and Du, C. (2019). On contributions by wind-induced mixing and eddy pumping to interannual chlorophyll variability during different ENSO phases in the northern south China Sea. *Limnol. Oceanogr.* 64, 503–514. doi: 10.1002/lno.11055

Zhang, Z., Tian, J., Qiu, B., Zhao, W., Chang, P., Wu, D., et al. (2016). Observed 3D structure, generation, and dissipation of oceanic mesoscale eddies in the south China Sea. *Sci. Rep.* 6, 24349. doi: 10.1038/srep24349

Zhang, X., Zhang, Z., McWilliams, J. C., Sun, Z., Zhao, W., and Tian, J. (2022). Submesoscale coherent vortices observed in the northeastern south China Sea. *J. Geophys. Res.: Oceans.* 127, e2021JC018117. doi: 10.1029/2021JC018117

Zhang, Z., Zhang, X., Qiu, B., Zhao, W., Zhou, C., Huang, X., et al. (2021). Submesoscale currents in the subtropical upper ocean observed by long-term high-resolution mooring arrays. *J. Phys. Oceanogr.* 51, 187–206. doi: 10.1175/JPO-D-20-0100.1

Zhong, Y., Bracco, A., Tian, J., Dong, J., Zhao, W., and Zhang, Z. (2017). Observed and simulated submesoscale vertical pump of an anticyclonic eddy in the south China Sea. *Sci. Rep.* 7, 44011. doi: 10.1038/srep44011

Zhou, K., Dai, M., Kao, S.-J., Wang, L., Xiu, P., Chai, F., et al. (2013). Apparent enhancement of 234Th-based particle export associated with anticyclonic eddies. *Earth Planetary. Sci. Lett.* 381, 198–209. doi: 10.1016/j.epsl.2013.07.039

frontiers | Frontiers in Marine Science

TYPE Data Report
PUBLISHED 16 August 2022
DOI 10.3389/fmars.2022.990351

Check for updates

OPEN ACCESS

EDITED BY
Dilip Kumar Jha,
National Institute of Ocean Technology, India

REVIEWED BY
Jun Bo,
State Oceanic Administration, China
Josephine Anthony,
Meenakshi Academy of Higher Education and Research, India

*CORRESPONDENCE
S. Elumalai
anandal@gmail.com
H. Thilagam
thilagampachaiyappas@gmail.com

†These authors have contributed equally to this work

SPECIALTY SECTION
This article was submitted to Marine Pollution, a section of the journal Frontiers in Marine Science

RECEIVED 09 July 2022
ACCEPTED 25 July 2022
PUBLISHED 16 August 2022

CITATION
Pandi P, Madhuvandhi J, Priya KK, Thiagarajan R, Gopalakrishnan S, Elumalai S and Thilagam H (2022) Weathered polyethylene microplastics exposure leads to modulations in glutathione-S-transferase activity in fish.
Front. Mar. Sci. 9:990351.
doi: 10.3389/fmars.2022.990351

COPYRIGHT
© 2022 Pandi, Madhuvandhi, Priya, Thiagarajan, Gopalakrishnan, Elumalai and Thilagam. This is an open-access article distributed under the terms of the Creative Commons Attribution License (CC BY). The use, distribution or reproduction in other forums is permitted, provided the original author (s) and the copyright owner(s) are credited and that the original publication in this journal is cited, in accordance with accepted academic practice. No use, distribution or reproduction is permitted which does not comply with these terms.

Weathered polyethylene microplastics exposure leads to modulations in glutathione-S-transferase activity in fish

P. Pandi[1†], J. Madhuvandhi[1†], KK. Priya[1], R. Thiagarajan[2], S. Gopalakrishnan[1,3], S. Elumalai[4*] and H. Thilagam[1*]

[1]Postgraduate and Research Department of Zoology, Pachaiyappa's College for Men, Chennai, India, [2]Department of Zoology, Ramakrishna Mission Vivekananda College (Autonomous), Chennai, India, [3]eProov Assessment Solution Pvt., Limited, Chennai, India, [4]Department of Biotechnology, University of Madras, Chennai, India

KEYWORDS

Weathered microplastics, Fish, GST, gene expression, enzyme

Introduction

Rapid urban and industrial expansion in recent years has significantly impacted coastal ecosystems across the world, including estuaries and bays (Jha et al., 2015; Dheenan et al., 2016). Their watersheds' high human population density adds to the toxins in the environment. The influence of plastic on coastal ecosystems and the organism has been documented (Janardhanam et al., 2022). Plastic has become the most frequent component of marine pollution and it has been widely spread in the different trophic levels of our ecosystem. Anthropogenic activity generates the majority of the plastics that after aging, weathering, and breaking become the principal sources of microplastics (Cole et al., 2011). Microplastic is often characterized as fibre particles with a size < 5mm and are difficult to get eliminated by a presently practiced sewage treatment protocol because of their tiny size (Hamidian et al., 2021), allowing them to seep into inland rivers and ultimately into marine habitats (Wang et al., 2021). A lot of research on the presence of microplastic in the environment and their consequences on marine species, in terms of physical harm, behavioral changes, tissue lesions, oxidative stress, and gene damage, has been conducted in recent years (Huang et al., 2020; 2021).

Several studies have documented that aquatic ecosystems across the world have been polluted with microplastic (Klein et al., 2015; Zhu et al., 2018; Hariharan et al., 2021; Janardhanam et al., 2022). Microplastics persistent at the water surface for several years, where it is being consumed and accumulated by a variety of species, causing biomagnification in the food chain (Li et al., 2016; Jabeen et al., 2017; Jin et al., 2018; Li et al., 2019). Further, studies have also reported that microplastic in the coastal environment constitutes a significant danger to the food web (Wright et al., 2013, Avio et al., 2015) and in terms of their presence in biological systems. Studies have demonstrated that 9.2 to 92.3% of fish had one or more microplastic within them (Davison and Asch, 2011; Neves et al., 2015; Jabeen et al., 2017).

Microplastics have also been seen in significant quantities around industrial cities along the intertidal zone. In addition, the microplastic also contains a large number of environmental pollutants that adhere to the surface which leads to hazardous effects on organisms (Chen et al., 2017, Guilhermino et al., 2018, Oliveira et al., 2018). It has been well documented that fish that consume microplastic exhibit physical changes as well as decreased development rates, immune defence mechanisms, antioxidant enzyme production, and even reproduction (Sussarellu et al., 2016; Rodriguez-Seijo et al., 2017; Jin et al., 2018; Pannetier et al., 2020). However, the toxicological consequences of weathered polyethylene (wPE) microplastic on aquatic life are difficult to comprehend owing to their size, shape, and manufacturing ingredients (Hariharan et al., 2021).

The glutathione S-transferases (GSTs, EC 2.5.1.18) comprise a supergene family of phase II detoxification enzymes that shield cells against the toxicity of many environmental toxins by enhancing reduced glutathione's (GSH) nucleophilic assault (Hayes et al., 2005). GSTs have been used as indicators of exposure to environmental contaminants in the majority of aquatic research (Schlenk et al., 2008). Differences in GST activity and expression, whether inherent or induced, may influence aquatic organisms against deleterious effects caused by environmental toxicants since GSTs are crucial for the detoxification of contaminants (Coles and Ketterer, 1990).

To characterize microplastic toxicity and link it to the organismal level of response, the molecular interactions between the microplastic and the biological target must be determined. Hariharan et al. (2021) demonstrated that exposure to weathered polyethylene (wPE) microplastics alters the antioxidant content in the green mussels (*Perna viridis*). However, to the best of our knowledge, there are no reports on the effect of wPE microplastics on biotransformation enzymes, especially GST in fish. Hence, in this study, we have attempted to understand the effect of wPE microplastics on the liver and gut GST activity in zebrafish.

Methodology

Three-month-old zebrafish *Danio albolineatus*, (240 numbers) were obtained from Kolathur fish farm, Tamil Nadu, India. The mean weight and length of fish were ranged between 1.5 - 2.1 g and 3.5- 4.8 cm respectively. The fish were acclimatized to laboratory conditions at a temperature of 27°C ± 1°C, pH 7.2 ± 0.2, and dissolved oxygen content of 5.0 ppm for 7 days prior to the experiment in 100-L glass tanks containing water treated using sand filtration. Fish were kept in a natural daylight cycle and fed with commercial flakes at 1% of body weight daily during the acclimation period.

Preparation of wPE microplastics was done following the methodology of Hariharan et al. (2021). Briefly, fishing ropes that had weathered were gathered from beaches close to Chennai's shore. Sand and dust particles on the surface layers of the materials were removed by washing them with UV-treated distilled water. The characterization of the worn ropes was done using Fourier Transform Infrared Spectroscopy-FTIR (PerkinElmer Spectrum Version 10.5.4). Characterized wPE debris was frozen at -80°C in Falcon tubes and then manually pulverized into tiny grains using a ball mill-sediment grinder. The wPE microplastic for experiments was then prepared by sieving the fine grains progressively through 32 µm test sieves and such particles were used for the wPE microplastic exposure. The exposure concentrations used for the current study comprised of two different sizes of particles; 1) lesser than 32 µm and 2) between 32 – 34 µm at the relative proportions of 30% and 70%, respectively. With repeated measurement, the dissolved number of wPE particles and the size ratio of the particles to the corresponding concentration per microgram of microplastics were determined. In sterile tubes, the wPE microplastics were carefully mixed with 1 ml milli-Q water to verify the number of particles (free from contaminations). The tubes were stirred briskly to encourage uniform mixing of the particles in the water, and then they were immediately transferred to a Sedgewick-Rafter counting slide and enumerated under a microscope (a Weswox) for counting. To standardize the number of particles in the prepared concentration, the tube was checked for particles that had adhered to their surfaces.

Before microplastic exposure, fish were divided into a batch of 40 fish (20 males and 20 females) and were acclimated in 50 L glass tanks for 1 week. The study consisted of two groups: 1) control and 2) microplastic exposed. For each group three tanks were maintained. The present study used 1 µg L^{-1} of wPE containing 1204 ± 117 microplastic/m^3 and this concentration was used as the sublethal concentration (Hariharan et al., 2021). To prevent the stratification of microplastic particles at the bottom/surface of the experimental chamber, the glass tank was provided with gentle aeration. The exposure lasted for 60 days, and samples were taken every 20 days. Fish behavior was regularly observed, and dead fish, if any, were removed right away from the test chambers. Additionally, utilizing a multi-parameter water quality probe, the physicochemical parameters including water temperature, pH, and dissolved oxygen were recorded twice a day (Hydrolab Quanta Multi-Probe Meter).

At the end of each exposure period, about twelve fish (6 male and 6 female) from each tank were dissected to isolate the internal organs such as the gut and liver for biochemical and mRNA expression study. Three fish were pooled together to ensure the required amount of sample for both enzyme activity and gene expression. Totally 36 fish were used for each time point for the study. The dissected organs were frozen in liquid nitrogen and maintained at −80°C until further analyses. Gut and liver samples were homogenized in ice-cold buffer (0.1 M Tris-HCl, 0.1 mM-EDTA, 0.1% Triton X-100 (v/v), pH 7.8). The homogenates were centrifuged, and the supernatants were collected. The supernatants were used for enzyme and protein analysis. The quantity of protein

was measured by the Bradford (1976) method using bovine serum albumin as a standard. GST activity was determined using the 1-Chloro-2,4-dinitrobenzene (CDNB) substrate after conjugating the acceptor substrate with glutathione, as reported by Habig et al. (1974).

Following the manufacturer's instructions, total RNA was extracted from samples of gut and liver tissues of fish that had been homogenized in TRIzol reagent. A NanoDrop reader was used to evaluate the amount and quality of the RNA samples (NanoDrop Technologies, Synergy). RNA samples with an OD 260/280 nm value between 1.8 and 2.0 were used for the cDNA conversion. Reverse transcription was performed on total RNA (1 µg/µL) in accordance with the manufacturer's instructions using a high-capacity cDNA reverse transcription kit. Utilizing Light Cycler 480, SYBR Premix Ex Taq TM II, and gene-specific primer pairs, quantitative real-time PCR was carried out using generated cDNAs as templates (Roche). The samples underwent denaturation (10 min at 95°C), amplification (40 cycles for 15 s at 95°C and 1 min at 60°C), quantification using a melting curve program (60 - 99°C) with a temperature rate of 0.1°C/s, and routine monitoring of fluorescence). At 60°C, the predesigned primers for RT-PCR were annealed. Before the primary reaction, all chosen primers were evaluated for efficacy and appropriate concentration. Each PCR reaction was carried out in triplicate, the housekeeping gene beta-actin was employed, and the variations in the abundances of each target gene's transcripts were represented as their ratio to the expression of the reference gene of *Danio rerio* are given in the Supplementary Table S1. Based on the $2^{-\Delta\Delta CT}$ relative responsive methods as described by Livak and Schmittgen (2001) were used to examine the relative fold change in gene expression.

The statistical analysis was carried out using SPSS software (version 20). The data were subjected to normality and homogeneity before a one-way analysis of variance (ANOVA) to test differences between the groups and the exposure periods. Multiple comparison *post hoc* tests were used to determine the statistical difference between different exposure periods and the p-value of less than 0.05 was considered significant.

Results and discussion

The GST mRNA expression patterns in the gut and liver of zebrafish were evaluated using qPCR (Figures 1, 2). As shown in

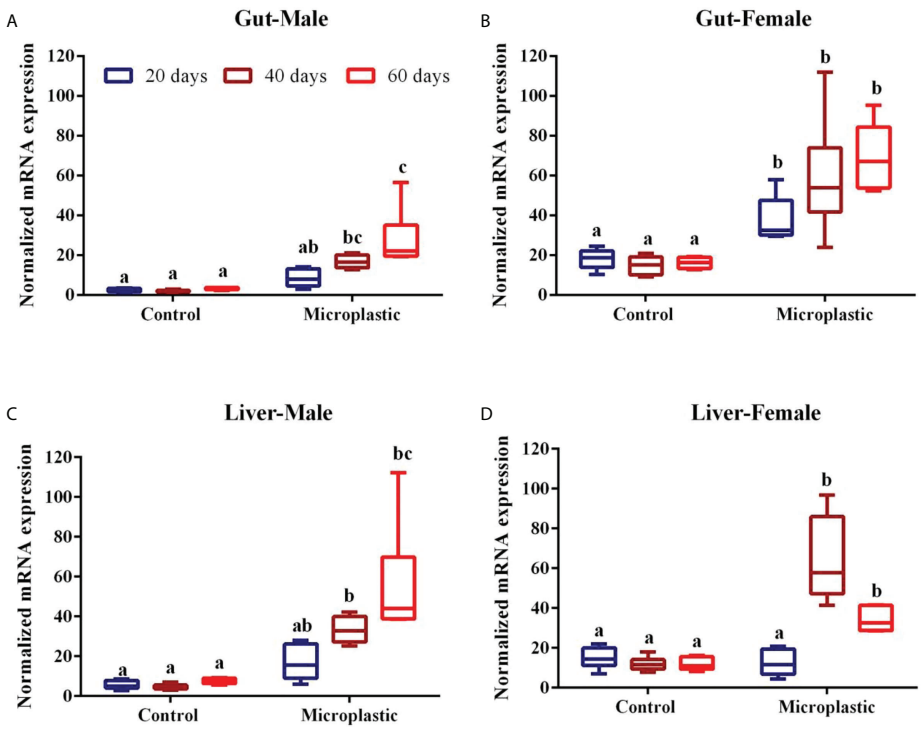


FIGURE 1
Showing the level of glutathione-S-transferase mRNA expression level in fish exposed to weathered polyethylene microplastics **(A)** Gut Male, **(B)** Gut Female, **(C)** Liver Male, **(D)** Liver Female. The line in each box represent median and whiskers represents the upper and lower 95% confidence intervals of the mean of six determinations using samples from different preparations. One-way analysis of variance (ANOVA) followed by Tukey's *post hoc* test was used. The significant ($P < 0.05$) differences between control and exposure groups were indicated by the alphabets; same alphabet shows no significant difference with respective control group. Different alphabet shows the significant difference with control respective group.

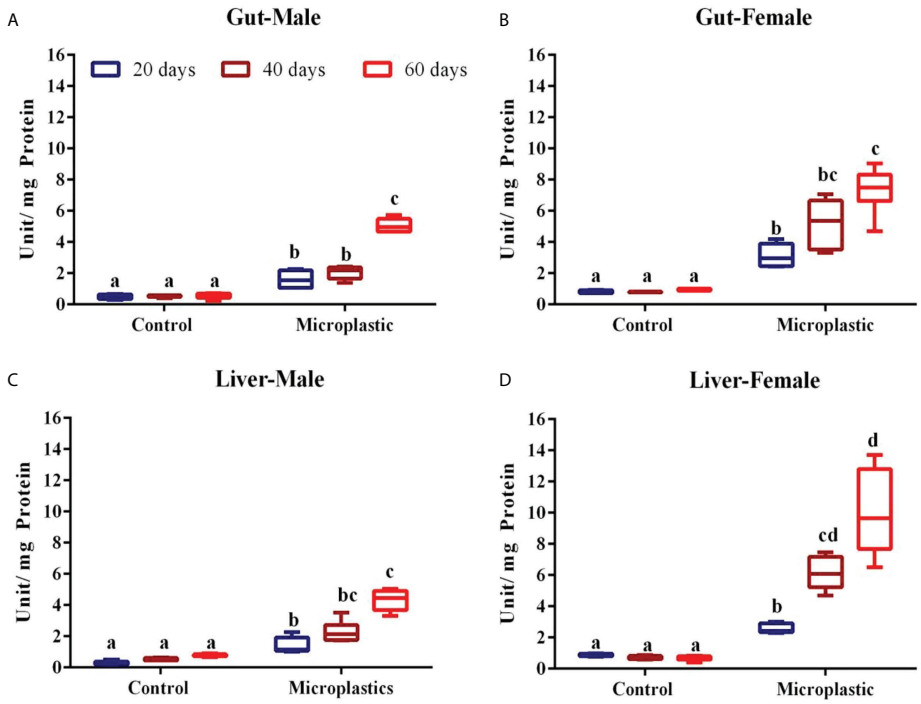


FIGURE 2
Showing the level of glutathione-S-transferase enzyme level in fish exposed to weathered polyethylene microplastics **(A)** Gut Male, **(B)** Gut Female, **(C)** Liver Male, **(D)** Liver Female. The line in each box represent median and whiskers represents the upper and lower 95% confidence intervals of the mean of six determinations using samples from different preparations. One-way analysis of variance (ANOVA) followed by Tukey's *post hoc* test was used. The significant ($P < 0.05$) differences between control and exposure groups were indicated by the alphabets; same alphabet shows no significant difference with respective control group. Different alphabet shows the significant difference with control respective group.

Figure 1(A), an upregulation of GST gene expression in the gut of zebrafish was observed at 40 and 60 d and it was induced up to 10-fold and 9-fold, respectively, in wPE microplastic exposed male zebrafish when compared with the respective control group. Fish exposed to wPE microplastic for 20 d showed an increase in GST gene expression but such an increase was not significantly different from the respective control group (Figure 1A). Similarly female fish exposed to wPE microplastic showed an upregulation of gene expression in the gut and such upregulation was up to 2-, 7- and 5-folds for 20, 40, and 60 d, respectively. All such inductions in GST in the female fishes were statistically significant ($p<0.05$) (Figure 1B).

Fish exposed to wPE microplastic showed upregulated GST gene expression in the liver of both male and female fish (Figures 1C, D). However female fishes showed the highest GST gene expression when compared to males with respective exposure periods. GST gene expression in male fish was induced by up to 4 and 10-folds after 40 and 60 d of wPE exposure, respectively (Figure 1C). Similarly, the female showed an upregulation of GST expression by up to 6 and 2-folds after 40 and 60 d of wPE exposure, respectively (Figure 1D). In both genders, after 20 days of exposure to wPE the liver GST gene expression was not statistically significant in the respective control group (Figure 1D).

The GST enzyme activity was considerably elevated in the gut and liver of fish exposed to wPE microplastic after respective exposure periods (Figures 2A–D). However, this induction level of the GST enzyme was observed as the exposure period of fish to wPE microplastic increased. The enzyme activity was higher in females exposed to wPE microplastics than in males. In both sexes, the liver has the highest GST activity of both the organs tested. In both male and female fish, the highest GST activity in both the organs was observed after 60 d exposure to wPE microplastics (Figures 2A–D).

Similar increases in GST enzyme activity due to wPE microplastic have been previously reported in mussels (Hariharan et al., 2021). Further Umamaheswari et al. (2021) reported that the microplastic exposure upregulated

the GST enzyme both at gene and protein levels in zebrafish. Fish living in increasingly polluted habitats exhibit a predisposition to adjust their GST activity due to the need for detoxification responses, which aids the fish in surviving in a highly contaminated environment (Chatterjee and Bhattacharya, 1984; Gopalakrishnan et al., 2011). The most crucial elements of the xenobiotic detoxification enzymes, GSTs are expressed in a variety of ways. Different basic structures, enzyme characteristics, and physiological roles may be found in members of the GST superfamily (Josephy, 2010). The distribution of each GST class in tissues may also differ and many studies have examined the pathogenic and physiological activities of GSTs as well as their tissue distribution (Ren et al., 2009; Kim et al., 2017). GSTs thus are crucial enzymes for phase II xenobiotic metabolism, and the stimulation of this enzyme would be a sign of host response to pollutants.

Although there was an increase in enzyme activity in the initial exposure period (after 20 d), the gene expression was not apparent. The induction of GST enzyme activity corresponds to GST gene expression at the latter stages of exposure to wPE microplastic. The significant increase in GST activity further supports the theory that this could be a response directly linked to microplastic exposure. Since it is well known that a higher GST activity can signal a greater capacity for detoxification (Bocedi et al., 2019) it can be inferred from our findings that the increased GST gene expression and activity could be part of antioxidant and biotransformation responses of the liver brought on by microplastics. As an antioxidant and second-phase detoxification enzyme, GST is crucial in the detoxification of a variety of electrophilic chemicals into hydrophilic molecules (Lushchak, 2012). Our findings demonstrated that exposure to wPE microplastics upregulated GST expression and activity levels in both the tissues of the fish and also in both genders. The current ecotoxicological risk assessment on zebra fish is a preliminary investigation that will be used to determine the initial health risks to MPs, which will then help to assess the health of the local aquatic organisms, which in turn will help in coastal conservation and fisheries management (Murugan et al., 2005; Kumar et al., 2009; Janardhanam et al., 2022) by developing a biochemical indicator tool for the coastal management.

Conclusion

The results of the current investigation demonstrated that zebrafish glutathione-S-transferase enzymes were modulated as a result of exposure to wPE microplastics. This study also found that exposure to wPE microplastic altered the levels of gene expression for the biotransformation enzymes, suggesting that these enzymes might serve as useful biochemical indicators for the assessment of microplastic exposure in coastal and marine ecosystems. More research is needed to understand the exact role and mechanism of action of GST enzymes in microplastic metabolism and animal survival in coastal environments.

Data availability statement

The original contributions presented in the study are included in the article/Supplementary Material. Further inquiries can be directed to the corresponding authors.

Ethics statement

Ethical review and approval was not required for the animal study because Commercially cultured and model fish.

Author contributions

PP, MJ, PK performed experiment and laboratory analysis. TH: conceptualization, experimental design, data validation. TR: manuscript corrections and critical suggestions. GKS: statistical analysis of data and manuscript correction. TH and ES: manuscript preparation, reviewing the manuscript and project administration. All authors contributed to the article and approved the submitted version.

Acknowledgments

The authors thank Head, Research department of Zoology and also the Principal Pachaiyappa's College for Men, Chennai-600 030 and Head Department of Biotechnology, University of Madras, Guindy Campus, Chennai-600 025 India. Staff from National Centre For Sustainable Coastal Management, Chennai-600 025 also acknowledged for the suggestions and help through the study.

Conflict of interest

Author GS was employed by eProov Assessment Solution Pvt., Limited.

The remaining authors declare that the research was conducted in the absence of any commercial or financial

relationships that could be construed as a potential conflict of interest.

Publisher's note

All claims expressed in this article are solely those of the authors and do not necessarily represent those of their affiliated organizations, or those of the publisher, the editors and the reviewers. Any product that may be evaluated in this article, or claim that may be made by its manufacturer, is not guaranteed or endorsed by the publisher.

Supplementary material

The Supplementary Material for this article can be found online at: https://www.frontiersin.org/articles/10.3389/fmars.2022.990351/full#supplementary-material.

References

Avio, CG, Gorbi, S, and Regoli, F. (2015). Experimental development of a new protocol for extraction and characterization of microplastics in fish tissues: First observations in commercial species from Adriatic Sea. *Mar. Environ. Res.* 111, 18–26. doi: 10.1016/j.marenvres.2015.06.014.

Bocedi, A., Noce, A., Marrone, G., Noce, G., Cattani, G., Gambardella, G., et al. (2019). Glutathione transferase P1-1 an enzyme useful in biomedicine and as biomarker in clinical practice and in environmental pollution. *Nutrients* 11 (8), 1741. doi: 10.3390/nu11081741

Bradford, M. M. (1976). A rapid and sensitive method for the quantification of microgram quantities of protein utilizing the principle of protein–dye binding. *Anal. Biochem.* 72, 248–254. doi: 10.1006/abio.1976.9999

Chatterjee, S., and Bhattacharya, S.. (1984). Detoxication of industrial pollutants by the glutathione glutathione-S-transferase system in the liver of Anabas testudineus (Bloch). *Toxicol. Lett.* 22 (2), 187–198. doi: 10.1016/0378-4274(84)90065-1

Chen, Q., Gundlach, M., Yang, S., Jiang, J., Velki, M., Yin, D., et al. (2017). Quantitative investigation of the mechanisms of microplastics and nanoplastics towardzebrafish larvae locomotor activity. *Sci. Total Environ.* 22 (2), 584–585, 1022-1032. doi: 10.1016/j.scitotenv.2017.01.156

Cole, M. P., Lindeque, P., Halsband, C., and Galloway, T. S. (2011). Microplastics as contaminants in the marine environment: A review. *Marine Pollution Bulletin* 62 (12), 2588–2597. doi: 10.1016/j.marpolbul.2011.09.025

Cole, M., Lindeque, P., Fileman, E., Halsband, C., Goodhead, R., Moger, J., et al. (2013). Microplastic ingestion by zooplankton, environmental science and technology *Environ. Sci. Technol.* 47, 12, 6646–6655. doi: 10.1021/es400663f

Coles, B., and Ketterer, B. (1990). The role of glutathione and glutathione transferases in chemical carcinogenesis. *Crit. Rev. Biochem. Mol. Biol.* 25 (1), 47–70. doi: 10.3109/10409239009090605

Davison, P., and Asch, R.. (2011). Plastic ingestion by mesopelagic fishes in the North Pacific Subtropical Gyre. *Mar. Ecol. Prog. Ser* 432, 173–180. doi: 10.3354/meps09142

Dheenan, P. S., Jha, D. K., Das, A. K., Vinithkumar, N. V., Prashanthi Devi, M., and Kirubagaran, R. (2016). Geographic information systems and multivariate analysis to evaluate fecal bacterial pollution in coastal waters of Andaman, India. *Environ. pollut.* 214, 45–53. doi: 10.1016/j.envpol.2016.03.065

Guilhermino, L, Vieira, LR, Ribeiro, D, Tavares, AS, Cardoso, V, Alves, A, et al. (2018). Uptake and effects of the antimicrobial florfenicol, microplastics and their mixtureson freshwater exotic invasive bivalve Corbicula fluminea, *Sci. Total Environ.* 622-623, 1131–1142. doi: 10.1016/j.scitotenv.2017.12.020

Gopalakrishnan, S., Nai, Z., Thilagam, H., Bei, C., Ding, J., Wang, X. H., et al. (2011). Biochemical responses and DNA damage in red sea bream from coastal fujian province, China. *Ecotoxicol. Environ. Saf.* 74 (6), 1526–1535. doi: 10.1016/j.ecoenv.2011.05.007

Habig, W. H., Pabst, M. J., and Jakoby, W. B. (1974). Glutathione s-transferases: the first enzymatic step in mercapturic acid formation. *J. Biol. Chem.* 249, 7130–7139.

Hamidian, A. H., Jafari, O. E., Feizi, F., Wu, C., Zhang, Y., and Yang, M. Y. (2021). A review on the characteristics of microplastics in wastewater treatment plants: A source for toxic chemicals. *J. Cleaner. Production.* 295, 126480. doi: 10.1016/j.jclepro.2021.126480

Hariharan, G., Purvaja, R., Anandavelu, I., Robin, R. S., and Ramesh, R. (2021). Accumulation and ecotoxicological risk of weathered polyethylene (wPE) microplastics on green mussel (Perna viridis). *Ecotoxicol. Environ. Saf.* 208, 111765. doi: 10.1016/j.ecoenv.2020.111765

Hayes, J. D., Flanagan, J. U., and Jowsey, I. R. (2005). Glutathione transferases. *Annu. Rev. Pharmacol. Toxicol.* 45:1, 51–88. doi: 10.1146 /annurev.pharmtox.45.120403.095857

Huang, W., Song, B., Liang, J., Niu, Q., Zeng, G., Shen, M., et al. (2021). Microplastics and associated contaminants in the aquatic environment: A review on their ecotoxicological effects, trophic transfer, and potential impacts to human health. *J. Hazard. Mater.* 405, 124187. doi: 10.1016/j.jhazmat.2020.124187

Huang, J. N., Wen, B., Meng, L. J., Li, X. X., Wang, M. H., Gao, J. Z., et al. (2020). Integrated response of growth, antioxidant defense and isotopic composition to microplastics in juvenile guppy (*Poecilia reticulata*). *J. Hazard. Mater.* 399, 123044. doi: 10.1016/j.jhazmat.2020.123044

Jabeen, K., Su, L., Li, J., Yang, D., Tong, C., Mu, J., et al. (2017). Microplastics and mesoplastics in fish from coastal and fresh waters of China. *Environ. pollut.* 221, 141–149. doi: 10.1016/j.envpol.2016.11.055

Janardhanam, M., Sivakumar, P., Srinivasan, G., Sivakumar, R., Marcus, P. N., Balasubramaniam, S., et al. (2022). Microplastics in demersal sharks from the southeast Indian coastal region. *Front. Mar. Sci.* 9. doi: 10.3389/fmars.2022.914391

Jha, D. K., Vinithkumar, N. V., Sahu, B. K., Dheenan, P. S., Das, A. K., Begum, M., et al. (2015). Multivariate and geo-spatial approach for seawater quality of chidiyatappu bay, south Andaman islands, India. *Mar. pollut. Bull.* 96(1–2), 463–470. doi: 10.1016/j.marpolbul.2015.05.004

Jin, Y., Xia, J., Pan, Z., Yang, J., Wang, W., and Fu, Z. (2018). Polystyrene microplastics induce *Microbiota dysbiosis* and inflammation in the gut of adult zebrafish. *Environ. pollut.* 235, 322–329. doi: 10.1016/j.envpol.2017.12.088

Josephy, P. D. (2010). Genetic variations in human glutathione transferase enzymes: significance for pharmacology and toxicology. *Hum. Genomics Proteomics* 2010, 876940. doi: 10.4061/2010/876940

Kim, Y., Cha, S. J., Choi, H. J., and Kim, K. (2017). Omega class glutathione s-transferase: Antioxidant enzyme in pathogenesis of neurodegenerative diseases. *Oxid. Med. Cell Longev.* 2017, 5049532. doi: 10.1155/2017/5049532

Klein, S., Worch, E., and Knepper, T. P. (2015). Occurrence and spatial distribution of microplastics in river shore sediments of the Rhine-main area in Germany. *Environ. Sci. Technol.* 49, 6070–6076. doi: 10.1021/acs.est.5b00492

Kumar, T. S., Vijayakumaran, M., Murugan, T. S., Jha, D. K., Sreeraj, G., and Muthukumar, S. (2009). Captive breeding and larval development of the scyllarine lobster petrarctusrugosus. *New Z. J. Mar. Freshw. Res.* 43:1, 101–112. doi: 10.1080/00288330909509985

Li, Y., Li, M., Li, Z., Yang, L., and Liu, X. (2019). Effects of particle size and solution chemistry on triclosan sorption on polystyrene microplastic. *Chemosphere* 231, 308–314. doi: 10.1016/j.chemosphere.2019.05.116

Li, J., Qu, X., Su, L., Zhang, W., Yang, D., Kolandhasamy, P., et al. (2016). Microplastics in mussels along the coastal waters of China. *Environ. pollut.* 214, 177–184. doi: 10.1016/j.envpol.2016.04.012

Livak, K. J., and Schittgen, T. D. (2001). Analysis of relative gene expression data using real-time quantitative PCR and the 2(-Delta Delta C(T)) Method. *Method. Methods (San Diego, Calif.)*, 25(4)402–408 doi: 10.1006/meth.2001.1262

Lushchak, V. I. (2012). Glutathione homeostasis and functions: potential targets for medical interventions. *J. Amino Acids* 2012, 736837. doi: 10.1155/2012/736837

Murugan, T. S., Remany, M. C., Mary Leema, T., Jha, D. K., Santhanakumar, J., Vijayakumaran, M., et al. (2005). Growth, repetitive breeding, and aquaculture

potential of the spiny lobster, panulirus ornatus. *New Z. J. Mar. Freshw.* 39:2, 311–315. doi: 10.1080/00288330.2005.9517311

Neves, D., Sobral, P., Ferreira, J. L., and Pereira, T.. (2015). Ingestion of microplastics by commercial fish off the Portuguese coast. *Mar. Pollut. Bull.* 101 (1), 191–126. doi: 10.1016/j.marpolbul.2015.11.008

Oliveira, P., Barboza, L. G. A., Branco, V., Figueiredo, N., Carvalho, C., and Guilhermino, L. (2018). Effects of microplastics and mercury in the freshwater bivalve *Corbicula fluminea* (Mülle): Filtration rate, biochemical biomarkers and mercury bioconcentration ecotoxicol. *Environ. Saf.* 164, 155–163. doi: 10.1016/j.ecoenv.2018.07.062

Pannetier, P., Morin, B., Le Bihanic, F. L., Dubreil, L., Clérandeau, C., Chouvellon, F., et al. (2020). Environmental samples of microplastics induce significant toxic effects in fish larvae. *Environ. Int.* 134, 105047. doi: 10.1016/j.envint.2019.105047

Ren, H. L., Xu, D. D., Gopalakrishnan, S., Qiao, K., Huang, W. B., and Wang, K. J. (2009). Gene cloning of a sigma class glutathione s-transferase from abalone (*Haliotis diversicolor*) and expression analysis upon bacterial challenge. *Dev. Comp. Immunol.* 33 (9), 980–990. doi: 10.1016/j.dci.2009.04.003

Schlenk, D., Celander, M., Gallagher, E., George, S., James, M., Kullman, S., et al. (2008). "Biotransformation in fishes," in *The toxicology of fishes*, vol. pp . Eds. R. T. Di Giulio and D. E. Hinton (New York: CRC press), 153–234.

Sussarellu, R., Suquet, M., Thomas, Y., Lambert, C., Fabioux, C., Pernet, M. E., et al. (2016). Oyster reproduction is affected by exposure to polystyrene microplastics. *Proceedings of the National Academy of Sciences of the UnitedStates of America* 113 (9), 2430–2435. doi: 10.1073/pnas.1519019113

Umamaheswari, S., Priyadarshinee, S., Bhattacharjee, M., Kadirvelu, K., and Ramesh, M. (2021). Exposure to polystyrene microplastics induced gene modulated biological responses in zebra fish (*Danio rerio*). *Chemosphere* 281, 128592. doi: 10.1016/j.chemosphere

Rodriguez-Seijo, A., Lourenço, J., Rocha-Santos, T., da Costa, J., Duarte, A. C., Vala, H., et al. (2017). Histopathological and molecular effects of microplastics in Eisenia andrei Bouché. *Environ. Pollut.* (Barking, Essex : 1987), 220 (Pt A), 495–503. doi: 10.1016/j.envpol.2016.09.092

Wang, Q., Zhu, X., Hou, C., Wu, Y., Teng, J., Zhang, C., et al. (2021). Microplastic uptake in commercial fishes from the bohai Sea, China. *Chemosphere* 263, 127962. doi: 10.1016/j.chemosphere.2020.127962

Wright, S. L., Thompson, R. C., and Galloway, T. S. (2013). The physical impacts of microplastics on marine organisms: A review. *Environ. pollut.* 178, 483–492. doi: 10.1016/j.envpol.2013.02.031

Zhu, L., Bai, H., Chen, B., Sun, X., Qu, K., and Xia, B. (2018). Microplastic pollution in north yellow Sea, China: Observations on occurrence, distribution and identification. *Sci. Total. Environ.* 636, 20–29. doi: 10.1016/j.scitotenv.2018.04.182

frontiers | Frontiers in Marine Science

TYPE Original Research
PUBLISHED 23 August 2022
DOI 10.3389/fmars.2022.977120

Check for updates

OPEN ACCESS

EDITED BY
Meilin Wu,
South China Sea Institute of Oceanology, Chinese Academy of Sciences, China

REVIEWED BY
Guo Wei,
East China University of Technology, China
Peixue Song,
Zaozhuang University, China
Zuobing Liang,
Sun Yat-sen University, China

*CORRESPONDENCE
Qingmei Zhu
zhuqingmei1987@163.com

SPECIALTY SECTION
This article was submitted to Marine Pollution, a section of the journal Frontiers in Marine Science

RECEIVED 24 June 2022
ACCEPTED 04 August 2022
PUBLISHED 23 August 2022

CITATION
Zhou X, Li Z, Chen C, Luo H, Zhu Q, Zeng Z and Lao Q (2022) The removal of atmospheric aerosols in a heavy industrial coastal city in China with frequent rainfall.
Front. Mar. Sci. 9:977120.
doi: 10.3389/fmars.2022.977120

COPYRIGHT
© 2022 Zhou, Li, Chen, Luo, Zhu, Zeng and Lao. This is an open-access article distributed under the terms of the Creative Commons Attribution License (CC BY). The use, distribution or reproduction in other forums is permitted, provided the original author (s) and the copyright owner(s) are credited and that the original publication in this journal is cited, in accordance with accepted academic practice. No use, distribution or reproduction is permitted which does not comply with these terms.

The removal of atmospheric aerosols in a heavy industrial coastal city in China with frequent rainfall

Xin Zhou[1,2], Zhiyang Li[3], Chunqing Chen[1,2], Huijie Luo[1,2], Qingmei Zhu[1,2,4]*, Zhen Zeng[1,2] and Qibin Lao[1,2]

[1]College of Ocean and Meteorology, Guangdong Ocean University, Zhanjiang, China, [2]Laboratory for Coastal Ocean Variation and Disaster Prediction, Guangdong Ocean University, Zhanjiang, China, [3]Guangdong AIB Polytechnic College, Guangzhou, China, [4]Key Laboratory of Climate, Resources and Environment in Continental Shelf Sea and Deep Sea of Department of Education of Guangdong Province, Guangdong Ocean University, Zhanjiang, China

Rapid urbanization and heavy industrialization generally result in serious aerosol pollution. Contrary to this conventional wisdom, Zhanjiang, one industrial city in the southernmost point of the Chinese mainland, is not accompanied by aerosol pollution and its air quality index always ranks high compared to other cities in China. To investigate this contradiction, 72-hour total suspended particles (TSPs) and water-soluble inorganic ions (WSIIs; including Mg^{2+}, Ca^{2+}, K^{+}, Na^{+}, NH_4^{+}, Cl^{-}, NO_3^{-}, and SO_4^{2-}) were collected in Zhanjiang, China, from November 2018 to November 2019. The relative humidity (RH) was higher than 80% throughout the whole year in Zhanjiang. However, the TSPs and WSIIs were not correlated with RH, indicating that RH can increase the particle size, but this had a minor impact on the dry deposition rate. The larger particles induced by RH were easily captured by wet precipitation, leading to a seasonal pattern with higher TSP and WSII mass concentrations during the dry and cool season and lower values during the hot and rainy season. This seasonal pattern and high aerosol acidity indicate that TSPs, WSIIs, and acidic gaseous precursors from the local sources were preferentially scavenged by the abundant rainfall and high precipitation frequency. Principal component analysis (PCA) results suggest that relatively clean marine emissions and secondary aerosols were the most important sources of TSPs and WSIIs. Our results indicate that the inconsistency between the heavy industrial activities and excellent air quality in Zhanjiang may be related to the high precipitation frequency (63%) and the marine dilution effect (27%).

KEYWORDS

aerosol, air quality improvement, water-soluble inorganic ions, precipitation, sources, Zhanjiang City

Introduction

One consequence of the rapid urbanization and industrialization in developing countries is the increase in the total suspended particles (TSPs) in the atmosphere, i.e., air quality deterioration (Seinfeld, 2004; Huang et al., 2014). TSPs have long been regarded as a global air pollution concern due to their significant impacts on climate change, atmospheric chemistry, air quality, acidification, and human health (Fuzzi et al., 2015; Xiao et al., 2017). The TSPs (also called atmospheric aerosols) are primarily composed of various chemical species and water-soluble inorganic ions (WSIIs) (Ali-Mohamed, 1991). Therefore, observations of WSIIs may provide valuable information for controlling aerosol pollution.

Secondary inorganic aerosols, such as SO_4^{2-} and NO_3^- particles, are important contributors to the WSIIs in the TSPs (Guo et al., 2014). The SO_4^{2-} and NO_3^- particles in the atmosphere are mainly generated from oxidation of their representative gaseous precursors (SO_2 and NOx) emitted from ambient fossil fuel combustion (Shon et al., 2012; Xu L. L. et al., 2017; Liu et al., 2019). These ions and gaseous precursors are largely linked to aerosol pollution and acidification (Cao et al., 2013; Weber et al., 2016; Liu et al., 2019; Tian et al., 2021). Previous studies have reported significant increases in the aerosol mass, which pose a potential threat to human health due to high fossil fuel combustion (Zhang et al., 2011). Additionally, Xiao and Liu (2004) found that air quality deterioration in Guiyang was caused by industrial activities, and some industries should be relocated to mitigate local haze pollution.

Zhanjiang city (20.00–21.58°N, 109.52–110.92°E), the site of our study, is located in Guangdong Province, southern China, and is a tropical coastal city close to the South China Sea (SCS,< 30 km). During the past decades, a variety of industries (especially heavy industries, i.e., petrochemical factory as well as iron and steel plant) have moved to and sprung up in Zhanjiang. Nowadays, Zhanjiang is a famous manufacturing and heavy industry base. According to the Guangdong Statistical Yearbook, the total output value of heavy industries above designated size in Zhanjiang accounts for ~50% of Zhanjiang's gross regional domestic product. Additionally, the Basf Zhanjiang Integrated Base, the Lianjiang Nuclear Power Plant, and the Jingxin Zhanjiang Donghai Thermal Power Plant are under construction. Marine pollution caused by the industrialization and urbanization *via* terrestrial input in this region has been recently reported (Sun et al., 2018; Peng et al., 2020; Li J. C. et al., 2020). However, the influence of industrialization and urbanization on ambient air quality in Zhanjiang are not reported and still needs to be clarified, as TSPs and WSIIs in the atmosphere can be captured by rainfall and then enter into the marine systems. This may pose a potential risk to marine systems, for example, eutrophication (Cui et al., 2020; Wang J. J. et al., 2020).

Although the sources and impact factors of the WSIIs in the TSPs have been studied extensively in order to lessen aerosol pollution (Xiao and Liu, 2004; Kundu et al., 2010; Zhang et al., 2011; Xiao et al., 2017; Wang Q. Q. et al., 2020), limited research has been conducted on the impact of precipitation on WSIIs, which is considered to be an important process for removing TSPs and soluble gases in the ambient atmosphere (Hou et al., 2018). Thus, we hypothesize that the shorter aerosol lifetime and shortage of gaseous precursors in the atmosphere caused by precipitation may contribute to reducing aerosol pollution, especially in tropical regions with frequent precipitation and plentiful rainfall.

To investigate this contradiction and to verify this speculation, we monitored the TSPs in the atmosphere for one year and analyzed the WSIIs in the TSPs in the tropical city of Zhanjiang, China. The objectives of this study are as follows: (1) to determine the TSP and WSII concentrations and seasonal variations; (2) to verify the aerosol removal effect of precipitation; and (3) to use principal component analysis (PCA) to identify the possible sources of the WSIIs.

Methods and materials

Sampling site and sample collection

Zhanjiang in the southernmost point of the Chinese mainland (Figure 1) has a typical tropical monsoon climate, with a cool dry season from October to March (dry season) and a hot wet season from April to September (rainy season; Chen et al., 2019). The average annual temperature and rainfall in the city is 23°C and 1689 mm, respectively (Chen et al., 2019). The sampling campaign was conducted from 1 November 2018 to 1 November 2019 at 1.5 m above the roof of a building in Guangdong Ocean University in rural Zhanjiang City (21.15°N, 110.30°E). The TSPs in the atmosphere were collected on a 450°C pre-baked quartz fiber filter (Type MK360, 203 x 254 mm, Munktell Filter, Sweden) using a high-volume air sampler (1.37 ± 0.25 m^3/min; KB-1000-180815, Xiamen, China), and the cumulative sampling time for each aerosol sample was about 72 hours. After sampling, the filter was stored at -20°C to prevent volatilization. A total of 116 aerosol samples were collected in this study.

pH measurements and analysis of the major WSIIs in the TSPs

The pH values of the samples were measured using a desktop pH meter (Orion STAR A211, Thermo Fisher Scientific, USA) immediately after obtaining the extracted aqueous solution. The remaining aqueous extracts were stored at -20°C until the water-soluble inorganic ions were analyzed.

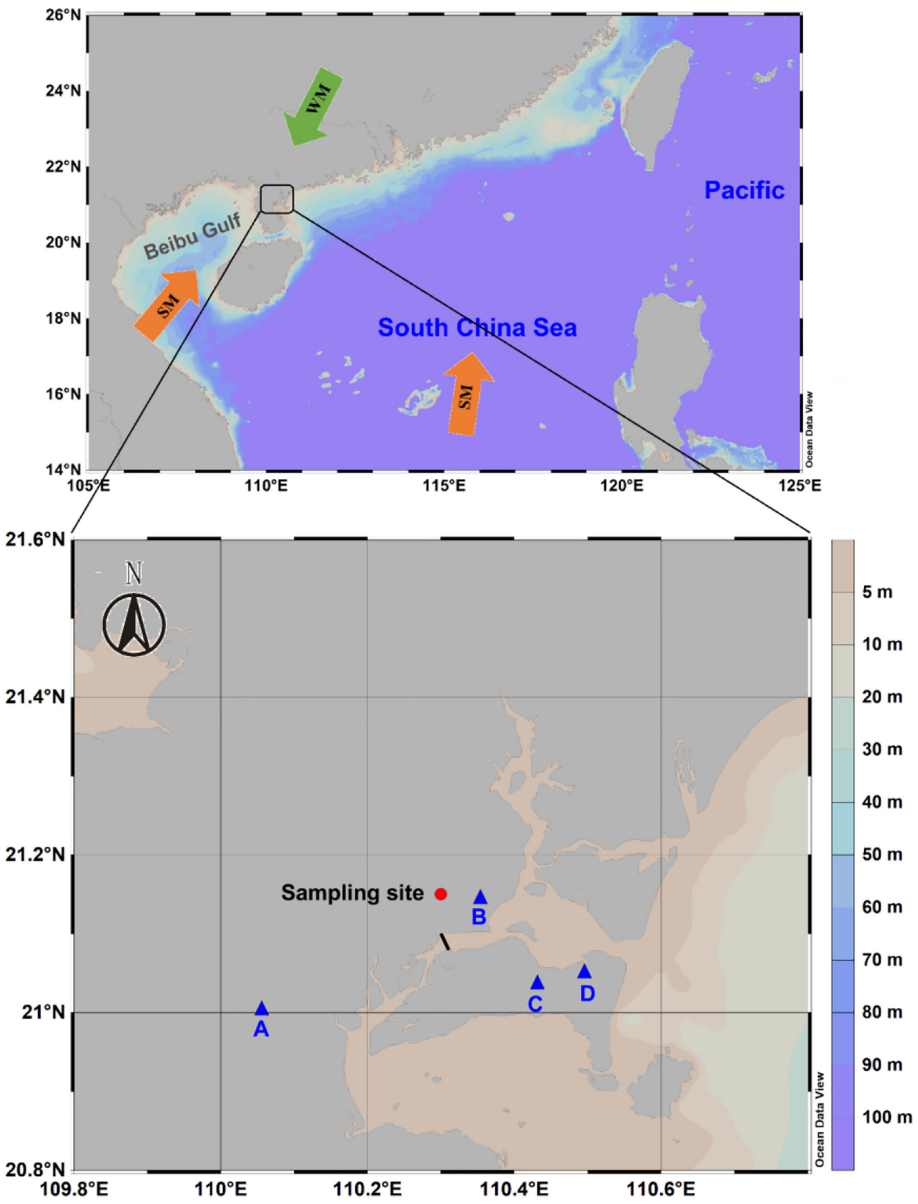


FIGURE 1
The sampling location of Zhanjiang (red dot). WM, winter monsoon; SM, summer monsoon. The blue triangles are the location of heavy industry. A, B, C, and D denote Chenming Paper Mill, Sinopec Zhanjiang Dongxing Petrochemcial Factory, Zhongke (Guangdong) Refinery & Petrochemical Factory, and Baosteel Zhanjiang Iron & Steel Plant, respectively.

Five cations (Mg^{2+}, Ca^{2+}, K^+, Na^+, and NH_4^+) and three anions (Cl^-, NO_3^-, and SO_4^{2-}) in the aqueous extracts of the aerosol samples were analyzed in this study. NH_4^+ and NO_3^- were determined using standard colorimetric methods (Grasshoff et al., 1999), and their detection limits were< 0.1 mg/L. The other ions were analyzed using ion chromatography (Dionex Aquion, Thermo Fisher Scientific), and their uncertainties were< 5%.

Meteorological data

Daily meteorological parameters, i.e., air temperature (°C), wind speed (km/h), and relative humidity (RH, %), were obtained from the local weather station (< 15 km southwest of the sampling site) during the sampling period. The precipitation was documented after each rainfall event. Detailed information on the rainfall sampling protocols can be found in our previously published papers (Chen

et al., 2019; Chen et al., 2020). The daily air pollutants, such as SO_2, NO_2, $PM_{2.5}$, and PM_{10}, presented during the sampling period in Zhanjiang were downloaded from https://www.zq12369.com/. A 72-hour average of the data described above (except for precipitation) was calculated and is presented in Figure 4.

Results

As shown in Figure 2, the mass concentration of the TSPs in the atmosphere ranged from 18.1 to 133.6 μg/m^3, with an average and standard deviation of 56.5 ± 24.3 μg/m^3. The average value of the TSPs falls within the recommended range of the international guidelines (150 to 230 μg/m^3). There were significantly seasonal variations in the mass concentrations of the TSPs (Figure 2 and Table 1). The mass concentration of the TSPs in the dry season (with an average value of 68.5 ± 23.0 μg/m^3; Table 1) were significantly higher than those in the rainy season (with an average value of 44.8 ± 19.2 μg/m^3; Table 1; ANOVA, $p< 0.01$).

The contents of the WSIIs in the TSPs increased in the order of $Mg^{2+} < Ca^{2+} < K^+ < Na^+ < NH_4^+ < Cl^- < NO_3^- < SO_4^{2-}$. SO_4^{2-} was the most abundant anion in the TSPs, followed by NO_3^- and Cl^-, which accounted for 56.2%, 27.2%, and 16.6%, respectively, of the total anions. The predominant cations were Na^+, NH_4^+, and K^+, accounting for 28.8%, 26.8%, and 20.4%, respectively, of the total cations. Similar seasonal variation pattern could be observed in the WSIIs. Significantly higher Mg^{2+}, Ca^{2+}, NH_4^+, NO_3^-, and SO_4^{2-} values occurred in the dry season, whereas lower values were observed in the rainy season (Figure 2D; Table 1; ANOVA, $p< 0.01$ for these ions). The mass concentrations of K^+ were stable throughout the sampling campaign (Figure 2B and Table 1; ANOVA, $p > 0.05$).

Discussion

Influences of meteorological factors

The average mass concentration of the TSPs in the rainy season (with an average value of 44.8 ± 19.2 μg/m^3) was 34.6% lower than that in the dry season (with an average of 44.8 ± 23.0 μg/m^3) (ANOVA, $p< 0.01$). The backward air mass trajectories during the same sampling periods in our published study (Luo et al., 2022)

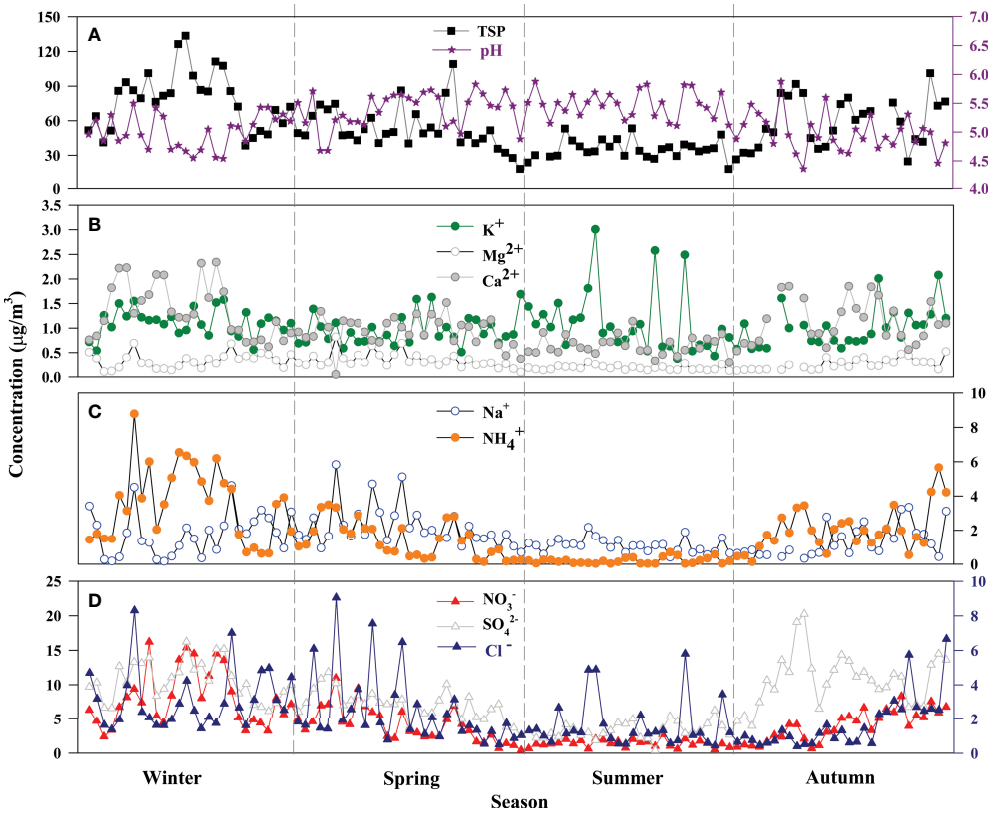


FIGURE 2
Seasonal variations in the pH, and mass concentrations of TSPs and WSIIs (i.e., K^+, Mg^{2+}, Ca^{2+}, Na^+, NH_4^+, NO_3^-, SO_4^{2-} and Cl^-) in the atmospheric aerosols in Zhanjiang.

TABLE 1 Seasonal variations in the WSIIs in the atmospheric aerosols in Zhanjiang.

	Rainy season	Dry season
n	58	58
Rainfall (mm)	1236.5	326.4
TSPs (μg/m^3)	44.8 ± 19.2	68.5 ± 23.0
Na^+ (μg/m^3)	1.3 ± 0.8	1.9 ± 1.2
NH_4^+ ($\mu g/m^3$)	0.7 ± 0.9	2.9 ± 1.8
K^+ (μg/m^3)	1.0 ± 0.5	1.1 ± 0.3
Mg^{2+} (μg/m^3)	0.2 ± 0.1	0.3 ± 0.1
Ca^{2+} (μg/m^3)	0.8 ± 0.4	1.2 ± 0.5
Cl^- (μg/m^3)	1.5 ± 1.3	2.9 ± 1.9
SO_4^{2-} ($\mu g/m^3$)	5.6 ± 3.7	10.3 ± 2.6
NO_3^- ($\mu g/m^3$)	2.0 ± 1.4	6.7 ± 3.5

showed that the air masses during the dry season could bring land-based aerosol to the Zhanjiang and the air parcels during the rainy season were mainly originated from the South China Sea. This suggested that the seasonal variation of TSPs concentrations in Zhanjiang were related to the air masses transition. However, it is hypothesized that this influence might be minor than local influences as discussed in the following sections. In addition, during the rainy season, the TSPs concentrations in the present study were lower than the value in the South China Sea (remote area, 60.4 ± 27.0 μg/m^3; Xiao et al., 2017), Guangzhou (urban area, 62.1 μg/m^3; Tan et al., 2009), and Guiyang (polluted area, 85.4 ± 29.1 μg/m^3; Li Q. et al., 2020). During the dry season, the TSPs concentrations in the present study were significantly lower than the concentration observed in the South China Sea (remote area, 114.7 ± 82.1 μg/m^3; Xiao et al., 2017), Shanghai (urban area, 94.64 μg/m^3; Gao et al., 2011), Xi'an (urban area, 130 μg/m^3; Gao et al., 2011), and Guiyang (polluted area, 140.2 ± 46.2 μg/m^3; Li Q. et al., 2020), and were similar to Guangzhou (urban area, 66.7 μg/m^3; Tan et al., 2009). These results implied that the seasonal variation of TSPs concentrations were greatly influenced by local conditions, for example, meteorological conditions (i.e., precipitation, temperature, wind speed, and RH) and local emissions (Gao et al., 2011; Meng et al., 2016; Xiao et al., 2017). Recent studies also found that local emission and meteorological factor have an important impact on air pollution (Wang et al., 2021; Zhou et al., 2022).

The meteorological conditions can affect chemical conversion and the deposition of TSPs (Meng et al., 2016) and thus affecting the mass fraction of WSIIs in TSPs. During the sampling periods, the mass fraction of WSIIs accounted for 35.7% of TSPs, displaying a higher fraction in the dry season (with an average value of 41.4%) and lower fraction in the rainy season (with an average value of 30.0%). This suggested that the seasonal variation of WSIIs was related to TSPs concentrations. The mass fraction of WSIIs in TSPs in the present study was higher than the value in the South China Sea (24.8%; Xiao et al., 2017), and were comparable to the value in urban Guangzhou (35%; Tao et al., 2017) and in suburban Zhuhai (34%; Tao et al., 2017). The significantly positive relationships between WSIIs and TSPs ($p< 0.01$ for NH_4^+, Ca^{2+}, Cl^-, NO_3^-, and SO_4^{2-}; $p< 0.05$ for Mg^{2+}; $p > 0.01$ for K^+ and Na^+; Table 2) also supported the concept that WSIIs were important constituents of TSPs. Therefore, WSIIs might play a significant role in TSPs in the present study.

During the sampling periods, the WSIIs concentrations were also higher during the dry season and were lower during the rainy season, with an average reduction rate of 42.3% (Table 1). This result is consistent with the seasonal pattern in Guiyang, that is, decreases in the TSPs (decrease of 18%) and WSIIs concentrations during the rainy season (Xiao and Liu, 2004). However, in contrast to the findings for Guiyang, the percentages of SO_4^{2-}, Cl^-, NO_3^-, and NH_{4^+} in the total WSIIs were lower in the rainy season than those in the dry season, indicating that in the particles, these ions tend to be coarser, so they have a shorter residence time than the finer components. Thus, they were readily captured by precipitation and were preferentially scavenged below the clouds (Xiao and Liu, 2004). Notably, in the precipitation characteristics shown in Figure 3, the precipitation frequency (precipitation frequency was calculated from the fraction of rain events in each month during sampling periods; rainfall > 0.5 mm/day as the criterion; Hou et al., 2018; data sourced from https://en.tutiempo.net/world.html) and the amount of rainfall were significantly higher in the rainy season (especially in summer) and lower in the dry season, which further suggests a removal process driven by frequent and large amounts of precipitation (Hou et al., 2018).

Temperature, wind speed, and RH also have impacts on the seasonal variations in the TSPs and WSIIs in atmospheric aerosols (Xiao and Liu, 2004; Xiao et al., 2017). In this study, the TSPs and WSIIs were strongly negatively correlated with the air temperature ($p< 0.01$ for TSPs, NH_4^+, Mg^{2+}, Ca^{2+}, Cl^-, NO_3^-, and SO_4^{2-}; $p > 0.05$ for K^+ and Na^+; Table 2), suggesting that the hot and rainy season helps reduce the amount of these particles in the atmosphere, leading to a decrease in the TSPs and WSIIs concentrations (Figure 2 and Table 1). Only the mass concentration of Ca^{2+} in the TSPs was affected by wind speed (Table 2), and the resultant positive correlation (Table 2, $p< 0.05$) suggests that strong winds can bring dust containing Ca^{2+}.

The high RH throughout the year (>80%) in Zhanjiang (Figure 4C) suggested that the particles in the atmospheric aerosols were wet and easily interacted with each other (Xiao and Liu, 2004), leading to an increase in particle size and the dry deposition rate (Tang et al., 2006). If the dry deposition rate increased during the sampling periods, a systematic decrease in the TSPs and WSIIs with increasing RH should be observed, and good correlations should be found among them. By contrast, the TSPs and WSIIs (with the exception of Na^+) were not correlated with RH in Zhanjiang (Table 2), indicating that the increase in particle size caused by the RH had little impact on the dry deposition rate.

TABLE 2 Correlation coefficients between pH, the WSIIs in the atmospheric aerosols, and the meteorological parameters in Zhanjiang.

	TSPs	Na^+	NH_4^+	K^+	Mg^{2+}	Ca^{2+}	Cl^-	NO_3^-	SO_4^{2-}	pH	WS	RH	T
TSPs	1	0.183	0.850**	0.120	0.330*	0.703**	0.293**	0.819**	0.799**	-0.512**	0.101	-0.006	-0.532**
Na^+		1	0.152	0.039	0.948**	-0.216*	0.813**	0.358**	0.136	0.163	0.048	0.212*	-0.146
NH_4^+			1	0.135	0.294**	0.576**	0.335**	0.849**	0.798**	-0.608**	0.083	-0.034	-0.589**
K^+				1	0.069	0.094	0.339**	0.102	0.002	0.004	0.000	-0.058	-0.061
Mg^{2+}					1	-0.029	0.807**	0.473**	0.292**	0.045	0.102	0.175	-0.292**
Ca^{2+}						1	-0.086	0.657**	0.478**	-0.418**	0.234*	-0.164	-0.535**
Cl^-							1	0.426**	0.158	0.088	0.084	0.124	-0.298**
NO_3^-								1	0.657**	-0.539**	0.144	0.000	-0.638**
SO_4^{2-}									1	-0.680**	0.049	-0.129	-0.447**
pH										1	-0.064	0.294**	0.340**

WS, wind speed (km/h), RH, relative humidity (%); T, air temperature (°C); **: correlation at the 0.01 level (two-tailed); *: correlation at the 0.05 level (two-tailed).

Indicators of aerosol acidity

In addition to the TSP and WSII concentrations, aerosol acidity is also a concerning environmental problem. Thus, the ion balance and neutralization factors were calculated to investigate the aerosol acidity (Xu J. S. et al., 2017; Agarwal et al., 2020). In order to evaluate the acid–base balance of the ions in the atmospheric aerosols, ion balance calculations, i.e., the ratio of the total anion equivalents to the total cations equivalents (Σ_{AE}/Σ_{CE}), have generally been conducted in previous studies (Zhang et al., 2011; Xu J. S. et al., 2017; Agarwal et al., 2020). The charge balance between the anions and cations was calculated as follows:

$$\Sigma_{AE} = [SO_4^{2-}]/48 + [NO_3^-]/62 + [Cl^-]/35.5, \quad (1)$$

$$\Sigma_{CE} = [Na^+]/23 + [NH_4^+]/18 + [K^+]/39 + [Mg^{2+}]/12 + [Ca^{2+}]/20. \quad (2)$$

Here, $[SO_4^{2-}]$, $[NO_3^-]$, $[Cl^-]$, $[Na^+]$, $[NH_4^+]$, $[K^+]$, $[Mg^{2+}]$, and $[Ca^{2+}]$ refer to the mass concentrations of the ions (μg/m^3).

The plot of Σ_{AE} vs Σ_{CE} is presented in Figure 5A. The slope of the linear regression for all of the TSP samples (R^2 = 0.87) was slightly higher than 1, indicating a cation deficient scenario, which may be the result of the omission of hydrogen ions from the calculations (Zhang et al., 2011). Furthermore, the average ratio of Σ_{AE}/Σ_{CE} in the four

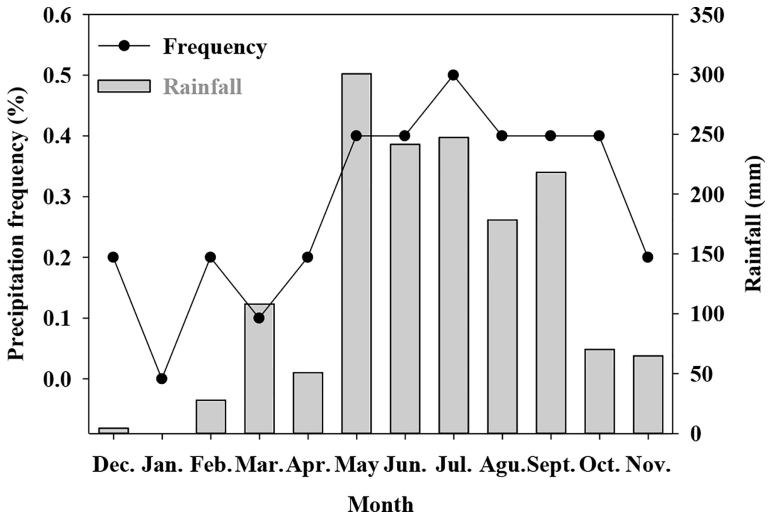


FIGURE 3
Monthly precipitation frequency and total rainfall amount in Zhanjiang. Precipitation frequency data was calculated from the fraction of rain events in each month during sampling periods (rainfall > 0.5 mm/day as the criterion; Hou et al., 2018; data sourced from https://en.tutiempo.net/world.html).

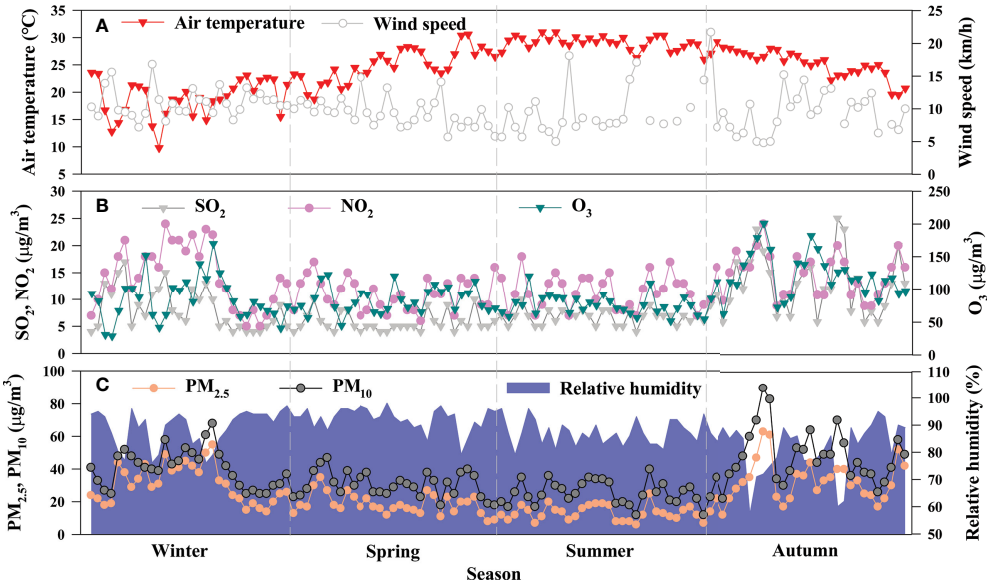


FIGURE 4
72-hour average values of air temperature, wind speed, SO_2, NO_2, O_3, $PM_{2.5}$, PM_{10}, and relative humidity in Zhanjiang.

seasons followed the order autumn (1.34) > winter (1.12) > summer (1.03) > spring (1.02), which is in good agreement with the seasonal pattern of the pH values (Figure 2A). Therefore, these results demonstrate that the aerosols are more acidic in autumn and winter and are less acidic in spring and summer in Zhanjiang. This seasonal variation is consistent with the aerosol research conducted in Guangzhou (GZ) and Hong Kong (HK), where the samples were found to have lower pH values (pH = 4.33 and 5.21 in GZ and HK, respectively) in winter and higher pH values (pH = 5.21 and 5.72 in GZ and HK, respectively) in summer (Cao et al., 2013).

The ratio of the NH_4^+ equivalent concentration to the sum of the equivalent SO_4^{2-} and NO_3^- concentrations (i.e., $[NH_4^+]/[SO_4^{2-}+NO_3^-]$) in the TSPs can be used to assess the neutralization reaction (secondary aerosol process) among NH_4^+, SO_4^{2-}, and NO_3^- (Xu J. S. et al., 2017). In this study, the equivalent ratios of $[NH_4^+]/[SO_4^{2-}+NO_3^-]$ of the samples were less than 1:1 (Figure 5B), which indicates an NH_4^+ deficiency in the ambient particles (Zhou et al., 2018). However, the measurements in this region are comparable to those on Jeju Island (average 1.7 ± 1.1 μg/m^3; Kundu et al., 2010) and in Guiyang (average 3.81 ± 1.64 μg/m^3; Xiao and Liu, 2004), are higher than those in Yurihonjo

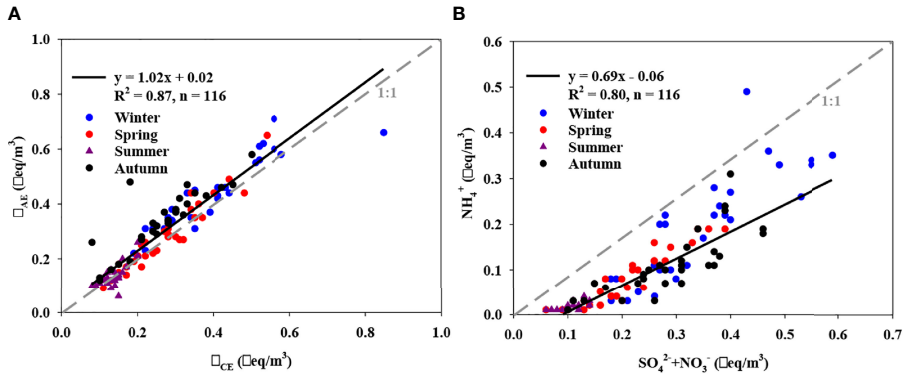


FIGURE 5
(A) Ion balance of the TSPs in Zhanjiang. **(B)** Relationship between the equivalent NH_4^+ concentration and the sum of the equivalent SO_4^{2-} + NO_3^- concentrations in the TSPs in Zhanjiang.

(rural site in Japan, average 0.38 ± 0.33 μg/m^3; Kawashima and Kurahashi, 2011) and NH_4^+ inadequate ambient (Jickells et al., 2003; Lin et al., 2016). This demonstrates that the NH_4^+ in the atmosphere in Zhanjiang is adequate. One possible reason for this discrepancy is that the equivalent concentrations of the acidifying anions were considerably more abundant. That is, SO_4^{2-} and NO_3^- were too abundant for the NH_4^+ in the atmospheric aerosols to be neutralized, and thus the acid status of the atmospheric aerosols can be ascribed to an excess of acidifying anions (Cao et al., 2020). Thus, the higher acidity in autumn and winter could be related to the higher concentrations of SO_4^{2-} and NO_3^- (Figure 2D).

Cations (NH_4^+, nss-K$^+$, nss-Mg^{2+}, and nss-Ca^{2+}) have individual neutralization capacities, and NH_4^+ plays a major role in decreasing aerosol acidity (Xu J. S. et al., 2017; Agarwal et al., 2020). Based on the similar mass concentrations of the cations in this study (Figure 2A–C), we hypothesize that there were other major neutralization ions in addition to NH_4^+. Thus, the neutralization factors (NFs) were investigated to determine the dominant neutralization cations. The contributions of Na$^+$ and Cl$^-$ to lessening the aerosol acidity are considered to be negligible since they are mainly sourced from sea salts (Safai et al., 2010; Satsangi et al., 2013). Although a good correlation was observed between Na$^+$ and Cl$^-$ ($p< 0.01$; Table 2), the corresponding ratios of [Na$^+$]/[Cl$^-$] were found to be lower than that of seawater (1.1) (Xu et al., 2014), suggesting that coal combustion was also a source of Cl$^-$ in addition to sea salt (Xue et al., 2016; Jain et al., 2017; Xu J. S.et al., 2017). Therefore, the contribution of Cl$^-$ to the neutralization should be taken into account, and the non-sea salt Cl$^-$ ([nss-Cl$^-$]) can be calculated by subtracting the sea salt Cl$^-$ ([ss-Cl$^-$] = [Na$^+$]/1.1). NFs in Zhanjiang were calculated using the following equations:

$$NF(NH_4^+) = [NH_4^+]/([NO_3^-] + [nss - Cl^-] + [nss - SO_4^{2-}]), \quad (3)$$

$$NF(nss - K^+) = [nss - K^+]/([NO_3^-] + [nss - Cl^-] + [nss - SO_4^{2-}]), \quad (4)$$

$$NF(nss - Mg^{2+}) = [nss - Mg^{2+}]/(2[NO_3^-] + 2[nss - Cl^-] + [nss - SO_4^{2-}]), \quad (5)$$

$$NF(nss - Ca^{2+}) = [nss - Ca^{2+}]/(2[NO_3^-] + 2[nss - Cl^-] + [nss - SO_4^{2-}]). \quad (6)$$

Here, $[NH_4^+]$, $[NO_3^-]$, [nss-Cl$^-$], $[nss - SO_4^{2-}]$, [nss-K$^+$], [nss-Mg^{2+}], and [nss-Ca^{2+}] refer to the mass concentration of the ions (μg/m^3). For cases with [Na$^+$]/[Cl$^-$] ratios higher than 1.1, [Cl$^-$] should be substituted for [nss-Cl$^-$]. The non-sea salt ions were calculated as follows (Balasubramanian et al., 2003; Nair et al., 2005):

$$[nss - K^+] = [K^+] - [Na^+] * 0.037, \quad (7)$$

$$[nss - Mg^{2+}] = [Mg^{2+}] - [Na^+] * 0.12, \quad (8)$$

$$[nss - Ca^{2+}] = [Ca^{2+}] - [Na^+] * 0.0385. \quad (9)$$

The NF values of the four cations (NH_4^+, nss-K$^+$, nss-Mg^{2+}, and nss-Ca^{2+}) are listed in Table 3. As speculated, there were three major neutralization ions in Zhanjiang. Nss-K$^+$ was the major neutralization ion in summer, which may be related to the fact that biomass burning is an important anthropogenic activity in rural sites (Xu J. S. et al., 2017; Agarwal et al., 2020). The NF values of NH_4^+ were the highest in winter, spring, and autumn, suggesting its dominant impact in neutralizing aerosol acidity. This result is supported by a previous study (Xu J. S. et al., 2017). Nss-Ca^{2+} was the second largest contributor to the neutralization of aerosol acidity, possibly due to the enhanced soil dust brought by strong wind, as suggested by the significant positive correlation between Ca^{2+} and the wind speed ($p< 0.01$; Table 2). Nearby agricultural fields and unpaved roads (Xu J. S. et al., 2017; Agarwal et al., 2020) could be the origins of this soil dust. The NF values of nss-Mg^{2+} were the lowest during the sampling periods, indicating that it had a minor neutralization effect.

The role of precipitation in chemical conversions

As was previously discussed, in this study, the aerosol acidity and concentration were correlated with excess NO_3^- and SO_4^{2-}. Knowledge of the origin and processes of these ions could help lessen aerosol pollution. Aerosol acidity is greatly affected by the

TABLE 3 The neutralization factors (NFs), i.e., NH_4^+, nss-K$^+$, nss-Mg^{2+}, and nss-Ca^{2+}, in the TSPs in Zhanjiang.

	NH_4^+	nss-K$^+$	nss-Mg^{2+}	nss-Ca^{2+}
Winter	0.11	0.04	0.01	0.05
Spring	0.07	0.06	0.01	0.06
Summer	0.02	0.20	0.01	0.09
Autumn	0.07	0.04	0.01	0.06
Average	0.07	0.08	0.01	0.07

oxidation of nitric oxide (NOx) to NO_3^- and of sulfur dioxide (SO_2) to SO_4^{2-} in the atmosphere (Cao et al., 2020). The nitrogen oxidation ratio (NOR) and the sulfur oxidation ratio (SOR) J. S. were estimated using the following equations (Lin, 2002; Xu et al., 2017) in order to gain a better understanding of the conversions of NO_3^- and SO_4^{2-}:

$$SOR = [nss - SO_4^{2-}]/([nss - SO_4^{2-}] + [SO_2]), \quad (10)$$

$$NOR = [NO_3^-]/([NO_3^-] + [NO_2]) \quad (11)$$

Here, $[nss - SO_4^{2-}]$, $[SO_2]$, $[NO_3^-]$, and $[NO_2]$ refer to the mass concentrations of the ions (μg/m^3). The higher SOR and NOR values observed (threshold: 0.1) suggest the presence of more gaseous precursors that generate sulfate- and nitrate-containing secondary aerosols through oxidation (Colbeck and Harrison, 1984; Ohta and Okita, 1990; Kaneyasu et al., 1995).

The monthly and seasonal variations in air temperature, NOR, SOR, and the amount of rainfall are presented in Figure 6. As can be seen, the monthly average values of NOR and SOR were higher than 0.1, indicating a considerable conversion of gaseous precursors to NO_3^- and SO_4^{2-} in the atmospheric aerosols during the sampling periods. The fact that NO_2 and SO_2 were relatively abundant in winter and autumn (Figure 4B) could contribute to the higher occurrences of NO_3^- and SO_4^{2-} (Figure 2D), which were seasonally consistent with the lower pH values (Figure 2A). The decreased production of secondary aerosols in summer is indicated by the valleys in the SOR and NOR curves (Figure 6). This seasonal pattern is contrary to the results of previous studies (Zhang et al., 2011; Xu J. S. et al., 2020). The ambient oxidant (O_3) for chemical conversion is relatively abundant (Figure 4B), so the different meteorological conditions may be the cause of the low conversion rates. The conversion of NO_2 to NO_3^- and SO_2 to SO_4^{2-} is favored by warm and humid ambient conditions (Zhang et al., 2011; Xu J. S. et al., 2020). Since the city investigated in this study is warmer and moister than Xi'an (Zhang et al., 2011), the chemical conversion of NO_2 and SO_2 occurred year-round, and the calculated oxidation ratio was higher than that in the abovementioned area. Additionally, the amount of rainfall in Zhanjiang is about twice than that in the abovementioned area and is mainly concentrated in summer (Figure 4), which gives rise to a precipitation-driven removal process. Therefore, the coexistence of low gaseous precursors (Figure 4B), low precursor conversions (Figure 6), and frequent plentiful rainfall (Figure 3) in summer in Zhanjiang may be related to the removal effect caused by the precipitation. Gaseous precursors can be captured by precipitation below the clouds (Chen et al., 2020), and a lack of reactants may induce low oxidation ratios (Jiang, 2016).

It has been reported that gaseous precursors are predominantly emitted by fossil fuel combustion (> 70%; Lv, 2019; Liu et al., 2019), and high concentrations of NO_2 and SO_2 in winter are influenced by additional coal combustion for heating (Zhang et al., 2011). Thus, the reduction in NO_2 and SO_2 in summer seems to suggest a decrease in fossil fuel usage in addition to the removal effect caused by precipitation. However, we believe that the reduced combustion in summer is unlikely to be based on the ratio of NO_3^- to SO_4^{2-} (NO_3^-/SO_4^{2-}) and power production.

The NO_3^-/SO_4^{2-} ratio of the atmospheric aerosols is recognized as an effective approach to assessing stationary and mobile sources of nitrogen and sulfur and has been widely used at various locations around the world (Arimoto et al., 1996; Tan et al., 2009; Safai et al., 2010; Begam et al., 2017). When this ratio is > 1, the emissions are considered to be produced by mobile sources; otherwise, they are emitted from stationary sources

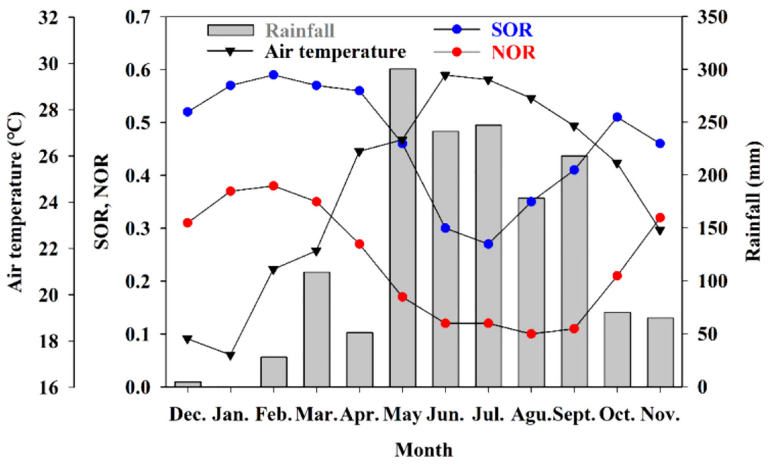


FIGURE 6
Monthly average values of air temperature, NOR, SOR, and amount of rainfall.

(Arimoto et al., 1996; Lv, 2019). As can be seen from Figure 7, the monthly average NO_3^-/SO_4^{2-} ratios during the sampling periods were<1 (from 0.05 to 2.57, averaged at of 0.55 ± 0.33), indicating that the predominance of stationary sources over mobile sources in Zhanjiang. Thus, the NO_2 and SO_2 in the atmosphere during the sampling periods were associated with local emissions.

China is a coal-fired country, and more than half of the coal is consumed by electric power plants, so power production can be considered to be an indicator of the local fossil fuel consumption. Power production continues at a high rate in summer; whereas it has a relatively low rate in winter and autumn (Figure 7), implying an adequate amount of gaseous precursors should be present in the hot and rainy season. However, the observations in summer showed low values (Figure 4B), which in turn supports the possibility of a precipitation-driven removal process.

Possible air quality improvement process and source identification in a heavy industry coastal city

Aerosol pollution is a significant global problem caused by rapid economic and industrial development. The inconsistency between heavy industrial activities and low aerosol concentrations during our sampling campaign in Zhanjiang may be related to a precipitation-driven removal effect (Hou et al., 2018) and the marine dilution effect. Aerosols from marine emissions are considered to be relatively clean (Jickells et al., 2003; Xiao et al., 2017; Zhou et al., 2019), which results in potential dilution and air quality improvement when mixed with polluted aerosols produced by terrestrial anthropogenic activities. Since the study area is bordered by the SCS, the marine effect should be taken into account in this region. Thus, the aerosols from non-sea salt contributions were evaluated, and the results are presented in Table 4. More than 50% of the Mg^{2+} in Zhanjiang was sourced from sea salt (Table 4), indicating that the Mg^{2+} is predominantly from marine emissions. The higher ratios (>90%) of nss-K^+/K^+, nss-Ca^{2+}/Ca^{2+}, and $nss-SO_4^{2-}/SO_4^{2-}$ found during sampling campaign (Table 4) indicate minor contributions from marine emissions to these WSIIs in the aerosols.

In order to investigate the effects of precipitation on the TSPs, linear regression analysis (SPSS version 22.0, IBM Corp.) was conducted to quantitatively describe the impacts of precipitation on the TSPs. The frequency and amount of precipitation were selected as the precipitation characteristics, as was suggested by Hou et al. (2018). As can be seen from the data shown in Figure 8, the TSPs were negatively affected by precipitation, indicating that the atmospheric aerosol lifetime was sensitive to precipitation (Hou et al., 2018), and precipitation significantly contributed (> 50%) to the decrease in the TSPs pollution in Zhanjiang. The high coefficient of determination (R^2 = 0.63) in Figure 8A further suggests that the precipitation frequency had a larger effect on the removal efficiency than the amount of precipitation. The model results of Hou et al. (2018) also highlight the importance of precipitation frequency in shortening aerosol lifetime.

Principal component analysis (PCA, SPSS version 22.0, IBM Corp.) was conducted in this study and presented in Table 5. Principal Components Analysis (PCA) is an algorithm to

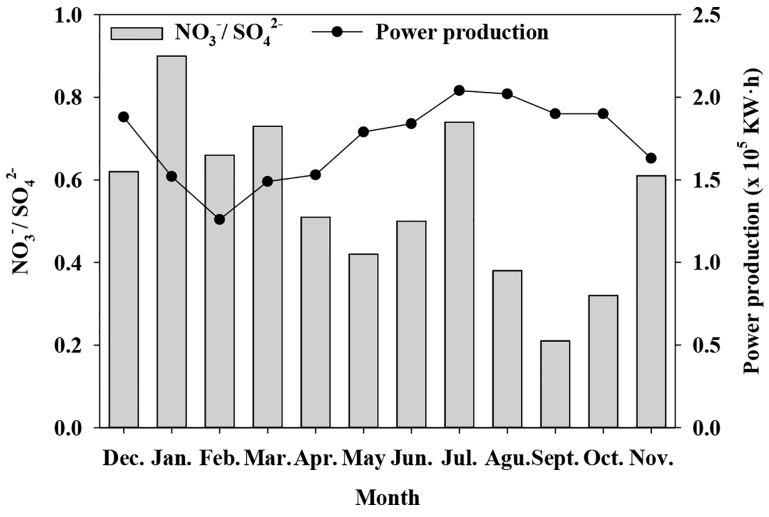


FIGURE 7
Monthly average values of the NO_3/SO_4^2 ratio (mass concentration ratio) and power production in Zhanjiang during the sampling periods (data from the Zhanjiang Bureau of Statistics, https://www.zhanjiang.gov.cn/tjj/).

TABLE 4 Non-sea salt ionic fractions in Zhanjiang.

	nss-K^+/K^+	nss-Mg^{2+}/Mg^{2+}	nss-Ca^{2+}/Ca^{2+}	$nss-SO_4^{2-}/SO_4^{2-}$
Winter	93%	45%	93%	96%
Spring	91%	27%	91%	92%
Summer	96%	33%	93%	89%
Autumn	94%	44%	94%	96%
Average	94%	37%	93%	93%

transform the columns of a dataset into a new set of features called Principal Components (PC). According to the results of PCA, a large chunk of the information across the full dataset is effectively compressed in fewer feature columns (i.e., PC1, PC2, PC3, etc.), while still preserving as much information as possible. This enables dimensionality reduction and ability to visualize the separation of classes or clusters (https://builtin.com/data-science/step-step-explanation-principal-component-analysis). The extracted PC with eigenvalue > 1.0 is retained for interpretation and the loading above 0.5 of each component is determined to be the major contribution to each of the PC scores (Gao et al., 2011; Zhang et al., 2011; Agarwal et al., 2020; Liu et al., 2021a; Liu et al., 2021b). In these studies, the determined component is regarded as tracer of certain source (Gao et al., 2011; Zhang et al., 2011; Agarwal et al., 2020; Liu et al., 2021a; Liu et al., 2021b). Similarly, the determined component can be used for tracing sources in the present study.

As presented in Table 5, three factors were identified (eigenvalue > 1.0) as PCs and accounted for 90.0% of the total data variance. PC1 was strongly loaded with TSPs, NH_4^+, Mg^{2+}, Ca^{2+}, Cl^-, NO_3^-, and SO_4^{2-}. NH_4^+, NO_3^-, and SO_4^{2-} were mainly from a secondary formation process (Agarwal et al., 2020). As was previously discussed, Cl^- reflects the influence of coal combustion (Xue et al., 2016; Jain et al., 2017; Xu J.S. et al., 2017). Ca^{2+} and Mg^{2+} reflect the contributions of soil dust and are the principal crustal elements (Gao et al., 2011; Zhang et al., 2011; Meng et al., 2016; Saxena et al., 2017; Jaiprakash et al., 2017). Therefore, PC1 was identified as a mixture of secondary aerosols, coal combustion, and soil dust. PC2 explained 27.4% of the total variance and was observed to be heavily loaded for Na^+, Mg^{2+}, and Cl^-, which were possibly influenced by sea salts. This is in agreement with the results for other coastal areas (Xu J. S. et al., 2017), that is, the aerosols in these areas exhibited oceanic characteristics. Thus, the presence of these ions indicates that PC2 was primarily sourced from marine emissions. PC3 was characterized by a high loading of K^+ and accounted for 11.5% of the variance. Moreover, K^+ was found to be uncorrelated with most of the WSIIs in Zhanjiang (Table 2), suggesting that the PC3 source is biomass burning.

We summarize the possible removal effect of TSPs in Zhanjiang in a conceptual diagram (Figure 9), showing frequent precipitation could remove a large amount of gas precursors and local secondary aerosols. The aerosols sourced from clean marine emissions therefore act as the supplement in the ambient, leading to the observance of relatively high contribution in the TSPs. This result may provide useful information for lessening aerosol pollution under the background of the pervasive anthropogenic aerosols pollution around the world, and the relocation site chosen for industrial activities.

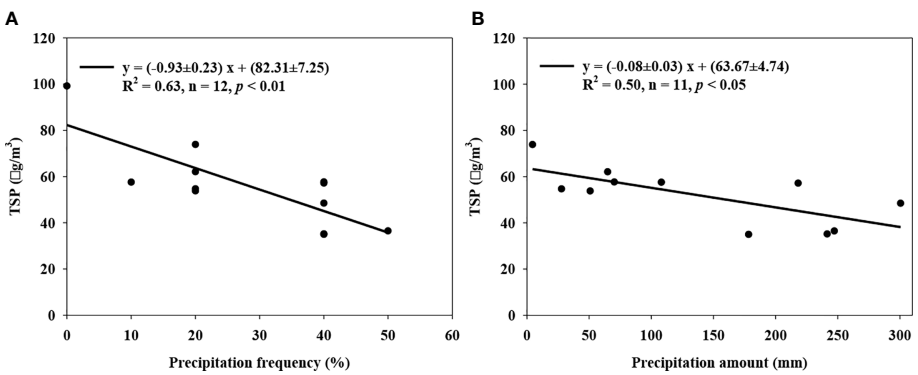


FIGURE 8
Linear regressions of **(A)** TSPs and precipitation frequency and **(B)** TSPs and amount of precipitation.

10.3389/fmars.2022.977120

TABLE 5 The results of the PCA for the mass concentrations of the TSPs and WSIIs in Zhanjiang.

	PC1	PC2	PC3
TSPs	**0.894**	-0.318	0.000
Na^+	0.496	**0.825**	-0.188
NH_4^+	**0.880**	-0.302	0.038
K^+	0.196	0.154	**0.959**
Mg^{2+}	**0.632**	**0.710**	-0.170
Ca^{2+}	**0.574**	-0.641	0.059
Cl^-	**0.598**	**0.710**	0.170
NO_3^-	**0.898**	-0.098	-0.055
SO_4^{2-}	**0.813**	-0.377	-0.132
Eigenvalue	4.413	2.468	1.038
% of variance	49.033	27.418	11.532
Cumulative variance	49.033	76.451	89.983
Factors	Secondary aerosol, coal combustion, and soil dust	Marine emission	Biomass burning

The bold values indicate strong loadings.

As stated above, gas precursors and local secondary aerosols can be captured by frequent precipitation and abundant rainfall. These materials thus enter the marine environment in the coastal area as atmospheric deposition, which may aggravate nutrients loading and even result in eutrophication and hypoxia (Duce et al., 2008; Chen et al., 2017; Wu et al., 2018; Cui et al., 2020). The impacts of atmospheric deposition on marine environment require attention and need further exploration.

Conclusions

The goal of this study was to clarify the discrepancy between industrial activities and low aerosol concentrations in a tropical coastal city due to a precipitation-driven removal process and the marine dilution effect. In Zhanjiang, 72h TSPs collection and WSIIs analysis were conducted during a one-year sampling campaign. The results of this investigation show that the TSP mass concentrations and the total WSII

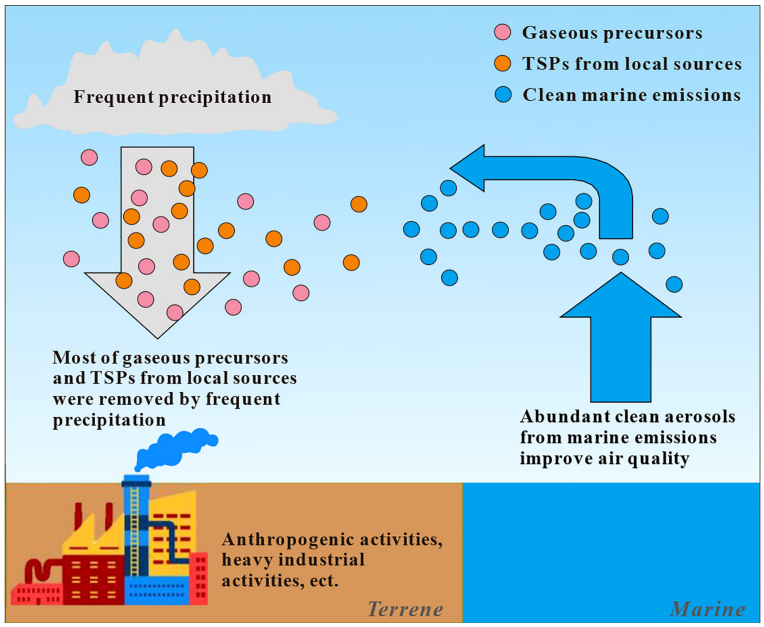


FIGURE 9
Conceptual diagram for TSPs removal process in Zhanjiang.

concentrations in Zhanjiang were lower in the spring and summer and were higher in the winter and autumn. This seasonal pattern and high aerosol acidity (indicated by the ion balance, neutralization factors, and pH values) further suggest that the TSPs, WSIIs, and acidic gaseous precursors were removed by frequent precipitation and abundant rainfall. The PCA results revealed that secondary aerosols and sea salts were important sources of the TSPs and WSIIs. One of the more significant findings of this study is that a combination of high precipitation frequency and marine dilution can lessen aerosol pollution in a heavy industrial city.

Data availability statement

The original contributions presented in the study are included in the article/Supplementary Material. Further inquiries can be directed to the corresponding author.

Author contributions

XZ Conceptualization, Writing-Original draft, Writing-Review and Editing. Data Curation, Visualization, Software. ZL Methodology, Project administration, Writing-Review and Editing. CC Investigation, Methodology, Writing-Review and Editing. HL Investigation, Writing-Review and Editing. QZ Methodology, Project administration, Writing-Review and Editing. ZZ Methodology, Writing-Review and Editing. QL Writing-Review and Editing. All authors contributed to the article and approved the submitted version.

Funding

This work was supported by National Natural Science Foundation of China (92158201, U1901213); Innovation and Entrepreneurship Project of Shantou (2021112176541391); Special Projects in Key Fields of Colleges and Universities in Guangdong Province (2020ZDZX1099); Guangdong Provincial College Innovation Team Project (2019KCXTF021), First-class Discipline Plan of Guangdong Province (080503032101, 231420003).

Conflict of interest

The authors declare that the research was conducted in the absence of any commercial or financial relationships that could be construed as a potential conflict of interest.

Publisher's note

All claims expressed in this article are solely those of the authors and do not necessarily represent those of their affiliated organizations, or those of the publisher, the editors and the reviewers. Any product that may be evaluated in this article, or claim that may be made by its manufacturer, is not guaranteed or endorsed by the publisher.

References

Agarwal, A., Satsangi, A., Lakhani, A., and Kumari, K. M. (2020). Seasonal and spatial variability of secondary inorganic aerosols in PM2.5 at Agra: Source apportionment through receptor models. *Chemosphere* 242, 125132. doi: 10.1016/j.chemosphere.2019.125132

Ali-Mohamed, A. Y. (1991). Estimation of inorganic particulate matter in the atmosphere of isa town, Bahrain, by dry deposition. *Atmos. Environ. Part B.* 25, 397–405. doi: 10.1016/0957-1272(91)90011-3

Arimoto, R., Duce, R. A., Savoie, D. L., Prospero, J. M., Talbot, R., Cullen, J. D., et al. (1996). Relationships among aerosol constituents from Asia and the north pacific during PEM-West a. *J. Geophys. Res. Atmos.* 101, 2011–2023. doi: 10.1029/95JD01071

Balasubramanian, R., Qian, W. B., Decesari, S., Facchini, M. C., and Fuzzi, S. (2003). Comprehensive characterization of PM2.5 aerosols in Singapore. *J. Geophys. Res. Atmos.* 108 (D16), 4523. doi: 10.1029/2002JD002517

Begam, G. R., Vachaspati, C. V., Ahammed, Y. N., Kumar, K. R., Reddy, R. R., Sharma, S. K., et al. (2017). Seasonal characteristics of water-soluble inorganic ions and carbonaceous aerosols in total suspended particulate matter at a rural semi-arid site, kadapa (India). *Environ. Sci. pollut. Res.* 24, 1719–1734. doi: 10.1007/s11356-016-7917-1

Cao, J. J., Tie, X. X., Dabberdt, W. F., Jie, T., Zhao, Z. Z., An, Z. S., et al. (2013). On the potential high acid deposition in northeastern China. *J. Geophys. Res. Atmos.* 118, 4834–4846. doi: 10.1002/jgrd.50381

Cao, Y. S., Zhang, Z. Y., Xiao, H. W., Xie, Y. J., Liang, Y., and Xiao, H. Y. (2020). How aerosol pH responds to nitrate to sulfate ratio of fine-mode particulate. *Environ. Sci. pollut. Res.* 27, 35031–35039. doi: 10.1007/s11356-020-09810-0

Chen, F. J., Chen, C. Q., Zhou, F. X., Lao, Q. B., Zhu, Q. M., and Zhang, S. W. (2017). Nutrients in atmospheric wet deposition in the zhanjiang bay. *China Environ. Sci.* 37 (6), 2055–2063.

Chen, F. J., Lao, Q. B., Jia, G. D., Chen, C. Q., Zhu, Q. M., and Zhou, X. (2019). Seasonal variations of nitrate dual isotopes in wet deposition in a tropical city in China. *Atmos. Environ.* 196, 1–9. doi: 10.1016/j.atmosenv.2018.09.061

Chen, F. J., Lao, Q. B., Li, Z. Y., Bian, P. W., Zhu, Q. M., Chen, C. Q., et al. (2020). Monthly variations of the nitrogen isotope of ammonium in wet deposition in a tropical city of south China. *Aerosol. Air. Qual. Res.* 20, 1062–1069. doi: 10.4209/aaqr.2019.06.0303

Colbeck, I., and Harrison, R. M. (1984). Ozone–secondary aerosol–visibility relationships in north-West England. *Sci. Total. Environ.* 34, 87–100. doi: 10.1016/0048-9697(84)90043-3

Cui, X., Huang, C. Z., Wu, J. P., Liu, X. H., and Hong, Y. G. (2020). Temporal and spatial variations of net anthropogenic nitrogen inputs (NANI) in the pearl river basin of China from 1986 to 2015. *PloS One* 15 (2), e0228683. doi: 10.1371/journal.pone.0228683

Duce, R. A., LaRoche, J., Altieri, K., Arrigo, K. R., Baker, A. R., Capone, D. G., et al. (2008). Impacts of atmospheric anthropogenic nitrogen on the open ocean. *Science* 320 (16), 893–897. doi: 10.1126/science.1150369

Fuzzi, S., Baltensperger, U., Carslaw, K., Decesari, S., Facchini, M. C., Fowler, D., et al. (2015). Particulate matter, air quality and climate: Lessons learned and future needs. *Atmos. Chem. Phys.* 14 (15), 8217–8299. doi: 10.5194/acp-15-8217-2015

Gao, X. M., Yang, L. X., Cheng, S. H., Gao, R., Zhou, Y., Xue, L. K., et al. (2011). Semi-continuous measurement of water-soluble ions in PM2.5 in jinan, China:

Temporal variations and source apportionments. *Atmos. Environ.* 45, 6048–6056. doi: 10.1016/j.atmosenv.2011.07.041

Grasshoff, K., Kremling, K., and Ehrhardt, M. (1999). Methods of seawater analysis, 3rd edn. *Wiley. New York.* pp, 159–228. doi: 10.1002/9783527613984

Guo, S., Hu, M., Zamora, M. L., Peng, J. F., Shang, D. J., Zheng, J., et al. (2014). Elucidating severe urban haze formation in China. *PNAS* 111, 17373–17378. doi: 10.1073/pnas.1419604111

Hou, P., Wu, S. L., McCarty, J. L., and Gao, Y. (2018). Sensitivity of atmospheric aerosol scavenging to precipitation intensity and frequency in the context of global climate change. *Atmos. Chem. Phys.* 18, 8173–8182. doi: 10.5194/acp-18-8173-2018

Huang, R. J., Zhang, Y. L., Bozzetti, C., Ho, K. F., Cao, J. J., Han, Y. M., et al. (2014). High secondary aerosol contribution to particulate pollution during haze events in China. *Nature* 514, 218–222. doi: 10.1038/nature13774

Jain, S., Sharma, S. K., Choudhary, N., Masiwal, R., Saxena, M., Sharma, A., et al. (2017). Chemical characteristics and source apportionment of PM2.5 using PCA/APCS, UNMIX, and PMF at an urban site of Delhi, India. *Environ. Sci. pollut. Res.* 24, 14637–14656. doi: 10.1007/s11356-017-8925-5

Jaiprakash,, Singhai, A., Habib, G., Raman, R. S., and Gupta, T. (2017). Chemical characterization of $PM_{1.0}$ aerosol in Delhi and source apportionment using positive matrix factorization. *Environ. Sci. pollut. Res.* 24, 445–462. doi: 10.1007/s11356-016-7708-8

Jiang, B. (2016). *Analysis of fine particle's chemical characteristics and secondary pollution formation at heshan atmospheric supersite. dissertation* (Guangzhou: Jinan University).

Jickells, T. D., Kelly, S. D., Baker, A. R., Biswas, K., Dennis, P. F., Spokes, L. J., et al. (2003). Isotopic evidence for a marine ammonia source. *Geophys. Res. Lett.* 30 (7), 1374. doi: 10.1029/2002GL016728

Kaneyasu, N., Ohta, S., and Murao, N. (1995). Seasonal variation in the chemical composition of atmospheric aerosols and gaseous species in Sapporo, Japan. *Atmos. Environ.* 29, 1559–1568. doi: 10.1016/1352-2310(94)00356-P

Kawashima, H., and Kurahashi, T. (2011). Inorganic ion and nitrogen isotopic compositions of atmospheric aerosols at yurihonjo, Japan: Implications for nitrogen sources. *Atmos. Environ.* 45, 6309–6316. doi: 10.1016/j.atmosenv.2011.08.057

Kundu, S., Kawamura, K., and Lee, M. (2010). Seasonal variation of the concentrations of nitrogenous species and their nitrogen isotopic ratios in aerosols at gosan, jeju island: Implications for atmospheric processing and source changes of aerosols. *J. Geophys. Res. Atmos.* 115, D20305. doi: 10.1029/2009JD013323

Li, J. C., Cao, R. X., Lao, Q. B., Chen, F. J., Chen, C. Q., Zhou, X., et al. (2020). Assessing seasonal nitrate contamination by nitrate dual isotopes in a monsoon-controlled bay with intensive human activities in south China. *Int. J. Environ. Res. Public Health* 17, 1921. doi: 10.3390/ijerph17061921

Li, Q., Li, X. D., Yang, Z., Cui, G., and Ding, S. (2020). Diurnal and seasonal variations in water-soluble inorganic ions and nitrate dual isotopes of $PM_{2.5}$: Implications for source apportionment and formation processes of urban aerosol nitrate. *Atmos. Res.* 248 (15), 105197. doi: 10.1016/j.atmosres.2020.105197

Lin, J. J. (2002). Characterization of water-soluble ion species in urban ambient particles. *Environ. Int.* 28, 55–61. doi: 10.1016/S0160-4120(02)00004-1

Lin, C. T., Jickells, T. D., Baker, A. R., Marca, A., and Johnson, M. T. (2016). Aerosol isotopic ammonium signatures over the remote Atlantic ocean. *Atmos. Environ.* 133, 165–169. doi: 10.1016/j.atmosenv.2016.03.020

Liu, M. Y., Chen, M., Duan, M., Lin, Y., Liu, X., Liang, J., et al. (2021b). Particulate export of PAHs firstly traced by $^{210}Po/^{210}Pb$ disequilibrium: Implication on the "Shelf sink effect" in the Arctic ocean. *J. Geophys. Res.: Oceans.* 126, e2021JC017384. doi: 10.1029/2021JC017384

Liu, M. X., Huang, X., Song, Y., Tang, J., Cao, J. J., Zhang, X. Y., et al. (2019). Ammonia emission control in China would mitigate haze pollution and nitrogen deposition, but worsen acid rain. *PNAS* 116, 7760–7765. doi: 10.1073/pnas.1814880116

Liu, M. Y., Zheng, H. W., Wang, W. M., Ke, H. W., Huang, P., Liu, S. G., et al. (2021a). Enhanced sinks of polycyclic aromatic hydrocarbons due to kuroshio intrusion: Implications on biogeochemical processes in the ocean-dominated marginal seas. *Environ. Sci. Technol.* 55 (10), 6838–6847. doi: 10.1021/acs.est.1c01009

Luo, H. J., Lao, Q. B., Chen, F. J., Chen, C. Q., Zhou, X., Jin, G. Z., et al. (2022). Nitrate sources and formation in aerosol and precipitation in a tropical city in south China: Insight from nitrate dual isotopes. *Atmos. Environ.* 278, 119087. doi: 10.1016/j.atmosenv.2022.119087

Lv, Z. (2019). *Chemical characteristics and source apportionment of water-soluble ions in PM2.5 in shijiazhuang. dissertation* (Nanchang: East China University of Technology).

Meng, C. C., Wang, L. T., Zhang, F. F., Wei, Z., Ma, S. M., Ma, X., et al. (2016). Characteristics of concentrations and water-soluble inorganic ions in PM2.5 in handan city, hebei province, China. *Atmos. Res.* 171, 133–146. doi: 10.1016/j.atmosres.2015.12.013

Nair, P. R., Parameswaran, K., Abraham, A., and Jacob, S. (2005). Wind-dependence of sea-salt and non-sea-salt aerosols over the oceanic environment. *J. Atmos. Sol. Terr. Phys.* 67, 884–898. doi: 10.1016/j.jastp.2005.02.008

Ohta, S., and Okita, T. (1990). A chemical characterization of atmospheric aerosol in Sapporo. *Atmos. Environ. Part A.* 24, 815–822. doi: 10.1016/0960-1686(90)90282-R

Peng, S. Y., Kong, D. M., Li, L. T., Zou, C. L., Chen, F. J., Li, M. J., et al. (2020). Distribution and sources of DDT and its metabolites in porewater and sediment from a typical tropical bay in the south China Sea. *Environ. pollut.* 267, 115492. doi: 10.1016/j.envpol.2020.115492

Safai, P. D., Budhavant, K. B., Rao, P. S. P., Ali, K., and Sinha, A. (2010). Source characterization for aerosol constituents and changing roles of calcium and ammonium aerosols in the neutralization of aerosol acidity at a semi-urban site in SW India. *Atmos. Res.* 98, 78–88. doi: 10.1016/j.atmosres.2010.05.011

Satsangi, A., Pachauri, T., Singla, V., Lakhani, A., and Kumari, K. M. (2013). Water soluble ionic species in atmospheric aerosols: Concentrations and sources at Agra in the indo-gangetic plain (IGP). *Aerosol. Air. Qual. Res.* 13, 1877–1889. doi: 10.4209/aaqr.2012.08.0227

Saxena, M., Sharma, A., Sen, A., Saxena, P., Saraswati,, Mandal, T. K., et al. (2017). Water soluble inorganic species of PM_{10} and $PM_{2.5}$ at an urban site of Delhi, India: Seasonal variability and sources. *Atmos. Res.* 184, 112–125. doi: 10.1016/j.atmosres.2016.10.005

Seinfeld, J. H. (2004). Air pollution: A half century of progress. *Energy Environ.* 50, 12. doi: 10.1002/aic.10102

Shon, Z. H., Kim, K. H., Song, S. K., Jung, K., Kim, N. J., and Lee, J. B. (2012). Relationship between water-soluble ions in $PM_{2.5}$ and their precursor gases in Seoul megacity. *Atmos. Environ.* 59, 540–550. doi: 10.1016/j.atmosenv.2012.04.033

Sun, R. X., Sun, Y., Li, Q. X., Zheng, X. B., Luo, X. J., and Mai, B. X. (2018). Polycyclic aromatic hydrocarbons in sediments and marine organisms: Implications of anthropogenic effects on the coastal environment. *Sci. Total. Environ.*, 640–641: 264-272. doi: 10.1016/j.scitotenv.2018.05.320

Tan, J. H., Duan, J. C., Chen, D. H., Wang, X. H., Guo, S. J., Bi, X. H., et al. (2009). Chemical characteristics of haze during summer and winter in guangzhou. *Atmos. Res.* 94, 238–245. doi: 10.1016/j.atmosres.2009.05.016

Tang, X., Zhang, Y., and Shao, M. (2006). *Atmospheric environmental chemistry. 2nd edition* (Beijing: Higher Education press).

Tao, J., Zhang, L. M., Cao, J. J., Zhong, L. J., Chen, D. S., Yang, Y. H., et al. (2017). Source apportionment of $PM_{2.5}$ at urban and suburban areas of the pearl river delta region, south China -with emphasis on ship emissions. *Sci. Total. Environ.* 574, 1559–1570. doi: 10.1016/j.scitotenv.2016.08.175

Tian, J., Guan, H., Zhou, Y. H., Zheng, N. J., Xiao, H. W., Zhao, J. J., et al. (2021). Isotopic source analysis of nitrogen-containing aerosol: A study of PM2.5 in guiyang (SW, China). *Sci. Total. Environ.* 760, 143935. doi: 10.1016/j.scitotenv.2020.143935

Wang, J. J., Beusen, A. H. W., Liu, X. C., Dingenen, R. V., Dentener, F., Yao, Q. Z., et al. (2020). Spatially explicit inventory of sources of nitrogen inputs to the yellow Sea, East China Sea, and south China Sea for the period 1970–2010. *Earth's. Future* 8, e2020EF001516. doi: 10.1029/2020EF001516

Wang, Q. Q., Li, J., Yang, J. X., Chen, Y., Li, Y. Y., Li, S. Y., et al. (2020). Seasonal characterization of aerosol composition and sources in a polluted city in central China. *Chemosphere* 258, 127310. doi: 10.1016/j.chemosphere.2020.127310

Wang, G., Zhu, Z. Y., Zhao, N., Wei, P., Li, G. H., and Zhang, H. Y. (2021). Variations in characteristics and transport pathways of PM2.5 during heavy pollution episodes in 2013–2019 in jinan, a central city in the north China plain. *Environ. Pollut.* 284, 117450. doi: 10.1016/j.envpol.2021.117450

Weber, R. J., Guo, H. Y., Russell, A. G., and Nenes, A. (2016). High aerosol acidity despite declining atmospheric sulfate concentrations over the past 15 years. *Nat. Geosci.* 9, 282–285. doi: 10.1038/ngeo2665

Wu, Y. C., Zhang, J. P., Liu, S. L., Jiang, Z. J., and Huang, X. P. (2018). Aerosol concentrations and atmospheric dry deposition fluxes of nutrients over daya bay, south China Sea. *Mar. Pollut. Bull.* 128, 106–114. doi: 10.1016/j.marpolbul.2018.01.019

Xiao, H. Y., and Liu, C. Q. (2004). Chemical characteristics of water-soluble components in TSP over guiyang, SW China 2003. *Atmos. Environ.* 38, 6297–6306. doi: 10.1016/j.atmosenv.2004.08.033

Xiao, H. W., Xiao, H. Y., Luo, L., Shen, C. Y., Long, A. M., Chen, L., et al. (2017). Atmospheric aerosol compositions over the south China Sea: temporal variability and source apportionment. *Atmos. Chem. Phys.* 17, 3199–3214. doi: 10.5194/acp-17-3199-2017

Xu, L. L., Duan, F. K., He, K. B., Ma, Y. L., Zhu, L. D., Zheng, Y. X., et al. (2017). Characteristics of the secondary water-soluble ions in a typical autumn haze in Beijing. *Environ. Pollut.* 227, 296–305. doi: 10.1016/j.envpol.2017.04.076

Xue, Y. F., Zhou, Z., Nie, T., Wang, K., Nie, L., Pan, T., et al. (2016). Trends of multiple air pollutants emissions from residential coal combustion in Beijing and its implication on improving air quality for control measures. *Atmos. Environ.* 142, 303–312. doi: 10.1016/j.atmosenv.2016.08.004

Xu, J. Z., Wang, Z. B., Yu, G. M., Qin, X., Ren, J. W., and Qin, D. H. (2014). Characteristics of water soluble ionic species in fine particles from a high altitude site on the northern boundary of Tibetan plateau: Mixture of mineral dust and anthropogenic aerosol. *Atmos. Environ.* 143, 43–56. doi: 10.1016/j.atmosres.2014.01.018

Xu, J. S., Xu, M. X., Snape, C., He, J., Behera, S. N., Xu, H. H., et al. (2017). Temporal and spatial variation in major ion chemistry and source identification of secondary inorganic aerosols in northern zhejiang province, China. *Chemosphere* 179, 316–330. doi: 10.1016/j.chemosphere.2017.03.119

Zhang, T., Cao, J. J., Tie, X. X., Shen, Z. X., Liu, S. X., Ding, H., et al. (2011). Water-soluble ions in atmospheric aerosols measured in Xi'an, China: Seasonal variations and sources. *Atmos. Res.* 102, 110–119. doi: 10.1016/j.atmosres.2011.06.014

Zhou, X., Luo, H. J., Chen, F. J., Chen, C. Q., Li, Z. Y., Zhu, Q. M., et al. (2022). Regime shift in aerosol ammonium between the rainy and dry season: Perspective from stable isotopes in bulk deposition. *Atmos. Pollut. Res.* 13, 101462. doi: 10.1016/j.apr.2022.101462

Zhou, X. D., Xu, Z. F., Liu, W. J., Wu, Y., Zhao, T., Jiang, H., et al. (2019). Chemical composition of precipitation in shenzhen, a coastal mega-city in south China: Influence of urbanization and anthropogenic activities on acidity and ionic composition. *Sci. Total. Environ.* 662, 218–226. doi: 10.1016/j.scitotenv.2019.01.096

Zhou, M., Zhang, Y. F., Han, Y., Wu, J. H., Du, X., Xu, H., et al. (2018). Spatial and temporal characteristics of $PM_{2.5}$ acidity during autumn in marine and coastal area of bohai Sea, China, based on two-site contrast. *Atmos. Res.* 202, 196–204. doi: 10.1016/j.atmosres.2017.11.014

frontiers | Frontiers in Marine Science

TYPE Original Research
PUBLISHED 24 August 2022
DOI 10.3389/fmars.2022.990113

Check for updates

OPEN ACCESS

EDITED BY
Dilip Kumar Jha,
National Institute of Ocean Technology, India

REVIEWED BY
Xinqing Zheng,
State Oceanic Administration, China
Wentao Niu,
Ministry of Natural Resources, China
Jiayuan Liang,
Guangxi University, China

*CORRESPONDENCE
Guowei Zhou
zhougw@scsio.ac.cn
Hui Huang
huanghui@scsio.ac.cn

SPECIALTY SECTION
This article was submitted to Marine Pollution, a section of the journal Frontiers in Marine Science

RECEIVED 09 July 2022
ACCEPTED 03 August 2022
PUBLISHED 24 August 2022

CITATION
Lei X, Liu C, Zhang Y, Yu X, Yang J, Luo Y, Zhou G and Huang H (2022) Spatial variability in the abundance and prey selection of the corallivorous snail *Drupella* spp. in the southeastern Hainan Island, China. *Front. Mar. Sci.* 9:990113. doi: 10.3389/fmars.2022.990113

COPYRIGHT
© 2022 Lei, Liu, Zhang, Yu, Yang, Luo, Zhou and Huang. This is an open-access article distributed under the terms of the Creative Commons Attribution License (CC BY). The use, distribution or reproduction in other forums is permitted, provided the original author(s) and the copyright owner(s) are credited and that the original publication in this journal is cited, in accordance with accepted academic practice. No use, distribution or reproduction is permitted which does not comply with these terms.

Spatial variability in the abundance and prey selection of the corallivorous snail *Drupella* spp. in the southeastern Hainan Island, China

Xinming Lei[1,2,3], Chengyue Liu[1,2,3], Yuyang Zhang[1,2,3], Xiaolei Yu[1,3], Jianhui Yang[1,3], Yong Luo[1,3], Guowei Zhou[1,3]* and Hui Huang[1,2,3]*

[1]CAS Key Laboratory of Tropical Marine Bio-Resources and Ecology, Guangdong Provincial Key Laboratory of Applied Marine Biology, South China Sea Institute of Oceanology, Innovation Academy of South China Sea Ecology and Environmental Engineering, Chinese Academy of Sciences, Guangzhou, China, [2]Southern Marine Science and Engineering Guangdong Laboratory (Guangzhou), Guangzhou, China, [3]CAS-HKUST Sanya Joint Laboratory of Marine Science Research and Key Laboratory of Tropical Marine Biotechnology of Hainan Province, Tropical Marine Biological Research Station in Hainan, Chinese Academy of Sciences, Sanya, China

Global climate change has caused extensive loss of biodiversity and ecosystem function globally, particularly in coral reefs in shallow tropical waters. As the corallivorous snails represent considerable disturbances to coral reefs across Indo-Pacific region, it is becoming a threat to coral health and recovery in the Hainan Island, South China Sea, but current-knowledge gap remains on the spatial distribution, prey preferences, and the influence factors related. Thus, we investigated the abundance distribution of *Drupella* spp. in relation to coral-prey selectivity, availability, and nutritional value. The snail density was heterogeneously distributed in the study area with an average of 0.72 ± 0.32 ind m^{-2} (varying from 0.09 ± 0.03 to 1.78 ± 0.39 ind m^{-2}), and the snail density was found generally higher in locations with higher coral cover, which resulted in much lower density where their preferred corals became scarce. Despite the snails showing a positive preference for Acroporidae corals, they displayed dietary plasticity by changing with prey abundance and availability. Further, we found the electivity index of the coral prey related to the substrate types, and the nutritional value of prey was an additional important determinant in the prey preference, suggesting that the specific reef habitat and environmental context may alter the prey preference of *Drupella* spp. Combined, these results provide preliminary evidence that *Drupella* spp. is among the common corallivories in the reef regions of Hainan Island, and we recommend that large-scale monitoring programs assess the spatial-temporal trends to better

understand the dynamics of predation linked to both anthropogenic and natural impacts.

KEYWORDS

Corallivory, coral, prey selection, spatial variation, *Drupella*

Introduction

Coral reefs are highly biodiverse but are among the most threatened habitats on Earth, facing unprecedented risk from global climate change, overfishing, and pollution (Hughes et al., 2018; Wolff et al., 2018; MacNeil et al., 2019). Due to these anthropogenic and natural disturbances, coral reefs are continuously deteriorating across the world (Gardner et al., 2003; Hoegh-Guldberg et al., 2007; Hughes et al., 2017). Although individual environmental threats (e.g., temperature, pH) to coral reefs have been well studied, the negative effect of corallivores could aggravate the reef degradation process (Rice et al., 2019). To mitigate losses in coral cover, it is essential to seek to identify the ecological processes and make well-informed conservation decisions that promote coral survivorship.

Feeding activities of corallivores have negative effects on coral growth and fitness, varying from minor to lethal damage and subsequently leading to fundamental changes in the reef state (Turner, 1994b; Rotjan and Lewis, 2008; Rice et al., 2019). For instance, an outbreak of crown-of-thorns starfish (*Acanthaster* spp., COTS) has caused high-coral mortality and reduced coral cover by up to 80% (Pratchett et al., 2017). High densities of other corallivores such as *Coralliophila* spp. and *Drupella* spp. have been reported to impact corals strongly in the Indo-Pacific, Western Indian Ocean, and Asia (Moyer et al., 1982; Boucher, 1986; Mcclanahan, 1994; Bruckner et al., 2017).

The genus *Drupella* is among the well-known corallivores occurring on coral reefs of the Indo-Pacific Ocean (Turner, 1994b; Claremont et al., 2011). Generally, these corallivorous gastropods are found in coral reef regions at a low density of 0–2 ind m^{-2} (Cumming, 1999; Cumming 2009a), while the outbreak of *Drupella* could reduce the live coral cover by more than 75% in the coral reef areas with a mean density of 14.73 ± 4.37 ind m^{-2} (Turner, 1994a; Turner 1994b). There were large aggregation or outbreak events of *Drupella* spp. have been observed in various regions, including Western Australia (Ayling and Ayling, 1987; Turner, 1994b), Great Barrier Reef (Cumming, 1999), Red Sea (Antonius and Riegl, 1998), Kenya (Mcclanahan, 1994), Thailand (Moerland et al., 2016; Scott et al., 2017), Maldives (Bruckner et al., 2017) and Hong Kong (Cumming and McCorry, 1998; Morton and Blackmore, 2009). Both anthropogenic (overfishing of natural predators, coral reef damage, and terrestrial run-off) and natural (changes in temperature and salinity) causes have been proposed to explain these events (Turner, 1994b; Turner, 1994a; Cumming, 2009b; Cumming, 2009a).

Previous studies have reported that these corallivorous snails display significant feeding selectivity and are affected by the relative abundance of each coral taxon (Morton and Blackmore, 2009). Many corallivores exhibit high dietary plasticity with respect to their coral prey, feeding on less preferred corals when their favored corals are not abundant. For instance, *Drupella* spp. had shifted their dietary preference for coral species of Acroporidae and Pocilloporidae to the less preferred fungiid corals after a major coral bleaching event in Thailand (Hoeksema et al., 2013; Moerland et al., 2016). Nevertheless, Morton et al. (2002) found that the snails of *D. rugosa* still preferred the low-abundance coral *Acropora* spp. in the reefs of Hong Kong despite being primarily dominated by massive corals. Hence, the coral assemblage composition might influence their diet varies as well. Additionally, the importance of the nutritional value of the prey species to prey preference has received attention in COTS (Pratchett et al., 2014; Keesing, 2021), while the data on the food selectivity of *Drupella* spp. is scarce.

In recent years, the aggregations of four species of *Drupella* spp., named *D. cornus*, *D. rugose*, *D. fragum*, and *D. margariticola* (Zhang and Zhang, 2007; Peng et al., 2014), have been constantly observed in the reef regions of Hainan Island. However, information regarding the snail aggregation and the coral status in these reef regions is still limited. Furthermore, the coral reefs in Hainan Island have suffered more from coastal development, pollution, overfishing, and destructive fishing practices than climate change (Hughes et al., 2013), which resulted in the live coral cover of the fringing reefs declining by more than 80% up to now. Nevertheless, both coral loss and recovery vary between each reef due to the different occurrence of disturbances (Lian et al., 2010; Zhang et al., 2016; Huang et al., 2020), and consequently, variation in both coral species abundance and cover may influence the ecology of the related organisms such as corallivores, in different ways.

The impact of corallivores in Hainan Province has recently attracted scientific attention, focusing on the outbreaks of *A. planci* (Li et al., 2019a; Li et al., 2019b). However, no information

is available on the spatial distribution of *Drupella* spp., and the feeding ecology of these corallivorous snails is still poorly described in Hainan Island. The study aimed to investigate the distribution patterns and prey selection of *Drupella* spp. and the associated factors influencing its feeding preference in the southeastern Hainan Island. In particular, we tested the hypotheses that (1) the abundance distribution of *Drupella* spp. varies with coral abundance; and (2) reef substrate types and the nutritional value of coral prey are related to the prey selection of the corallivores.

Materials and methods

Study area

A field study was conducted from July 2019 to December 2020 along the coast of the southeastern Hainan Island, South China Sea. Our study area included five locations (Figure 1) with the intensive distribution of reef coral communities to enable convenient sampling and detection of *Drupella* spp. (Mollusca, Gastropoda, Muricidae).

Xiaozhou Island (XZD) and Xiaodonghai (XDH) are located at the east and west sides of the Luhuitou Peninsula of Sanya, respectively, and the marine environments are significantly affected severely by intensive human activities (e.g., coastal works, tourists activities, sewage discharges) (Titlyanov et al., 2019). Wuzhizhou Island (WZZ) is a small uninhabited island located about 2.7 km off the northern coast of Sanya. However, the marine environments are influenced by direct human activities (e.g., constructions, marine traffic, diving activities) (Huang et al., 2020). Fenjiezhou Island (FJZ) is a small island located at the junction of Lingshui County and Wanning City, and 2.2 km off the east coast of Hainan Island. Due to its exceptional coastal and diving tourism resources, the marine environment of this uninhabited island is affected by coastal construction, tourist activities, and disordered harvesting of marine resources, etc. (Bai et al., 2016). Dazhou Island (DZD) is another uninhabited small island located about 11 km away from the coast, and it has been the National Marine Ecological and Climatic Nature Reserve since September 1990. There are no constructive activity being conducting on it. Therefore, there are two types of sample sites among the five research stations: inshore sites (XZD and XDH) and offshore sites (WZZ, FJZ, and DZD).

Biological and environmental data collection

The shells of the snails are often encrusted with crustose coralline algae and other epifauna, which makes their *in situ* identification difficult. To avoid misidentification, the snail taxa were identified to the genus level and pooled as *Drupella* spp.

To examine the effects of variation in coral cover, abundance, and substrate pattern on the population structure, prey preferences, and spatial distribution of *Drupella* spp., we surveyed five locations along the southeast coast of Hainan Island. According to the accessibility of each site, three replicate belt transects of 20 m in length and 2.5 m on either side, lying parallel to the shoreline, were randomly selected at a depth of 1–3 m at each sample station. The survey depth was set in accordance with the previous studies, which reported that *Drupella* spp. is mainly distributed in shallower reef areas (Turner, 1994a; Cumming, 2009a; Scott et al., 2017; Hamman, 2018).

The benthic reef community composition was determined by the linear point intercept (LPI) method (Nadon and Stirling, 2006)

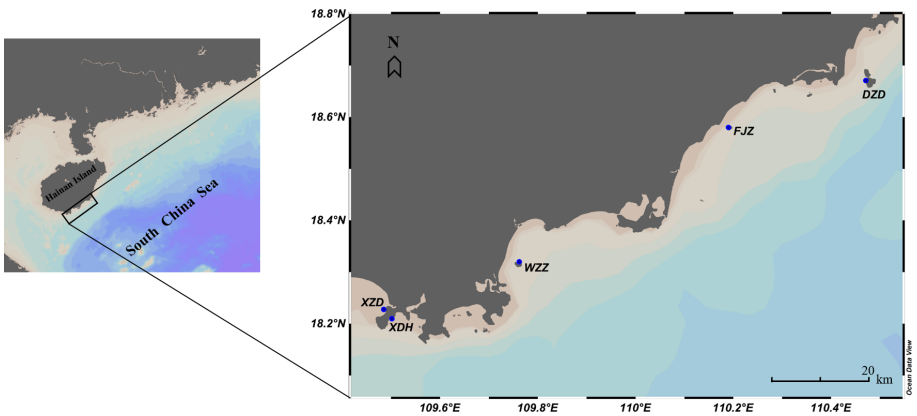


FIGURE 1
Research stations along the southeastern part of Hainan Island.

on the same belt transects. Within each transect, types of substrate were identified as live coral, dead coral, rock, sand, macroalgae, and other sessile invertebrates. During the survey, special emphasis was given to the substrate directly under the *Drupella* individuals, while the corals were identified to species level to study the detailed prey preference and to broad categories for all other substrate types. *Drupella* spp. was considered relating to corals whether they were in an aggregation over the living tissue or a dead part of a living coral colony or near the feeding scar, because they should move from one coral colony to another to find food or shelter (Cumming, 1999; Morton et al., 2002).

Statistical analysis

Statistical comparisons of the spatial variation of the predator density and percentage of live coral cover between stations were analyzed using the permutational multivariate analysis of variance (PERMANOVA) with 999 permutations. Furthermore, the feeding preferences of *Drupella* spp. were investigated using the Ivlev (1961) electivity index (E_i). E_i was estimated using the formula:

$$E_i = \frac{r_i - p_i}{r_i + p_i}$$

For this equation, r_i represents the proportion of prey in the diet and p_i represents the proportion of prey in the environment. Values of E_i range between 1 (maximum preference) and −1 (maximum avoidance), whereby 0 indicates random feeding. We calculated r_i as the frequency of corallivorous snails on a specific i species or genus of coral in relation to all the preyed colonies within each station.

The distribution and abundance of coral species, especially the species used as prey by *Drupella* spp., are likely to influence the distribution and abundance of the predator. Therefore, the similarity of coral species distribution for stations was analyzed using the ANOSIM test based on the Bray–Curtis similarity coefficient (Clarke and Gorley, 2015). Non-parametric multi-dimensional scaling (nMDS) ordinations were used to visualize the similarities and dissimilarities in coral community composition between stations, with a bubble plot showing the coral species preyed upon by *Drupella* spp. (E_i >0.5) in each sample station. We took the percentage of live coral cover as the relative abundance of corals at every station.

To explore the relationship between the electivity of coral prey and the benthic variables at each study station, we employed a nonparametric distance-based linear model (DISTLM) along with distance-based redundancy ordination analysis (dbRDA). The DISTLM models the relationship between these variables mentioned and the multivariate E_i of the coral dataset based on a multiple regression model as a way to determine the linear combination of variables that explains the greatest amount of variation in the elected coral community dataset, and it examines the amount of variance explained by each variable. Before analysis, benthic variable data were averaged, and a Draftsman plot was used to assess the collinearity between variables. Variables with a high degree of collinearity (Spearman's correlation coefficient |r| >0.85) were removed from the DISTLM analyses. Additionally, DISTLM was initially used to analyze the marginal effects of each variable, followed by the application of the "best" model building process with a R^2 selection to identify the best set of factors explaining the variation in the preferred coral community.

Additionally, principal component analysis (PCA) was used to investigate the features of the nutritional value of prey of the coral genus. The PCA multivariate analysis of the coral genera nutritional value of prey data, including lipid content (mg cm^{-2}), protein content (mg cm^{-2}), tissue biomass (ash-free dry weight, mg cm^{-2}), *Symbiodinium* density ($\times 10^6$ cells cm^{-2}), Chlorophyll-a content (Chl-a, μg cm^{-2}), tissue thickness (mm), and polyp density (polyps cm^{-2}). These data were obtained from the Coral Trait Database (Madin et al., 2016) and some published studies (Achituv et al., 1994; Loya et al., 2001; Anthony and Hoegh-Guldberg, 2003; Leuzinger et al., 2003; Edmunds et al., 2014; Qin et al., 2020; Keesing, 2021). The obtained species data were averaged as genus values, and the missing values were filled out using linear regression (Table S2).

All analyses were performed using PRIMER v7 software, including the PERMANOVA+ add-on package (Anderson et al., 2008; Clarke and Gorley, 2015).

Results

Abundance and spatial distribution

During the survey period, we counted individuals of *Drupella* spp. with an overall average density of 0.72 ± 0.32 ind m^{-2}. Snail density was higher at the offshore sites (WZZ, FJZ, and DZD) compared to the inshore sites (XZD, XDH) (Figure 2A). The variation of snail densities among the stations was found to be statistically significant ($p<0.05$), with mean densities ranging from 0.09 ± 0.03 ind m^{-2} at station XDH, up to 1.78 ± 0.39 ind m^{-2} at station DZD. Similarly, the percent live hard coral cover varied significantly among the stations as well ($p<0.05$), with the mean value ranging from 0.83 ± 0.60% at station XDH, up to 37.52 ± 0.07% at station WZZ (Figure 2B). The mean number of individuals per aggregation was 4.56 ± 1.28 for all *Drupella* spp. individuals pooled together; ranging from a minimum of 1 to a maximum of 38 individuals found on a single coral species, *Acropora hyacinthus* (at DZD).

There were 70 coral species in the total found among the five research stations (Table S1), of which 30 species belonging to 10 genera were preyed on by *Drupella* spp. (Tables 1, 2). The number of coral species ranged from four at XDH to 38 at WZZ, and the other benthic reef substrate variables showed

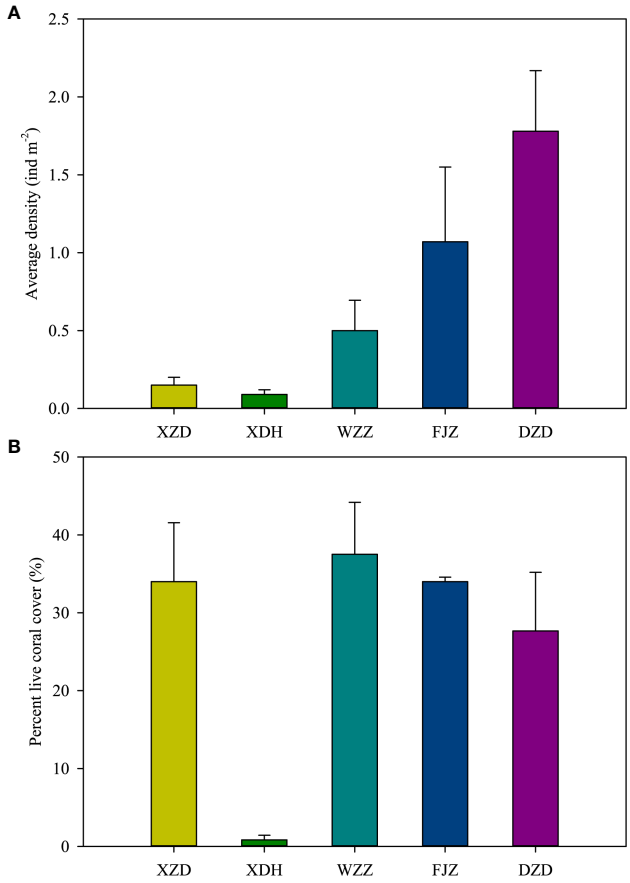


FIGURE 2
Spatial differences in **(A)** average snail density and **(B)** average percent live coral cover for each station. Bars indicate standard error.

significant differences among the research stations, except for sand, macroalgae, and the other sessile invertebrates (Table 3). The top three genera with the highest proportion at each station were *Favites* (30.39%), *Acropora* (25.00%), and *Platygyra* (15.20%) in XZD, *Oulastrea* (40.00%), *Montipora* (20.00%), and *Favites* (20.00%) in XDH, *Porites* (32.16%), *Acropora* (24.78%), and *Montipora* (13.19%) in WZZ, *Galaxea* (37.09%), *Porites* (24.48%), and *Platygyra* (7.09%) in FJZ, *Acropora* (22.29%), *Favites* (17.47%), and *Acanthastrea* (12.05%) in DZD, respectively. The coral community structure varied significantly among the research stations (ANOSIM, global R = 0.62, p = 0.001) (Figure 3).

Prey selection and preferences

Prey preference varied at different stations according to the availability of coral prey. Coral species belonging to the family Acroporidae (*Acropora* and *Montipora*) were all preferred positively by *Drupella* spp. among the sample stations. Considering the preferred coral prey (E_i >0.5 at any station) of the snail, there were 20 coral species, and the abundance and distribution of these species were different in the sample stations (ANOSIM, global R = 0.52, p = 0.001), with species *A. gemmifera*, *Montipora* sp., and *P. lobata* being more abundant in the stations XZD and DZD, while the other eight species (*A. cytherea*, *A. formosa*, *A. hyacinthus*, *A. intermedia*, *Acropora* sp., *G. fascicularis*, *Goniastrea* sp., and *Porites* sp.) were more abundant in the stations WZD and FJZ (Figure 3, Table 1).

Species belonging to the genera *Acropora*, *Echinophyllia*, *Favites*, *Montipora*, and *Pocillopora* had positive values of the electivity index (E_i) in the five sample stations, while the other species had at least one negative value of the index in all stations (Table 1). At the genus level, all the genera of coral prey had positive values of E_i in the sample stations, except for the genera of *Galaxea*, *Porites*, *Platygyra*, and *Lobophyllia*, which were the avoided prey by *Drupella* spp. in the station FJZ (Table 2).

TABLE 1 Feeding preferences of *Drupella* spp. according to the Ivlev's electivity index (E_i) considering the coral species preyed upon at each station.

Species	XZD	XDH	WZZ	FJZ	DZD
Acropora cytherea	–	–	0.79	–	–
Acropora digitifera	–	–	–	–	1.00
Acropora formosa	–	–	0.79	–	1.00
Acropora gemmifera	–	–	1.00	–	–
Acropora hyacinthus	–	–	–	–	1.00
Acropora intermedia	–	1.00	0.74	–	1.00
Acropora microclados	–	–	–	–	1.00
Acropora robusta	0.09	–	–	–	–
Acropora sp.	–	–	1.00	0.77	–
Echinophyllia aspera	–	–	–	0.58	–
Favites abdita	0.18	–	–	0.58	–
Favites flexuosa	–	–	–	0.58	–
Favites micropentagonus	0.58	–	–	–	–
Favites sp.	0.04	–	–	–	–
Galaxea fascicularis	–	–	0.33	−0.10	0.73
Goniastrea retiformis	–	–	–	−0.14	–
Goniastrea sp.	–	–	–	1.00	–
Lobophyllia corymbosa	–	–	–	−0.03	–
Montipora efflorescens	–	–	–	1.00	–
Montipora informis	–	–	–	–	1.00
Montipora sp.	–	–	–	0.77	–
Montipora turgescens	–	–	–	1.00	–
Montipora venosa	0.01	–	–	–	–
Platygyra pini	0.40	–	–	–	–
Platygyra sinensis	–	–	–	−0.33	–
Platygyra sp.	−0.11	–	–	–	–
Pocillopora damicornis	0.30	–	–	–	0.31
Porites lobata	–	–	–	–	1.00
Porites lutea	–	–	–	−0.20	−0.22
Porites sp.	–	–	–	–	1.00

XZD, Xiaozhoudao; XDH, Xiaodonghai; WZZ, Wuzhizhou; FJZ, Fenjiezhou; DZD, Dazhoudao.

TABLE 2 Feeding preferences of *Drupella* spp. according to the Ivlev's Electivity Index (E_i) considering the coral genera preyed upon at each station.

Genera	XZD	XDH	WZZ	FJZ	DZD
Acropora	0.09	1.00	0.82	0.77	1.00
Montipora	0.01	–	–	0.85	1.00
Galaxea	–	–	0.33	−0.10	0.73
Echinophyllia	–	–	–	0.58	–
Favites	0.30	–	–	0.58	–
Pocillopora	0.30	–	–	–	0.31
Porites	–	–	–	−0.20	0.31
Goniastrea	–	–	–	0.20	–
Platygyra	0.09	–	–	−0.33	–
Lobophyllia	–	–	–	−0.03	–

XZD, Xiaozhoudao; XDH, Xiaodonghai; WZZ, Wuzhizhou; FJZ, Fenjiezhou; DZD, Dazhoudao.

10.3389/fmars.2022.990113

TABLE 3 Benthic reef substrate variables at each station. mean ± SE.

Variable	XZD	XDH	WZZ	FJZ	DZD	p-value
Average live coral cover	34.00 ± 7.57	0.83 ± 0.60	37.52 ± 6.68	34.00 ± 0.58	27.67 ± 7.54	<0.001
Number of coral species	21 ± 2.2	4 ± 0.9	38 ± 2.5	30 ± 2.3	22 ± 2.1	0.003
Dead coral cover	2.50 ± 0.00	66.50 ± 15.40	43.56 ± 3.09	35.00 ± 0.00	2.50 ± 1.61	<0.001
Rock	59.50 ± 6.51	0.00 ± 0.00	3.00 ± 3.00	4.00 ± 0.00	49.50 ± 5.11	<0.001
Sand	0.67 ± 0.67	6.34 ± 3.28	6.33 ± 4.10	7.00 ± 0.00	12.17 ± 11.43	0.67
Other sessile invertebrate	3.33 ± 2.03	0.00 ± 0.00	9.42 ± 5.89	19.50 ± 0.00	8.17 ± 2.05	0.23
Macroalgae	0.00 ± 0.00	26.33 ± 14.17	0.17 ± 0.17	0.50 ± 0.00	0.00 ± 0.00	0.07

XZD, Xiaozhoudao; XDH, Xiaodonghai; WZZ, Wuzhizhou; FJZ, Fenjiezhou; DZD, Dazhoudao.

Relationship between feeding behavior and benthic variables

The benthic variables were different among the sample stations (SIMPEROF, global π = 0.59, p = 0.001). The Draftsman plots indicated that the number of coral species, other sessile invertebrate and macroalgae were all highly correlated with live coral cover (|r| >0.85, Table S3), and so these variables were excluded from the DISTLM analysis. Additionally, as the dead coral cover was highly correlated with rock (r = −0.95, Table S3), the rock was kept in the analysis based on the forward factor selection process.

The DISTLM analysis indicated that the three benthic variables, including live coral cover, rock, and sand, had a strong relationship with the electivity index of the coral prey at the research stations, although the marginal test showed no statistical significance (p >0.05). The dbRDA included vectors corresponding to these three variables on two axes that explained 91.6% of the fitted variation and 62.4% of the total variation (Figure 4). When considering the variables alone and ignoring all other variables, sand contributed to explaining the highest percentual variance, accounting for 21.03% of the variability in the coral prey communities, followed by rock, accounting for 13.51%, and live coral cover, accounting for 8.79%. The samples corresponding to the relatively high live coral cover stations were distributed along the dbRDA1 axis, while the samples of the different types of stations were dispersed along the dbRDA2 axis.

Comparative analysis of food value of coral prey

PCA analyses revealed that the coral prey species fell into four significantly different groups (Figure 5). The first group comprised the genus *Montipora*, characterized by high Chl-a content and delivering high-polyp density, tissue biomass, and a low *Symbiodinium* density. The second group, comprising the genera *Acropora*, *Pocillopora*, and *Porites*, fell out together along axes of high *Symbiodinium* density, low Chl-a content, and

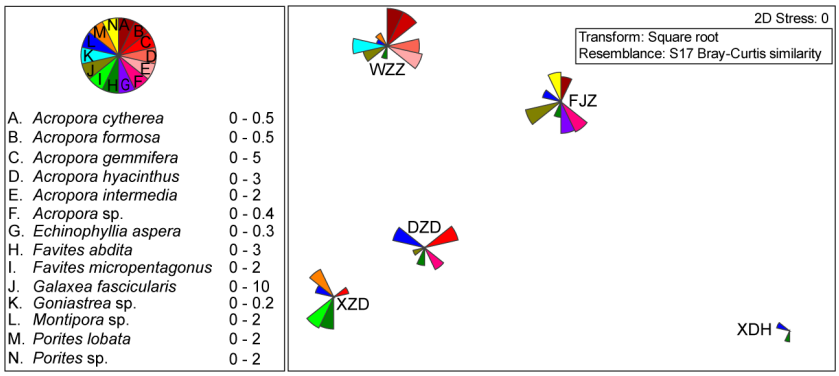


FIGURE 3
Non-parametric multi-dimensional scaling (nMDS) ordinations visualized the similarities and dissimilarities in coral community composition (living coral cover served as the abundance) between stations, with a bubble plot showing the live cover of the coral species preferred by *Drupella* spp. (Ei >0.5 at any station) in each sample station (XZD, Xiaozhoudao; XDH, Xiaodonghai; WZZ, Wuzhizhou; FJZ, Fenjiezhou; and DZD, Dazhoudao).

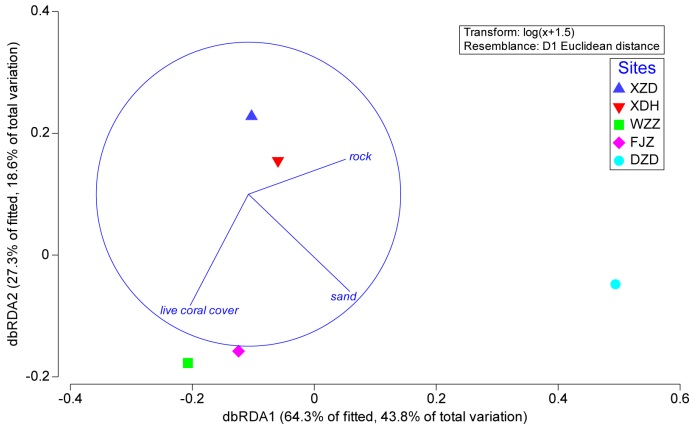


FIGURE 4
Distance-based redundancy analysis (dbRDA) of the Iviev's electivity index (E_i) considering the coral prey for each station shows vector overlays of coral species preyed included in the best model by DISTLM analysis (XZD, Xiaozhoudao; XDH, Xiaodonghai; WZZ, Wuzhizhou; FJZ, Fenjiezhou; DZD, Dazhoudao).

delivering high-polyp density. The third group, comprising the genera *Favites*, *Galaxea*, and *Platygyra*, was correlated with high-tissue thickness, low-polyp density, and delivered high-lipid content and *Symbiodinium* density. The fourth group comprised the genera *Goniastrea* and *Lobophyllia*, characterized by high-lipid content, protein content, and tissue biomass, and delivered high-tissue thickness, high Chl-a content, and low-polyp density.

Discussion

In recent years, the overabundance of corallivores has become an increasing threat to coral reef ecosystems across the Indo-Pacific Ocean. In the South China Sea, especially in the near-shore coral reef area, more and more aggregations of *Drupella* spp. have been observed, which would become a potential roadblock to the regional efforts to recover and restore the degraded coral communities in China. This study revealed the spatial differences in density and prey selection of the corallivorous snail *Drupella* spp. in the southeastern Hainan Island, South China Sea. Prey preferences of *Drupella* spp. vary in different stations according to the abundance and availability of coral prey. Corals of the family Acroporidae were preferred positively by *Drupella* spp. among all research stations, and their favored coral preys are of meaty, nutrition-packed, and vegetarian characteristics. Benthic variables, including live coral cover, rock, and sand, had a strong relationship with the coral prey communities among the research stations.

In this study, the overall mean density of *Drupella* spp. was lower than that in previous studies (Ayling and Ayling, 1987; Turner, 1994a; Cumming, 1999; Cumming, 2009b; Schoepf et al., 2010; Moerland et al., 2016), but higher than that in a recent study (Saponari et al., 2021). The corallivores did not outbreak because the mean density in each study site (0.09–1.78 ind m^{-2}) never exceeded the outbreak threshold of >3 ind m^{-2} defined by (Cumming 2009a; Cumming, 2009b). However, the mean density exceeded the level of 0.62 ind m^{-2} suggested by Bessey et al. (2018) that the snails could outbreak on their preferred coral species if the density exceeded this level. In particular, we found there was a maximum of 38 individuals of a single coral species, *Acropora hyacinthus* at DZD. Thus, the high current density of the snails remained potentially destructive to the coral communities in the study regions.

The heterogeneity in the density of *Drupella* spp. recorded at different sites may have been responsible for the anthropogenic activities, such as over-fishing or boating traffic (Ayling and Ayling, 1987; Turner, 1994a), especially the coral collapse in XDH. Additionally, the snail density was found to be higher in the stations with relatively high coral cover than that in the stations with low coral cover across all sites surveyed, such as in FJZ and DZD, independently of the number of coral species. This finding was consistent with the theory of optimal foraging, which assumed that predators fed in such a way as to trade-off between the alternative available prey abundances (Cumming, 2009a; Keesing, 2021). However, we found that the coral cover was relatively high in XZD but with lower snail density. Hence, these between-site variations in the densities of *Drupella* were apparently not just dependent on the differences in the live coral cover at each station. Specifically, our statistical results indicated that the live coral cover only contributed to explaining the percentual variance of 8.79% for the electivity index of the

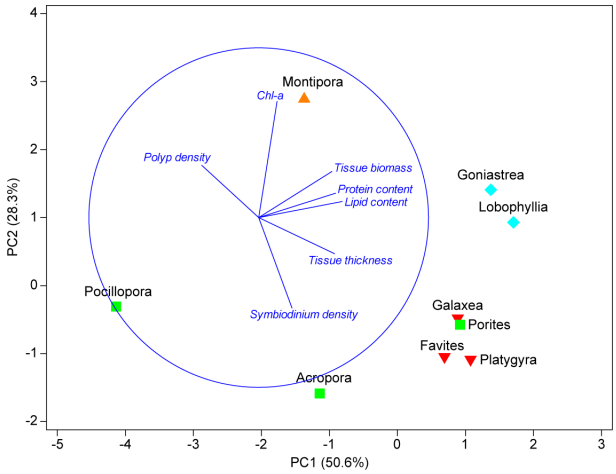


FIGURE 5
Principal components analysis (PCA) plot of multivariate analysis of coral genera nutritional value of prey data: lipid content, protein content, tissue biomass, *Symbiodinium* density, Chl-a content, tissue thickness, and polyp density. PCA analyses are based on the data obtained from the Coral Trait Database and published studies. The missing values were filled using a linear regression. The genus *Echinophyllia* was excluded in these analyses because the data were not available. The triangle, upside-down triangle, square, and diamond symbols indicate the four groups of significant different coral genera based on the SIMPEROF test.

coral prey, which highlights that the coral cover would not always be the main factor. Additionally, the different abundance of their preferred coral species (*Acropora* and *Montipora*) in each station may have been responsible (Morton and Blackmore, 2009). Although they are more mobile, the encounter probability with their preferred prey is probably an additional explanation. Thus, factors other than the live coral cover are probably important in controlling the density of *Drupella* in different reef regions.

For instance, the highest proportion of the coral taxa we found in each research station may be involved in the impact factors. For instance, the highest proportion of the genera *Favites* resulted in positive feeding in XZD, although they are the massive growth form of corals. Prior studies reported that the coral growth forms and intraspecific attraction probably played additional roles in the food selection of *Drupella* spp. (McClanahan, 1997; Schoepf et al., 2010). Corals with branching growth forms were always used as food and shelter (Ayling and Ayling, 1987; Hamman, 2018), especially for the juvenile snail *Drupella* spp. (McClanahan, 1997; Schoepf et al., 2010; Hamman, 2018).

Our study showed there were significant differences in the coral community composition among the research stations. The different *Drupella* densities in each site were probably correlated to the distribution pattern of the coral assemblage (Schoepf et al., 2010). Moreover, variation among coral assemblages has also been linked to the snail relative density because the abundance and distribution of their preferred coral prey were different in each sample station. Specifically, the low abundance of their preferred prey (*Acropora* and *Montipora*) at XZD was probably responsible for the low density of *Drupella*. Previous studies revealed that a decrease in the abundance of preferred coral species might result in a higher density of snails in the reefs (Schoepf et al., 2010). Nonetheless, *Acropora* abundance does not always explain the distribution pattern of *Drupella* (Turner, 1994b), for the snails could aggregate on the remaining corals if the coral population decreased (Hoeksema et al., 2013; Saponari et al., 2021).

Results from our analysis of spatially explicit data of 30 prey species demonstrated that the corallivorous snail displayed dietary plasticity, consistent with the previous findings that they were able to switch to their less preferred corals in the areas where their preferred prey became scarce (Turner, 1994b; Shafir et al., 2008; Schoepf et al., 2010; Hoeksema et al., 2013; Tsang and Ang, 2015; Saponari et al., 2021). In this study, we found coral species of the family Acroporidae were preyed on positively where the abundance of them was relatively high, such as at WZZ, FJZ, and DZD. However, the snails were confined to their less favorite prey. For instance, they had to prey on *Favites* spp. and *Platygyra* spp. when the coral species of Acroporidae were less available at XZD. Similarly, previous observations revealed that *Drupella* were restricted to preying on massive or encrusting corals where branching corals were not available (Mcclanahan, 1994; Cumming and McCorry, 1998; Morton et al., 2002; Hoeksema et al., 2013; Moerland et al., 2016). Moreover, as found in our study, the snails were found

expanding their prey range from branching corals (*Acropora* and *Pocillopora*) to a few massive corals (*Porites*, *Favites*, *Galaxea*, etc.) in the Maldives (Bruckner et al., 2017; Saponari et al., 2021) according to the availability of their preferred prey.

Interestingly, previous studies found that some coral species that were not preferentially preyed upon by *Drupella*, such as corals of the genus *Porites* (Morton et al., 2002; Hamman, 2018), while they had a positive tendency to be preyed on in the station DZD in this investigation. These results showed that the complex change of coral community composition in this study area influenced the predation preference of the snail *Drupella*. Additionally, during the survey period, we also found the snails preferred aggregating near the freshly damaged tissues of the corals, which supports evidence from previous observations (Morton et al., 2002; Bright et al., 2015; Bruckner et al., 2017; Hamman, 2018). Kita et al. (2005) reported that the chemicals in the mucus released by damaged coral tissue showed potent feeding-attractant activity toward *D. cornus*.

Besides the influence factors to the prey preferences of the snail *Drupella* spp. proposed by previous studies above, other researches indicated that coral growth forms, such as branching growth form, could strongly influence their feeding preferences (Turner, 1994a; Cumming and McCorry, 1998; Cumming, 1999; Schoepf et al., 2010; Saponari et al., 2021). In this research, we found that benthic variables, including live coral cover, rock, and sand, had a strong relationship with the electivity index of the coral prey at the research stations. This indicated that the substrata condition played an important role in determining the prey preference of *Drupella* spp. This finding is consistent with the reports that the snails showed different reef habitat preferences (Turner, 1994a; Cumming, 1999), such as a high cover of rubble and dead coral (Moerland et al., 2016). However, the correlation was not statistically significant in the present study. This was presumably due to the insufficient sample collection and/or some remaining unclear drivers, although various aspects had been discussed in previous studies, such as coral communities (Morton and Blackmore, 2009; Schoepf et al., 2010; Saponari et al., 2021); depth (Schoepf et al., 2010; Saponari et al., 2021); reef status (Mcclanahan, 1994; Morton et al., 2002). Furthermore, prey selection by *Drupella* spp. could not only be considered in the multivariable analysis because coral species tested were insufficient. Additionally, environmental stressors, including elevated seawater temperature, reduced salinity, mechanical damage, and coral diseases, were also correlated with the feeding preference of *Drupella* (Morton et al., 2002; Al-Horani et al., 2011; Nicolet et al., 2013; Tsang and Ang, 2019).

The comparative analysis suggested that the preferred coral genera were composed of the theoretically favorable traits of high nutritional value, such as high protein content, lipid content, tissue biomass, and thickness. (Keesing, 2021; Keesing, 1990) reported that the nutritional value of coral prey was an important determinant in the evolution of the prey preferences of crown-of-thorns starfish. Our results here demonstrate that the favored coral preys of *Drupella* spp. were among those with high nutritional value, e.g., high protein content, lipid content, tissue biomass, and thickness. In particular, their preferred corals (*Acropora* and *Montipora*) contained high Chl-a content, *Symbiodinium* density, polyp density, and intermediate tissue nutritional value. These indicated that, to a certain extent, the corallivorous snails were smart and their preferred coral prey were full of nutritional value with the features of being meaty, energy-enriching, and vegetarian. However, the location of energy reserves in the coral tissue varied from species to species. For instance, the lipid was typically deposited in the basal half to one-third of the polyp column in hard corals (Stimson, 1987). This would explain why the corals with massive growth form, such as *Porites* spp., had resulted in a random prey choice, because the lipid reserved in polyps penetrating further down into the skeleton (Keesing, 2021). This suggests that linking feeding preference to food nutritional value for *Drupella* spp. feeding on numerous coral species in such a complex environment as coral reef requires more than an assessment of the absolute nutritional content of food.

Conclusions

Overall, our surveys revealed that the abundance of corallivorous snails, *Drupella* spp., varied spatially on the reefs throughout southeastern Hainan Island, South China Sea, while the snail density was found generally related to coral cover, independent of the number of coral species. However, the high coral cover was not always responsible for the high density of the snails. *Drupella* spp. showed a positive preference for Acroporidae corals, and random choice resulted for *Porites*, *Galaxea*, *Platygyra*, and *Lobophyllia* corals, when their favored taxa were abundant in situ. The results of our study suggest that the prey preference of *Drupella* spp. exhibits a dietary plasticity according to the abundance and availability of their favored coral prey, as well as the encounter probability between them. Furthermore, benthic types, including live coral cover, rock, and sand, had a strong relationship with the electivity index of the coral prey, reflecting the prey preference of *Drupella* spp. related to the substrata condition. The nutritional value of coral preys was an additional important determinant in their prey preference, while the location of the nutrient deposits in the corals and the complex environmental context should not be ignored.

As the corals in the shallow water suffering increasing influences, further works should focus on larger geographical areas, and expend to the deeper areas of the coral reefs to make a better understanding of the spatial distribution of *Drupella* spp. In addition, the prey preference and the microhabitat use in each

life stage should be well studied. With the future research on how to increase the local predators of the corallivorous snails, there will be more benefit to reducing the cost and need for human interventions.

Data availability statement

The original contributions presented in the study are included in the article/Supplementary Material. Further inquiries can be directed to the corresponding authors. Data pertaining to this study are available at South China Sea Ocean Data Center, National Earth System Science Data Center, National Science & Technology Infrastructure of China(http://data.scsio.ac.cn/metaData-detail/1534808395246669824)..

Author contributions

XL: Conceptualization, methodology, investigation, data acquisition and curation, formal analysis, and writing-original draft. CL: Investigation, data acquisition and curation, writing-review and editing. YZ: Analytic tools, investigation, data acquisition, and curation. XY: Investigation, data acquisition, and curation. JY: Investigation, data acquisition, and curation. YL: Investigation, data acquisition, and curation. GZ: Methodology, funding, supervision, writing–review and editing. HH: Funding, supervision, writing–review and editing. All authors contributed to the article and approved the submitted version.

Acknowledgments

This research was funded by the National Natural Science Foundation of China (41876192, 41976120), the Guangdong Basic and Applied Basic Research Foundation (2019A1515011532 and 2019A1515111045), the Key Research and Development Project of Hainan Province, China (ZDYF2020200), the Science and Technology Planning Project of Guangdong Province, China (2020B1212060058), the Innovation Academy of South China Sea Ecology and Environmental Engineering, Chinese Academy of Sciences (ISEE2021ZD03), and the Key Special Project for Introduced Talent Teams of Southern Marine Science and Engineering Guangdong Laboratory (Guangzhou) (GML2019ZD0404). The authors thank the staff of Tropical Marine Biological Research Station in Hainan for their logistical and administrative support. We appreciate the constructive comments from the reviewers and the editor who have greatly improved the initial manuscript. We also thank the data archive support from the National Earth System Data Center, National Science & Technology Infrastructure of China (http://www.geodata.cn).

Conflict of interest

The authors declare that the research was conducted in the absence of any commercial or financial relationships that could be construed as a potential conflict of interest.

Publisher's note

All claims expressed in this article are solely those of the authors and do not necessarily represent those of their affiliated organizations, or those of the publisher, the editors and the reviewers. Any product that may be evaluated in this article, or claim that may be made by its manufacturer, is not guaranteed or endorsed by the publisher.

Supplementary material

The Supplementary Material for this article can be found online at: https://www.frontiersin.org/articles/10.3389/fmars.2022.990113/full#supplementary-material

References

Achituv, Y., Ben-Zion, M., and Mizrahi, L. (1994). Carbohydrate, lipid, and protein composition of zooxanthellae and animal fractions of the coral pocillopora damicornis exposed to ammonium enrichment. *Pacific Sci.* 48 (3), 224–233.

Al-Horani, F. A., Hamdi, M., and Al-Rousan, S. A. (2011). Prey selection and feeding rates of drupella cornus (Gastropoda: Muricidae) on corals from the Jordanian coast of the gulf of aqaba, red Sea. *Jordan J. Biol. Sci.* 4 (4), 191–198.

Anderson, M. J., Gorley, R. N., and Clarke, K. R. (2008). *PERMANOVA+ for PRIMER: Guide to software and statistical methods* (Plymouth, UK: PRIMER-E Ltd).

Anthony, K. R. N., and Hoegh-Guldberg, O. (2003). Variation in coral photosynthesis, respiration and growth characteristics in contrasting light microhabitats: an analogue to plants in forest gaps and understoreys? *Funct. Ecol.* 17, 246–259. doi: 10.1046/j.1365-2435.2003.00731.x

Antonius, A., and Riegl, B. (1998). Coral diseases and drupella cornus invasion in the red Sea. *Coral Reefs* 17 (1), 48–48. doi: 10.1007/s003380050093

Ayling, T., and Ayling, A. L. (1987). *Ningaloo marine park: preliminary fish density assessment and habitat survey: with information on coral damage due to drupella cornus grazing* (Western Australia: Department of Conservation and Land Management).

Bai, L., Zhao, Z., Liu, Q., and Cui, J. (2016). Investigation on shellfish species living in the intertidal zone to subtidal zone of fenjiezhou island of hainan. *Agric. Sci. Technol.* 17 (5), 1204–1210. doi: 10.16175/j.cnki.1009-4229.2016.05.037

Bessey, C., Babcock, R. C., Thomson, D. P., and Haywood, M. D. E. (2018). Outbreak densities of the coral predator drupella in relation to *in situ* acropora

growth rates on ningaloo reef, Western Australia. *Coral Reefs* 37 (4), 985–993. doi: 10.1007/s00338-018-01748-7

Boucher, L. M. (1986). Coral predation by muricid gastropods of the genus drupella at enewetak, Marshall islands. *Bull. Mar. Sci.* 38 (1), 9–11.

Bright, A. J., Cameron, C. M., and Miller, M. W. (2015). Enhanced susceptibility to predation in corals of compromised condition. *PeerJ* 3, e1239. doi: 10.7717/peerj.1239

Bruckner, A. W., Coward, G., Bimson, K., and Rattanawongwan, T. (2017). Predation by feeding aggregations of drupella spp. inhibits the recovery of reefs damaged by a mass bleaching event. *Coral Reefs* 36 (4), 1181–1187. doi: 10.1007/s00338-017-1609-2

Claremont, M., Reid, D. G., and Williams, S. T. (2011). Evolution of corallivory in the gastropod genus drupella. *Coral Reefs* 30 (4), 977–990. doi: 10.1007/s00338-011-0788-5

Clarke, K. R., and Gorley, R. N. (2015). *Primer v7: User Manual/Tutorial* (Plymouth, UK: PRIMER-E Ltd).

Cumming, R. L. (1999). Predation on reef-building corals: multiscale variation in the density of three corallivorous gastropods, drupella spp. *Coral Reefs* 18 (2), 147–157. doi: 10.1007/s003380050170

Cumming, R. L. (2009a). *Case study: impact of drupella spp. on reef-building corals of the great barrier reef* (Townsville, QLD, Australia: Great Barrier Reef Marine Park Authority).

Cumming, R. L. (2009b). *Population outbreaks and large aggregations of drupella on the great barrier reef* (Townsville, QLD, AustraliaGreat Barrier Reef Marine Park Authority).

Cumming, R. L., and McCorry, D. (1998). Corallivorous gastropods in Hong Kong. *Coral Reefs* 17 (2), 178–178. doi: 10.1007/s003380050112

Edmunds, P. J., Burgess, S. C., Putnam, H. M., Baskett, M. L., Bramanti, L., Fabina, N. S., et al. (2014). Evaluating the causal basis of ecological success within the scleractinia: an integral projection model approach. *Mar. Biol.* 161 (12), 2719–2734. doi: 10.1007/s00227-014-2547-y

Gardner, T. A., Cote, I. M., Gill, J. A., Grant, A., and Watkinson, A. R. (2003). Long-term region-wide declines in Caribbean corals. *Science* 301 (5635), 958–960. doi: 10.1126/science.1086050

Hamman, E. A. (2018). Aggregation patterns of two corallivorous snails and consequences for coral dynamics. *Coral Reefs* 37 (3), 851–860. doi: 10.1007/s00338-018-1712-z

Hoegh-Guldberg, O., Mumby, P. J., Hooten, A. J., Steneck, R. S., Greenfield, P., Gomez, E., et al. (2007). Coral reefs under rapid climate change and ocean acidification. *Science* 318 (5857), 1737–1742. doi: 10.1126/science.1152509

Hoeksema, B. W., Scott, C., and True, J. D. (2013). Dietary shift in corallivorous drupella snails following a major bleaching event at koh Tao, gulf of Thailand. *Coral Reefs* 32 (2), 423–428. doi: 10.1007/s00338-012-1005-x

Huang, J. Z., Wang, F. X., Zhao, H. W., Xu, H. L., Liu, S., Xu, Q., et al. (2020). Reef benthic composition and coral communities at the wuzhizhou island in the south China Sea: The impacts of anthropogenic disturbance. *Estuarine Coast. Shelf. Sci.* 243, 106863. doi: 10.1016/j.ecss.2020.106863

Hughes, T. P., Barnes, M. L., Bellwood, D. R., Cinner, J. E., Cumming, G. S., Jackson, J. B. C., et al. (2017). Coral reefs in the anthropocene. *Nature* 546 (7656), 82–90. doi: 10.1038/nature22901

Hughes, T. P., Huang, H., and Young, M. A. L. (2013). The wicked problem of china's disappearing coral reefs. *Conserv. Biol.* 27 (2), 261–269. doi: 10.1111/j.1523-1739.2012.01957.x

Hughes, T. P., Kerry, J. T., Baird, A. H., Connolly, S. R., Dietzel, A., Eakin, C. M., et al. (2018). Global warming transforms coral reef assemblages. *Nature* 556 (7702), 492–496. doi: 10.1038/s41586-018-0041-2

Keesing, J. K. (1990). *Feeding biology of the crown-of-thorns starfish, acanthaster planci (Linnaeus) doctor PhD, James cook university*.(Townsville: James Cook University of North Queensland).

Keesing, J. K. (2021). Optimal foraging theory explains feeding preferences in the Western pacific crown-of-thorns sea star acanthaster sp. *Biol. Bull.* 241 (3), 303–329. doi: 10.1086/718141

Kita, M., Kitamura, M., Koyama, T., Teruya, T., Matsumoto, H., Nakano, Y., et al. (2005). Feeding attractants for the muricid gastropod drupella cornus, a coral predator. *Tetrahedron Lett.* 46 (49), 8583–8585. doi: 10.1016/j.tetlet.2005.09.182

Leuzinger, S., Anthony, K. R., and Willis, B. L. (2003). Reproductive energy investment in corals: scaling with module size. *Oecologia* 136 (4), 524–531. doi: 10.1007/s00442-003-1305-5

Lian, J. S., Huang, H., Huang, L. M., and Wang, D. R. (2010). *Coral reef and its biodiversity of sanya* (Beijing: Marine Press).

Li, Y. C., Liang, J. L., Wu, Z. J., and Chen, S. Q. (2019a). Outbreak and prevention of acanthaster planci (in Chinese). *Ocean Dev. Manag.* 8, 9–12.

Li, Y. C., Wu, Z. J., Liang, J. L., Chen, S. Q., and Zhao, J. M. (2019b). Analysis on the outbreak period and cause of acanthaster planci in xisha islands in recent 15 years (in Chinese). *Chin. Sci. Bull.* 64, 3478–3484. doi: 10.1360/TB-2019-0152

Loya, Y., Sakai, K., Yamazato, K., Nakano, Y., Sambali, H., and van Woesik, R. (2001). Coral bleaching: the winners and the losers. *Ecol. Lett.* 4 (2), 122–131. doi: 10.1046/j.1461-0248.2001.00203.x

MacNeil, M. A., Mellin, C., Matthews, S., Wolff, N. H., McClanahan, T. R., Devlin, M., et al. (2019). Water quality mediates resilience on the great barrier reef. *Nat. Ecol. Evol.* 3 (4), 620–627. doi: 10.1038/s41559-019-0832-3

Madin, J. S., Anderson, K. D., Andreasen, M. H., Bridge, T. C., Cairns, S. D., Connolly, S. R., et al. (2016). The coral trait database, a curated database of trait information for coral species from the global oceans. *Sci. Data* 3, 160017. doi: 10.1038/sdata.2016.17

Mcclanahan, T. R. (1994). Coral-eating snail drupella cornus population increases in Kenyan coral reef lagoons. *Mar. Ecol. Prog. Ser.* 115 (1-2), 131–137. doi: 10.3354/meps115131

McClanahan, T. R. (1997). Dynamics of drupella cornus populations on Kenyan coral reefs. *Proc. 8th Coral Reef. Sym.* 1, 633–638.

Moerland, M. S., Scott, C. M., and Hoeksema, B. W. (2016). Prey selection of corallivorous muricids at koh Tao (Gulf of Thailand) four years after a major coral bleaching event. *Contrib. Zool.* 85 (3), 291–309. doi: 10.1163/18759866-08503003

Morton, B., and Blackmore, G. (2009). Seasonal variations in the density of and corallivory by drupella rugosa and cronia margariticola (Caenogastropoda: Muricidae) from the coastal waters of Hong Kong: 'plagues' or a'ggregations'? *J. Mar. Biol. Assoc. U. K.* 89 (1), 147–159. doi: 10.1017/s002531540800218x

Morton, B., Blackmore, G., and Kwok, C. T. (2002). Corallivory and prey choice by drupella rugosa (Gastropoda : Muricidae) in Hong Kong. *J. Molluscan Stud.* 68, 217–223. doi: 10.1093/mollus/68.3.217

Moyer, J. T., Emerson, W. K., and Ross, M. (1982). Massive destruction of scleractinian corals by the muricid gastropod, drupella in Japan and the Philippines. *Nautilus* 96 (2), 69–82.

Nadon, M. O., and Stirling, G. (2006). Field and simulation analyses of visual methods for sampling coral cover. *Coral Reefs* 25 (2), 177–185. doi: 10.1007/s00338-005-0074-5

Nicolet, K. J., Hoogenboom, M. O., Gardiner, N. M., Pratchett, M. S., and Willis, B. L. (2013). The corallivorous invertebrate drupella aids in transmission of brown band disease on the great barrier reef. *Coral Reefs* 32 (2), 585–595. doi: 10.1007/s00338-013-1010-8

Peng, F. M., Wu, Z. H., Shen, Y. C., Li, Z. M., and Liu, L. (2014). Systematic observation on morphological structure of drupella margariticola (Broderip 1833). *J. Guangdong Ocean Univ.* 34 (6), 12–17.

Pratchett, M. S., Caballes, C. F., Rivera-Posada, J. A., and Sweatman, H. P. A. (2014). Limits to understanding and managing outbreaks of crown-of-thorns starfish (Acanthaster spp.). *Oceanography Mar. Biol.: Annu. Rev.* 52, 133–199. doi: 10.1201/b17143

Pratchett, M., Caballes, C., Wilmes, J., Matthews, S., Mellin, C., Sweatman, H., et al. (2017). Thirty years of research on crown-of-thorns starfish, (1986–2016): scientific advances and emerging opportunities. *Diversity* 9 (4), 1–49. doi: 10.3390/d9040041

Qin, Z., Yu, K., Liang, Y., Chen, B., and Huang, X. (2020). Latitudinal variation in reef coral tissue thickness in the south China Sea: Potential linkage with coral tolerance to environmental stress. *Sci. Total Environ.* 711, 134610. doi: 10.1016/j.scitotenv.2019.134610

Rice, M. M., Ezzat, L., and Burkepile, D. E. (2019). Corallivory in the anthropocene: interactive effects of anthropogenic stressors and corallivory on coral reefs. *Front. Mar. Sci.* 5. doi: 10.3389/fmars.2018.00525

Rotjan, R. D., and Lewis, S. M. (2008). Impact of coral predators on tropical reefs. *Mar. Ecol. Prog. Ser.* 367, 73–91. doi: 10.3354/meps07531

Saponari, L., Dehnert, I., Galli, P., and Montano, S. (2021). Assessing population collapse of drupella spp. (Mollusca: Gastropoda) 2 years after a coral bleaching event in the republic of Maldives. *Hydrobiologia* 848 (11), 2653–2666. doi: 10.1007/s10750-021-04546-5

Schoepf, V., Herler, J., and Zuschin, M. (2010). Microhabitat use and prey selection of the coral-feeding snail drupella cornus in the northern red Sea. *Hydrobiologia* 641 (1), 45–57. doi: 10.1007/s10750-009-0053-x

Scott, C. M., Mehrotra, R., Hein, M. Y., Moerland, M. S., and Hoeksema, B. W. (2017). Population dynamics of corallivores (Drupella and acanthaster) on coral

reefs of koh Tao, a diving destination in the gulf of Thailand. *Raffles Bull. Zool.* 65, 68–79.

Shafir, S., Gur, O., and Rinkevich, B. (2008). A drupella cornus outbreak in the northern gulf of eilat and changes in coral prey. *Coral Reefs* 27 (2), 379–379. doi: 10.1007/s00338-008-0353-z

Stimson, J. S. (1987). Location, quantity and rate of change in quantity of lipids in tissue of Hawaiian hermatypic corals. *Bull. Mar. Sci.* 41 (3), 889–904.

Titlyanov, E. A., Titlyanova, T. V., Scriptsova, A. V., Ren, Y. X., Li, X. B., and Huang, H. (2019). Interannual and seasonal changes in the benthic algae flora of coral reef in xiaodong hai (Hainan island, China). *J. Mar. Sci. Eng.* 7 (8), 243. doi: 10.3390/jmse7080243

Tsang, R. H. L., and Ang, P. (2015). Cold temperature stress and predation effects on corals: their possible roles in structuring a nonreefal coral community. *Coral Reefs* 34 (1), 97–108. doi: 10.1007/s00338-014-1210-x

Tsang, R. H. L., and Ang, P.Jr. (2019). Resistance to temperature stress and drupella corallivory may promote the dominance of platygyra acuta in the marginal coral communities in Hong Kong. *Mar. Environ. Res.* 144, 20–27. doi: 10.1016/j.marenvres.2018.11.009

Turner, S. J. (1994a). The biology and population outbreaks of the corallivorous gastropod drupella on indo-pacific reefs. *Oceanography Mar. Biol.: Annu. Rev.* 32, 461–530.

Turner, S. J. (1994b). Spatial variability in the abundance of the corallivorous gastropod drupella cornus. *Coral Reefs* 13 (1), 41–48. doi: 10.1007/Bf00426434

Wolff, N. H., Mumby, P. J., Devlin, M., and Anthony, K. R. N. (2018). Vulnerability of the great barrier reef to climate change and local pressures. *Global Change Biol.* 24 (5), 1978–1991. doi: 10.1111/gcb.14043

Zhang, Y. Y., Huang, H., Huang, J. Y., You, F., Lian, J. S., Yang, J. H., et al. (2016). The effects of four transplantation methods on five coral species at the sanya bay. *Acta Oceanol. Sin.* 35 (10), 88–95. doi: 10.1007/s13131-016-0916-8

Zhang, S. P., and Zhang, F. S. (2007). Study on species of drupa and drupella (Gastropoda, muricidae, rapaninae) from China coasts. *Mar. Sci.* 31 (9), 62–66. doi: 10.3969/j.issn.1000-3096.2007.09.012

frontiers | Frontiers in Marine Science

TYPE Data Report
PUBLISHED 26 August 2022
DOI 10.3389/fmars.2022.987067

Check for updates

OPEN ACCESS

EDITED BY
Dilip Kumar Jha,
National Institute of Ocean Technology, India

REVIEWED BY
Thilagam Harikrishnan,
Pachaiyappa's College for Men, India
Rajamanickam Krishnamurthy,
Arignar Anna Government Arts and Science College Chennai, India

*CORRESPONDENCE
Uma Sankar Panda
uspanda@nccr.gov.in

SPECIALTY SECTION
This article was submitted to Marine Pollution, a section of the journal Frontiers in Marine Science

RECEIVED 05 July 2022
ACCEPTED 01 August 2022
PUBLISHED 26 August 2022

CITATION
Pradhan U, Panda US, Naik S, Mishra P, Kumar DS, Begum M and Murthy MVR (2022) Coupled hydrodynamic and water quality modeling in the coastal waters off Chennai, East Coast of India. *Front. Mar. Sci.* 9:987067. doi: 10.3389/fmars.2022.987067

COPYRIGHT
© 2022 Pradhan, Panda, Naik, Mishra, Kumar, Begum and Murthy. This is an open-access article distributed under the terms of the Creative Commons Attribution License (CC BY). The use, distribution or reproduction in other forums is permitted, provided the original author(s) and the copyright owner(s) are credited and that the original publication in this journal is cited, in accordance with accepted academic practice. No use, distribution or reproduction is permitted which does not comply with these terms.

Coupled hydrodynamic and water quality modeling in the coastal waters off Chennai, East Coast of India

Umakanta Pradhan, Uma Sankar Panda*, Subrat Naik, Pravakar Mishra, D. Satish Kumar, Mehmuna Begum and M. V. Raman Murthy

National Centre for Coastal Research, Ministry of Earth Sciences, NIOT Campus, Chennai, India

KEYWORDS

coastal water quality, hydrodynamics, modelling, prediction, chennai

Introduction

Coastal waters are inherently dynamic due to river discharge, industrial effluents, shipping, dredging, waste dumping, and sewage disposal. Population growth in urban cities, climate change and variability, and changes in land-use practices all contribute to pressure on coastal water quality (Sekovski et al., 2012; Miller and Hutchins, 2017; Kumar et al., 2020; Vijay Prakash et al., 2021). Anthropogenic activity is evident around these estuaries and coastal and open ocean environments. Hence, it is important to assess the water quality on a regular basis and provide mitigation measures for coastal pollution (Yuvaraj et al., 2018). Improving water quality and variability in coastal waters is necessary and should be prioritized. Observational programs, which are more expensive and time-consuming, aid in understanding the status of water quality and its trends. Many countries have coastal programs that use predictive systems to inform the public and stakeholders about coastal health. Hydrodynamic processes are an integral part of complex surface water systems. The main factor that determines the concentration of pollutants is hydrodynamic transport, which includes advection, dispersion, vertical mixing, and convection (James, 2002). The flow and circulation patterns have a great influence not only on the distribution of temperature, nutrients, and dissolved oxygen (DO) but also on the aggregation and distribution of sediments and pollutants. When a load of pollutants is discharged into coastal waters, it is affected by the fate and transportation processes that change its concentration.

Several studies have been conducted to evaluate the coastal water quality spatiotemporally along the east coast of Indian coastal waters using site-specific data and model configuration (Panda et al., 2006; Bharathi et al., 2017; Naik et al., 2020;

Mohanty et al., 2021). Through numerical modeling and remote sensing, estimation is user-friendly and low-cost in evaluating any water quality (Fallconer, 1993; Kageyama and Nishida, 2000; Brando and Dekker, 2003; El-Din et al., 2013); still, the field data are essential to validate the model and correct of ground value to the remote data. *In situIn-situ* sampling and laboratory analysis are more accurate than modeling and remote sensing data, while the remote sensing data provide better spatiotemporal resolution than the data obtained from *in situ* samplings (Miller and McKee, 2004; Wu et al., 2014), and numerical modeling infers spatiotemporal and water column information. However, satellite image data cannot consistently obtain the information due to the limitations of weather conditions, date of the pass, and its swath (Song et al., 2018); similarly, numerical modeling required accurate time series boundary information. Water temperature and salinity play a substantial role in regulating the processes in the aquatic system (Mogaddam et al., 2019). The physical and biological processes are under influence by little changes in salinity and temperature in the water column through land runoff (van Beusekom et al., 2009; Deininger et al., 2016), precipitation (Ackerman and Weisberg, 2003), and storm (Noble et al., 2003), which resulted in the coastal water quality and biomass such as diversity, local species composition, and bloom.

Knowing that the coastal environment is highly dynamic and ecologically complex, therefore, an integrated modeling system is required to address the coastal water quality issues. Currently, there is no real-time water quality information system for beach goers, tourists, and coastal stakeholders. Unless a site-specific model is set up to generate as per the coastal user's requirement, there will be a scientific–societal gap in information. As a result, spatiotemporal collection of time series information is easy to evaluate with model-based water quality prediction. The predictive approach is basically followed by a three-step procedure that includes a) monitoring of various environmental conditions, b) simulation and observational validation of the model, and c) dissemination of the predictive information in the public domain. Therefore, the present study aimed to set up the coastal water quality model at the beach level, which simulates and forecasts the water quality as a public information system.

Study area

Chennai city, spreading over an area of 176 km^2, is located on the western seaboard of the Bay of Bengal (BoB) and covers three major tourist beaches, *viz*., Marina, Elliot, and Thiruvanmiyur, along the east coast of India (Figure 1A). Two rivers, *viz*., Cooum and Adyar, flow crisscrossing the city, carrying a major share of domestic sewage, a part of this industrial, port, and harbor effluents into the coast are highly significant. To develop a model to achieve forecasting of coastal water quality, a comprehensive program was designed, which includes *in situ* measurements, the development of a model, and an information dissemination system.

Data and methods

The *in situ* monitoring stations were carefully located keeping in view of discharge points, off-tourist beaches, transition zones, and the surf zone dynamics. A total of 30 sampling stations were fixed (Figure 1A), among which three are at the river inlets, which act as point sources discharging urban runoff, 21 stations in nearshore waters, i.e., 1 km from the coast wherein the concentration of land inputs are apparent, and nine stations are at a distance of 2 km from the beaches where concentrations are significantly reduced (Mishra et al., 2015).

The *in situ* monitoring stations were strategically fixed to include discharge points, off-tourist beaches, transition zones, and the dynamics of the surf zone. The observations were made for the period 2013–2016, at above 30 locations and further up to 2019 at seven stations right on the beaches (Figure 1A). In each sampling, 11 water quality variables were collected such as water temperature, salinity, pH, DO, biological oxygen demand (BOD), nitrate, nitrite, total nitrogen, phosphate, total phosphorus, and chlorophyll-*a*, following standard protocols of seawater quality analysis (Strickland and Parsons, 1972). The discharges of all inlets were calculated using the change in water level, current speed and direction, and geomorphology of inlets. Hourly meteorology data from an automated weather station at Ennore (a coastal observatory) were used for model validation, while National Centre for Medium-Range Weather Forecast (NCMRWF) data were used to forecast water quality for the next 3 days. The model required coastal oceanography data such as tide and current for different seasons (2013 to 2015). The primary goals of oceanographic data collection have traditionally been to understand and describe the state of the coastal ocean and its variability, whereas the current study is primarily concerned with model forcing (input) and validation. The tide gauge (Valeport make) was used to collect sea-level changes (Tide), while the current meter was used to collect current data (RCM, Aanderaa make). A water quality buoy (WQB) mounted with YSI Exo-2 water quality sensors and MaxiMet meteorological sensors provide a 10-min interval of uninterrupted time series data. The data are transmitted on GSM mode and received through FTP. These time series (60-min interval) data have been used to understand the variability and validation of the model.

Model description

Water quality models have evolved into an important tool for identifying water environmental pollution, as well as the fate

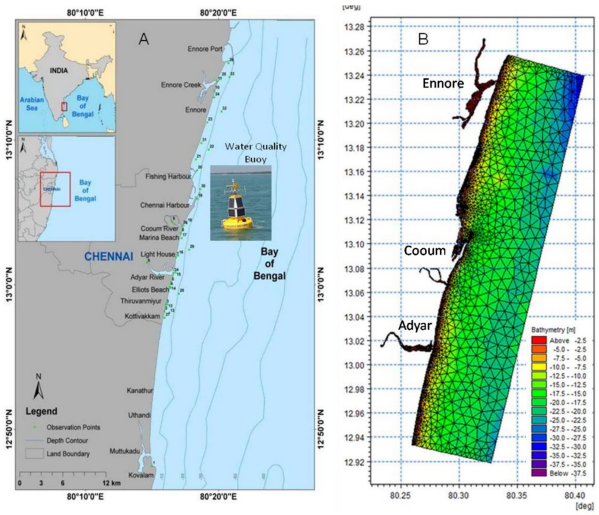


FIGURE 1
(A) Study area. **(B)** Model domain.

and transport of pollutants in the coastal water environments. With the advancement of model theory and the fast-updating computer technique, an increasing number of water quality models with various model algorithms have been developed. In the present study, a cell-centered finite volume method was adapted to compute the hydrodynamics with a very high resolution near the coast. As the river inlets are very fragile and more dynamic with siltation processes along this coast, hence continuous inlet monitoring (width) has been carried out for a couple of years, and an average width of river inlet is considered for model domain preparation (Figure 1B). An open equation solver water quality module (Ecolab) has been developed to model the fate of coastal waters at different spatiotemporal scales. Formulation of coastal water quality models requires fine-resolution bathymetry, proper initial conditions, boundary forcing, point discharge quantities, and water quality information (Supplementary Figure S1). The real-time observational data are assimilated into the models for better forecast results.

Three boundaries, *viz.*, a) open ocean, b) point sources at the land interface, and c) atmospheric inputs, were configured in the model. The time series boundary condition for the open ocean is given from the regional ocean model reanalysis provided by Indian National Center for Ocean Information Services (INCOIS). The fluxes at point sources were computed from the observations, and the atmospheric forcing on forecast mode is given by the National Centre for Medium Range Weather Forecast (NCMRWF). A spatial varying bed resistance in terms of Chezy coefficient computed with respect to the depth profiles and coefficient for viscosity is 0.5 by Smagorinsky formulation (Supplementary Table 1). Various sensitivity analyses were carried out to develop an optimized model for the coastal waters off the Chennai coast.

Model skill and forecast accuracy

Proper model validation is highly necessary, while the output of the model is used as input for other models or real applications. The establishment of the model should be confirmed by agreement between observation and model output. In the present study, the correlation coefficient and root mean absolute error (RMAE) are used for the model skill test and the forecasting accuracy estimation, respectively. The correlation coefficient ($r = S_{xy}/S_xS_y$, where $S_x$and $S_y$are the sample standard deviations and $S_{xy}$is the sample covariance) describes the degree of colinearity, and their range is 1 to −1, which is an index of the degree of learner relationship between observed and predicted values. When $r = 1$ or $r = -1$, a perfect positive and perfect negative relationship exists, while $r = 0$ indicates no linear relationship. The relative means absolute error ($RMAE = ||P| - |O||/|P|$; where P is the simulated value and O is the observed value) gives the relative error between the observed and predicted values and is extensively used to evaluate the numerical model performance. The accuracy of daily water quality forecasts was estimated through correlation coefficient by using the 10-min interval time series data from an automated sensor-based water quality buoy platform.

Results and discussion

Hydrodynamic

The hydrodynamic plays a key role in the variation of water quality in the nearshore region. The nearshore circulation along the east coast of India is mainly season-dependent with reversal wind, varying wave regimes, and river runoff (Shetye and Shenoi, 1988). The advection and dispersion along the coastal water are mainly subject to tidal action, wind, and river discharge. The advection and dispersion modules (particle tracking and Ecolab) coupled with hydrodynamic modeling were carried out for 15 days in each season, i.e., northeast monsoon (NEM: December 2013) and southwest monsoon (SWM: September 2015), and validated with observed data of sea-level changes (tide) and depth-averaged current (speed and direction).

The tidal analysis of the measured water level that clears the tide is micro (<2 m) and semi-diurnal. During December (NEM), the tidal range is ~1.25 m on a spring tide and 0.5 m on the neap phase, while it is ~1 m during spring and 0.5 m in the neap phase in September (SWM). The tide is classified as micro-tidal (Rao et al., 2009; Kankara et al., 2013). Though the rivers are small and semi-perennial, there is no significant variation of tidal amplitude throughout the domain. The harmonic analysis of measure tides generated 18 tidal constituents, out of which five important constituents are used in the prediction and validation (Supplementary Table S2). The dominant tidal constituents are principal lunar semidiurnal (M2), principal solar semidiurnal (S_2), lunisolar declinational diurnal (K_1), and principal lunar declinational diurnal (O_1), which are used to calculate the tidal form number ($F = O_1 + K_1/M_2 + S_2$). The form number is <0.25, which describes the tide as mostly semi-diurnal. Figures 2A1 and B1 depict the validation of water levels for both seasons. The simulated amplitude and phase of tide are in agreement with the observations. The simulated current patterns (Supplementary Figure S2A, B) are in line with the East India Coastal Current (EICC), which is dominated by seasonal reversing. EICC is northward during SWM, while it is southward during NEM (Shetye et al., 1996; Babu et al., 2003; Gangopadhyay et al., 2013; Kankara et al., 2013). The validation of the current speed and direction for the NEM and SWM is shown in Supplementary Figure S2 (A2, B2, A3, B3), respectively. The observed current speed ranged from 0 to 0.38 and from 0 to 0.55 m/s during September and December, respectively, whereas the simulated speed ranged from 0 to 0.35 m/s in September and from 0 to 0.65 m/s in December. The current direction during December is varied from 200 to 280° and 200 to 218° for observation and modeling, respectively. The hydrodynamic model result indicates that the coastal current is primarily driven by wind, with no evidence of the tide's sinusoidal nature. The combined action of northerly longshore current and micro tide triggers the inlet siltation and blocking along the coasts. The model has the potential to simulate hydrodynamics precisely.

Discharge

The accurate quantification of discharge at the point source, *viz*., Adyar and Cooum river inlets, is critical information because it directly affects coastal water quality and prediction. A current meter is placed in the mid of the inlet for 15 days. The cross-section and depth of the active inlet opening and water levels were considered to calculate the discharge values. For continuous-time series discharge information, the same data have been used in the model to develop probabilistic input of discharges calculated for a different season, tidal condition, and variable geomorphology of the inlets. The probabilistic inputs were calculated as $d = a * d * v$, where d is the discharge (m^3/s), a is the cross-sectional area (m^2), and v is the speed (m/s), while −ve discharge indicates discharge from sea to river during the flooding phase of the tide, and +ve discharge indicates discharge from the river to sea during the ebb phase of the tide. The coastal orientation (16°) is taken as considered in the discharge calculation. Supplementary Figure S3 shows the estimated discharge for Adyar and Cooum rivers. The higher discharged values from October to February are due to the major precipitations received during NEM over Chennai, which increase due to the increase in the land runoffs.

Water quality

The simulated water quality parameters at different spatiotemporal scales were generated for different seasons (Supplementary Figure S4) for water temperature, salinity, DO and Chl-*a*, and validated with the *in situ* measurements. The seasonal dispersion pattern of concentrations for distinct wind regimes, *viz*., NEM (northward) and SWM (southward), for the year 2020 agree with the wind pattern. This implies the coastal current is the driving factor for the fate and transport of pollutants along this coast. The higher concentration of all the parameters is nearly parallel to the coast and is intense near the river inlets (Supplementary Figure S4). Further, the dispersion depends on the local circulation pattern, which subsequently affects the adjacent coast.

Spatial variation of the Water Temperature (WT) is higher in coastal water compared to the deeper during SWM, while it reverses during NEM, because of the influence of variation in atmospheric temperature, land runoff, and land–sea interaction. The observed water temperature at the Marina nearshore region varied from 25.4°C to 30.9°C during December and April, respectively. The higher order of WT variation (~3.3°C) was recorded during the NEM compared to other seasons

(Figure 2A). The maximum average WT (29.3°C to 29.8°C) was observed from the end of May to early September, while it is minimum (27°C to 28.6°C) from November to February. During the survey, the standard deviation of WT is 0.4°C to 1.1°C during March and December, respectively. The maximum diurnal variation in air temperature, rainfall, and a cloudy sky is the triggering factor in reducing the surface WT during the NEM period. The northeast monsoonal rain over Chennai brought huge fresh cold water to the nearshore region. The validation of WT was assessed by comparing observed (2013 to 2019) and model results (2020) on a monthly basis (Figure 2A) and found a very good agreement in trend. The WT trend is better fitting, while the average WT variation between the observed and model results is ±0.5°C. The quality of model fit was evaluated by calculating the correlation coefficient (r) by using the monthly average of the analyzed month. The correlation coefficient (r) is 0.75, and the model performance is very good (Figure 2B). Similarly, the correlation coefficient (r) between observed time series water quality buoy and simulated data of water temperature is 0.8 (Figure 2C).

The salinity off Marina beach ranges between 25 and 35.4. The highest salinity was recorded in July, while the lowest was recorded in December. The salinity structure of this coastal water increased from January to July and then decreased till December. Early research indicated that the EICC transports freshwater southward along India's east coast beginning in September and that this freshwater plume reaches the extreme southern part of India in November (Sengupta et al., 2006; Akhil et al., 2014). The freshwater from the riverine system to the coastal water along India's east coast is freshening up to 100 km from the coast, causing the salinity to decrease (Vinayachandran and Kurian, 2007). From June to September, monsoonal rain-derived freshwater is predominant in the extreme northern part of BoB, and the southern current pattern (November, December, and January) begins transporting freshwater southward along the shore (Shetye et al., 1996; Jensen, 2001; Rao, 2003). The southward freshwater plume through EICC and rainfall during the NEM are the most noticeable features of salinity variation along Chennai coastal water. As the vertical stratification began in early January along the east coast of the Indian nearshore waters, the average salinity increased from January to July (Shetye and Shenoi, 1988). The observed salinity trends are easily captured by regional modeling through a proper validation of coastal current. Figure 2D depicts that the model salinity trend (2020) is matching with the observed salinity trend (2013–2019). The correlation coefficient (r) of salinity (monthly average) is 0.9 (Figure 2E), and for time series, it is 0.85 (Figure 2F), and the performance of validation is excellent.

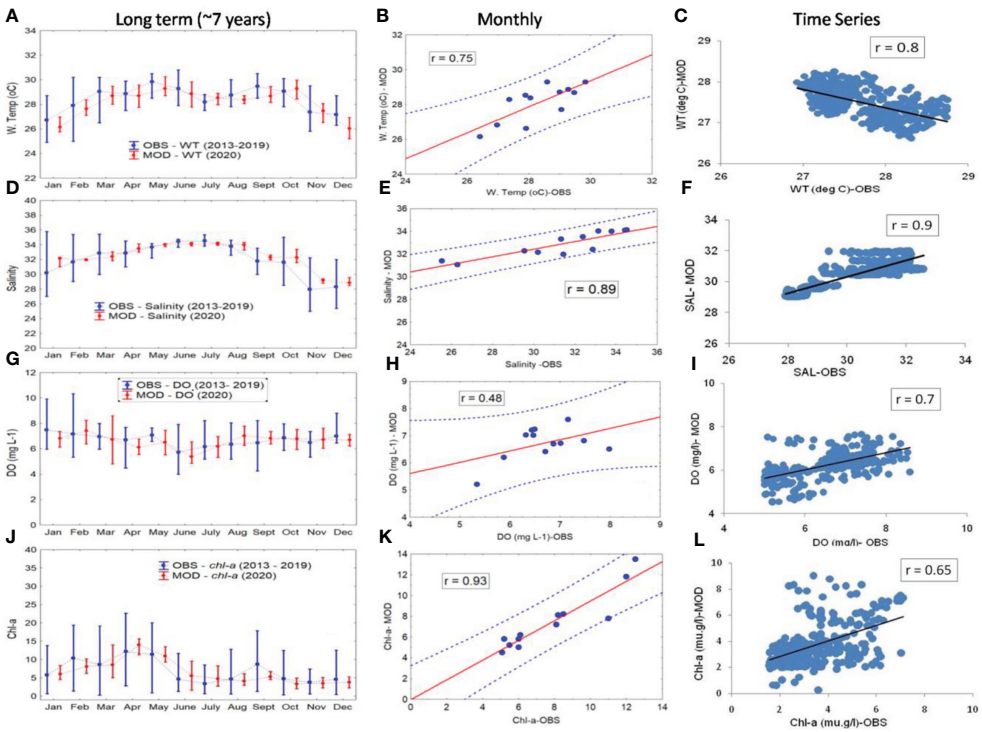


FIGURE 2
Validation of water temperature: **(A)** long term, **(B)** monthly, and **(C)** time series. Salinity: **(D)** long term, **(E)** monthly, and **(F)** time series. Dissolved oxygen: **(G)** long term, **(H)** monthly, and **(I)** time series. Chl-*a*: **(J)** long term, **(K)** monthly, and **(L)** time series.

DO concentrations ranged from 4.1 to 10.5 mg/L during the annual cycle. There were no seasonal variations in water temperature or salinity. During the investigation, the average DO value ranged from 5.5 to 7.5 mg/L. High winds blow during the southwest monsoon, but DO is lower than in other seasons. The high DO concentration was recorded in January, which could be due to the higher photosynthetic rate and air–sea interaction (Carignan et al., 2000; Naik et al., 2020). From January onwards, the DO decreases steadily until June, when it slowly increases again until January. During the NEM period, the deviation of the DO value is high (January and February). A minimum variation in DO was observed (0.6 mg/L) during the validation plot between observed DO (2013 to 2019) and model DO (2020) (Figure 2G). Figure 2H shows a positive correlation between model and monthly average DO (r = 0.5), while the model DO versus time series observation (r = 0.7) was recorded (Figure 2I). The model results for DO show within the range. The variation of DO between model and observation is subjected to photosynthesis, local wind patterns, and urban discharge.

The Chl-*a* concentration in Chennai coastal water varied from 0.5 to 23.8 mg/m^3. The maximum concentration was observed during April, while the minimum was in November. The Chl-*a* concentration is found to be higher during April, which might be due to the pre-monsoon convection process that brings nutrient-rich bottom water to the surface and or regenerated resources, which is responsible for this enhancement of the biological production (Jha et al., 2013; Naik et al., 2020). It follows an increasing trend from January to May and then started decreasing till November with an abrupt increase in September. A similar trend also reported for the Chl-*a* concentration along Puducherry coastal water is reported by Bharathi et al. (2017). The seasonal rainfall and cloudy days during November and December bring nutrient-rich freshwater to the coastal waters and reduced sunlight at the sea surface, which makes it more turbid and less productive and causes less Chl-*a* concentrations. Light conditions also play an important role in influencing the seasonal development of Chl-*a* (Yang and Ye, 2022). From January onwards, the existence of high water nutrients in coastal water will favor increasing the Chl-*a* concentration, and a similar study was also reported for Brahmani estuarine region by Palleyi et al. (2010). The observed average Chl-*a* value ranged from 3.5 to 13.4 mg/m^3, while the model value ranged from 3.5 to 14.0 mg/m^3 (Figure 2J). The validation for Chl-*a* between observed and model follows the same trend with an excellent correlation coefficient (r = 0.93) and a maximum deviation of ±0.75 mg/m^3 (Figure 2K), while the correlation (r) between model and observed data in the time series is 0.63 (Figure 2L).The exercise confirms, with long-term validation, that the seasonal trends are well captured by the model and in short-term comparison agree with *in situ* observations.

Prediction performance

Predictive models of coastal water quality supplement traditional monitoring by providing timely and adequate information for public health protection and coastal ecosystem management. It is critical to choose an appropriate model type and metrics to reduce errors and ensure that the predicted outcome is reliable. The development of an optimized model is the result of intensive sampling to collect a sufficient amount of data, analysis and processing, sensitivity analyses, and model calibration. However, as prediction duration increases, the uncertainty in the forcing parameters increases, resulting in a wide variation in the forecast range (Counillon et al., 2021; Džal et al., 2021). The model in this study simulates up to 8 days in advance, but the RMSE skill scores are acceptable for up to 3 days after which the ranges widen (Supplementary Figures S5A–D). The forecast skills are varied when considering individual parameters. RMSE skill scores for water temperature, salinity, DO, and Chl-*a* follow similar trends. The bias error is significantly increasing from the fifth day onwards; therefore, the forecast is considered for up to 3 days.

Conclusion

Coastal water quality modeling is of great environmental interest and scientific value and is an efficient tool for developing water quality information for beachgoers, stakeholders, and coastal managers. A coupled hydrodynamic-water quality model was setup to simulate and forecast coastal water quality parameters. The *in situ* measured data and sensor-based time series data were used to calibrate and validate the model. The skill test confirms that the model performance for hydrodynamics and water quality are in the acceptable ranges up to 3 days of forecast. Sensor-based data assimilation, high frequency of point source quantities, estimation of non-point source components, and data assimilation in the model will improve forecast accuracy. This paper attempted to predict the coastal water quality, which is highly dynamic and complex and paves the way for future improvements. The data generated assist beachgoers and coastal stakeholders during any abnormalities in water quality. This is an imperative study to achieve the targets under United Nations' Sustainable Development Goal (SDG)-14 and will assist coastal managers in the sustainable management of coastal regions.

Data availability statement

The original contributions presented in the study are included in the article/Supplementary Material. Further inquiries can be directed to the corresponding author.

Ethics statement

All applicable international, national, and/or institutional guidelines for the care and use of animals were followed by the authors.

Author contributions

UKP: fieldwork, data analysis, modeling, and writing original draft. USP: review, modeling, and manuscript writing. SN: fieldwork, literature review, data analysis, and interpretation. PM: final draft and supervision. DK: model data analysis. MB: review and data interpretation. MVR: review and project administration. All authors revised and edited the manuscript. All authors contributed to the article and approved the submitted version.

Acknowledgments

The authors are grateful to The Secretary, Ministry of Earth Sciences (MoES), Government of India, for his continuous support and encouragement. This manuscript has an NCCR contribution no. NCCR/MS 388.

Conflict of interest

The authors declare that the research was conducted in the absence of any commercial or financial relationships that could be construed as a potential conflict of interest.

Publisher's note

All claims expressed in this article are solely those of the authors and do not necessarily represent those of their affiliated organizations, or those of the publisher, the editors and the reviewers. Any product that may be evaluated in this article, or claim that may be made by its manufacturer, is not guaranteed or endorsed by the publisher.

Supplementary material

The Supplementary Material for this article can be found online at: https://www.frontiersin.org/articles/10.3389/fmars.2022.987067/full#supplementary-material

References

Ackerman, D., and Weisberg, S. B. (2003). Relationship between rainfall and beach bacterial concentrations on Santa Monica bay beaches. *J. Water Health* 1, 85–89. doi: 10.2166/wh.2003.0010

Akhil, V. P., Durand, F., Lengaigne, M., Vialard, J., Keerthi, M. G., Gopalakrishna, V. V., et al. (2014). A modeling study of the processes of surface salinity seasonal cycle in the bay of Bengal. *J. Geophys. Res. Ocean.* 119, 3926–3947. doi: 10.1002/2013jc009632

Babu, M. T., Sarma, Y. V. B., Murty, V. S. N., and Vethamony, P. (2003). On the circulation in the bay of Bengal during northern spring inter-monsoon. *Deep Sea Res. Part {II} Top. Stud. Oceanogr.* 50, 855–865. doi: 10.1016/s0967-0645(02)00609-4

Bharathi, M. D., Patra, S., Sundaramoorthy, S., Madeswaran, P., and Sundaramanickam, A. (2017). Elucidation of seasonal variations of physicochemical and biological parameters with statistical analysis methods in puducherry coastal waters. *Mar. pollut. Bull.* 122, 432–440. doi: 10.1016/j.marpolbul.2017.05.048

Brando, V. E., and Dekker, A. G. (2003). Satellite hyperspectral remote sensing for estimating estuarine and coastal water quality. *IEEE Trans. Geosci. Remote Sens.* 41, 1378–1387. doi: 10.1109/tgrs.2003.812907

Carignan, R., Planas, D., and Vis, C. (2000). Planktonic production and respiration in oligotrophic Shield lakes. *Limnol. Oceanogr.* 45, 189–199. doi: 10.4319/lo.2000.45.1.0189

Counillon, F., Keenlyside, N., Toniazzo, T., Koseki, S., Demissie, T., Bethke, I., et al. (2021). Relating model bias and prediction skill in the equatorial Atlantic. *Clim. Dyn.* 56, 2617–2630. doi: 10.1007/s00382-020-05605-8

Deininger, A., Faithfull, C. L., Lange, K., Bayer, T., Vidussi, F., and Liess, A. (2016). Simulated terrestrial runoff triggered a phytoplankton succession and changed seston stoichiometry in coastal lagoon mesocosms. *Mar. Environ. Res.* 119, 40–50. doi: 10.1016/j.marenvres.2016.05.001

Džal, D., Kosović, I. N., Mastelić, T., Ivanković, D., Puljak, T., and Jozić, S. (2021). Modelling bathing water quality using official monitoring data. *Water* 13, 3005. doi: 10.3390/w13213005

El-Din, M. S., Gaber, h., Koch, M., Ahmed, R. S., and Bahgat, I. (2013). Remote sensing application for water quality assessment in lake timsah, Suez canal, Egypt. *J. Remote Sens. Technol.* 1(3), 61–74. doi: 10.18005/jrst0103002

Fallconer, R. A. (1993). Application of numerical models for water quality studies. *Proc. Inst. Civ. Eng. - Civ. Eng.* 97, 163–170. doi: 10.1680/icien.1993.25304

Gangopadhyay, A., Raj, G. N. B., Chaudhuri, A. H., Babu, M. T., and Sengupta, D. (2013). On the nature of meandering of the springtime western boundary current in the bay of Bengal. *Geophys. Res. Lett.* 40, 2188–2193. doi: 10.1002/grl.50412

James, I. D. (2002). Modelling pollution dispersion, the ecosystem and water quality in coastal waters: A review. *Environ. Model. Software* 17, 363–385. doi: 10.1016/S1364-8152(01)00080-9

Jensen, T. G. (2001). Arabian Sea And bay of Bengal exchange of salt and tracers in an ocean model. *Geophys. Res. Lett.* 28, 3967–3970. doi: 10.1029/2001gl013422

Jha, D. K., Prashanthi Devi, M., Vinithkumar, N. V., Das, A. K., Dheenan, P. S., Venkateshwaran, P., et al. (2013). Comparative investigation of water quality parameters of aerial & rangat bay, Andaman islands using in-situ measurements and spatial modelling techniques. *Water Qual. Expo. Heal.* 5, 57–67. doi: 10.1007/s12403-013-0086-2

Kageyama, Y., and Nishida, M. (2000). Water quality analysis based on remote sensing data and numerical model. *J. Geogr. (Chigaku Zasshi)* 109, 27–36. doi: 10.5026/jgeography.109.27

Kankara, R. S., Mohan, R., and Venkatachalapathy, R. (2013). Hydrodynamic modelling of chennai coast from a coastal zone management perspective. *J. Coast. Res.* 29, 347–357. doi: 10.2307/23353632

Kumar, S. S., Panda, U. S., Pradhan, U. K., Mishra, P., and Murthy, M. V. R. (2020). Web-based decision support system for coastal water quality. *J. Coast. Res.* 89, 139–144. doi: 10.2112/SI89-023.1

Miller, J. D., and Hutchins, M. (2017). The impacts of urbanisation and climate change on urban flooding and urban water quality: A review of the evidence concerning the united kingdom. *J. Hydrol. Reg. Stud.* 12, 345–362. doi: 10.1016/j.ejrh.2017.06.006

Miller, R. L., and McKee, B. A. (2004). Using MODIS Terra 250 m imagery to map concentrations of total suspended matter in coastal waters. *Remote Sens. Environ.* 93, 259–266. doi: 10.1016/j.rse.2004.07.012

Mishra, P., Panda, U. S., Pradhan, U., Kumar, C. S., Naik, S., Begum, M., et al. (2015). Coastal water quality monitoring and modelling off chennai city. *Proc. Eng.* 116, 955–962. doi: 10.1016/j.proeng.2015.08.386

Mogaddam, S. F., Bidokhti, A. A., Givi, F. A., and Ezam, M. (2019). Evaluation of physical changes (temperature and salinity) in the Persian gulf waters due to climate change using field data and numerical modeling. *Int. J. Environ. Sci. Technol.* 17, 2141–2152. doi: 10.1007/s13762-019-02532-y

Mohanty, A. K., Sathishkumar, R. S., Sahu, G., Suriyaprakash, R., Arunachalam, K. D., and Venkatesan, R. (2021). Spatial and seasonal variations in coastal water characteristics at kalpakkam, western bay of Bengal, southeast India: a multivariate statistical approach. *Environ. Monit. Assess.* 193, 366. doi: 10.1007/s10661-021-09115-w

Naik, S., Mishra, R. K., Sahu, K. C., Lotliker, A. A., Panda, U. S., and Mishra, P. (2020). Monsoonal influence and variability of water quality, phytoplankton biomass in the tropical coastal waters – a multivariate statistical approach. *Front. Mar. Sci.* 7. doi: 10.3389/fmars.2020.00648

Noble, R. T., Weisberg, S. B., Leecaster, M. K., McGee, C. D., Dorsey, J. H., Vainik, P., et al. (2003). Storm effects on regional beach water quality along the southern California shoreline. *J. Water Health* 1, 23–31. doi: 10.2166/wh.2003.0004

Palleyi, S., Kar, R. N., and Panda, C. R. (2010). Seasonal variability of phytoplankton population in the brahmani estuary of orissa, India. *J. Appl. Sci. Environ. Manage.* 12, 19–23. doi: 10.4314/jasem.v12i3.55474

Panda, U., Sundaray, S., Rath, P., Nayak, B., and Bhatta, D. (2006). Application of factor and cluster analysis for characterization of river and estuarine water systems – a case study: Mahanadi river (India). *J. Hydrol.* 331, 434–445. doi: 10.1016/j.jhydrol.2006.05.029

Rao, R. R. (2003). Seasonal variability of sea surface salinity and salt budget of the mixed layer of the north Indian ocean. *J. Geophys. Res.* 108, 3009. doi: 10.1029/2001jc000907

Rao, V. R., Murthy, M. V. R., Bhat, M., and Reddy, N. T. (2009). Littoral sediment transport and shoreline changes along ennore on the southeast coast of India: Field observations and numerical modeling. *Geomorphology* 112, 158–166. doi: 10.1016/j.geomorph.2009.05.015

Sekovski, I., Newton, A., and Dennison, W. C. (2012). Megacities in the coastal zone: Using a driver-pressure-state-impact-response framework to address complex environmental problems. *Estuar. Coast. Shelf Sci.* 96, 48–59. doi: 10.1016/j.ecss.2011.07.011

Sengupta, D., Raj, G. N. B., and Shenoi, S. S. C. (2006). Surface freshwater from bay of Bengal runoff and Indonesian throughflow in the tropical Indian ocean. *Geophys. Res. Lett.* 33, L22609. doi: 10.1029/2006gl027573

Shetye, S. R., Gouveia, A. D., Shankar, D., Shenoi, S. S. C., Vinayachandran, P. N., Sundar, D., et al. (1996). Hydrography and circulation in the western bay of Bengal during the northeast monsoon. *J. Geophys. Res. Ocean.* 101, 14011–14025. doi: 10.1029/95jc03307

Shetye, S. R., and Shenoi, S. S. C. (1988). Seasonal cycle of surface circulation in the coastal north Indian ocean. *Proc. Indian Acad. Sci. - Earth Planet. Sci.* 97, 53–62. doi: 10.1007/BF02861627

Song, N., Wang, N., Lin, W., and Wu, N. (2018). Using satellite remote sensing and numerical modelling for the monitoring of suspended particulate matter concentration during reclamation construction at dalian offshore airport in China. *Eur. J. Remote Sens.* 51, 878–888. doi: 10.1080/22797254.2018.1498301

Strickland, J. D. H., and Parsons, T. R. (1972). *A practical handbook of seawater analysis, issue 167; issue 1977* (Fisheries Research Board of Canada, Ottawa).

van Beusekom, J. E. E., Loebl, M., and Martens, P. (2009). Distant riverine nutrient supply and local temperature drive the long-term phytoplankton development in a temperate coastal basin. *J. Sea Res.* 61, 26–33. doi: 10.1016/j.seares.2008.06.005

Vijay Prakash, K., Geetha Vimala, C. S., Preethi Latha, T., Jayaram, C., Nagamani, P. V., and Laxmi, C. N. V. (2021). Assessment of water quality along the southeast coast of India during COVID-19 lockdown. *Front. Mar. Sci.* 8. doi: 10.3389/fmars.2021.659686

Vinayachandran, P. N., and Kurian, J. (2007). Hydrographic observations and model simulation of the bay of Bengal freshwater plume. *Deep Sea Res. Part I Oceanogr. Res. Pap.* 54, 471–486. doi: 10.1016/j.dsr.2007.01.007

Wu, G., Liu, L., Chen, F., and Fei, T. (2014). Developing {MODIS}-based retrieval models of suspended particulate matter concentration in dongting lake, China. *Int. J. Appl. Earth Obs. Geoinf.* 32, 46–53. doi: 10.1016/j.jag.2014.03.025

Yang, C., and Ye, H. (2014). Enhanced Chlorophyll-a in the coastal waters near the Eastern Guangdong during the Downwelling Favorable Wind Period. *Remote Sens.* 14, 1138. doi: 10.3390/rs14051138

Yuvaraj, P., Satheeswaran, T., Damotharan, P., Karthikeyan, V., Jha, D. K., Dharani, G., et al. (2018). Evaluation of the environmental quality of parangipettai, southeast coast of India, by using multivariate and geospatial tool. *Mar. pollut. Bull.* 131, 239–247. doi: 10.1016/j.marpolbul.2018.04.022

frontiers | Frontiers in Marine Science

TYPE Original Research
PUBLISHED 29 August 2022
DOI 10.3389/fmars.2022.987685

Check for updates

OPEN ACCESS

EDITED BY
Meilin Wu,
South China Sea Institute of Oceanology, (CAS), China

REVIEWED BY
Yanpei Zhuang,
Jimei University, China
Miming Zhang,
State Oceanic Administration, China
Zuhao Zhu,
Ministry of Natural Resources, China

*CORRESPONDENCE
Shuwen Zhang
zhangsw@stu.edu.cn

SPECIALTY SECTION
This article was submitted to Marine Pollution, a section of the journal Frontiers in Marine Science

RECEIVED 06 July 2022
ACCEPTED 08 August 2022
PUBLISHED 29 August 2022

CITATION
Jian X, Zhang S, Lao Q, Chen F, Huang P, Chen C and Zhu Q (2022) Using dual water isotopes to quantify the mixing of water masses in the Pearl River Estuary and the adjacent northern South China Sea. *Front. Mar. Sci.* 9:987685. doi: 10.3389/fmars.2022.987685

COPYRIGHT
© 2022 Jian, Zhang, Lao, Chen, Huang, Chen and Zhu. This is an open-access article distributed under the terms of the Creative Commons Attribution License (CC BY). The use, distribution or reproduction in other forums is permitted, provided the original author(s) and the copyright owner(s) are credited and that the original publication in this journal is cited, in accordance with accepted academic practice. No use, distribution or reproduction is permitted which does not comply with these terms.

Using dual water isotopes to quantify the mixing of water masses in the Pearl River Estuary and the adjacent northern South China Sea

Xiaoyu Jian[1,2], Shuwen Zhang[1,2*], Qibin Lao[3], Fajin Chen[3], Peng Huang[3], Chunqing Chen[3] and Qingmei Zhu[3]

[1]Institute of Marine Science, Shantou University, Shantou, China, [2]Guangdong Provincial Key Laboratory of Marine Disaster Prediction and Protection, Shantou University, Shantou, China, [3]College of Ocean and Meteorology, Guangdong Ocean University, Zhanjiang, China

The mixing of different water masses is important for local physical and biogeochemical processes as well as for ecosystems in the ocean. In this study, a new dataset of stable water isotopes (δD and $\delta^{18}O$) combined with temperature–salinity profiles was used to quantitatively understand the mixing of water masses in the Pearl River Estuary (PRE) and the adjacent northern South China Sea (SCS). Based on hydrographic characteristics and the isotope–salinity relationships in the water column, three water masses, namely, low isotopic values (<1.5‰ for δD and <0‰ for $\delta^{18}O$) with a salinity of <33.20 for PRE water (PREW), high isotopic values (>2.0‰ for δD and >0.6‰ for $\delta^{18}O$) with a salinity of >34.60 for SCS Kuroshio Branch (SCSKB), and higher isotopic values (>3.0‰ for δD and <0.4‰ for $\delta^{18}O$) with a salinity of >33.30 for SCS water (SCSW), were identified in the PRE and the adjacent SCS. The mixing of the three water masses in the PRE and the adjacent SCS was mainly from SCSW (71%), followed by the SCSKB (23%), and the proportion of PREW only accounted for 6%. However, different water layers and regions are affected differently by these three water masses. The surface water is mainly influenced by the PREW, whereas the subsurface water is mainly influenced by the intrusion of SCSKB (100–300 m). The mixing process of water masses in the west side of the study area (<115°E) is mainly contributed by the SCSW (86%), whereas the contributions of PREW and SCSKB are only 4% and 10%, respectively. By contrast, the mixing of water masses in the east side (>115°E) is mainly influenced by the Kuroshio intrusion (50%). This study reveals that dual water isotopes are exquisitely sensitive to determine the complex hydrological process in the PRE and the adjacent SCS, and water masses on marine environment should deserve more attention.

KEYWORDS

δD, $\delta^{18}O$, water mass, Pearl River Estuary, kuroshio

Introduction

The mixing of water masses plays an important role in the storage and redistribution of freshwater, heat, and biogenic elements, and may have a large impact on the local marine ecology (Legrande and Schmidt, 2006; Oka and Qiu, 2012; Lian et al., 2016; Lao et al., 2022a; Zhuang et al., 2022). For example, transport of different water masses with the substances will lead to a change in biogeochemical processes after mixing, thus affecting the carbon and nitrogen cycle, and climate change (Deshpande et al., 2013; Durack, 2015; Wang et al., 2017; Xu et al., 2018; Yu et al., 2022). Thus, the study of water mass processes contributes to a better understanding of the impact of marine biogeochemical processes and marine primary productivity (Xu et al., 2018; Lao et al., 2022a).

Traditionally, temperature–salinity (T–S) relationships have been used to distinguish the characteristics of marine water masses for a long time (Helland-Hansen and Nansen, 1926; Harvey, 1982), and are still widely used recently (Xie et al., 2011; Liu et al., 2017; Karati et al., 2019). However, such traditional method has some limitations to trace the mixing of water masses because the salinity and temperature are not the characteristic of water itself (Bigg and Rohling, 2000; Lao et al., 2022a). It is difficult to identify the mixing of water masses with the same salinity in the oceans, particularly in the coastal areas (Lao et al., 2022a and Lao et al., 2022b). In coastal waters, water masses are mixed from different freshwater masses, and these water masses may have similar or even the same temperature and salinity, thus making it difficult to distinguish their contribution (Bigg & Rohling, 2000; Lao et al., 2022a and Lao et al., 2022b). By contrast, $\delta^{18}O$ and δD are properties of the water itself, and they are less influenced by biogeochemical processes (Lian et al., 2016; Jin et al., 2018; Chen et al., 2020b; Lao et al., 2022a). They have a sensitive signal, which could be modified by physical processes, such as precipitation, runoff input, evaporation, advection, or upwelling (Craig and Gordon, 1965; Rohling, 2007; Lian et al., 2016). The response of $\delta^{18}O$ and salinity to physical processes is similar, which is lower in freshwater and higher in seawater (Benetti et al., 2017). In addition, the $\delta^{18}O$ and δD both decrease with increased freshwater flushing/precipitation and increase with evaporation/seawater intrusion (Frew et al., 2000; Deshpande et al., 2013; Richardson et al., 2018). Thus, the composition of different water masses would have different δD–$\delta^{18}O$ and $\delta^{18}O$–salinity relationships, which can indicate the degree of complexation of different water masses with each other (Sengupta et al., 2013; Benetti et al., 2017; Kumar et al., 2018; Chen et al., 2020b). Moreover, since isotopes are less influenced by biogeochemical processes, the contribution of water masses can be quantified using stable isotope mixing models (Chen et al., 2020b; Wu et al., 2021; Lao et al., 2022a). For example, the water mass processes are quantitatively identified between the western Pacific Ocean and the South China Sea (SCS) (>3,700 m) by using the dual water isotopes combined with temperature–salinity profiles (Wu et al., 2021). In the coastal oceans, the mixing of different water sources and the intrusion of the high salinity to the coastal waters (Lian et al., 2016; Chen et al., 2020), and their impacts on the groundwater (Tran et al., 2019; Zhang et al., 2022) and coastal ecological environment, such as the distribution of nutrient and primary productivity (Lao et al., 2022a) and the mariculture activities (Lao et al., 2022b), were also identified by the dual water isotopes. Thus, the isotope tool has been successfully used to track the movement and mixing of water masses (Legrande and Schmidt, 2006; Deshpande et al., 2013; Sengupta et al., 2013; Lian et al., 2016; Benetti et al., 2017; Chen et al., 2020b).

The Pearl River Estuary (PRE) is located at the southern end of the Chinese mainland, and it is the largest river in south China (Fang and Wang, 2022). The mixing of water masses in the PRE and the adjacent northern SCS is quite complex, which is not only influenced by the river diluted water and SCS water (Chen et al., 2022), but also influenced by the saline Kuroshio intrusion (Wu et al., 2021). Based on the dual water isotopes combined with the salinity, the proportion of Kuroshio intrusion into the northern SCS through the Luzon Strait was quantified, which accounts for 15%. The mixing of three water masses, the Pearl River freshwater, the SCS water, and the Kuroshio water, has a great impact on the regional ecosystem (Chen et al., 2019). For example, the Kuroshio intrusion into the SCS formed a strong front due to interactions with northern SCS water, which has supplied external high Chl *a* and nutrients in the subsurface SCS water and increasing phytoplankton productivity in the frontal area (Deshpande et al., 2013; Wang et al., 2017; Xu et al., 2018). In addition, there are varying degrees of seawater backflow to the PRE each year (Liu et al., 2017; Liu et al., 2019). In the northern SCS, the intrusion of the Kuroshio subsurface water to the continental slope was identified by using seawater $\delta^{18}O$ (Chen et al., 2020b). Based on the $\delta^{18}O$–salinity relationship, the SCS Warm Current in the northeastern SCS mainly originated from the upslope deflection of the slope current formed by the Kuroshio subsurface water intrusion into the SCS, rather than from the west segment of the SCS Warm Current formed to the Hainan Island (Chen et al., 2020b). In the PRE, by using dual water isotopes, the study suggested that the saline groundwater mainly originated from the seawater intrusion in the past, whereas the fresh groundwater was mainly from the modern meteoric precipitation recharge (Wu et al., 2020). However, in the PRE and the adjacent SCS with complex hydrodynamic forces, there is still no quantitative understanding of the mixing of different water masses, which will provide a better understanding of the impact of the biogeochemical processes and the impact of the water mass composition on the primary productivity of the ocean (Xu et al., 2018).

In this study, we present a new dataset of dual water isotopes ($\delta^{18}O$ and δD), temperature, and salinity in the water column of the PRE during fall (September) in 2015. We attempted to

identify and quantify the mixing of different water masses in the PRE and the adjacent northern SCS. This study will provide a deeper understanding of the physical processes in the PRE and the adjacent northern SCS, providing a new insight into the impact of water mass mixing on biogeochemical processes of the marginal sea.

Materials and methods

Study area and sampling

During fall (September) 2015, a cruise was carried out in the PRE and adjacent northern SCS. A total of 24 stations on three sections were sampled in the study area (Figure 1). Seawater samples (a total of 108) were collected in the water column for given depths (i.e., 0.5, 5, 25, 50, 75, 100, 150, 200, 300, 500, and 800 m) using a rosette sampler fitted with 10-L Niskin bottles. The pretreatment of seawater samples refers to that of Lao et al. (2022a). The seawater samples for dual water isotopes were filtered through acetate membranes (0.45 μm pore size) to avoid the influence of bio-processes on water isotopes after sampling. The filtrate was transferred to a precleaned high-density polyethylene bottle, and the bottle was wrapped by a parafilm (PM-996, USA) to reduce biological effects and avoid isotopic fractionation by volatilization of the water, and then stored at −20°C for analysis. Seawater temperature, salinity, and depth were measured using a CTD (SBE911, Seabird) on site.

Stable isotope measurement

The most abundant isotope pairs in seawater are the ratios of the stable isotopes of hydrogen, i.e., ^{2}H and ^{1}H, and the stable isotopes of oxygen, i.e., ^{18}O and ^{16}O. The ratios are reported in unit of per mill (i.e., ‰) deviations from Vienna Standard Mean Ocean Water (V-SMOW), denoted δD and $\delta^{18}O$:

$$\delta^{18}O \ \ or \ \ \delta D = \frac{R_{sample} - R_{V-SMOW}}{R_{V-SMOW}} \times 1000 \qquad (1)$$

where R_{sample} and $R_{V\text{-}SMOW}$ indicate the ratio of $^{18}O/^{16}O$ and D/H (i.e., $^{2}H/^{1}H$, ^{2}H also named deuterium with acronym of D) of the sample and V-SMOW, respectively.

The seawater samples for $\delta^{18}O$ and δD were measured by using the equilibration method. The detailed process can be found in Lao et al., 2022a and Lao et al., 2022b). In brief, samples were equilibrated with H_2 or CO_2, and the equilibrated gas was measured by an elemental analysis isotope ratio mass spectrometer (Gasbench II-IRMS) (Gasbench II interfaced with a 253 plus mass spectrometer). For the analysis of seawater for δD, platinum (Pt) catalyst (200 μl) was added to the samples, and the H_2 (2% H_2/He) was introduced to ensure that D/H in water and D/H in H_2 are in isotopic equilibrium. The procedure of the equilibrium of δD was at 28°C for 40 min. The analysis of the seawater sample for $\delta^{18}O$, CO_2 (1% CO_2/He) is introduced into a 500-μl sample to ensure that $^{18}O/^{16}O$ in water and $^{18}O/^{16}O$ in CO_2 are in isotopic equilibrium. The procedure of the equilibrium of $\delta^{18}O$ was at 24°C for 24 h. During the measurement, a standard sample ($\delta^{18}O_{V\text{-}SMOW}$ for 0‰ and $\delta D_{V\text{-}SMOW}$, VSMOW2 for 0‰) was inserted every 12 samples to confirm the stability of the instrument. Based on the results of each standard sample, the precision and accuracy calculated for $\delta^{18}O$ were 0.1‰ and ±0.1‰, respectively. The precision and accuracy calculated for δD were 0.6‰ and ±0.5‰, respectively.

The Bayesian mixing model

The proportion of contribution from different water masses can be quantified by using a Bayesian stable isotope mixing model. The details of the model are as follows (Moore and Semmens, 2008):

$$X_{ij} = \sum_{k=1}^{k} P_k \left(S_{jk} + c_{jk}\right) + \epsilon_{ij} \qquad (2)$$

$$S_{jk} \sim N\left(\mu_{jk}, \ \omega_{jk}^2\right) \qquad (3)$$

$$c_{jk} \sim N\left(\lambda_{jk}, \ \tau_{jk}^2\right) \qquad (4)$$

$$\epsilon_{jk} \sim N\left(0, \ \sigma_j^2\right) \qquad (5)$$

where X_{ij} and S_{jk} represent the $\delta^{18}O$ and δD of a mixed water sample and isotope signature values of water mass sources, respectively; S_{jk} represents normal distribution with standard deviation ω_{jk} and mean deviation μ_{jk}; P_k represents the proportion of different water masses; c_{jk} represents the fractionation factor for δD and $\delta^{18}O$ of different water masses, normally distributed, with mean λ_{jk} and standard deviation τ_{jk}; ϵ_{jk} represents the residual error of the addition of an unquantified change between samples, normally distributed, with mean 0 and standard deviation σ_j. Since the $\delta^{18}O$ and δD in seawater are less affected by biogeochemical processes (Fairbanks, 1982; Hattori, 1997; Lian et al., 2016; Wang et al., 2018), the Bayesian mixing model was successfully applied to quantify the mixing contribution of water masses (Lao et al., 2022a and Wu et al., 2021; Lao et al., 2022b). The advantage of the Bayesian mixing model compared to other methods, such as the model MixSIR, is the residual error term in the form of standard deviation included in the model (Jackson et al., 2009).

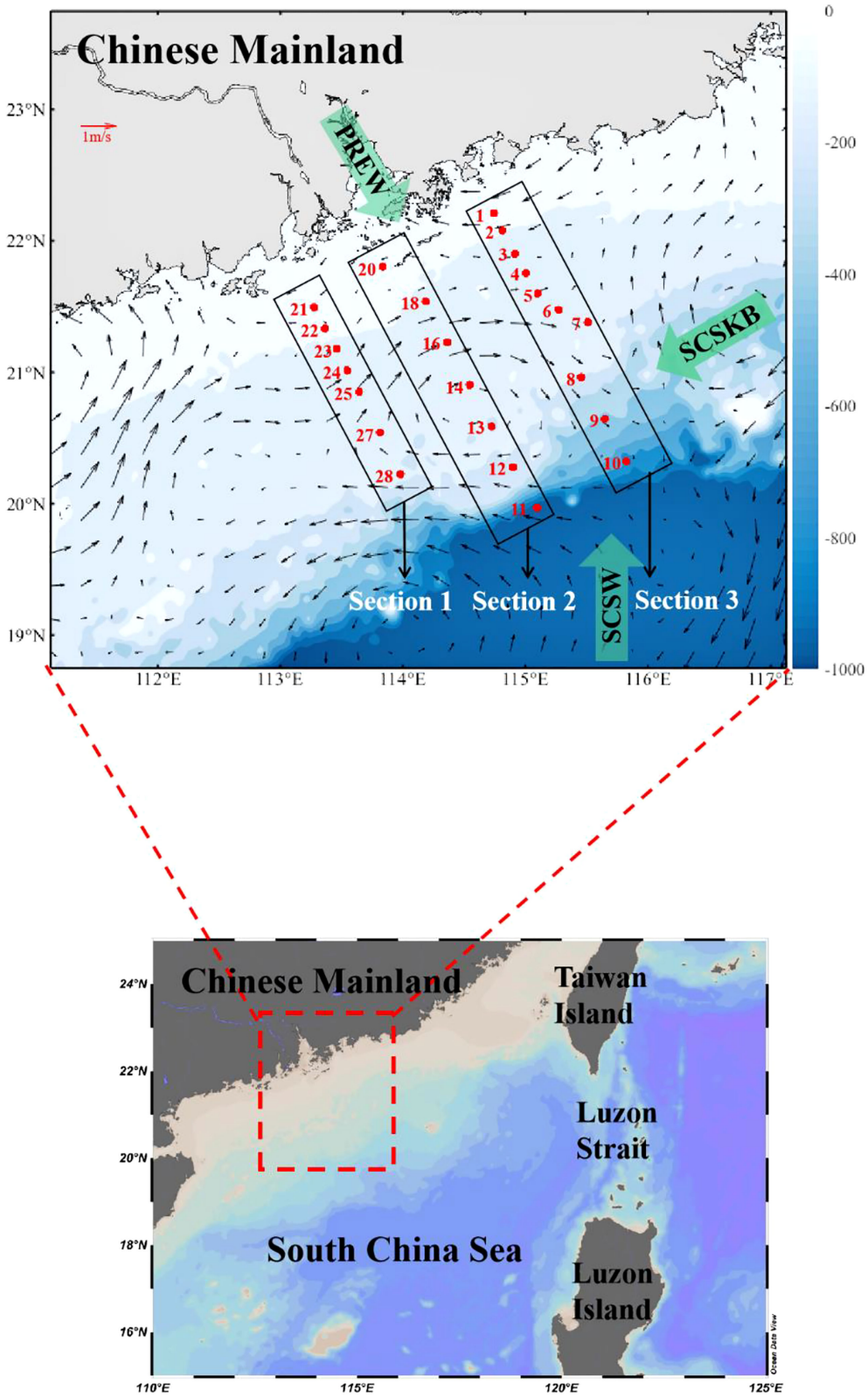


FIGURE 1
Sampling stations in the Pearl River Estuary during September 2015.The surface current vectors were also plotted. PREW, Pearl River flushing water; SCSW, South China Sea water; SCSKB, South China Sea Kuroshio Branch.

Results

Hydrography properties

The vertical distributions of temperature and salinity along the three sections are shown in Figure 2. A thermal stratification can be clearly seen in the PRE and the adjacent northern SCS. Temperature decreased gradually with depth in the water column, with the highest temperature of 30.33°C in the surface and the lowest temperature of 5.32°C in the bottom.

The salinity is characterized by low salinity in the surface layer (minimum salinity value of 32.35) and high salinity in the bottom layer. Notably, the maximum salinity is presented in the subsurface layer (maximum salinity value of 34.71), with an average of 34.16. The lowest salinity (<33.5) was found in the nearshore area of Sections 2 and 3 (Figure 2). The high temperature (>25°C) and low salinity (<34) in the surface water extend from the nearshore area to the outer sea, suggesting that this may be influenced by the coastal diluted water. However, in the subsurface water of the offshore area, the higher salinity and temperature may be influenced by the Kuroshio intrusion in the northern SCS (Chen et al., 2020b; Wu et al., 2021).

Stable isotope distributions

$\delta^{18}O$ and δD ranged from −0.2‰ to 0.9‰ and from −6.7‰ to 18.5‰, with an average value of 0.3‰ and 5.5‰, respectively. The distribution of $\delta^{18}O$ and δD exhibited a wide range spanning the surface and middle layers (both maximum and minimum values occur in the middle layer or in both the middle and surface layers) (Figures 3, 4); lower values were found in the nearshore areas whereas higher values were found in the offshore areas (Figure 3). Similar to the distribution of salinity, $\delta^{18}O$ and δD showed lower values in the surface water and higher values in the mid and bottom water. In addition, lower values were found in the nearshore area, whereas higher values were found in the offshore area. Notably, significantly high $\delta^{18}O$ values were found in the offshore area of Section 3, which may be influenced by the Kuroshio water intrusion since the Kuroshio water was characterized by significantly positive $\delta^{18}O$ in the eastern Luzon Strait (Wu et al., 2021).

Identification of water masses in the PRE and the adjacent northern SCS

Based on the salinity, temperature, and stable oxygen and hydrogen isotope of the PRE, three water masses can be identified that affect the PRE and adjacent northern SCS waters (Figure 5). The PRE flushing water is derived from continental runoff with high temperature (>26.5°C) but low salinity (<33.2) and isotope values (<1.5‰ for δD and <0‰ for $\delta^{18}O$), forming PREW end-member. The bottom water of the SCS is mainly derived from the northern part of the SCS, with low-temperature (<10°C) but high-salinity water (>33.30), forming South China Sea bottom water (SCSBW) end-member. A further water mass, with high salinity (>34.6) and isotope values (>2.0‰ for δD and >0.6‰ for $\delta^{18}O$), is located in the subsurface layer. The salinity and isotopic characteristics of this water mass follow those of the Kuroshio waters (Chen et al., 2020a; Wu et al., 2021), forming SCSBW end-member.

Isotope–salinity/isotope relationships

The correlation of δD–$\delta^{18}O$, δD–salinity, and $\delta^{18}O$–salinity relationships for the three sections is shown in Figure 6. Those relationships exhibited higher slopes in Sections 1 and 2, and lower slope in Section 3. These indicated that the water mass processes were similar between Sections 1 and 2, while Section 3 was significantly different from the two sections. The vertical distribution of δD and $\delta^{18}O$ in Section 3 is also noticeably different from the other two sections, which also indicates that the water mass process in Section 3 is significantly different from the other two sections (Figure 4). Section 3 is located to the east of the PRE and probably more affected by the Kuroshio intrusion than Sections 1 and 2.

Discussion

δD–$\delta^{18}O$ and $\delta^{18}O$–salinity in different sections

In Section 1, the significant correlation of $\delta^{18}O$–salinity ($\delta^{18}O$ = 0.28S-9.47; R^2 = 0.38, p < 0.01) and δD–$\delta^{18}O$ (δD = 12.65$\delta^{18}O$+4.31; R^2 = 0.39, p < 0.01) was found (Figures 6A, C). A high-slope but low-intercept $\delta^{18}O$–salinity relationship indicated the influence of the strong overland runoff or strong rainfall (Lao et al., 2022a and Singh et al., 2010; Kumar and Ramesh, 2016; Kumar et al., 2018; Lao et al., 2022b). In addition, the slope of observed δD–$\delta^{18}O$ is significantly higher than that of the global meteoric water line (GMWL: δD = 8.00$\delta^{18}O$+10) (Craig, 1961) and the global ocean water line (GOWL: δD = 7.37$\delta^{18}O$-0.72) (Rohling, 2007), indicating that this section is mixed with freshwater or high rainfall, or both (Figure 6C). Notably, lower temperature and higher salinity compared to the surface water at the other stations were found in the coastal water (Station 21) of Section 1, which is similar to the subsurface water column characteristics of the others (Figures 2A, D). This may be because the coastal upwelling transports to the

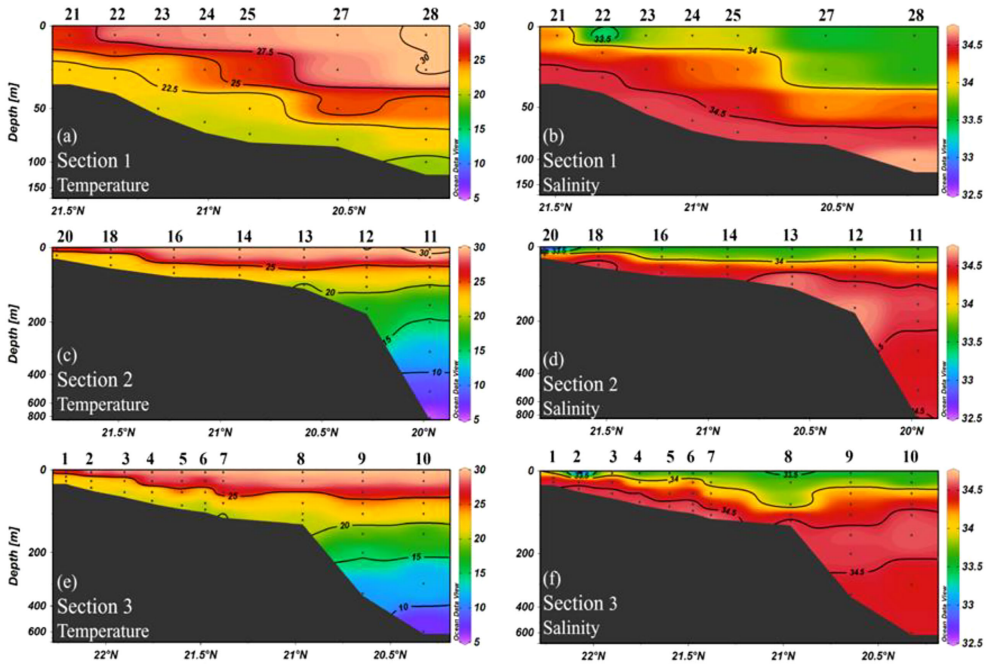


FIGURE 2
Vertical distribution of temperature and salinity in three sections as defined in Figure 1. Note that the depth scale is not linear where the upper 400 m was stretched.

subsurface waters (Xia et al., 2018). Nevertheless, the overall influence of coastal currents in western Guangdong is more important in freshwater (Ying et al., 2003). Thus, the surface salinity decreased in outer Station 21 (Figure 2B). The vertical distribution of salinity showed less influence of intrusion of high-salinity seawater, which may be due to the shallow sampling depth (less than 200 m). High values of salinity and $\delta^{18}O$ were found at the base of Station 28, but due to the shallowness of the station, it is difficult to determine whether these two high values originated from SCSKB or not. Thus, the mixing of water masses in Section 1 is mainly influenced by PREW and SCSW (offshore).

Section 2 is slightly different from Section 1, and the coastal water (Station 20) is characterized by low temperatures and low salinity (Figures 2C, D), indicating a significant impact from PREW. The slope of δD–$\delta^{18}O$ ($\delta D = 10.78\delta^{18}O+4.61$; $R^2 = 0.13$, $p < 0.1$) for this section is higher than GMWL and GOWL (Figure 6C), indicating the presence of freshwater or heavy rainfall. However, the slope of the $\delta^{18}O$–salinity ($\delta^{18}O = 0.25S-8.31$; $R^2 = 0.66$, $p < 0.001$) in Section 2 is slightly lower than that in Section 1, indicating that in addition to freshwater input, this section is also influenced by the saline water intrusion. This also supports the view that the PREW is more likely to flow to the west of the PRE (Ying et al., 2003; Lao et al., 2019a) and, as a result of the influence on Section 1, which is located to the west, is more significant. However, it is also possible that this is due to the greater depth of the station in Section 2 (up to 850 m), which is more affected by the high salinity of seawater. High salinity values (>34.5) and high $\delta^{18}O$ values (>0.4‰) were observed at the bottom (100–150 m) at Stations 12 and 13 (Figures 2D, 4D); this may be due to the intrusion of SCSKB into the subsurface and intermediate layers with high salinity and high $\delta^{18}O$ water. Offshore stations are affected by the SCSW on both the surface and bottom layers. Thus, the mixing process of water masses in Section 2 is mainly influenced by PREW, SCSW, and SCSKB (offshore).

In Section 3, the salinity of the water is relatively high compared to the other two sections from the coast to offshore (Figure 2F), with an average of 34.13. The slope of δD–$\delta^{18}O$ ($\delta D = 4.68\delta^{18}O+1.43$; $R^2 = 0.12$, $p < 0.1$) for this section is lower than GMWL and GOWL (Figure 6C), indicating intrusion of high-salinity seawater or strong evaporation, or both. In addition, compared to the other two sections, the slope of δD–$\delta^{18}O$ is relatively lower. The low slope and high intercept of the $\delta^{18}O$–salinity ($\delta^{18}O = 0.24S-7.6$; $R^2 = 0.26$, $p < 0.001$) regression line for Section 3 indicated that water mass processes in this section are mainly influenced by high-salinity seawater (Figure 6C). Section 3 is located on the eastern side of the PRE, while PREW

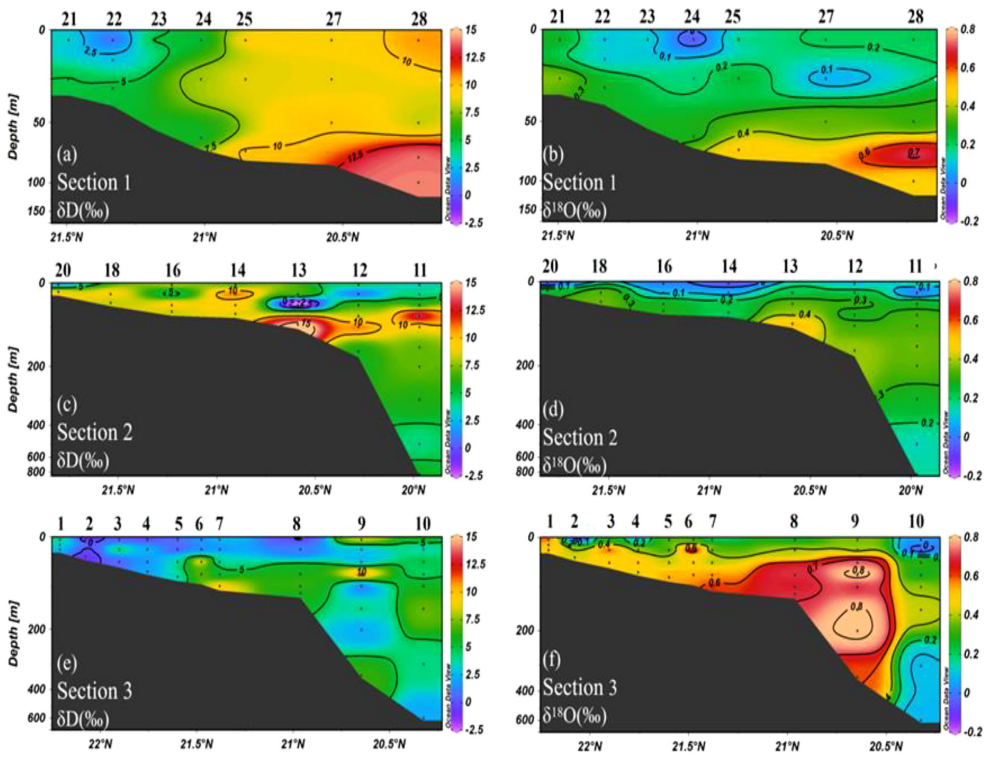


FIGURE 3
Vertical distribution of $\delta^{18}O$ and δD in three sections as defined in Figure 1. Note that the depth scale is not linear where the upper 400 m was stretched.

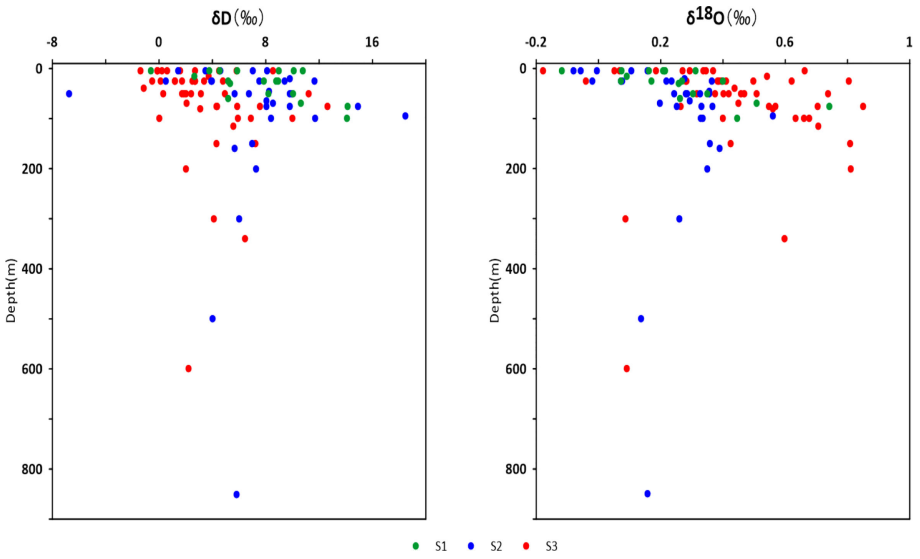


FIGURE 4
Vertical profiles of $\delta^{18}O$ and δD in the three sections of the PRE and the adjacent SCS.

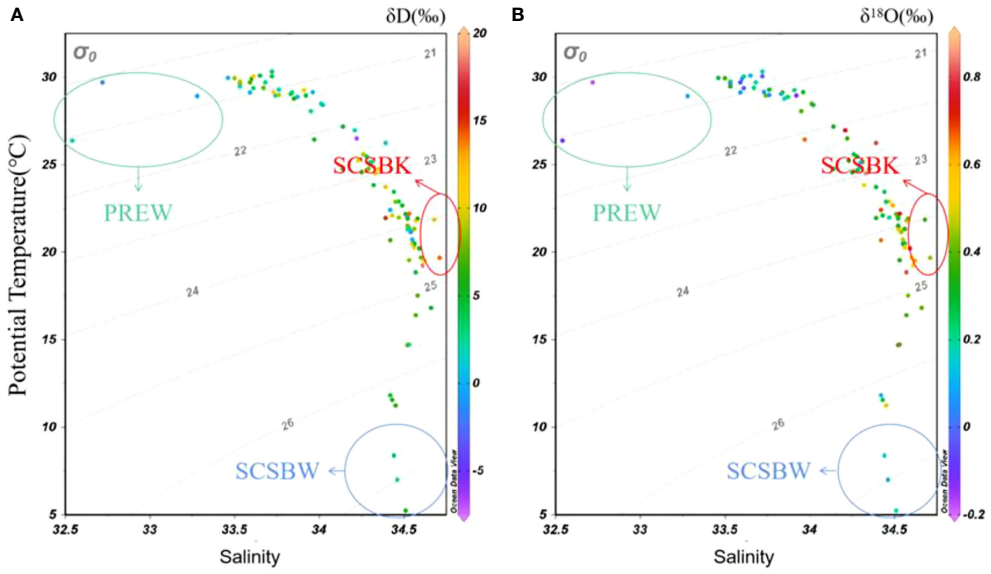


FIGURE 5
Plots of potential temperature (°C) versus salinity for water column of the Pearl River Estuary. Colors indicate **(A)** δD and **(B)** $\delta^{18}O$ values. Three water masses, PREW, SCSKB, and SCSDW, were also marked with ellipses. PREW, Pearl River flushing water; SCSKB, South China Sea Kuroshio Branch; SCSBW, South China Sea bottom water.

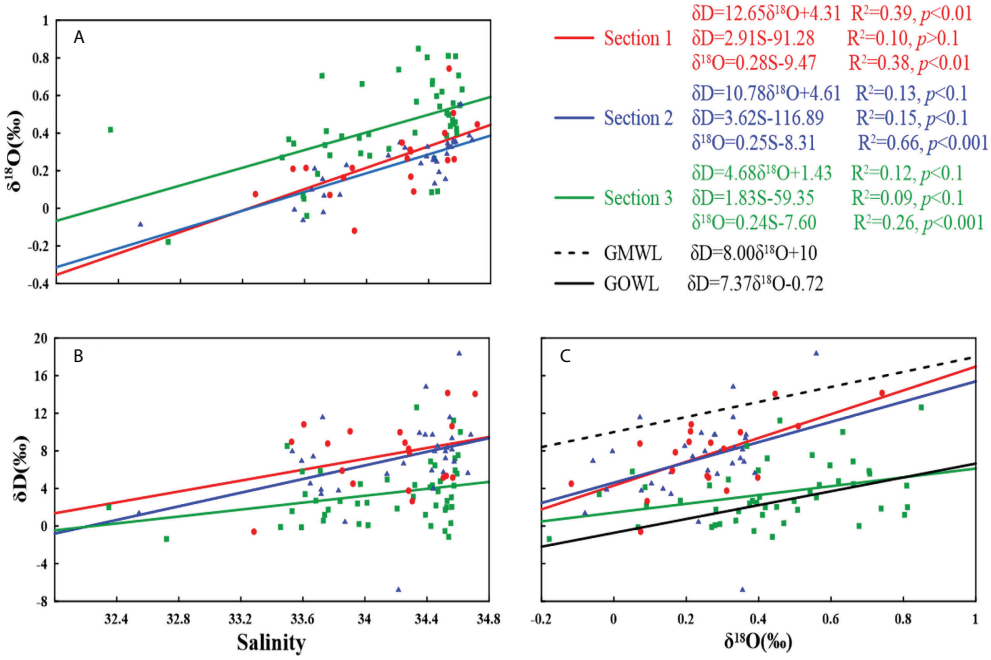


FIGURE 6
(A) $\delta^{18}O$ vs. salinity, **(B)** δD vs. salinity, and **(C)** δD–$\delta^{18}O$ relationship for selected sections as defined in Figure 1. The GMWL was from Craig (1961); the GOWL was from Rohling (2007).

is more likely to flow to the west (Lao et al., 2019a; Chen et al., 2021). These indicate that the effect of PREW may be less on Section 3. The offshore stations (Stations 7–10) in Section 3 showed a high salinity and $\delta^{18}O$ at 100 m to 150 m (Figures 2F, 4F), indicating a significant influence of SCSKB in the subsurface of the section, particularly at a depth of 100–340 m in Station 9, which exhibited the highest salinity (average of 34.49) and $\delta^{18}O$ value (average of 0.7‰). Notably, the $\delta^{18}O$ values in Station 9 were still higher than the Kuroshio end-member in the surface and subsurface water of the eastern Luzon Strait (Wu et al., 2021). There may be two reasons for this phenomenon. Firstly, after the Kuroshio Water intruded into the northern SCS, the continuous evaporation of seawater led to isotopic fractionation during water transportation. The cruise is carried out in summer (June and July), which is during the rainy season and has a large rainfall (Wu et al., 2021). However, the cruise in this study was carried out in fall (September), during which rainfall decreased and seawater volatilization gradually increased. Secondly, the formation of typhoon will carry away a large amount of moisture on the sea surface and transport it to remote areas (Chen et al., 2021; Lao et al., 2022a). Those processes lead to the continuous evaporation of seawater during the Kuroshio water transportation in the SCS. There are two typhoons generated in SCS during September 2015, namely, Vamcon and Mujigae (Chen et al., 2021). Thus, the Kuroshio water may have been fractionated after entering the SCS, resulting in a higher $\delta^{18}O$ value in this study than that in the previous study (Wu et al., 2021). Thus, the mixing process of water masses in Section 3 is different from Sections 1 and 2, which is mainly influenced by SCSW and SCSKB.

Deuterium excess in the PRE

The deuterium excess (*d-excess* = $\delta D\text{-}8\times\delta^{18}O$) is a derived parameter that depends on kinetic fractionation processes of isotopes associated with evaporation (Deshpande et al., 2013). The *d-excess* in continental runoff is about 10‰, while in seawater, it is about 0‰ (Kumar et al., 2018). Even small inputs from continental sources or evaporation of seawater can lead to *d-excess* values >0‰. Only kinetic fractionation during evaporation can result in low *d-excess* values; 0.5‰ can be considered a critical value higher than which the mixing of water masses can be considered not significantly influenced by evaporation or precipitation (Deshpande et al., 2013). The sampling period was September; the runoff was still higher during that period, while the mean value of the *d-excess* in the surface waters of the Pearl River Estuary was 3.08‰. In addition, *d-excess* showed no correlation with $\delta^{18}O$ in the three sections (Figure 7). This suggested a relatively lower effect of kinetic evaporation on seawater in the study area. Thus, the mixing processes of the water masses in the PRE and the adjacent northern SCS are mainly influenced by coastal water in PRE and higher-salinity seawater from SCS and SCSKB.

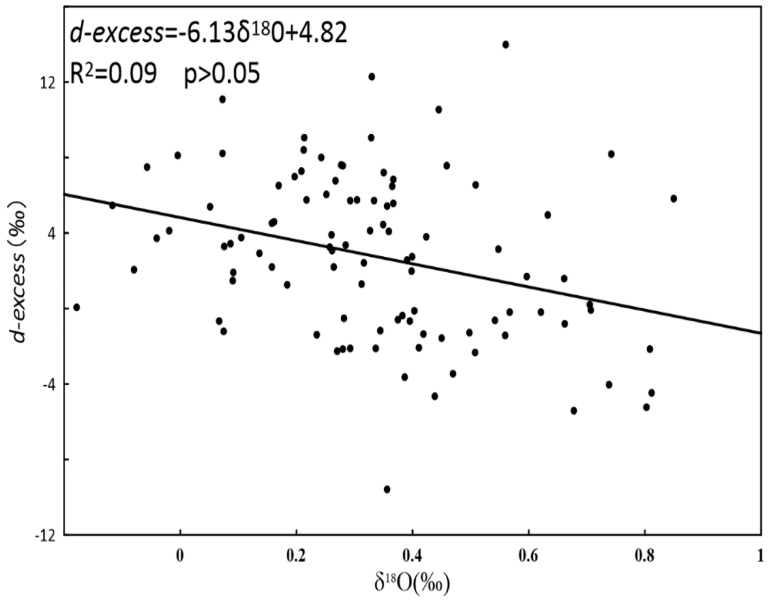


FIGURE 7
d-excess–$\delta^{18}O$ relationship for seawater samples collected in different sections.

Quantification of different water masses and their contributions

As discussed above, the mixing in Section 3 is different from Sections 1 and 2. The seawater in Section 3 may be more influenced by the mixing with SCSW and SCSKB, while Sections 1 and 2 are influenced by the mixing of the three water masses. It is not appropriate to use the Bayesian stable isotope mixing model to quantify the contribution of different water masses if isotopic fractionation is present. However, the dual water isotopes are conservative and less influenced by biological processes (Lian et al., 2016; Jin et al., 2018; Chen et al., 2020; Lao et al., 2022a and Lao et al., 2022b); thus, the $\delta^{18}O$–salinity and δD–$\delta^{18}O$ relationships have been used to determine the mixing of ocean water with runoff, large-scale ocean mixing, sea ice, and glacier melting (Bigg and Rohling, 2000; Benetti et al., 2017). In addition, we found that the correlation between *d-excess* and $\delta^{18}O$ was weak, indicating the lower influence of kinetic fractionation. Thus, we believe that the variation of isotopic compositions and relationships of $\delta^{18}O$–S and δD–$\delta^{18}O$ is mainly influenced by the mixing processes of different water masses, and the Bayesian approach can be used to calculate the relative contribution of different water masses based on the isotopic characteristics of each end-member. To quantify the contribution of mixing between different water masses in the study area, Station 20 characterized by the lowest surface water salinity was selected as a PREW end-member; Station 11 has lower water temperatures but higher salinity at depths of 200–850 m and is very far from the coast, so the 200–850 m of this station was selected as the SCSW end-member; Station 9 with high salinity and isotopic values of water at 100–340 m was selected as the SCSKB end-member. Since *d-excess* and $\delta^{18}O$ are not correlated, indicating little effect from kinetic fractionation, it is feasible to calculate the contribution of different water masses by using dual water isotopes in the Bayesian mixing model. The hydrological and isotopic characteristics of the three end-members are summarized in Table 1. The isotopic values from the three end-members were used to calculate the proportion of the mixing water masses in the PRE and the adjacent northern SCS. The results are presented in Figure 8. The results showed that the seawater mainly contributed from the SCSW (accounting for 71%), followed by the SCSKB (accounting for 23%), while the contribution of PREW only accounted for 6%. However, in Section 3, the seawater mainly contributed from SCSKB (accounting for 50%), which was significantly higher than that in Sections 1 and 2. This suggested that the Kuroshio intruded into the northern SCS has a great impact on Section 3, but has a lesser impact on the other two sections. This result is consistent with a previous study that suggested that the Kuroshio water could intrude the continental slope in the southwestern Taiwan Strait (about 117°E) (Chen et al., 2020b). Moreover, the SCS water in the southwestern Taiwan Strait mainly originated from the upslope deflection of the slope current formed by the Kuroshio water intrusion into the SCS, but not from the west segment of the SCS water formed to the east of Hainan Island (Chen et al., 2020b). However, this study found that the great impact of the Kuroshio intrusion can even reach 115.5°E (in Section 3), which brings a new understanding to the influence of the Kuroshio intrusion into the northern SCS.

TABLE 1 The isotopic characteristics of the PREW, SCSW, and SCSKB in the PRE and the adjacent northern SCS.

	PREW	SCSW	SCSKB
Salinity	32.54 ± 0	34.47 ± 0.04	34.49 ± 0.06
Temperature	26.39 ± 0	10.02 ± 3.51	16.84 ± 4.20
δD (‰)	1.4 ± 0	5.8 ± 1.3	3.2 ± 2.8
$\delta^{18}O$ (‰)	−0.1 ± 0	0.2 ± 0.1	0.8 ± 0.1

The implications of the water masses mixing in the local environment

In this study, we investigated the mixing of water masses in the PRE and the adjacent SCS according to the relationship between δD, $\delta^{18}O$, and salinity. The mixing of water masses in the PRE and adjacent SCS is mainly contributed by SCSW (71%), SCSKB (23%), and PREW (6%). The characteristics of high temperature but low salinity and low isotope values of PREW are mainly influenced by the surface water. The influence of SCSW water on the mixing of water masses in the PRE and the adjacent SCS is mainly through surface intrusion from the bottom of the offshore. The SCSKB that originated from the Kuroshio with high salinity and high isotopic values is mainly influenced by the subsurface water (100–300 m). In the PRE, the signal of the SCSKB water was weak, because of the high density with high temperature and high salinity sinking to the subsurface layer (100–300 m) after intrusion of the Kuroshio Branch into SCS. However, this study found that the signals of the Kuroshio Branch were only captured in the east of 115°E (Section 3) (the contribution of Kuroshio water accounting for 50%), whereas the west of 115°E (Sections 1 and 2) was mainly affected by the PREW (mainly in the surface water) and SCSW. The mixing of different water masses with the elements carried by the transportation processes may greatly impact environmental factors and local marine ecosystems (Lao et al., 2022a and Lao et al., 2022b). For example, the high absorption and fluorescence of dissolved organic matter (CDOM and FDOM) in the subsurface layer of SCS were mainly modulated by the Kuroshio intrusion (Wang et al., 2017). In addition, a stable input of external nutrients from different water masses, such as the West Guangdong coastal current and SCS water, was observed to sustain primary production in the Beibu Gulf throughout the year (Lao et al., 2022a). However, a high

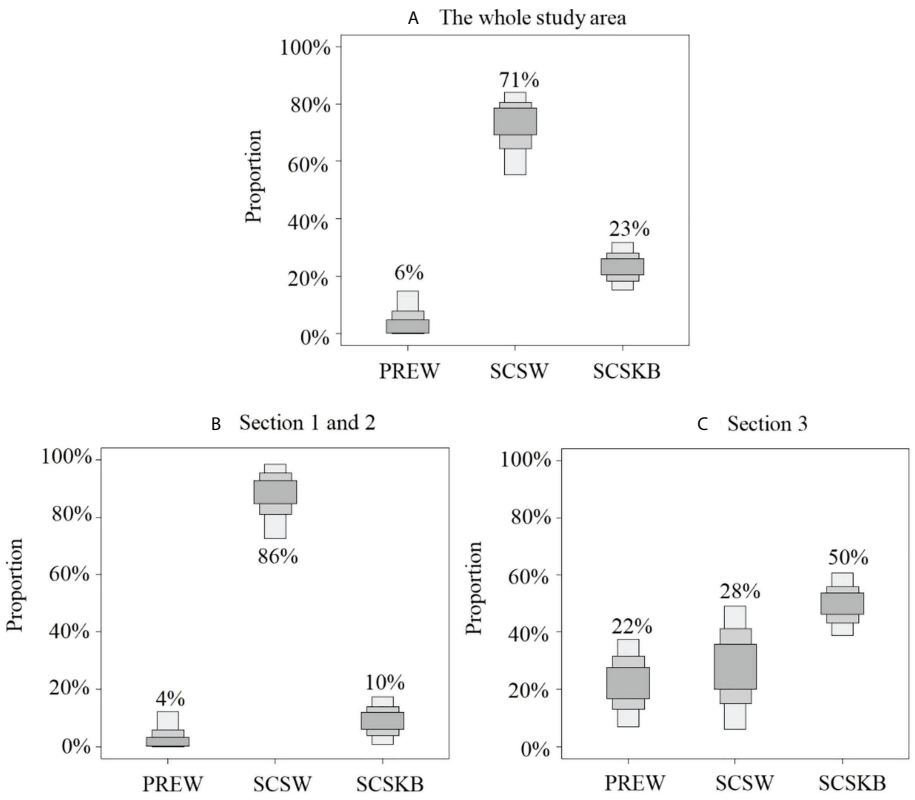


FIGURE 8
Proportional contribution of different water masses to the seawater of the PRE and the adjacent northern SCS. **(A)** The whole study area; **(B)** Section 1 and 2; **(C)** Section 3.

nutrient supplied from the West Guangdong coastal current to the Beibu Gulf during the dry season also resulted in the frequent algal blooms in the central gulf (Lao et al., 2022a). By contrast, as the dominant water source during the rainy seasons, the coastal current in the Beibu Gulf can input a large number of land-based pollutants into the coastal oceans (Lao et al., 2019b; Lao et al., 2022a), thereby intensifying water pollution, such as eutrophication (Lao et al., 2021). Moreover, increasing intrusion of high-salinity water has altered the mariculture activities in the coastal bays because it increased the salinity and seriously retained the pollutants of freshwater in the coastal bays (Lao et al., 2022b). Thus, the results of this study also provide a new idea for the study of physical dynamic and biogeochemical cycles in this region.

Conclusion

This study presents a new dataset, including δD and $\delta^{18}O$, for the water mass processes from the PRE and the adjacent northern SCS. Based on hydrographic observations and the relationship between isotopes of hydrogen, oxygen, and salinity in the water column, we have identified and quantified the mixing processes in the water column at PRE and the adjacent northern SCS. The seawater in the PRE and the adjacent northern SCS is significantly influenced by PREW (6%), SCSKB (23%), and SCSW (71%). However, the influence of PREW mainly occurred in the surface water, whereas the SCSKB with high salinity and high isotopic values is mainly influenced by the subsurface water (100–300 m). The mixing process of water masses in Sections 1 and 2 is similar, which is mainly contributed by the SCSW (86%), while the contribution of PREW and SCSKB is only 4% and 10%, respectively. By contrast, the mixing process of water masses in Section 3 is mainly influenced by the Kuroshio intrusion (50%). In addition, this study found that the great impact of the Kuroshio intrusion can reach 115.5°E (in Section 3), which brings a new understanding to the influence of the Kuroshio intrusion into the northern SCS.

Data availability statement

The original contributions presented in the study are included in the article/supplementary materials. Further inquiries can be directed to the corresponding author.

Author contributions

SZ was responsible for the conceptualization. XJ and QL prepared and wrote the original draft. XJ, QL and FC wrote, reviewed, and edited the manuscript. PH were responsible for the data curation. XJ, CC, QZ were responsible for the experimental operation. XJ, CC were responsible for field sampling. FC and SZ funded the acquisition. All authors contributed to the article and approved the submitted version.

Acknowledgments

We would like to thank Professor Jie Xu for his support in collecting water samples. This work was supported by the National Natural Science Foundation of China (92158201 and U1901213), the Scientific Research Start-Up Foundation of Shantou University (NTF20006), the Innovation and Entrepreneurship Project of Shantou (2021112176541391), and the Guangdong Natural Science Foundation of China (2019B1515120066).

Conflict of interest

The authors declare that the research was conducted in the absence of any commercial or financial relationships that could be construed as a potential conflict of interest.

Publisher's note

All claims expressed in this article are solely those of the authors and do not necessarily represent those of their affiliated organizations, or those of the publisher, the editors and the reviewers. Any product that may be evaluated in this article, or claim that may be made by its manufacturer, is not guaranteed or endorsed by the publisher.

References

Benetti, M., Reverdin, G., Aloisi, G., and árny Erla, S. R. (2017). Stable isotopes in surface waters of the Atlantic ocean: Indicators of ocean-atmosphere water fluxes and oceanic mixing processes. *J. Geophys. Res. Oceans.* 122 (6), 4723–4742. doi: 10.1002/2017JC012712

Bigg, G. R., and Rohling, E. J. (2000). An oxygen isotope data set for marine waters. *J. Geophys. Res.: Ocean.* 105 (C4), 8527–8535. doi: 10.1029/2000JC900005

Chen, F., Deng, Z., Lao, Q., Bian, P., Jin, G., Zhu, Q., et al. (2022). Nitrogen cycling across a salinity gradient from the pearl river estuary to offshore: Insight from nitrate dual isotopes. *J. Geophys. Res.: Biogeosci.* 127 (5), e2022JG006862. doi: 10.1029/2022JG006862

Chen, F., Huang, C., Lao, Q., Zhang, S., Chen, C., Zhou, X., et al. (2021). Typhoon control of precipitation dual isotopes in southern China and its palaeoenvironmental implications. *J. Geophys. Res.: Atmosph.* 126 (14), e2020JD034336. doi: 10.1029/2020JD034336

Chen, F., Lao, Q., Zhang, S., Bian, P., and Chen, C. (2020b). Nitrate sources and biogeochemical processes identified using nitrogen and oxygen isotopes on the eastern coast of hainan island. *Cont. Shelf. Res.* 207, 104209. doi: 10.1016/j.csr.2020.104209

Chen, D., Lian, E., Shu, Y., Yang, S., Li, Y., Liu, P, et al. (2020a). Origin of the springtime south China Sea warm current in the southwestern Taiwan strait: Evidence from seawater oxygen isotope. *Sci. China: Earth Sci.* 63 (10), 1564–1576. doi: 10.1007/s11430-019-9642-8

Chen, F., Zhou, X., Lao, Q., Wang, S., Jin, G., Chen, C., et al. (2019). Dual isotopic evidence for nitrate sources and active biological transformation in the northern south China Sea in summer. *PloS One* 14 (1), e0209287. doi: 10.1371/journal.pone.0209287

Craig, H. I. (1961). Isotopic variations in meteoric waters. *Science* 133, 1702–1703. doi: 10.1126/science.133.3465.1702

Craig, H., and Gordon, L. I. (1965). Deuterium and oxygen 18 variation in the ocean and the marine atmosphere in *Stable Isotopes in Oceanographic Studies and Paleotemperatures*. Edited by. E. Tongiorgi, 9–130. (Pisa, Italy: Conisglio Naz. delle Ric., Lab. di Geol. Nucl).

Deshpande, R. D., Muraleedharan, P. M., Singh, R. L., Kumar, B., Rao, M. S., Dave, M., et al. (2013). Spatio-temporal distributions of $\delta^{18}O$, δD and salinity in the Arabian Sea: Identifying processes and controls. *Mar. Chem.* 157 (dec.20), 144–161. doi: 10.1016/j.marchem.2013.10.001

Durack, P. J. (2015). Ocean salinity and the global water cycle. *Oceanography* 28 (1), 20–31. doi: 10.5670/oceanog.2015.03

Fairbanks, R. G. (1982). The origin of continental shelf and slope water in the new York bight and gulf of Maine: Evidence from $H_2\ ^{18}O/H_2\ ^{16}O$ ratio measurements. *J. Geophys. Res.: Ocean.* 87 (C8), 5796–5808. doi: 10.1029/JC087iC08p05796

Fang, Z., and Wang, W. (2022). Dynamics of trace metals with different size species in the pearl river estuary, southern China. *Sci. Tot. Environ.* 807 (P1), 150712. doi: 10.1016/J.SCITOTENV.2021.150712

Frew, R. D., Dennis, P. F., Heywood, K. J., Meredith, M. P., and Boswell, S. M. (2000). The oxygen isotope composition of water masses in the northern north Atlantic. *Deep-Sea. Res. Part I.* 47 (12), 2265–2286. doi: 10.1016/S0967-0637(00)00023-6

Harvey, J. (1982). θ-s relationships and water masses in the eastern north Atlantic. *Deep. Sea. Res. Part A. Oceanog. Res. Pap.* 29 (8), 1021–1033. doi: 10.1016/0198-0149(82)90025-5

Hattori, K. 1997(1997). *Stable isotope geochemistry: Jochen hoefs. 4th ed* (Berlin: Springer-Verlag), 201 pp. doi: 10.1002/qj.49705322213

Helland-Hansen, B., and Nansen, F. (1926). The eastern north Atlantic. *Geofys Publikasjonen.* 4, 76.

Jackson, A. L., Inger, R., Bearhop, S., and Parnell, A. (2009). Erroneous behaviour of MixSIR, a recently published Bayesian isotope mixing model: a discussion of Moore & semmens, (2008). *Ecol. Lett.* 12 (3), E1–E5. doi: 10.1111/j.1461-0248.2008.01233.x

Jin, K., Rao, W., Tan, H., Song, Y., Yong, B., Zheng, F., et al. (2018). H-O isotopic and chemical characteristics of a precipitation-lake water-groundwater system in a desert area. *J. Hydrol.* 559, 848–860. doi: 10.1016/j.jhydrol.2018.03.005

Karati, K. K., Ashadevi, C. R., Rasheed, K., Vineetha, G., Smitha, B. R., Vimalkumar, K. G., et al. (2019). Influence of the coastal circulation and water-mass characteristics in structuring the zooplankton community of the eastern Arabian Sea. *Reg. Stud. Mar. Sci.* 31, 100761. doi: 10.1016/j.rsma.2019.100761

Kumar, P. K., and Ramesh, R. (2016). Revisiting reconstructed Indian monsoon rainfall variations during the last ~25 ka from planktonic foraminiferal $\delta^{18}O$ from the Eastern Arabian Sea. *Quat. Int.* 443, 29–38. doi: 10.1016/j.quaint.2016.07.012

Kumar, P. K., Singh, A., and Ramesh, R. (2018). Controls on $\delta^{18}O$, δD and $\delta^{18}O$–salinity relationship in the northern Indian ocean. *Mar. Chem.* 207, 55–62. doi: 10.1016/j.marchem.2018.10.010

Lao, Q., Chen, F., Liu, G., Chen, C., Jin, G., Zhu, Q., et al. (2019b). Isotopic evidence for the shift of nitrate sources and active biological transformation on the western coast of guangdong province, south China. *Mar. pollut. Bull.* 142, 603–612. doi: 10.1016/j.marpolbul.2019.04.026

Lao, Q., Liu, G., Shen, Y., Su, Q., and Lei, X. (2021). Biogeochemical processes and eutrophication status of nutrients in the northern beibu gulf, south China. *J. Earth Sys. Sci.* 130 (4), 1–14. doi: 10.1007/s12040-021-01706-y

Lao, Q., Su, Q., Liu, G., Shen, Y., Chen, F., Lei, X., et al. (2019a). Spatial distribution of and historical changes in heavy metals in the surface seawater and sediments of the beibu gulf, China. *Mar. pollut. Bull.* 146, 427–434. doi: 10.1016/j.marpolbul.2019.06.080

Lao, Q., Wu, J., Chen, F., Zhou, X., Li, Z., Chen, C., et al. (2022b). Increasing intrusion of high salinity water alters the mariculture activities in zhanjiang bay during the past two decades identified by dual water isotopes. *J. Environ. Manage.* 320, 115815. doi: 10.1016/j.jenvman.2022.115815

Lao, Q., Zhang, S., Li, Z., Chen, F., Zhou, X., Jin, G., et al. (2022a). Quantification of the seasonal intrusion of water masses and their impact on nutrients in the beibu gulf using dual water isotopes. *J. Geophys. Res.: Ocean.* 127, e2021JC018065. doi: 10.1029/2021JC018065

Legrande, A. N., and Schmidt, G. A. (2006). Global gridded data set of the oxygen isotopic composition in seawater. *Geophys. Res. Lett.* 33 (12), 12604–1-12604-5. doi: 10.1029/2006GL026011

Lian, E., Yang, S., Wu, H., Yang, C., Li, C., and Liu, J. T. (2016). Kuroshio subsurface water feeds the wintertime Taiwan warm current on the inner East China Sea shelf. *J. Geophys. Res.: Oceans.* 121 (7), 4790–4803. doi: 10.1002/2016JC011869

Liu, B., Liao, Y., Yan, S., and Yan, H. (2017). Dynamic characteristics of saltwater intrusion in the pearl river estuary, China. *Nat. Haz.* 89 (3), 1097–1117. doi: 10.1007/s11069-017-3010-4

Liu, B., Peng, S., Liao, Y., and Wang, H. (2019). The characteristics and causes of increasingly severe saltwater intrusion in pearl river estuary. *Estuar. Coast. Shelf. Sci.* 220, 54–63. doi: 10.1016/j.ecss.2019.02.041

Moore, J. W., and Semmens, B. X. (2008). Incorporating uncertainty and prior information into stable isotope mixing models. *Ecol. Lett.* 11 (5), 470–480. doi: 10.1111/j.1461-0248.2008.01163.x

Oka, E., and Qiu, B. (2012). Progress of north pacific mode water research in the past decade. *J. Oceanogr.* 68 (1), 5–20. doi: 10.1007/s10872-011-0032-5

Richardson, L. E., Middleton, J. F., James, N. P., Kyser, T. K., and Opdyke, B. N. (2018). Water masses and their seasonal variation on the Lincoln shelf, south Australia. *Limnol. Oceanogr.* 63 (5), 1944–1963. doi: 10.1002/lno.10817

Rohling, E. J. (2007). Progress in paleosalinity: Overview and presentation of a new approach. *Paleoceanography* 22 (3), A3215–1-A3215-9. doi: 10.1029/2007PA001437

Sengupta, S., Parekh, A., Chakraborty, S., Kumar, K. R., and Bose, T. (2013). Vertical variation of oxygen isotope in bay of Bengal and its relationships with water masses. *J. Geophys. Res.: Oceans.* 118 (12), 6411–6424. doi: 10.1002/2013JC008973

Singh, A., Jani, R. A., and Ramesh, R. (2010). Spatiotemporal variations of the $\delta^{18}O$–salinity relation in the northern Indian ocean. *Deep-Sea. Res. Part I.* 57 (11), 1422–1431. doi: 10.1016/j.dsr.2010.08.002

Tran, D. A., Tsujimura, M., Vo, L. P., Nguyen, V. T., Nguyen, L. D., and Dang, T. D. (2019). Stable isotope characteristics of water resources in the coastal area of the Vietnamese Mekong delta. *Isotope. Environ. Health Stud.* 55 (6), 566–587. doi: 10.1080/10256016.2019.1673746

Wang, C., Guo, W., Li, Y., Stubbins, A., Li, Y., Song, G., et al. (2017). Hydrological and biogeochemical controls on absorption and fluorescence of dissolved organic matter in the northern south China Sea. *J. Geophys. Res.: Biogeosci.* 122 (12), 3405–3418. doi: 10.1002/2017JG004100

Wang, B., Zhang, H., Xia, L., Li, X., and Wang, F. (2018). Cumulative effects of cascade dams on river water cycle: Evidence from hydrogen and oxygen isotopes. *J. Hydrol.* 568, 604–610. doi: 10.1016/j.jhydrol.2018.11.016

Wu, J., Lao, Q., Chen, F., Huang, C., Zhang, S., Wang, C., et al. (2021). Water mass processes between the south China Sea and the Western pacific through the Luzon strait: Insights from hydrogen and oxygen isotopes. *J. Geophys. Res.: Ocean.* 126 (8), e2021JC017484. doi: 10.1029/2021JC017484

Wu, X., Zhang, L., Hu, B. X., Wang, Y., and Xu, Z. (2020). Isotopic and hydrochemical evidence for the salinity origin in the coastal aquifers of the pearl river delta, guangzhou, China. *J. Contam. Hydrol.* 235 (prepublish), 103732. doi: 10.1016/j.jconhyd.2020.103732

Xia, Y., Liu, C., and Wang, D. (2018). Pearl river flushing freshwater driven upwelling in summer 2006. *Haiyang. Xuebao.* 40 (07), 43–54. doi: 10.3969/j.issn.0253-4193.2018.07.004

Xie, L., Tian, J., Zhang, S., Zhang, Y., and Yang, Q. (2011). An anticyclonic eddy in the intermediate layer of the Luzon strait in autumn 2005. *J. Oceanogr.* 67 (1), 37–46. doi: 10.1007/s10872-011-0004-9

Xu, M. N., Zhang, W., Zhu, Y., Liu, L., Zheng, Z., Wan, X. S., et al. (2018). Enhanced ammonia oxidation caused by lateral kuroshio intrusion in the boundary zone of the northern south China Sea. *Geophys. Res. Lett.* 45 (13), 6585–6593. doi: 10.1029/2018GL077896

Ying, Y. S., Wen, B. X., Sheng, C. C., Fei, C.Hangzhou, China, Qingdao, and China (2003). Analysis on characteristics and mechanism of current system in west coast of guangdong province in the summer. *Acta Oceanol. Sin.* 25 (6), 1–8. doi: 10.1007/s11769-003-0089-1

Yu, X., Zhuang, Y., Cai, X, and Qi, D. (2022). Role of marginal seas in deep ocean regeneration of dissolved silica: A case study in the marginal seas of the Western pacific. *Front. Mar. Sci.* 9. doi: 10.3389/fmars.2022.925919

Zhang, Y., Li, Q., Luo, Y., Yan, L., Peng, K., Liu, Z., et al. (2022). Groundwater salinization in a subtropical region, beihai, southern China: Insights from hydrochemistry and multiple isotopes (H, O, s, Sr). *Appl. Geochem.* 141, 105323. doi: 10.1016/j.apgeochem.2022.105323

Zhuang, Y., Jin, H., Cai, W.-J., Li, H., Qi, D., and Chen, J. (2022). Extreme nitrate deficits in the western Arctic ocean: Origin, decadal changes, and implications for denitrification on a polar marginal shelf. *Global Biogeochem. Cycle.* 36, e2022GB007304. doi: 10.1029/2022GB007304

frontiers | Frontiers in Marine Science

TYPE Original Research
PUBLISHED 02 September 2022
DOI 10.3389/fmars.2022.986379

Check for updates

OPEN ACCESS

EDITED BY
Dilip Kumar Jha,
National Institute of Ocean Technology, India

REVIEWED BY
Qiao Yongmin,
Jinan University, China
Feng Jiang,
Sun Yat-sen University, China
Balasubramaniam Sujatha,
Pachaiyappa's College for Men, India

*CORRESPONDENCE
Wen Zhou
zhouwen@scies.org

SPECIALTY SECTION
This article was submitted to Marine Pollution, a section of the journal Frontiers in Marine Science

RECEIVED 05 July 2022
ACCEPTED 15 August 2022
PUBLISHED 02 September 2022

CITATION
Geng B, Zhou W, Lu L, Cao Q, Hong M and Wen D (2022) Risk assessment of offshore oil spill in the northern South China Sea: A stochastic scenario modeling approach.
Front. Mar. Sci. 9:986379.
doi: 10.3389/fmars.2022.986379

COPYRIGHT
© 2022 Geng, Zhou, Lu, Cao, Hong and Wen. This is an open-access article distributed under the terms of the Creative Commons Attribution License (CC BY). The use, distribution or reproduction in other forums is permitted, provided the original author(s) and the copyright owner(s) are credited and that the original publication in this journal is cited, in accordance with accepted academic practice. No use, distribution or reproduction is permitted which does not comply with these terms.

Risk assessment of offshore oil spill in the northern South China Sea: A stochastic scenario modeling approach

Bingxu Geng[1,2], Wen Zhou[3]*, Lingyan Lu[4], Qian Cao[3], Man Hong[3] and Ding Wen[3]

[1]Marine Environmental Engineering Center, South China Sea Institute of Oceanology, Chinese Academy of Sciences, Guangzhou, China, [2]Southern Marine Science and Engineering Guangdong Laboratory (Guangzhou), Guangzhou, China, [3]South China Institute of Environmental Sciences, Ministry of Ecology and Environment of the People's Republic of China, Guangzhou, China, [4]Guangdong Center for Marine Development Research, Guangzhou, China

The coastal area in the northern South China Sea (nSCS) is one of China's most economically active regions. The fast-growing industry of marine sector and the shipping has increased the probability of oil spill accidents. An oil spill is a usually unexpected incident that is harmful to the ecological environment and marine organisms of the coastal area. As a result, utilizing a numerical model to simulate the fate and transport trajectory of spilled oil and to assess the potential risk of an oil spill accident to the coastal marine environment is of great necessity. The present study aimed to examine the impact of the risk of oil spills on the coastal environment in the nSCS. We built a hydrodynamic model and an oil spill dispersion model based on MIKE21 FM to study the tidal dynamics and oil spill dispersion in the coastal area in the nSCS. Moreover, the stochastic approach was used to simulate and predict the fastest arrival time and the probability distribution of the pollution of the oil film to the surrounding environment in the coastal regions of the nSCS. We examined the mechanisms for the influences of tides and wind on the fastest arrival time of oil film and the spatial distribution of the pollution probability of oil spill incidents at different locations in the nSCS based on the model. The results showed that the wind direction has a dominating effect on the direction of the oil dispersion. Due to the differences in the tidal dynamics in different regions, the migration and dispersion of the oil are also affected by the tidal current. This research provides guidance on the risk assessment of oil spill accidents for marine environmental management.

KEYWORDS

oil spill accident, The northern South China Sea, risk assessment, stochastic scenario simulation, Numerical modeling

Introduction

Oil exploration and transportation activities have been promoted due to the increase in petroleum demand and consumption in recent decades. The frequent production and transportation activities on the sea increase the potential for the risk of oil spills to the marine environment. Man-made errors and failures, such as collisions of construction and shipping vessels, ship groundings, and crude oil pipeline ruptures, emit tons of crude oil to the ocean (Chen et al., 2019). A sudden oil spill accident can have a devastating effect on the marine environment and marine ecosystem because of the high concentration of the contaminants and the difficulties with treatment (Law and Hellou, 1999; Fisher et al., 2016; Wang et al., 2020). The oil film spreading on the sea surface will hinder water reaeration and decrease the dissolved oxygen concentration in the water column and would finally deteriorate the bottom hypoxia (Rabalais et al., 2018). Generally, oil spills harm ocean life in two ways: *via* fouling/oiling (Alkhatib et al., 2021) or oil toxicity (Demiguel-Jiménez et al., 2021). Fouling or oiling happens when oil physically harms plants or animals (Camphuysen and Heubeck, 2015; Troisi et al., 2016; Chen et al., 2020). It can cover a bird's wings, causing it to be unable to fly. Additionally, oil has many different toxic compounds that lead to severe health problems (Ferguson et al., 2020). Thus, the prediction and risk assessment of oil spill incidents are important for marine environment protection. The coastal area of the northern South China Sea (nSCS), centered on the Greater Bay Area (Guangdong–Hong Kong–Macao Great Bay Area), is one of the most active areas in China's national economic development (Yu, 2021). A lot of marine constructions are built to provide offshore services, leading to intense maritime traffic carrying oil and petroleum during shipping (Chen et al., 2018). Any leakage of the oil into the environment can cause the long-term contamination to the environment and finally spoil the delicate balance of the offshore ecology. Meanwhile, the research indicates that oil spill incidents that occurred many years ago still affect the environment and impact the local ecosystems (Beyer et al., 2016; Gao et al., 2018). Major concerns were raised about the potential influence of oil spilling accidents on the marine environment. Thus, the study on the impact of offshore oil spills in the nSCS can provide basic knowledge for offshore environmental protection.

A numerical simulation of the trajectory of an oil spill is the main method for the analysis and assessment of oil spill hazards (Prasad et al., 2018; Balogun et al., 2021). Depending on different hydrodynamic and meteorological conditions, the numerical simulation of oil spill risk is generally divided into a typical scenario simulation and a stochastic scenario simulation (Keramea et al., 2021). Among them, a typical scenario simulation is more widely used (Kampouris et al., 2021). Generally, a dominant and unfavorable wind direction are the only two conditions that are considered in a typical scenario simulation. Tidal dynamic conditions only include flooding and ebb-tidal periods. The above meteorological and hydrological conditions are combined into several typical scenarios. The oil spill trajectory model is used to predict the drift trajectory of the oil film and the fastest time for the oil spill to reach the environmentally sensitive regions forced by the meteorological and hydrological conditions given for each typical scenario. Samuels et al. (2013) developed an oil spill modeling system that can be applied on a global scale. Prakash et al. (2015) used oil weathering processes to predict critical slick properties such as viscosity and density.

However, the hydrographic and meteorological conditions of the ocean change at any time, and the occurrence of oil spills is random. The deterministic approach cannot reflect the oil spills' stochasticity and the uncertain impact of oil spills on the marine environment. Therefore, more and more researchers have started to use the stochastic approach to simulate and assess the pollution risk of oil spills to the sea in recent years (Al-Rabeh et al., 1989; Amir-Heidari et al., 2019; Saçu et al., 2021). The stochastic scenario simulation is a method developed based on probability theory by numerically simulating the oil spill drift trajectory with hundreds of random scenario combinations for potential oil spill incidents. Meteorological and hydrological conditions were randomly selected from the wind and tidal fields at any time in the past years with uncertainty in the time of the occurrence of each random scenario. For each stochastic scenario, data such as the elapsed time of pollutants and oil film thickness at each moment are calculated and recorded for each model grid (Toz, 2017). Finally, with the statistical information on the probability of pollution and the fastest arrival time of the oil film for each model grid under the influence of the oil spill, combined with the distribution location of sensitive environmental targets around the study area, we can obtain the pollution probability and the fastest arrival time of the oil film for each sensitive environmental target or the oil spill (Zacharias et al., 2021).

From the above analysis, it can be seen that the use of the stochastic approach and the combined use of stochastic and typical scenario simulation methods to predict the impact of oil spills on the marine ecosystem have been widely used in recent years (Niu et al., 2016; Saçu et al., 2021). However, the existing research lacks in-depth studies on the dynamic mechanisms of the spatial distribution of pollution probability and the fastest arrival time of the oil film in oil spill accidents obtained from the simulation of the stochastic scenario method, which cannot provide a scientific basis for the marine management department to formulate scientific and effective countermeasures for the risk management of oil spill accidents.

Therefore, this study used a stochastic approach to predict the pollution probability and shortest arrival time of the

nearshore oil spill incident in the nSCS to the surrounding marine environment. The driving mechanism of tidal dynamics, the wind field on the spatial distribution of pollution probability and the shortest arrival time were analyzed to provide a deeper understanding of oil's impact on the nSCS. This can be used to improve the accuracy of the risk assessment of coastal oil spills in the nSCS and the decision support for the marine management department to develop effective risk management countermeasures for oil spill incidents.

Methodology

This research selected the coastal area near Shantou in the nSCS to study the impact of oil spill risk based on a stochastic scenario simulation. The MIKE21 FM model was used to numerically simulate the tidal dynamics and the oil spill trajectory in the study area. This section will briefly introduce the tidal dynamic model, the oil spill dispersion model, and the setup of the stochastic scenario simulation.

Hydrodynamic model setup and validation

Figure 1 shows the model domain and model grid in the coastal area of the nSCS. The model used an unstructured triangular mesh. The entire model domain consists of 2840 nodes and 5091 triangular cells, with a minimum horizontal resolution of ~25 m. The coastline and water depth of the model were obtained by digitizing and interpolating the latest nautical chart data. The open boundary of the model is driven by the hourly tidal elevation. The driving data are interpolated from the global tidal inversion model (TPXO7.2) developed by Oregon State University (OSU) in the USA. The model's simulation period starts from 1 September 2020 to 30 September 2020.

A 25-hour tidal elevation series at station T1, and a 25-hour tidal current with observations of the direction and velocity at stations V1 and V2 was used to validate the tidal dynamic model in the nSCS. The location of each station is shown in Figure 1. The modeled time-series of the tidal elevation, velocity and direction of tidal currents were compared with the observed data, and the results are shown in Figures 2, 3. The time-series distribution of the tidal elevation and current velocity simulated by the tidal dynamics model is consistent with the distribution trends observed in the field. The model successfully simulates the trends of high and low tides at the observed stations. Quantitative statistics show that the average error of the tide level is 0.08 m. Overall, the hydrodynamic model in the nSCS can better reproduce the tidal dynamic process in our model domain. The results can be applied to the nearshore oil spill trajectory and the oil spill risk assessment study in the nSCS.

Setup of the oil spill model

We use the MIKE model's OS oil spill model to simulate the accidental oil spill's fate and transport trajectory. In our oil spill model, the oil spill enters the water body after the oil spill accident. It first expands in all directions due to gravity, inertia force, viscosity, and surface tension, forming a large area of oil film. After that, it starts drifting and spreading under the effect of environmental factors such as tidal currents and sea surface wind. The oil from the spilling accident contains various components with different vapor pressure, solubility, viscosity, and surface tension. The highly volatile components evaporate quickly, some of the lighter carbon components will gradually dissolve in water, and the non-volatile parts will remain on the sea surface. After the accident happens, the oil film spreads and migrates on the sea surface affected by the wind and tide, while evaporation, emulsification, and dissolution processes occur.

The oil spill model is based on the model of "oil particles", which treats the oil spill as being many oil spill particles. It uses the Lagrange random walk approach and the particle cloud principle to describe the process of oil spill diffusion and considers the processes of the evaporation, emulsification, dissolution, and biodegradation of the oil spill. The hydrodynamic field calculated by the tidal model provides the corresponding turbulent diffusion coefficients for the oil spill model to simulate oil particles' drift and diffusion processes. Since the offshore wind conditions (wind speed and direction) significantly influence the motion of the oil film, the effect of

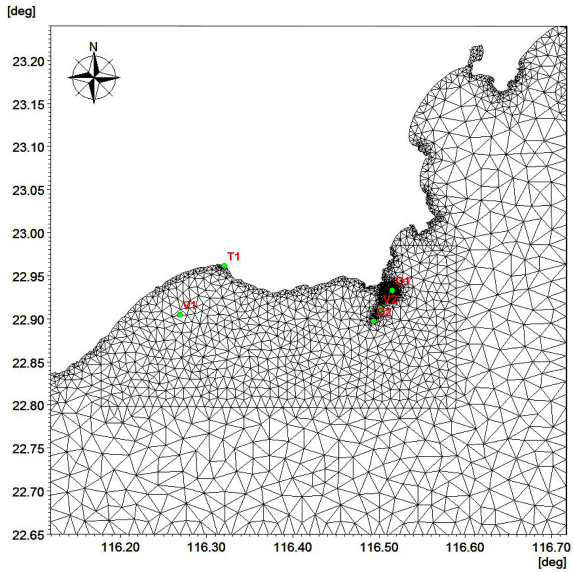


FIGURE 1
Model domain and model grid of the coastal tidal dynamic model in the northern South China Sea.

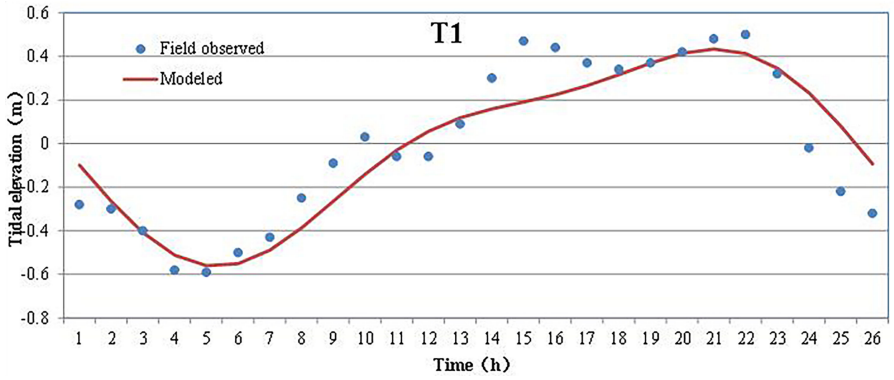


FIGURE 2
Comparison of the hourly tide levels calculated by the tidal model with the tide levels observed at station T1.

wind on the motion of the oil film is considered in the simulation.

In this paper, the oil spill is set to occur at two locations, named O1 and O2 in Figure 1, and the accidental oil spill volume is assumed to be 3000 tons. The oil spill is taken as the continuous point source with a duration of 1 hour.

Setup of the stochastic oil spill risk scenario

Based on the tidal dynamics and the oil spill model constructed in the previous section, this section sets up stochastic scenarios for oil spills occurring at stations O1 and O2. About 300 stochastic scenarios with random hydrodynamics and wind forcing fields were set up. For each stochastic scenario, 6-day continuous hydrodynamic data were randomly selected from the 30-day hourly field of tidal dynamics calculated by the hydrodynamic model. Moreover, a 6-day continuous wind speed and direction were randomly selected from the daily average wind vectors at the sea surface over 3 years (1 January 2017–31 December 2019) of NCEP/NCAR data. The above randomly selected tidal dynamic field and sea surface wind field boundary conditions were used as the lateral open and surface momentum boundary conditions of the model, respectively, to simulate the oil spill dispersion at O1 and O2 for each stochastic scenario. In each stochastic scenario simulation, we record information on the oil film thickness for each grid of the model to determine whether the grid is contaminated by the oil spill and the time when the oil spill reaches the grid. Finally, the oil spill contamination probability (P) and the fastest oil spill arrival time (T) are statistically calculated for each grid based on the results of 300 simulations of random scenarios. The following equations are used to calculate P and T:

$$P(i) = \frac{M(i)}{N} \times 100\,\% \tag{1}$$

$$T(i) = \min\{T(i)_n\},\ n = 1,\ 2,\ \cdots,\ N \tag{2}$$

where i is the grid cell number of the model; P(i) is the probability of the pollution of grid cell i by the oil spill; n is

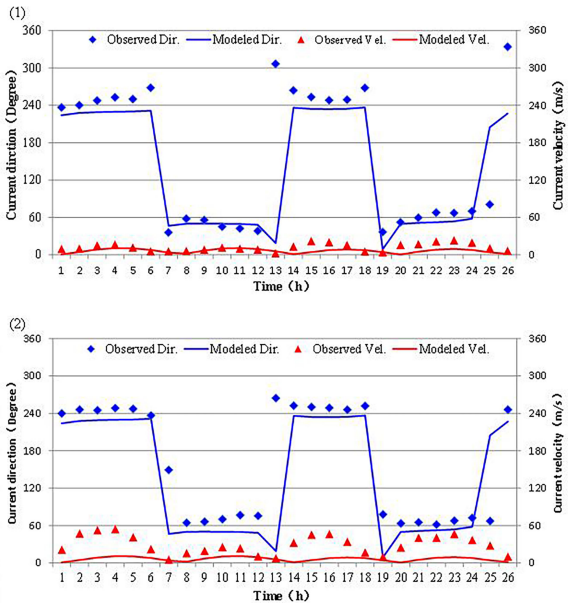


FIGURE 3
Comparison of tidal flow velocity and direction calculated by the tidal model with the observations conducted at a) Station V1 and b) Station V2.

the total number of simulations (n=300); M(i) is the number of times the accidental oil spill contaminated grid cell i in N runs of the simulation; and T(i) is the minimum time for the oil spill to spread to grid cell i in N runs of the simulation.

Results and discussion

Distribution of the tidal currents

This study analyzes the spatial distribution characteristics of nearshore tidal dynamics in the nSCS based on the modeled hourly tidal field. Figures 4, 5 show the model's simulated tidal velocity vectors and speed distributions during peak flood and ebb-tidal periods. The study area is dominated by SW and NE directions of the flood and ebb tidal currents, and the tidal current is mainly a reciprocal flow. Among them, the tidal flood flow is mainly in the SW direction and the ebb-tidal flow is mainly in the NE direction. The spatial distribution of tidal currents is significantly influenced by the coastline and topography, and the direction of tidal currents is basically parallel to the coastline. The maximum tidal velocity at the flood and ebb tide is about 0.5 m/s. The maximum tidal flow at the ebb tide is slightly higher than that at the flood tide.

Results of the stochastic stimulation

Figures 6–9 show the distribution of the fastest arrival time (T) and pollution probability (P) of the oil film caused by the oil spill incident at sites O1 and O2, respectively, based on the stochastic simulation. From the prediction results, when an oil spill occurs at point O1, both the northeast and southwest sea areas at the spill location have a higher probability of being contaminated by the oil spill (maximum contamination probability >10%), and the time for the oil film to reach the area is shorter.

When an oil spill occurs at the O2 site, the southwest area of the spill location has a higher probability of being contaminated by the oil spill and has a shorter time for the oil film to reach the area.

Mechanism analysis

Based on the wind speed and direction data of 300 randomly selected cases from the above 3-year daily averaged NCEP/NCAR wind field data, the wind frequency of the study area, and the average wind speed within the corresponding wind frequency were statistically obtained to form the wind rose diagram (Figure 10). The maximum wind frequency in the study area is northeast, and the wind frequency in this direction is greater than 8%. The maximum wind frequency corresponds to the maximum speed. The maximum wind speed in the northeast direction exceeds 10 m/s. In general, the prevailing wind direction in the study area is northeast, and the wind speed is high.

The distribution of the fastest arrival time of the oil film and the probability of the contamination of the oil spill at the two stations are consistent with the distribution of the prevailing

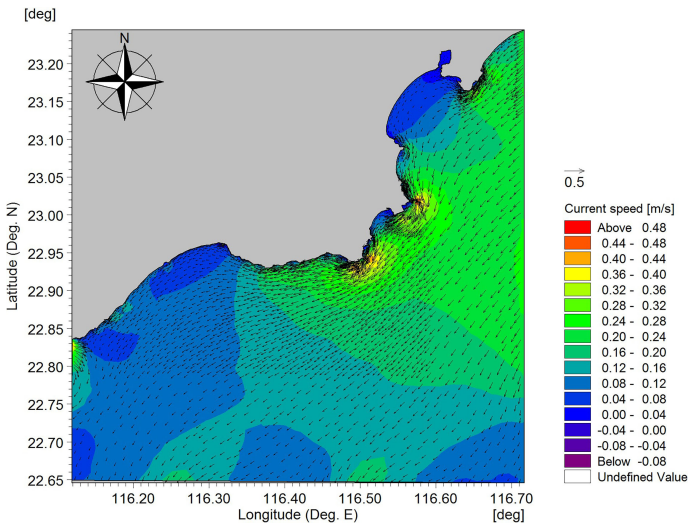


FIGURE 4
Tidal current distribution during the peak flood tidal period in the northern South China Sea calculated by tidal model (The arrow is the tidal velocity vector, and the color filled graph is the current speed distribution).

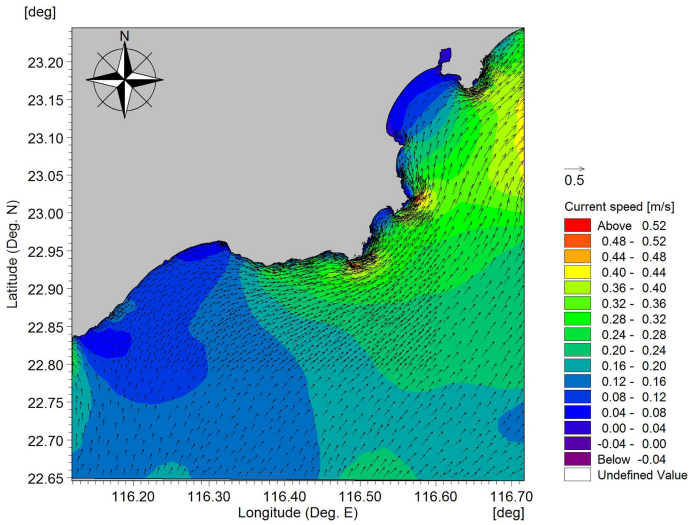


FIGURE 5
Tidal current distribution during the peak ebb tidal period in the northern South China Sea calculated by tidal model (The arrow is the tidal velocity vector, and the color filled graph is the current speed distribution).

wind direction in the region. Under the influence of the prevailing wind (northeast wind), the oil spill mainly spreads to the southwest, and the southwest of the accident site has a high probability of being contaminated by the oil spill. The wind direction has a significant effect on the direction of the dispersion of the oil spill. However, the probability of oil spill contamination at site O1 and the fastest arrival time of the oil film are also larger to the northeast of the spill site. It indicates that some of the oil film also spreads to the northeast of the accident site, which is opposite to the prevailing wind direction, indicating that the tidal dynamic process in the region may also play a role in the spread of the oil film.

Figure 11 shows the distribution of 30-day hourly tidal currents at stations O1 and O2 calculated by the tidal model in the nSCS. The tidal current distribution in site O1 and site O2 demonstrates significant differences. The breakwater built to the

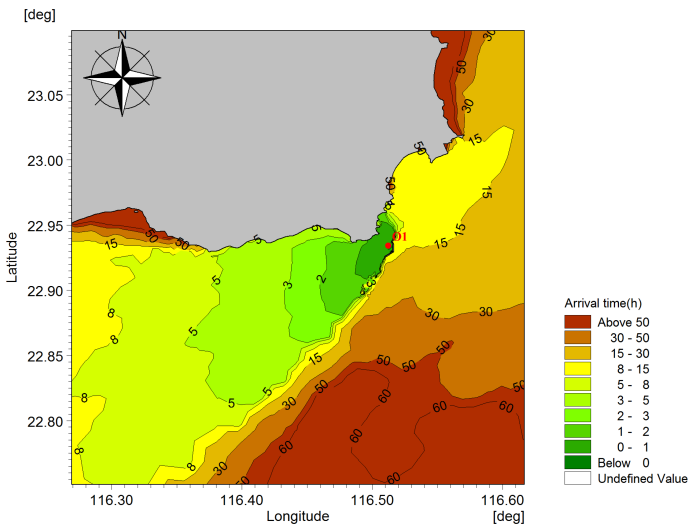


FIGURE 6
Distribution of the fastest arrival time (T) for the oil film from the oil spill accident occurred at site O1.

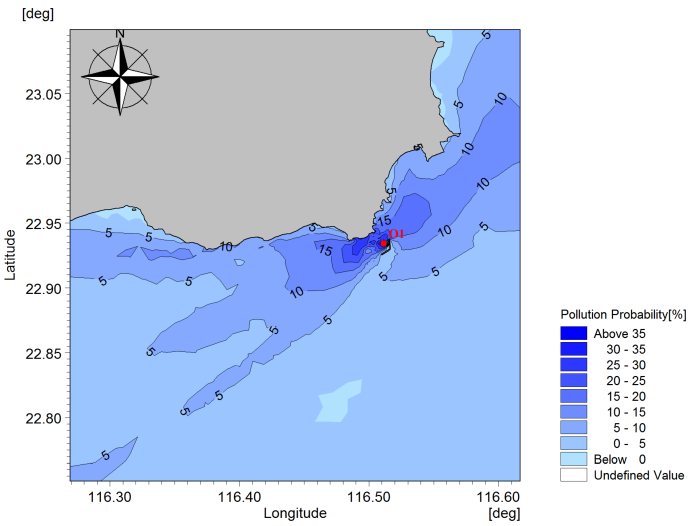


FIGURE 7
Distribution of pollution probability (P) for the oil film from the oil spill accident occurred at site O1.

northeast of site O1 has resulted in a change in the tide at that location. The tide at site O1 flows mainly in the north–west direction, and the maximum tidal current velocity is about 0.25 m/s. The tidal current at site O2 is a typical reciprocal flow, flowing southwestward at high tide and northeastward at low tide. The tidal current velocity is high, with a maximum speed greater than 0.3 m/s. The relatively strong northwesterly tidal current velocity at site O1 has an influence on the spread of the oil spill, causing part of the oil spill at this site to spread to the northeast. Although the reciprocal flow is more dominant at site O2, the spreading of the oil spill at this site is mainly affected by the wind.

In summary, the oil film dispersion caused by the nearshore oil spill accident in the nSCS is mainly influenced by the wind. Due to the difference in tidal dynamic conditions in different regions, the dispersion of oil spills from accidents in some regions is also influenced by tidal processes.

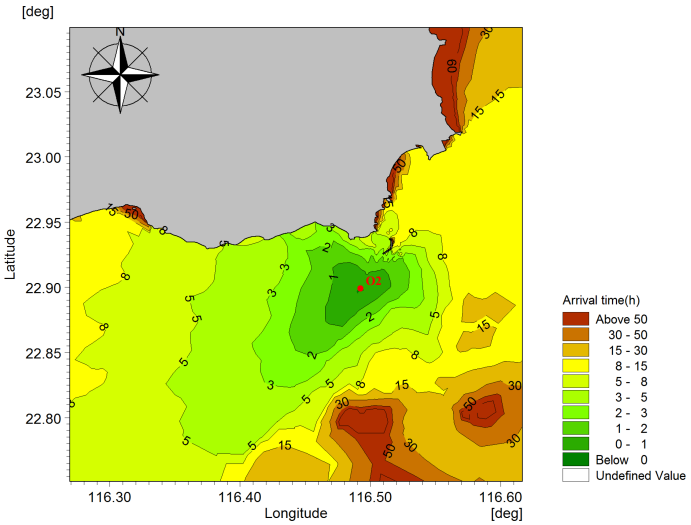


FIGURE 8
Distribution of the fastest arrival time (T) for the oil film from the oil spill accident occurred at site O2.

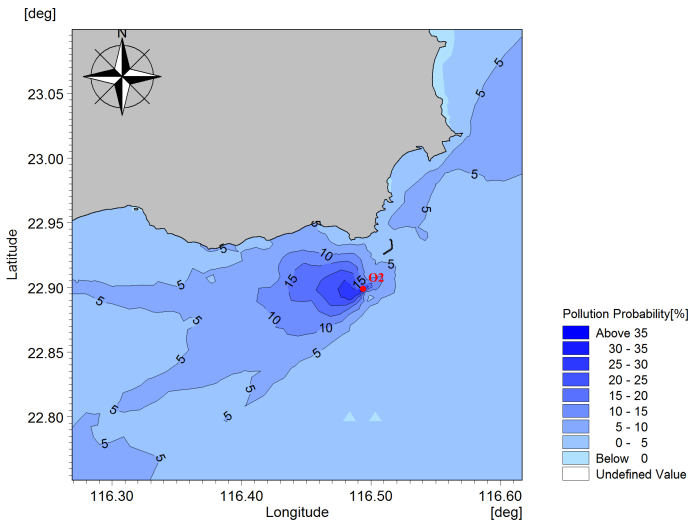


FIGURE 9
Distribution of pollution probability (P) for the oil film from the oil spill accident occurred at site O2.

Conclusion

In the present study, a coastal tidal dynamics model was developed for the nSCS, and the model was validated using the field observed data. An oil spill dispersion forecasting model based on "oil particles" was built. Based on the above models, the stochastic approach was used to simulate the fastest arrival time of the oil film and the probability of contamination distribution to the surrounding marine environment from oil spills at the nearshore O1 and O2 sites in the nSCS.

Based on the simulation results of the fastest arrival time of the oil film (T) and the probability of contamination (P), the accidental oil spill, affected by wind forcing and tidal dynamic processes, mainly influences the northeast and southwest areas of the accidental site. The wind has a significant effect on the dispersion direction of the accidental oil spill, and both the

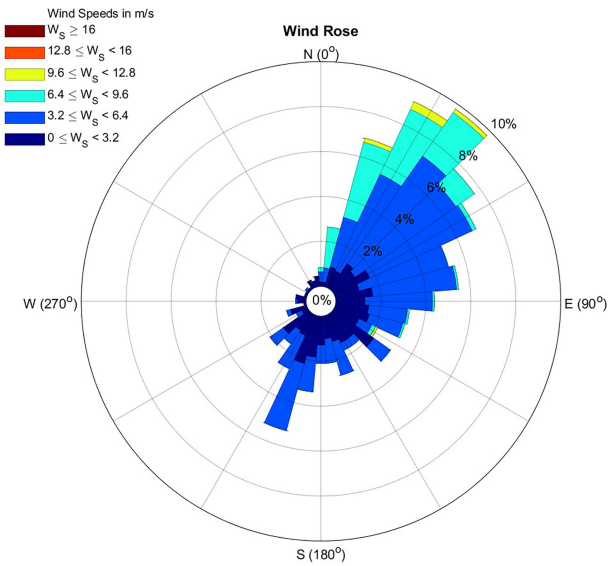


FIGURE 10
Wind rose diagram based on 300 randomly selected scenarios from 3-year daily averaged NCEP/NCAR wind data.

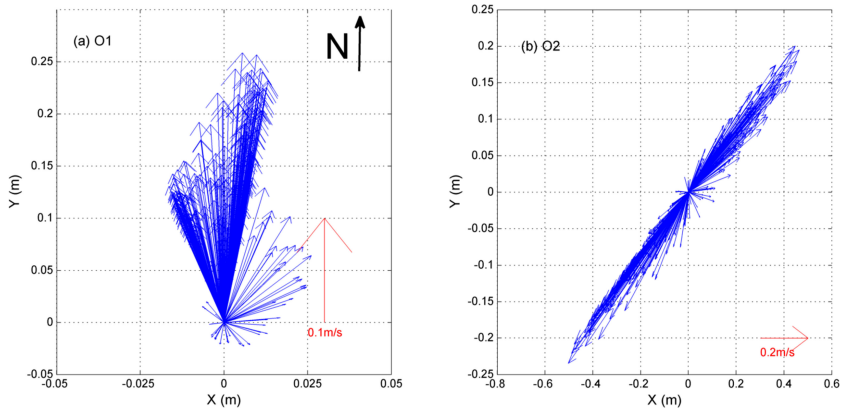


FIGURE 11
30-day hourly tidal current distributions at stations: **(a)** O1 and **(b)** O2, calculated by tidal model in the northern South China Sea.

migration and dispersion of accidental oil spills in some regions are also influenced by tidal processes.

We suggest using a stochastic scenario approach to predict the potential threat of an accidental oil spill to the surrounding marine environment and develop a scientific risk management strategy.

Data availability statement

The raw data supporting the conclusions of this article will be made available by the authors, without undue reservation.

Author contributions

BG: Conceptualization, Methodology, Writing - Original Draft. WZ: Methodology, Writing - Original Draft. LL: Data Curation. QC: Writing - Review & Editing. MH: Investigation. DW: Formal analysis. All authors contributed to the article and approved the submitted version.

Funding

This study is supported by the Guangdong Basic and Applied Basic Research Foundation (No. 2019A1515012108), the research fund from the State Key Laboratory of Tropical Oceanography (LTOZZ2101), and by the Key Special Project for Introduced Talents Team of Southern Marine Science and Engineering Guangdong Laboratory (Guangzhou) (GML2019ZD0404).

Conflict of interest

The authors declare that the research was conducted in the absence of any commercial or financial relationships that could be construed as a potential conflict of interest.

Publisher's note

All claims expressed in this article are solely those of the authors and do not necessarily represent those of their affiliated organizations, or those of the publisher, the editors and the reviewers. Any product that may be evaluated in this article, or claim that may be made by its manufacturer, is not guaranteed or endorsed by the publisher.

References

Alkhatib A., Ayari M. A., Hawari A. H. (2021). Fouling mitigation strategies for different foulants in membrane distillation. *Chem. Eng. and Processing Process Intensification* 167, 108517. doi: 10.1016/j.cep.2021.108517

Al-Rabeh A., Cekirge H., Gunay N. (1989). A stochastic simulation model of oil spill fate and transport. *Appl. Math. Model.* 13, 322–329. doi: 10.1016/0307-904X(89)90134-0

Amir-Heidari P., Arneborg L., Lindgren J. F., Lindhe A., Rosén L., Raie M., et al. (2019). A state-Of-The-Art model for spatial and stochastic oil spill risk assessment: A case study of oil spill from a shipwreck. *Environ. Int.* 126, 309–320. doi: 10.1016/j.envint.2019.02.037

Balogun A.-L., Yekeen S. T., Pradhan B., Yusof K. B. W. (2021). Oil spill trajectory modelling and environmental vulnerability mapping using gnome model and gis. *Environ. pollut.* 268, 115812. doi: 10.1016/j.envpol.2020.115812

Beyer J., Trannum H. C., Bakke T., Hodson P. V., Collier T. K. (2016). Environmental effects of the deepwater horizon oil spill: A review. *Mar. pollut. Bull.* 110, 28–51. doi: 10.1016/j.marpolbul.2016.06.027

Camphuysen K., Heubeck M. (2015). Beached bird surveys in the north Sea as an instrument to measure levels of chronic oil pollution. *Oil pollut. In North Sea* 41, 193–208. doi: 10.1007/698_2015_435

Chen Q., Bao B., Li Y., Liu M., Zhu B., Mu J., et al. (2020). Effects of marine oil pollution on microbial diversity in coastal waters and stimulating indigenous microorganism bioremediation with nutrients. *Regional Stud. In Mar. Sci.* 39, 101395. doi: 10.1016/j.rsma.2020.101395

Chen J., Zhang W., Li S., Zhang F., Zhu Y., Huang X. (2018). Identifying critical factors of oil spill in the tanker shipping industry worldwide. *J. Of Cleaner Production* 180, 1–10. doi: 10.1016/j.jclepro.2017.12.238

Chen J., Zhang W., Wan Z., Li S., Huang T., Fei Y. (2019). Oil spills from global tankers: Status review and future governance. *J. Of Cleaner Production* 227, 20–32. doi: 10.1016/j.jclepro.2019.04.020

Demiguel-Jiménez L., Etxebarria N., Lekube X., Izagirre U., Marigómez I. (2021). Influence of dispersant application on the toxicity to Sea urchin embryos of crude and bunker oils representative of prospective oil spill threats in Arctic and Sub-Arctic seas. *Mar. pollut. Bull.* 172, 112922. doi: 10.1016/j.marpolbul.2021.112922

Ferguson A., Solo-Gabriele H., Mena K. (2020). Assessment for oil spill chemicals: Current knowledge, data gaps, and uncertainties addressing human physical health risk. *Mar. pollut. Bull.* 150, 110746. doi: 10.1016/j.marpolbul.2019.110746

Fisher C. R., Montagna P. A., Sutton T. T. (2016). How did the deepwater horizon oil spill impact deep-Sea ecosystems? *Oceanography* 29, 182–195. doi: 10.5670/oceanog.2016.82

Gao W., Yin X., Mi T., Zhang Y., Lin F., Han B., et al. (2018). Microbial diversity and ecotoxicity of sediments 3 years after the jiaozhou bay oil spill. *Amb Express* 8, 1–10. doi: 10.1186/s13568-018-0603-6

Kampouris K., Vervatis V., Karagiorgos J., Sofianos S. (2021). Oil spill model uncertainty quantification using an atmospheric ensemble. *Ocean Sci.* 17, 919–934. doi: 10.5194/os-17-919-2021

Keramea P., Spanoudaki K., Zodiatis G., Gikas G., Sylaios G. (2021). Oil spill modeling: A critical review on current trends, perspectives, and challenges. *J. Of Mar. Sci. and Eng.* 9, 181. doi: 10.3390/jmse9020181

Law R. J., Hellou J. (1999). Contamination of fish and shellfish following oil spill incidents. *Environ. Geosci.* 6, 90–98. doi: 10.1046/j.1526-0984.1999.08039.x

Niu H., Li S., King T., Lee K. (2016). "Stochastic modeling of oil spill in the salish Sea," in *The 26th International Ocean And Polar Engineering Conference*, International Society of Offshore and Polar Engineers, 758–754

Prakash B., Kedia A., Mishra P. K., Dubey N. (2015). Plant essential oils as food preservatives to control moulds, mycotoxin contamination and oxidative deterioration of agri-food commodities–potentials and challenges. *Food Control* 47, 381–391. doi: 10.1016/j.foodcont.2014.07.023

Prasad S., Nair B., Rahaman H., Shenoi S., Vijayalakshmi T. (2018). An assessment on oil spill trajectory prediction: Case study on oil spill off ennore port. *J. Of Earth System Sci.* 127, 1–8. doi: 10.1007/s12040-018-1015-3

Rabalais N. N., Smith L. M., Turner R. E. (2018). The deepwater horizon oil spill and gulf of Mexico shelf hypoxia. *Continental Shelf Res.* 152, 98–107. doi: 10.1016/j.csr.2017.11.007

Saçu Ş., Şen O., Erdik T. (2021). A stochastic assessment for oil contamination probability: A case study of the bosphorus. *Ocean Eng.* 231, 109064. doi: 10.1016/j.oceaneng.2021.109064

Samuels W. B., Amstutz D. E., Bahadur R., Ziemniak C. (2013). Development of a global oil spill modeling system. *Earth Sci. Res.* 2, 52. doi: 10.5539/esr.v2n2p52

Toz A. C. (2017). Modelling oil spill around bay of samsun, Turkey, with the use of oilmap and adios software systems. *Polish Maritime Res.* 3 (95), 115–125. doi: 10.1515/pomr-2017-0096

Troisi G., Barton S., Bexton S. (2016). Impacts of oil spills on seabirds: Unsustainable impacts of non-renewable energy. *Int. J. Of Hydrogen Energy* 41, 16549–16555. doi: 10.1016/j.ijhydene.2016.04.011

Wang Y., Lee K., Liu D., Guo J., Han Q., Liu X., et al. (2020). Environmental impact and recovery of the bohai Sea following the 2011 oil spill. *Environ. pollut.* 263, 114343. doi: 10.1016/j.envpol.2020.114343

Yu H. (2021). The guangdong-Hong Kong-Macau greater bay area in the making: Development plan and challenges. *Cambridge Rev. Of Int. Affairs* 34, 481–509. doi: 10.1080/09557571.2019.1679719

Zacharias D. C., Gama C. M., Harari J., Da Rocha R. P., Fornaro A. (2021). Mysterious oil spill on the Brazilian coast–part 2: A probabilistic approach to fill gaps of uncertainties. *Mar. pollut. Bull.* 173, 113085. doi: 10.1016/j.marpolbul.2021.113085

frontiers | Frontiers in Marine Science

TYPE Data Report
PUBLISHED 20 September 2022
DOI 10.3389/fmars.2022.1011149

Check for updates

OPEN ACCESS

EDITED BY
Prashanthi Devi Marimuthu,
Bharathidasan University, India

REVIEWED BY
Obulisamy Parthiba Karthikeyan,
South Dakota School of Mines and Technology, United States
Rajakumar S.,
Bharathidasan University, India

*CORRESPONDENCE
Sujatha Balasubramaniam
sujathapachaiyappas@gmail.com
Gopalakrishnan Singaram
gopalthilagam@gmail.com
Thilagam Harikrishnan
thilagampachaiyappas@gmail.com

†These authors have contributed equally to this work

SPECIALTY SECTION
This article was submitted to Marine Pollution, a section of the journal Frontiers in Marine Science

RECEIVED 03 August 2022
ACCEPTED 05 September 2022
PUBLISHED 20 September 2022

CITATION
Marcus PN, Sivakumar P, Srinivasan G, Sivakumar R, Harikrishnan T, Balasubramaniam S and Singaram G (2022) Immunomodulatory response of Asian seabass *Lates calcarifer* in an *ex situ* environment: Implications for future ocean acidification scenario. *Front. Mar. Sci.* 9:1011149. doi: 10.3389/fmars.2022.1011149

COPYRIGHT
© 2022 Marcus, Sivakumar, Srinivasan, Sivakumar, Harikrishnan, Balasubramaniam and Singaram. This is an open-access article distributed under the terms of the Creative Commons Attribution License (CC BY). The use, distribution or reproduction in other forums is permitted, provided the original author(s) and the copyright owner(s) are credited and that the original publication in this journal is cited, in accordance with accepted academic practice. No use, distribution or reproduction is permitted which does not comply with these terms.

Immunomodulatory response of Asian seabass *Lates calcarifer* in an *ex situ* environment: Implications for future ocean acidification scenario

Priscilla Niranjani Marcus[1†], Priya Sivakumar[1†], Gomathi Srinivasan[1†], Rekha Sivakumar[1], Thilagam Harikrishnan[1*], Sujatha Balasubramaniam[1*] and Gopalakrishnan Singaram[2*]

[1]Postgraduate and Research Department of Zoology, Pachaiyappa's College for Men, Chennai, India, [2]Department of Biotechnology, Dwaraka Doss Goverdhan Doss Vaishnav College, Chennai, India

KEYWORDS

Asian seabass, ocean acidification, marine environment, immunomodulation, carbon dioxide, leukocytes, respiratory burst

Introduction

Global warming and ocean acidification (OA) are being brought on by an increase in atmospheric carbon dioxide (CO_2) concentration (Feely et al., 2004; Orr et al., 2005), and both are now widely acknowledged as significant factors in modulating physiological systems in the marine organism (Srinivasan et al., 2022). Increased CO_2 levels in the surface waters result in a drop in seawater pH, and changes in the chemistry of carbonates, and can have an impact on the bioavailability of contaminants (Bijma et al., 2013). Although OA has a significant impact on the acid-base balance, energy metabolism, and biomineralization of marine organisms (Kroeker et al., 2010), its effects on immune functions are still poorly understood (Calder-Potts et al., 2008), which makes it difficult to predict how susceptible marine fish to overcome the parasites and diseases attack as the ocean physicochemical concentration changes.

The survival of marine organisms are significantly influenced by good seawater quality (Jha et al., 2013), diseases and parasites free suitable locations, which are regarded as the main risk factor in both fish farms and the open ocean (Kumar et al., 2009; Jha et al., 2017). The resistance of aquatic organisms to parasites and diseases can be modulated by environmental stresses, such as fluctuations in temperature, salinity, and pollution (Galloway and Depledge, 2001; Marcogliese, 2008). Fish that live in water are

constantly exposed to a variety of pathogenic and non-pathogenic microorganisms; as a result, they may evolve powerful defence systems that aid in their survival. Aquatic organism immune systems, like that of fish, are constantly impacted by periodic or unanticipated changes in their surroundings. Fish health status may be negatively impacted by adverse environmental circumstances either acutely or chronically, either by changing certain biochemical parameters or by regulating innate and adaptive immune responses (Domingueza et al., 2004). Fish may therefore serve as significant indicator in the biomonitoring of water quality, particularly immunotoxic environmental contaminants, depending on their biological factors related to immunity.

The available literature regarding the alteration of immunity in shellfish because of ocean acidification shows that earlier studies were focused on marine invertebrates since the shellfish are more vulnerable to acidified environment since most of the higher invertebrates rely more on these environment for calcification (Ivanina et al., 2014). Our previous study documented that acidified environment impairs haematological and serum biochemical parameters in *Lates calcarifer* (Srinivasan et al., 2022). In the present study, it was further observed that long-term chronic exposure to acidified medium modulated the immunocompetence of fish in terms of the change in immune-associated parameters tested. To our knowledge, negligible work has been carried out to observe the impact of seawater acidification on immunomodulation in fish with different size groups. Therefore the present study investigated the effect of acidification on the nonspecific immune-associated parameters, including respiratory burst, myeloperoxidase (MPO) activity, bactericidal activity, circulating total immunoglobulin, and on cellular components (leukocytes) in two different size groups (fish fry and fingerlings) of *Lates calcarifer*.

Methods

The collection of fish and experimental design were explained in detail as described in Srinivasan et al., 2022. Briefly, a total of 360 fish were used for this study (180 fry and 180 fingerlings). The control, pH 7.7, and pH 7.4 were three groups and for time point, we used 18 fish per experimental group. Sampling was done at 20, 40, and 60 days (d) of exposure. Fish were anesthetized for 30 seconds in ice-cold aquarium water before collecting the blood. Blood samples were split into two aliquots; one was heparinized (at a concentration of 50 IU/ml blood), and the other was left to coagulate at room temperature for 30 minutes before being stored at 4°C for 24 hours. The serum was extracted from the clotted sample by centrifuging it at 3,500 rpm for 5 minutes at 4°C, and it was then kept at -20°C until it was used. Heparinized blood was utilised for Nitroblue tetrazolium assay and differential leukocyte counts. The University of Madras' Animal Ethics Committee authorized the aforementioned animal procedures.

Differential leukocyte count was done according to the method described by Horton and Okamura (2003). Briefly, by preparing a blood smear on a slide by using 20 µL of heparinized blood, the slide was then fixed in 95% methanol before staining with Giemsa for 5 min. The slides were washed gently in tap water and allowed to dry before microscopic examination. The percentage of monocytes, lymphocytes, neutrophils, and thrombocytes in the blood was determined by counting leukocytes under a microscope randomly until the count reached 100 cells per slide.

Respiratory burst activity was assessed by following the modified method described by Thilagam et al. (2009) and Havixbeck et al. (2016). About 50 µL of heparinized blood was incubated at 37°C for 1 h to facilitate adhesion of cells in the Eppendorf tube followed by washing with phosphate buffer. About 50 µL of nitroblue tetrazolium was added to the tube and incubated for a further 1 h. The tubes were shaken well and centrifuged at 1000 rpm for 15 minutes, after which the supernatant was removed. Absolute methanol was used to fix the cells followed by washing in 30% methanol. The tubes were air dried and extraction fluid of 2 mL (potassium hydroxide and dimethyl sulfoxide) was added to each tube to dissolve the precipitate. Tubes were then centrifuged at 6,000 rpm for 10 minutes to collect the supernatant and read at 630 nm optical density.

Myeloperoxidase (MPO) was measured in the serum following the method described by Quade and Roth (1997). A serum sample (10 µL) and 140 µL of Hank's balanced salt solution (Ca^{2+} and Mg^{2+} free) were added to a 96- well plate. The 50 µL of 20 mM 3,3',5,5' tetra methyl benzidine, and 5 mM H_2O_2 were added to initiate the reaction. After 2 minutes the reaction was stopped by adding 50 µL of 4 M sulphuric acid and the absorbance was measured at 450 nm in a microplate reader.

The procedure described by Siwicki and Anderson (1993) was adapted to test the total immunoglobulin level. Briefly, polyethylene glycol was used to precipitate immunoglobulin. Blood serum was incubated with equal volume polyethylene glycol solution for two hours at room temperature followed by spinning the sample tube at 3,000 rpm for 15 minutes, the supernatant was used for measuring the protein content using Bradford method (1976). The quantity of measured protein was subtracted from the serum protein content to determine the total immunoglobulin level.

Serum bactericidal activity was measured following a modified method described by Rainger and Rowley (1993). A pellet of *Aeromonas hydrophila* was washed and suspended in phosphate buffer. The absorbance of the suspension was adjusted to 0.500 at 600 nm and the suspension was serially diluted (1:10) with phosphate buffer. The bactericidal activity was determined by incubating 2 µL of the *A. hydrophila* suspension with 20 µL of serum in a microvial for 1 h at 37°C.

In control group, phosphate buffer was used in place of serum sample and nutrient broth was used in place of the serum for positive control. By counting the colonies that appeared on a nutrient agar plate after 24 hours at 37°C following incubation, the number of live bacteria was ascertained.

SPSS software was used to perform the statistical analysis (version 20). Graph pad prism (version 8) was used to plot the graph. Prior to using a two-way analysis of variance (ANOVA) to assess differences between the groups, the data were normalized, and homogeneity test also conducted. The statistical difference between various treatment groups was assessed using Tukey's multiple comparison *post hoc* tests, and a p-value of less than 0.05 was regarded as significant.

Results and discussion

Leukocytes count in fish fry and fingerlings are given in Figures 1A–D. Monocyte counts in the fish fry and fingerlings increased significantly ($p<0.05$) when the fish were exposed to pH 7.4. All the exposure periods showed a significant rise in monocyte counts (Figure 1A). There were no discernible changes between the respective control and fish fry or fingerling exposed to pH 7.7. In contrast, the neutrophil counts decreased significantly in fry exposed to pH 7.7 and pH 7.4 after 20 d (Fig. 1B). Both fry and fingerlings exposed to pH 7.7 reduced neutrophil counts after 40 d of exposure. However, fish exposed to both pH (7.7 and 7.4) for 60 d showed no significant difference with respective control groups (Figure 1B)

After 20 d and 40 d of exposure, fish fry exposed to pH 7.7 and pH 7.4 had considerably less thrombocytes than the corresponding control group. However, fingerlings exposed to pH 7.7 and pH 7.4 exhibits a rise in thrombocytes that was statistically significant over 40 d (Figure 1C) of exposure. With respect to the control groups, fingerling exposed to pH 7.4 for 60 d exhibits an increase in thrombocytes but no discernible change. After 20 d and 40 d of exposure to pH 7.7 and pH 7.4, the lymphocyte counts in fry dramatically dropped, but after 60 d of exposure, there was no discernible change observed (Figure 1D). Fish fingerlings subjected to pH 7.7 and pH 7.4 did not significantly differ from the corresponding control in terms of lymphocyte count, except for fish fingerlings exposed to pH 7.4 for 60 d (Figure 1D). Reduced circulating lymphocyte count were a sign that immunosuppression had taken place in fish exposed to the lower pH, as documented by Machado et al. (2020). Additionally, after 20 d of exposure, neutrophils in fish fry drastically reduced, but not in fingerling for the same exposure period. On the contrary monocytes, the count was increased when the fish were exposed to pH 7.4. Increase in circulating lymphocyte and thrombocyte count were a sign of nonspecific immunological activation (Machado et al., 2020) and the drastic change in these leukocyte counts in fish may lead to immunomodulation (Thilagam et al., 2009).

The increase in respiratory burst activity in fish is a measure of the amount of oxidative radicals produced as a result of acidified exposure (1 E). When the fish fingerlings and fry were exposed to pH 7.7 and pH 7.4 respiratory burst activity increased significantly after 20 d and 40 d respectively compared to the respective control group of *L. calcarifer* (Figure 1E). Interestingly fish fry exposed to both pHs (7.7 and 7.4) showed no significant change after 60 d of exposure when compared to the respective groups showing that the fish might adapt to the acidified environment.

In recent times, respiratory burst activity has been utilised to examine how fish's immune systems respond to exposure to environmental factors (Barbosa et al., 2020). An indicator of the modulation of nonspecific immunity is the increase in respiratory burst activity in fish, which is a measure of oxidative radical production due to environmental stress (Thilagam et al., 2009). Furthermore, the ROS produced during the respiratory burst activity are thought to be potent microbicidal agents. The current investigation found that exposure of fish to acidified environment increased respiratory burst activity in both groups and that the increase depended on the amount of acidity and the length of exposure. It's interesting to see that the prolonged acidification exposure (60 d) to the fish fry did not significantly increase the ROS. Though both fry and fingerlings were shown to be more vulnerable to acidified environment, according to the findings of the current study and these modulations in ROS generation after prolonged exposure could be either fish adaptability to the environmental condition or due to enhance the antioxidant defence of the fish and needs to be elucidated.

The MPO activity increased when fish fry and fingerlings were exposed to acidified environment throughout the exposure period as compared to the corresponding control group (Figure 1F). At 20 d, both groups exposed to pH 7.4 showed greater MPO activity. MPO activity had a similar pattern to that of the respiratory burst. In many situations where neutrophils play a role in pathological diseases, MPO levels, and neutrophil activation can be connected. A significant association between the respiratory burst and MPO was found (Figures 2A, B), indicating that most of the O_2^- produced during this respiratory burst was transformed to the bactericidal oxidant hypochlorous acid *via* a sequence of events involving superoxide dismutase and MPO (Thilagam et al., 2009).

Total immunoglobulin levels in fish exposed to acidified environment is given in Figure 1G. Both the fry and fingerling groups showed a drop in total immunoglobulin levels after exposure to acidified medium, however, only fish exposed to pH 7.4 experienced a significant drop in total immunoglobulin during the exposure period. Fingerling exposed to pH 7.7 showed a noticeable rise in total immunoglobulin levels, but such increase was not statistically significant. Environmental influences are thought to interact with cell nucleoproteins and nucleic acids, changing protein synthesis and cell integrity.

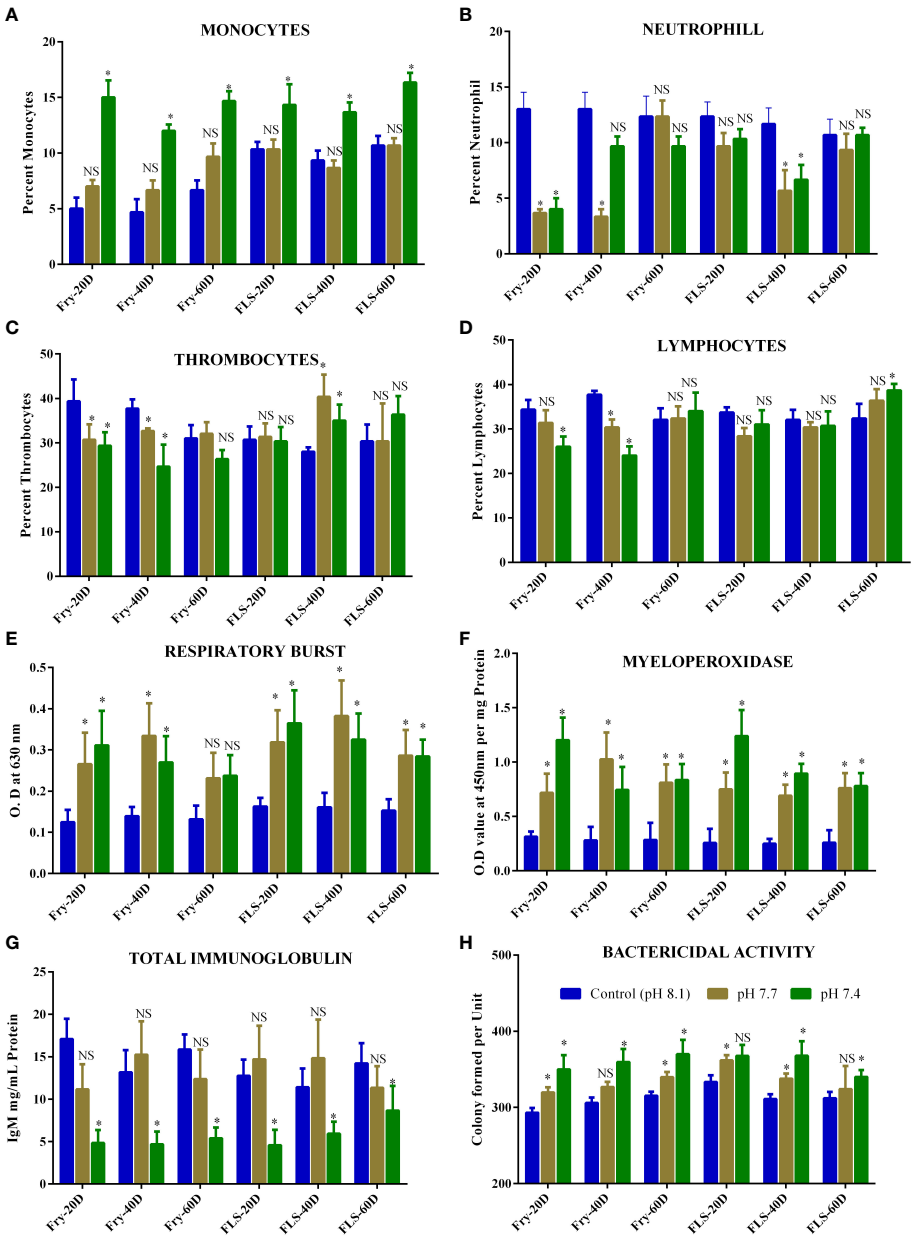


FIGURE 1
(A–D) is the data representing the biochemical components such as **(A)** Monocytes **(B)** Neutrophil **(C)** Thrombocytes **(D)** Lymphocytes **(E)** Respiratory burst **(F)** Myeloperoxidase **(G)** Immunoglobulin **(H)** Bactericidal activity in fish fry and fingerling of Asian seabass exposed for 60 d under different acidified conditions. Each bar represents mean ± standard deviation of six samples. Two-way analysis of variance followed by Tukey's *post hoc* test was used. The asterisk indicates significant difference between the exposure and control groups whereas NS letters No significant difference ($p < 0.05$) between different groups.

Changes in blood protein levels as a result of environmental stress have been documented (Dominguez et al., 2004; Srinivasan et al., 2022). Except for fish fingerlings exposed to pH 7.7 in the current investigation, the total immunoglobulin level was significantly lower in fish exposed to experimentally acidified environment compared to the respective control group. When Nile tilapia were exposed to acidified environment it was observed that there was no appreciable change in immunoglobulin levels (Dominguez et al., 2004), but the fish did react to changes in salinity and temperature. Machado et al. (2020) recorded a decrease in total immunoglobulin when Senegalese sole exposed to acidified seawater and in the present study decrease in total immunoglobulin was statistically significant ($p < 0.05$) in the fish fry which supports

A FRY

	Monocytes	*Neutrophil*	*Thrombocytes*	*Lymphocytes*	*ROS*	*MPO*	*IgL*	*Bactericidal*
Monocytes	1.0000							
Neutrophil	-0.0212	1.0000						
Thrombocytes	-0.4169	0.3059	1.0000					
Lymphocytes	-0.0465	0.4386	0.4506	1.0000				
ROS	0.2590	-0.5877	-0.4164	-0.4345	1.0000			
MPO	0.4369	-0.5447	-0.4597	-0.4168	0.7362	1.0000		
IgL	-0.4162	0.2321	0.6342	0.4744	-0.4115	-0.4659	1.0000	
Bactericidal	0.5386	-0.1896	-0.7236	-0.3329	0.4071	0.5851	-0.7035	1.0000

B FINGERLINGS

	Monocytes	*Neutrophil*	*Thrombocytes*	*Lymphocytes*	*ROS*	*MPO*	*IgL*	*Bactericidal*
Monocytes	1.0000							
Neutrophil	0.0806	1.0000						
Thrombocytes	0.1362	-0.4552	1.0000					
Lymphocytes	0.3653	0.1325	0.3230	1.0000				
ROS	0.3521	-0.3991	0.4128	0.1564	1.0000			
MPO	0.5452	-0.1766	0.2028	0.1400	0.7147	1.0000		
IgL	-0.4865	-0.0430	0.0283	-0.1142	-0.2180	-0.4823	1.0000	
Bactericidal	0.3850	-0.1814	0.2494	0.0912	0.5737	0.6751	-0.3195	1.0000

FIGURE 2
Correlation Analysis and heat map showing the relationship between the immune associated parameters when the Asian seabass *L. calcarifer* exposed to OA for 60 d. **(A)** Fry **(B)** Fingerlings. The values and colour depict the relationship between the parameters.

the previous study by Machado et al. (2020) and revealed that decrease in total immunoglobulin could be attributed to increasing acidification in the oceanic environment. The discrepancy in the results for fish fry and fingerlings could be attributed to the adaptability of different size groups to the acidified environment and subsequent stress.

Figure 1H illustrates how exposure to acidified environment affected the serum bactericidal activity in both fish fry and fingerlings. When the fry was exposed to pH 7.7 and pH 7.4 for 20 d, 40 d, and 60 d, the serum bactericidal activity drastically reduced. Similarly declines in bactericidal activity were observed in fingerling serum at both pH (7.7 and 7.4) after 20 and 40 d. However, fingerling exposed to pH 7.7 after 60 d did not exhibit any significant differences from the respective control group. The decrease in serum bactericidal activity at all exposure periods in both groups as compared to the respective control group can be used to explain why fish exposed to acidified environment developed less resistance to A. hydrophila.

Statistically significant ($p< 0.05$) associations were observed between parameters of the immune system in the blood components of fish (Figure 2). There were statistically significant correlations between leukocyte counts and other parameters studied in both fish fry and fingerlings. A significant positive correlation was found between the leukocytes (Monocytes and Lymphocytes) with most of the immune associated parameters in fish fingerlings and the same was negative correlated in fish fry. This discrepancy might due to the size variation or adaptation of the fingerling to the acidified environment needs to elucidate further.

This is the first comparison study of how the immune system in *L. calcarifer* modulated when two different size groups of fish are exposed to an acidified environment. In light of the findings of current study, we hypothesised that seawater acidification might have an impact on the structure and immune function of *L. calcarifer* leukocytes. Acidification exposure led to an excess of ROS, which was responsible for causing oxidative stress in the leukocytes, and at the same time, the acidified environment induced further accumulation of ROS by inhibiting the activity of the antioxidant system and these changes might result in immune system dysfunction, which could have negative effects including decreased disease resistance, growth impairment, and poorer survival rates. Furthermore it has been demonstrated that the increasing H^+ level is just one of several stressors brought on by the CO_2-induced acidification of seawater. In order to clarify the underlying processes, further study should concentrate on analysing the energy metabolism, oxidative stress and antioxidant defense of *L. calcarifer* subjected to acidified environment.

Data availability statement

The original contributions presented in the study are included in the article/supplementary material. Further inquiries can be directed to the corresponding authors.

Ethics statement

Ethical review and approval was not required for the animal study because only commercial fish were used with no ethical issues.

Author contributions

PM, PS, GS, RS: Sample collection, laboratory analysis, data processing. TH: Data validation and manuscript preparation. SB, GS: Review the manuscript, suggestion, and project administration. All authors contributed to the article and approved the submitted version.

Acknowledgments

The authors thank the Head, Research Department of Zoology and also the Principal Pachaiyappa's College for Men, Chennai- 600 030 and Department of Biotechnology and the Principal Dwaraka Doss Goverdhan Doss Vaishnav College, Chennai, 600106, Tamil Nadu, India for extending their support through the experiment.

Conflict of interest

The authors declare that the research was conducted in the absence of any commercial or financial relationships that could be construed as a potential conflict of interest.

Publisher's note

All claims expressed in this article are solely those of the authors and do not necessarily represent those of their affiliated organizations, or those of the publisher, the editors and the reviewers. Any product that may be evaluated in this article, or claim that may be made by its manufacturer, is not guaranteed or endorsed by the publisher.

References

Barbosa, L. M. G., Moraes, G., Anibal, F. F., and Machado, C. M. M. (2020). Effect of environmental thermal fluctuations on innate immune responses in pacu *Piaractus mesopotamicus* juveniles. *Aquac Rep.* 17, 100303. doi: 10.1016/j.aqrep.2020.100303

Bijma, J., Pörtner, H. O., Yesson, C., and Rogers, A. D. (2013). Climate change and the oceans–what does the future hold? *Mar. Pollut. Bull.* 74 (2), 495–505. doi: 10.1016/j.marpolbul.2013.07.022

Bradford, M. M. (1976). A rapid and sensitive method for the quantitation of microgram quantities of protein utilizing the principle of protein-dye binding. *Anal Biochem.* 72, 248–254. doi: 10.1006/abio.1976.9999

Calder-Potts, R., Widdicombe, S., Parry, H., Spicer, J., and Pipe, R. (2008). Effects of ocean acidification on the immune response of the blue mussel *Mytilus edulis*. *Aquat. Biol. - AQUAT Biol.* 2, 67–74. doi: 10.3354/ab00037

Dominguez, M., Takemurab, A., Tsuchiyaa, M., and Nakamura, S. (2004). Impact of different environmental factors on the circulating immunoglobulin levels in the Nile tilapia, *Oreochromis niloticus*. *Aquaculture* 241, 491–500. doi: 10.1016/j.aquaculture.2004.06.027

Feely, R. A., Sabine, C. L., Lee, K., Berelson, W., Kleypas, J., Fabry, V. J., et al. (2004). Impact of anthropogenic CO2 on the CaCO3 system in the oceans. *Science* 305, 362–366. doi: 10.1126/science.1097329

Galloway, T. S., and Depledge, M. H. (2001). Immunotoxicity in invertebrates: measurement and ecotoxicological relevance. *Ecotoxicol (London England)* 10 (1), 5–23. doi: 10.1023/a:1008939520263

Havixbeck, J. J., Rieger, A. M., Wong, M. E., Hodgkinson, J. W., and Barreda, D. R. (2016). Neutrophil contributions to the induction and regulation of the acute inflammatory response in teleost fish. *J. Leukoc Biol.* 99 (2), 241–252. doi: 10.1189/jlb.3HI0215-064R

Horton, T., and Okamura, B. (2003). Post-haemorrhagic anaemia in sea bass, dicentrarchus labrax (L.), caused by blood feeding of ceratothoa oestroides (Isopoda: Cymothoidae). *J. Fish Dis.* 26 (7), 401–406. doi: 10.1046/j.1365-2761.2003.00476.x

Ivanina, A. V., Hawkins, C., and Sokolova, I. M. (2014). Immunomodulation by the interactive effects of cadmium and hypercapnia in marine bivalves crassostrea virginica and mercenaria. *Fish Shellfish Immunol.* 37 (2), 299–312. doi: 10.1016/j.fsi.2014.02.016

Jha, D. K., Devi, M. P., Vinithkumar, N. V., Das, A. K., Dheenan, P. S., Venkateshwaran, P., et al. (2013). Comparative investigation of water quality parameters of aerial & rangat bay, Andaman islands using in-situ measurements and spatial modelling techniques. *Water Qual. Expo. Health* 5, 57–67. doi: 10.1007/s12403-013-0086-2

Jha, D. K., Rajaprabhu, G., Kirubagaran, R., Sendhil Kumar, R., Dharani, G., Das, A. K., et al. (2017). Estimation of potential zones for offshore mariculture in the Indian Sea using geographical information system as a management tool. *J. Coast. Conserv.* 21, 893–902. doi: 10.1007/s11852-017-0556-y

Kroeker, K. J., Kordas, R. L., Crim, R. N., and Singh, G. G. (2010). Meta-analysis reveals negative yet variable effects of ocean acidification on marine organisms. *Ecol. Lett.* 13 (11), 1419–1434. doi: 10.1111/j.1461-0248.2010.01518.x

Kumar, T. S., Vijayakumaran, M., Murugan, T. S., Jha, D. K., Sreeraj, G., and Muthukumar, S. (2009). Captive breeding and larval development of the scyllarine lobster *Petrarctus rugosus*. n. *Z. J. Mar. Freshw. Res.* 43, 101–112. doi: 10.1080/00288330909509985

Machado, M., Arenas, F., Svendsen, J. C., Azeredo, R., Pfeifer, L. J., Wilson, J. M., et al. (2020). Effects of water acidification on Senegalese sole solea senegalensis health status and metabolic rate: Implications for immune responses and energy use. *Front. Physiol.* 11. doi: 10.3389/fphys.2020.00026

Marcogliese, D. J. (2008). The impact of climate change on the parasites and infectious diseases of aquatic animals. *Rev. sci tech (Int Office Epizootics)* 27 (2), 467–484. doi: 10.20506/rst.27.2.1820

Orr, J., Fabry, V., Aumont, O., Bopp, L., Doney, S. C., Feely, R. A., et al. (2005). Anthropogenic ocean acidification over the twenty-first century and its impact on calcifying organisms. *Nature* 437, 681–686. doi: 10.1038/nature04095

Quade, M. J., and Roth, J. A. (1997). A rapid, direct assay to measure degranulation of bovine neutrophil primary granules. *Vet Immunol. immunopathol* 58 (3-4), 239–248. doi: 10.1016/s0165-2427(97)00048-2

Rainger, G. E., and Rowley, A. F. (1993). Antibacterial activity in the serum and mucus of rainbow trout, oncorhynchus mykiss, following immunization with *Aeromonas salmonicida*. *Fish Shellfish Immunol.* 3, 475–482. doi: 10.1006/fsim.1993.1046

Siwicki, A. K., and Anderson, D. P. (1993). *Nonspecific defence mechanisms assay in fish II; potential killing activity of neutrophils and manocytes, lysozyme activity in serum and organs and total immunoglobulin (Ig) level in serum* (Olsztyn, Poland: Olsztyn: Wydawnictwo Instytutu Rybactwa Strodladowego).

Srinivasan, G., Marcus, P. N., Sivakumar, P., Paramasivam, P., Sivakumar, R., Harikrishnan, T., et al. (2022). Ocean acidification impact on haematological and serum biochemical parameters in lates calcarifer. *Front. Mar. Sci.* 9. doi: 10.3389/fmars.2022.940573

Thilagam, H., Gopalakrishnan, S., Bo, J., and Wang, K.-J. (2009). Effect of 17β-estradiol on the immunocompetence of japanese sea bass (*Lateolabrax japonicus*). *Environ. Toxicol. Chem.* 28, 1722–1731. doi: 10.1897/08-642.1

frontiers | Frontiers in Marine Science

TYPE Original Research
PUBLISHED 23 September 2022
DOI 10.3389/fmars.2022.1004235

Check for updates

OPEN ACCESS

EDITED BY
Meilin Wu,
South China Sea Institute of Oceanology, (CAS), China

REVIEWED BY
Wen-zhuo Zhu,
Zhejiang Ocean University, China
Xianbiao Lin,
Ocean University of China, China

*CORRESPONDENCE
Jibiao Zhang
zhangjb@gdou.edu.cn

SPECIALTY SECTION
This article was submitted to Marine Pollution, a section of the journal Frontiers in Marine Science

RECEIVED 27 July 2022
ACCEPTED 26 August 2022
PUBLISHED 23 September 2022

CITATION
Zhang P, Ou S, Zhang J, Zhao L and Zhang J (2022) Categorizing numeric nutrients criteria and implications for water quality assessment in the Pearl River Estuary, China.
Front. Mar. Sci. 9:1004235.
doi: 10.3389/fmars.2022.1004235

COPYRIGHT
© 2022 Zhang, Ou, Zhang, Zhao and Zhang. This is an open-access article distributed under the terms of the Creative Commons Attribution License (CC BY). The use, distribution or reproduction in other forums is permitted, provided the original author(s) and the copyright owner(s) are credited and that the original publication in this journal is cited, in accordance with accepted academic practice. No use, distribution or reproduction is permitted which does not comply with these terms.

Categorizing numeric nutrients criteria and implications for water quality assessment in the Pearl River Estuary, China

Peng Zhang[1,2], Shujun Ou[1], Junxiao Zhang[2,3], Lirong Zhao[1] and Jibiao Zhang[1]*

[1]College of Chemistry and Environmental Science, Guangdong Ocean University, Zhanjiang, China, [2]Key Laboratory of Marine Environmental Survey Technology and Application, Ministry of Natural Resource, Guangzhou, China, [3]South China Sea Marine Technology and Survey Center, State Oceanic Administration, Guangzhou, China

Coastal eutrophication, the over-enrichment of water with nutrients, has become a global ecological problem. As coastal waters are subjected to great pressure due to anthropogenic influences and climate change, establishing numeric nutrient criteria for coastal waters has been exceedingly complex at present. To control and improve the water quality of the Pearl River Estuary (PRE), based on the data from 2015 to 2020, the nutrient criteria of the PRE and adjacent waters were established using frequency statistical analysis. Based on the spatiotemporal salinity patterns, the coastal waters of the PRE were divided in three subareas namely freshwater (Zone I), mixed (Zone II), and seawater (Zone III) using cluster analysis. The recommended criteria values of dissolved inorganic nitrogen (DIN) were 0.573, 0.312, and 0.134 mg·L^{-1} in Zones I, II, and III, respectively. The total nitrogen (TN) criterion for Zone III (0.222 mg·L^{-1}) was much lower than those for Zone I (0.902 mg·L^{-1}) and Zone II (0.885 mg·L^{-1}).The dissolved inorganic phosphorus (DIP) criteria were different for the three Zones, ranging from 0.004 to 0.009 mg·L^{-1}, and the total phosphorus (TP) recommended criteria in Zones I, II, and III were 0.039, 0.028, and 0.020 mg·L^{-1}, respectively. In the water quality assessment, the categorizing numeric nutrients criteria can be referred and applied into fresh, mixed, and seawater zones of PRE. The results of this study provide a new nutrient reference condition in the PRE, which could be helpful in establishing integrated land-ocean unified nutrient criteria and water quality assessment, and implementing effective coastal eutrophication control in the future.

KEYWORDS

coastal eutrophication, nutrient criteria, water quality, assessment, Pearl River estuary

Introduction

Nitrogen (N) and Phosphorus (P) are the material foundations for the growth and reproduction of phytoplankton, and their composition, concentration, and distribution directly affect the primary productivity of the ocean and food chain (Ryther and Dunstan, 1971, Anderson et al., 2002; Conley et al., 2009; Davidson et al., 2014; Lin G. and Lin X., 2022). In marine environments, N and P nutrients exist in various forms of inorganic and organic matter (Zhang et al., 2019a, Ge et al., 2021). Dissolved inorganic nitrogen (DIN, including NO_3^--N, NO_2^--N and NH_4^+-N) is the main form of N, and its concentration change is the main factor controlling the change in total nitrogen (TN) content (Wei et al., 2014; Zhang et al., 2020b; Hong et al., 2019). In addition, dissolved organic nitrogen (DON) is an important potential direct or indirect nitrogen source for microorganisms and phytoplankton (Lu et al., 2016; Luo, 2017; Luo et al., 2017; Zhang et al., 2020c). As ocean is one of the largest nitrogen pools, its important role in the marine nitrogen cycle has been widely recognized (Luo et al., 2017). The main form of P is dissolved inorganic phosphorus (DIP), which accounts for more than 50% of total phosphorus (TP), and is not only the most preferred phosphorus source for organisms, but also a limiting factor for most of the marine ecosystems (Li, 2017; Zhang et al., 2017; Zhang et al., 2019a; Zhang et al., 2020). When DIP cannot meet the needs of phytoplankton, heterotrophic bacteria in the ocean supplement DIP by hydrolyzing dissolved organic phosphorus (DOP) using alkaline phosphatase (Zhang et al., 2021). With the rapid development of industry and agriculture, the use of pesticides, fertilizers, and fossil fuels has increased significantly, and a large amount of nitrogen and phosphorus nutrients have been transported to the estuaries and coasts through river flow, atmospheric deposition, and groundwater discharge, resulting in severe eutrophication (Herbeck et al., 2013; Li et al., 2014; Ménesguen, 2014; Wang et al., 2018; Zhang et al., 2019b; Zhang et al., 2020a; Peng et al., 2021). Nutrient criteria representing the enrichment status of surface waters that are minimally impacted by human development maybe defined as the threshold value that supports a particular beneficial designated use (US EPA, 1998; US EPA, 2001). Coastal eutrophication has caused serious damage to the ecosystem and disturbed the balance of original ecosystem, resulting in outbreak of harmful algal blooms and the formation of hypoxic or anoxic zones (DePinto and Verhoff, 1977; Boynton et al., 1982; Burkholder et al., 1992; Arai, 2001; Wu, 2007; Lin et al., 2018; Xu, 2020; Ke et al., 2022; Zhang et al., 2022; Cai et al., 2011). Therefore, developing and categorizing the numeric nutrients criteria played an important role in assessing the attainment of designated uses and measuring progress toward achieving water quality goals (US EPA, 1998; US EPA, 2001; Huo et al., 2015; Yang et al., 2019).

Estuaries are mixed areas of freshwater and seawater, and the interaction of hydrodynamic environment, biochemical processes, and human activities here is very complex (Zhang et al., 2017; Li et al., 2018; Lu et al., 2018; Li et al., 2013; Liu et al., 2011). Estuaries and coastal waters are particularly vulnerable to pollution because they are the final receiving waters of most rivers in the upper reaches. Estuarine zoning is the most effective tool for coastal marine resource management, which can identify different types of estuarine, so as to different standards can be used to manage estuarine resources (Hume and Herdendorf, 1988). It is also the premise for the formulation of nutrient criteria (Liu et al., 2011). To reduce and prevent the further aggravation of eutrophication, it is necessary and urgent to develop estuarine nutrient criteria. In the 1960s, the United States carried out research on water quality criteria, published a series of literatures on water quality criteria, and issued technical guidelines for nutrient water criteria for different water bodies (such as lakes, rivers, wetlands), which had a profound impact on the formulation of nutrient criteria or standards for every American state and other countries around the world (Xu, 2020; Department of Ecology and Environment of Jiangsu Province, 2021b). The reference condition approach, mechanistic modelling, and stressor-response analysis are commonly recommended for setting nutrient criteria globally (US EPA, 2000). The US EPA applied the reference state method and mechanical model method to formulate the TN nutrient criteria values for the Tampa Bay and Florida Bay, respectively, while the European Union pioneered the transition node identification method to determine the Baltic Sea nutrient criteria (Florida Department of Environment Protection, 2007; Florida Department of Environment Protection, 2011; Wang et al., 2020; Xu, 2020). The research on nutrient criteria in China started relatively late and began at the beginning of the 20th century (Xu, 1981; Xia and Zhang, 1990). Some progress has been made in establishing nutrient criteria for lakes based on foreign experience (Huo et al., 2009; Huo et al., 2017; Liang et al., 2021). However, systematic studies on nutrient criteria in estuaries are limited (Su et al., 2016; Liu et al., 2018a; Yang et al., 2019). In addition, the existing standards involving nutrient indicators include Environmental quality standards for surface water (GB3838-2002) applicable to freshwater and Seawater Quality Standard (GB3097-1997) applicable to seawater, but they are not applicable to the estuarine area where salt and fresh water are mixed, and the latter only includes two indicators of DIN and DIP, lacking the assessment of TN and TP (Douglas and Mclaughlin, 2014; Su et al., 2017). Some studies have used reference state method to establish nutrient criteria in the Liaohe Estuary and coastal waters (Hu et al., 2011; Su et al., 2016). On the basis of the segmentation of the Jiulong River Estuary, whose nutrient criteria was determined using reference conditions, statistical

model analysis, and cumulative frequency distributions (Liu et al., 2018a), a nutrient criteria for the Yangtze Estuary and coastal waters was developed using population distribution approach (Yang et al., 2019). Therefore, categorizing numeric nutrients criteria for the estuarine transitional zones can be developed based on the segmentation of estuary.

The Pearl River Estuary (PRE) is characterized by superior natural conditions, dense population, and developed economy (Yin et al., 2000; Zhou et al., 2018; Li et al., 2020; Huang et al., 2021). With the development of social and economic activities and high-intensity human activities, the wastewater and sewage discharge to the PRE continues to increase, which intensifies the enrichment of nutrients in local waters (Lu et al., 2009). This results in the frequent occurrence of red tide disasters and the increasing degree and expansion of hypoxia phenomenon (Glibert et al., 2018; Geeraert et al., 2021; Ke et al., 2022). The amount of TN discharged from land sources in the PRE is still high, and the water quality has been inferior to Grade IV (DIN > 0.5mg $mg{\cdot}L^{-1}$ or DIP > 0.045mg/L) for a long time. DIN and DIP are the main factors exceeding the standard, among which DIN exceeds the standard by 1.7–5.9 times (Moffat, 1998; Tong et al., 2015; South China Sea Branch of the State Oceanic Administration, 2017; State of Oceanic Administration, 2018; Yan and Li, 2018; Department of Ecology and Environment of Guangdong Province, 2022a). In the summer of 2019, the concentrations of DIN and DIP in the PRE were 0.168-1.247 $mg{\cdot}L^{-1}$ and 0.011-0.044 $mg{\cdot}L^{-1}$, respectively, and 25% of the monitoring stations were over-eutrophication (Ma and Zhao, 2021). In addition, from 1981 to 1998 and 2000 to 2009, nearly 116 red tides were recorded in the PRE affecting more than 2850 km^2 of coastal waters (Wei et al., 2012). Many red tides had a long duration and high toxicity, endangering the habitat environment of aquatic organisms (Lai et al., 2018). At present, the PRE has been listed as one of the three major areas in the "14^{th} Five-Year Plan" national key sea area of comprehensive management battle, which will drive the overall improvement of the quality of marine ecological environment (Ministry of Ecology and Environment of the People's Republic of China, 2022b). The government and Guangdong Province have also successively put forward plans to prevent and control pollution in estuaries and coastal waters, comprehensively implementing the principle of "coordinating land and sea, taking into account river and sea", strengthening the linkage between land pollution control and comprehensive treatment of marine environment, adhering to both pollution prevention and control and ecosystem protection, so as to realize the whole chain of pollution control from source to end (Ministry of Ecology and Environment of the People's Republic of China, 2022a; Department of Ecology and Environment of Guangdong Province, 2022b). Therefore, to control and improve water quality, provide effective management measures, it is urgent and critical to establish effective nutrients criteria.

Based on the seasonal data of the PRE and adjacent waters from 2015 to 2020, the study objectives were (1) to establish nutrient criteria using the frequency distribution method, (2) to establish water quality standards based on nutrient criteria to evaluate and verify it, and (3) to estimate the background concentrations of N and P and implement zoning management in the PRE. This study can provide a scientific basis for effectively solving the problem of eutrophication, evaluating water quality in coastal waters, and joint prevention and control of water pollution land-ocean coordination.

Materials and methods

Study areas

The Pearl River originates from Mashen Mountain in the Wumeng Mountain System of the Yunnan-Guizhou Plateau, with a total drainage area of 453690 km^2, and flows through Yunnan, Guizhou, Guangxi, Guangdong, Hunan, Jiangxi, and northern Vietnam (Zhao, 1989; Cui et al., 2020). The Pearl River is rich in water, with an annual inflow of 326 billion steres and an annual runoff of over 330 billion steres, followed by the Yangtze River. It is the largest water system in southern China (Zeng et al., 2020). The runoff of the Pearl River varies greatly, and the annual distribution of runoff is corresponding to the rainy season. The runoff in the wet season accounts for 70-80% of the total amount of the whole year, which is characterized by the wet > normal > dry season, indicating that the runoff is of the type of precipitation replenishment (Zhao, 1989; Yuan, 2005). The PRE is more than 80 km long, from north to south, and covers an area of 2100 km^2. It borders Guangzhou in the north, Shenzhen and Hong Kong in the east, Zhuhai and Macao in the west, and is located in the core of the Guangdong-Hong Kong-Macao Greater Bay Area (Huang X. and Huang L., 2002) (Figure 1A). The tidal nature of the PRE belongs to irregular semi diurnal mixed tide. The surface flow velocity is higher than the bottom flow velocity, and the summer flow velocity is higher than the winter flow velocity (Xia and Zhou, 2021). With the rapid development of industry and agriculture along the PRE and the continuous influx of population, pollutants such as nitrogen, phosphorus, and other nutrients enter the PRE through artificial discharge, river carrying, precipitation, and other means, resulting in eutrophication and deterioration of water quality (Niu et al., 2020a, Niu et al., 2020b, Qiu et al., 2010, Yin et al., 2013). The environmental quality of the PRE ecosystem needs to be improved urgently (Strokal et al., 2017; Zeng et al., 2020).

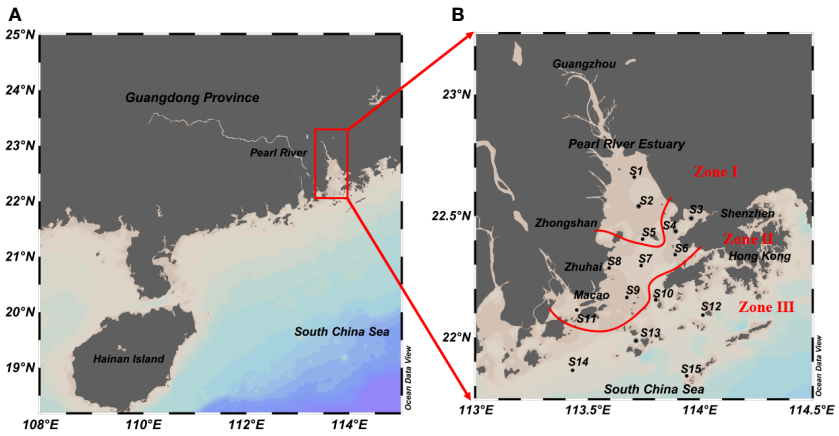


FIGURE 1
Study area **(A)** and monitoring stations **(B)** of the Pearl River Estuary coastal water.

Data sources and chemical analysis

Monitoring data in the PRE were acquired from the Department of Ecology and Environment of Guangdong Province. During the six years from 2015 to 2020, the study area was sampled in the dry (April), wet (July), and normal (October) water flow seasons every year, totaling to 18 sampling seasons. A total of 15 stations were set in the study area (Figure 1B) and 921 datasets were collected, including 262 groups of DIN, 90 groups of TN, DIP groups of 262, TP groups of 90, and 217 groups of salinity. Water samples were collected using cleaned polyethylene bottles or hard glass bottles and promptly brought back to the laboratory for filtration within 24 h. The relative standard deviations (RSD) of repeated determinations of selected samples were less than 5%. The details of analytical methods, processes and instruments in this study had been described in the Specification of Oceanographic Survey (China National Standardization Management Committee, 2007; China National Standardization Management Committee, 2007b; Ministry of Environmental Protection of the PRC, 2009).

Analytical approach of nutrients criteria

Combined with domestic and foreign experience, the frequency distribution method was used to establish nutrient water criteria in the PRE. In the case of sufficient data or good habitat condition, the corresponding value of the 25th percentile (or other suitable percentile) of the nutrient index frequency distribution curve was used as the criteria value. The selection of specific percentage point is only a suggestion and can be determined according to the habitat of the study area. If the area is heavily polluted, the corresponding value of the 5th percentile (or other appropriate percentile) on the frequency distribution curve of nutrient indicators can be selected as the criteria value (Hu et al., 2011; McLaughlin, 2014; Yang, 2015). After processing and integrating the experimental data, the K-S test (Kolmogorov-Smirnov test) was conducted to determine whether the data conformed to a normal distribution. If it conformed ($P \geq 0.05$), a frequency distribution diagram was drawn. If not ($P < 0.05$), the partial maximum or minimum values were removed or logarithmic transformation was carried out before testing, and then the corresponding frequency distribution diagram was drawn. Based on the figure, reference to the historical data and the data of this study, water quality criteria were determined, and then compared with Seawater Quality Standard to evaluate, interpret, and correct the recommended water quality criteria. The detailed process is illustrated in Figure 2 (US EPA, 1998; US EPA, 2001; Meng et al., 2008; Li et al., 2019).

Data processing methods

Microsoft Excel 2016 was used to record and organize the data, and Statistical Product and Service Solution (SPSS) software was used for salinity clustering analysis to complete the estuary division. The establishment of the nutrient criteria adopted the frequency distribution method, and the normal distribution test of each nutritional index was performed using SPSS to determine the criteria. Ocean Data View (4.0) (Schlitzer, 2002) was used to draw a schematic diagram of the monitoring stations and a spatiotemporal distribution map. Other images,

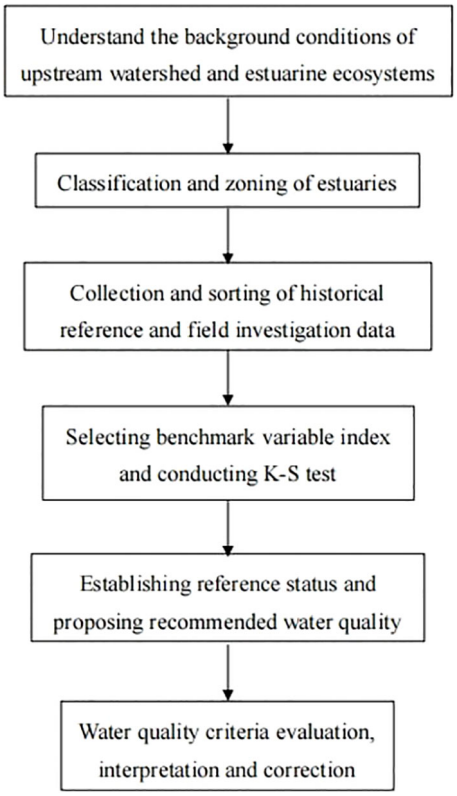


FIGURE 2
Framework of establishing water quality criteria in the PRE coastal water (Li et al., 2019).

such as the frequency distribution curve and salinity cluster analysis dendrogram, were drawn using Origin Lap 2021 software. The average data used in this study are expressed as mean ± standard deviation (mean ± SD).

Results

Spatiotemporal salinity variations and segmentation solutions in the PRE coastal water

Among the three periods in the PRE, the average salinity was 18.48 ± 8.86 PSU, and the maximum and minimum salinity were 32.48 PSU in the dry season and 2.23 PSU in the wet season, respectively. The salinity in the PRE decreased from dry to wet water flow period, and then remarkable increased during the normal water flow period. The salinity range in surface seawater in the dry season was 5.47–32.48 PSU, with an average value of 19.92 ± 8.74 PSU. In the wet season, salinity in the surface water had a range from 2.23–27.99 PSU, and the average was 14.31 ± 8.06 PSU, which differed from the other two seasons and was the lowest. The average salinity in the normal season was 21.21 ± 8.73 PSU, which ranged from 5.71–32.15 PSU. Spatially, the distribution of salinity was similar during the three water flow periods, and it was low in the upper part of the estuary and gradually increased to the open sea (Figure 3).

Applying the SPSS cluster analysis model with salinity as the reference condition, the PRE can be divided in three zones (Figure 4). The first subsection contained S1, S2, and S5, which included the upper estuary, whose water characteristics are mainly freshwater, and the average salinity value was 6.93 ± 2.56 PSU. The second subsection contains S3, S4, S6, S7, S8, S9, and S11. This area belongs to the middle of the estuary and is the largest area where salt water and fresh water are mixed in different proportions, with an average salinity of 16.71 ± 1.49 PSU. The third subsection contained S10, S12, S13, S14, and S15, which are the ocean-dominated areas in the lower part of the estuary with an average salinity of 27.96 ± 2.56 PSU. As a result, based on the morphological characteristics of the estuary and the

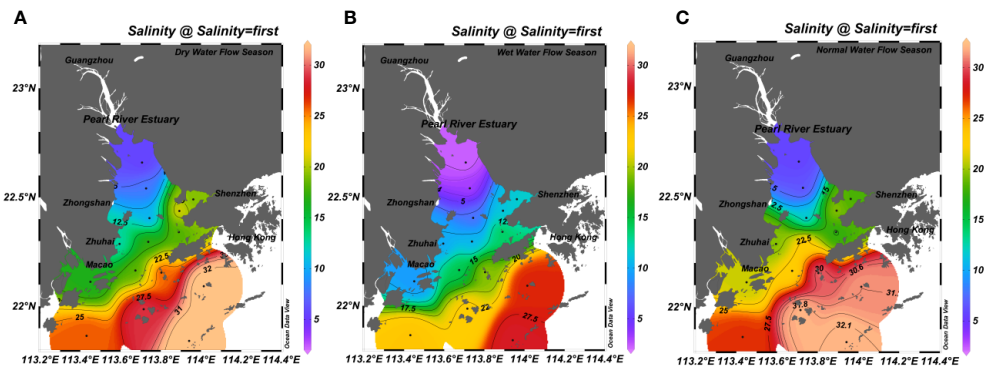


FIGURE 3
Spatial and temporal distribution of salinity along the PRE coastal water in the dry **(A)**, wet **(B)**, normal **(C)** season.

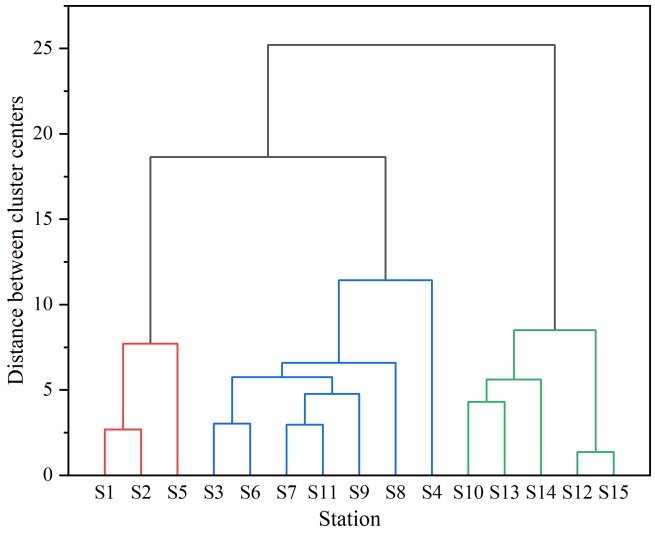


FIGURE 4
Cluster analysis tree of salinity.

spatial distribution of salinity (Figure 3), the PRE can be divided in Zone I (S1, S2, S5), Zone II (S3, S4, S6, S7, S8, S9, S11), and Zone III (S10, S12, S13, S14, S15).

DIN and TN criteria in the PRE coastal water

The frequency distributions of nitrogen and phosphorus nutrients in the PRE was obtained through a normal distribution test and frequency distribution analysis of the partitioned data (Figure 5, Table 1, and Table A1).

In Zone I, the average value of DIN in the three water flow seasons was 1.459 mg·L^{-1}, with a median of 1.445 mg·L^{-1}, varying from 0.098 to 3.237 mg·L^{-1}. The average value and median of TN were 1.832 mg·L^{-1} and 1.783 mg·L^{-1}, respectively, and the variation range was 0.177–3.220 mg·L^{-1} from the dry to the normal season. According to the Bulletin on Marine Environment of Guangdong Province from 2015 to 2017 and the Bulletin on Ecological Environment of Guangdong Province from 2018 to 2020, the water quality of coastal waters along the PRE is poor. Zone I is located in the estuary, and the water quality of most sea areas was Grade IV or inferior. In recent years, DIN has exceeded standard limits. Therefore, for DIN and TN the corresponding value of the 5th percentage point of the frequency distribution curve was selected as the reference state to propose the criteria value, which were 0.573 mg·L^{-1} for DIN and 0.902 mg·L^{-1} for TN (Figure 6).

In Zone II, the average value of DIN in the three water flow seasons was 0.953 mg·L^{-1} and the median was 0.912 mg·L^{-1}, varying from 0.116 to 2.379 mg·L^{-1}. The average and median values of TN were 1.287 mg·L^{-1} and 1.270 mg·L^{-1}, respectively, and the variation range was 0.286–2.480 mg·L^{-1}. Based on the Bulletin on Marine Environment of Guangdong Province from 2015 to 2017 and the Bulletin on Ecological Environment of Guangdong Province from 2018 to 2020, the water quality of coastal waters along the PRE was poor, but it was Grade I or Grade II in most of the sea area of Zone II, which was better than Zone I. The 15th percentage point of the water quality frequency distribution curve was selected as the reference state to propose the recommended water quality criteria, which were 0.312 mg·L^{-1} for DIN and 0.885 mg·L^{-1} for TN (Figure 6).

In Zone III, the average value of DIN in the three water flow seasons was 0.217 mg·L^{-1} and the median was 0.250 mg·L^{-1}, varying from 0.020 to 1.049 mg·L^{-1}. The average and median values of TN were 0.432 mg·L^{-1} and 0.347 mg·L^{-1}, respectively, and the variation range was 0.038–1.340 mg·L^{-1}. It can be seen from the data that nutrient pollution in Zone III was not as serious as that in Zones I and II. It may be due to the distance from the estuary, the reduction of the influence of terrestrial input and the physical mixing process of ocean currents (Liu et al., 2020). However, it is possible that there is a negative correlation between salinity and nitrogen and phosphorus nutrients (Hu et al., 2016; Zhou et al., 2022; Ke et al., 2022). Therefore, the 25th percentile under the water quality frequency distribution curve was selected as the reference state, and the recommended water quality criteria were proposed as 0.134 mg·L^{-1} for DIN and 0.222 mg·L^{-1} for TN (Figure 6).

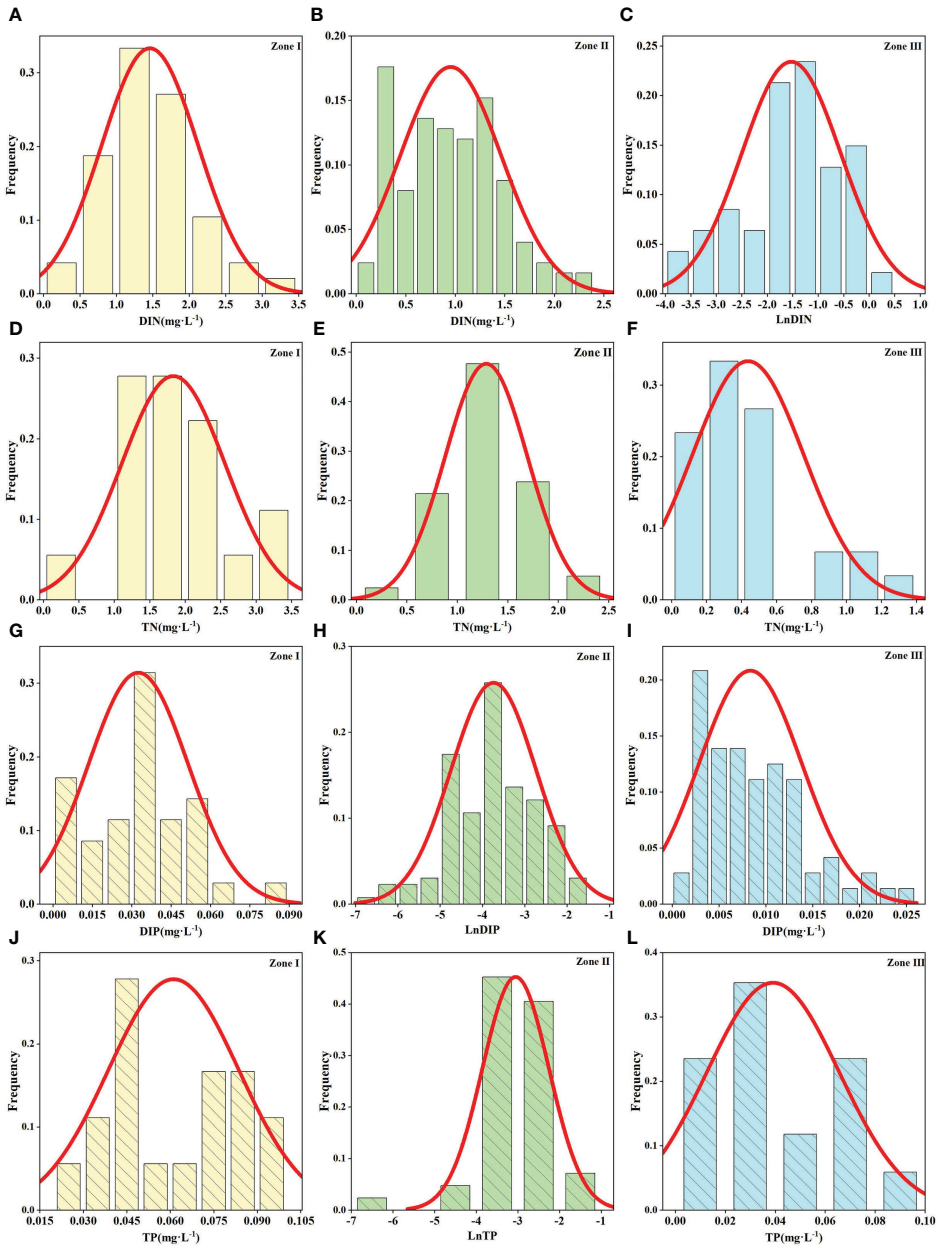


FIGURE 5
Frequency distributions of DIN **(A–C)**, TN **(D–F)**, DIP **(G–I)**, and TP **(J–L)** in the PRE coastal water.

DIP and TP criteria in the PRE coastal water

In Zone I, the average value of DIP in all three seasons was 0.033 mg·L^{-1}, with a median of 0.033 mg·L^{-1}, ranging from 0.002 to 0.086 mg·L^{-1}. The mean value of the TP concentration during the three seasons was 0.039 mg·L^{-1}, the median was 0.059 mg·L^{-1}, and the variation range was 0.028–0.098 mg·L^{-1}. For DIP and TP the corresponding value of the 15th percentage point of the frequency distribution curve was selected as the reference state to propose the criteria value, which were 0.009 mg·L^{-1} for DIP and 0.039 mg·L^{-1} for TP (Figure 7).

In Zone II, during the three water flow seasons, the average value of DIP was 0.024 mg·L^{-1}, with a median of 0.024 mg·L^{-1}, ranging from 0.001 to 0.201 mg·L^{-1}. The mean value of the TP concentration was 0.047 mg·L^{-1}, the median was 0.049 mg·L^{-1}, and the variation range was 0.002–0.259 mg·L^{-1}. The 15th percentage point of the water quality frequency distribution

TABLE 1 Frequency distribution results of DIN, TN, DIP and TP in the PRE coastal water (mg·L^{-1}).

Area	Nutrient	Number	5%	15%	20%	25%	50%	75%	85%
Zone I	DIN	48	0.573	0.790	0.924	1.019	1.445	1.798	2.108
	TN	18	0.902	1.247	1.289	1.377	1.783	2.166	2.402
	DIP	35	0.004	0.009	0.015	0.019	0.033	0.046	0.051
	TP	18	0.035	0.039	0.040	0.041	0.059	0.082	0.085
Zone II	DIN	125	0.230	0.312	0.402	0.565	0.912	1.320	1.492
	TN	42	0.745	0.885	0.935	1.035	1.270	1.513	1.626
	DIP	132	0.005	0.009	0.010	0.011	0.024	0.049	0.067
	TP	42	0.018	0.028	0.032	0.033	0.048	0.076	0.102
Zone III	DIN	47	0.038	0.073	0.127	0.134	0.249	0.414	0.628
	TN	30	0.117	0.160	0.190	0.222	0.347	0.521	0.743
	DIP	72	0.002	0.002	0.003	0.004	0.008	0.012	0.013
	TP	17	0.001	0.016	0.017	0.020	0.035	0.063	0.070

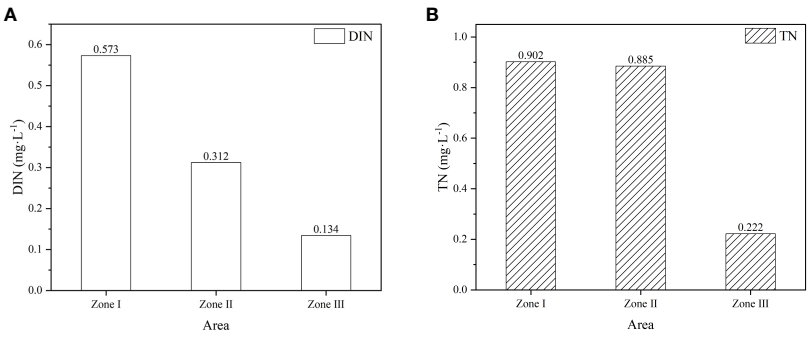


FIGURE 6
Recommended criteria for DIN **(A)** and TN **(B)** in the PRE coastal water.

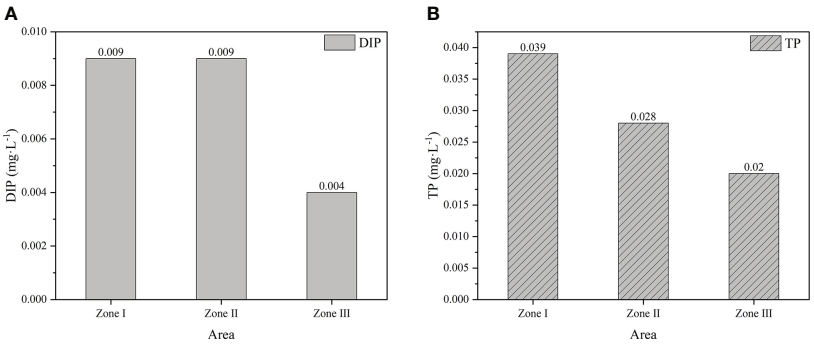


FIGURE 7
Recommended criteria for DIP **(A)** and TP **(B)** in the PRE coastal water.

curve was selected as the reference state to propose the recommended water quality criteria, which were 0.009 mg·L^{-1} for DIP and 0.028 mg·L^{-1} for TP (Figure 7).

In Zone III, the average DIP value in all three seasons was 0.008 mg·L^{-1}, with a median of 0.008 mg·L^{-1}, ranging from 0.001 to 0.024 mg·L^{-1}. The mean value of the TP concentration was 0.039 mg·L^{-1}, the median was 0.035 mg·L^{-1}, and the variation range was 0.001–0.085 mg·L^{-1}. The 25th percentile under the water quality frequency distribution curve was selected as the reference state, and the recommended water quality criteria were proposed as 0.004 mg·L^{-1} for DIP and 0.020 mg·L^{-1} for TP (Figure 7).

Water quality assessment standard for DIN, TN, DIP and TP in the PRE coastal water

According to the sea water quality standard and different applicable functions and protection objectives, the coastal waters of the PRE were divided in four functional areas (Table A2), and the marine water quality standards of DIN, TN, DIP, and TP were formulated.

For the water quality standard limits of nitrogen and phosphorus applicable to class I marine functional areas, the seawater quality standard needs to be stricter because it involves areas with special needs to be protected, such as marine nature reserves and rare and endangered marine biological reserves. The sea water and environmental quality standards for surface water stipulate relatively strict water quality requirements for areas requiring special protection, such as nature reserves. Therefore, it was formulated with reference to the water quality criteria for coastal waters in the PRE (Table 2).

For the water quality standard limits of nitrogen and phosphorus applicable to class II marine functional areas, considering the accessibility and economic factors of the standards and the large amount of nutrients required for aquaculture biological bait in aquaculture areas, the standard values of nitrogen and phosphorus should be relaxed appropriately. The nutrient water quality standards for fishery waters in the seawater quality standard and the environmental quality standards for surface water are considerably higher than those for nature reserves. The nutrient indicators in Zones I and II can be formulated with reference to a cumulative frequency of 25% in the results of the frequency distribution curve, and Zone III can be formulated with reference to a cumulative frequency of 50% in the results of the frequency distribution curve (Table 2).

Classes III and IV include general industrial water use areas, coastal scenic tourism areas, marine port waters, and marine development operation areas. As the nutrient index has relatively little impact on the use function and protection objectives of the two types of marine functional areas and considering the accessibility and economic factors of the standard, the nutrient standard limit should be more relaxed. Similar situations are reflected in the seawater quality standards and environmental quality standards for surface water. The standard was developed with reference to the values of 50% and 70% of the cumulative frequency in the statistical results of the frequency distribution curve in Zones I and II, whereas Zone III is formulated with reference to the cumulative frequencies of 75% and 85% in the statistical results of the frequency distribution curve method (Table 2).

Discussion

Comparison of nutrients by reference condition

During the 40 years from 1980 to 2020, nutrients in the PRE showed different trends (Long et al., 2020). The concentration of DIN showed a very significant increasing trend, while the DIP

TABLE 2 Sea water quality standard in coastal waters of the PRE (mg·L^{-1}).

Area	Nutrient	I Grade	II Grade	III Grade	IV Grade
Zone I	DIN	0.573	1.019	1.445	1.789
	TN	0.902	1.377	1.783	2.166
	DIP	0.009	0.019	0.033	0.046
	TP	0.039	0.041	0.059	0.082
Zone II	DIN	0.312	0.565	0.912	1.320
	TN	0.885	1.035	1.270	1.513
	DIP	0.009	0.011	0.024	0.049
	TP	0.028	0.033	0.048	0.076
Zone III	DIN	0.134	0.249	0.414	0.628
	TN	0.222	0.347	0.521	0.743
	DIP	0.004	0.008	0.012	0.013
	TP	0.020	0.035	0.063	0.070

concentration began to decrease after a significant increase, and then remained unchanged (Howarth, 2008; Huang, 2008; Long et al., 2020; Ma et al., 2009). In the early 1980s, the concentration of DIN was only 0.120 mg·L^{-1} (Yuan, 2005), and 0.270 mg·L^{-1} in 1986 (He et al., 2004), which is close to the DIN criteria of the PRE seawater area (0.134 mg·L^{-1}) and the mixing area (0.312 mg·L^{-1}); therefore, the DIN concentration in the PRE without pollution was roughly between 0.120 mg·L^{-1} and 0.312 mg·L^{-1}. Before 1990, the DIN concentration in the PRE increased slowly and reached as high as 0.510 mg·L^{-1} in 1995 (Dang et al., 2019). Then, it began to increase explosively and reached a peak of 1.256 mg·L^{-1} in 2017, increasing more than 10 times. The concentration of DIP was maintained between 0.008 and 0.015 mg·L^{-1} before 1990 (Yuan, 2005), which was comparable to the DIP criteria proposed in this study for the PRE seawater area (0.004 mg·L^{-1}), mixing area (0.009 mg·L^{-1}), and freshwater area (0.009 mg·L^{-1}). The DIP concentration in the PRE without pollution was approximately 0.004–0.015 mg·L^{-1}. After 1990, the DIP began to increase remarkably, reaching 0.070 mg·L^{-1} in 2010 (Dang et al., 2019), which had increased more than eight times in the past 30 years. It then began to fluctuate at a high level, showing an oscillatory downward trend.

Some studies have shown that the water quality of the PRE has gradually changed from exceeding the standard of heavy metals to nutrients around 1990, and excessive pollutants were mainly DIN and DIP (Yuan, 2005; Dang et al., 2019). However, owing to the lack of long-term continuous monitoring data and seawater quality assessment for TN and TP, the phenomenon of exceeding the standard may have occurred earlier. In recent years, the Guangdong Provincial Department of Ecology and Environment and many studies have monitored TN and TP in the PRE. The results suggested that the average concentrations of TN and TP were 1.113 and 0.050 mg·L^{-1} in 2019-2020, respectively (Department of Ecology and Environment of Guangdong Province, 2020; Department of Ecology and Environment of Guangdong Province, 2021). Compared with 2014, TN decreased, while TP was relatively constant (Zhang et al., 2015). In addition, TN/TP can also reflect the demand of phytoplankton for nutrients, reflecting the total amount of nutrients that may be absorbed and utilized by phytoplankton in the sea area (Redfield et al., 1963; Huang and Hong, 1999; Chen et al., 2013; Jin and Liu, 2013). Therefore, it is necessary to establish the relationship between DIN and TN, DIP and TP, and to calculate the background concentration of TN and TP to evaluate the criteria of TN and TP, to better understand their impact on eutrophication.

There is a negative correlation between DIN and DIP and salinity in the PRE, indicating that the terrigenous nutrients are strongly influenced by the mixing of sea and fresh water (Lan et al., 2014; Ke et al., 2022; Hong, 2022; Smith et al., 1999). The runoff input regulates the distribution of N and P to the sea, resulting in a gradual decrease in DIN and DIP from south to north. Therefore, the N and P nutrient criteria values (except DIP) are shown as Zone I > Zone II > Zone III.

Comparison of numeric nutrient criteria

The numerical nutritional standards for the different estuaries and coastal waters were different (Table 3). This may be due to the natural characteristics of different estuaries, such as dilute water, water residence time, and vertical stratification (US EPA, 2001), as well as differences in methods of deriving nutrient criteria in different countries (Wang et al., 2020). The recommended nutrient criteria in the PRE were comparable to those found in most of the estuaries as listed in the Table 3. The research on water criteria in China mainly focuses on DIN and DIP, while the international studies focus on TN and TP (Raymond et al., 2011; Evans-white et al., 2013), and the criteria values of TN and TP compared with those in the coastal waters of estuaries of China, are relatively strict. Among these the TN criteria of the coastal waters of the Yangtze River Estuary are more than 10 times that of the coast of Hawaii, and that of the freshwater area of the PRE is about six times (Table 3). Compared to other estuaries in China, the Yangtze River Estuary is the largest estuary in China and is located in the core area of the Yangtze River Delta economy. It is also the most developed area for industry and agriculture in China. In recent years, the impact of rapid economic development on near-shore water quality has become increasingly evident. Moreover, coastal waters of the Yangtze River estuary are affected by water masses such as the Yangtze River flushing fresh water, Jiangsu-Zhejiang coastal current, northern Jiangsu coastal current, and Taiwan warm current, and the hydrological environment is relatively complex (Li et al., 2022). They all resulted in lower DIN, TN, DIP, and TP nutritional criteria than those for other estuarine areas in China. There are few differences in the DIP and TP criteria between the PRE and Liaohe River Estuary, which may indicate that the two estuaries have similar phosphorus distribution characteristics, both of which are phosphorus limited (Wu et al., 2017; Zeng et al., 2020; Chen et al., 2020; Ke et al., 2022). Some studies have shown that nitrogen in the PRE ranks first among many estuaries in China (Huang et al., 2003; Lai et al., 2018). To alleviate nitrogen pollution, the recommended standards for DIN and TN are relatively strict.

Recommended standard certification and analysis of results

In this study, the monitoring data of DIN and DIP in the near-shore waters of the PRE from 2015 to 2020 were used to evaluate the new standards proposed in this study, while the

TABLE 3 Reference condition or criteria in different coastal water and estuaries worldwide (mg·L^{-1}).

Zone		DIN	TN	DIP	TP	References
Coastal water of Jiangsu Province	mixed area		0.95		0.074	Department of Ecology and Environment of Jiangsu Province, 2021a
	seawater area		0.41		0.042	
Jiulong River Estuary	fresh water area	0.896		0.028		Liu et al., 2018
	mixed area	0.294		0.024		
	seawater area	0.196		0.028		
Yangtze River Estuary		1.05-1.24	1.56-1.85	0.030-0.036	0.060-0.072	Yang et al., 2019
Liaohe River Estuary		0.77	1.11	0.005	0.037	Su et al., 2016
Hawaii	coastal waters		0.15		0.020	US EPA, 2009
	estuarine area		0.20		0.025	
Biscayne Bay			0.24-0.38		0.005-0.009	Briceo et al., 2010
Europe	Baltic coast		0.013-0.033			Helcom, 2015; Helcom, 2017; Herrero et al., 2019
	Mediterranean coast		0.0115-0.0186			
	estuary		0.089-0.105			
Pearl River Estuary	fresh water area	0.573	0.902	0.009	0.039	This study
	mixed area	0.312	0.885	0.009	0.028	
	seawater area	0.134	0.222	0.004	0.020	

exceedances of DIN and DIP in the same period were analyzed using the seawater quality standard (GB3097-1997). If the seawater quality standard was adopted for assessment, the DIN concentration in the three seasons did not meet the Grade IV water quality standard by more than 50%, especially in the dry season, which was 56.67%. At the same time, only approximately 40% of the DIN concentration met the Grade I, II, or III water quality standards. Using the recommended water quality standard proposed in this study, the concentration of DIN did not meet the Grade IV water quality standard decreased by nearly 75% in the normal period, while DIN concentration met Grade I, Grade II, and Grade III water quality standards and increased to more than 60%, and up to 76% in the normal water flow season (Figure 8A). As for DIP, if the seawater quality standard was employed, the DIP concentration in the dry, wet, and normal seasons met the water quality standards of Grade I and Grade II, reaching approximately 70%, and the water quality in the inferior Grade IV was less than 20%. If the water quality standard recommended in this study was used, the proportion of DIP concentration that met Grade I and Grade II water quality standards during the three seasons considerably decreased and dropped by half in the dry season, while the proportion of DIP concentration in Grade IV or inferior increased by 59% in the dry season (Figure 8B).

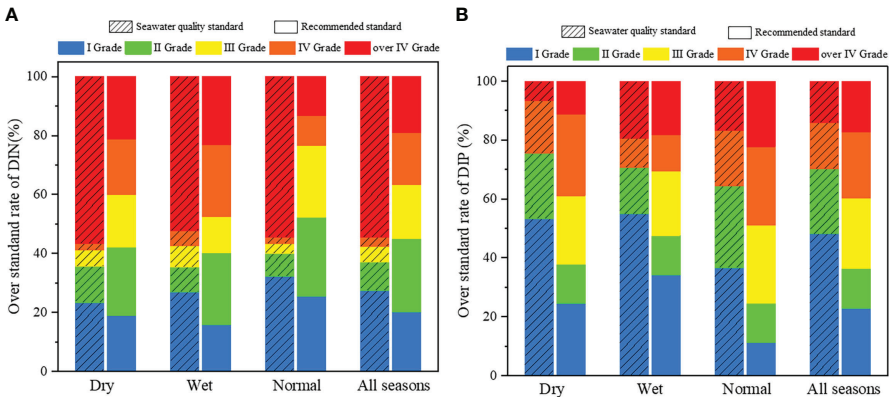


FIGURE 8
Seawater quality standard and the recommended standard assessment DIN **(A)** and DIP **(B)**.

Currently, there are no seawater assessment standards for TN and TP in China. The study also used monitoring data from the PRE in 2019 and 2020 to verify the TN and TP specified in this standard. The proportions of TN and TP failed to meet the Grade IV water quality standard, which was the highest in the wet season. Overall, TN and TP met the Grade III water quality standard (Figure 9). The compliance rate of TP meeting the Grade III water quality standard was higher than that of DIN, TN, and DIP. As shown in the picture, using the recommended standard to evaluate DIN, TN, DIP and TP, the annual compliance of each index was almost the same, the proportion of each nutrient standard to reach Grade III water quality standard was more than 60%. Therefore, it can be tentatively judged that there may be "over-protection" for DIN and "under-protection" for DIP in the current seawater quality standard of the PRE. Therefore, from the management perspective, the new standard had no obvious impact on the assessment of seawater quality in the coastal waters of the PRE. From a scientific point of view, the standard is formulated based on the monitoring data of PRE over the years and conforms to the status of the environmental quality of PRE. Since the standard is a recommended local standard and was first explored in China, it is scientifically reasonable and operable, although it cannot consider all aspects.

Implications of establishing estuarine nutrients criteria for alleviating eutrophication

There are differences in the nutrient monitoring indicators stipulated in China's current seawater quality standard and environmental quality standards for surface water, and they are applicable to seawater and freshwater, respectively (Ministry of Ecology and Environment of the People's Republic of China, 1997; Ministry of Ecology and Environment of the People's Republic of China, 2002). However, they may not be fully applicable to estuaries in which seawater and freshwater are mixed (Su et al., 2016; Li et al., 2020). Therefore, the significance of establishing estuarine nutrient criteria for eutrophication mitigation is as follows: first, the water quality index system is unified, supplementing the seawater quality assessment of TN and TP, and the nutrient pollution status and source of nutrient pollution are objectively assessed (Yang, 2015); second, the management of estuaries by zoning and classification has been realized, and the establishment of a joint mechanism for pollution prevention and control of watershed, estuary, and coastal sea area waters has been promoted (Song et al., 2021); finally, the establishment of estuarine nutrient criteria realizes the overall planning of land and sea, and takes into account rivers and seas, which promotes water pollution prevention and control, water ecological protection, and water resources management, which is of great significance to further realize the construction of beautiful estuaries and bays and high-quality development of the marine economy (Liu et al., 2017; Ministry of Ecology and Environment of the People's Republic of China, 2022). In addition, land-based pollution will lead to nutrient enrichment in estuaries, which will cause great damage to the marine environment (Wu et al., 2019). Based on the fact that the PRE is a typical estuarine ecosystem with high N and low P, and has been in a P-limited state for a long term, it is appropriate to adopt the pollution control mode of land and sea integration (Redfield et al., 1963). Establishing estuarine nutrient criteria can estimate the background concentration of nutrient, and formulate scientific water quality standard for assessment, which can strictly control the discharge of land-based pollutant, reduce the total amount of nutrients entering to the sea, and reduce the contribution of land-based pollution to the PRE from the source (Hu et al., 2020). At the same time, it is necessary to strengthen the comprehensive management of

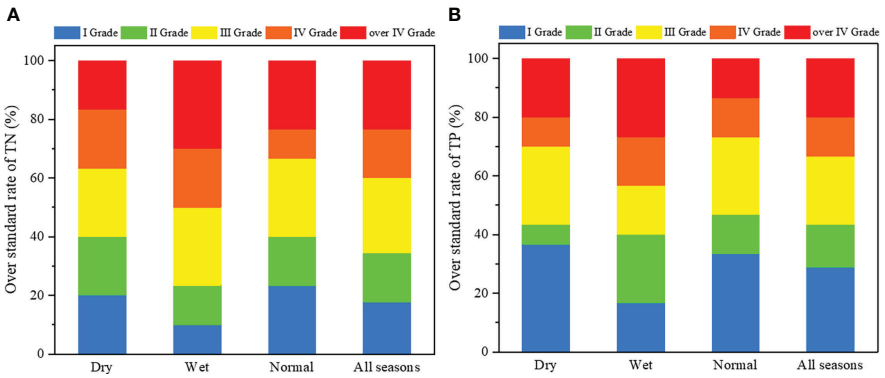


FIGURE 9
Recommended standard assessment TN **(A)** and TP **(B)**.

rivers flowing into the PRE, and reinforce the real-time monitoring of water quality in the PRE, accurately identify the sudden changes in water quality in the PRE, and provide a scientific basis for the improvement of water quality in the PRE (Hong, 2022).

Therefore, this study considers that long-term monitoring should be carried out in the coastal waters of various estuaries, such as the Pearl River Estuary, Yangtze River Estuary, and Yellow River Estuary, to accumulate rich reference data to provide data support for the formulation of nutrient criteria in China (Su et al., 2016). Simultaneously, corresponding nutrient control standards and management strategies should be put forward based on the actual situation of different estuaries (Huo et al., 2018; Zhou et al., 2020). Under the background of "Strengthening the environmental protection and restoration of estuaries and bays, implementing the comprehensive management of one bay and one policy in estuaries and adjacent bays, and building a number of beautiful bays by implementing classified policies", establish zoning management and control of nutrients in the basin-estuary-coastal water, achieve the goal of fine water quality management and control, make full use of the self-purification capacity of water bodies, and improve the eutrophication of estuarine coastal water (Department of Ecology and Environment of Guangdong Province, 2022b).

Conclusions

In this study, the PRE was divided in three segments based on salinity, corresponding to freshwater, mixed, and seawater areas, with increasing salinity from north to south. Frequency statistical analysis was applied to establish the recommended nutrient criteria. The recommended DIN, TN, DIP, and TN criteria in the freshwater area were 0.573, 0.902, 0.009, and 0.039 $mg{\cdot}L^{-1}$, respectively; the recommended DIN, TN, DIP, and TN criteria in the mixed area were 0.312, 0.885, 0.009, and 0.028 $mg{\cdot}L^{-1}$, respectively; and the recommended DIN, TN, DIP, and TP criteria in the seawater area were 0.134, 0.222, 0.004, and 0.020 $mg{\cdot}L^{-1}$, respectively. The DIN concentration in the PRE without pollution was approximately between 0.120 $mg{\cdot}L^{-1}$ and 0.312 $mg{\cdot}L^{-1}$, and the DIP concentration without pollution was approximately 0.004–0.015 $mg{\cdot}L^{-1}$. It is necessary to establish the relationship between DIN and TN, DIP and TP to better understand their impact on eutrophication. Under the integrated management mode of land and ocean, the emissions of land-based pollutants should be strictly controlled to reduce the impact on estuaries and coastal waters. At present, the Sea Water Quality Standard may have "over-protection" problems in the assessment of DIN of the PRE, while there may be "under-protection" problems in the DIP assessment. As a result, the establishment and application of nutrient water quality criteria unified the water quality monitoring indicator for land and ocean, is the basis for setting water quality standards, an effective measure to prevent eutrophication of water bodies, and a scientific basis for comprehensive monitoring, assessment, and management of nutrients in estuaries, which is of great significance for building beautiful estuaries and bays in China and worldwide. In the future, long-term monitoring should be carried out in the coastal waters of various estuaries, such as the Pearl River Estuary, Yangtze River Estuary, and Yellow River Estuary, to accumulate rich reference data to provide data support for the formulation of nutrient criteria in China.

Data availability statement

The original contributions presented in the study are included in the article/Supplementary Material. Further inquiries can be directed to the corresponding author.

Author contributions

Conceptualization: PZ; Methodology: PZ and JBZ; Software: SO; Validation: PZ, JXZ, and LZ; Formal analysis: PZ, JXZ, and LZ; Writing-original draft preparation: PZ and SO; Writing-review and editing: PZ and SO; Visualization: PZ and JBZ; Supervision: PZ and JBZ; Project management: PZ and JXZ; Funding acquisition: PZ and JBZ. All listed authors made substantial, direct, and intellectual contributions to the work and are approved for publication.

Funding

This research was financially supported by Key Laboratory of Marine Environmental Survey Technology and Application, Ministry of Natural Resource, P.R. China (MESTA-2020-B014); Research and Development Projects in Key Areas of Guangdong Province (2020B1111020004); Guangdong Ocean University Fund Project (R18021); First-class Special Fund (231419018); Innovation Strong School Project of Guangdong Ocean University (230420021).

Acknowledgments

The authors are grateful for the anonymous reviewers' careful review and valuable suggestions to improve the manuscript.

Conflict of interest

The authors declare that the research was conducted in the absence of any commercial or financial relationships that could be construed as a potential conflict of interest.

Publisher's note

All claims expressed in this article are solely those of the authors and do not necessarily represent those of their affiliated organizations, or those of the publisher, the editors and the reviewers. Any product that may be evaluated in this article, or claim that may be made by its manufacturer, is not guaranteed or endorsed by the publisher.

Supplementary material

The Supplementary Material for this article can be found online at: https://www.frontiersin.org/articles/10.3389/fmars.2022.1004235/full#supplementary-material

References

Anderson, D. M., Glibert, P. M., and Burkholder, J. M. (2002). Harmful algal blooms and eutrophication: nutrient sources, composition, and consequences. *Estuaries* 25, 704–726. doi: 10.1007/BF02804901

Arai, M. N. (2001). Pelagic coelenterates and eutrophication: a review. *Hydrobiologia* 451 (1-3), 69–87. doi: 10.1023/A:1011840123140

Boynton, W. R., Kemp, W. M., and Keefe, C. W. (1982). "A comparative analysis of nutrients and other factors influencing estuarine phytoplankton production," in *Estuarine comparisons* (New York, USA: Academic Press), 69–90.

Briceo, H., Boyer, J., and Harlem, P. (2010). *Proposed methodology for the assessment of numeric nutrient criteria for south Florida estuaries and coastal waters* (USA: Florida International University, Southeast Environmental Research Center).

Burkholder, J. M., Noga, E. J., Hobbs, C. H., Glasgow, H. B., and Smith, S. A. (1992). New 'phantom' dinoflagellate is the causative agent of major estuarine fish kills. *Nature* 358 (6385), 407–410. doi: 10.1038/360768e0

Cai, W. J., Hu, X., Huang, W. J., Murrell, M. C., Lehrter, J. C., Lohrenz, S. E., et al. (2011). Acidification of subsurface coastal waters enhanced by eutrophication. *Nat. Geosci.* 4, 766. doi: 10.1038/ngeo1297

Chen, M. Y., Chen, D., Zheng, A. R., Shi, X. Y., Li, Q. D., Jiang, P., et al. (2020). Distribution features of nitrogen, phosphorus, chlorophyll-a and their relationships with environmental factors in the jiulongjiang river estuary sea area. *J. Xiamen University(Natural Science)* 59 (S1), 99–106.

Chen, N., Peng, B., Hong, H., Turyaheebwa, N., Cui, S., and Mo, X. (2013). Nutrient enrichment and n: P ratio decline in a coastal bay-river system in southeast China: the need for a dual nutrient (N and p) management strategy. *Ocean Coast. Manag.* 81, 7–13. doi: 10.1016/j.ocecoaman.2012.07.013

China National Standardization Management Committee (2007). *The specification for marine monitoring*. China: Standards Press of China.

China National Standardization Management Committee (2007b). *Specification for oceanographic survey-part 4: Survey of chemical parameters in sea water*. China: Standards Press of China.

Conley, D. J., Paerl, H. W., Howarth, R. W., Boesch, D. F., Seitzinger, S. P., Havens, K. E., et al. (2009). Controlling eutrophication on: nitrogen and phosphorus. *Science* 323 (5917), 1014–1015.

Cui, X., Huang, C., Wu, J., Liu, X., and Hong, Y. (2020). Temporal and spatial variations of net anthropogenic nitrogen inputs (NANI) in the pearl river basin of China from 1986 to 2015. *PloS One* 15 (2), e0228683. doi: 10.1371/journal.pone.0228683

Dang, E. S., Tang, J. Y., Zhou, L. N., Ye, C., and Bao, C. G. (2019). Water quality assessment and eutrophication analysis in coastal waters of pearl river estuary. *J. Dalian Ocean Univ.* 34 (4), 580–587.

Davidson, K., Gowen, R. J., Harrison, P. J., Fleming, L. E., Hoagland, P., and Moschonas, G. (2014). Anthropogenic nutrients and harmful algae in coastal waters. *J. Environ. Manage.* 146, 206–216. doi: 10.1016/j.jenvman.2014.07.002

Department of Ecology and Environment of Guangdong Province (2020). *Seawater monitoring information in coastal waters of guangdong province in 2019*. Guangzhou, Guangdong: Guangdong Environmental Monitoring Center.

Department of Ecology and Environment of Guangdong Province (2021). *Seawater monitoring information in coastal waters of guangdong province in 2020*. Guangzhou, Guangdong: Guangdong Environmental Monitoring Center.

Department of Ecology and Environment of Guangdong Province (2022a). *2021 report on the state of guangdong provincial ecology and environment*. Guangzhou, Guangdong: Guangdong Provincial Department of ecology and environment.

Department of Ecology and Environment of Guangdong Province (2022b). *The "14th five-year plan" for marine ecological environmental protection in guangdong province*. Guangzhou, Guangdong: Department of Ecology and Environment of Guangdong Province.

Department of Ecology and Environment of Jiangsu Province (2021a). *Evaluation standard for seawater quality of jiangsu province, total nitrogen and total phosphorus*. Nanjing, Jiangsu: Department of Ecology and Environment of Jiangsu Province.

Department of Ecology and Environment of Jiangsu Province (2021b). *Specification for compilation of total nitrogen and total phosphorus of marine water quality assessment standard (draft for public comment)*. Jiangsu, China: Department of Ecology and Environment of Jiangsu Province.

DePinto, J. V., and Verhoff, F. H. (1977). Nutrient regeneration from aerobic decomposition of green algae. *Environ. Sci. Technol.* 11 (4), 371–377. doi: 10.1021/es60127a002

McLaughlin., D. B. (1977). Maximizing the accuracy of field-derived numeric nutrient criteria in water quality regulations. *Integrated Environmental Assessment and Management* 10 (1), 133–137.

McLaughlin, D. B. (2014). Maximizing the accuracy of field-derived numeric nutrient criteria in water quality regulations. Integrated environmental assessment and management. 10 (1), 131–137.

Evans-white, M. A., Haggard, B. E., and Scott, J. T. (2013). A review of stream nutrient criteria development in the united states. *J. Environ. Qual.* 42 (4), 1002–1014. doi: 10.2134/jeq2012.0491

Florida Department of Environment Protection (FDEP) (2007). *State of Florida numeric nutrient criteria development plan*. USA: Florida Department of Environment Protection.

Florida Department of Environment Protection (FDEP) (2011). *Site-specific information in support of establishing numeric nutrient criteria for Biscayne bay, Florida bay, Florida keys, and whitewater bay-ten thousand islands*. USA: Florida Department of Environment Protection.

Geeraert, N., Archana, A., Xu, M. N., Kao, S. J., Baker, D. M., and Thibodeau, B. (2021). Investigating the link between pearl river-induced eutrophication and hypoxia in Hong Kong shallow coastal waters. *Sci. Total Environ.* 772, 145007. doi: 10.1016/j.scitotenv.2021.145007

Ge, T. T., Wang, X. Y., Tan, L. J., and Li, T. (2021). Effect of stratification and tides on the transport of particulate nitrogen and phosphorus near the changjiang river estuary in summer. *Mar. Sci.* 45 (08), 1–9. doi: 10.11759/hykx20210319003

Glibert, P. M., Al-Azri, A., Icarus Allen, J., Bouwman, A. F., Beusen, A. H., Burford, M. A., et al. (2018). "Key questions and recent research advances on harmful algal blooms in relation to nutrients and eutrophication," in *Global ecology and oceanography of harmful algal blooms*, 229–259. doi: 10.1007/978-3-319-70069-4_12

Helcom (2015)HELCOM eutrophication assessment. Available at: http://helcom.fi/helcom-at-work/projects/eutro-oper/.

Helcom (2017)HELCOM core indicator report. Available at: www.helcom.fi.

Herbeck, L. S., Unger, D., Wu, Y., and Jennerjahn, T. C. (2013). Effluent, nutrient and organic matter export from shrimp and fish ponds causing eutrophication in coastal and back-reef waters of NE hainan, tropical China. *Cont. Shelf Res.* 57, 92–104. doi: 10.1016/j.csr.2012.05.006

Herrero, F. S., Teixeira, H., and Poikane, S. (2019). A novel approach for deriving nutrient criteria to support good ecological status: application to coastal and transitional waters and indications for use. *Front. Mar. Sci.* 6 (255). doi: 10.3389/fmars.2019.00255

He, G. F., Yuan, G. M., and Li, F. Q. (2004). Effect of economic development on water quality in zhujiang estuary. *Mar. Environ. Sci.* 23 (4), 50–52. doi: 10.2174/0929866043478455

Hong, X. Y. (2022). Analysis of the long-term dynamics of nutrients linking to terrestrial pollution in xiamen bay. *J. Appl. Oceanogr.* 41 (02), 249–258.

Hong, Y., Wu, J., Guan, F., Yue, W., and Long, A. (2019). Nitrogen removal in the sediments of the pearl river estuary, China: Evidence from the distribution and forms of nitrogen in the sediment cores. *Mar. pollut. Bull.* 138, 115–124. doi: 10.1016/j.marpolbul.2018.11.040

Howarth, R. W. (2008). Coastal nitrogen pollution: A review of sources and trends globally and regionally. *Harmful Algae.* 8 (1), 14–20. doi: 10.1016/j.hal.2008.08.015

Huang, Y. F. (2008). Nutrient limitation of eutrophication in guangzhou Sea area (Qingdao, Shandong: Ocean University of China).

Huang, B. Q., and Hong, H. S. (1999). Alkaline phosphatase activity and utilization of dissolved organic phosphorus by algae in subtropical coastal waters. *Mar. pollut. Bull.* 39 (1/12), 205–211. doi: 10.1016/S0025-326X(99)00006-5

Huang, X. P., and Huang, L. M. (2002). Temporal and spatial variation characteristics of inorganic nitrogen and active phosphorus in zhujiang estuary. *J. Oceanogr. Taiwan Strait* 21 (4), 6. doi: 10.3969/j.issn.1000-8160.2002.04.005

Huang, X. P., Huang, L. M., and Yue, W. Z. (2003). The characteristics of nutrients and eutrophication in the pearl river estuary, south China. *Mar. pollut. Bull.* 47 (1), 30–36. doi: 10.1016/S0025-326X(02)00474-5

Huang, F., Lin, X., Hu, W., Zeng, F., He, L., and Yin, K. (2021). Nitrogen cycling processes in sediments of the pearl river estuary: Spatial variations, controlling factors, and environmental implications. *Catena* 206, 105545. doi: 10.1016/j.catena.2021.105545

Hume, T. M., and Herdendorf, C. E. (1988). A geomorphic classification of estuaries and its application to coastal resource management a new Zealand example. *Ocean Shoreline Manage.* 11 (3), 294–274. doi: 10.1016/0951-8312(88)90022-7

Huo, S. L., Chen, Q., Xi, B. D., Guo, X. J., Chen, Y. Q., and Liu, H. L. (2009). A literature review for lake nutrient criteria development. *Ecol. Environ. Sci.* 18 (2), 743–748.

Huo, S. L., Ma, C. Z., Xi, B. D., and He, Z. S. (2017). Progress in research on lake nutrient criteria. *J. Environ. Eng. Technol.* 7 (2), 125–133.

Huo, S., Ma, C., Xi, B., He, Z., Su, J., and Wu, F. (2015). Nonparametric approaches for estimating regional lake nutrient thresholds. *Ecol. Indic.* 58, 225–234. doi: 10.1016/j.ecolind.2015.05.065

Huo, S. L., Ma, C. Z., Xi, B. D., Zhang, Y. L., Wu, F. C., and Liu, H. L. (2018). Development of methods for establishing nutrient criteria in lakes and reservoirs: A review. *J. Environ. Sci.* 67 (05), 54–66. doi: 10.1016/j.jes.2017.07.013

Hu, Q., Qu, L., Huang, B. G., Li, Q., and You, Q. M. (2016). Status and evaluation on nutrients for the adjacent sea water of the yellow river estuary in autumn of 2014. *Mar. Environ. Sci.* 35 (05), 732–738.

Hu, Y. Y., Wang, J. Y., Zhang, Z. F., Zong, H. M., and Chen, S. M. (2011). Approach of nutrient criteria establishment and application in coastal area of liaohe estuary. *China Environ. Sci.* 31 (6), 996–1000. doi: 10.3724/SP.J.1011.2011.00468

Hu, P., Yan, S. Q., Shi, P., Zheng, Z. Y., and Lin, L. R. (2020). The situation and protection suggestions of marine ecological environment in guangdong province. *Ocean Dev. Manage.* 37 (06), 115–120.

Jin, J., and Liu, S. M. (2013). Advances in studies of phosphorus utilization by marine phytoplankton. *Adv. Earth Sci.* 28 (02), 253–261. doi: 10.11867/j.issn.1001-8166.2013.02.0253

Ke, S., Zhang, P., Ou, S. J., Zhang, J. X., Chen, J. Y., and Zhang, J. B. (2022). Spatiotemporal nutrient patterns, composition, and implications for eutrophication mitigation in the pearl river estuary, China. *Estuar. Coast. Shelf Sci.* 266, 107749. doi: 10.1016/j.ecss.2022.107749

Lai, Z. N., Wang, C., Gao, Y., Zeng, Y. Y., Liu, Q. F., Peng, S. Y., et al. (2018). *Aquatic ecological environment of pearl river estuary* (Beijing: China Agricultural Press), 29–30.

Lan, W. L., Li, T. S., and Han, L. J. (2014). Distribution and seasonal variation of nutrient in the adjacent waters of tieshangang bay in guangxi. *Mar. Sci.* 38 (7), 64–69.

Liang, Z. Y., Xu, Y. Y., Qiu, Q. L. L., Liu, Y., Lu, W. T., and Wagner, T. (2021). A framework to develop joint nutrient criteria for lake eutrophication management in eutrophic lakes. *J. Hydrol.* 594, 125883. doi: 10.1016/j.jhydrol.2020.125883

Li, K. Q., He, J., Li, J., Guo, Q., Liang, S. K., Li, Y. B., et al. (2018). Linking water quality with the total pollutant load control management for nitrogen in jiaozhou bay, China. *Ecol. Indic.* 85, 57–66. doi: 10.1016/j.ecolind.2017.10.019

Li, R. H., Liu, S. M., Li, Y. W., Zhang, G. L., Ren, J. L., and Zhang, J. (2014). Nutrient dynamics in tropical rivers, lagoons, and coastal ecosystems of eastern hainan island, south China Sea. *Biogeosciences* 11 (2), 481. doi: 10.5194/bg-11-481-2014

Li, R. H., Liu, S. M., Zhang, G. L., Ren, J. L., and Zhang, J. (2013). Biogeochemistry of nutrients in an estuary affected by human activities: The wanquan river estuary, eastern hainan island, China. *Cont. Shelf Res.* 57, 18–31. doi: 10.1016/j.csr.2012.02.013

Li, Y. D., Lu, C. C., Li, H. L., Chang, L., Lin, J., and Shen, M. (2022). Distribution and diurnal variation of main nutrients in the Yangtze river estuary and its adjacent based on GOCI. *Mar. Forecasts* 39 (02), 1–13.

Lin, X. J., Gao, S., Zhang, T. Y., and Liu, G. M. (2018). Researching progress and application status of eutrophication evaluation method of seawater. *Adv. Earth Sci.* 33 (04), 373–384.

Lin, G. M., and Lin, X. B. (2022). Bait input altered microbial community structure and increased greenhouse gases production in coastal wetland sediment. *Water Res.* 218, 118520. doi: 10.1016/j.watres.2022.118520

Li, M. M., Pang, B. J., Lan, W. L., and Fu, J. X. (2020). Study on estuarine mixed zone delimitation and nutrient standard limits construction method. *Environ. Monit. China* 36 (03), 74–82.

Liu, B. L., Cao, W. Z., Huang, Z., Chen, W. H., Chen, H. H., and Liu, L. S. (2018). Developing nutrient criteria for the jiulong river estuary, southeast China. *Acta Oceanol. Sin.* 37 (2), 1–13. doi: 10.1007/s13131-017-1121-0

Liu, C. L., Jin, S. L., Ma, Y. F., and Li, S. (2020). Nutrient concentrations and distribution characteristics in the Yangtze river estuary adjacent sea are in summer. *J. Xiamen Univ. (Natural Science)* 59 (S1), 75–80. doi: 10.19316/j.issn.1002-6002.2020.03.09

Liu, J., Liu, L. S., and Zheng, B. H. (2017). Problems and countermeasures of water environmental management in estuaries. *Res. Environ. Sci.* 30 (5), 645–653. doi: 10.13198/j.issn.1001-6929.2017.02.28

Liu, S. M., Li, R. H., Zhang, G. L., Wang, D. R., Du, J. Z., Herbeck, L. S., et al. (2011). The impact of anthropogenic activities on nutrient dynamics in the tropical wenchanghe and wenjiaohe estuary and lagoon system in East hainan, China. *Mar. Chem.* 125 (1), 49–68. doi: 10.1016/j.marchem.2011.02.003

Liu, L. S., Zheng, B. H., Meng, W., and Cai, W. Q. (2011). Sub-Areas compartmentalization of changjiang estuary based on the natural geographical characteristics. *Acta Ecol. Sin.* 31 (17), 5042–5054.

Li, R., Xu, J., Li, X., Shi, Z., and Harrison, P. J. (2017). Spatiotemporal variability in phosphorus species in the pearl river estuary: Influence of the river discharge. *Sci. Rep.* 7 (1), 649–648. doi: 10.1038/s41598-017-13924-w

Li, Z.Y., Yu, R.C., Liu, Z.T., Li, A.F., Hu, H., Wang, L., et al (2019). Technical guide for nutrient criteria in estuarine water bodies. *Chinese Society for Oceanology and Limnology*. Available at: http://csol.qdio.ac.cn/xhdtDetail.aspx?id=2640

Long, Y. X., Sun, Q., and Yang, K. (2020). Research on trend of nutrients and its response to human activities in the pearl river estuary. *E3S Web Conf.* 145, 02081. doi: 10.1051/e3sconf/202014502081

Lu, Z., Gan, J., Dai, M., Liu, H., and Zhao, X. (2018). Joint effects of extrinsic biophysical fluxes and intrinsic hydrodynamics on the formation of hypoxia west off the pearl river estuary. *J. Geophys. Res.: Oceans* 123 (9), 6241–6259. doi: 10.1029/2018JC014199

Lu, F. H., Ni, H. G., Liu, F., and Zeng, E. Y. (2009). Occurrence of nutrients in riverine runoff of the pearl river delta, south China. *J. Hydrol.* 376 (1), 107–115. doi: 10.1016/j.jhydrol.2009.07.018

Luo, Y. (2017). Spatial and temporal variations of dissolved organic nitrogen in typical seas and theirs effects on phytoplankton communities (Xiamen, Fujian: Third Institute of Oceanography, Ministry of Nature Resources). Available at: https://xueshu.baidu.com/usercenter/paper/show?paperid=53a334552d4d5254155a8f2b115e3741&site=xueshu_se

Luo, Y., Chen, B. H., Lin, H., Sun, X. W., Chen, W. F., Dong, X., et al. (2017). Spatial and temporal distribution of dissolved organic nitrogen and composition of total dissolved nitrogen in xiamen waters in autumn and winter. *J. Appl. Oceanogr.* 36 (02), 210–220.

Lu, D. L., Yang, N. N., Liang, S. K., Li, K. Q., and Wang, X. L. (2016). Comparison of land-based sources with ambient estuarine concentrations of total dissolved nitrogen in jiaozhou bay (China). *Estuar. Coast. Shelf Sci.* 180, 82–90. doi: 10.1016/j.ecss.2016.06.032

Ma, Y., Wei, W., Xia, H. Y., Yu, B., Wang., D., Ma, Y., et al. (2009). History change and influence factor of nutrient in lingdingyang sea area of zhujiang river estuary. *Acta Oceanol. Sin.* 31 (02), 69–77. doi: 10.3321/j.issn 0253-4193.2009.02.010

Ma, B., and Zhao, H. (2021). Distribution characteristics of chlorophyll *a* and nutrients in the pearl river estuary in summer and their relationship with environmental factors. *Mar. Environ. Sci.* 40 (5), 707–716.

McLaughlin, D. B. (2014). Maximizing the accuracy of field-derived numeric nutrient criteria in water quality regulations. *Integr. Environ. Assess. Manage.* 10 (1), 133–137. doi: 10.1002/ieam.1485

Ménesguen, A. (2014). "Eutrophication of the marine environment," in *The land-Sea interactions*, 71–191. John Wiley & Sons, Inc.

Meng, W., Wang, L. J., Zheng, B. H., and Lei, K. (2008). Methods for developing nutrient criteria in estuarine waters. *Acta Ecol. Sin.* 28 (10), 5133–5140. doi: 10.3321/j.issn:1000-0933.2008.10.061

Ministry of Ecology and Environment of the People's Republic of China (1997). *Sea Water quality standard (GB 3097-1997)*. China: Ministry of Ecology and Environment of the People's Republic of China.

Ministry of Ecology and Environment of the People's Republic of China (2002). *Environmental quality standards for surface water (GB 3838-2002)*. China: Ministry of Ecology and Environment of the People's Republic of China.

Ministry of Ecology and Environment of the People's Republic of China (2022a). *Action plan for comprehensive management of key sea areas*. China: Ministry of Ecology and Environment of the People's Republic of China.

Ministry of Ecology and Environment of the People's Republic of China (2022b). *The "14th five-year plan" for marine ecological environmental protection*. China: Ministry of Ecology and Environment of the People's Republic of China.

Ministry of Environmental Protection of the PRC (2009). *Specification for offshore environmental monitoring: HJ 442–2008* (China: China Environment Science Press), 19.

Moffat, A. S. (1998). Global nitrogen overload problem grows critical. *Science* 279 (5353), 988–989.

Niu, L., Luo, X., Hu, S., Liu, F., Cai, H., Ren, L., et al. (2020a). Impact of anthropogenic forcing on the environmental controls of phytoplankton dynamics between 1974 and 2017 in the pearl river estuary, China. *Ecol. Indic.* 116, 106484. doi: 10.1016/j.ecolind.2020.106484

Niu, L., van Gelder, P., Luo, X., Cai, H., Zhang, T., and Yang, Q. (2020b). Implications of nutrient enrichment and related environmental impacts in the pearl river estuary, China: Characterizing the seasonal influence of riverine input. *Water* 12 (11), 3245. doi: 10.3390/w12113245

Peng, H. H., Geng, H. Y., Mao, X. Y., Shi, J., and Lv, X. Q. (2021). Study on total control of total nitrogen in the laizhou bay. *Water* 13 (17), 2439–2439. doi: 10.3390/w13172439

Qiu, D., Huang, L., Zhang, J., and Lin, S. (2010). Phytoplankton dynamics in and near the highly eutrophic pearl river estuary, south China Sea. *Cont. Shelf Res.* 30 (2), 177–186. doi: 10.1016/j.csr.2009.10.015

Raymond, P., Morgan, I., and Kathleen, M. (2011). Nutrient concentrations in Maryland non-tidal streams. *Environ. Monit. Assess.* doi: 10.1007/s10661-010-1684-0

Redfield, A. C., Ketchum, B. H., and Richards, F. A. (1963). "The influence of organisms on the composition of sea-water," in *The Sea*. Ed. M. N. Hill (New York: Interscience), 26–77.

Ryther, J. H., and Dunstan, W. M. (1971). Nitrogen, phosphorus, and eutrophication in the coastal marine environment. *Science* 171 (3975), 1008–1013. doi: 10.2307/1731314

Schlitzer, R. (2002). Interactive analysis and visualization of geoscience data with ocean data view. *Comput. Geosci.* 28 (10), 1211–1218. doi: 10.1016/S0098-3004(02)00040-7

Smith, V. H., Tilman, G. D., and Nekola, J. C. (1999). Eutrophication: impacts of excess nutrient inputs on freshwater, marine, and terrestrial ecosystems. *Environ. Pollut.* 100 (1), 179–196. doi: 10.1016/S0269-7491(99)00091-3

Song, S., Guo, L. F., Zhang, H., and Zhang, H. (2021). Research on pollution control mechanism of watershed, estuary and coastal sea areas. *Mar. Environ. Sci.* 40 (06), 838–842.

South China Sea Branch of the State Oceanic Administration (2017). *South China Sea marine environment bulletin in 2016*. 29. China: South China Sea Branch of S.O.A.

State of Oceanic Administration (2018). *Bulletin of China marine ecological environment status in 2017*. 7–8. China: State Oceanic Administration.

Strokal, M., Kroeze, C., Wang, M., and Ma, L. (2017). Reducing future river export of nutrients to coastal waters of China in optimistic scenarios. *Sci. Total Environ.* 579, 517–528. doi: 10.1016/j.scitotenv.2016.11.065

Su, J., Ji, D. F., Lin, M., Chen, Y. Q., Sun, Y. Y., Huo, S. L., et al. (2017). Developing surface water quality standards in China. *Res. Conserv. Recy* 117, 294–303. doi: 10.1016/j.resconrec.2016.08.003.

Su, J., Yang, F. X., Su, R. G., and Yao, Q. Z. (2016). Approach of nutrient criteria establishment and application in the liaohe estuary. *Periodical Ocean Univ. China* 46 (9), 78–84.

Tong, Y., Zhao, Y., Zhen, G., Chi, J., Liu, X., Lu, Y., et al. (2015). Nutrient loads flowing into coastal waters from the main rivers of china, (2006-2012). *Sci. Rep.* 5, 16678. doi: 10.1038/srep16678

US EPA (1998). *National strategy for the development of regional nutrient criteria* (Washington, DC: USEPA).

US EPA (2000). "Nutrient criteria technical guidance manual lakes and reservoirs," in *Water quality criteria for the protection of human health*. Washington, DC: U.S. Environmental Protection Agency, Office of Water.

US EPA (2001). *Nutrient criteria technical guidance manual: Estuarine and coastal marine waters* (Washington, DC: U.S. Environmental Protection Agency, Office of Water).

US EPA (2009). *National recommended water quality criteria* (USA: United States Environmental Protection Agency, Office of Water, Office of Science and Technology).

Wang, L., Chan, Y. Y., Bian, J. C., and Li, Z. Y. (2020). Study on derivation of nutrient for the daliaohe estuary. *Mar. Sci.* 44 (12), 1–13.

Wang, B. D., Xin, M., Wei, Q. S., and Xie, L. P. (2018). A historical overview of coastal eutrophication in the China seas. *Mar. pollut. Bull.* 136, 394–400. doi: 10.1016/j.marpolbul.2018.09.044

Wei, M. X., Fang, H. Q., He, B. M., Cao, Q., Li, Z., and Pan, L. H. (2014). Biogeochemical characteristics of nitrogen in seawater and its ecological effect at mangrove areas in bays, guangxi. *Wetland Sci.* 12 (04), 441–450. doi: 10.13248/j.cnki.wetlandsci.2014.04.006

Wei, G. Q., Wang, H., Cai, W. X., and Yi, B. (2012). 10-year retrospective analysis on harmful algal blooms in the pearl river estuary. *Mar. Sci. Bull.* 31 (04), 466–474. doi: 10.1007/s11783-011-0280-z

Wu, D. (2007). *Comprehensive eutrophication assessment for estuaries and coastal waters based on the PSR framework* (Dalian Maritime University).

Wu, G., Cao, W., Wang, F., Su, X., Yan, Y., and Guan, Q. (2019). Riverine nutrient fluxes and environmental effects on china's estuaries. *Sci. Total Environ.* 661, 130–137 China. doi: 10.1016/j.scitotenv.2019.01.120

Wu, G. J., Cao, W. Z., Zheng, H., Kao, C. M., Chang, C. T., Chiang, P. C., et al. (2017). Decadal changes in nutrient fluxes and environmental effects in the jiulong river estuary. *Mar. pollut. Bull.* 124 (2), 871–877. doi: 10.1016/j.marpolbul.2017.01.071

Xia, Q., and Zhang, X. H. (1990). *Water quality standards manual* (China: China Environmental Press).

Xia, W., and Zhou, Z. Q. (2021). Analysis of meteorological and hydrological elements in the sea around the pearl river estuary based on observed data in summer. *Trans. Oceanol. Limnol.* 43 (5), 60–65.

Xu, Z. R. (1981). *Water quality assessment criteria* (China: China Architecture & Building Press).

Xu, H. Y. (2020). *Regime shift of trophic status and nutrient criteria in the bohai Sea* (China: The First Institute of Oceanography, Ministry of Nature Resources).

Yang, F. X. (2015). *Approaches of nutrient criteria establishment and its influencing factors in the daliaohe estuary* (Qingdao, Shandong: Ocean University of China).

Yang, F. X., Mi., T. Z., Chen, H. T., and Yao, Q. Z. (2019). Developing numeric nutrient criteria for the Yangtze river estuary and adjacent waters in China. *J. Hydrol.* 579, 124188. doi: 10.1016/j.jhydrol.2019.124188

Yan, S. H., and Li, T. (2018). Assessment of the pearl river estuary by water comprehensive pollution index. *China Resour. Compr. Util.* 36 (7), 173–175. doi: CNKI:SUN:ZWZS.0.2018-07-059

Yin, K., Qian, P. Y., Chen, J. C., Hsieh, D. P. H., and Harrison, P. J. (2000). Dynamics of nutrients and phytoplankton biomass in the pearl river estuary and adjacent waters of Hong Kong during summer: preliminary evidence for phosphorus and silicon limitation. *Mar. Ecol.-Prog. Series.* 194, 295–305, England. doi: 10.3354/meps194295

Yin, K., XU, J., Lai, Z., and Harrison, P. J. (2013). "Dynamics of phytoplankton blooms and nutrient limitation in the pearl river (Zhujiang) estuarine coastal waters," in *Biogeochemical dynamics at major river-coastal interfaces*. Eds. T. Bianchi, M. Allison and W. Cai (Cambridge University Press), 274–295.

Yuan, G. M. (2005). *The effect of economic development of zhujiang delta on the water environment at zhujiang estuary* (Qingdao, Shandong: Ocean University of China).

Zeng, D. N., Niu, L. X., Tao, W., Fu, L. X., and Yang, Q. S. (2020). Nutrient dynamics in pearl river estuary and their eutrophication evaluation. *J. Guangdong Ocean Univ.* 40 (3), 73–82. doi: 10.3969/j.issn.1673-9159.2020.03.010

Zhang, P., Chen, Y., Peng, C., Dai, P., Lai, J., Zhao, L., et al. (2020b). Spatiotemporal variation, composition of DIN and its contribution to eutrophication in coastal waters adjacent to hainan island, China. *Reg. Stud. Mar. Sci.* 37, 101332. doi: 10.1016/j.rsma.2020.101332

Zhang, P., Peng, C. H., Zhang, J. B., Zhang, J. X., Chen, J. Y., and Zhao, H. (2022). Long-term harmful algal blooms and nutrients patterns affected by climate change and anthropogenic pressures in the zhanjiang bay, China. *Front. Mar. Sci.* 9, 849819. doi: 10.3389/fmars.2022.849819

Zhang, P., Peng, C. H., Zhang, J. B., Zou, Z. B., Shi, Y. Z., Zhao, L. R., et al. (2020c). Spatiotemporal urea distribution, sources, and indication of DON bioavailability in zhanjiang bay, China. *Water* 12 (3). doi: 10.3390/w12030633

Zhang, P., Ruan, H., Dai, P., Zhao, L., and Zhang, J. (2020a). Spatiotemporal river flux and composition of nutrients affecting adjacent coastal water quality in hainan island, China. *J. Hydrol.* 591, 125293. doi: 10.1016/j.jhydrol.2020.125293

Zhang, P., Su, Y., Liang, S. K., Li, K. Q., Li, Y. B., and Wang, X. L. (2017). Assessment of long-term water quality variation affected by high-intensity land-

based inputs and land reclamation in jiaozhou bay, China. *Ecol. Indic.* 75, 210–219. doi: 10.1016/j.ecolind.2016.12.035

Zhang, W., Sun, J., Nie, H. T., Jiang, G. Q., and Tao, J. H. (2015). Seasonal and spatial variation of nutrient and the response of phytoplankton in PRE and adjacent sea areas. *Acta Ecol. Sin.* 35 (12), 4034–4044. doi: 10.5846/stxb201308262158

Zhang, J. H., Wang, D., Liu, G. X., Wang, Y., Dong, H. Z., Han, X. Y., et al. (2020). Phosphorus species in the Yangtze river estuary adjacent sea area in summer of 2016. *J. Xiamen Univ. (Natural Science)* 59 (S1), 99–92. doi: 10.6043/j.issn.0438-0479.202007113

Zhang, P., Wei, L. R., Lai, J. Y., Dai, P. D., Chen, Y., and Zhang, J. B. (2019b). Concentration, composition and fluxes of land-based nitrogen and phosphorus source pollutants input into zhanjiang bay in summer. *J. Guangdong Ocean Univ.* 39 (4), 63–72.

Zhang, J. B., Zhang, P., Dai, P. D., Lai, J. Y., and Chen, Y. (2019a). Spatiotemporal distributions of DIP and the eutrophication in hainan island adjacent coastal water. *China Environ. Sci.* 39 (6), 2541–2548. doi: 10.19674/j.cnki.issn1000-6923.2019.0303

Zhang, J. B., Zhang, Y. C., Zhang, P., Li, Y., Li, J. X., Xu, J. L., et al. (2021). Seasonal phosphorus variation in coastal water affected by the land-based sources input in the eutrophic zhanjiang bay, China. *Estuar. Coast. Shelf Sci.* 252, 107277. doi: 10.1016/j.ecss.2021.107277

Zhao, H. T. (1989). Hydrological and sedimentary characteristics of the pearl river estuary. *Trop. Geogr.* 9 (3), 201–212.

Zhou, F. X., Chen, F. J., Li, Z. Y., Zhu, Q. M., Meng, Y. F., and Zhang, S. W. (2018). Environmental characteristics of nutrients in the pearl river estuary in spring 2014. *J. Guangdong Ocean Univ.* 38 (3), 42–48. doi: 10.3969/j.issn.1673-9159.2018.03.007

Zhou, Y., Wang, L. L., Zhou, Y. Y., and Mao, X. Z. (2020). Eutrophication control strategies for highly anthropogenic influenced coastal waters. *Sci. Total Environ.* 705, 135760. doi: 10.1016/j.scitotenv.2019.135760

Zhou, C. F., Yuan, G. W., Peng, M., and Zhang, P. (2022). Distributions, compositions of nitrogen and phosphorus nutrients and nutriture evaluation in the coastal area of qidong, jiangsu. *Environ. pollut. Control* 44 (01), 104–110.

frontiers | Frontiers in Marine Science

TYPE Original Research
PUBLISHED 03 October 2022
DOI 10.3389/fmars.2022.1010909

Check for updates

OPEN ACCESS

EDITED BY
Meilin Wu,
South China Sea Institute of Oceanology, Chinese Academy of Sciences (CAS), China

REVIEWED BY
Juan Chen,
Hohai University, China
Yafen Wang,
China University of Geosciences Wuhan, China

*CORRESPONDENCE
Paul K. S. Shin
paulksshin@gmail.com

†These authors have contributed equally to this work and share first authorship

SPECIALTY SECTION
This article was submitted to Marine Pollution, a section of the journal Frontiers in Marine Science

RECEIVED 03 August 2022
ACCEPTED 12 September 2022
PUBLISHED 03 October 2022

CITATION
Xu W, Fleddum AL, Shin PKS and Sun J (2022) Impact of and recovery from seabed trawling in soft-bottom benthic communities under natural disturbance of summer hypoxia: A case study in subtropical Hong Kong. *Front. Mar. Sci.* 9:1010909. doi: 10.3389/fmars.2022.1010909

COPYRIGHT
© 2022 Xu, Fleddum, Shin and Sun. This is an open-access article distributed under the terms of the Creative Commons Attribution License (CC BY). The use, distribution or reproduction in other forums is permitted, provided the original author(s) and the copyright owner(s) are credited and that the original publication in this journal is cited, in accordance with accepted academic practice. No use, distribution or reproduction is permitted which does not comply with these terms.

Impact of and recovery from seabed trawling in soft-bottom benthic communities under natural disturbance of summer hypoxia: A case study in subtropical Hong Kong

Wenzhe Xu[1,2†], Anne Lise Fleddum[3†], Paul K. S. Shin[3*] and Jun Sun[1,2,4,5]

[1]College of Marine and Environmental Sciences, Tianjin University of Science and Technology, Tianjin, China, [2]Research Centre for Indian Ocean Ecosystem, Tianjin University of Science and Technology, Tianjin, China, [3]Department of Biology and Chemistry, City University of Hong Kong, Hongkong, Hong Kong SAR, China, [4]College of Marine Science and Technology, China University of Geosciences (Wuhan), Wuhan, China, [5]Institute for Advanced Marine Research, China University of Geosciences, Guangzhou, China

Bottom trawling has widespread impact on the structure and composition of benthic communities. In this study, soft-bottom macrofauna in a heavily trawled area and an adjacent marine park that has been closed to bottom trawling for more than ten years were sampled, allowing to investigate the impact of and recovery from trawling. Both areas were equally affected by seasonal summer hypoxia. Polychaetes were the most abundant at trawled (78-86%) and non-trawled (85-94%) sites in both summer and winter. The non-trawled sites inside the marine park area had a lower level of species composition and abundance as compared to the trawled sites in summer, whereas in winter the benthic communities at these trawled and non-trawled sites appeared much similar with the majority of the identified taxa being dominated by new recruiting juveniles in both sampling areas. Results of permutational multivariate analysis of variance (PERMANOVA) on transformed infaunal abundance and biomass data revealed significant differences ($p<0.05$) between trawled and non-trawled treatments and seasons, as well as their interactions. Pair-wise *a posteriori* PERMANOVA further indicated significant differences for the abundance and biomass data in summer but insignificant differences in winter. PERMANOVA of the biological traits of infauna weighted with transformed biomass also confirmed significant difference for seasons only. Such findings imply that the effect of season was more important than that of trawling especially on the biological trait structure of the benthic communities. In addition, bottom trawling may contribute to a higher level of dissolved oxygen when the area suffered from hypoxia, resulting a higher biodiversity in the trawled area in summer. By comparing data taken prior to

closure of the marine park from trawling, the recovery of infaunal community has been slow over the 12 years as a trawl-free area. Apart from natural disturbance of summer hypoxia, such recovery could also be complicated with the presence of artificial reefs deployed within the marine park, which may affect the hydrodynamics of the benthic environment and modify the community structure and function.

KEYWORDS

bottom trawling, benthic community, biological trait analysis, hypoxia, recovery

Introduction

Bottom trawling is the most widespread anthropogenic disturbance to the seabed globally (Halpern et al., 2008). When heavy trawling gear is dragged along the seabed, sediments are resuspended (O'Neill and Ivanović, 2016; Hiddink et al., 2017), seafloor habitats are damaged (Cook et al., 2013), and the benthic community structure is disrupted (Kaiser et al., 2000). Effects of bottom trawling, including reduced ecosystem functioning, decreased biomass and lowered diversity of benthic organisms, have been well documented in marine ecosystems, which eventually lead to an overall reduction in productivity in the long term (Queirós et al., 2006; Hinz et al., 2009; Sköld et al., 2018; Ramalho et al., 2020; McLaverty et al., 2021).

The degree of such impact depends on the characteristics of the trawling gear (Steele et al., 2002; Rijnsdorp et al., 2015), type of benthic habitat (Koslow et al., 2001; Kenchington et al., 2006; Queirós et al., 2006), trawling frequencies (Enticknap, 2002), size of the trawled area (Watling and Norse, 1998), and natural disturbances such as seasonal changes in water quality and hydrodynamics in the local environment (Ortega et al., 2018). Bottom trawling in vulnerable habitats, e.g., coral reefs, can be particularly damaging and cause substantial declines in associated benthic communities (Althaus et al., 2009; Cook et al., 2013; Williams et al., 2020). However, effects of trawling in coastal soft-bottom areas under frequent natural disturbances may not be so obvious or even negligible as community response to both anthropogenic (e.g., trawling) and natural disturbance (e.g., hypoxic events) could be similar (Moritz et al., 2015; Szostek et al., 2016). For example, frequent natural disturbance resulting from seasonal storm events has led to an increase in the abundance of small-bodied, opportunistic and short-lived (r-selected) species with a concomitant loss of larger-bodied, longer-lived and slower growing (K-selected) species (Anderlini and Wear, 1992). Similarly, bottom trawling can also cause a shift of trait composition of benthic species with the dominance of r-selected characters (Mangano et al., 2013; Kaiser et al., 2018). Hence the impact of trawling on the benthic communities may not be easily observed in areas where natural disturbance frequently occurs (van Denderen et al., 2015; Ortega et al., 2018).

Although the adverse consequences of trawling on the seabed fauna are widely documented, relative few studies have been conducted on the recovery of benthic communities from cessation of trawling operations (Hiddink et al., 2006b; Hiddink et al., 2017). The difficulty of following such a recovery process is that trawling has usually operated for a long time and there are little or no data prior to trawling for comparison (Thrush and Dayton, 2002). By collating available data from 24 comparative and 46 experimental studies of trawling impacts on communities of soft-bottom macroinvertebrates, Hiddink et al. (2017) estimated that the recovery rates of benthic communities after trawling is stopped would range between 1.9 and 6.4 years. A meta-analysis of 122 experiments on the effects of bottom trawling to evaluate rates of recovery following disturbance also revealed that sessile and low mobility biota with longer life-spans, such as sponges, soft corals and bivalves, would take longer (>3 years) to recover from bottom trawling than mobile biota (<1 year) with shorter life-spans, such as polychaetes and most crustaceans (Sciberras et al., 2018). However, these estimations were based on the assumption that the observed state of biota is in equilibrium with the reported trawling effort. Other environmental drivers which may exist and mask the impact caused by trawling, such as natural disturbance resulting from seasonal hypoxic events, were not explicitly considered. Hence, empirical studies are needed to determine the trawling impacts and recovery of benthic ecosystems in areas where natural disturbance phenomena, such as seasonal hypoxia, are frequent.

Hong Kong lies within the subtropical region in the northern part of the South China Sea and is influenced by the estuary of the Pearl River from the west and seasonal currents and monsoons from the east. The territory is known to have a long fishing history with heavy trawling in most areas around the coast. A port survey, conducted by the Agriculture, Fisheries and

Conservation Department (AFCD) of the Government of the Hong Kong Special Administrative Region (HKSAR), China, has shown that nearly all Hong Kong's territorial waters have been trawled, except for a few small protected areas and shipping channels (Agriculture, Fisheries and Conservation Department, 2006). In 2010, up to 400 trawlers operated partly or wholly within the Hong Kong waters accounting for 80% of the total fishing efforts estimated to be 93% higher than the maximum sustainable fishing yield (Wang et al., 2021). In order to rehabilitate the damaged habitats and depletion of marine resources, the HKSAR Government imposed a permanent territory-wide ban on all types of trawling operations since the end of 2012.

Hoi Ha Wan Marine Park is a semi-enclosed bay within Tolo Channel on the northeast of Hong Kong (Figure 1). The park, covering an area of 260 hectares, is a sheltered bay with pristine water quality and provides a good marine environment for nurturing a great variety of organisms and habitats, including coral reef, hard rock, mangroves, sandy and soft muddy bottom. It is also a trawl-free area since the designation of the marine park in 1996. In contrast, outside the park boundary, the seabed of Tolo Channel has been intensively trawled until the ban started at the end of 2012. Both the park and channel, however, have been affected by seasonal changes of water quality due to heavy rainfall and limited water exchanges with frequent occurrences of hypoxia in the summer (Wu, 1988; Fleddum et al., 2011). These two sites thus provided an opportunity to investigate the potential changes in structure and function of soft-bottom benthic communities through comparison of data obtained from the park (i.e., non-trawled area) and channel (i.e., trawled area), so as to decipher possible community recovery from cessation of trawling under seasonal disturbance. Such studies are relatively lacking in tropical and subtropical waters (Wang et al., 2021).

The aims of this study were to (1) investigate the trawling impact on the structure and function of infaunal communities in

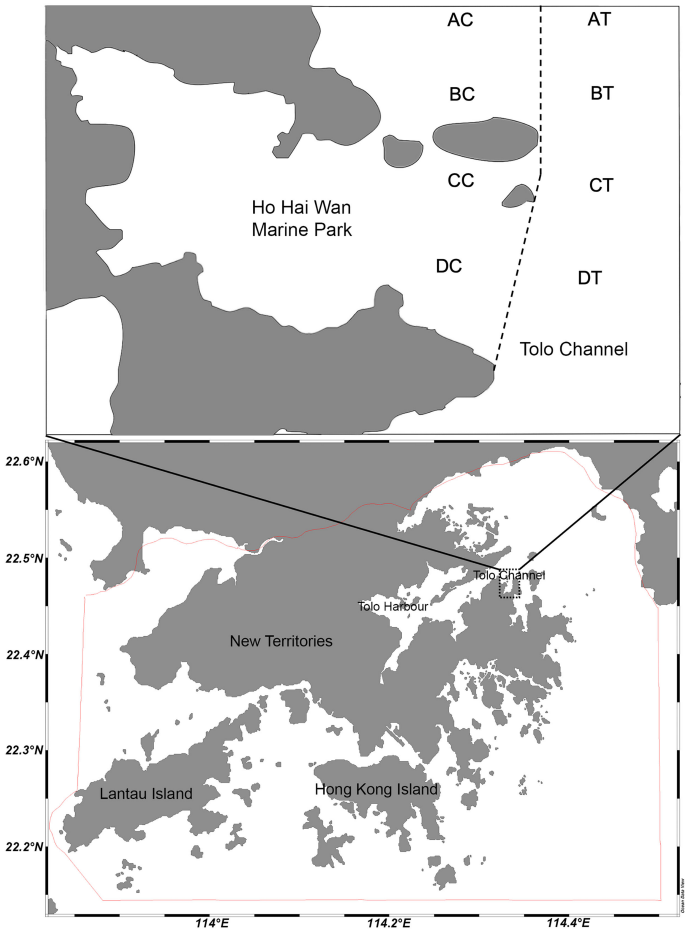


FIGURE 1
Map showing sampling sites AC-DC in the non-trawled area inside the Hoi Ha Wan Marine Park and AT-DT in the trawled area along the Tolo Channel. The dotted line indicates the boundary of the marine park and the red line shows the boundary of territorial waters of Hong Kong.

subtropical waters that experience significant seasonal changes in dissolved oxygen, and (2) address the possibility of recovery inside the marine park by comparing with the heavily-trawled area nearby. Since benthic organisms generally have a life cycle time between 40 days to 10 years (Watling and Norse, 1998), it is expected that the seabed environment has been stabilized from previous historical trawling operations and has undergone various successional stages after the area has been protected as a marine park since 1996. It is hypothesized that biodiversity, with higher biomass and more rare species (i.e., species with one individual recorded), would have increased in the park during the protected time and larger, longer-lived species would dominate. Our findings could provide new evidence regarding the recovery of benthic communities from bottom trawling in subtropical coastal waters where natural disturbance such as seasonal hypoxia is frequent.

Materials and methods

Design of the case study

Figure 1 and Table S1 show the location and information of the eight sampling sites for macrobenthic infauna in Hoi Ha Wan Marine Park and nearby Tolo Channel, with four non-trawled sites AC to DC inside the park boundary and four trawled sites AT to DT along the channel. During the study period, two paired Chinese traditional shrimp trawlers with six connected bottom nets (each of about 2 m width) were observed in the morning and in the afternoon, covering the whole area of the Tolo Channel during the day. This fishing pattern was regular in this particular area except at AT where some large stones are located at the bottom and trawling frequency was lower. The trawling intensity was, on average, five trawls a week for the trawled sites BT, CT and DT and one time a week for site AT (WWF Hong Kong, pers. comm.). Artificial reefs and coral communities are located in the marine park area. Hence, the location of sampling sites AC to DC was chosen carefully to minimize interference with these structures.

Field sampling and environmental measurements

Five replicates of 0.1 m^2 van Veen grab were used to collect infaunal samples at each of the trawled (AT, BT, CT and DT) and non-trawled sites (AC, BC, CC and DC), respectively, at the beginning of October 2008 (end of summer, wet season) and at the beginning of March 2009 (end of winter, dry season) before the implementation of territory-wide trawl ban at the end of 2012. Additionally three replicate samples were taken for measurement of total organic carbon (TOC) and for particle size analysis in the laboratory. Prior to field sampling, a diver went down to the seabed at each site and took photographs of the sediment surface to make sure that those designated trawled sites along the channel had actually been trawled with evidence of track marks while those non-trawled sites within the park were not disturbed. Water depth, temperature and dissolved oxygen (DO) were also measured at the surface of the bottom sediment at each site by a diver using a hand-held digital depth gauge, thermometer and optical dissolved oxygen sensor (model D-Opto, Zebra-Tech Ltd., USA) respectively. Each replicate of grab sediments collected for faunal analysis was washed over a sieve with a 0.5 mm mesh opening on board. All residues were preserved in 70% ethanol and stained with Rose Bengal.

Laboratory analyses

Upon arrival to the laboratory, the sediment samples for TOC were frozen at 20°C for 24 h followed by freeze-drying. The freeze-dried sediments were homogenized to<0.25 mm with a mechanical homogenizer and stored in a desiccator for further analyses. TOC in sediment was then measured following the Walkley–Black wet titration method (Walkley and Black, 1934). For particle size analysis, the wet-sieving method was performed according to Buchanan (1984). A geometric grade scale modified by Wentworth in Φ values (Buchanan, 1984) was used to classify the grain size, in which higher Φ values represent finer sediments (Table S2).

The residues collected from the infaunal samples were sorted under a dissecting microscope and animals were picked, and later identified to lowest possible taxa and counted. The biomass (wet weight) was measured using an electronic balance for each species, after blotting the animals on filter paper for one minute before weighing to the nearest 0.01 g, since most of the animals were small and juvenile. Larger animals were blotted on filter paper for 2-3 minutes according to Jennings et al. (2002). Tube-forming polychaetes were removed from tubes before weighing. For damaged specimens, the following procedures, according to Jennings et al. (2002), were applied: (1) 'complete' animals were assembled from fragments in the sample as far as possible and recorded as single individuals and (2) if fragments of an animal constituted less than 30% of the expected mass of a complete animal, they were discarded.

Classification of biological traits

Macrofaunal genera and species were classified into seven biological traits according to the body size, larval type, mobility, body form, degree of attachment, living habit and feeding habit. These traits were subdivided into 36 categories (Table S3) and each category was scored according to the affinity of each individual taxon for each trait category, ranging from 0 - 3, with 0 being no affinity and 3 being total affinity, which is

referred as fuzzy-coding (Chevene et al., 1994). Information of biological traits was referenced from Fleddum (2010), based on various literature sources including scientific publications, theses, web databases and expert knowledge. When there was no trait information for a species, with the exception of the body size, the trait scores from the same genus were used since it is generally accepted that there are similar traits between species of the same genus (Fleddum, 2010). In this study, changes in functional composition on biomass were adopted in the biological trait analysis as many important ecological processes are strongly affected by the biomass of important functional groups within the benthic community (Tillin et al., 2006).

Data treatment and statistical analysis

Six environmental parameters including depth, DO, temperature, trawling intensity, TOC and sediment median diameter (MD Φ) were examined using normalized principal component analysis (PCA) with Euclidean distance to investigate the variance within the sampling sites and between the trawled and non-trawled treatments for each season (Pielou, 1984). Percentage of TOC was arcsine transformed before data being normalized. Permutational multivariate analysis of variance (PERMANOVA) was also performed to test for significant differences in environmental variables between trawled and non-trawled treatments and between summer and winter seasons (Anderson et al., 2008).

The infaunal data of five grab replicates at each site were pooled as one sample. Both abundance and biomass data were square-root transformed to reduce the effect of species with high abundance or biomass, and the dominant taxa groups were calculated as percentages, Shannon diversity (*H'*) and Pielou evenness (*J'*) of the infauna for each site were determined based on the transformed pooled abundance data (Schratzberger and Jennings, 2002). Principal coordinate analysis (PCoA) of the transformed, pooled biomass was applied to elucidate community structure between treatments and seasons (Anderson et al., 2008). In the present study, biomass data were adopted for PCoA, as many important ecological processes are strongly affected by the biomass of important functional groups within the benthic community (Tillin et al., 2006). PERMANOVA was also conducted to test for differences in infaunal abundance and biomass between treatments and seasons, with "treatments" (fixed factor) crossed with "seasons" (fixed factor). Where differences or interactions were significant, pair-wise permutation tests were used to further explore these differences and the contribution of species to the average Bray-Curtis dissimilarity between treatments and seasons were further examined with similarity percentage (SIMPER) analysis (Clarke and Gorley, 2006). The species abundance data were also categorized in $\log_2$ classes to depict the distribution of commonly and rarely occurring species for both treatments and seasons.

Similarly, to evaluate the biological trait relationship from the infaunal samples, PCoA of the weighted biological traits with square-root transformed biomass was conducted between trawled and non-trawled treatments and seasons. PERMANOVA was also applied to test differences for weighted biological traits between treatments and seasons, followed by pair-wise permutation tests if significant differences or interactions were found. The contribution of biological trait categories to the average Bray-Curtis dissimilarity was further examined with SIMPER analysis and the categories in each biological trait were compared using the Mann-Whitney U test, if significant differences were noted between treatments and seasons from PERMANOVA. The biological trait contribution for rare species from summer and winter (trawled and non-trawled treatments) was also presented as percent of the whole trait pool. Although such rare species occur in less abundance, they collectively contribute to, and exert a greater effect, on ecosystem functioning (Ellingsen et al., 2007).

All the above multivariate analyses were performed with PRIMER-E v.6 and its add-on package PERMANOVA+ (PRIMER-E, Plymouth Marine Laboratory, UK), whereas the determination of Mann-Whitney U test was conducted through STATISTICA v.8 (StatSoft, Oklahoma, USA).

Results

Environmental variables

The entire study area was considered to be fairly uniform with respect to bottom depth, temperature, DO, TOC and sediment median diameter (MD Φ) during the sampling period within each season (Table 1). Water depth at the trawled sites was between 18 and 23 m, whereas at the non-trawled sites between 14 and 16 m. The temperature ranged from 26.66 to 27.18°C in summer and 19.01 to 19.86°C in winter across all the sampling sites. The DO at the seabed was higher in winter (>8 ppm) than summer (~5-6 pm) for both trawled and non-trawled sites, and slightly higher DO was registered for the non-trawled sites (summer 6.29-6.56, winter 8.85-9.05 ppm) than the trawled sites (summer 5.31-6.50 ppm, winter 8.38-8.91 ppm). The percentage of TOC was higher for both trawled and non-trawled sites in summer (2.03-2.54%) than winter (1.06-1.94%). Across all the sampling sites, the sediment was classified as silt (Table S2) with sediment median diameter between 5.72 and 6.21 Φ, with exception at the trawled site AT (4.65-5.56 Φ). Figure 2 depicts the relationship between the sampling sites and environmental variables from the PCA results. The first two axes from the PCA plot contributed to 85% (eigenvalue = 2.64 and 2.46) of the variance in summer (Figure 2A) and 87.3%

10.3389/fmars.2022.1010909

TABLE 1 Summary of the environmental characteristics and trawling intensity per week of all the sampling sites in trawled and non-trawled treatments and seasons.

			Summer					
Environmental factor	**AT**	**BT**	**CT**	**DT**	**AC**	**BC**	**CC**	**DC**
Depth (m)	22	23	20	18	16	14	16	16
DO (ppm)	6.50	5.92	5.67	5.31	6.29	6.50	6.62	6.56
Temp (°C)	27.18	27.14	27.05	26.66	27.22	27.17	26.99	26.76
TI (week)	1	5	5	5	0	0	0	0
TOC (%)	2.03	2.33	2.54	2.42	2.33	2.36	2.49	2.41
MD (Φ)	5.56	5.72	6.19	6.12	6.09	6.15	6.20	6.19
			Winter					
Environmental factor	**AT**	**BT**	**CT**	**DT**	**AC**	**BC**	**CC**	**DC**
Depth (m)	22	23	20	18	16	14	16	16
DO (ppm)	8.39	8.38	8.91	8.84	8.91	8.95	8.85	9.05
Temp (°C)	19.38	19.53	19.04	19.01	19.86	19.84	19.65	19.82
TI (week)	1	5	5	5	0	0	0	0
TOC (%)	1.06	1.94	1.82	1.77	1.68	1.65	1.80	1.80
MD (Φ)	4.65	6.03	6.18	6.14	6.05	6.13	6.21	6.19

DO, dissolved oxygen; Temp, temperature; TOC, total organic carbon; TI, trawling Intensity; MD, median diameter of particle size.

(eigenvalue = 3.1 and 2.14) in winter (Figure 2B). The grouping of the sampling sites was quite similar for both seasons, with the trawled sites being positioned to the right and non-trawled sites at the upper left. Except for AT, the grouping of the other three trawled sites was correlated with water depth, trawling intensity and, to a lesser extent, TOC, whereas for the four non-trawled sites, they were correlated with DO and median sediment diameter. The trawled site AT showed a different pattern than the other trawled sites with lower trawling intensity and coarser sediment (Table 1).

A PERMANOVA test showed significant differences in environmental factors between trawled and non-trawled treatments (pseudo-F = 7.900, df = 1, p = 0.001) and seasons (pseudo-F = 12.610, df = 1, p = 0.001) but not significant for the interaction between treatments and seasons (pseudo-F = 0.110, df = 1, p = 0.927).

Macrobenthic community structure

A total of 77 species were identified for both seasons and treatments (41 in summer and 57 in winter, sharing 20 of the same taxa). Polychaetes were the most dominant taxa for all the sampling sites (non-trawled area: summer 94%; winter 85%; trawled area: summer 78%; winter 86% of total species) (Table S4). The highest percentage composition of crustaceans was found at the trawled sites in summer (14%), whereas the highest percentage composition of molluscs was recorded at these same sites in winter (7%).

In summer, the non-trawled sites inside the protected marine park area had a low level of species composition and abundance (Table 2). Among these four sites, BC recorded the highest species number (11/0.5 m^2), total biomass (4.79 g/0.5 m^2), number of individuals (17/0.5 m^2), *J'* (0.95) and $\log_e$ *H'* (2.28). In comparison with the non-trawled sites, except for *J'*, higher species richness, abundance, biomass and diversity index were recorded at the trawled sites with BT recording the highest species composition (23/0.5 m^2), total biomass (3.87 g/0.5 m^2) and $\log_e$ *H'* (2.84). Amongst these four trawled sites, AT also had the highest number of individuals (63/0.5 m^2) and CT the highest *J'* value (0.93). In contrast to summer, the macrobenthic community structure showed changes in winter (Table 2), in which the most of the identified taxa were dominated by new recruiting juveniles in both sampling areas. All the diversity indices increased at all sites with the exception of BT, which had a smaller species composition but more individuals. The infauna recorded from both trawled and non-trawled sites also revealed more similarities in winter for all other measurements, except for AT, which had lower trawling intensity but highest species number (31/0.5 m^2), total biomass (21.53 g/0.5 m^2) and number of individuals (353/0.5 m^2).

The results from PCoA showed that the first axis contributed 25.4% of the total data variation and the second axis 13.3% (Figure 3). The PCoA plot of infaunal samples depicted distinct separation between seasons with winter samples located at the left side, closer to PCo2, while the summer samples located at the right side of the plot. Although the non-trawled site CC in summer had only one species with the largest contribution to the data variance, its position on the PCoA plot was still closer to other non-trawled sites than those trawled sites in summer.

PERMANOVA on the transformed abundance data identified significant differences between trawled and non-

10.3389/fmars.2022.1010909

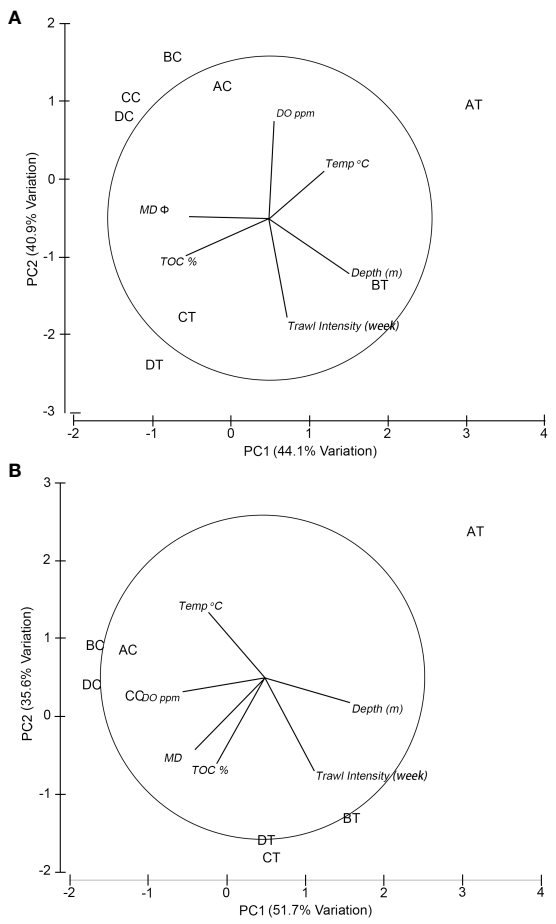


FIGURE 2
Principal component analysis (PCA) of normalised environmental factors using Euclidean distance for **(A)** summer and **(B)** winter. The lines show the direction of the environmental factors that are related to the sampling sites. AT-DT, trawling sites; AC-DC, non-trawled sites; Temp, temperature; DO, dissolved oxygen; TOC, total organic carbon; MD Φ, median sediment diameter in Φ scale (see Table S2).

trawled treatments (pseudo-F = 2.899, df = 1, p = 0.002), seasons (pseudo-F = 6.354, df = 1, p = 0.001) and the interaction between treatments and seasons (pseudo-F = 2.438, df = 1, p = 0.004). Similarly, PERMANOVA of the transformed biomass data also indicated significant differences between treatment (pseudo-F = 2.024, df = 1, p = 0.007), seasons (pseudo-F = 4.598, df = 1, p = 0.001) and interaction between treatments and seasons (pseudo-F = 1.950, df = 1, p = 0.016). Pair-wise *a posteriori* PERMANOVA between trawled and non-trawled sites for abundance and biomass data revealed significant differences for the biomass and abundance in summer but insignificant differences in winter (Table S5).

SIMPER analysis revealed that some of the same species, including the polychaetes *Chaetozone setosa*, *Aglaophamus dibranchis* and *Sigambra hanaokai*, and the ribbon worm (Nemertea) Cerebratulidae sp., occurred in both treatments and/or in both seasons with slight differences in cumulative percentages in abundance (Table 3). Other most numerically dominant species recorded in summer were the polychaete *Heteromastus filiformis* at the non-trawled sites and the polychaete *Euryothoe* sp. and the tube-building amphipod *Jassa marmorata* from the trawled sites; whereas in winter, these comprised the polychaetes *Prionospio ehlersi*, *P. malmgreni* and *Schistomeringos rudolphi* at the non-trawled sites and the bivalves *Tellina* sp. and the peanut worm (Sipuncula) *Apionsoma trichocephalus* from the trawled areas.

The infauna from the summer sampling consisted more rare species (i.e., represented only by one individual) in the pooled samples than that from winter for the non-trawled sites (13/2 m^2 versus 7/2 m^2), whereas an opposite trend was noted for the trawled sites (13/2 m^2 versus 19/2 m^2) (Figure 4). The distributions of the abundance classes were overall similar at both the trawled and non-trawled sites in winter compared to summer, as there were fewer species and individuals recorded at the non-trawled sites in summer.

Biological trait analysis

The results from PCoA of biological traits showed that the first axis contributed to 44.5% of the total variation and the second axis 27% (Figure 5). The distance between seasons in the plot decreased after traits were weighed in with the biomass. With only one species, and low trait contribution, the non-trawled site CC was positioned closest to PCo1 and had the largest contribution to data variance. There was no clear grouping between the trawled and non-trawled treatments in summer or winter.

PERMANOVA of the weighted trait data showed no significant differences between treatments (pseudo-F = 1.419, df = 1, p = 0.179) and interaction between treatments and seasons (pseudo-F = 1.939, df = 1, p = 0.066), but significant difference for seasons (pseudo-F = 5.793, df = 1, p = 0.003). Further exploration of the results from SIMPER and significant biological traits with Mann-Whitney U test between seasons is listed in Table 4. Nineteen of the 36 biological trait categories analyzed had up to 90% contribution to Bray-Curtis dissimilarity of 64.6% between seasons. The total rare species contributions to the biological trait pool were also lower for the non-trawled compared to the trawled sites in summer (Figure 6). However, in winter, the total rare species contribution at the non-trawled sites increased in several biological trait categories and was higher than that at the trawled sites, including species with smaller body size (<5 mm to 1 cm), planktotrophic or direct larval development, less motility, laterally flat or ball shape, temporary or permanent attachment, sessile life or surface crawling, and suspension or scavenger feeding (Figure 6; Table S3).

10.3389/fmars.2022.1010909

TABLE 2 Univariate analysis of pooled abundance data (0.5 m^2) for summer and winter sampling.

Sample	S	B	Summer N	J'	H'(log_e)
AC	5	0.08	7	0.96	1.55
BC	11	4.79	17	0.95	2.28
CC	1	0.00	4	0.00	0.00
DC	4	0.29	6	0.89	1.24
AT	17	0.67	63	0.72	2.05
BT	23	3.87	42	0.90	2.84
CT	8	0.20	15	0.93	1.93
DT	10	0.52	19	0.86	1.98
Sample	**S**	**B**	**Winter N**	**J'**	**H'(log_e)**
AC	24	1.73	56	0.91	2.91
BC	21	0.51	87	0.83	2.55
CC	16	1.84	66	0.76	2.11
DC	24	11.74	67	0.89	2.84
AT	31	21.53	353	0.52	1.81
BT	16	4.89	79	0.67	1.87
CT	19	5.32	72	0.72	2.14
DT	17	7.93	97	0.72	2.06

S, species (S/0.5 m^2); B, total biomass (g/0.5 m^2); N, number of individuals (N/0.5 m^2); *J'*, Pielou's eveness; *H'*, log_e Shannon diversity.

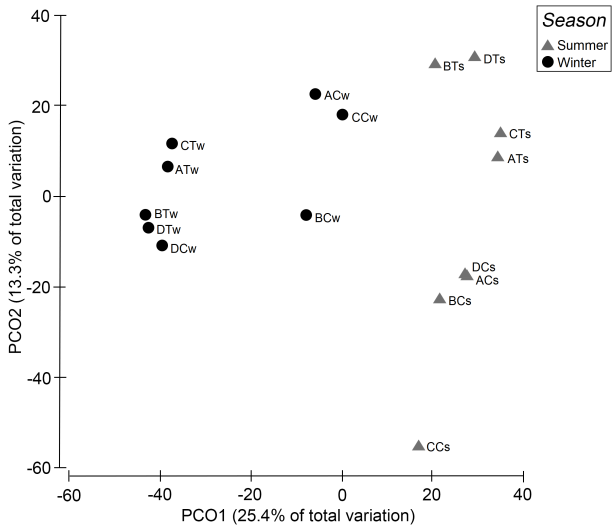


FIGURE 3
Principal coordinate analysis (PCoA) of the transformed pooled biomass (g/0.5 m^2) for treatments (AT-DT = trawled sites, AC-DC = non-trawled sites) and seasons (s, summer; w, winter).

TABLE 3 The top five species contribution from SIMPER (Similarity Percentages) for summer and winter sampling.

Species	Average abundance (ind./0.5m^2)	Average similarities (%)	Contribution (%)	Cumulative(%)
Non-trawled area: summer				
Sigambra hanaokai	1.29	12.26	55.85	55.85
Chaetozone setosa	0.79	2.62	11.91	67.76
Cerebratulidae sp.	0.60	1.85	8.42	76.18
Aglaophamus dibranchis	0.50	1.74	7.94	84.12
Heteromastus filiformis	0.50	1.74	7.94	92.06
Trawled area: summer				
Aglaophamus dibranchis	1.87	9.54	22.00	22.00
Jassa marmorata	1.70	7.14	16.45	38.46
Euryothoe sp.	2.41	6.83	15.74	54.20
Chaetozone setosa	1.46	6.68	15.41	69.61
Cerebratulidae sp.	1.62	2.66	6.13	75.74
Non-trawled area: winter				
Chaetozone setosa	3.55	8.50	19.19	19.19
Sigambra hanaokai	3.00	7.71	17.42	36.60
Prionospio ehlersi	2.32	4.97	11.23	47.83
Prionospio malmgreni	1.80	3.05	6.88	54.71
Schistomeringos rudolphi	1.25	2.05	4.64	59.35
Trawled area: winter				
Chaetozone setosa	8.28	15.62	28.28	28.28
Aglaophamus dibranchis	3.55	7.00	12.67	40.95
Sigambra hanaokai	2.31	5.31	9.61	50.56
Telinna sp.	2.05	4.81	8.72	59.28
Apionsoma trichocephalus	1.82	3.85	6.98	66.26

Discussion

Environmental parameters in trawled and non-trawled areas

The entire study area was considered uniform with respect to the measured environmental variables during the sampling period within summer and winter. The DO at the bottom was slightly higher in winter and the *in-situ* DO measurements in summer at the sampling time showed no signs of hypoxia. However, the study area is well-known for hypoxic periods during summer. Earlier DO measurements in the same sampling area taken during summer confirmed low oxygen (DO<2 ppm) at certain times of the year (Wu and Richards, 1979; Horikoshi and Thompson, 1980; Wu, 1982; Wu, 1988; Fleddum et al., 2011). Seasonal changes of other water quality parameters such as NO_3^-, NH_4^+ and PO_4^{3-} in the study area were minimal based on the online EPD monitoring database (2022). To better detect the effects of changes in macrobenthic community structure for each season, the end of summer and the end of winter were chosen for this study. This could be the reason for relatively higher DO recorded at the bottom during the end of summer, despite possibly lower DO occurrences during the mid-summer period, prior to the present field sampling. There were significant differences in environmental factors between trawled and non-trawled treatments and seasons but not for the interaction between treatments and seasons. This suggested that seasons are important in environmental changes for the whole sampling area but are not the only cause of the differences between trawled and non-trawled treatments. The trawled site AT, which had lower trawling intensity and coarser sediment, showed a different pattern than the other trawled sites

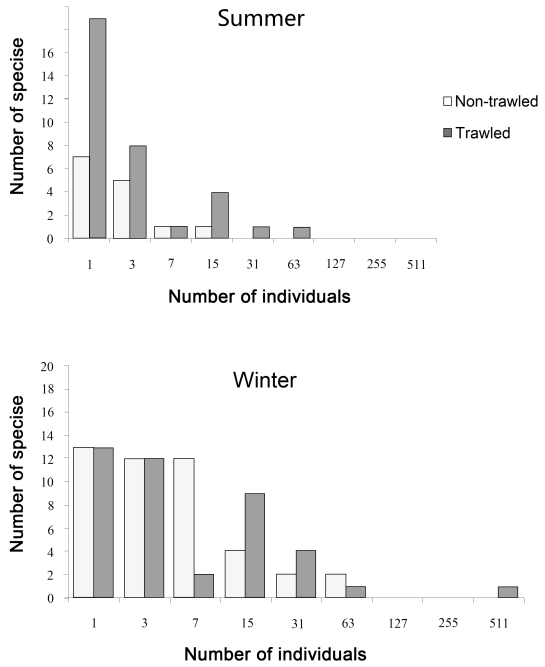


FIGURE 4
Species abundance distribution for each season and each treatment (trawled and non-trawled). The x-axis is in logarithmic scale (modified $\log_2$ classes). Class 1 represents 1 individual, 3 represents between 2-3 individuals, 7 represents 4-7 individuals, etc.

in macrobenthic composition. The largest difference between the trawled and non-trawled areas was the trawling intensity. Trawling is known to change environmental factors, such as grain size moving towards finer fractions (Pilskaln et al., 1998; Reiss et al., 2009), TOC towards higher percentage levels (Tuck et al., 1998; Reiss et al., 2009) and DO towards higher levels (De Borger et al., 2021). However, the trend of decrease in median sediment diameter and increase in TOC in the trawled area as compared to the non-trawled area was not clear in the present study (Table 1). In addition, as the present field sampling was conducted at the end of summer instead of mid-summer when hypoxic events can be more frequent, the increase in DO caused by bottom trawling was not clearly demonstrated.

Effects of trawling on macrobenthic community

The largest differences between the trawled and non-trawled treatments were found during summer, with significantly higher abundance, biomass, biodiversity and numbers of rare species in the trawled area. The non-trawled sites inside the marine park had a lower level of species composition and abundance, and several of the grab samples were void of macrofauna. In summer, the structure and biological trait composition of macrobenthic communities in the trawled area were also significantly more diverse than that in the non-trawled area. Such differences in

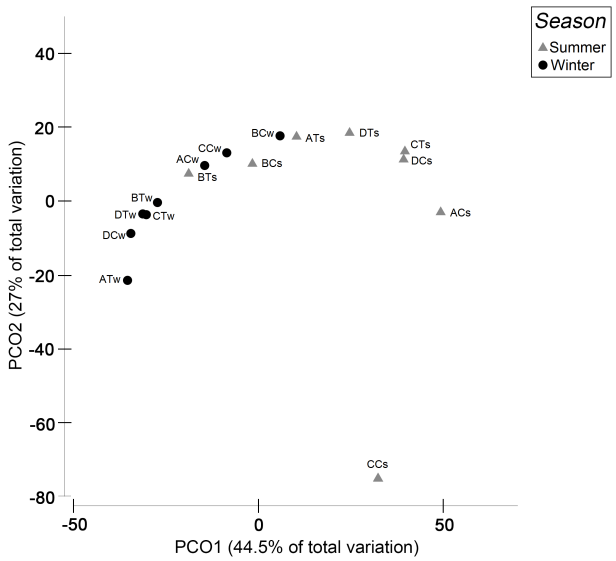


FIGURE 5
Principal coordinate analysis (PCoA) of weighted biological traits with square-root transformed biomass for treatments (AT-DT = trawled sites, AC-DC = non-trawled sites) and seasons (s, summer; w, winter).

TABLE 4 Results of contribution of biological trait categories from SIMPER analysis and Mann-Whitney U test between seasons.

Category	Average abundance (ind./0.5m^2)		Contribution (%)	Cumulative (%)	Rank summer	Rank winter	U	p level
	Summer	Winter						
DA1	4.43	18.86	11.16	11.16	40	96	4	**0.003**
AH4	2.85	16.17	9.87	21.03	38	98	2	**0.001**
AM2	2.51	54	6.96	27.98	40	96	4	**0.003**
FH4	0.83	9.84	6.74	34.72	38	98	2	**0.001**
LT2	2.33	10.00	6.17	40.90	42	94	6	**0.006**
LT1	2.10	9.23	5.91	46.81	40	96	4	**0.003**
BF1	2.55	9.78	5.72	52.53	40	96	4	**0.003**
BF2	0.87	7.21	4.75	57.28	36	100	0	**< 0.001**
FH8	1.63	6.89	4.30	61.58	41	95	5	**0.004**
NS4	1.97	7.23	4.26	65.84	41	95	5	**0.004**
NS5	0.99	6.57	4.10	69.94	45	91	9	**0.015**
NS3	1.29	5.70	3.64	73.58	36	100	0	**< 0.001**
FH3	1.18	5.04	3.20	76.78	41	95	5	**0.004**
BF5	3.19	5.19	2.89	79.68	53	83	17	0.115
AH5	2.32	4.49	2.73	82.40	52	84	16	0.092
AM4	1.69	4.02	2.39	84.79	46	90	10	**0.020**
FH1	1.89	3.21	2.33	87.12	59	77	23	0.343
AM3	0.92	3.09	1.81	88.94	48	88	12	**0.035**
NS6	1.45	2.34	1.72	90.66	57	79	21	0.247

DA1, none attachment; AH4, burrower; AM2, low mobility; FH4, subsurface deposit feeder; LT2, lecitotrophic larval type; LT1, planktotrophic larval type; BF1, cylindrical body form; BF2, dorsally flat body form; FH8, carnivore/omnivore feeding type; NS4, 3-6 cm in adult size; NS5, 6-10 cm in adult size; NS3, 1-3 cm in adult size; FH3, surface deposit feeder; AM4, high mobility; and AM3, medium mobility (see Table S3).
Cut off for low contribution is 90%. Significant level ($p < 0.05$) is shown in bold.

benthic community in favour of trawling during summer in the present study were unexpected. This finding was not in line with the hypothesis that intensive trawling activity results in a shift from K-selected to r-selected species, with a decrease in species diversity and rare species (de Juan and Demestre, 2012; Kaiser et al., 2018). It appeared that in Tolo Channel, summer may be favourable to trawling disturbances, relative to the environment in the protected, non-trawled area. Trawling can modify macrobenthic community structure and a higher abundance of opportunistic species is known to occur (Thrush and Dayton, 2002; McLaverty et al., 2020). However, higher abundance does not necessarily mean that the community is not disturbed. Watling and Norse (1998) compared trawling activities to forest cutting. Forest cutting is a change in the habitat from one type of community to another. The forest goes through different successional stages until, after several years, it reaches a similar habitat and community to what it was before, if the disturbance ceases. In that process, the biodiversity of opportunistic species increases until the strongest organisms inhabit and displace the weaker ones. This can be compared to trawling, in which the disturbed habitat may change its environmental factors and, in turn, affects the structure of the community. Intermediate disturbance hypothesis proposed by Connell (1978) has often been associated with some level of the successional stages and can be the reason for the highest biodiversity at the trawled site AT, where trawling occurred, but at a lower intensity. The succession that the benthic marine environment goes through will depend on the type of bottom and how it has been changed (Lu and Wu, 2000). The coral community may take decades to be repaired (MacNeil et al., 2015). Communities at the continental shelves and slopes, which have fewer natural disturbances, also have a slower recovery time, compared to areas with natural disturbances (Watling and Norse, 1998; Dernie et al., 2003). For communities in muddy environments, a few years should be enough to restore it back to what it was pre-trawled (Allen and Clarke, 2007; Sciberras et al., 2018). In the present study, repeated low summer DO events, coupled with heavy trawling activities, may have modified the macrobenthic community structure in Tolo Channel. Soft-bottom benthic communities with natural disturbances, such as hypoxia, could benefit from trawling in harsh times (in this case, wet, summer in Hong Kong) to some extent. One can consider that there is a trade-off between trawling and hypoxia. In winter, when DO was high and there was no occurrence of hypoxia, there were no significant differences in community structure between the trawled and non-trawled areas. Hypoxia is a natural event in the area and it is known to reduce the biodiversity drastically in the summer for both epi- and infauna; however, a rapid recovery of community structure to normal conditions has been noted in winter (Wu, 1988; Fleddum et al., 2011). It is thus suggested that trawling could contribute to a higher level of DO in a time when the area suffers from hypoxia (De Borger et al., 2021), thus increasing

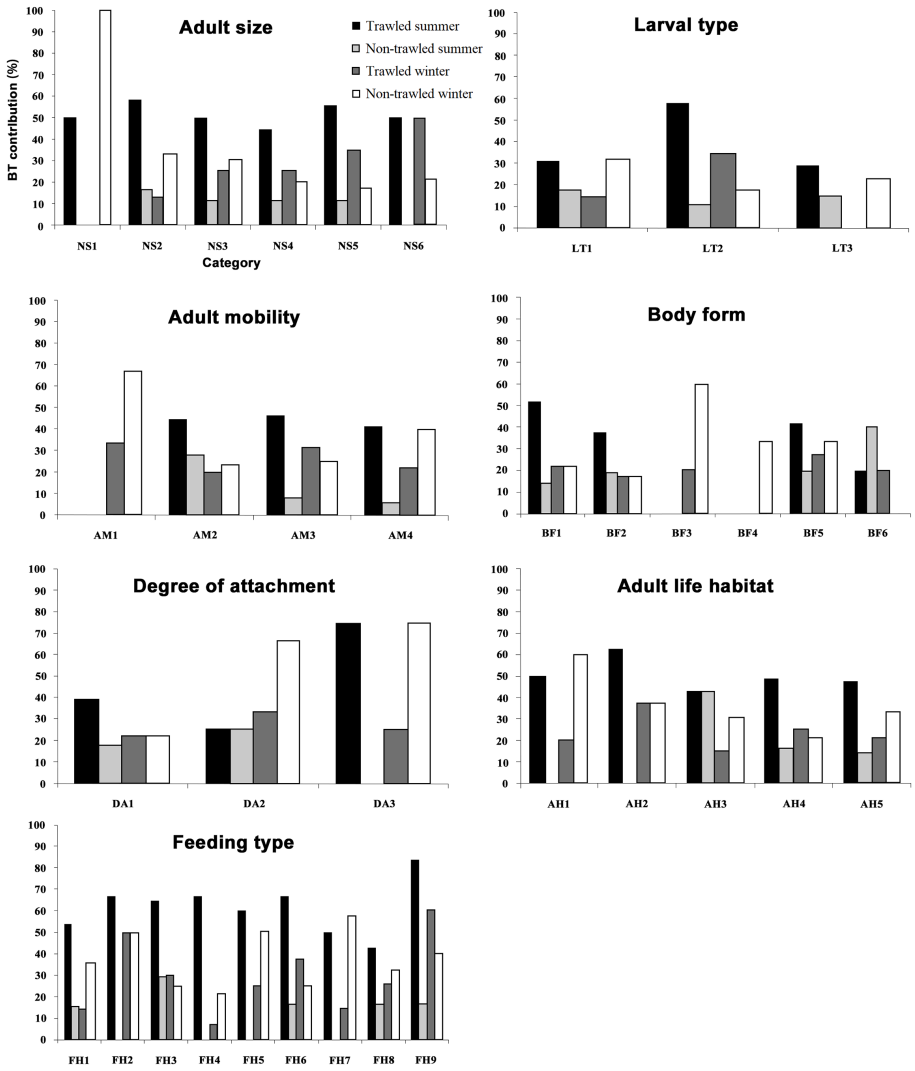


FIGURE 6
Biological trait (BT) contribution for rare species from summer and winter (trawled and non-trawled treatments) measured as percent of the whole trait pool. The biological trait is ranked as presence/absence. (Size, NS1:< 5 mm; NS2: 5 mm-1 cm; NS3: 1-3 cm; NS4: 3-6 cm; NS5: 6-10 cm; NS6: > 10 cm; Larval type, LT1: Planktotroph; LT2: Lecitotroph; LT3: Direct development; Mobility, AM1: None; AM2: Low; AM3: Medium; AM4: High; Body form, BF1: Short/cylindrical; BF2: Dorsally flat; BF3: Laterally flat; BF4: Ball shape; BF5: Long thin; BF6: Irregular; Attachment, DA1: None; DA2: Temporary; DA3: Permanent; Life Habitat, AH1: Sessile; AH2: Tube (permanent); AH3: Tube (semi-permanent); AH4: Burrower; AH5: Surface crawler; Feeding, FH1: Suspension/filter; FH2: Scraper/grazer; FH3: Surface deposit feeder; FH4: Subsurface deposit feeder; FH5: Dissolved matter/symbiont; FH6: Large detritus/sand licker; FH7: Scavenger; FH8: Carnivore/omnivore;FH9: Parasitic/commensal).

the chance of survival for the benthic animals. This might be an explanation of the higher biodiversity in summer in the trawled area as compared to the non-trawled sites. In a study of benthic communities in the southern Baltic Sea, van Denderen et al. (2022) reported that hypoxia may impact the community structure more significantly than trawling. Another explanation for the present findings could be that trawling may enhance the conditions of the seabed by removing large sessile organisms, such as sponges and soft corals, disturb the sea bottom and make food more available for some fish species (Rijnsdorp and Vingerhoed, 2001), which prey on invertebrates, such as polychaetes and crustaceans. However, it is difficult to estimate the exact impact of trawling in any study. Pitcher et al. (2000) removed seven tonnes of epifaunal biomass from the seabed in north-eastern Australia and still did not find any significant differences in the benthic communities in the trawled areas, which is an example of what is obvious but is not detectable (Thrush and Dayton, 2002).

It is complicated to evaluate the effects in areas with high natural disturbances (Drabsch et al., 2001; Kaiser et al., 2006). Natural disturbances can be factors such as wave forces, severe

storms, earthquakes, volcanic activities and seasonal changes including hypoxia and heavy rainfall or large temperature differences during summer or winter. The marine fauna are affected by these natural factors and, therefore, it may be difficult to distinguish trawling from the effects of natural disturbances (Rijnsdorp et al., 2015). van Denderen et al. (2015) examined the effects of trawling and natural disturbance on benthic communities over gradients of commercial bottom trawling effort in the North and Irish Seas. They found that the impact of trawling was greatest in areas with low levels of natural disturbance, while similar impact was small in areas with high level of natural disturbance.

Recovery from trawling in the marine park

Recovery is a return of environmental variables and species composition to a state that existed before the disturbance occurred. Recovery from trawling depends on types of habitat (Collie et al., 2000; Eno et al., 2013), frequency of disturbance compared with natural changes (Hiddink et al., 2006a; van Denderen et al., 2015), species and life history characteristics (Hiddink et al., 2018) and the size of the area disturbed (Preciado et al., 2019). There are hardly any data on the macrobenthic community inside the Hoi Ha Wan Marine Park before the Government closed the area to trawling in 1996. However, Mackie et al. (1993) performed a survey in Hoi Ha Wan and Tolo Channel in April 1989 using duplicate 0.1 m^2 van Veen grab (pool of two replicates) to investigate the macrofaunal community. This is the only set of data that can be used to compare with those obtained from the present study, since the four non-trawled sampling sites were located in the same survey area. In general, the abundance, number of species and Shannon diversity H' were higher in 1989, while the evenness J' was higher in this study, indicating a stronger similarity in abundance among the species and fewer numerically dominant species were found in the present case. Mackie et al. (1993) recorded the dominance of the polychaete *Minuspio* sp. in Hoi Ha Wan and Tolo Channel, which can serve as an indicator of organic pollution. In this study, there were only two individuals of *Minuspio cirrifera* found inside the protected marine park in summer and none in the trawled area along the Tolo Channel. The polychaetes *Sigambra* sp. and *Aglaophamus* sp. in the 1989 survey were among the top five abundant species, similar to this study, but the abundance was quite different. Among top five species, the abundance ranged from 11-260/0.2 m^2 in April 1989, while 0-4/0.5 m^2 were recorded in summer and 11-25/0.5 m^2 in winter in the present study. Only three individuals of *Chaetozone* sp. were observed in the same area in 1989, while in this study the species *C. setosa* were among the most numerically dominant. Polychaetes were found to dominate in both studies. The trend in the infaunal communities of subtropical Hong Kong is known to exhibit low species richness and biodiversity, but high abundance and evenness, in undisturbed localities when compared to temperate regions (Mackie et al., 1993). This trend is not fully understood, but some factors, such as reduced salinity, large annual temperature fluctuations, intense biological interactions, high sediment silt-clay content, sediment instability and negative redox potential could be contributing to this state (Shin and Thompson, 1982; Shin, 1989).

Through a review of trawling data of experimental and comparative studies mainly from temperate waters, Hiddink et al. (2017) estimated the recovery rates of biota after trawling would range between 1.9 and 6.4 years. Using a similar review approach, Sciberras et al. (2018) further indicated that for motile and short life-span species, such as polychaetes and most crustaceans, the recovery rate from trawling could be less than 1 year. Hence, the implication from such estimations is that biota within Hoi Ha Wan Marine Park should have had enough time to recover from trawling after 12 years as a trawl-free area. However this was not the case, according to the data obtained in the present study. The low biomass of infauna recorded in the marine park was surprising and contradicted to our hypothesis that a higher biodiversity with larger body-sized and longer-lived species would be found in the non-trawled marine park area, as compared to the heavily trawled area in Tolo Channel. The marine park covers 260 hectares; however, there is no prior knowledge on what extent of seabed within the park was affected by bottom trawling in the past as recovery from trawling would depend on the size of the area that has been disturbed (Thrush et al., 1998; Sciberras et al., 2013). A recent study, conducted in subtropical Hong Kong by comparing of surveys conducted in June 2012 (before the territory-wide trawl ban in Hong Kong) and June 2015 (2.5 years after the ban), revealed a significant increase in site-based abundance, species richness, functional diversity and among-site similarity of macrobenthos after the trawl ban, except in Tolo Harbour and Tolo Channel which is influenced by seasonal hypoxic events (Wang et al., 2021). With natural disturbances, such as an annual hypoxic season, the non-trawled sites in Ho Hai Wan Marine Park would need several more years in order to achieve a recovery back to its former state. However, the recruitment rate in the non-trawled area appeared to be rapid since the biodiversity managed to restore itself during winter.

The hypoxic situation in the marine park area is a natural phenomenon, which is likely not the reason for the decreasing trend in biodiversity. Another important consideration is that the marine park itself may have contributed to the changes through time. It is now widespread that marine protected areas are effective tools for conserving marine ecosystems (Kelleher, 1999; Lubchenco et al., 2003; Palumbi, 2003). Studies have observed ranges of responses to such protected waters, such as increases in total biodiversity (Edgar and Barrett, 1999), abundance or biomass (Russ et al., 2004; Abesamis and Russ,

2005), frequency of aggressive interactions between adults within the same species (Abesamis and Russ, 2005), and mean body size (Edgar and Barrett, 1999; Tuya et al., 2000; Abesamis and Russ, 2005). However, there could be short- and long-term consequences to marine protected areas that have been exposed to impact, in varying degrees. After the Government closed the area for trawling, several artificial reefs have been deployed inside the marine park, with the intention to increase fish biodiversity (Wilson et al., 2002). These reefs are in a distance of at least 15 m from the four non-trawled sampling sites; however, whether or not the reef structures would affect the infuanl community around through changes in hydrodynamics of the benthic environment (Shin et al., 2014) is not clear. Hence in the present study, apart from seasonal hypoxic events, the infaunal community within the marine park may also be influenced by the presence of the artificial reefs over these years.

Conclusion

The present study was conducted in a heavily trawled area and a nearby marine park which has been closed to bottom trawling for more than 10 years, enabling the examination of the impact of and recovery from trawling on benthic communities. As the study sites were influenced by summer hypoxia, the results obtained imply that natural disturbance may exert a greater influence on the community structure and function than from trawling. Moreover, bottom trawling may contribute to a higher level of DO in a time when the area suffers from hypoxia, thus favouring the survival of benthic animals. By comparing data taken prior to closure of the marine park from trawling, the recovery of infaunal community appeared to be slow over the 12 years as a trawl-free area. Such recovery could also be complicated with the presence of artificial reefs deployed within the marine park, which may affect the hydrodynamics of the benthic environment and modify the community structure and function. Further studies on the structure and function of benthic communities, both on spatial changes around the artificial reefs and temporal changes over time, are thus suggested within the marine park area and in adjacent waters, so as to investigate the longer-term recovery progress of benthic ecosystems after the trawl ban.

Data availability statement

The raw data supporting the conclusions of this article will be made available by the authors, without undue reservation.

Author contributions

PS designed the study and finalized the manuscript. WX assisted in the study and revised the manuscript. AF conducted the field and laboratory work and wrote the manuscript. JS provided comments on the drafts of the manuscript. All authors contributed to the article and approved the submitted version.

Funding

This research was supported by a postgraduate studentship awarded to AF at City University of Hong Kong, Hong Kong SAR, China.

Acknowledgments

Thanks for Paul Hodgson and his diving team for *in-situ* measurements of water depth, temperature and DO and checking the seabed condition prior to field sampling over the study period.

Conflict of interest

The authors declare that the research was conducted in the absence of any commercial or financial relationships that could be construed as a potential conflict of interest.

Publisher's note

All claims expressed in this article are solely those of the authors and do not necessarily represent those of their affiliated organizations, or those of the publisher, the editors and the reviewers. Any product that may be evaluated in this article, or claim that may be made by its manufacturer, is not guaranteed or endorsed by the publisher.

Supplementary material

The Supplementary Material for this article can be found online at: https://www.frontiersin.org/articles/10.3389/fmars.2022.1010909/full#supplementary-material

References

Abesamis, R. A., and Russ, G. R. (2005). Density-dependent spillover from a marine reserve: Long-term evidence. *Ecol. Appl.* 15 (5), 1798–1812. doi: 10.1890/05-0174

Agriculture, Fisheries and Conservation Department (2006) *Agriculture, fisheries and conservation department port survey*. Available at: https://www.afcd.gov.hk/english/fisheries/fish_cap/fish_cap_latest/fish_cap_latest.html.

Allen, J. I., and Clarke, K. R. (2007). Effects of demersal trawling on ecosystem functioning in the north Sea: A modelling study. *Mar. Ecol. Prog. Ser.* 336, 63–75. doi: 10.3354/meps336063

Althaus, F., Williams, A., Schlacher, T. A., Kloser, R. J., Green, M. A., Barker, B. A., et al. (2009). Impacts of bottom trawling on deep-coral ecosystems of seamounts are long-lasting. *Mar. Ecol. Prog. Ser.* 397, 279–294. doi: 10.3354/meps08248

Anderlini, V. C., and Wear, R. G. (1992). The effect of sewage and natural seasonal disturbances on benthic macrofaunal communities in Fitzroy bay, Wellington, new Zealand. *Mar. pollut. Bull.* 24 (1), 21–26. doi: 10.1016/0025-326X(92)90312-T

Anderson, M. J., Gorley, R. N., and Clarke, K. R. (2008). *PERMANOVA+ for PRIMER: Guide to software and statistical methods* (Plymouth, UK: PRIMER-E).

Buchanan, J. B. (1984). "Sediment analysis," in *Methods for the study of marine benthos. IBP handbook second ed, 2nd ed.*, vol. vol. 16 . Eds. N. A. Holme and A. D. McIntyre (Oxford, UK: Blackwell Scientific Publications), 41–65.

Chevene, F., Doledec, S., and Chessel, D. (1994). A fuzzy coding approach for the analysis of long-term ecological data. *Freshw. Biol.* 31, 295–309. doi: 10.1111/j.1365-2427.1994.tb01742.x

Clarke, K. R., and Gorley, R. N. (2006). *PRIMER v6: User Manual/Tutorial* (Plymouth, UK: PRIMER-E).

Collie, J. S., Hall, S. J., Kaiser, M. J., and Poiner, I. R. (2000). A quantitative analysis of fishing impacts on shelf-sea benthos. *J. Anim. Ecol.* 69, 785–798. doi: 10.1046/j.1365-2656.2000.00434.x

Connell, J. H. (1978). Diversity in tropical rain forests and coral reefs: high diversity of trees and corals is maintained only in a nonequilibrium state. *Science* 199, 1302–1310. doi: 10.1126/science.199.4335.1302

Cook, R., Fariñas-Franco, J. M., Gell, F. R., Holt, R. H. F., Holt, T., Lindenbaum, C., et al. (2013). The substantial first impact of bottom fishing on rare biodiversity hotspots: A dilemma for evidence-based conservation. *PloS One* 8, e69904. doi: 10.1371/journal.pone.0069904

De Borger, E., Tiano, J., Braeckman, U., Rijnsdorp, A. D., and Soetaert, K. (2021). Impact of bottom trawling on sediment biogeochemistry: a modelling approach. *Biogeosciences* 18, 2539–2557. doi: 10.5194/bg-18-2539-2021

de Juan, S., and Demestre, M. (2012). A trawl disturbance indicator to quantify large scale fishing impact on benthic ecosystems. *Ecol. Indic.* 18, 183–190. doi: 10.1016/j.ecolind.2011.11.020

Dernie, K. M., Kaiser, M. J., and Warwick, R. M. (2003). Recovery rates of benthic communities following physical disturbance. *J. Anim. Ecol.* 72 (6), 1043–1056. doi: 10.1046/j.1365-2656.2003.00775.x

Drabsch, S. L., Tanner, J. E., and Connell, S. D. (2001). Limited infaunal response to experimental trawling in previously untrawled areas. *Ices. J. Mar. Sci.* 58 (6), 1261–1271. doi: 10.1006/jmsc.2001.1105

Edgar, G. J., and Barrett, N. S. (1999). Effects of the declaration of marine reserves on Tasmanian reef fishes, invertebrates and plants. *J. Exp. Mar. Biol. Ecol.* 242 (1), 107–144. doi: 10.1016/S0022-0981(99)00098-2

Ellingsen, K. E., Hewitt, J. E., and Thrush, S. F. (2007). Rare species, habitat diversity and functional redundancy in marine benthos. *J. Sea. Res.* 58 (4), 291–301. doi: 10.1016/j.seares.2007.10.001

Eno, N. C., Frid, C. L. J., Hall, K., Ramsay, K., Sharp, R. A. M., Brazier, D. P., et al. (2013). Assessing the sensitivity of habitats to fishing: from seabed maps to sensitivity maps. *J. Fish. Biol.* 83 (4), 826–846. doi: 10.1111/jfb.12132

Enticknap, B. (2002). *Trawling the North Pacific. Understanding the effects of bottom trawl. Fisheries on alaska's living seafloor*. (Anchorage, AK:Alaska marine conservation council, fisheries project coordinator). 22 pp.

EPD (2022) *Marine water quality data* (Hong Kong S.A.R: Environmental Protection Department). Available at: https://cd.epic.epd.gov.hk/EPICRIVER/marine/ (Accessed 1 September 2022).

Fleddum, A. L. (2010). *Effects of human disturbance on biological traits and structure of macrobenthic communities. PhD thesis* (Hong Kong: City University of Hong Kong), 325 pp.

Fleddum, A. L., Cheung, S. G., Hodgson, P., and Shin, P. K. S. (2011). Impact of hypoxia on the structure and function of benthic epifauna in tolo harbour, Hong Kong. *Mar. pollut. Bull.* 63, 221–229. doi: 10.1016/j.marpolbul.2011.03.019

Halpern, B. S., Walbridge, S., Selkoe, K. A., Kappel, C. V., Micheli, F., D'Agrosa, C., et al. (2008). A global map of human impact on marine ecosystems. *Science* 319, 948–952. doi: 10.1126/science.1149345

Hiddink, J. G., Jennings, S., and Kaiser, M. J. (2006a). Indicators of the ecological impact of bottom-trawl disturbance on seabed communities. *Ecosystems* 9, 1190–1199. doi: 10.1007/s10021-005-0164-9

Hiddink, J. G., Jennings, S., Kaiser, M. J., Queirós, A. M., Duplisea, D. E., and Piet, G. J. (2006b). Cumulative impacts of seabed trawl disturbance on benthic biomass, production, and species richness in different habitats. *Can. J. Fish. Aquat. Sci.* 63 (4), 721–736. doi: 10.1139/f05-266

Hiddink, J. G., Jennings, S., Sciberras, M., Bolam, S. G., Cambiè, G., McConnaughey, R. A., et al. (2018). Assessing bottom trawling impacts based on the longevity of benthic invertebrates. *J. Appl. Ecol.* 56 (5), 1075–1084. doi: 10.1111/1365-2664.13278

Hiddink, J. G., Jennings, S., Sciberras, M., Szostek, C. L., Hughes, K. M., Ellis, N., et al. (2017). Global analysis of depletion and recovery of seabed biota after bottom trawling disturbance. *Proc. Natl. Acad. Sci. U.S.A.* 114, 8301–8306. doi: 10.1073/pnas.1618858114

Hinz, H., Prieto, V., and Kaiser, M. J. (2009). Trawl disturbance on benthic communities: chronic effects and experimental predictions. *Ecol. Appl.* 19 (3), 761–773. doi: 10.1890/08-0351.1

Horikoshi, L. B., and Thompson, G. B. (1980). "Distribution of subtidal molluscs collected by trawling in tolo harbour and tolo channel, Hong Kong, with special reference to habitat segregation in two venerid bivalves," in *The malacofauna of Hong Kong and southern China*. Ed. B. Morton (Hongkong, China:Hong Kong University Press), 149–162.

Jennings, S., Nicholson, M. D., Dinmore, T. A., and Lancaster, J. E. (2002). Effects of chronic trawling disturbance on the production of infaunal communities. *Mar. Ecol. Prog. Ser.* 243, 251–260. doi: 10.3354/meps243251

Kaiser, M. J., Clarke, K. R., Hinz, H., Austen, M. C. V., Somerfield, P. J., and Karakassis, I. (2006). Global analysis of response and recovery of benthic biota to fishing. *Mar. Ecol. Prog. Ser.* 311, 1–14. doi: 10.3354/meps311001

Kaiser, M. J., Hormbrey, S., Booth, J. R., Hinz, H., and Hiddink, J. G. (2018). Recovery linked to life history of sessile epifauna following exclusion of towed mobile fishing gear. *J. Appl. Ecol.* 55, 1060–1070. doi: 10.1111/1365-2664.13087

Kaiser, M. J., Ramsay, K., Richardson, C. A., Spence, F. E., and Brand, A. R. (2000). Chronic fishing disturbance has changed shelf sea benthic community structure. *J. Anim. Ecol.* 69, 494–503. doi: 10.1046/j.1365-2656.2000.00412.x

Kelleher, G. (1999). *Guidelines for marine protected areas* (Switzerland and Cambridge UK: IUCN, Gland), 107 pp.

Kenchington, E. L. R., Gilkinson, K. D., Kevin, G., MacIsaac, K. G., Bourbonnais-Boyce, C., Kenchington, T. J., et al. (2006). Effects of experimental otter trawling on benthic assemblages on Western bank, northwest Atlantic ocean. *J. Sea. Res.* 56, 249–270. doi: 10.1016/j.seares.2006.03.010

Koslow, J. A., Gowlett-Holmes, K., Lowry, J. K., O'Hara, T., Poore, G. C. B., and Williams, A. (2001). Seamount benthic macrofauna off southern Tasmania: community structure and impacts of trawling. *Mar. Ecol. Prog. Ser.* 213, 111–125. doi: 10.3354/meps213111

Lubchenco, J., Palumbi, S. R., Gaines, S. D., and Andelman, S. (2003). Plugging a hole in the ocean: The emerging science of marine reserves. *Ecol. Appl.* 13, 3–7. doi: 10.1890/1051-0761(2003)013[0003:PAHITO]2.0.CO;2

Lu, L., and Wu, R. S. S. (2000). An experimental study on recolonization and succession of marine macrobenthos in defaunated sediment. *Mar. Biol.* 136, 291–302. doi: 10.1007/s002270050687

Mackie, A. S. Y., Oliver, P. G., and Kingston, P. F. (1993). "The macrobenthic infauna of hoi ha wan and tolo channel, Hong Kong," in *Proceedings of the first international conference on the marine biology of Hong Kong and the south China Sea, Hong Kong*. Ed. B. Morton (Hong Kong: Hong Kong University Press), 657–674. 28 October - 3 November 1990.

MacNeil, M. A., Graham, N. A., Cinner, J. E., Wilson, S. K., Williams, I. D., Maina, J., et al. (2015). Recovery potential of the world's coral reef fishes. *Nature* 520, 341–344. doi: 10.1038/nature14358

Mangano, M. C., Kaiser, M. J., Porporato, E. M., and Spanò, N. (2013). Evidence of trawl disturbance on mega-epibenthic communities in the southern tyrrhenian Sea. *Mar. Ecol. Prog. Ser.* 475, 101–117. doi: 10.3354/meps10115

McLaverty, C., Dinesen, G. E., Gislason, H., Brooks, M. E., and Eigaard, O. R. (2021). Biological traits of benthic macrofauna show size-based differences in response to bottom trawling intensity. *Mar. Ecol. Prog. Ser.* 671, 1–19. doi: 10.3354/meps13790

McLaverty, C., Eigaard, O. R., Dinesen, G. E., Gislason, H., Kokkalis, A., Erichsen, A. C., et al. (2020). High-resolution fisheries data reveal effects of

bivalve dredging on benthic communities in stressed coastal systems. *Mar. Ecol. Prog. Ser.* 642, 21–38. doi: 10.3354/meps13330

Moritz, C., Gravel, D., Savard, L., McKindsey, C. W., Brêthes, J. C., and Archambault, P. (2015). No more detectable fishing effect on northern gulf of St Lawrence benthic invertebrates. *ICES. J. Mar. Sci.* 72, 2457–2466. doi: 10.1093/icesjms/fsv124

O'Neill, F. G., and Ivanović, A. (2016). The physical impact of towed demersal fishing gears on soft sediments. *ICES. J. Mar. Sci.* 73, i5–i14. doi: 10.1093/icesjms/fsv125

Ortega, I., Colling, L. A., and Dumont, L. F. C. (2018). Response of soft-bottom macrobenthic assemblages to artisanal trawling fisheries in a subtropical estuary. *Estuar. Coast. Shelf. Sci.* 207, 142–153. doi: 10.1016/j.ecss.2018.04.007

Palumbi, S. R. (2003). Population genetics, demographic connectivity, and the design of marine reserves. *Ecol. Appl.* 13, 146–158. doi: 10.1890/1051-0761(2003)013[0146:PGDCAT]2.0.CO;2

Pielou, E. C. (1984). *The interpretation of ecological data: A primer on classification and ordination* (New York, USA: John Wiely & Sons), 263 pp.

Pilskaln, C. H., Churchill, J. H., and Mayer, L. M. (1998). Resuspension of sediment by bottom trawling in the gulf of Maine and potential geochemical consequences. *Conserv. Biol.* 12 (6), 1223–1229. doi: 10.1046/j.1523-1739.1998.0120061223.x

Pitcher, C. R., Poiner, I. R., Hill, B. J., and Burridge, C. Y. (2000). Implications of the effects of trawling on sessile megazoobenthos on a tropical shelf in northeastern Australia. *ICES. J. Mar. Sci.* 57, 1359–1368. doi: 10.1006/jmsc.2000.0911

Preciado, I., Arroyo, N. L., González-Irusta, J. M., López-López, L., Punzón, A., Muñoz, I., et al. (2019). Small-scale spatial variations of trawling impact on food web structure. *Ecol. Indic.* 98, 442–452. doi: 10.1016/j.ecolind.2018.11.024

Queirós, A. M., Hiddink, J. G., Kaiser, M. J., and Hinz, H. (2006). Effects of chronic bottom trawling disturbance on benthic biomass, production and size spectra in different habitats. *J. Exp. Mar. Bio. Ecol.* 335, 91–103. doi: 10.1016/j.jembe.2006.03.001

Ramalho, S. P., Lins, L., Soetaert, K., Lampadariou, N., Cunha, M. R., Vanreusel, A., et al. (2020). Ecosystem functioning under the influence of bottom-trawling disturbance: An experimental approach and field observations from a continental slope area in the West Iberian margin. *Front. Mar. Sci.* 7. doi: 10.3389/fmars.2020.00457

Reiss, H., Simon, P. R., Greenstreet, S. P. R., Sieben, K., Ehrich, S., Piet, G. J., et al. (2009). Effects of fishing disturbance on benthic communities and secondary production within an intensively fished area. *Mar. Ecol. Prog. Ser.* 394, 201–213. doi: 10.3354/meps08243

Rijnsdorp, A. D., Bastardie, F., Bolam, S. G., Buhl-Mortensen, L., Eigaard, O. R., Hamon, K. G., et al. (2015). Towards a framework for the quantitative assessment of trawling impacts on the sea bed and benthic ecosystems. *ICES. J. Mar. Sci.* 73 (1), 27–38. doi: 10.1093/icesjms/fsv207

Rijnsdorp, A. D., and Vingerhoed, B. (2001). Feeding of plaice, *Pleuronectes platessa* l. and sole *Solea solea* (L.) in relation to the effects of bottom trawling. *J. Sea. Res.* 45 (3-4), 219–229. doi: 10.1016/S1385-1101(01)00047-8

Russ, G. R., Alcala, A. C., Maypa, A. P., Calumpong, H. P., and White, A. T. (2004). Marine reserve benefits local fisheries. *Ecol. Appl.* 14 (2), 597–606. doi: 10.1890/03-5076

Schratzberger, M., and Jennings, S. (2002). Impacts of chronic trawling disturbance on meiofaunal communities. *Mar. Biol.* 141, 991–1000. doi: 10.1007/s00227-002-0895-5

Sciberras, M., Hiddink, J. G., Jennings, S., Szostek, C. L., Hughes, K. M., Kneafsey, B., et al. (2018). Response of benthic fauna to experimental bottom fishing: A global meta-analysis. *Fish. Fish. (Oxf.)* 19 (4), 698–715. doi: 10.1111/faf.12283

Sciberras, M., Jenkins, S. R., Kaiser, M. J., Hawkins, S. J., and Pullin, A. S. (2013). Evaluating the biological effectiveness of fully and partially protected marine areas. *Environ. Evid.* 2 (1), 1–31. doi: 10.1186/2047-2382-2-4

Shin, P. K. S. (1989). Natural disturbance of benthic infauna in the offshore waters of Hong Kong. *Asian Mar. Biol.* 6, 193–207.

Shin, P. K. S., Cheung, S. G., Tsang, T. Y., and Wai, H. Y. (2014). "Ecology of artificial reefs in the subtropics," in *Advances in marine biology 68*. Ed. M. P. Lesser (Oxford, UK: Academic Press), 1–63, ISBN: .

Shin, P. K. S., and Thompson, G. B. (1982). Spatial distribution of the infaunal benthos of Hong Kong. *Mar. Ecol. Prog. Ser.* 10, 37–47. doi: 10.3354/meps010037

Sköld, M., Göransson, P., Jonsson, P., Bastardie, F., Blomqvist, M., Agrenius, S., et al. (2018). Effects of chronic bottom trawling on soft-seafloor macrofauna in the kattegat. *Mar. Ecol. Prog. Ser.* 586, 41–55. doi: 10.3354/meps12434

Steele, J., Alverson, D. L., Auster, P., Collie, J., DeAlteris, J. T., Deegan, L., et al. (2002). *Effects of trawling and dredging on seafloor habitat* (Washington, DC.: National Academy Press), 126 pp.

Szostek, C. L., Murray, L. G., Bell, E., Rayner, G., and Kaiser, M. J. (2016). Natural vs. fishing disturbance: drivers of community composition on traditional king scallop, *Pecten maximus*, fishing grounds. *ICES. J. Mar. Sci.* 73 (supplement 1), i70–i83. doi: 10.1093/icesjms/fsv152

Thrush, S. F., and Dayton, P. K. (2002). Disturbance to marine benthic habitats by trawling and dredging: implications for marine biodiversity. *Annu. Rev. Ecol. Evol. Syst.* 33, 449–473. doi: 10.1146/annurev.ecolsys.33.010802.150515

Thrush, S. F., Hewitt, J. E., Cummings, V. J., Dayton, P. K., and Cryer, M. (1998). Disturbance of the marine benthic habitat by commercial fishing: impacts at the scale of the fishery. *Ecol. Appl.* 8, 866–879. doi: 10.1890/1051-0761(1998)008[0866:DOTMBH]2.0.CO;2

Tillin, H. M., Hiddink, J. G., Jennings, S., and Kaiser, M. J. (2006). Chronic bottom trawling alters the functional composition of benthic invertebrate communities on a sea-basin scale. *Mar. Ecol. Prog. Ser.* 318, 31–45. doi: 10.3354/meps318031

Tuck, I. D., Hall, S. J., Robertson, M. R., Armstrong, E., and Basford, D. J. (1998). Effects of physical trawling disturbance in a previously unfished sheltered Scottish sea loch. *Mar. Ecol. Prog. Ser.* 162, 227–242. doi: 10.3354/meps162227

Tuya, F. C., Soboil, M. L., and Kido, J. (2000). An assessment of the effectiveness of marine protected areas in the San Juan islands, Washington, USA. *ICES. J. Mar. Sci.* 57 (4), 1218–1226. doi: 10.1006/jmsc.2000.0808

van Denderen, P. D., Bolam, S. G., Hiddink, J. G., Jennings, S., Kenny, A., Rijnsdorp, A. D., et al. (2015). Similar effects of bottom trawling and natural disturbance on composition and function of benthic communities across habitats. *Mar. Ecol. Prog. Ser.* 541, 31–43. doi: 10.3354/meps11550

van Denderen, P. D., Törnroos, A., Sciberras, M., Hinz, H., Friedland, R., Lasota, R., et al. (2022). Effects of bottom trawling and hypoxia on benthic invertebrate communities. *Mar. Ecol. Prog. Ser.* 694, 13–27. doi: 10.3354/meps14094

Walkley, A., and Black, I. A. (1934). An examination of the degtjareff method for determining soil organic matter, and a proposed modification of the chromic acid titration method. *Soil Sci.* 37, 29–38. doi: 10.1097/00010694-193401000-00003

Wang, Z., Leung, K. M., Sung, Y. H., Dudgeon, D., and Qiu, J. W. (2021). Recovery of tropical marine benthos after a trawl ban demonstrates linkage between abiotic and biotic changes. *Commun. Biol.* 4 (1), 1–8. doi: 10.1038/s42003-021-01732-y

Watling, L., and Norse, E. A. (1998). Disturbance of the seabed by mobile fishing gear: A comparison to forest clearcutting. *Conserv. Biol.* 12, 1180–1197. doi: 10.1046/j.1523-1739.1998.0120061180.x

Williams, A., Althaus, F., Maguire, K., Green, M., Untiedt, C., Alderslade, P., et al. (2020). The fate of deep-sea coral reefs on seamounts in a fishery-seascape: What are the impacts, what remains, and what is protected? *Front. Mar. Sci.* 7. doi: 10.3389/fmars.2020.567002

Wilson, K. D., Leung, A. W., and Kennish, R. (2002). Restoration of Hong Kong fisheries through deployment of artificial reefs in marine protected areas. *ICES. J. Mar. Sci.* 59, 157–163. doi: 10.1006/jmsc.2002.1186

Wu, R. S. S. (1982). Periodic defaunation and recovery in a sub-tropical epibenthic community, in relation to organic pollution. *J. Exp. Mar. Biol. Ecol.* 64, 253–269. doi: 10.1016/0022-0981(82)90013-2

Wu, R. S. S. (1988). Marine pollution in Hong Kong: A review. *Asian Mar. Biol.* 5, 1–23.

Wu, R. S. S., and Richards, J. (1979). *Mass mortality of benthos in tolo harbour. fisheries occasional paper 21* (Hong Kong, China: Hong Kong Agriculture and Fisheries Department).

frontiers | Frontiers in Marine Science

TYPE Data Report
PUBLISHED 04 October 2022
DOI 10.3389/fmars.2022.1012541

Check for updates

OPEN ACCESS

EDITED BY
Chee Kong Yap,
Putra Malaysia University, Malaysia

REVIEWED BY
Thilagam Harikrishnan,
Pachaiyappa's College for Men, India
Rajamanickam Krishnamurthy,
Arignar Anna Government Arts and Science College Chennai, India

*CORRESPONDENCE
Shrivarshini Vasudevan
shrivarshiniv17@gmail.com

SPECIALTY SECTION
This article was submitted to Marine Pollution, a section of the journal Frontiers in Marine Science

RECEIVED 05 August 2022
ACCEPTED 05 September 2022
PUBLISHED 04 October 2022

CITATION
Koduvayur MV, Vasudevan S, Pandey V, Santhanakumar J, Jha DK and Dharani G (2022) Comparative evaluation of heavy metal concentration in different organs of the asian seabass: A multivariate approach. *Front. Mar. Sci.* 9:1012541. doi: 10.3389/fmars.2022.1012541

COPYRIGHT
© 2022 Koduvayur, Vasudevan, Pandey, Santhanakumar, Jha and Dharani. This is an open-access article distributed under the terms of the Creative Commons Attribution License (CC BY). The use, distribution or reproduction in other forums is permitted, provided the original author(s) and the copyright owner(s) are credited and that the original publication in this journal is cited, in accordance with accepted academic practice. No use, distribution or reproduction is permitted which does not comply with these terms.

Comparative evaluation of heavy metal concentration in different organs of the asian seabass: A multivariate approach

Manasi Venkat Koduvayur[1], Shrivarshini Vasudevan[1]*, Vikas Pandey[2], Jayapal Santhanakumar[2], Dilip Kumar Jha[2] and Gopal Dharani[2]

[1]School of Chemical and Biotechnology, Sastra University, Thanjavur, India, [2]Ocean Science and Technology for Islands, National Institute of Ocean Technology, Ministry of Earth Sciences, Government of India, Chennai, India

KEYWORDS

fish, metal toxicity, Asian seabass, multivariate approach, Tamil Nadu coast

Introduction

India's coastal ecosystems have been severely damaged in recent years as a result of increased urban and industrial development (Dheenan et al., 2014; Dheenan et al., 2016; Yuvaraj et al., 2018; Jha et al., 2022). The contaminants that originate from these anthropogenic actions have the potential to negatively impact various ecosystems such as corals (Jha et al., 2011; Jha et al., 2013a), mangroves (Das et al., 2014), and the ecological health and functioning of coastal regions (Pandey et al., 2022) as well as estuaries (Pandey et al., 2021). Previous studies have also shown that the areas subjected to minimal human interference generally contain better seawater quality (Jha et al., 2012; Jha et al., 2013b; Jha et al., 2015). Among the various contaminants such as nutrient eutrophication, microbial pollution, and pesticide, metal contamination plays a significant role in regulating the fisheries dynamics in the coastal regions (Jha et al., 2021). Because of their abundance, persistence, bioaccumulation, and toxicity, trace metals have been proven to influence coastal ecosystems (Ali et al., 2013; Jha et al., 2018). Fish are at the end of the aquatic food chain and thus can accumulate metals and pass them on to humans *via* the food chain, causing severe health problems (Al-Yousuf et al., 2000). The coastal population is highly dependent on fish and related products for their dietary supplement, and hence, it is important to estimate the metal concentration in the different organs of fish for better health management.

Seabass is protandric and generally grows up to 150 cm in size tolerating a wide range of salinity up to 40 ppt making it euryhaline (Mozanzadeh et al., 2021), and reproduces through catadromous migration (Noakes, 1988). However, these attributes, i.e., the high

salinity tolerance and reproductive migration, also make them prone to various contaminations. It is well known that natural processes such as mineral weathering, volcanic eruptions, dust deposition, human-caused activities such as mining, burning fossil fuels, agriculture, industry, marine traffic, urban development, and sewage, can all contribute to metal pollution in the near-shore environment. Some metals are essential, at optimal concentration, for biological functions whereas others have no known biological role and are recognized for their toxic effects on aquatic organisms, even at environmental concentrations (Mason, 2013). The toxicity of non-essential metals such as aluminum (Al), cadmium (Cd), mercury (Hg), and lead (Pb) increases with concentration. These metals are thought to be more bio-available in their dissolved ionic form, causing toxicity. On the other hand, toxic effects of essential metals such as copper (Cu), zinc (Zn), chromium (Cr), nickel (Ni), cobalt (Co), and iron (Fe) occur either at metabolic deficiencies or at high concentrations. Fishes mostly absorb metals through their gills and digestive tract, and little amounts are absorbed through their skin (Sfakianakis et al., 2015). Heavy metals act as neurotoxins and can alter the brain and neurological systems if consumed in higher concentrations through the food chain (Fu and Xi, 2020). Considering the commercial importance and high demand of *Lates cacarifer* for food, this study aimed to examine the concentration of heavy metals in the different organs such as the 1) muscle, 2) liver, 3) intestine, and 4) gills. Through multivariate statistical analysis, our study estimates heavy metal contamination in the different organs of fish and helps in the assessment of environmental conditions.

Methods

Seawater and sediment were also collected with the fish samples from the Rameswaram coastal region, Tamil Nadu (Figure 1A). The area is a known religious destination in India and thousands of pilgrims visit every day. The sewage, fuel combustion, cosmetics etc., resulting from domestic and industrial discharge increase various contaminants in the nearshore environment.

Sample collection and analysis

Niskin and Van Veen Grab samplers that had been acid-cleaned were used to collect surface seawater (30–50 cm depth) and sediment samples, respectively. The samples were collected during monsoon (MON) (June to September). The collected seawater and sediment samples were transferred into acid-cleaned polypropylene bottles and polyethylene airtight bags, respectively. The seawater samples were promptly brought to pH 2–3 using supra-pure HNO_3, and then stored at 4°C until analysis. Following the prescribed procedure, the sediment samples were first dried, crushed in an agate pestle and mortar, and then sieved through a 2 mm sieve (USEPA, 2001). A significant quantity of seawater and sediment in triplicates were taken and kept in an ice box for metal analysis (USEPA, 2001).

Forty-two fish of similar size groups were collected and transported to the laboratory in an ice box for further processing and subsequent analyses. In the laboratory, after recording the length and weight of fishes, they were dissected from their anal aperture using a sterile dissection knife and forceps to collect the organs like 1) muscle, 2) liver, 3) intestine and 4) gills. The organs were stored in labeled pre acid-cleaned falcon tubes at −20°C until analysis. Analytical-grade chemicals and Milli-Q water (Elix UV5 and Milli-Q, Millipore, USA) were used to prepare the solution and reagent. The Teflon container and polypropylene containers were cleaned by soaking in 5% HNO_3 for 24 h, followed by a rinse in Milli-Q water and drying. Following the standard digestion protocol, 1 g of dried sediment was digested at 140°C with 5 mL HNO_3 (Suprapur®, Merck) in a microwave digestion system (Anton Paar) (APHA, 2005). After digestion, the clear solution was transferred to centrifuge tubes, and 10 mL of Milli-Q water (Millipore, resistivity: 18.2 M/cm) was added to make the volume equal (Cortada and Collin, 2013). Similar procedures were used to add 5 mL of concentrated HNO_3 to a 5 mL seawater sample before microwave digestion. Fish organs were digested in 5 mL of pure HNO_3 and diluted to 20 mL with Milli-Q water for trace metal analysis. Inductively coupled plasma mass spectrometry (ICP-MS) was used to measure the concentrations of trace elements (Agilent 7500). Samples, certified reference materials (CRM), and duplicate analytical blanks were all examined for any potential contamination as per the procedure followed by Jha et al. (2019). The reference value (seawater and sediment), as well as the analyzed mean and standard deviation of the elemental values obtained for the CRM [NIST CRM048 (sediment) and NIST CRM QC3163 (seawater)], is adopted from Jha et al. (2019). By comparing the analyzed value to the CRM value, the precision and correctness of the analysis were confirmed. The metal concentrations in seawater were represented as ppb, whereas in sediment and fish organs as ppm.

Seawater was tested for pH, salinity, and temperature using the multi-parameter water quality probes (HANNA, HI98194) (APHA, 2005). The data collected for seawater, sediment, and fish were subjected to descriptive statistics to estimate the metal concentration. An analysis of variance (ANOVA, one-way) test was used to examine the significant differences ($\alpha = 0.05$) among the different organs of fish. Though a detailed analysis was carried out for the seawater, sediment, and fish organs, the major focus was on metal concentration in the fish organs. Box-whisker plots and correlation between metal levels in various organs of the fish were determined. Hierarchical clustering was performed using Ward's method, through squared Euclidean distances as a measure of the dissimilarity matrix. All multivariate analyses were carried out using the SPSS software (version 18).

Results and discussion

The length and body weight of *L. calcarifer* ranged from 10.2 to 12.4 cm and 10.93 to 23 g, respectively. Trace metal concentrations and bioavailability in coastal environments are heavily influenced by water quality characteristics such as pH, salinity, and organic matter, since they can precipitate as fresh/estuarine water interacting with seawater (Jha et al., 2019). The seawater temperature variation (29.00°C–30.65°C), pH (7.95–8.15), and salinity (30.5–31.5 PSU) were measured during the study. The trace metal percentage of CRM for seawater and sediment are given in Supplementary Table S1. The trace metal concentration in seawater and sediment are summarized in Table S2. However, trace metal concentrations in different fish organs are summarized in Table S3. Heavy metals like Cd, Hg and Pb were below detection level (BDL) in seawater and sediment samples. However, Fe had comparatively higher concentrations in seawater, sediment, and also in fish samples.

The concentration of Nickel (Ni) in seawater varied from 1.86 to 5.43 ppb, whereas it ranged from 6.9 to 7.62 ppm in sediment. Further, in fish organs, gills showed a higher value (1.31–4.89 ppm) whereas muscle showed BDL. The variation of Ni was significant ($p < 0.05$, $F = 11.915$) in various fish organs.

Copper (Cu) and zinc (Zn) enter the coastal ecosystem mostly through anthropogenic wastes such as fertilizers, algaecides, fungicides, and molluscicides, which in turn are deposited in the atmosphere and return to the sea through precipitation (Srichandan et al., 2016). Copper concentration varied from 24.3 to 96.6 ppb in seawater, while the concentration ranged from 1.5 to 10.6 ppm in sediment. This could be attributed to the application of biocides (antifouling paints) in ships and boats to prevent the growth of potential fouling organisms and also due to organic inputs from anthropogenic activities such as agriculture and industry in the coastal regions (Anbuselvan et al., 2018). Cu showed a higher value in the gills (10–48.26 ppm) whereas it was least in the muscle (0.85–4.49 ppm) of the fish. Zinc varied from 16.24 to 24.30 ppb in seawater, while the concentration ranged from 3.91 to 4.86 ppm in sediment. Ships and boats use anticorrosive paint, in which zinc sulphate is one of the chemical component (Yasar et al., 2001). The Zn showed a higher value in gills (16.4–24 ppm) and lower value was observed in the liver (5.44–11.09 ppm).

Manganese (Mn) is a transition metal that is essential in low concentrations but toxic in high concentrations (Srichandan et al., 2016). Its concentration in seawater ranged from 12.69 to 26.38 ppb and from 231 to 243 ppm in sediment. Further, in fish organs, liver showed a higher concentration (2.44–102.39 ppm) whereas it was least in the intestine (0.001–0.43 ppm), followed by muscle (0.82–1.6 ppm). Mn variation was significant ($p < 0.05$, $F = 8.828$) in various fish organs.

The concentration of cobalt (Co) in seawater was below detection level (BDL), whereas it ranged from 3.2 to 3.49 ppm in sediment. Further, fish organs, gills, and liver showed a similar value of 0.72 ppm whereas muscle and intestine showed negligible value. It is reported that (Tovar-Sánchez and Flegal, 2004) Co reaches to the coastal environment through the estuary system. During the current investigation, Co variation was insignificant ($p > 0.05$, $F = 2.774$) in various fish organs.

Total aluminum (Al) normally exists in relatively low amounts (5 ppb) in seawater; but in river water, it may reach 400 ppb (Jha et al., 2019). It is toxic to fish at 1500 ppb level in seawater (https://www.lenntech.com/periodic/water/aluminum/aluminum-and-water.htm). Total Al concentrations in seawater varied from 3.30 to 5.47 ppb, whereas in sediment it ranged from 3759 to 4918 ppm. Further, in fish organs, gill showed a higher concentration (16.95–68 ppm) whereas it was least in the muscle (0.96–1.89 ppm). During the current investigation, Al variation was significant ($p < 0.05$, $F = 15.589$) in various fish organs. The seawater contained higher concentrations of Iron (Fe) (355–463 ppb). Similarly, in sediment also higher Fe concentration was recorded ranging from 3665 to 4986 ppm. However, in fish, the maximum value of Fe was observed (43–159 ppm) in the gills compared to the other organs and it was least in the muscle (11.74–19.89 ppm). The concentration in the muscle was well within the permissible level as per the guidelines of WHO (1989).

The main sources of Cr are river drainage, dredging sludge, and dumping of industrial wastes (Jha et al., 2019). The concentration of Cr varied from 0.40 to 0.58 ppb in seawater, while it ranged from 15.48 to 16.80 ppm in sediment. Further, in fish organs, gills showed a higher value of 2.6 to 78 ppm whereas it was least in the muscle (0.001 to 0.55 ppm). The concentration of lead (Pb) varied from 2 to 4.6 ppb in seawater, while it ranged from 3.57 to 4.60 ppm in sediment. It enters the coastal ecosystem mainly by atmospheric deposition (Mukai et al., 1993), fly ash (Selvaraj et al., 2003), coal combustion (Anbuselvan et al., 2018), and anthropogenic activities. The Pb concentration in the fish organ was observed as BDL.

The rank order distribution in terms of mean metal concentration in seawater was: Fe (424 ppb) > Cu (56.67 ppb) > Mn (17.89 ppb) > Al (4.32 ppb) > Ni (3.83 ppb) > Pb (3.1 ppb) > Cr (0.46 ppb) > Co (BDL). In comparison, the rank order of metals in sediment was: Al (4226 ppm) > Fe (4117 ppm) > Mn (236 ppm) > Cr (15.95 ppm) > Ni (7.26 ppm) > Cu (5.66 ppm) > Zn (4.52 ppm) > Pb (3.97 ppm) > Co (3.32 ppm). The concentration of each metal varied considerably based on different organs (Table S3); however, the overall rank order of mean concentration of metals in fish was: Fe (56.99 ppm) > Mn (22.27 ppm) > Cr (13.82 ppm) > Zn (12.31 ppm) > Al (11.91 ppm) > Cu (9.02 ppm) > Ni (1.33 ppm) > Co (0.26 ppm) > Pb (BDL).

The box-whisker plots for trace metals in fish organs are given in Figures 1B–H. Ni, Cu, Fe, Cr, Al, Co (Figures 1B–G), and Mn (Figure 2A) show that the underlying distribution is skewed toward high concentration in the fish organs and has long whiskers at the top of the box. Overall, the concentration of metals was found higher in gills compared to other organs. The mild outliers (circles) and extreme outliers (asterisks), which are

randomly distributed, suggest the natural variability of metal in different organs of the fish. The one-way ANOVA results showed that apart from Co ($p > 0.05$), the concentration of all the metals significantly varied ($p < 0.05$) between different organs of the fish (Table S5).

The hierarchical clustering (Figure 2B) grouped the fish organs in the same or different clusters based on similarity or dissimilarity in the concentration of each metal. The resultant dendrogram produced one cluster keeping the intestine and muscle together whereas the gills and liver corresponded to

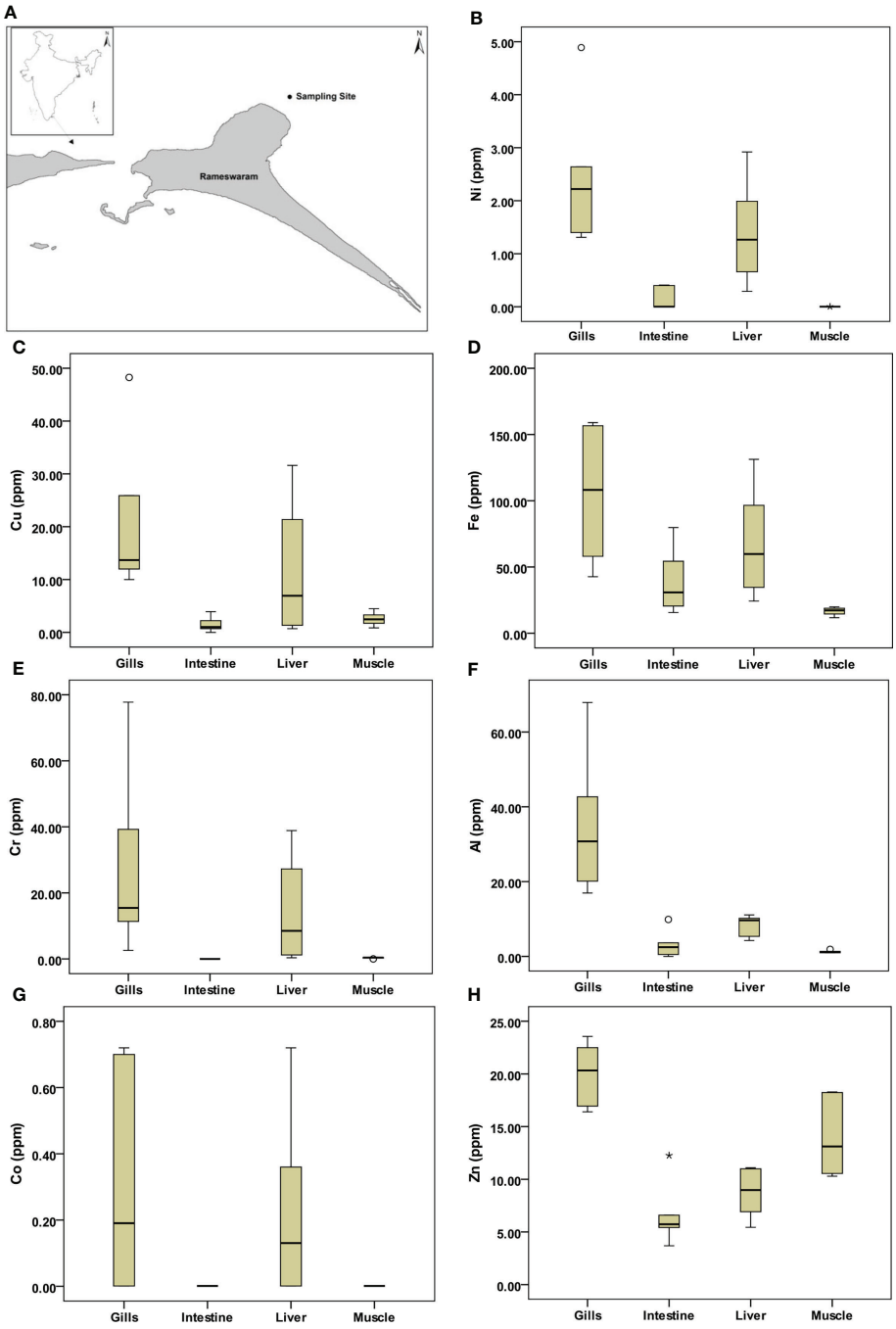


FIGURE 1
Study area map and box-whisker plots for selected metal variables in different parts of fish. **(A)** Sampling location, **(B)** Nickel, **(C)** Copper, **(D)** Iron, **(E)** Chromium, **(F)** Aluminum, **(G)** cobalt, and **(H)** Zinc. In each plot, the median is represented by the central point, the interval is represented by the rectangle (i.e. 25% and 75% percentiles), and the range is indicated by the whisker (*: extreme outlier; ∘: mild outlier).

outliers. The concentration of metals in gills was significantly different from that of other organs; therefore, it formed an outlier in the dendrogram. The metal concentration in the intestine and muscle was quite similar to each other; therefore, they formed a separate cluster. The concentration of metals in the liver showed similarity with the gills and therefore formed a separate cluster associated with the gills.

The concentration of metals in each organ of the fish was analyzed using Pearson's correlation to establish their relationship, and the results are shown in Table S4. Except for a few, all metals showed a significant positive correlation ($p < 0.05$) with each other. The correlation of Zn with Mn and Co was not significant ($p > 0.05$); Al and Cr were also not significantly correlated. This could be attributed to

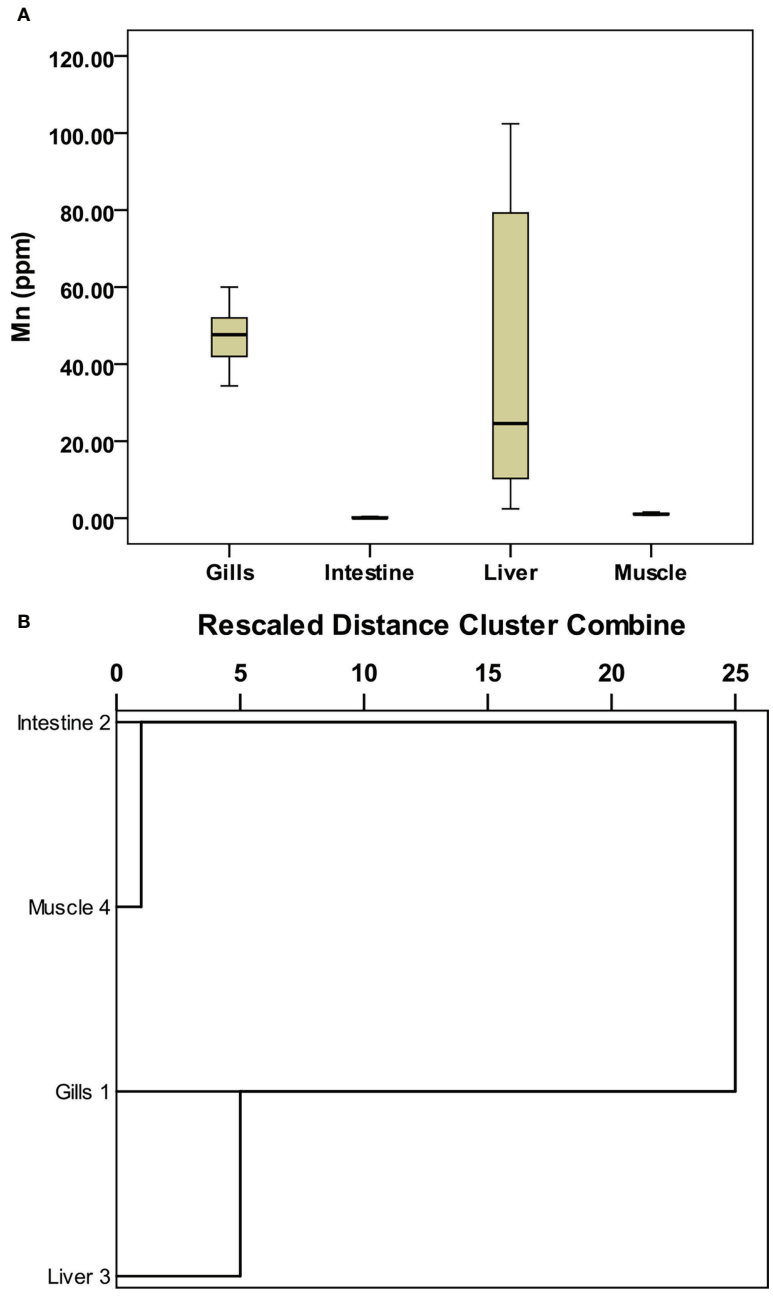


FIGURE 2
Box-whisker plots for selected metal variables in different parts of fish and Cluster analysis. **(A)** Manganese, and **(B)** dendrogram of the metal variables in different organs of the fish.

different concentrations of these metals in different organs of the fish.

The heavy metal concentration in fish muscle was found in trace quantities for essential metals whereas toxic metals such as Pb, Hg, and Cd were BDL. The mean concentration of trace metals in fish organs, seawater, and sediment was well within the permissible level as per the guidelines (WHO, 1989). However, considering that this location is a tourist hotspot, regular monitoring is required to estimate the metal concentration, develop a mitigation plan for promoting healthy habitats for flora and fauna, and contribute to coastal conservation and fisheries management (Murugan et al., 2005; Vijayakumaran et al., 2005; Kumar et al., 2009; Jha et al., 2017; Pandey et al., 2021; Pandey et al., 2022).

Conclusion

The study reveals that heavy metal concentrations of cadmium, lead, and mercury were below detection level, whereas other metal concentrations especially for the fish muscle were well within the permissible level. The highest heavy metal concentrations were found in gills and the lowest concentration occurred in the muscle. Since fish muscle is a consumable part, metal contamination may be harmful to human beings. Results indicate that the level of metals in the fish muscle is well within the standard levels and safe for human consumption. Although the concentration of heavy metals is negligible, routine metal toxicology studies must be conducted to evaluate the health of the coastal ecosystem and fish stock assessment in the region.

Data availability statement

The original contributions presented in the study are included in the article/Supplementary Material. Further inquiries can be directed to the corresponding author.

Ethics statement

Commercial fish does not require ethical committee approval.

Author contributions

SV and MK: Collection of samples, analysis of samples, processing of data, and writing-original draft. JS: Sample collection and dissection; VP: Statistical analysis and reviewing the manuscript; DJ: Conceptualization, sampling design, method validation, reviewing the manuscript and guidance; GD: Administration and project management. All authors contributed to the article and approved the submitted version.

Acknowledgments

The authors are thankful to Dr. G. A. Ramadass, Director, NIOT, Chennai, for allowing the student internship project at NIOT. We also like to thank the scientific and supporting staffs of MBT Groups in Chennai, India, for their timely help.

Conflict of interest

The authors declare that the research was conducted in the absence of any commercial or financial relationships that could be construed as a potential conflict of interest.

Publisher's note

All claims expressed in this article are solely those of the authors and do not necessarily represent those of their affiliated organizations, or those of the publisher, the editors and the reviewers. Any product that may be evaluated in this article, or claim that may be made by its manufacturer, is not guaranteed or endorsed by the publisher.

Supplementary material

The Supplementary Material for this article can be found online at: https://www.frontiersin.org/articles/10.3389/fmars.2022.1012541/full#supplementary-material

References

APHA (American Public Health Association) (2005). *Standard Methods for the Examination of Water and Wastewater. 21th edition* (Washigton, D.C: American Works Association and Water Environmental Federation).

Ali, A., Dahanukar., N., and Raghavan, R. (2013). Length-weight and length-length relationship of three species of snakehead fish, channa diplogramma, C. marulius and C. striata from the riverine reaches of lake vembanad, Kerala, India, CEPF Western ghats special series. *J. Threatened Taxa* 5 (13), 4769–4773. doi: 10.11609/JoTT.o3353.4769-73

Al-Yousuf, M. H., El-Shahawi, M. S., and Al-Ghais, S. M. (2000). Trace metals in liver, skin and muscle of lethrinus lentjan fish species in relation to body length and sex. *Sci. Total Environ.* 256, 87–94. doi: 10.1016/S0048-9697(99)00363-0

Anbuselvan, N., D., S. N., and Sridharan, M. (2018). Heavy metal assessment in surface sediments off coromandel coast of India: Implication on marine pollution. *Mar. pollut. Bull.* 131, 712–726. doi: 10.1016/J.MARPOLBUL.2018.04.074

Cortada, U., and Collin, M. (2013). The nature and contamination of sediments in the Plentzia estuary (Biscay province, Spain). *Geogaceta* 54, 147–150.

Das, A. K., Jha, D. K., Devi, M. P., Sahu, B.K., Vinithkumar, N.V., Kirubagaran, R., et al. (2014). Post tsunami mangrove evaluation in coastal vicinity of Andaman Islands, India. *J. Coast. Conserv.* 18, 249–255. doi: 10.1007/s11852-014-0312-5

Dheenan, P. S., Jha, D. K., Das, A. K., Vinithkumar, N. V., Prashanthi Devi, M., Kirubagaran, R., et al. (2016). Geographic information systems and multivariate analysis to evaluate fecal bacterial pollution in coastal waters of Andaman, India. *Environ. pollut.* 214 (7), 45–53. doi: 10.1016/j.envpol.03.065

Dheenan, P. S., Jha, D. K., Vinithkumar, N. V., Ponmalar, A. A., Venkateshwaran, P., and Kirubagaran, R. (2014). Spatial variation of physicochemical and bacteriological parameters elucidation with GIS in rangat bay, middle andaman. India. *J. Sea Res.* 85, 534–541. doi: 10.1016/j.seares.2013.09.001

Fu, Z., and Xi, S. (2020). The effects of heavy metals on human metabolism. *Toxicol. Mech. Methods* 30 (3), 167–176. doi: 10.1080/15376516.2019.1701594

Jha, D. K., Begum, M., Das, A. K., Sahu, B. K., and Kirubagaran., R. (2012). Environmental quality assessment of treis island, nicobar, india. J. *Mater. Environ. Sci.* 3, 800–807. Available at: http://www.jmaterenvironsci.com/Document/vol3/vol3_N5/81-JMES-211-2012-Jha.pdf.

Jha, D. K., Kirubagaran, R., Vinithkumar, N. V., Dharani, G., and Madeswaran, P. (2018). *"The Andaman and Nicobar Islands" in World seas: An environmental evaluation, ed* (UK and USA: Charles Sheppard (Academic press), 185–209.

Jha, D. K., Dharani, G., Verma., P., Ratnam, K., Senthil Kumar., R., and Rajaguru, S. (2021). Evaluation of factors influencing the trace metals in puducherry and diu coasts of India through multivariate techniques. *Mar. pollut. Bull.* 167 (6), 2021. doi: 10.1016/j.marpolbul.2021.112342

Jha, D. K., Pandey, V., Muthukumar, C., Sathish Kumar, P., Venkatnarayanan, S., Jebakumar, J. P. P., et al. (2022). Investigation of coastal water characteristics along the southeast coast of India: A multivariate approach. *Front. Mar. Sci.* 9, 945495. doi: 10.3389/fmars.2022.945495

Jha, D. K., Prashanthi Devi, M., Vinithkumar, N. V., Das, A. K., Kumar, A., Dheenan, P. S., et al. (2013b). Comparative investigation of water quality parameters of aerial & rangat bay, Andaman islands using *In-situ* measurements and spatial modelling techniques. *Water Qual. Expo. Health* 5, 57–67. doi: 10.1007/s12403-013-0086-2

Jha, D. K., Ratnam, K., Rajaguru, S., Dharani, G., Devi, M. P., and Kirubagaran, R. (2019). Evaluation of trace metals in seawater, sediments, and bivalves of nellore, southeast coast of India, by using the multivariate and ecological tool. *Mar. pollut. Bull.* 146, 1–10. doi: 10.1016/J.MARPOLBUL.2019.05.044

Jha, D. K., Vinithkumar, N. V., Marimuthu, N., Baskar, B., Sahu, B., Das, A. K., et al. (2013a). Field and GIS based post-tsunami assessment of scleractinian coral cover in the aerial bay group of islands, north Andaman, India. *J. Coast. Conserv.* 17, 671–677. doi: 10.1007/s11852-013-0266-z

Jha, D. K., Vinithkumar, N. V., Sahu, B. K., Dheenan, P. S., Das, A. K., Begum, M., et al. (2015). Multivariate and geo-spatial approach for seawater quality of chidiyatappu bay, south Andaman islands, India. *Mar. pollut. Bull.* 96, 1–2. doi: 10.1016/j.marpolbul.2015.05.004

Jha, D. K., Vinithkumar, N. V., Santhnakumar, J., Nazar, A. K. A., and Kirubagaran, R. (2011). Assessment of post tsunami coral reef resource in pongi balu coast, south Andaman islands. *Curr. Sci.* 100 (4), 530–534. Available at: https://www.currentscience.ac.in/Volumes/100/04/0530.pdf.

Jha, D. K., Rajaprabhu, G, Kirubagaran,, R., Sendhil Kumar, R., Dharani, G., and Das, A. K. (2017). Estimation of potential zones for offshore mariculture in the Indian Sea using geographical information system as a management tool. *J. Coast. Conserv.* 21, 893–902. doi: 10.1007/s11852-017-0556-y

Kumar, T. S., Vijayakumaran, M., Murugan, T. S., Jha, D. K., Sreeraj, G., and Muthukumar, S. (2009). Captive breeding and larval development of the scyllarine lobster petrarctusrugosus, New Zealand. *J. Mar. Freshw. Res.* 43 (1), 101–112. doi: 10.1080/00288330909509985

Mason, R. P. (2013). *Trace Metals in Aquatic Systems*. Blackwell Publishing Ltd.

Mukai, H., Furuta, N., Fujii, T., Ambe, Y., Sakamoto, K., and Hashimoto, Y. (1993). Characterization of sources of lead in the urban air of Asia using ratios of stable lead isotopes. *Environ. Sci. Technol.* 27, 1347–1356. doi: 10.1021/es00044a009

Mozanzadeh, M. T., Safari, O., Oosooli, R., Mehrjooyan, S., Najafabadi, M. Z., Hoseini, S. J., et al. (2021). The effect of salinity on growth performance, digestive and antioxidant enzymes, humoral immunity, and stress indices in two euryhaline fish species: Yellowfin seabream (Acanthopagrus latus) and Asian seabass (Lates calcarifer). *Aquaculture* 534, 736329. doi: 10.1016/J.AQUACULTURE.2020.736329

Murugan, T. S., Remany, M. C., Mary Leema, T., Jha, D. K., Santhanakumar, J., Vijayakumaran, M., et al. (2005). Growth, repetitive breeding, and aquaculture potential of the spiny lobster, panulirus ornatus, new Zealand. *J. Mar. Freshw.* 39 (2), 311–315. doi: 10.1080/00288330.2005.9517311

Noakes, D. (1988). Common strategies of anadromous and catadromous fishes. American fisheries society symposium 1. *Trans. Am. Fish. Soc.* 117 (5), 515–518. doi: 10.1577/1548-8659-117.5.515

Pandey, V., Jha, D. K., Sathish Kumar, P., Santhanakumar, J., Venkatnarayanan, S., Jebakumar, J., et al. (2022). "Effect of multiple stressors on the functional traits of sub-tidal macrobenthic fauna: A case study of the southeast coast of India". *Mar. pollut. Bull.* 175, 113355. doi: 10.1016/j.marpolbul.2022.113355

Pandey, V., Venkatnarayanan, S., Sathish Kumar, P., Ratnam, K., Jha, D. K., Rajaguru, S., et al. (2021). Assessment of ecological health of swarnamukhi river estuary, southeast coast of India, through AMBI indices and multivariate tools. *Mar. pollut. Bull.* 164, 112031. doi: 10.1016/j.marpolbul.2021.112031

Selvaraj, K., Ram Mohan, V., Jonathan, M. P., Siddartha, R., and Srinivasalu, S. (2003). Distribution of nondetrital trace metals in sediment cores from Ennore Creek, Southeast coast of India. *J. Geol. Soc India* 62, 191–204.

Sfakianakis, D. G., Renieri, E., Kentouri, M., and Tsatsakis, A. M. (2015). Effect of heavy metals on fish larvae deformities: A review. *Environ. Res.* 137, 246–255. doi: 10.1016/J.ENVRES.2014.12.014

Srichandan, S., Panigrahy, R. C., Baliarsingh, S. K., Rao B., S., Pati, P., Sahu, B. K., et al. (2016). Distribution of trace metals in surface seawater and zooplankton of the bay of Bengal, off rushikulya estuary, East coast of India. *Mar. pollut. Bull.* 111 (1–2), 468–475. doi: 10.1016/J.MARPOLBUL.2016.06.099

Tovar-Sánchez, A., Sergio, A., and Russell, A. (2004). Temporal and spatial variations in the biogeochemical cycling of cobalt in two urban estuaries: Hudson River estuary and San Francisco Bay. *Estuar. Coast. Shelf Sci.* 60, 717–728. doi: 10.1016/j.ecss.2004.03.010

USEPA (2001). *Methods for collection, storage and manipulation of sediments for chemical and toxicological analyses: Technical manual* (Office of Water, Washington, DC: USEPA).

Vijayakumaran, M., Murugan, T. S., Remany, M. C., Mary Leema, T., Jha, D. K., Santhanakumar, J., et al. (2005). Captive breeding of the spiny lobster, panulirus homarus, New Zealand. *J. Mar. Freshw. Res.* 39 (2), 325–334. doi: 10.1080/00288330.2005.9517313

WHO (World Health Organization) (1989). Heavy Metals Environmental Aspects. *Environ. Health Criteria* (Geneva, Switzerland) 85.

Yasar, D., Aksu, A. E., and Uslu, O. (2001). Anthropogenic pollution in Izmit Bay: heavy metals in surface sediments. *Turk. J. Eng. Environ. Sci.* 25, 299–313.

Yuvaraj, P., Satheeswaran, T., Damotharan, P., Karthikeyan, V., Jha, D. K., Dharani, G., et al. (2018). Evaluation of the environmental quality of parangipettai, southeast coast of India, by using multivariate and geospatial tool. *Mar. pollut. Bull.* 131 (6), 239–247. doi: 10.1016/j.marpolbul.2018.04.022

frontiers | Frontiers in Marine Science

TYPE Original Research
PUBLISHED 07 October 2022
DOI 10.3389/fmars.2022.1008912

Check for updates

OPEN ACCESS

EDITED BY
Meilin Wu,
South China Sea Institute of Oceanology (CAS), China

REVIEWED BY
Thilagam Harikrishnan,
Pachaiyappa's College for Men, India
Abdul Jaleel,
Council of Scientific and Industrial Research (CSIR), India
Marília Cunha-Lignon,
São Paulo State University, Brazil

*CORRESPONDENCE
Behara Satyanarayana
satyam2149@gmail.com
Dipti Raut
raut.dipti2@gmail.com

SPECIALTY SECTION
This article was submitted to Marine Pollution, a section of the journal Frontiers in Marine Science

RECEIVED 01 August 2022
ACCEPTED 20 September 2022
PUBLISHED 07 October 2022

CITATION
Nayak A, Equbal J, Rout SS, Dash B, Thiruchitrambalam G, Bhadury P, Satyanarayana B and Raut D (2022) Macrobenthic community of an anthropogenically influenced mangrove associated estuary on the East coast of India: An approach for ecological assessment.
Front. Mar. Sci. 9:1008912.
doi: 10.3389/fmars.2022.1008912

COPYRIGHT
© 2022 Nayak, Equbal, Rout, Dash, Thiruchitrambalam, Bhadury, Satyanarayana and Raut. This is an open-access article distributed under the terms of the Creative Commons Attribution License (CC BY). The use, distribution or reproduction in other forums is permitted, provided the original author(s) and the copyright owner(s) are credited and that the original publication in this journal is cited, in accordance with accepted academic practice. No use, distribution or reproduction is permitted which does not comply with these terms.

Macrobenthic community of an anthropogenically influenced mangrove associated estuary on the East coast of India: An approach for ecological assessment

Aswini Nayak[1], Jawed Equbal[2], Sonali Sanghamitra Rout[1], Bhagyashree Dash[1], Ganesh Thiruchitrambalam[2], Punyasloke Bhadury[3], Behara Satyanarayana[4,5,6]* and Dipti Raut[1]*

[1]Center of Excellence in Environment and Public Health, Environmental Science Laboratory, Department of Zoology, Ravenshaw University, Cuttack, Odisha, India, [2]Department of Ocean Studies and Marine Biology, Pondicherry University, Port Blair, India, [3]Integrative Taxonomy and Microbial Ecology Research Group, Department of Biological Sciences, Indian Institute of Science Education and Research Kolkata, Mohanpur, West Bengal, India, [4]Mangrove Research Unit (MARU), Institute of Oceanography and Environment, Universiti Malaysia Terengganu, Kuala Nerus, Malaysia, [5]Systems Ecology and Resource Management Research Unit, Université Libre de Bruxelles, Brussels, Belgium, [6]Mangrove Specialist Group (MSG), Species Survival Commission (SSC), International Union for the Conservation of Nature (IUCN), c/o Zoological Society of London, London, United Kingdom

The Mahanadi Estuarine System (MES), with a complex network of freshwater channels, rivers, and mangroves, is a leading seaport in State Odisha on the east coast of India, but subjected to intense human activity in recent years. Such anthropic impingements are known to impact sediment-dwelling biota adversely. However, information on the macrobenthic community of the MES is not well documented yet. Therefore, the primary objectives of this study (February 2013-March 2017) were to address knowledge gaps on the macrobenthic community structure vis-à-vis local environmental conditions and to evaluate the extent of anthropogenic disturbances on macrobenthos. The results from 264 benthic grab samples (van Veen, 0.04 m^2; 2 replicates × 12 GPS fixed locations × 3 seasons) revealed 73 taxa representing 64 genera and 48 families of macrobenthic fauna. The polychaetes (81.41%) and crustaceans (15.42%) were significant faunal groups that contributed mainly to the benthic population and diversity. Multivariate approaches using benthic community attributes and biotic indices (AMBI and M-AMBI) as proxy measures of environmental disturbances proved effective for appraisal. The correlations between the environmental parameters (temperature, pH, salinity) and community estimates were statistically significant. Hierarchical clustering analysis disclosed three major groups (Global R 0.70; $p < 0.002$) influenced by tolerant/opportunist species. The lower abundance, richness, diversity, and dominance of opportunistic species mark the signs of environmental stress.

The community health status remained unbalanced, as indicated by AMBI scoring. M-AMBI analysis contributed best in differentiating areas exposed to diverse impacts and indicated polluted community health status with moderate ecological quality. Our results reiterate the effective use of macrobenthos as bioindicators for ecological status and monitoring. The findings could be utilized for future monitoring assessments, translated into valuable information, and designed into well-defined sustainable management strategies for the MES.

KEYWORDS

macrobenthos, pollution monitoring, Mahanadi estuary, Odisha, Bay of Bengal, AMBI, M-AMBI

Highlights

- Comprehensive assessment of the macrobenthic fauna from a tropical mangrove-associated estuary in India.
- Differential benthic responses to anthropogenic interference examined through a suite of univariate and multivariate analyses.
- Less diverse benthic communities and more opportunistic species marked signs of local environmental stress.
- AMBI and M-AMBI indices differentiated benthic community health/ecological quality in relation to various anthropogenic impacts.
- Macrobenthos effective as bioindicators for habitat monitoring and assessment of the estuary.
- Recommendations for conservation and management of the Mahanadi estuary outlined.

Introduction

Estuaries are naturally stressed bionetworks that exhibit a high degree of variability in their environmental conditions (Elliott and Quintino, 2007). These highly productive ecosystems have been the focal points for various human activities, of which rapid industrialization and indiscriminate urbanization are accountable for divergent pressures and ecosystem degradation (Lotze et al., 2006; John et al., 2017; Dash et al., 2021). Together with extreme climatic events, unprecedented demands of a rapidly increasing population for space, development, and resources have resulted in changes across global estuaries and started questioning the future of the estuaries (Kennish, 2002; Wetz and Yoskowitz, 2013; Elliott et al., 2019). Given the limitations of physicochemical approaches for determining the effects of such disturbances, the importance of macrobenthic investigations are frequently emphasized (Dauvin et al., 2016; Belal, 2019).

With extended life spans, sedentary lifestyles, and varying thresholds of sensitivity to ambient water/sediment conditions, benthic organisms are excellent bioindicators of prolonged environmental variations, mirrored through fluctuations in species composition and abundance (Veiga et al., 2016; Sany et al., 2018a). Furthermore, the distribution patterns of macrobenthos are susceptible to a wide range of anthropogenic interferences and show spatial and temporal shifts accordingly (Dash et al., 2021). Therefore, studies on the macrobenthic communities are increasingly adopted for assessing the health of the aquatic ecosystems (Mulik et al., 2017; Borja et al., 2019; Mulik et al., 2020a; Mulik et al., 2020b; Pandey et al., 2021; Dauvin et al., 2021; Subramanian et al., 2021).

Many tropical estuaries, particularly in South and Southeast Asia, are polluted and over-exploited (Bae et al., 2017; Sarathy et al., 2022). In India, the estuaries have been reported with altered or degraded environmental quality owing to the inadvertent growth of industries and metropolises on the banks of the major rivers (Sigamani et al., 2015; Feebarani et al., 2016; Mulik et al., 2017; Mitra et al., 2018; Mulik et al., 2020a; Mulik et al., 2020b). The increased loads of municipal and industrial effluents, in amounts higher than the assimilatory capacity of the system, are accumulating pollutants and causing hypoxia-like conditions (Mitra et al., 2018; Mulik et al., 2020a; Kumar et al., 2021). Despite the large deltas with some luxuriant estuarine mangrove cover along the east coast of India (in contrast to the west coast), studies that have looked at the effects of changed environmental conditions on macrobenthic fauna are largely limited (Raut et al., 2005; Ansari et al., 2017; Bhowmik and Mandal, 2021; Dash et al., 2021; Pandey et al., 2021).

The Mahanadi estuary at Paradip in the State of Odisha (Figure 1), a leading maritime gateway on the east coast of India, is not exempt from the severe anthropogenic disturbances in recent times (Nayak, 2020). Port/harbor expansion, dredging, increased marine traffic, loss of mangroves, and aquaculture development, amongst others, are some regularly seen activities in the vicinity. Such events, not to mention the additional burdens of pollution and changes in physicochemical conditions of the estuary, show adverse impacts on the sediment-dwelling benthic communities (Nayak et al., 2018), making this study highly relevant.

Identifying the differential response of macrobenthos to environmental changes is crucial for their habitat protection. In this perspective, a suite of univariate and multivariate data analyses remains invaluable (e.g., Clarke et al., 2014; Sany et al., 2018b; Mulik et al., 2020a). Among others, the biotic indices such as AMBI (AZTI's Marine Biotic Index) and M-AMBI (Multivariate AMBI) are robust and used widely for coastal environmental monitoring and benthic quality assessment (Borja et al., 2000; Bald et al., 2005; Muxika et al., 2007; Borja et al., 2014). In addition, these indices glean complex ecological information into easily communicable and understandable scores for possible conservation/management insights (Pinto et al., 2009).

The present study was primarily aimed to provide a state-of-the-art appraisal of the macrobenthos at Mahanadi estuary. The objectives were - (i) to identify macrobenthic communities and their composition in relation to local environmental conditions as an approach for ecological assessment and (ii) to evaluate the extent of anthropogenic disturbances on macrobenthos through the application of marine biotic indices as proxy measures of environmental degradation. This is the first long-term investigation of the hitherto poorly explored Mahanadi Estuarine System (MES). Therefore, it can form the basis for future environmental monitoring, assessment, and management of the region.

Materials and methods

Study area

River Mahanadi, together with its three tributaries - Daya, Nuna, and Bhargavi, discharges into the Bay of Bengal in the State of Odisha on the east coast of India (20°17'08" N; 86°42'24" E) (Figure 1). The mixed semi-diurnal tides with a range of 1.45 to 2.20 m (mean, 1.29 m) reach 13 km upstream (depth 5.19 ± 1.11m) and support a rich diversity of the estuarine (mangrove) flora and fauna (Dey et al., 2013; Palei et al., 2014). According to the Indian Water Resources Information System (I-WRIS, 2021), Mahanadi is one of India's largest and longest (494 km) river systems, with a catchment area of over 65,628 km^2. The leading seaport, 'Paradip' - located 8 km south of the river mouth- is a hub for regional sea-borne trade. With a steadily rising population, the port township is fast developing as a core investment region for petroleum and chemicals (Hazra et al., 2020). Several industries like Indian Farmers and Fertilizers Cooperative Ltd., Paradip Phosphates Limited, Pellet Plant, Indian Oil Corporation Limited, Essar Steel, Ice manufacturing plants, Sea Food Processing units, besides many others, have sprung up in the immediate vicinity, with near denudation of once dense mangrove vegetation fringing the mudflats. Although fishing and cultivation are the traditional livelihood choices of the coastal residents, lucrative shrimp farming has gained precedence in recent years. As a result, the chemicals used for enhancing aquaculture production have been rampant. With the leaching of such substances into the waters, impacts on the estuary are imminent. Besides the untreated sewage from the township, effluents containing oil sludge, sulfur, ash, and gypsum released from industries are proven deterrent to the estuarine ecosystem (Hazra et al., opp. cit. and references therein; SPBO, 2020; Acharyya et al., 2021a; Acharyya et al., 2021b). Overall, the MES has become vulnerable to increased anthropogenic pressures and necessitates further assessment studies.

The climate of Mahanadi Delta is influenced by the premonsoon (March-May), postmonsoon (September-November), and winter (December-February) seasons every year. The southwest monsoon is the major monsoon season during which southwest directional winds blow from June to September. The northwest directional winds influence the winter months (December to February). The weather is typically marked by hot and humid conditions (31.46°C) in April-June and cool and dry (28.66°C) in December-January (https://www.worldweatheronline.com/). The southwest or summer monsoon (mid-June to September) brings heavy precipitation (average, 417.75 mm). The Mahanadi in spate discharges about 45,000 m^3 s^{-1} into the Bay of Bengal (Mohanti and Swain, 2005), reducing salinity and increasing fluvial loads in the nearshore waters. Furthermore, the southwest monsoon winds generate waves up to ~3 m high or more (Dash et al., 2020). As a result, the coast remains wave-dominated throughout the southwest monsoon and mixed wave and tide-dominated in the non-monsoon periods (Mohanti and Swain, opp. cit.).

Samples collection and laboratory analyses

Both biotic (macrobenthos) and abiotic (water and sediment) samples were collected trimonthly for nearly five years, covering the premonsoon, postmonsoon, and winter seasons (February 2013– March 2017). However, the pre-and postmonsoon sampling in 2016-2017 could not be completed due to logistic constraints.

A total of 12 sampling stations - from the river mouth to 13 km upstream (Figure 1), were fixed and reached with the

help of a handheld GPS (Garmin Etrex 72H, Taiwan). The geographic location of the stations also represents various land-use land-cover types and habitat functioning in the vicinity. For instance, St. 1 (river mouth), St. 2 (adjacent to fishing harbor), and St. 11 (upstream area) act as migratory bird's foraging zone (BFZ). Similarly, Sts. 3-8 (adjoining mangroves) are the mangrove-associated zone (MAZ). Intensive shrimp farming (at Sts. 3, 6, and 7) and a factory named Indian Farmers Fertiliser Cooperative Limited (IFFCO) (at St. 8) are also present in the MAZ. The remaining Sts. 9, 10, and 12 adjacent to the country boat berthing facility and Essar Steel India Limited, a leading manufacturer and supplier of steel products and iron ore pellets, stand for the mangrove denuded zone (DZ). In addition, the two bifurcates of River Mahanadi at St. 12 bring considerable freshwater influx at the confluence (Figure 1).

Altogether, 264 sediment samples (in replicates) were collected with the help of a van Veen grab (0.04 m^2). After separating a small fraction of the sediment (~25g) for textural and organic matter analyses, each grab sample was transferred to a 500 µm sieve and gently washed with the seawater for macrobenthos. All specimens retained on the sieve were fixed in 5% buffered formaldehyde with 1% Rose Bengal for further processing and identification in the laboratory. Species-level identification of the macrobenthos (where possible) was carried out under a stereomicroscope (Leica, E24W, Germany) by following the standard literature (Fauvel, 1953; Fauchald, 1977; Abbott and Dance, 1982; Subba Rao et al., 1991; Blake et al., 2009; Yokoyama and Sukumaran, 2012; Muir and Hossain, 2014; Hutchings and Kupriyanova, 2018). The World Register of Marine Species (http://www.marinespecies.org/index.php) was followed to validate the scientific names. The faunal density at each station was expressed as ind. m^{-2}. Further, to estimate the wet biomass (gm^{-2}), preserved specimens were separated into different groups, kept on a mesh, and then moisture blotted out carefully with absorbent paper and weighed (OHAUS PAJ603 electronic balance).

Sand, silt, and clay (%) compositions in the sediment were determined by the pipette method (Krumbein and Pettijohn, 1938) and assigned the textural classes (Shepard, 1954). The organic matter (OM) (%) was estimated by the modified Walkey-Black wet-oxidation method (Gaudette et al., 1974). In the case of hydrographical parameters, salinity (psu), dissolved oxygen (DO) (mg l^{-1}), nitrite-nitrogen (NO_2^-) (µmol l^{-1}), and orthophosphate (PO_4^-) (µmol l^{-1}) were estimated by following the standard protocols (APHA, 1989; Grasshoff et al., 1999). Water temperature (using a mercury-filled thermometer of 0.5°C sensitivity), pH (using a Hanna HI 98107 with ±0.1 accuracy), depth (m) (using echo sounder), and transparency (m) (using a Secchi disc) were measured *in situ*. The instruments were calibrated before recording *in situ* variables in the field.

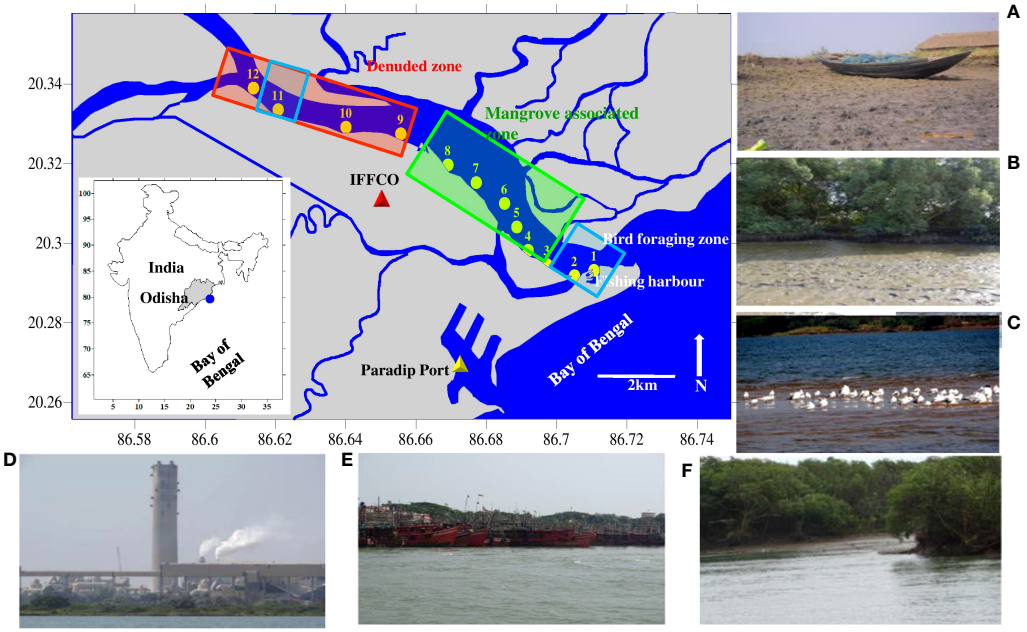


FIGURE 1
Mahanadi estuary in State Odisha on the east coast of India. The sampling stations (1-12) cover the ecotone influenced by the tides, i.e., from the river mouth to 13 km upstream. Examples of each habitat and sources of disturbances are denoted. **(A)** Denuded zone; **(B, C)** Mud flat and bird foraging zone, **(D)** IFFCO factory; **(E)** Fishing harbour, and **(F)** Mangrove associated zone.

Data treatment and statistical analyses

The faunal diversity indices such as mean abundance, species richness (*S*), and Shannon-Wiener index (*H'*) were computed using the PRIMER *v*.7 software (Plymouth Routines in Multivariate Ecological Research) (Clarke and Gorley, 2015). The (square root-transformed) data were used for Bray-Curtis similarity (clustering through hierarchical group-average linking) and non-metric multidimensional scaling (nMDS) ordinations. The significance of sample groupings was tested through the Analysis of Similarities (ANOSIM), whereas confirmatory evidence of the faunal assemblages was provided through the Similarity Profile Analysis (SIMPROF) (Clarke and Ainsworth, 1993). The species abundance matrix was represented by a shade plot where the gradation of shade from grey to black is linearly proportional to the increase in species abundance (Clarke and Gorley, 2015). The unconstrained binary divisive clustering (UNCTREE) analysis further examined both sample and species associations. The environmental data were normalized and subjected to Principal Component Analysis (PCA) to distinguish the sampling sites in relation to their (local) environmental conditions. The analysis of variance (ANOVA) tests was used to probe the spatial and temporal differences. The PCA was carried out using PRIMER *v*.7.

Biotic indices for environmental assessment

AMBI and M-AMBI indices were used to assess the gradient of anthropogenic stress across the MES. The index scores were derived from the AMBI *v*.6 software (http://www.ambi.azti.es). AMBI index is a univariate measure that uses a 'differential weighting' algorithm based on the classification of benthic species into five Ecological Groups (EGs) (i.e., EGI - species very sensitive; EGII - indifferent to enrichment; EGIII - tolerant to excess OME (organic matter enrichment); EGIV - second-order opportunistic species and, EGV -first-order opportunistic species) (Grall and Glémarec, 1997). The macrobenthos of Mahanadi estuary were assigned to different EGs by following the AMBI *v*.6 December 2020 taxa list. In addition, a few taxa not identified up to species level or not found in the AMBI database were also assigned for their respective EGs availing the WORMS database. However, 18.7% of total taxa were either not assigned to any EG or ignored due to irrelevant species (cf. Borja and Muxika, 2005).

The scores of the AMBI index were used to categorize the ecological quality of the estuary into five classes based on a scale from 0 to 7 (0-1.2: high, 1.2-3.3: good, 3.3-4.3: moderate, 4.3-5.5: poor and, >5.5: bad). On the other hand, M-AMBI is a multimetric index that derives scores from multiple factors (species richness, Shannon-Weiner diversity index, and AMBI scores). Further, it requires setting a reference condition (Muxika et al., 2007) of a high ecological quality ratio (EQR) of environmental and biological parameters specific to the habitat (Borja et al., 2012). Reference conditions are characterized by high biological and environmental quality elements giving the site a high ecological quality ratio (EQR) compared to the impacted site (Bigot et al., 2008). The Water Framework Directive (WFD) offers four criteria to select reference conditions: (1) pristine or minor disturbance, (2) historical data, (3) predictive modelling, and (4) expert judgment (Basset et al., 2013). Since finding the less disturbed or pristine environment is as difficult as getting the historical data in the era of 'Anthropocene,' it is always prudent to perform predictive modelling for setting the reference condition. Therefore, an internal control with high diversity, richness, and low AMBI from the dataset was used to set the reference target, and the M-AMBI scores were calculated as suggested by Muxika et al. (2007). The scores of M-AMBI were used to qualify the samples into five grades based on a scale from 0 to 1 (>0.77: high, 0.77–0.53: good, 0.53–0.38: moderate, 0.38–0.20: poor, and <0.20: bad). Procedures adopted to estimate indices scores, algorithm, boundary limits, and community health/ecological quality classifications were based on the WFD scale of indices detailed by Equbal et al. (2017).

The pairwise Mann–Whitney U test was applied to assess differences on a seasonal scale within the faunal groups. Differences were considered significant at $p<0.05$ for all power test analyses. Finally, Pearsons' correlation coefficient test was carried out to find the possible influence of environmental parameters on biotic indices (Graph Pad Software, USA).

Results

Physico-chemical characteristics of water

The water temperature ranged from 21.5 to 36.0°C (mean, 28.34 ± 1.08°C), with the lowest measurements during winter and the highest during premonsoon (Table 1). The upper reaches were relatively warmer than the lower reaches of the estuary (Figure 2). The water pH was slightly alkaline - especially downstream (>7.5), and varied significantly between the seasons (two-way ANOVA $F = 19.89$, $p < 0.01$). With increasing salinity from upstream to downstream, brackish water conditions (9.26 ± 1.87 psu) prevailed along the estuary's entire (13 km long) stretch. Seasonal salinity changed in the order of winter > premonsoon > postmonsoon. The sampling stations in the proximity of industries (e.g., Sts. 8, 9, 10) showed less DO than those adjoining mangroves (Sts. 5, 6, 7). There was a

TABLE 1 Hydrographical and sediment characteristics of Mahanadi estuary during February 2013-March 2017.

Environmental parameters	Premonsoon (n = 36)	Postmonsoon (n = 36)	Winter (n = 60)	Mean (n = 132)
Water				
Temperature (°C)	26.00-37.00	24.00-35.00	21.00-31.00	21.50-36.00
	(31.38 ± 1.49)	(30.03 ± 1.22)	(25.51 ± 1.19)	(28.34 ± 1.08)
pH	1.33-7.96	3.75-8.32	5.93-9.23	2.27-9.19
	(6.86 ± 0.45)	(7.34 ± 0.39)	(7.86 ± 0.26)	(7.44 ± 0.24)
Salinity (psu)	2.49-22.41	0.13-7.04	3.07-24.98	0.13-23.38
	(10.69 ± 1.55)	(0.98 ± 0.48)	(13.37 ± 1.78)	(9.26 ± 1.87)
Dissolved oxygen (mg l^{-1})	0.16-7.52	2.40-8.00	0.80-8.96	1.04-8.56
	(4.31 ± 0.73)	(5.26 ± 0.69)	(4.44 ± 0.81)	(4.63 ± 0.44)
Nitrite-nitrogen (µmol l^{-1})	0.84-34.83	0.29-6.98	0.32-25.24	0.34-21.23
	(4.21 ± 1.51)	(1.90 ± 0.38)	(3.31 ± 1.21)	(3.17 ± 0.75)
Orthophosphate (µmol l^{-1})	0.08-29.16	0.08-20.60	0.37-23.74	0.31-22.62
	(5.55 ± 2.18)	(4.34 ± 1.55)	(3.79 ± 1.19)	(4.42 ± 1.06)
Transparency (m)	0.34-0.85	0.21-0.55	0.64-1.77	0.21-1.77
	(0.55 ± 0.05)	(0.35 ± 0.03)	(0.95 ± 0.09)	(0.62 ± 0.18)
Depth (m)	2.00-7.00	5.00-12.00	3.00-9.00	2.00-12.00
	(4.00 ± 0.60)	(7.00 ± 0.70)	(5.00 ± 0.53)	(5.19 ± 1.11)
Sediment				
Sand (%)	14.11-98.85	3.27-94.14	5.94-95.64	3.27-98.85
	(45.80 ± 9.83)	(41.99 ± 13.60)	(53.00 ± 8.46)	(48.03 ± 6.52)
Silt (%)	1.10-85.79	5.84-96.28	4.31-93.99	1.10-96.28
	(53.94 ± 9.86)	(57.86 ± 13.57)	(46.90 ± 8.45)	(51.81 ± 6.51)
Clay (%)	0.04-0.76	0.02-0.76	0.00-0.76	0.00-0.76
	(0.26 ± 0.11)	(0.15 ± 0.09)	(0.10 ± 0.04)	(0.16 ± 0.05)
Organic matter (%)	0.24-6.63	0.28-4.05	0.07-5.08	0.07-6.63
	(1.70 ± 0.37)	(1.96 ± 0.44)	(1.67 ± 0.28)	(1.76 ± 0.24)

Values are given as minimum-maximum (mean ± standard error).

significant difference in DO between pre-and postmonsoon periods (one-way ANOVA F =4.61, p< 0.05).

The distribution of dissolved nutrients revealed higher concentrations of NO_2^- (3.17 ± 0.75 µmol l^{-1}) and PO_4^- (4.22 ± 1.06 µmol l^{-1}) at the stations close to shrimp farms and industries (e.g., Sts. 7, 8, 11). Nutrient enrichment was high during the premonsoon, followed by postmonsoon and winter seasons (Table 1). The sampling stations subjected to higher anthropogenic intervention and upstream fluvial loads (Sts. 7-12) also had a lower water column transparency. The waters are more turbid for postmonsoon (0.35 ± 0.03) than premonsoon (0.55 ± 0.05) or winter (0.95 ± 0.09). Station-wise environmental parameters for each year and season are provided as Supplementary Data (STable 1).

Sediment characteristics

The estuarine sediments were comprised mostly of sand (48.03 ± 6.52) and silt (51.81 ± 6.51) (Table 1), with three distinct textural classes (i.e., silty sand, sandy silt, and silt). The OM ranged from 0.07 to 6.63% and was rather high at the creek/canal confluence locations (Figure 2). The correlation between textural grades and OM was clear. For instance, sediments from the river mouth (St. 1) and upstream (St. 12) with a high sand composition contained less OM in contrast to the mangrove sediments (Sts. 2-9) with a high silt composition. Seasonally, silt was distinctive of the postmonsoon. The sediment textural classes also indicated significant spatial and temporal variations (two-way ANOVA, sand F=3.23, $p < 0.05$; silt F=3.18, $p < 0.05$; clay F=10.89, $p < 0.01$).

The PCA revealed significant eigenvalues (>1), and the percentage of variance was 31.9% for PC1, followed by 26.9% for PC2. While most stations in the MAZ with silt and OM were on the positive side of the two axes, the sites of the DZ with a sand abundance were on the negative side (Figure 3). Overall, the first axis had segregation of stations based on their sediment nature, and the second axis was based on their water characteristics. The stations belonging to BFZ were closely associated with the water quality (salinity, DO, pH, NO_2^-) (Figure 3).

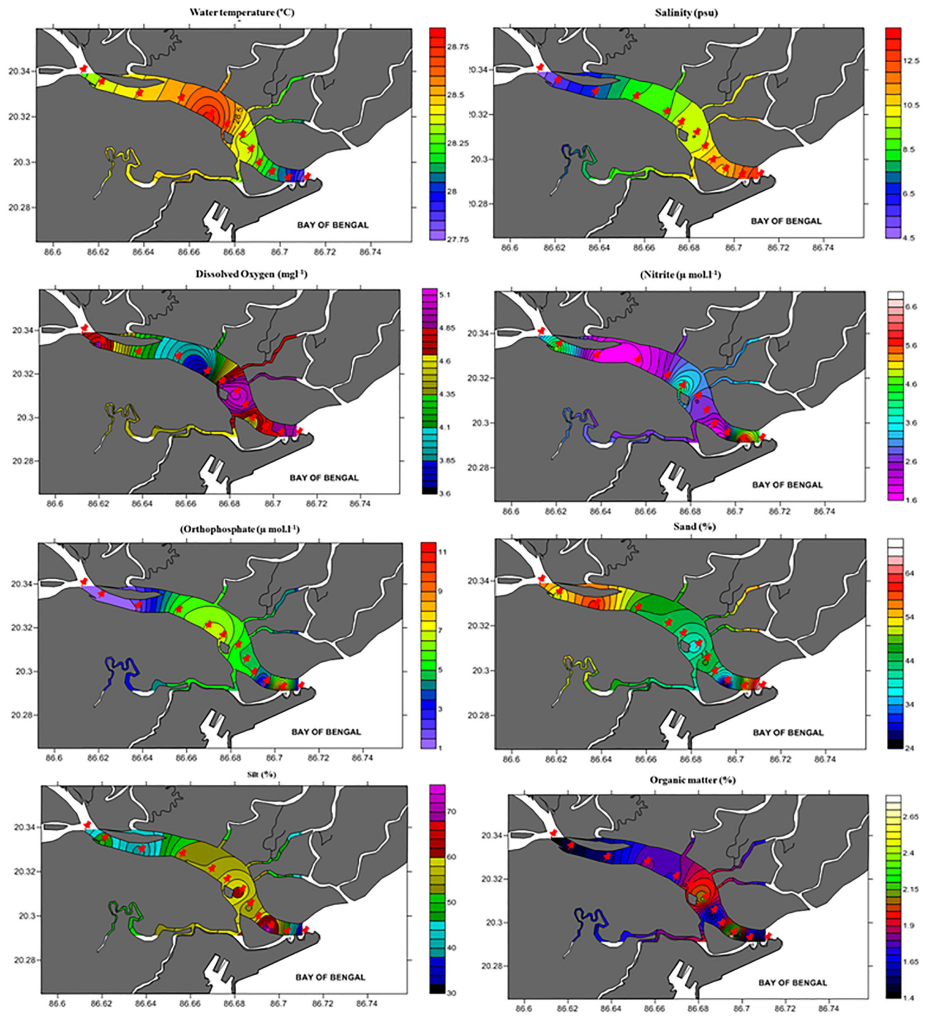


FIGURE 2
Spatial distribution patterns of hydrographical (water temperature, salinity, dissolved oxygen, nitrite, and orthophosphate) and sediment (sand, silt, and organic matter) variables in Mahanadi estuary.

Macrobenthic community

The present study recorded 100,500 individuals from 73 taxa, 64 genera, and 48 families represented by major faunal groups such as Polychaeta, Brachiopoda, Sipuncula, Crustacea, Mollusca, Echinodermata, and Pisces. However, polychaetes (81.41%), and crustaceans (15.42%) were found to be important in terms of their abundance (Table 2). Within Polychaeta, families such as Spionidae (9 species), Capitellidae (4 species), and Nereididae (4 species) were the most diverse and dominant groups, contributing 48% to the total population. The notable species of polychaetes were nereid *Perinereis cavifrons*, nephtyid *Micronephthys oligobranchia*, spionids *Dipolydora coeca*, *Malacoceros indicus*, and *Polydora cornuta*. The important species of crustacean and molluscs included *Victoriopisa chilkensis*, *Psammacoma gubernaculum*, and *Nassarius stolatus*, with their juvenile populations (Table 2).

The macrobenthic faunal abundance ranged between 50 and 3,213 ind. m^{-2} (760 ± 727) (Table 2) was high at the BFZ in winter (mean, 2,288 ind. m^{-2}) and postmonsoon (3,213 ind. m^{-2}). In particular, the prevalence of *P. cavifrons* for these two seasons (773-970 ind. m^{-2}) is noteworthy. The faunal abundance of the BFZ varied significantly between premonsoon and postmonsoon (Mann–Whitney test, $p = 0.00$), whereas it differed between premonsoon and winter for the MAZ (Mann–Whitney, $p = 0.03$). The wet weight biomass was low in upstream (e.g., 0.03 gm^{-2} at St. 9) than in the downstream areas (25 gm^{-2} at St. 2). The macrobenthic faunal abundance data (Polychaeta, Mollusca, and Crustacea) tested for seasonal, species and station wise changes together with their interaction effects revealed significant

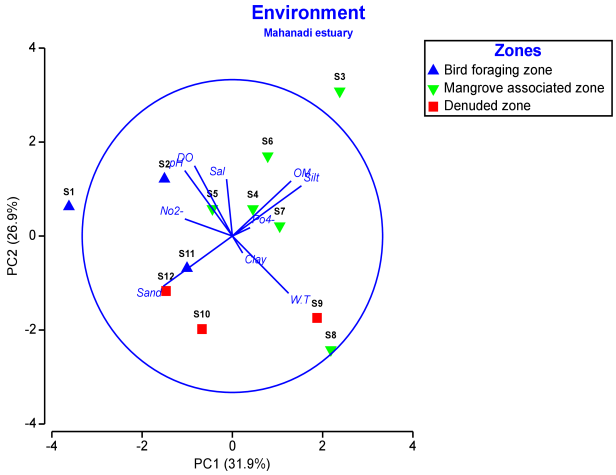


FIGURE 3
Principal Component Analysis (PCA) depicting the influence of environmental variables on the sampling (1-12) sites of the Mahanadi estuary during 2013-2017.The circle represents the correlation circle, and the orientation of the environmental parameters (lines) approximate their correlation to each other and to the ordination axes (DO = dissolved oxygen, Sal = salinity, OM = total organic matter, NO_2^- = nitrite-nitrogen, $PO4^-$ = orthophosphate, WT = water temperature). The MAZ (n = 66) – Mangrove associated zone includes St. 3, 4, 5, 6, 7, and 8, The BFZ (n = 33) – Birds foraging zone includes St. 1, 2 and 11, and the DZ (n = 33) – Denuded zone is represented by St. 9, 10 and 12.

differences, particularly for the molluscs (Table 3). Station-wise data on macrobenthic faunal abundance for each season were provided in the supplementary information (STable 2).

Macrobenthic assemblages

The abundance and distribution of 49 macrobenthic species at one or more sampling stations in the estuary accounted for ≥1% of the total population. Hierarchical clustering and nMDS plots have shown a clear-cut separation of the sampling stations into three major faunal groups (Global R 0.70; $p < 0.002$) (Figure 4). Group I, representing the BFZ (Sts. 1, 2, and 11), was dominated by *Perinereis cavifrons*, *Cossura coasta*, and *Dendronereis aestuariana* species ($\pi = 1.07$, $p < 0.07$), whereas Group II, for the MAZ (Sts. 3-8), is characterized by *Micronephtys-Victoriopisa-Heteromastus* assemblage. The sampling sites of DZ (Sts. 9, 10, and 12) as Group III contained *Cossura-Dipolydora-Malacoceros* assemblage. The UNCTREE analysis further confirmed the presence of these three faunal clusters (BFZ - Global *R*: 1, B%: 31.1, π: 2.59; MAZ- Global *R*: 0.61, B%: 48, π:1.06; DZ - Global *R*: 1, B%: 64.2, π: 1.07 (Figure 5).

Ecological groups (EGs)

Altogether, 61 macrobenthic species (out of 73) were categorized into their corresponding EGs (Table 2). Except for EGV (one species), the other groups were diverse and represented by 12-17 taxa. The highest faunal (mean) density was contributed by EGIV (36.4%), followed by EGII (20.8%), EGIII (20.5%), EGI (19.5%), and EGV (2.7%). The species such as *Heteromastus filiformis*, *C. coasta*, *D. coeca* (of EGIV), *P. cavifrons* (EGIII), *M. oligobranchia* (EGII), and *V. chilkensis* (EGI) were abundant, and collectively formed 60% of the total population. The faunal composition of MAZ (41.5%) and DZ (38.3%) was dominated by EGIV organisms, while BFZ (36.6%) by the EGIII (Figure 6). Seasonally, both premonsoon (41.7%) and winter (35.3.%) periods were characterized by EGIV and the postmonsoon (35.3.%) by EGIII species.

AMBI and M-AMBI indices

According to the AMBI scores, the estuary's ecological quality was *good* throughout except for St. 8, which had *moderate* conditions (Table 4). The AMBI scores improved from the premonsoon to the winter period. In this context, the samples with *poor* to *moderate* status from MAZ and BFZ (Sts. 2 and 7-9) in the premonsoon were represented by *moderate* to *good* status during the postmonsoon and winter (Figure 6B). The differences between premonsoon and winter were significant (Mann-Whitney, $p = 0.01$). Also, the sampling stations in the DZ were depicted with *good* ecological quality. However, in terms of community health, the estuary was unbalanced and polluted (Table 4).

In contrast to AMBI, the M-AMBI scores classified around 60% of the samples as *moderate* and 33.3% as *good* quality. M-AMBI followed a trend similar to that of AMBI, improving sample grades from the premonsoon to the winter period (Figure 6C). Except for St. 12 and St. 9 (DZ), where samples

10.3389/fmars.2022.1008912

TABLE 2 Numerical abundance of macrobenthic fauna and their assignment to ecological groups (EGs-Ecological groups, NA-Not assigned, IG-Ignored, SD-standard deviation).

Species/Taxa	EGs	Mean (ind.m^{-2})	SD	Min	Max	% Contribution	% Relative frequency
Polychaeta							
Orbinia sp.	IV	0.9	3.5	13	25	0.11	6.06
Aricidea sp.	NA	11.9	28.7	13	150	1.57	31.06
Cossura coasta	IV	48.6	194.3	13	1388	6.38	17.42
Cossura sp.	IV	24.5	80.6	13	550	3.22	24.24
Boccardia sp.	III	0.2	2.2	13	25	0.02	0.76
Heterospio sp.	II	1.1	8.5	13	75	0.15	2.27
Malacoceros indicus	III	23.6	73.1	13	713	3.10	38.64
Dispio sp.	III	0.5	2.4	13	13	0.06	3.79
Magelona cincta	I	7.7	23.3	13	138	1.01	12.12
Polydora cornuta	IV	22.8	210	13	2388	3.00	6.82
Dipolydora coeca	IV	47.3	127.8	13	900	6.22	38.64
Pseudopolydora kempi	IV	2.9	10.2	13	75	0.39	10.61
Paraprionospio sp.	IV	5.7	32.7	13	363	0.75	11.36
Prionospio polybranchiata	III	8	33.6	13	250	1.04	12.88
Cirriformia filigera	IV	0.8	5.9	13	63	0.10	2.27
Capitella species complex	V	10.1	35.2	13	288	1.33	15.91
Heteromastus filiformis	IV	61	112.6	13	588	8.01	48.48
Mediomastus sp.	III	7.2	39.9	13	388	0.94	6.82
Notomastus aberans	III	2.8	12.8	13	88	0.37	6.06
Euclymene annandalei	I	6.1	31.5	13	288	0.80	9.09
Hypereteone barantollae	II	0.7	2.8	13	13	0.09	5.30
Pisione sp.	I	0.3	1.9	13	13	0.04	2.27
Hesione sp.	II	0.3	2.4	13	25	0.04	1.52
Ancistrosyllis sp.	III	0.3	3.3	38	38	0.04	0.76
Hermundura annandalei	II	9	28.3	13	188	1.18	18.18
Syllis sp.	II	0.8	3.4	13	25	0.10	5.30
Perinereis cavifrons	III	126.9	467.3	13	2788	16.66	19.70
Namalycastis indica	IV	0.3	2.4	13	25	0.04	1.52
Dendronereis aestuarina	III	22.4	83.2	13	800	2.95	28.03
Neanthes chingrighattensis	IV	21.8	54.1	13	300	2.86	36.36
Glycera alba	IV	10.6	22.2	13	125	1.39	29.55
Glycera sphyrabrancha	II	16.4	45.4	13	300	2.15	20.45
Micronephthys oligobranchia	II	80	138.7	13	1000	10.51	56.06
Nephtys polybranchia	II	0.9	8.8	13	100	0.12	2.27
Cryptonome parvecarunculata	IG	1	8	13	88	0.14	3.03
Diopatra sp.	I	4.1	14.2	13	88	0.53	9.85
Lumbrineris simplicis	II	2.3	6.3	13	38	0.30	13.64
Lumbrinereis sp.	II	0.6	3.4	13	25	0.07	3.03
Sternaspis sp.1	III	8.4	42.3	13	375	1.11	9.85
Sternaspis sp. 2	III	3	15.1	13	100	0.40	5.30
Melinna aberrans	III	5.3	18.9	13	150	0.70	12.12
Pectinaria sp.	I	0.4	2.6	13	25	0.05	2.27
Terebella ehrenbergi	III	0.9	3.8	13	25	0.11	5.30
Myriochele sp.	II	4.8	18.3	13	150	0.63	12.12
Fabriciola sp.	I	4.8	15.1	13	88	0.63	15.15
Brachiopoda							
Lingula sp.	I	2.3	10	13	88	0.30	7.58

(Continued)

TABLE 2 Continued

Species/Taxa	EGs	Mean (ind.m^{-2})	SD	Min	Max	% Contribution	% Relative frequency
Sipunculida							
Sipunculid sp.	I	0.9	6.9	13	75	0.11	2.27
Crustacea							
Belzebub hanseni	NA	0.2	1.5	13	13	0.02	1.52
Paracaprella pusilla	I	2.6	7.4	13	38	0.34	12.88
Corophium volutator	III	12.6	129.6	25	1488	1.65	3.79
Victoriopisa chilkensis	I	76.6	172	13	1525	10.06	69.70
Cumacid sp.	I	6.3	39.1	13	413	0.82	9.09
Cyathura sp.	III	5.3	34.1	13	275	0.70	6.82
Exosphaeroma parva	III	3.3	23.2	13	250	0.44	4.55
Sphaeroma sp.	II	3	18.3	13	150	0.40	5.30
Harpacticid sp.	IG	0.5	5.4	63	63	0.06	0.76
Macrobrachium sp.	NA	5.7	16.5	13	88	0.75	15.91
Clibanarius sp.	IG	0.5	2.4	13	13	0.06	3.79
Crab juveniles	IG	0.9	4.3	13	38	0.12	6.06
Gastropoda							
Paratectonatica tigrina	II	0.7	7.6	88	88	0.09	0.76
Pirenella cingulata	I	0.4	2.6	13	25	0.05	2.27
Nassarius foveolatus	II	0.2	2.2	25	25	0.02	0.76
Nassarius stolatus	II	2.3	8	13	63	0.30	9.85
Agaronia gibbosa	IG	0.2	1.5	13	13	0.02	1.52
Gastropod juveniles	NA	2.5	6.4	13	38	0.32	15.91
Bivalvia							
Nucula sp.	I	0.2	2.2	25	25	0.02	0.76
Acrosterigma variegatum	III	0.1	1.1	13	13	0.01	0.76
Psammacoma gubernaculum	I	3.9	18.8	13	175	0.51	10.61
Meretrix sp.	I	0.3	1.9	13	13	0.04	2.27
Bivalve juveniles	IG	2.5	6.8	13	38	0.32	13.64
Echinoderms							
Ophiuroid juveniles	II	1.4	5	13	38	0.19	9.09
Pisces							
Periophthalmus sp.	IG	3.9	10.9	13	88	0.51	18.18
Boleophthalmus boddarti	IG	1.3	10.2	13	113	0.17	3.79
Diversity indices							
Abundance (ind. m^{-2})		760.6	727.9	50	3213		
Biomass (g m^{-2})		1.8	3.4	0.03	25		
Species richness (*S*)		8.7	4.6	2	24		
Shannon-Weiner index ($H'log_2$)		2.2	0.8	0.1	3.9		

The sample size n = 132 (mean of duplicate 264 grab samples).

were downgraded from *good* (premonsoon) to *moderate* (postmonsoon and winter) and *moderate* (premonsoon and postmonsoon) to *poor* condition (winter). A unidirectional shift in quality grades was observed at St. 2 (BFZ), where samples upgraded from *poor* (premonsoon) to *moderate* (postmonsoon) and *good* condition (winter). In contrast, the samples from Sts. 6, 7, and 8 (MAZ) and St. 10 (DZ) showed quality improvement only during the winter period (Figure 6C). Both spatial and temporal differences in the M-AMBI scores of the BFZ (ANOVA F=9.2, P <0.001) and the MAZ were significant (F=.3, P=0.04).

Relationship between the estuarine environment and macrobenthos

The Pearson's correlation coefficients indicate a significant relationship between water quality parameters and benthic (AMBI

TABLE 3 Result of three-way ANOVA of macrobenthic faunal abundance data (Polychaeta, Mollusca, and Crustacea): Comparing the significance of seasonal, species, station differences, and their interaction effects (*p< 0.05, **p< 0.01, ***p< 0.001).

Group	Source	Degrees of Freedom	Mean Sum of Squares	Snedecor's F ratio	Remarks
Polychaeta	Between seasons (A)	2	72.63	2.38	p > 0.05
	Between species (B)	44	159.52	5.23***	p< 0.001
	Between stations (C)	11	99.99	3.28**	p< 0.01
	AB interaction	88	67.44	2.21**	p< 0.01
	BC interaction	484	48.28	1.58**	p< 0.01
	AC interaction	22	20.02	0.66	p> 0.05
	Error	968	30.52		
Mollusca	Between seasons (A)	2	0.45	7.74**	p< 0.01
	Between species (B)	10	0.30	5.14**	p< 0.01
	Between stations (C)	11	0.14	2.51**	p< 0.01
	AB interaction	20	0.11	1.94**	p< 0.01
	BC interaction	110	0.07	1.25*	p < 0.05
	AC interaction	22	0.11	1.86**	p< 0.01
	Error	220	0.06		
Crustacea	Between seasons (A)	2	1.09	0.14	p> 0.05
	Between species (B)	13	87.27	11.07***	p< 0.001
	Between stations (C)	11	9.64	1.22	p> 0.05
	AB interaction	26	5.15	0.65	p>0.05
	BC interaction	143	10.04	1.27*	p<0.05
	AC interaction	22	10.88	1.38	p> 0.05
	Error	286	7.89		

and M-AMBI) indices, whereas sedimentary attributes did not show any marked association (Table 5). Among the water quality parameters, temperature, pH, and salinity were influential in assessing community health. The distribution of macrobenthos in EGI, EGIII, and EGIV seems to have been governed by temperature, pH, salinity, and DO conditions (Table 5).

Discussion

Environmental status of Mahanadi estuary

As physically controlled ecosystems, estuaries are characterized by wide variabilities in their local environmental conditions. The environment, however, becomes imbalanced and stressed when exposed to increased anthropogenic stressors (Kennish, 2005; Brown et al., 2022; Suzzi et al., 2022).

Among the environmental variables observed for the MES, the water temperature was strongly marked by seasonality. In this case, other atmospheric influences, such as precipitation, nearshore sea temperatures, and river run-offs, are likely to influence its variability (Leal Filho et al., 2022). High water temperature in the premonsoon was evident in the present study. The other traceable stressors like municipal wastes, sewage, and litter from Paradip port city, fisher hamlets, and fishing harbour that enter the estuary through Atharbanki, a mangrove channel, are also found to affect the water quality to a greater extent. Nutrient enrichment at the stations close to BFZ, shrimp farms, and the fertilizer industry (Sts. 1-3 and 6-8) can be explained by avifaunal excrements and untreated effluents. The low pH in the proximity of industries (Sts. 8-9) is attributable to the influx of acidic wastes (Sundaray et al., 2009; Acharyya et al., 2021a; Acharyya et al., 2021b). On the other hand, (acidic) humic substances carried by freshwater in colloidal suspension get coagulated upon meeting the seawater and can shift the pH to an alkaline condition (Beer, 1996). The latter was apparent from the downstream measurements at the Mahanadi estuary and was similar to findings from other estuaries elsewhere (Mohanty, 2018; Habib et al., 2021; Jabir et al., 2021).

The east-flowing rivers in India, the Brahmaputra, Ganges, Irrawaddy, Godavari, Mahanadi, Krishna, and Cauvery, contribute significantly to the total freshwater discharge into the Bay of Bengal (BoB) (from 1.5×10^{12} m^3 to 1.83×10^{13} m^3 per year) (Varkey et al., 1996; Thadathil et al., 2002). These rivers have a maximum climatological discharge between July and September when the southwest monsoon rainfall is at its peak and decreases gradually to a minimum during the winter and premonsoon (Sandeep and Pant, 2019). Hence, salinity with an increasing gradient towards the mouth of the estuary was low for the wet (monsoon) season and high for the dry (winter) season. Higher DO at Sts. 5-7 of the MAZ could be due to

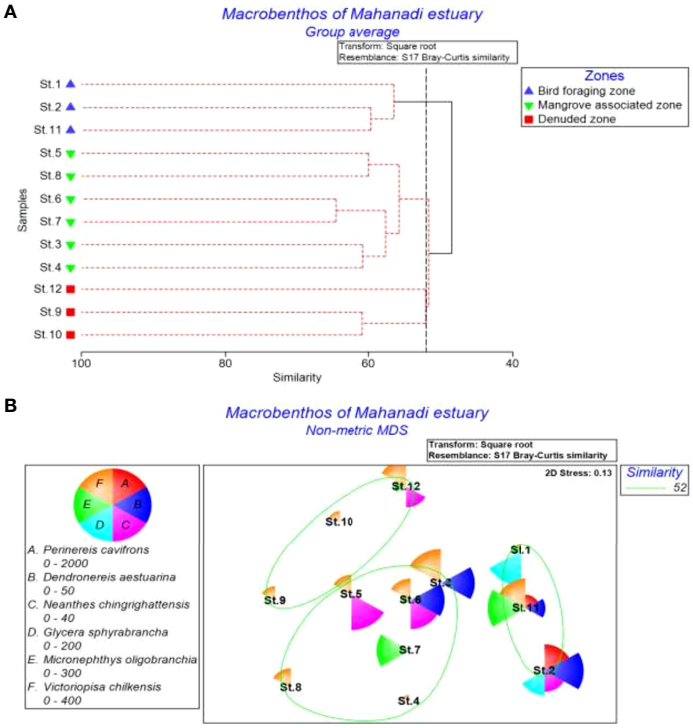


FIGURE 4
(A) Bray-Curtis similarity and **(B)** n-MDS ordination showing sampling (1-12) site groupings based on macrobenthic abundance data in the Mahanadi estuary (similarity: 48.7%).

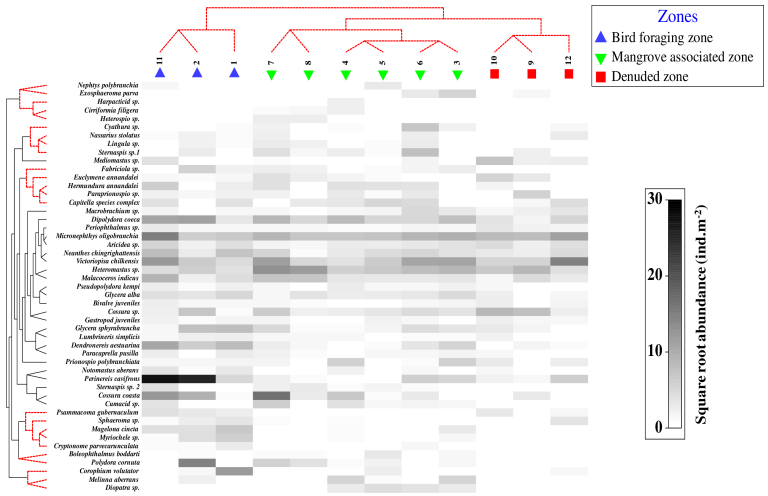


FIGURE 5
Macrobenthic communities of Mahanadi estuary in 2013-2017: Shade plot, a visual representation of abundances (averaged over seasons) of 49 macrobenthic species accounting for ≥ 1% or ~1% of the total abundance at one or more sampling sites. Groups are named Bird foraging zone, Mangrove associated zone, and Denuded zone with linear greyscale intensity proportional to square root transformation abundance (ind.m^{-2}). The three significantly different sub-clusters marked by SIMPROF-powered UNCTREE analysis (X-axis) are evident.

sustained autotrophic production in the waters. This process originates through nutrient-rich outwelling from the adjacent mangroves during inundation regimes (Cohen et al., 2004; Prasad and Ramanathan, 2008). However, land-based sulphate leaching from the gypsum dumps (heaped close to the fertilizer industry), and industrial effluents, besides others, are the drivers of near hypoxia conditions at Sts. 8-10 (cf. Nayak et al., 2018; Taillardat et al., 2020; Sharma et al., 2022). Depletion in DO is a strong indicator of poor water quality (Costa et al., 2018). Such low DO can prolong hypoxia and affect major estuarine ecosystem-level processes, including fluxes and rates linked to carbon and nitrogen biogeochemical cycling. Therefore, maintaining the best possible conditions across the river basins, including coastal and offshore waters, is essential (Karydis and Kitsiou, 2013; Barletta et al., 2019) and crucial for ecosystem functioning and maintaining estuarine biodiversity (Ghosh et al., 2022).

Fine sediment deposition is difficult in the regions where strong water currents persist (Mitchell, 2020). Low fine particle accretion, sandy texture, and lesser OM at seaward (St. 1) and near confluence sites (Sts. 10, 12) support this phenomenon in the study area. Similarly, mud (silt and clay) accruals occurred mainly in sheltered seascapes (mangrove-fringed sites, Sts. 3-8) due to weak tidal currents and land-based fine particle sources. Muddy sediments retained more OM (>2%) than sandy sediments because of the better adsorption capacity of the fine-grained particles (Gaonkar et al., 2021; Haddout et al., 2022). Furthermore, litter from mangrove vegetation (leaves, propagules, and twigs) and subsurface root growth significantly deliver organic carbon to mangrove sediments (Alongi, 1998). Therefore, sites adjoining mangroves revealed higher OM arising from autogenic sources and outwelling (Hossain et al., 2014; Mohanty et al., 2019).

Reliable information on aquatic resources is key to improving their management (Karydis and Kitsiou, 2013). Furthermore, the competence in accommodating changes (episodic or permanent) to managerial plans requires an in-depth understanding of the drivers of water quality deviations and the availability of natural resources at different timescales (Costa et al., 2018). Anthropogenic activities have significantly threatened the Mahanadi estuary's water quality and biota. As a result, continuous monitoring and potential corrective measures are required to mitigate such effects.

Macrobenthos of Mahanadi estuary

Studies on the macrobenthos of the MES and adjacent mangrove waterways/intertidal mudflats are confined mainly to taxonomic accounts, without much inference to the local environmental conditions (Deb, 1998; Pattanayak and Haldar, 1998; Rao, 1998; Surya Rao and Maitra, 1998; Nayak et al., 2018; Tudu et al., 2018; Mohanty et al., 2022). In recent years, industrial expansion has become disproportionately rapid along major waterways due to well-connected transport hubs and habitation sites, as is the case for the MES. The complex network of creeks and canals acting as vectors and sink for the effluents released from the port town, fishing harbour/landing centers, industrial units, etc. (Rodgers et al., 2020) shows significant consequences on the benthic communities.

Macrobenthic diversity and dominance patterns in the Mahanadi estuary reflected varying degrees of natural and man-induced stressors. Spatial and temporal benthic faunal distribution appeared to be primarily structured by sediment texture, OM, salinity, and pH. For instance, the abundance of polychaetes in the estuary could represent their tolerance to a wide array of (shifting/changing) environmental conditions (Sanchis et al., 2021). The deposit-feeding *P. cavifrons* is an important link between detritus accumulation and higher trophic levels. As an opportunist, *P. cavifrons* can repopulate in defaunated areas where the perturbations like dredging (St. 2, opposite to fishing harbour) and mangrove denudation (sites in the proximity of industries) occur. Furthermore, the capitellids, including *Heteromastus*, spionids, and *Magelona* spp., exhibit a natural proliferation in fine-muddy sediments (Afli et al., 2008; Sivadas and Ingole, 2016), while *Paraprionospio* and *Magelona* spp. survive in hypoxic and lesser competitive environments inhospitable to their predators and competitors (Sivadas et al., 2021). The impoverished faunal trends noticed towards the estuary mouth (St. 1) and upstream (St.12) also confirm the observations of Shirodkar and Nayak (2010). Macrobenthos in the proximity of shrimp farms and industries (IFFCO, Essar Steel) could represent the impacted environmental conditions as pollution indicators (Borja et al., 2000; Dauvin et al., 2012; Albano et al., 2013; Shivarudrappa et al., 2019). Seasonally varied diversity indices are perceptible, with maximum abundance in the winter (Kundu et al., 2010). The findings of this study were consistent with other regional (Mulik et al., 2017; Dias et al., 2018; Rehitha et al., 2019; Sivadas et al., 2021; Subramanian et al., 2021; Kumar et al., 2022; Rehitha et al., 2022) and global (Abrogueña et al., 2021; Bravo et al., 2021; Dauvin et al., 2021; Salimi et al., 2021; Sánchez-Ovando et al., 2021; Kanhai, 2022) benthic evaluations.

An estuary is a dynamic environment where the macrobenthos are adapted to live in widely shifting environmental conditions over relatively short distances (Ortega et al., 2018). The benthic assemblages of Mahanadi estuary are distinct in relation to the local environmental settings. For example, the heterogeneity in *Micronephtys-Victoriopisa-Heteromastus* assemblage of the MAZ could represent anthropic interventions (through industries, ferry traffic, mangrove destruction, and shrimp farms) modifying the habitat and its preference for the sediment composed of silty-sand and high OM. Also, *Cossura-Dipolydora-Malacoceros* assemblage of the DZ, under similar man-made disturbances (boat berthing, Essar steel), occupied the sediment with silt and

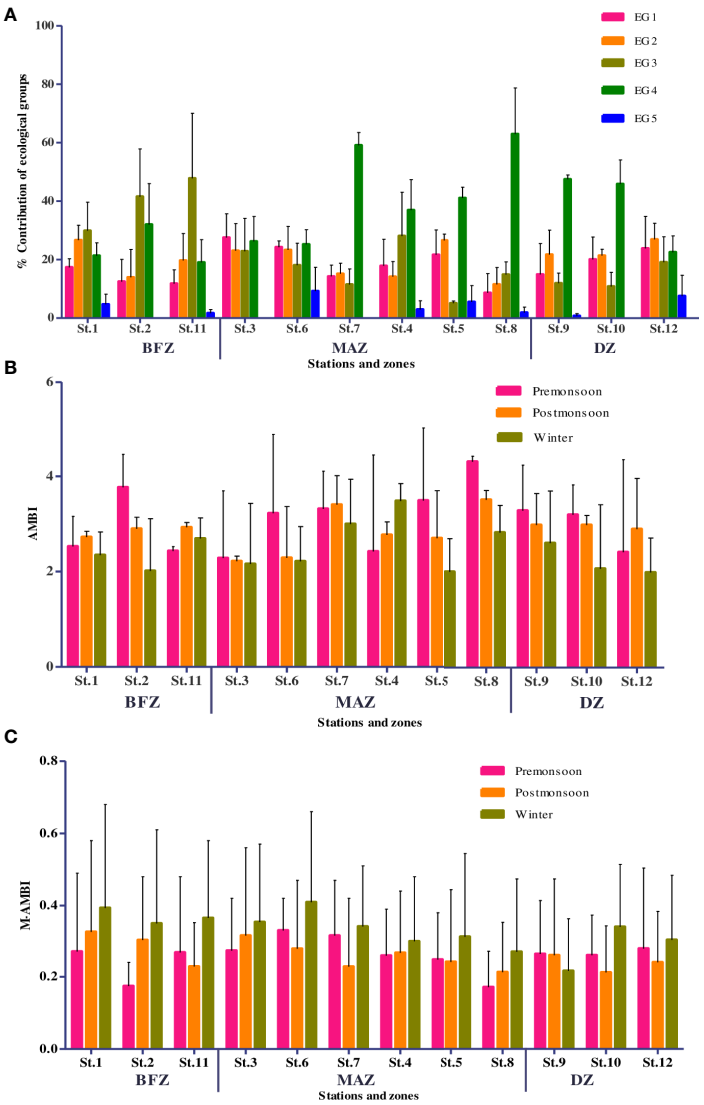


FIGURE 6
(A) Ecological groups associated with stations/zones of Mahanadi estuary; **(B)** AMBI and **(C)** M-AMBI seasonal variations across stations/zones in Mahanadi estuary.

high OM. Therefore, each zone showed the macrofaunal responses to diverse stressors in the vicinity. The effect could be revealed through a low diversity, which testifies to the relationship between biodiversity loss and human-induced disturbances (D'Alessandro, 2020).

Benthic quality status of the Mahanadi estuary

Apart from the anthropogenic interventions, monsoon-mediated perturbations also lead to a high degree of substrate heterogeneity and changes in the structure and function of biological communities in the estuary (Sivadas et al., 2011). The benthic community attributes such as abundance, richness, and diversity fluctuate mostly through defaunation, migration, and spawning of species with recovery followed by stable conditions, recruitment, and resettlement (Gaonkar et al., 2013; Sivadas et al., 2021). As a result, tolerant or opportunist species often dominate these communities, exhibiting a highly dynamic population under specific situations (Sivadas et al., 2016). The health assessment of the MES based on the biotic indices demonstrated a high agreement with inferences extracted from benthic community structures against natural or anthropogenic disturbances.

TABLE 4 Results of AMBI, M-AMBI and biodiversity of macrobenthos from Mahanadi estuary, during February 2013-March 2017.

Stations	EG I (%)	EG II (%)	EG III (%)	EG IV (%)	EG V (%)	Mean AMBI	Disturbance classification (based on AMBI)		N (ind.m^2)	S	H'log$_2$	Mean M-AMBI	Disturbance classification (based on M-AMBI)	
							CHs	EQs					CHs	EQs
St.1	17.98	28.21	26.99	22.46	4.36	2.50	Unbalanced	Good	716.27	12.00	2.84	0.60	Unbalanced	Good
St.2	15.16	17.40	37.29	30.14	0.00	2.74	Unbalanced	Good	1507.18	10.55	1.88	0.48	Polluted	Moderate
St.3	30.25	19.71	22.15	27.59	0.00	2.21	Unbalanced	Good	654.82	9.36	2.36	0.53	Unbalanced	Good
St.4	16.28	15.54	24.05	40.09	4.04	3.02	Unbalanced	Good	430.91	7.55	2.13	0.45	Polluted	Moderate
St.5	24.59	26.14	4.91	39.83	4.55	2.60	Unbalanced	Good	353.64	7.45	2.23	0.47	Polluted	Moderate
St.6	25.02	22.61	20.23	24.27	7.92	2.51	Unbalanced	Good	694.55	11.09	2.44	0.55	Unbalanced	Good
St.7	15.23	15.91	10.18	58.68	0.00	3.18	Unbalanced	Good	1092.18	9.27	2.33	0.48	Polluted	Moderate
St.8	11.08	12.37	15.55	58.44	2.57	3.44	Polluted	Moderate	396.73	6.27	1.93	0.38	Heavily polluted	Poor
St.9	18.66	18.74	11.87	47.97	0.64	2.90	Unbalanced	Good	355.91	6.09	1.81	0.40	Polluted	Moderate
St.10	22.83	22.05	9.93	43.71	0.00	2.64	Unbalanced	Good	430.91	6.82	2.02	0.43	Polluted	Moderate
St.11	12.18	20.16	45.45	20.63	1.56	2.51	Unbalanced	Good	1933.18	10.55	2.02	0.49	Polluted	Moderate
St.12	25.05	28.16	17.27	23.13	6.37	2.36	Unbalanced	Good	573.00	7.73	2.03	0.46	Polluted	Moderate

The mean sample n = 11 at each Station (St. 1 – St. 12).
CHs, Community Health status; EQs, Ecological Quality status; N, Abundance; S, Species richness; H'log$_2$, Shannon-Weiner index.

The dominance of *P. cavifrons, Heteromastus filiformis*, and *Dipolydora coeca* in organically rich and contaminated sediments consequently changed the ecological quality status of MAZ and DZ from *poor* to *moderate*. In contrast, *good* to *moderate* conditions at sandy sediments (BFZ) suggest that low organic content is also favourable to EGI and EGIII forms (Sigamani et al., 2015). Overall, the present study affirms both MAZ and DZ as polluted, with benthic communities of tolerant (EGIII) and second-order opportunistic (EGIV) species. The Odisha Pollution Control Board (OSPCB) estimates untreated domestic wastewater discharge from urban settlements in the Mahanadi basin at 3,45,000 m^3 (m^3 = 1000 liters) per day, producing biochemical oxygen demand (BOD) load of about 68.8 tonnes daily. The water quality index (WQI) of the Paradip coastal waters (riverine and estuarine stretch) also indicated a deteriorating trend from "grade C" in 2013-15 to "grade D" in 2017 (SPCB report card, 2020).

The benthic indices obtained through quality-based evaluation in the present study reflect different stages of the estuarine environmental conditions. Large-scale variability in the environmental parameters and ecological quality status of the benthic habitat at each station (or zone) could be attributable to the heterogeneous MES (Elliott and Quintino, 2007). Temporal variation of macrobenthic communities was evident through either increased or decreased benthic indices depending upon life strategy (r-selected and k-selected) and niche

TABLE 5 Relationship between biotic indices and environmental variables.

Pearsons linear r

Variables	Biomass	N	S	H'(log$_2$)	AMBI	M-AMBI	EGI	EGII	EGIII	EGIV	EGV
Temperature (°C)	-0.323	-0.087	**-0.537****	**-0.448****	**0.475***	**-0.593*****	**-0.439****	-0.156	0.132	0.142	0.221
pH	0.227	0.165	**0.392****	0.304	**-0.643*****	**0.489****	**0.514****	0.19	0.097	-0.534	0.046
Salinity (psu)	0.217	-0.213	0.252	0.213	-0.109	0.264	**0.394***	-0.031	**-0.394***	0.162	0.157
Dissolved Oxygen (mgl^{-1})	0.135	**0.344***	0.121	0.039	-0.261	0.117	0.025	0.099	0.31	**-0.409***	-0.025
Nitrite (μ mol.l^{-1})	0.229	0.164	0.077	-0.133	0.041	-0.034	-0.042	0.094	-0.098	0.101	-0.027
Orthophosphate (μ mol.l^{-1})	0.226	-0.076	-0.084	-0.127	**0.434****	-0.215	-0.29	-0.052	-0.275	0.548	-0.136
Organic matter (%)	-0.121	0.059	0.02	0.012	-0.092	0.042	-0.012	-0.101	0.196	-0.053	-0.299
Sand %	0.171	-0.073	0.207	0.267	-0.176	0.248	0.155	0.314	-0.232	-0.123	0.233
Silt %	-0.171	0.074	-0.206	-0.267	0.175	-0.247	-0.153	-0.314	0.232	0.122	-0.233
Clay %	-0.032	-0.047	-0.153	-0.131	0.219	-0.183	-0.232	-0.05	0.049	0.156	-0.068

Values are Pearson's correlation coefficient; bold font denotes correlations are significant at $p < 0.05$. n = 132.

performance (sensitive, indifferent and tolerant) of the individual species (Equbal et al., 2017). The improved sample quality between premonsoon and winter is suggestive of satisfactory performance by the benthic indices during stable, less turbulent, and low seasonal impact periods (Kröncke and Reiss, 2010; Karakassis et al., 2013; Sigamani et al., 2015; Bae et al., 2016; Chan et al., 2016; Feebarani et al., 2016; Sivadas et al., 2016; Mulik et al., 2017). In fact, for many estuaries on the east coast of India, premonsoon exhibit the most stressed conditions with excess and continuous accumulation of contaminants (Mitra et al., 2018). However, a good flush-out of pollutants is only possible during the monsoon season (Mulik et al., 2020a), aided further by a breakdown of contaminants owing to changing redox chemistry and consequences on benthic-pelagic coupling (Ghosh et al., 2022).

The applied biotic indices evaluated the benthic quality status by discriminating the highly disturbed from the less disturbed areas of the estuary. While the robustness of the M-AMBI (compared to AMBI) in sample quality assessment was explained by several researchers (Khan et al., 2014; Equbal et al., 2017; Pandey et al., 2021), a few others have observed its reverse performance due to lack of reference conditions and spatial benthic variability, heterogeneity within the estuarine complexes (Sigamani et al., 2015). According to Borja and Tunberg (2011), both AMBI and M-AMBI are sensitive to detecting human-mediated disturbances modified by natural disturbances. However, for regions strongly influenced by season, coastal dynamics, and anthropogenic disturbances, the univariate AMBI could show a high degree of variability than the multimetric M-AMBI (Kröncke and Reiss, 2010). The temporal variability of AMBI was indeed found to be less than M-AMBI (Equbal et al., 2018). Nevertheless, the marine biotic index, especially the M-AMBI, appeared to be more robust and realistic in grading the habitat quality into different classes. Therefore M-AMBI index can be used as far as the assessment of benthic habitat quality of the MES is concerned.

Recommendations for conservation and management

Considering the Mahanadi estuary's polluted health status, some holistic management initiatives are required immediately. The government can enforce authority and share responsibilities with local stakeholders, academic institutions, and non-governmental organizations as partners (Romañach et al., 2018). Regular monitoring of the environmental conditions and mangrove cover through advanced research (by observing heavy metal concentrations, application of Remote Sensing and GIS, and others) and citizen science approaches are essential (Zauki et al., 2019; Wolswijk et al., 2020; Durango-Cordero et al., 2021; Gopalakrishnan et al., 2021; Wolswijk et al., 2022). Afforestation of degraded mangrove zones, embankment of tidal rivers - without affecting zonation/succession of the wetland species, and biodiversity conservation (as mandated by the Department of Forest and Environment, Government of Odisha) are some crucial endeavours in the right direction. Moreover, the impact of local pollution on human health should be apprised through appropriate awareness campaigns. The approaches of this kind would be able to lessen the present-day waste discharge, habitat fragmentation, and ecological functioning damages.

Conclusions

The present study unveiled the macrobenthic community of the mangrove-associated MES and demonstrated the impacts of anthropogenic intervention through an ecological approach. Significant sources of anthropic stressors (municipal wastes, sewage, litter, acidic discharges from industries, nutrients, and shrimp farm run-offs) were influential in structuring the macrobenthic assemblages of the MES on spatial and temporal scales. The dominance of opportunistic (second-order opportunists, EGIV) and tolerant (EGIII) species marked the signs of environmental stress, regardless of the sources of disturbance, i.e., natural or anthropogenic. The higher (mean) abundance of opportunists and tolerant species in the MAZ and DZ was mainly caused by OM enrichment that was further modified by the industrial and shrimp farming effluents. Marine biotic indices, especially the M-AMBI, informed the MES's current state of ecological quality. The improved benthic community health from *moderate* to *good* in the premonsoon and winter was largely due to stable environmental conditions, allowing multiple species to co-exist in the light of reduced tolerant/opportunist species. The findings of this study also identified a set of environmental factors (water temperature, nutrient enrichment, salinity, DO, pH) influencing the macrobenthic assemblages of the MES. Evaluating the structure of macrobenthos in relation to anthropogenic/natural pressures and impacts provided the much-needed breadth of knowledge to help the management authorities formulate appropriate conservation strategies/policies. Given the importance of aquatic ecosystems for livelihood and climate change mitigation, the coastal and estuarine ecosystems must be protected so that their goods and services are sustainably utilized in the present and also availed by future generations.

Data availability statement

The original contributions presented in the study are included in the article/Supplementary Material. Further inquiries can be directed to the corresponding authors.

Author contributions

AN: Methodology, Field Investigation, Laboratory analysis, Data curation. JE: Software, Data curation, writing. SS: Field Investigation, Laboratory analysis, Figures. BD: Field Investigation, Laboratory analysis, Figures. GT: Software validation, manuscript preparation. DR: Conceptualization, Original draft preparation, and writing. BS: review and editing. PB: review and editing. All authors contributed to the article and approved the submitted version.

Funding

The University Grants Commission, New Delhi, India (File No. 41-64/2012 (SR) dated 11-JUL-2012) funded the research. The Open Access funding was provided by the Mangrove Research Unit (MARU), Institute of Oceanography and Environment, Universiti Malaysia Terengganu, Malaysia.

Acknowledgments

The University Grants Commission, New Delhi, India (File No. 41-64/2012 (SR) dated 11-JUL-2012) funded the research. The authors are grateful to the Principal Chief Conservator of Forests (Wildlife) and Chief Wildlife Warden, Government of Odisha, for their kind permission to conduct this research work at Mahanadi estuary. Laboratory facilities at the Department of Zoology, Ravenshaw University, are appreciated. Thanks to the reviewers for the suggestions and comments that immensely helped to improve the manuscript.

Conflict of interest

The authors declare that the research was conducted in the absence of any commercial or financial relationships that could be construed as a potential conflict of interest.

Publisher's note

All claims expressed in this article are solely those of the authors and do not necessarily represent those of their affiliated organizations, or those of the publisher, the editors and the reviewers. Any product that may be evaluated in this article, or claim that may be made by its manufacturer, is not guaranteed or endorsed by the publisher.

Supplementary material

The Supplementary Material for this article can be found online at: https://www.frontiersin.org/articles/10.3389/fmars.2022.1008912/full#supplementary-material

References

Abbott, R. T., and Dance, S. P. (1982). *Compendium of seashells* (New York: EP Dutton. Inc.), 411.

Abrogueña, J. B. R., Joydas, T. V., Pappathy, M., Cali, N. A., Alcaria, J., and Shoeb, M. (2021). Structure and composition of the macrobenthic community associated to shallow mangrove-seagrass habitat along the Southern Red Sea coast, Saudi Arabia. *Egypt. J. Aquat. Res.* 47, 61–66. doi: 10.1016/J.EJAR.2020.10.001

Acharyya, T., Sudatta, B. P., Raulo, S., Singh, S., Srichandan, S., Baliarsingh, S. K., et al. (2021a). "A systematic review of biogeochemistry of Mahanadi river estuary: Insights and future research direction," in *Estuarine biogeochemical dynamics of the East coast of India* (Switzerland: Springer, Cham), 57–80.

Acharyya, T., Sudatta, B. P., Srichandan, S., Baliarsingh, S. K., Lotliker, A. A., Raulo, S., et al. (2021b). Deciphering long-term seasonal and tidal water quality trends in the Mahanadi estuary. *J. Coast. Conserv.* 25, 1–16. doi: 10.1007/s11852-021-00843-2

Afli, A., Ayari, R., and Zaabi, S. (2008). Ecological quality of some Tunisian coast and lagoon locations, by using benthic community parameters and biotic indices. *Estuar. Coast. Shelf Sci.* 80, 269–280. doi: 10.1016/J.ECSS.2008.08.010

Albano, M. J., da Cunha Lana, P., Bremec, C., Elías, R., Martins, C. C., Venturini, N., et al. (2013). Macrobenthos and multi-molecular markers as indicators of environmental contamination in a south American port (Mar del Plata, southwest Atlantic). *Mar. Pollut. Bull.* 73, 102–114. doi: 10.1016/J.MARPOLBUL.2013.05.032

Alongi, D. M. (1998). *Coastal ecosystem processes* (Boca Raton: CRC Press).

Ansari, K. G. M. T., Pattnaik, A. K., Rastogi, G., and Bhadury, P. (2017). Multiple spatial scale analysis provide an understanding of benthic macro-invertebrate community structure across a lagoonal ecosystem. *Wetlands* 37, 277–287. doi: 10.1007/s13157-016-0866-0

APHA (1989). *Standard methods for the examination of water and wastewater. 17th Ed* (Washington DC: American Public Health Association), 1550.

Bae, M. J., Chun, J. H., Chon, T. S., and Park, Y. S. (2016). Spatio-temporal variability in benthic macroinvertebrate communities in headwater streams in south Korea. *Water* 8 (3), 99. doi: 10.3390/w8030099

Bae, H., Lee, J. H., Song, S. J., Park, J., Kwon, B. O., Hong, S., et al. (2017). Impacts of environmental and anthropogenic stresses on macrozoobenthic communities in Jinhae Bay, Korea. *Chemosphere* 171, 681–691. doi: 10.1016/J.CHEMOSPHERE.2016.12.112

Bald, J., Borja, A., Muxika, I., Franco, J., and Valencia, V. (2005). Assessing reference conditions and physico-chemical status according to the European water framework directive: A case-study from the Basque country (Northern Spain). *Mar. Pollut. Bull.* 50, 1508–1522. doi: 10.1016/J.MARPOLBUL.2005.06.019

Barletta, M., Lima, A. R. A., and Costa, M. F. (2019). Distribution, sources and consequences of nutrients, persistent organic pollutants, metals and microplastics in south American estuaries. *Sci. Total Environ.* 651, 1199–1218. doi: 10.1016/J.SCITOTENV.2018.09.276

Basset, A., Barbone, E., Borja, A., Elliott, M., Jona-Lasinio, G., Marques, J. C., et al. (2013). Natural variability and reference conditions: Setting type-specific classification boundaries for lagoon macroinvertebrates in the Mediterranean and Black Seas. *Hydrobiologia* 704 (1), 325–345. doi: 10.1007/s10750-012-1273-z

Beer, T. (1996). *Environmental Oceanography. 2nd ed* (Boca Raton: CRC Press). doi: 10.1201/9780203756980

Belal, A. A. M. (2019). Macro-benthic invertebrates as a bio-indicator for water and sediment quality in Suez Bay, Red Sea. *Egypt. J. Aquat. Res.* 45, 123–130. doi: 10.1016/j.ejar.2019.03.003

Bhowmik, M., and Mandal, S. (2021). Do seasonal dynamics influence traits and composition of macrobenthic assemblages of Sundarbans estuarine system, India? *Oceanologia* 63, 80–98. doi: 10.1016/j.oceano.2020.10.002

Bigot, L., Grémare, A., Amouroux, J. M., Frouin, P., Maire, O., and Gaertner, J. C. (2008). Assessment of the ecological quality status of soft-bottoms in Reunion Island (tropical southwest Indian Ocean) using AZTI marine biotic indices. *Mar. Pollut. Bull.* 56, 704–722. doi: 10.1016/J.MARPOLBUL.2007.12.020

Blake, J. A., Maciolek, N. J., Ota, A. Y., and Williams, I. P. (2009). Long-term benthic infaunal monitoring at a deep-ocean dredged material disposal site off northern California. *Deep Sea Res. Part II Top. Stud. Oceanogr.* 56, 1775–1803. doi: 10.1016/J.DSR2.2009.05.021

Borja, A., Chust, G., and Muxika, I. (2019). *Forever young: The successful story of a marine biotic index. 1st ed* (United Kingdom: Elsevier Ltd). doi: 10.1016/bs.amb.2019.05.001

Borja, Á., Dauer, D. M., and Grémare, A. (2012). The importance of setting targets and reference conditions in assessing marine ecosystem quality. *Ecol. Indic.* 12, 1–7. doi: 10.1016/J.ECOLIND.2011.06.018

Borja, A., Franco, J., and Pérez, V. (2000). A marine biotic index to establish the ecological quality of soft-bottom benthos within European estuarine and coastal environments. *Mar. Pollut. Bull.* 40, 1100–1114. doi: 10.1016/S0025-326X(00)00061-8

Borja, Á., Marín, S., Núñez, R., and Muxika, I. (2014). Is there a significant relationship between the benthic status of an area, determined by two broadly-used indices, and best professional judgment? *Ecol. Indic.* 45, 308–312. doi: 10.1016/J.ECOLIND.2014.04.015

Borja, A., and Muxika, I. (2005). Guidelines for the use of AMBI (AZTI's marine biotic index) in the assessment of the benthic ecological quality. *Mar. Pollut. Bull.* 7, 787–789. doi: 10.1016/j.marpolbul.2005.04.040

Borja, A., and Tunberg, B. G. (2011). Assessing benthic health in stressed subtropical estuaries, eastern Florida, USA using AMBI and m-AMBI. *Ecol. Indic.* 11, 295–303. doi: 10.1016/J.ECOLIND.2010.05.007

Bravo, G., Livore, J. P., Battini, N., Gastaldi, M., Lauretta, D., Brogger, M., et al. (2021). Rocky reef biodiversity survey: Punta Pardelas, Argentina. *Biodivers. Data J.* 9, e72081. doi: 10.3897/BDJ.9.e72081

Brown, A. M., Bass, A. M., and Pickard, A. (2022). Anthropogenic-estuarine interactions cause disproportionate greenhouse gas production: A review of the evidence base. *Mar. Pollut. Bull.* 174, 113240. doi: 10.1016/j.marpolbul.2021.113240

Chan, A. K. Y., Xu, W. Z., Liu, X. S., Cheung, S. G., and Shin, P. K. S. (2016). Sediment characteristics and benthic ecological status in contrasting marine environments of subtropical Hong Kong. *Mar. Pollut. Bull.* 103, 360–370. doi: 10.1016/J.MARPOLBUL.2015.12.032

Clarke, K. R., and Ainsworth, M. (1993). A method of linking multivariate community structure to environmental variables. *Mar. Ecol. Prog. Ser.* 92, 205–205. doi: 10.3354/meps092205

Clarke, K. R., and Gorley, R. N. (2015). *Getting started with PRIMER v7* (United Kingdom: PRIMER-E).

Clarke, K. R., Tweedley, J. R., and Valesini, F. J. (2014). Simple shade plots aid better long-term choices of data pre-treatment in multivariate assemblage studies. *J. Mar. Biolog. Assoc. U.K.* 94, 1–16. doi: 10.1017/S0025315413001227

Cohen, M. C. L., Lara, R. J., Szlafsztein, C., and Dittmar, T. (2004). Mangrove inundation and nutrient dynamics from a GIS perspective. *Wetl. Ecol.* 12, 81–86. doi: 10.1023/B:WETL.0000021668.25445.41

Costa, C. R., Costa, M. F., Dantas, D. V., and Barletta, M. (2018). Interannual and seasonal variations in estuarine water quality. *Front. Mar. Sci.* 5. doi: 10.3389/fmars.2018.00301

D'Alessandro, M., Porporato, E. M. D., Esposito, V., Giacobbe, S., Deidun, A., Nasi, F., et al. (2020). Common patterns of functional and biotic indices in response to multiple stressors in marine harbours ecosystems. *Environ. Pollut.* 259, 113959. doi: 10.1016/J.ENVPOL.2020.113959

Dash, C., Jaiswal, M. K., Pati, P., Patel, N. K., Singh, A. K., and Shah, R. A. (2020). Fluvial response to late quaternary sea level changes along the Mahanadi delta, east coast of India. *Quat. Int.* 553, 60–72. doi: 10.1016/j.quaint.2020.07.033

Dash, B., Rout, S. S., Lovaraju, A., Charan Kumar, B., Bharati, A., Ganesh, T., et al. (2021). Macrobenthic community of a tropical Bay system revisited: Historical changes in response to anthropogenic forcing. *Mar. Pollut. Bull.* 171, 112775. doi: 10.1016/j.marpolbul.2021.112775

Dauvin, J. C., Alizier, S., Rolet, C., Bakalem, A., Bellan, G., Gesteira, J. L. G., et al. (2012). Response of different benthic indices to diverse human pressures. *Ecol. Indic.* 12, 143–153. doi: 10.1016/J.ECOLIND.2011.03.019

Dauvin, J. C., Andrade, H., De-La-Ossa-Carretero, J. A., Del-Pilar-Ruso, Y., and Riera, R. (2016). Polychaete/amphipod ratios: An approach to validating simple benthic indicators. *Ecol. Indic.* 63, 89–99. doi: 10.1016/j.ecolind.2015.11.055

Dauvin, J. C., Fersi, A., Pezy, J. P., Bakalem, A., and Neifar, L. (2021). Macrobenthic communities in the tidal channels around the Gulf of Gabès, Tunisia. *Mar. Pollut. Bull.* 162, 111846. doi: 10.1016/J.MARPOLBUL.2020.111846

Deb, M. (1998). Crustacea. In Fauna of Mahanadi estuary. *Estuar. Ecosystem Ser.* 3, 129–159.

Dey, M., Chowdhury, C., Pattnaik, A. A., Ganguly, D., Mukhopadhyay, S. K., De, T. K., et al. (2013). Comparison of Monsoonal change of water quality parameters between 1983 and 2008 in a tropical estuary in Northeastern India: Role of phytoplankton and community metabolism. *Mar. Ecol.* 34, 14–29. doi: 10.1111/j.1439-0485.2012.00519.x

Dias, H. Q., Sukumaran, S., Srinivas, T., and Mulik, J. (2018). Ecological quality status evaluation of a Monsoonal tropical estuary using benthic indices: comparison via a seasonal approach. *Environ. Sci. Pollut. Res.* 25, 22672–22688. doi: 10.1007/s11356-018-2344-0

Durango-Cordero, J., Satyanarayana, B., Chan, J. C. W., Bogaert, J., and Dahdouh-Guebas, F. (2021). Distinguishing original and non-original stands at the Zhanjiang Mangrove National Nature Reserve (P.R. China): Remote sensing and GIS for conservation and ecological research. *Remote Sens.* 13, 2781. doi: 10.3390/rs13142781

Elliott, M., Day, J. W., Ramachandran, R., Wolanski, E., Fang, Q., Sheehan, M. R., et al. (2019). A synthesis: What is the future for coasts, estuaries, deltas and other transitional habitats in 2050 and beyond? *Coasts Estuaries Futur.* 2019, 1–28. doi: 10.1016/B978-0-12-814003-1.00001-0

Elliott, M., and Quintino, V. (2007). The estuarine quality paradox, environmental homeostasis and the difficulty of detecting anthropogenic stress in naturally stressed areas. *Mar. Pollut. Bull.* 54, 640–645. doi: 10.1016/j.marpolbul.2007.02.003

Equbal, J., Lakra, R. K., Savurirajan, M., Satyam, K., and Thiruchitrambalam, G. (2018). Testing performances of marine benthic biotic indices under the strong seasonality in the tropical intertidal habitats, South Andaman, India. *Mar. Pollut. Bull.* 135, 266–282. doi: 10.1016/J.MARPOLBUL.2018.07.034

Equbal, J., Thiruchitrambalam, G., Lakra, R. K., Savurirajan, M., and Satyam, K. (2017). Assessing the ecological quality of the Port Blair coast (South Andaman, India) using different suites of benthic biotic indices. *Mar. Biolog. Assoc. U.K.* 97 (5), 1007–1021. doi: 10.1017/S0025315417000753

Fauchald, K. (1977). The polychaete worms. definitions and keys to the orders, families and genera. *Natural History Museum Los Angeles County Sci. Ser.* 28, 1–188. http://hdl.handle.net/10088/3435

Fauvel, P. (1953). "The fauna of India including Pakistan, Ceylon, Burma and Malaya," in *Annelida: Polychaeta* (Delhi: The Indian Press), 507.

Feebarani, J., Joydas, T. V., Damodaran, R., and Borja, A. (2016). Benthic quality assessment in a naturally- and human-stressed tropical estuary. *Ecol. Indic.* 67, 380–390. doi: 10.1016/j.ecolind.2016.03.005

Gaonkar, C. V., Nasnodkar, M. R., and Matta, V. M. (2021). Assessment of metal enrichment and contamination in surface sediment of Mandovi estuary, Goa, West coast of India. *Environ. Sci. Pollut. Res.* 28 (41), 57872–57887. doi: 10.1007/s11356-021-14610-1

Gaonkar, U. V., Sivadas, S. K., and Ingole, B. S. (2013). Effect of tropical rainfall in structuring the macrobenthic community of Mandovi estuary, west coast of India. *J. Mar. Biolog. Assoc. U.K.* 93 (7), 1727–1738. doi: 10.1017/S002531541300026X

Gaudette, H. E., Flight, W. R., Toner, L., and Folger, D. W. (1974). An inexpensive titration method for the determination of organic carbon in recent sediments. *J. Sediment. Res.* 44, 249–253. doi: 10.1306/74D729D7-2B21-11D7-8648000102C1865D

Ghosh, A., Woodward, E. M. S., Nelson, C. E., Saha, R., and Bhadury, P. (2022). Nitrogen driven niche differentiation in bacterioplankton communities of northeastern coastal Bay of Bengal. *Environ. Res. Commun.* 4, 1–15. doi: 10.1088/2515-7620/ac5a69

Gopalakrishnan, L., Satyanarayana, B., Chen, D., Wolswijk, G., Amir, A. A., Vandegehuchte, M. B., et al. (2021). Using historical archives and landsat imagery to explore changes in the mangrove cover of Peninsular Malaysia between 1853 and 2018. *Remote Sens.* 13, 3403. doi: 10.3390/rs13173403

Grall, J., and Glémarec, M. (1997). Using biotic indices to estimate macrobenthic community perturbations in the Bay of Brest. *Estuar. Coast. Shelf Sci.* 44, 43–53. doi: 10.1016/S0272-7714(97)80006-6

Grasshoff, K., Kremling, K., and Ehrardt, M. (1999). *Methods of seawater analysis. 3rd ed.* Vol. 407 (Weinhein: VerlagChemie).

Habib, S., Hossain, M. B., Hossain, M. S., Jolly, Y. N., and Sarker, S. (2021). Ecological risk evaluation in bottom-surface sediments and sub-surface water in the subtropical Meghna estuarine system. *Heliyon* 7, e08324. doi: 10.1016/J.HELIYON.2021.E08324

Haddout, S., Priya, K. L., Casila, J. C. C., and Samad, B. (2022). Assessment of heavy metal contamination in the surficial sediments from the Sebou river estuary, Morocco, environ. *Forensics* 23:1-2, 23–31. doi: 10.1080/15275922.2021.1887970

Hazra, S., Das, S., Ghosh, A., Raju, P. V., and Patel, A. (2020). The Mahanadi delta: A rapidly developing delta in India. *In Deltas Anthropocene Palgrave Macmillan Cham*, 53–77. doi: 10.1007/978-3-030-23517-8_3

Hossain, M. S., Chowdhury, S. R., Navera, U. K., Hossain, M. A. R., Imam, B., and Sharifuzzaman, S. M. (2014). Opportunities and strategies for ocean and river resources management. Dhaka: Background paper for preparation of the 7th five year plan. *Plann. Commission Ministry Planning Bangladesh*. 1–66.

Hutchings, P., and Kupriyanova, E. (2018). Cosmopolitan polychaetes–fact or fiction? personal and historical perspectives. *Invertebr. Syst.* 32, 1–9. doi: 10.1071/IS17035

I-WRIS (2021) *Water resources information system of India*. Available at: https://indiawris.gov.in/wris/#/Basin (Accessed 16 January2022, 021).

Jabir, T., Vipindas, P. V., Jesmi, Y., Divya, P. S., Adarsh, B. M., Miziriya, H. N., et al. (2021). Influence of environmental factors on benthic nitrogen fixation and role of sulfur reducing diazotrophs in a eutrophic tropical estuary. *Mar. Pollut. Bull.* 165, 112126. doi: 10.1016/j.marpolbul.2021.112126

John, S. E., Rajimol, T. R., Mohan S, V., Maya, K., and Padmalal, D. (2017). Environmental degradation of a tropical estuary due to human interferences-a case study from Southern Kerala, SW India. *Arab. J. Geosci.* 10, 1–15. doi: 10.1007/s12517-017-3112-z

Kanhai, A. (2022). Spatial and seasonal variation in polychaete communities according to their trophic categories in southwest Tobago, West Indies. *Neotrop. Biodivers.* 8 (1), 8–20. doi: 10.1080/23766808.2021.2021051

Karakassis, I., Dimitriou, P. D., Papageorgiou, N., Apostolaki, E. T., Lampadariou, N., and Black, K. D. (2013). Methodological considerations on the coastal and transitional benthic indicators proposed for the water framework directive. *Ecol. Indic.* 29, 26–33. doi: 10.1016/J.ECOLIND.2012.12.020

Karydis, M., and Kitsiou, D. (2013). Marine water quality monitoring: A review. *Mar. Pollut. Bull.* 77, 23–36. doi: 10.1016/J.MARPOLBUL.2013.09.012

Kennish, M. J. (2002). Environmental threats and environmental future of estuaries. *Environ. Conserve.* 29, 78–107. doi: 10.1017/S0376892902000061

Kennish, M. J. (2005). "Estuaries, anthropogenic impacts," in *Encyclopedia of earth sciences series* (Netherlands: Springer), 434–436). doi: 10.1007/978-3-319-48657-4_140-2

Khan, S. A., Manokaran, S., and Lyla, P. S. (2014). Assessment of ecological quality of Vellar and Uppanar estuaries, southeast coast of India, using benthos. *Indian J. Geo-Marine Sci.* 43, 1989–1995.

Kröncke, I., and Reiss, H. (2010). Influence of macrofauna long-term natural variability on benthic indices used in ecological quality assessment. *Mar. Pollut. Bull.* 60, 58–68. doi: 10.1016/J.MARPOLBUL.2009.09.001

Krumbein, W. C., and Pettijohn, F. J. (1938). *Manual of sedimentary petrography* (New York: Appleton Century Crofts Inc.), 549.

Kumar, M. R., Krishnan, K. A., Vimexen, V., Faisal, A. K., Mohind, M., and Arun, V. (2022). Heavy metal impression in surface sediments and factors governing the fate of macrobenthic communities in tropical estuarine ecosystem, India. *Environ. Sci. Pollut. Res.* 29, 38567–38590. doi: 10.1007/s11356-021-18394-2

Kumar, C., Ghosh, A., Yash Debnath, M., and Bhadury, P. (2021). Seasonal dynamicity of environmental variables and water quality index in the lower stretch of the River Ganga. *Environ. Res. Commun.* doi: 10.1088/2515-7620/ac10fd

Kundu, S., Mondal, N., Lyla, P. S., and Ajmal Khan, S. (2010). Biodiversity and seasonal variation of macro-benthic infaunal community in the inshore waters of Parangipettai coast. *Environ. Monit. Assess.* 163 (1), 67–79. doi: 10.1007/s10661-009-0817-9

Leal Filho, W., Nagy, G. J., Martinho, F., Saroar, M., Erache, M. G., Primo, A. L., et al. (2022). Influences of Climate Change and Variability on Estuarine Ecosystems: An Impact Study in Selected European, South American and Asian Countries. *Int. J. Environ. Res. Public Health* 19 (1), 585. doi: 10.3390/ijerph19010585

Lotze, H. K., Lenihan, H. S., Bourque, B. J., Bradbury, R. H., Cooke, R. G., Kay, M. C., et al. (2006). Depletion, degradation, and recovery potential of estuaries and coastal seas. *Science* 312, 1806–1809. doi: 10.1126/science.1128035

Mitchell, S. (2020). Sediment transport and Marine Protected Areas. *Marine Protected Areas*, 587–598. doi: 10.1016/B978-0-08-102698-4.00030-7

Mitra, S., Ghosh, S., Satpathy, K. K., Bhattacharya, B. D., Sarkar, S. K., Mishra, P., et al. (2018). Water quality assessment of the ecologically stressed Hooghly river estuary, India: A multivariate approach. *Mar. Pollut. Bull.* 126, 592–599. doi: 10.1016/j.marpolbul.2017.09.053

Mohanti, M., and Swain, M. R. (2005). "Mahanadi river delta, east coast of India: an overview on evolution and dynamic processes," in *Department of Geology* (Vani Vihar: Utkal University).

Mohanty, B. (2018). *Taxonomy and Ecology of Brachyuran Crabs of Devi Estuary and Associated Mangrove Environment, Astarang, East Coast of India (Doctoral dissertation, Ravenshaw University)*.

Mohanty, B., Nayak, A., Dash, B., Rout, S. S., Charan Kumar, B., Patnaik, L., et al. (2019). Biodiversity and ecological considerations of brachyuran crabs (Crustacea: Decapoda) from Devi estuary–mangrove region on the east coast of India. *Reg. Stud. Mar. Sci.* 32, 100865. doi: 10.1016/j.rsma.2019.100865

Mohanty, B., Raut, D., Dev Roy, M. K., Patnaik, L., Rout, S. S., Dash, B., et al. (2022). Brachyuran Crabs of Devi estuary: *Taxonomic perspective* (India: Odisha Biodiversity Board), 120.

Muir, A. I., and Hossain, M. M. M. (2014). The intertidal polychaete (Annelida) fauna of the Sitakunda coast (Chittagong, Bangladesh), with notes on the Capitellidae, Glyceridae, Lumbrineridae, Nephtyidae, Nereididae and Phyllodocidae of the "Northern Bay of Bengal ecoregion". *ZooKeys* 1, 1–419. doi: 10.3897/zookeys.419.7557

Mulik, J., Sukumaran, S., and Dias, H. Q. (2020a). Can the ecological status of three differentially impacted Monsoonal tropical estuaries in NW India, be adequately assessed by a common estuarine benthic index? *Ecol. Indic.* 119, 106807. doi: 10.1016/J.ECOLIND.2020.106807

Mulik, J., Sukumaran, S., and Dias, H. Q. (2020b). Is the benthic index AMBI impervious to seasonality and data transformations while evaluating the ecological status of an anthropized Monsoonal estuary? *Ocean Coast. Manage.* 186, 105080. doi: 10.1016/J.OCECOAMAN.2019.105080

Mulik, J., Sukumaran, S., Srinivas, T., and Vijapure, T. (2017). Comparative efficacy of benthic biotic indices in assessing the ecological quality status (EcoQS) of the stressed Ulhas estuary, India. *Mar. Pollut. Bull.* 120, 192–202. doi: 10.1016/J.MARPOLBUL.2017.05.014

Muxika, I., Borja, Á., and Bald, J. (2007). Using historical data, expert judgement and multivariate analysis in assessing reference conditions and benthic ecological status, according to the European water framework directive. *Mar. Pollut. Bull.* 55, 16–29. doi: 10.1016/J.MARPOLBUL.2006.05.025

Nayak, A. (2020). Benthic macrofauna of Mahanadi estuary Odisha, East coast of India, doctoral thesis submitted to Ravenshaw university. 406. Available at: http://hdl.handle.net/10603/355684.

Nayak, A., Charan Kumar, B., Lovaraju, A., Raut, D., Sanghamitra Rout, S., Dash, B., et al. (2018). Benthic infauna from mudflats of Atharbanki mangrove waterway in Odisha, India. *J. Mar. Biol. Assoc. India.* 60, 33–39. doi: 10.6024/jmbai.2018.60.1.2026-05

Ortega, I., Colling, L. A., and Dumont, L. F. C. (2018). Response of soft-bottom macrobenthic assemblages to artisanal trawling fisheries in a subtropical estuary. estuar. *Coast. Shelf Sci.* 207, 142–153. doi: 10.1016/J.ECSS.2018.04.007

Palei, N. C., Rath, B. P., Pradhan, S. D., Swain, K. K., and Pati, M. (2014). The water birds of Paradeep Phosphate limited (PPL) campus of Jagatsinghpur District in Odisha, India. *World J. Zool.* 9 (3), 208–213. doi: 10.5829/idosi.wjz.2014.9.3.8552

Pandey, V., Venkatnarayanan, S., Kumar, P. S., Ratnam, K., Jha, D. K., Rajaguru, S., et al. (2021). Assessment of ecological health of Swarnamukhi river estuary, southeast coast of India, through AMBI indices and multivariate tools. *Mar. Pollut. Bull.* 164, 112031. doi: 10.1016/J.MARPOLBUL.2021.112031

Pattanayak, J. G., and Haldar, B. P. (1998). Other groups. In Fauna of Mahanadi estuary, Orissa, Estuarine Ecosystem Series, Rec. *Zool. Surv. India* 3, 215–218.

Pinto, R., Patrício, J., Baeta, A., Fath, B. D., Neto, J. M., and Marques, J. C. (2009). Review and evaluation of estuarine biotic indices to assess benthic condition. *Ecol. Indic.* 9, 1–25. doi: 10.1016/J.ECOLIND.2008.01.005

Prasad, M., and Ramanathan, A. L. (2008). Dissolved organic nutrients in the Pichavaram mangrove waters of east coast of India. *Indian J. Geo-Marine Sci.* 37, 141–145.

Rao, C. A. N. (1998). Polychaete, in Fauna of Mahanadi estuary, Orissa. *Estuar. Ecosystem Series Rec. Zool. Surv. India.* 3, 199–209.

Raut, D., Ganesh, T., Murty, N. V. S. S., and Raman, A. V. (2005). Macrobenthos of Kakinada bay in the Godavari delta, East coast of India: Comparing decadal changes. *Estuar. Coast. Shelf Sci.* 62, 609–620. doi: 10.1016/j.ecss.2004.09.029

Rehitha, T. V., Madhu, N. V., Vineetha, G., Vipindas, P. V., Resmi, P., and Revichandran, C. (2019). Spatio-temporal variability in macrobenthic communities and trophic structure of a tropical estuary and its adjacent coastal waters. *Environ. Monit. Assess.* 191 (6), 1–18. doi: 10.1007/s10661-019-7460-x

Rehitha, T. V., Vineetha, G., and Madhu, N. V. (2022). Ecological habitat quality assessment of a tropical estuary using macrobenthic functional characteristics and biotic indices. *Environ. Sci. Pollut. Res.* 29, 1–18. doi: 10.1007/s11356-022-19295-8

Rodgers, K., McLellan, I., Peshkur, T., et al. (2020). The legacy of industrial pollution in estuarine sediments: Spatial and temporal variability implications for ecosystem stress. *Environ Geochem Health* 42, 1057–1068. doi: 10.1007/s10653-019-00316-4

Romañach, S. S., DeAngelis, D. L., Koh, H. L., Li, Y., Teh, S. Y., Raja Barizan, R. S., et al. (2018). Conservation and restoration of mangroves: Global status, perspectives, and prognosis. *Ocean Coast. Manage.* 154, 72–82. doi: 10.1016/J.OCECOAMAN.2018.01.009

Salimi, E., Sakhaei, N., Nurinezhad, M., Savari, A., and Ghaemmaghami, S. S. (2021). Composition, biomass and secondary production of the macrobenthic invertebrate assemblage in a mangrove forest in Nayband Bay, Persian Gulf. *Reg. Stud. Mar. Sci.* 42, 101636. doi: 10.1016/J.RSMA.2021.101636

Sánchez-Ovando, J. P., Benítez-Villalobos, F., and Bastida-Zavala, J. R. (2021). Early development of two species of *Spirobranchus* Blainville, 1818 (Polychaeta: Serpulidae) from the Southern Mexican Pacific. *Invertebr. Reprod. Dev.* 65, 188–200. doi: 10.1080/07924259.2021.1932614

Sanchis, C., Soto, E. H., and Quiroga, E. (2021). The importance of a functional approach on benthic communities for aquaculture environmental assessment: Trophic groups – a polychaete view. *Mar. Pollut. Bull.* 167, 112309. doi: 10.1016/J.MARPOLBUL.2021.112309

Sandeep, K. K., and Pant, V. (2019). Riverine freshwater plume variability in the Bay of Bengal using wind sensitivity experiments. *Deep Sea Res. Part II Top. Stud. Oceanogr.* 168, 104649. doi: 10.1016/J.DSR2.2019.104649

Sany, T. S. B., Hashim, R., Tajfard, M., and Rahman, M. A. (2018a). Assessing the ecological health status using macrobenthic communities of tropical coastal water. *Hum. Ecol. Risk Assess. (HERA)* 24, 1761–1785. doi: 10.1080/10807039.2017.1422974

Sany, T. S. B., Tajfard, M., Hashim, R., Rezayi, M., Rahman, M. A., and Karlen, D. J. (2018b). The response of macrobenthic communities to environmental variability in tropical coastal waters. *Estuaries Coast.* 41, 1178–1192. doi: 10.1007/s12237-017-0346-7

Sarathy, P. P., Bharathidasan, V., Murugesan, P., Selvaraj, P., and Punniyamoorthy, R. (2022). Seasonal carbonate system vis-à-vis pH and salinity in selected tropical estuaries: Implications on polychaete diversity and composition towards predicting ecological health. *Oceanologia* 64, 346–362. doi: 10.1016/J.OCEANO.2022.01.001

Sharma, D., Rao, K., and Ramanathan, A. L. (2022). A systematic review on the impact of urbanization and industrialization on Indian coastal mangrove ecosystem. *Coast. Ecosyst.* 38, 175–199. doi: 10.1007/978-3-030-84255-0_8

Shepard, F. P. (1954). Nomenclature based on sand-silt-clay ratios. *J. sediment. Res.* 24, 151–158. doi: 10.1306/D4269774-2B26-11D7-8648000102C1865D

Shirodkar, S. R., and Nayak, V. N. (2010). Distribution and seasonal abundance of macro benthos of Gangavali estuary, Uttar Kannada, West coast of India. *J. Ecobiotechnol.* 2 (5), 80–84. Available at: https://updatepublishing.com/journal/index.php/jebt/article/view/41.

Shivarudrappa, S. K., Rakocinski, C. F., and Briggs, K. B. (2019). Vertical distribution of macrobenthos in hypoxia-affected sediments of the northern Gulf of Mexico: Applying functional metrics. *Estuaries Coast.* 42, 250–263. doi: 10.1007/s12237-018-0446-z

Sigamani, S., Perumal, M., Arumugam, S., Preetha Mini Jose, H. M., and Veeraiyan, B. (2015). AMBI indices and multivariate approach to assess the ecological health of Vellar–Coleroon estuarine system undergoing various human activities. *Mar. Pollut. Bull.* 100, 334–343. doi: 10.1016/J.MARPOLBUL.2015.08.028

Sivadas, S. K., Gupta, G. V. M., Kumar, S., and Ingole, B. S. (2021). Trait-based and taxonomic macrofauna community patterns in the upwelling ecosystem of the southeastern Arabian Sea. *Mar. Environ. Res.* 170, 105431. doi: 10.1016/J.MARENVRES.2021.105431

Sivadas, S. K., and Ingole, B. S. (2016). Biodiversity and biogeography pattern of benthic communities in the coastal basins of India. *Mar. Biol. Res.* 12 (8), 797–816. doi: 10.1080/17451000.2016.1203949

Sivadas, S., Ingole, B., and Nanajkar, M. (2011). Temporal variability of macrofauna from a disturbed habitat in Zuari estuary, west coast of India. *Environ. Monit. Assess.* 173 (1), 65–78. doi: 10.1007/s10661-010-1371-1

Sivadas, S. K., Nagesh, R., Gupta, G. V. M., Gaonkar, U., Mukherjee, I., Ramteke, D., et al. (2016). Testing the efficiency of temperate benthic biotic indices in assessing the ecological status of a tropical ecosystem. *Mar. Pollut. Bull.* 106 (1-2), 62–76. doi: 10.1016/j.marpolbul.2016.03.026

State Pollution Control Board, Odisha (2020). *Health card of Paradeep coastal stretch. State Pollution Control Board, Odisha, Coastal Management Cell, Integrated Coastal Zone Management Programme.* Odisha, State Pollution Control Board

Subba Rao, N. V., Surya Rao, K. V., and Maitra, S. (1991). Marine molluscs. In Fauna of Orissa, esturine ecosystem series, rec. *Zool. Surv. India.* 1, 1–175.

Subramanian, R., Retnamma, J., Nagarathinam, A., Loganathan, J., Singaram, P., and Chandrababu, V. (2021). Seasonality of macrobenthic assemblages and the biotic environmental quality of the largest Monsoonal estuary along the west coast of India. *Environ. Sci. Pollut. Res.* 28 (28), 37262–37278. doi: 10.1007/s11356-021-13144-w

Sundaray, S. K., Nayak, B. B., and Bhatta, D. (2009). Environmental studies on river water quality with reference to suitability for agricultural purposes: Mahanadi river estuarine system, India–a case study. *Environ. Monit. Assess.* 155 (1), 227–243. doi: 10.1007/s10661-008-0431-2

Surya Rao, K. V., and Maitra, S. (1998). Mollusca In Fauna of Mahanadi estuary Orissa, estuarine ecosystem series, Rec. *Zool. Surv. India* 3, 161–197.

Suzzi, A. L., Gaston, T. F., McKenzie, L., Mazumder, D., and Huggett, M. J. (2022). Tracking the impacts of nutrient inputs on estuary ecosystem function. *Sci. Total Environ.* 811, 152405. doi: 10.1016/j.scitotenv.2021.152405

Taillardat, P., Marchand, C., Friess, D. A., Widory, D., David, F., Ohte, N., et al. (2020). Respective contribution of urban wastewater and mangroves on nutrient dynamics in a tropical estuary during the monsoon season. *Mar. Pollut. Bull.* 160, 111652. doi: 10.1016/j.marpolbul.2020.111652

Thadathil, P., Gopalakrishna, V. V., Muraleedharan, P. M., Reddy, G. V., Araligidad, N., and Shenoy, S. (2002). Surface layer temperature inversion in the Bay of Bengal. *Deep Sea Res. Part I Oceanogr. Res.* 49, 1801–1818. doi: 10.1016/S0967-0637(02)00044-4

Tudu, P. C., Yennawar, P., Ghorai, N., Tripathy, B., and Mohapatra, A. (2018). An updated checklist of marine and estuarine mollusc of Odisha coast. *Indian J. Geo-Marine Sci.* 47, 1537–1560.

Varkey, M. J., Murty, V. S. N., and Suryanarayana, A. (1996). Physical oceanography of the Bay of Bengal and Andaman Sea. *Oceanogr. Mar. Biol.* 5, 413. Available at: https://updatepublishing.com/journal/index.php/jebt/article/view/41.

Veiga, P., Torres, A. C., Aneiros, F., Sousa-Pinto, I., Troncoso, J. S., and Rubal, M. (2016). Consistent patterns of variation in macrobenthic assemblages and environmental variables over multiple spatial scales using taxonomic and functional approaches. *Mar. Environ. Res.* 120, 191–201. doi: 10.1016/j.marenvres.2016.08.011

Wetz, M. S., and Yoskowitz, D. W. (2013). An "extreme" future for estuaries? effects of extreme climatic events on estuarine water quality and ecology. *Mar. Pollut. Bull.* 69, 7–18. doi: 10.1016/j.marpolbul.2013.01.020

Wolswijk, G., Satyanarayana, B., Siau, Y. F., Ali, A. N. B., Saliu, I. S., Fisol, M. A. B., et al. (2020). Distribution of mercury in sediments, plant and animal tissues in Matang Mangrove Forest Reserve, Malaysia. *J. Hazard. Mater.* 387, 121665. doi: 10.1016/j.jhazmat.2019.121665

Wolswijk, G., Trullols, A. B., Hugé, J., Otero, V., Satyanarayana, B., Lucas, R., et al. (2022). Can mangrove silviculture be carbon neutral? *Remote Sens.* 14, 2920. doi: 10.3390/rs14122920

Yokoyama, H., and Sukumaran, S. (2012). First records of three *Paraprionospio* species (Polychaeta: Spionidae) from Indian waters. *Cah. Biol. Mar.* 53, 279–287. Available at: http://drs.nio.org/drs/handle/2264/4047.

Zauki, N. A. M., Satyanarayana, B., Fairuz-Fozi, N., Nelson, B. R., Martin, M. B., Akbar-John, B., et al. (2019). Citizen Science Frontiers horseshoe crab population regain at their spawning beach in East Peninsular Malaysia. *J. Environ. Manage* 232, 1012–1020. doi: 10.1016/j.jenvman.2018.12.002

frontiers | Frontiers in Marine Science

TYPE Original Research
PUBLISHED 19 October 2022
DOI 10.3389/fmars.2022.1005442

Check for updates

OPEN ACCESS

EDITED BY
Meilin WU,
South China Sea Institute of Oceanology (CAS), China

REVIEWED BY
Sanjeevan V. N.,
Kerala University of Fisheries and Ocean Studies, India
Edyta Zawisza,
Institute of Geological Sciences (PAN), Poland

*CORRESPONDENCE
Ho Young Soh
hysoh@chonnam.ac.kr

SPECIALTY SECTION
This article was submitted to Marine Pollution, a section of the journal Frontiers in Marine Science

RECEIVED 28 July 2022
ACCEPTED 06 October 2022
PUBLISHED 19 October 2022

CITATION
Lee EH, Choi SY, Seo MH and Soh HY (2022) Impacts of hypoxia on the mesozooplankton community structure in a semi-enclosed bay. *Front. Mar. Sci.* 9:1005442. doi: 10.3389/fmars.2022.1005442

COPYRIGHT
© 2022 Lee, Choi, Seo and Soh. This is an open-access article distributed under the terms of the Creative Commons Attribution License (CC BY). The use, distribution or reproduction in other forums is permitted, provided the original author(s) and the copyright owner(s) are credited and that the original publication in this journal is cited, in accordance with accepted academic practice. No use, distribution or reproduction is permitted which does not comply with these terms.

Impacts of hypoxia on the mesozooplankton community structure in a semi-enclosed bay

Eun Hye Lee[1], Seo Yeol Choi[2], Min Ho Seo[3] and Ho Young Soh[1,2]*

[1]Department of Environmental Oceanography, Chonnam National University, Yeosu, South Korea, [2]Department of Ocean Integrated Science, Chonnam National University, Yeosu, South Korea, [3]Department of Marine Ecology, Marine Ecology Research Center, Yeosu, South Korea

Gamak Bay is frequently affected by hypoxia in summer. Therefore, this study aimed to examine the effect of hypoxia on the mesozooplankton community of this region. Mesozooplankton samples were obtained biweekly (28 times) at a hypoxic station (inner bay) and a normoxic station (middle bay) using a conical net (mesh size 200 μm; mouth diameter 30 cm) from April 2020 to April 2021. In the inner bay, hypoxia was observed a total of five times between early June and late September, whereas no instances of hypoxia were detected in the middle bay. During the hypoxic period, mesozooplankton abundance was higher in the inner bay than the middle bay ($p < 0.05$). During the normoxic period, there was no difference between the inner bay and the middle bay ($p > 0.05$). The dominant species in the hypoxic period were three species of cladocerans (*Pleopis polyphemoides*, *Pseudoevadne tergestina*, *Penilia avirostris*) and the copepod *Acartia sinjiensis*. The abundance of cladocerans was higher in the inner bay, and that of *A. sinjiensis* was higher in the middle bay ($p < 0.05$). In addition to water temperature, salinity, and size-fractionated Chl-*a* concentration, mesozooplankton abundance was also significantly correlated with the bottom DO concentration. Collectively, our findings suggest that hypoxia can affect mesozooplankton abundance and occurrence times.

KEYWORDS

dissolved oxygen (DO), environmental condition, cladocera, copepoda, hypoxic period, tolerance

Introduction

Global warming caused by the Industrial Revolution has severely impacted terrestrial and marine environments, resulting in serious socio-economic and political issues (IPCC, 2013). Hypoxia caused by global warming (dissolved oxygen concentration of 2 mg L^{-1} or less) is one of the most widespread harmful anthropogenic effects on coasts and estuaries

(Diaz and Rosenberg, 2008), and is classified as a major global environmental problem, along with ocean acidification, overfishing, and habitat loss (Breitburg et al., 2018). In marine ecosystems, climate change induces an increase in sea levels and water temperature, as well as changes in precipitation and wind patterns, driving environmental changes in coasts and estuaries (Altieri and Gedan, 2015). Additionally, a growing body of evidence has demonstrated that global warming induces hypoxia in coastal regions and estuaries (Bendtsen and Hansen, 2013; Carstensen et al., 2014; Jenny et al., 2014; Altieri and Gedan, 2015).

Dissolved oxygen changes in the ocean are mainly driven by factors such as decreased oxygen solubility, increased stratification, and increased biological respiration (Keeling et al., 2010). Additionally, the increase in hypoxic regions over the past half century is largely due to excessive anthropogenic nutrient loading, which stimulates eutrophication (Kemp et al., 2005). This increases the supply of organic matter to deeper water layers and sediments, causing low oxygenation in the bottom water and resulting in the occurrence of 'dead zones' (Diaz and Rosenberg, 2008; Conley et al., 2009). The area range of coastal hypoxia has increased significantly in recent decades due to the increase in coastal eutrophication (Diaz, 2001; Diaz and Rosenberg, 2008; Conley et al., 2009; Rabalais et al., 2010). An assessment of the literature shows that the number of coastal areas with reported hypoxia have increased over time at an exponential growth rate of 5.5% per year (Vaquer-Sunyer and Duarte, 2008). This growth rate may be partly due to increased observational efforts, but the prevalence of hypoxia is expected to increase further due to the combined effects of eutrophication and climate change (Conley et al., 2009).

Hypoxia can be a serious stressor for marine organisms and ecosystems, resulting in community structure changes through increased dominance of less sensitive species or a decrease in the growth of sensitive species (Marcus et al., 2004; Richmond et al., 2006; Roman et al., 2019; Keister et al., 2020). Particularly, mesozooplankton plays a pivotal role in the food web and is a major component of the biological carbon pump. Hypoxia can directly or indirectly affect mesozooplankton community structure, and the tolerance of mesozooplankton to hypoxia varies in a taxon- and stage-dependent manner (Roman et al., 1993; Marcus, 2001; Richmond et al., 2006; Grodzins et al., 2016; Pan et al., 2018). Several studies have focused on the effects of zooplankton in relation to hypoxia. Elliott et al. (2012) found that the abundance of zooplankton was low in the hypoxic bottom waters, but abundant in the upper normoxic waters. Roman et al. (2012) noted that zooplankton shifted the vertical distribution to the upper water column during the day in the Gulf of Mexico where bottom hypoxia occurs. Shi et al. (2019) showed that in regions where hypoxia was observed, the zooplankton biomass was relatively high and the taxonomic diversity was lower. Slater et al. (2020) showed that hypoxia clearly contributed to a decrease in copepods and planktivorous fish, and an increase in gelatinous zooplankton. However, among the various taxonomic groups experiencing hypoxia, some species may respond strongly to these conditions, but the overall effect on the communities is less clear. Therefore, more research is clearly needed to understand the relationship between hypoxia and the various taxonomic groups that inhabit coastal areas.

Mesozooplankton abundance tends to fluctuate greatly within a short period due to the temporal differences in the life strategies of each taxon (Klais et al., 2016). For example, the population of copepods may increase in weeks or months (Hansen et al., 2006), whereas the population of cladocerans may increase in days or weeks (Egloff et al., 1997; Park and Marshall, 2000). Particularly, cladocerans have a very short generation time compared to copepods, and therefore determining their seasonal abundance requires an in-depth understanding of their reproductive characteristics through frequent sampling (Omorii and Ikeda, 1984; Mullin and Onbé, 1992; Atienza et al., 2008). Therefore, to quantitatively evaluate mesozooplankton populations and communities, the survey period and interval must be considered by reflecting the reproductive characteristics of taxonomic groups (Omorii and Ikeda, 1984; Klais et al., 2016).

Keister et al. (2020) reported that the two most common effects of hypoxia in the Hood Canal (Washington, USA) were lower total abundance and biomass of zooplankton and higher abundance of gelatinous zooplankton. However, the hypothesis that hypoxia leads to a dominance of cyclopoid copepods relative to calanoid copepods was not clearly demonstrated. In Masan Bay, Korea, where hypoxia commonly occurs in summer, a cladoceran species was positively correlated with low DO, suggesting that hypoxia could have an effect on the population growth of cladocerans (Jang et al., 2015). Moreover, copepods and cladocerans predominate in eutrophic coastal and estuarine environments depending on the region (Soh et al., 2002; Isinibilir et al., 2008; Isinibilir, 2009; Rakhesh et al., 2013; Li et al., 2022). However, despite their high abundance, few studies have investigated the effect of hypoxia on copepods and cladocerans.

Gamak Bay has been the subject of intensive research in relation to hypoxia in recent decades (Kim et al., 2010; Seo et al., 2012; Shin et al., 2013; Lee et al., 2016; Lee et al., 2019). Unlike detailed studies focusing on the response and abundance of taxonomic groups of mesozooplankton according to hypoxia, very few studies have characterized the relationship between mesozooplankton and hypoxia in Gamak Bay. Moon et al. (2006) demonstrated that mesozooplankton abundance decreased significantly when hypoxia occurred in summer, with the highest abundances occurring in the surface layer. However, the effects of hypoxia on specific taxonomic groups remains unknown. Therefore, our study focused on the composition of mesozooplankton populations (mainly cladocerans and copepods), abundance, and occurrence patterns that respond rapidly to changes in the environment.

Furthermore, to determine whether hypoxia decreases or increases the abundance of mesozooplankton and changes its community structure, samples were collected from the inner bay (hypoxic zone) and middle bay (normoxic zone) areas of the study site and then compared. The specific goals of this study were to evaluate the effect of hypoxia on (1) the composition of the mesozooplankton community, (2) the abundance of mesozooplankton, and (3) the occurrence pattern of the dominant species in the hypoxic period.

Materials and methods

Study area

Gamak Bay is a semi-enclosed bay located in the center of the southern coast of Korea (Figure 1). The study area is oval-shaped (approximately 9 km in width and 15 km in length) and is surrounded by the Yeosu Peninsula and Dolsan Island to the east. The submarine topography is divided into two basins around the ridge in the center of the bay. The central part of the bay is approximately 6–7 m deep, and the northern part from the center of the bay is concave and deeper, reaching a 9–11 m depth. Depth increases from the center of the bay to the south. Seawater exchange is primarily through the southern entrance to the bay and additionally through a narrow northeast channel. Particularly, the submarine topography of the northern waters of Gamak Bay causes stagnation and prevents seawater exchange (Lee and Cho, 1990). Moreover, there are several densely populated mussel and oyster farms nearby, resulting in severe excrement and feed residue contamination from the farmed organisms. Also, eutrophication occurs due to the inflow of seawater and domestic sewage (Noh, 2003). To solve this problem, the amount of domestic sewage inflow is reduced through sewage terminal treatment, and the oxygen demand of the sediment is reduced by dredging the contaminated sediment.

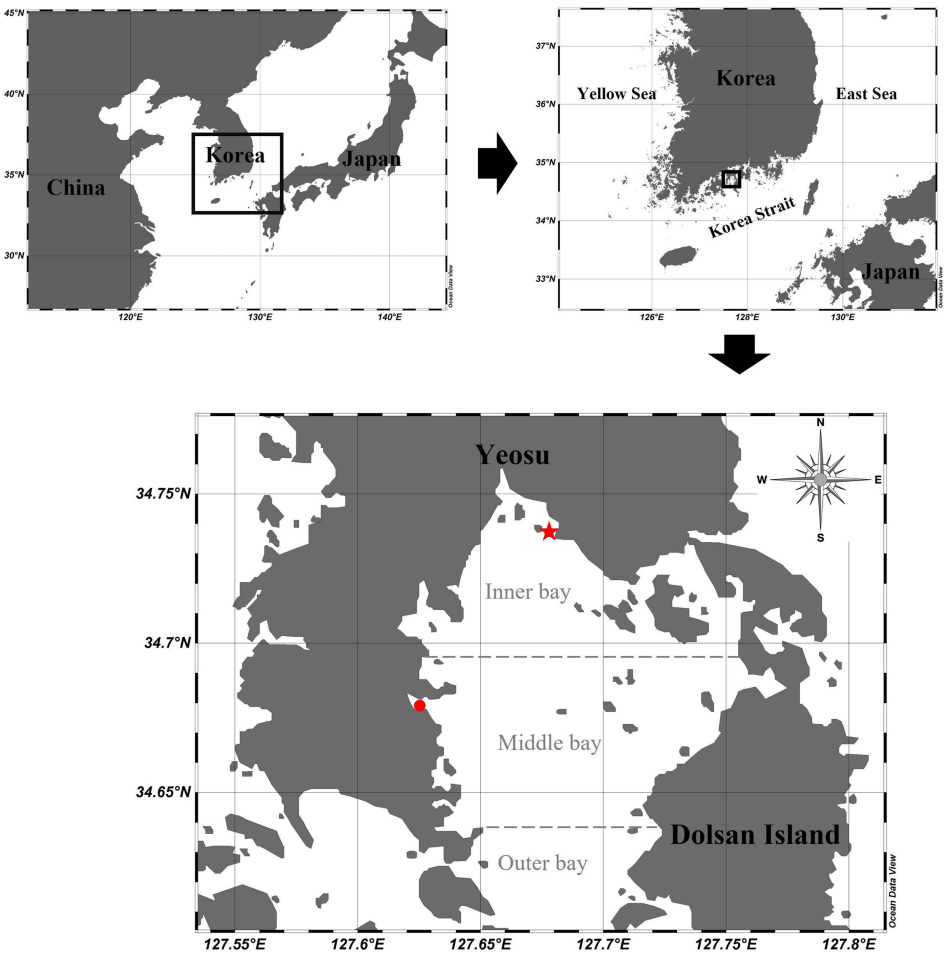


FIGURE 1
Sampling stations in Gamak Bay: a red star dot for the inner bay station and a red circle dot for the middle bay station.

However, despite these efforts, a large amount of organic matter is supplied, which raises concerns about potential eutrophication (NIFS, 2010). The largest contributor to hypoxia in northern Gamak Bay is the occurrence of a stratified bottom water mass formed by slow seawater flow. A large amount of phytoplankton is produced under the thermocline in summer due to an abundance of nutrients and sufficient solar radiation, both of which are required for photosynthesis. Although this study did not provide information on CTD and nutrient profiles according to water depth, Kim et al. (2006) and Kim et al. (2011) observed that the thermocline was mainly formed at depths of 3–5 m and 2–5 m. In turn, the organic matter that sinks to the bottom is decomposed and oxygen consumption rates increase. Additionally, the oxygen consumption rate of sediments increases, which further exacerbates hypoxia (Kim et al., 2006). However, hypoxia does not occur in the southern part of Gamak Bay because the water is constantly flowing and the oxygen supply is consistent, although the oxygen consumption rate of the sediments is high (Lee, 2015).

Environmental variables

The study was conducted at two fixed stations (inner bay: 34° 48′55″ N 127°24′40″ E, middle bay: 34°40′42″ N 127°37′26″ E) in Gamak Bay, Korea. A total of 28 mesozooplankton samples were collected at each station at high tide every two weeks from April 2020 to April 2021. The depth of the study stations were 10 m and 5 m in the inner bay and middle bay, respectively. Environmental variables were measured on the surface layer and the bottom layer (bottom depth−1 m), whereas the total chlorophyll-*a* (Chl-*a*) concentration was measured only in the surface layer. Water temperature, salinity, and dissolved oxygen (DO) were measured using an YSI multimeter (600QS, YSI Inc., OH, USA). To measure the total Chl-*a* concentration, seawater (500 ml) was immediately filtered through 47-mm-diameter GF/F glass-fiber filters (Whatman, Maidstone, UK). Chl-*a* concentration was measured in 3 size categories (> 20 μm, 3–20 μm, < 3 μm), representing microphytoplankton, nanophytoplankton, and picophytoplankton, respectively. To measure the size-fractionated Chl-*a* concentration, 500 ml of seawater was filtered through 20 μm filter paper and 3 μm PC membrane filter paper, respectively, and then filtered again using GF/F filter paper. The filter was placed in a 15 ml tube and frozen at −20°C until analysis. The pigment was extracted in the laboratory for 24 h in 90% acetone and Chl-*a* concentrations were determined fluorometrically (10AU, Turner Designs, Sunnyvale, CA, USA) (Parsons et al., 1984).

Mesozooplankton samples

Mesozooplankton samples were vertically collected with a conical net (mouth diameter, 30 cm; mesh size, 200 μm; Manufacturer, DAIHAN SCIENTIFIC CO., LTD.) from near the bottom (bottom depth−1 m) to the surface at a speed of 1 m/s. A flowmeter (Hydro-Bios, 438115, Kiel, Germany) was attached to the mouth of the conical net to measure the volume of the filtered water. After collection, the samples were preserved in 5% neutral formalin seawater solution. The samples were then subsampled using a Folsom splitter until approximately 200 individuals of the dominant taxa were obtained and dispensed into Bogorov-Rass counting chambers. All specimens from subsamples were identified by species or the lowest classification level and counted under a dissecting microscope (Nikon SMZ645, Nikon, Tokyo, Japan). When more detailed observation was needed for species identification, observations were conducted under a high-magnification optical microscope (Nikon eclipse E200, Nikon, Tokyo, Japan). Mesozooplankton abundance was standardized based on the volume of filtered water and expressed as the number of individuals per cubic meter (indiv. m^{-3}).

Data analysis

The Mann-Whitney U-test was used to statistically examine the spatial differences in environmental variables (water temperature, salinity, DO concentration, total Chl-*a* concentration, and size-fractionated Chl-*a* concentration) and zooplankton abundance for the inner and the middle bay during the hypoxic (June to September) and normoxic (from October to May) periods. Additionally, differences in dominant species abundance in the hypoxic period were compared in the inner and middle bay (SPSS 18.0 software, SPSS Inc., CHICAGO, IL, United States). Redundancy analysis (RDA) was conducted to investigate the correlation between the species dominating the hypoxic period and environmental variables (CANOCO 4.5, Wageningen UR, Netherlands) (Ter Braack and Šmilauer, 2002). The data were log transformed and centered prior to the analysis. The significance of the variability explained by individual environmental variables was tested using the Monte Carlo permutation test with 499 random permutations. The results are presented as a biplot where dominant species and environmental variables are plotted together.

Results

Environmental variables

Water temperature ranged from 4.4 to 30.0°C at the surface and from 4.8 to 24.5°C at the bottom of the inner bay (Figure 2A). From June to September, when hypoxia occurs, the temperature difference between the surface and bottom was up to 4°C due to the increase in surface water temperature. When hypoxia was not observed, there was no significant

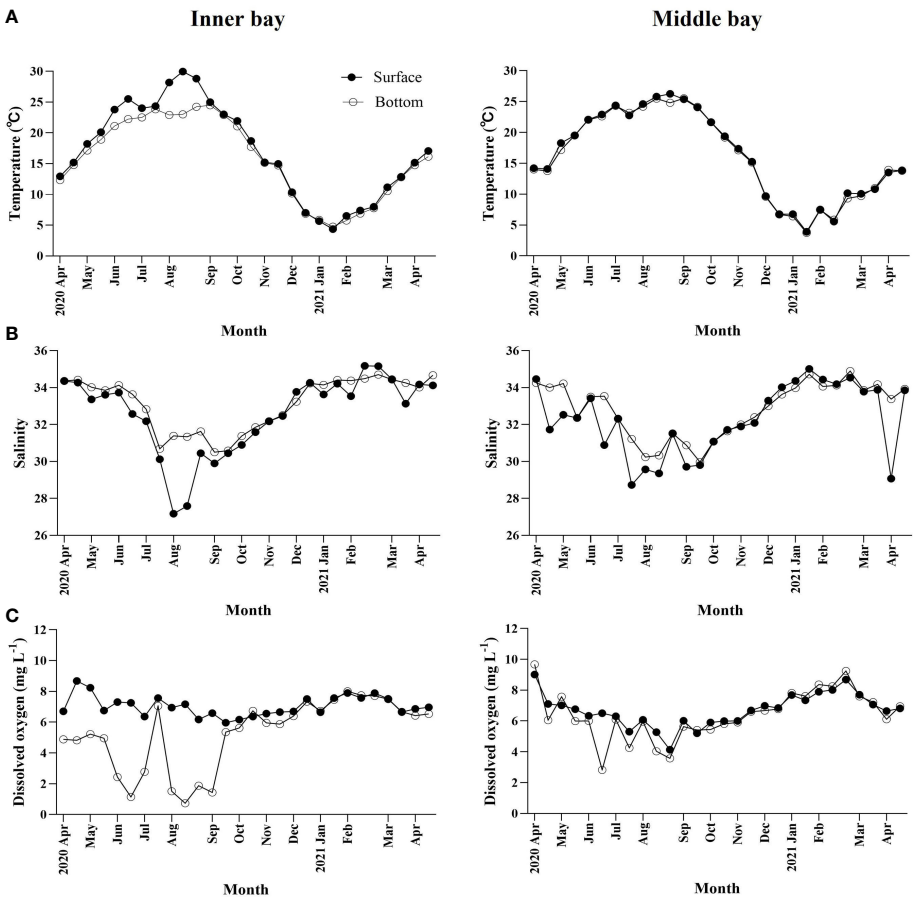


FIGURE 2
Temporal variations in environmental variables including **(A)** water temperature (°C), **(B)** salinity, and **(C)** dissolved oxygen concentration in Gamak Bay from April 2020 to April 2021.

difference between the surface and bottom temperature. In the middle bay, water temperature ranged from 3.9 to 26.3°C at the surface and from 3.7 to 25.5°C at the bottom. The difference in water temperature between the surface and the bottom was approximately 1°C throughout the sampling period. In both regions, the lowest temperature occurred in February, whereas the highest occurred in September.

Salinity ranged from 27.2 to 35.2 at the surface and from 30.5 to 34.7 at the bottom of the inner bay, (Figure 2B). In June, when hypoxic conditions began, the salinity of the surface and bottom reached 33 or higher, but gradually decreased and reached its lowest point in August. In August, the difference in salinity between the surface and the bottom was also greatest, reaching up to 4.2. Afterward, the salinity in the surface increased gradually when the hypoxic conditions completely disappeared. In the middle bay, the salinity at the surface and the bottom ranged from 28.7 to 34.5 and from 30.0 to 34.9, respectively, and the difference between the surface and the bottom was less than 2 during most of the sampling period.

DO concentration ranged from 6.0 to 8.6 mg L^{-1} at the surface and from 0.7 to 8.0 mg L^{-1} at the bottom of the inner bay (Figure 2C). In spring and summer, DO concentration was high in the surface. Hypoxia in which the bottom DO concentration decreased to less than 2 mg L^{-1} was observed five times from June to September when the surface water temperature was high. In autumn and winter, DO concentration was similar in the surface and bottom. In the middle bay, DO concentration ranged from 4.1 to 9.0 mg L^{-1} at the surface and from 2.8 to 9.7 mg L^{-1} at the bottom, and DO concentrations did not decrease below 2 mg L^{-1}.

Total Chl-*a* concentration ranged from 0.7 μg L^{-1} to 7.8 μg L^{-1} (Figure 3A) in the inner bay. Total Chl-*a* concentration also appeared as two peaks in mid-August and late-September (7.8 μg L^{-1} and 7.6 μg L^{-1}, respectively). In December and January, two peaks were observed, which were relatively lower than in summer. In the middle bay, the total Chl-*a* concentration ranged from 0.5 μg L^{-1} to 5.3 μg L^{-1}, reaching a peak in late-June (5.3 μg L^{-1}), and the fluctuation range was lower than that of the inner bay.

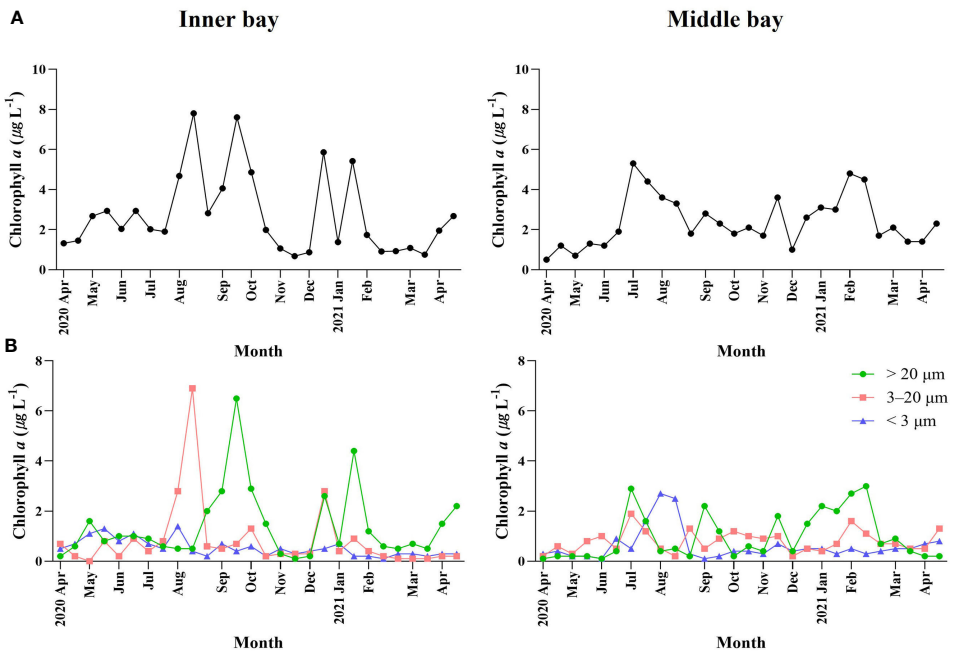


FIGURE 3
Temporal variations environmental variables including **(A)** total Chl-*a* concentration and **(B)** size-fractionated Chl-*a* concentration in Gamak Bay from April 2020 to April 2021.

The proportions of different phytoplankton size fractions varied throughout the sampling period (Figure 3B). In the inner bay, the < 3 μm size fraction accounted for 3.3%–50.7% (average 25.6%) of the total Chl-*a* concentration and accounted for the highest proportion of total Chl-*a* concentration in late-November and the lowest proportion in mid-January. The 3–20 μm size fraction accounted for 1.2%–88.6% (average 25.1%) of the total Chl-*a* concentration and accounted for the highest proportion of total Chl-*a* concentration in mid-August and the lowest proportion in mid-May. The > 20 μm size fraction accounted for 6.2%–80.9% (average 49.3%) of the total Chl-*a* concentration and accounted for the highest proportion of total Chl-*a* concentration in late-November and the lowest proportion in mid-January. In the middle bay, the < 3 μm size fraction accounted for 4.9%–76.7% (average 27.6%) of the total Chl-*a* concentration and accounted for the highest proportion of total Chl-*a* concentration in mid-August and the lowest proportion in early-September. The 3–20 μm size fraction accounted for 7.4%–83.8% (average 37.3%) of total Chl-*a* concentration and accounted for the highest proportion of total Chl-*a* concentration in early-June and the lowest proportion in mid-August. The > 20 μm size fraction accounted for 5.1%–77.4% (average 35.0%) of the total Chl-*a* concentration and accounted for the highest proportion of total Chl-*a* concentration in early-September and the lowest proportion in early-June.

The spatial difference in environmental variables between the inner and middle bay during the hypoxic (June to September) and normoxic (October to May) period was identified (Table 1). During the hypoxic period, there was no significant difference in water temperature, salinity, total Chl-*a* concentration, and the three size categories of Chl-*a* concentration in the inner and middle bay. However, there was a significant difference in the surface and bottom DO concentration in the inner and middle bay (Mann-Whitney U-test, $p < 0.01$). During the normoxic period, there was no significant difference in water temperature, salinity, DO concentration, and total Chl-*a* concentration in the inner and middle bay, but there was a significant difference in the 3–20 μm categories of Chl-*a* concentration (Mann-Whitney U-test, $p < 0.05$).

Temporal variation in mesozooplankton composition

The mesozooplankton that appeared in the two regions were identified as copepods, cladocerans planktonic larvae, and other zooplankton (chaetognaths, appendicularians, amphipods, hydromedusae, etc.). A total of 45 and 52 taxa of mesozooplankton were identified in the inner and middle bay, respectively (Supplementary Table 1). Copepods were most

TABLE 1 Spatial differences in environmental variables were tested with Mann-Whitney U-tests.

		Inner bay		Middle bay	
		z-value	*p*-value	z-value	*p*-value
Temperature	surface	-1.347	0.200	-0.450	0.667
	bottom	-1.540	0.139	-0.323	0.749
Salinity	surface	-0.289	0.815	-0.450	0.667
	bottom	-1.058	0.321	-1.166	0.247
DO	surface	-3.079	0.001**	-0.590	0.569
	bottom	-2.598	0.008**	-1.869	0.061
Total Chl-*a* concentration	surface	-0.385	0.743	-0.295	0.214
> 20 μm		-0.770	0.481	-1.271	0.771
3–20 μm		-0.048	0.963	-2.570	0.010*
< 3 μm		-0.192	0.888	-0.787	0.444

Asterisks stand for significant-difference levels between inner and middle bay: *$P < 0.05$; **$P < 0.01$.

dominant in the inner bay (60.1%), followed by cladocerans (24.4%), larvae (8.3%), and other zooplankton (7.2%). In the middle bay, copepods were most dominant (81.9%), followed by larvae (9.4%), other zooplankton (4.8%), and cladocerans (4.0%).

The temporal variation of mesozooplankton composition was different in the two regions. In the inner bay, In April and May, during the normoxic period, copepods were high (64.7%–96.2%), whereas cladocerans were very low (< 3%) (Figure 4A). In June, when hypoxic conditions began, copepods began to decrease, reaching their lowest point in August (6.7%). Conversely, cladocerans gradually increased in June, and they were the highest in August (74%). Hypoxic conditions persisted until early-September but cladocerans decreased sharply to 4%, whereas copepods sharply increased to 61.8%. Additionally, planktonic larvae and other zooplankton increased to 20.5% and 13.7%, respectively. From late-September to early-October, during the normoxic period, planktonic larvae and other zooplankton were high at an average of 29.8% and 23% respectively, and cladocerans were very low at less than 2.5%. In November, copepods were very high at 81.7% and gradually decreased from March. Conversely, planktonic larvae and other zooplankton decreased to an average of 12.3% and 0.8%, respectively, and gradually increased from March.

In the middle bay, copepods were very high (87.7%–99.1%) from April to June (Figure 4B). From July to November, they were repeated to be high and low in the range of 44 to 90.8%, and continued to be very high after December (91%). In contrast, cladocerans were very low (0.2%–3.7%) from May to July but increased in August, reaching their highest at 49.6% in mid-September. Afterward, they reached a small peak (29.7%) in early-November and decreased sharply thereafter, reaching undetectable levels in December. Planktonic larvae were the lowest at 0.9% to 13.1% from April to June, and the highest at 33.1% in early-September. After that, they appeared throughout the sampling period with an average of 3.2%. Other zooplankton were lower than 1% from April to June, and increased gradually, reaching a maximum of 32.5% in mid-August. Afterward, they remained low (4.5%) throughout the sampling period.

Spatial differences in mesozooplankton abundance in the two regions during the hypoxic and normoxic periods

During the hypoxic period, mesozooplankton abundance was significantly higher in the inner bay than in the middle bay (Mann-Whitney U-test, $p < 0.01$) (Figure 5A). The abundance ranged from 2,862 to 13,905 indiv. m^{-3} (6,877 ± 3,421 indiv. m^{-3} on average) in the inner bay and from 535 to 5,137 indiv. m^{-3} (3,029 ± 1,627 indiv. m^{-3}) in the middle bay. During the normoxic period, the abundance ranged from 231 to 8,293 indiv. m^{-3} (2,022 ± 2,198 indiv. m^{-3} on average) in the inner bay and from 364 to 7,829 indiv. m^{-3} (2,316 ± 2,580 indiv. m^{-3}) in the middle bay (Figure 5B). There was no significant difference in mesozooplankton abundance between the inner and the middle bay (Mann-Whitney U-test, $p > 0.05$).

The appearance of dominant species during the hypoxic period

During the hypoxic period, the dominant species in the two regions included three cladocerans (*Pleopis polyphemoides*, *Pseudoevadne tergestina*, *Penilia avirostris*) and one copepod (*Acartia sinjiensis*). The abundances of these species exhibited distinct differences between the inner and the middle bay. *P. polyphemoides* ranged from 10 to 2,315 indiv. m^{-3} (1,018 ± 992 indiv. m^{-3} on average) in the inner bay and from 0 to 157 indiv. m^{-3} (35 ± 54 indiv. m^{-3} on average) in the middle bay (Figure 6A), and this difference was found to be statistically significant (Mann-Whitney U-test, $p < 0.01$). The abundance of

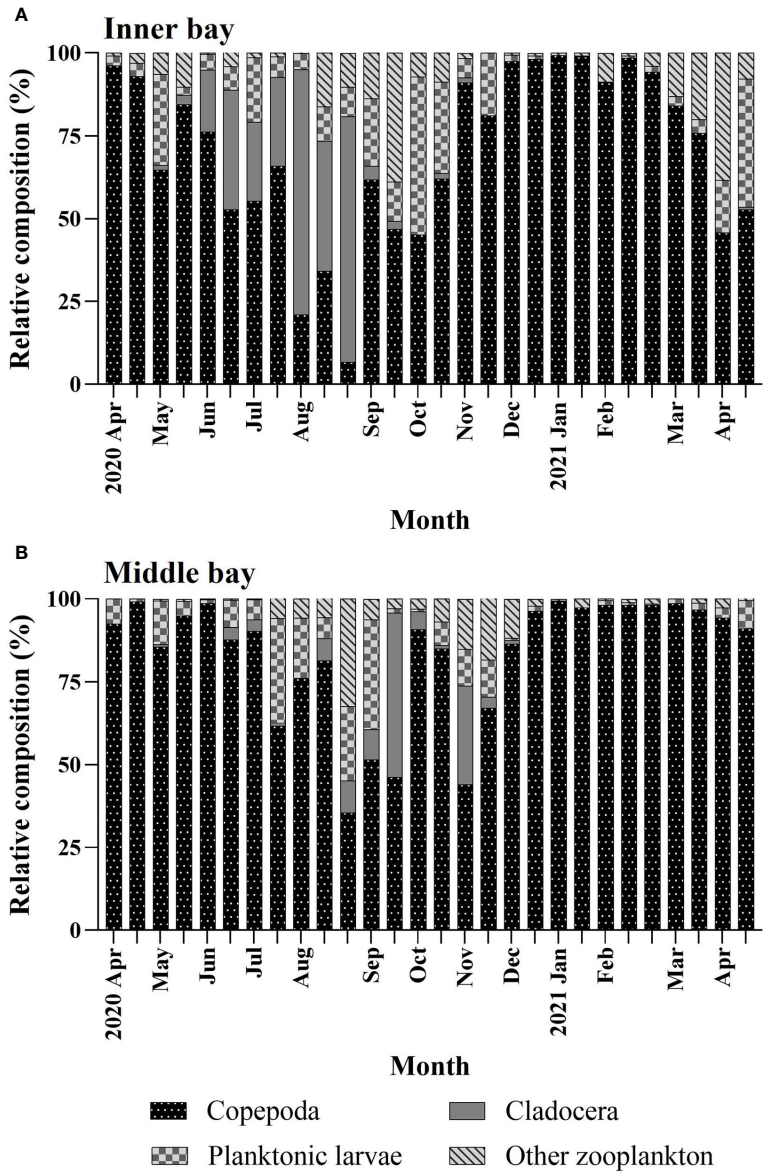


FIGURE 4
Temporal variations in percentages of mesozooplankton composition in the **(A)** inner bay and **(B)** middle bay in Gamak Bay from April 2020 to April 2021.

P. tergestina ranged from 0 to 5,008 indiv. m^{-3} (1,408 ± 1,810 indiv. m^{-3} on average) in the inner bay and from 0 to 340 indiv. m^{-3} (79 ± 143 indiv. m^{-3} on average) in the middle bay (Figure 6B), and this difference was found to be statistically significant (Mann-Whitney U-test, $p < 0.05$). The abundance of *P. avirostris* ranged from 0 to 2,373 indiv. m^{-3} (461 ± 852 indiv. m^{-3} on average) in the inner bay and from 0 to 265 indiv. m^{-3} (60 ± 115 indiv. m^{-3} on average) in the middle bay (Figure 6C); however, this difference was not statistically significant (Mann-Whitney U-test, $p > 0.05$). Furthermore, the abundance of copepods was higher in the middle bay. Specifically, *A. sinjiensis* ranged from 0 to 483 indiv. m^{-3} (91 ± 172 indiv. m^{-3} on average) in the inner bay and from 4 to 1767 indiv. m^{-3} (568 ± 735 indiv. m^{-3} on average) in the middle bay (Figure 6D), and this difference was found to be statistically significant (Mann-Whitney U-test, $p < 0.05$).

The two taxonomic groups differed in occurrence times between the inner and the middle bay. Compared with *A. sinjiensis*, three cladocerans appeared approximately a month earlier in the inner bay than in the middle bay, and disappeared earlier. Interestingly, *P. polyphemoides* showed similar patterns between the two regions (Figure 7A). In the inner bay, they

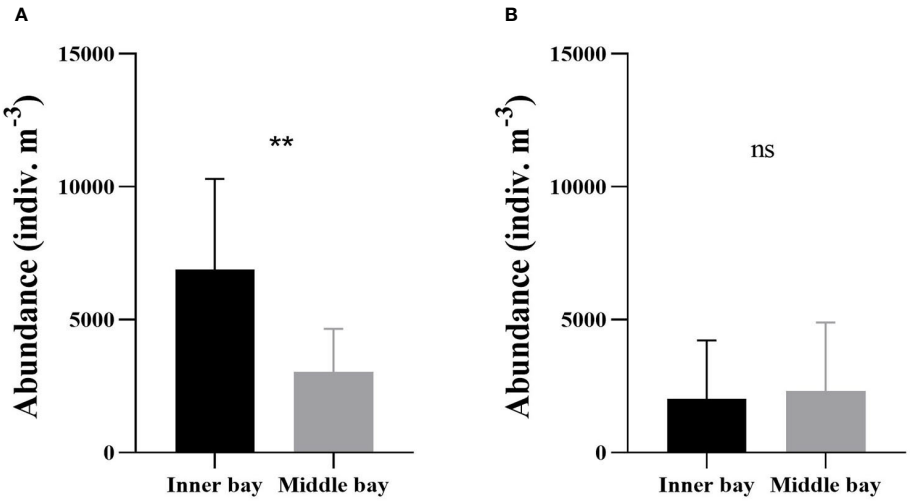


FIGURE 5
Mean mesozooplankton abundance in the inner bay and the middle bay of Gamak Bay during the **(A)** hypoxic period (from June to September) and **(B)** normoxic period (from October to May). Spatial differences in mesozooplankton abundance were tested with Mann-Whitney U-tests. Asterisks stand for significant-difference levels between inner and middle bay: $^{**}p < 0.01$; ns, not significant.

appeared in May and showed the first peak of 2,156 indiv. m^{-3} in mid-June when the bottom was hypoxic. In early July, before the temporary disappearance of hypoxia, they sharply decreased to 40 indiv. m^{-3}, and in early-August, they showed a second peak of 2,315 indiv. m^{-3}. They appeared in small numbers after hypoxia had completely disappeared and did not appear after early-November. In the middle bay, they appeared in May, and the abundance increased and decreased repeatedly. The maximum abundance was 993 indiv. m^{-3} in early-November. After that, they decreased sharply and did not appear after early-December. *P. tergestina* appeared approximately a month earlier in the inner bay compared to the middle bay, and disappeared a month earlier (Figure 7B). In the inner bay, *P. tergestina* appeared in mid-June (25 indiv. m^{-3}) when the bottom was hypoxic, and the maximum abundance was 5,008 indiv. m^{-3} in late-August. After mid-September, when hypoxia had completely disappeared, the abundance decreased sharply and *P. tergestina* was not detected in November. In the middle bay, 52 indiv. m^{-3} appeared in mid-July, and the maximum abundance was 340 indiv. m^{-3} in late-August. After that, they decreased sharply and did not appear from late-September to October, then appeared again in November and did not appear from December onward. *P. avirostris* in the inner bay appeared approximately one month earlier in the inner bay compared to the middle bay, and disappeared two months earlier (Figure 7C). In the inner bay, it appeared in mid-July, when hypoxia had temporarily disappeared, and in mid-August, when hypoxia occurred again, the maximum abundance was 2,373 indiv. m^{-3}. From this point, they decreased sharply and disappeared in September. In the middle bay, they appeared 262 indiv. m^{-3} in mid-August, and the maximum abundance was 265 indiv. m^{-3} in mid-September. Since then, they decreased sharply and disappeared in November. Compared to cladocerans, copepods exhibited the opposite pattern. *A. sinjiensis* appeared approximately a month and a half earlier in the middle bay than in the inner bay, and disappeared a month earlier (Figure 7D). In the inner bay, they appeared in mid-July, when hypoxia had temporarily disappeared, and in mid-August, when hypoxia occurs again, the maximum abundance was 483 indiv. m^{-3}. After that, they decreased sharply, and appeared in small abundances, and disappeared after early-November. In the middle bay, 11 indiv. m^{-3} appeared in early-June, after which they reached 1,700 indiv. m^{-3} throughout July. After that, they gradually decreased and disappeared after early-October.

Relationship between dominant species during the hypoxic period and environmental variables

The relationship between the dominant species of the hypoxic period and environmental variables (Temperature, salinity, DO concentration, total Chl-*a* concentration and size-fractionated Chl-*a* concentration) was analyzed using RDA. In the inner bay, the model explained 75.4% of the variance of dominant species and environmental data on the first two axes (Table 2). Furthermore, the species-environment correlations of axes 1 (0.92) and 2 (0.80) were relatively high. The environmental variables in axes 1 and 2 explained 97% of the variance in dominant species. The eigenvalues of the RDA were

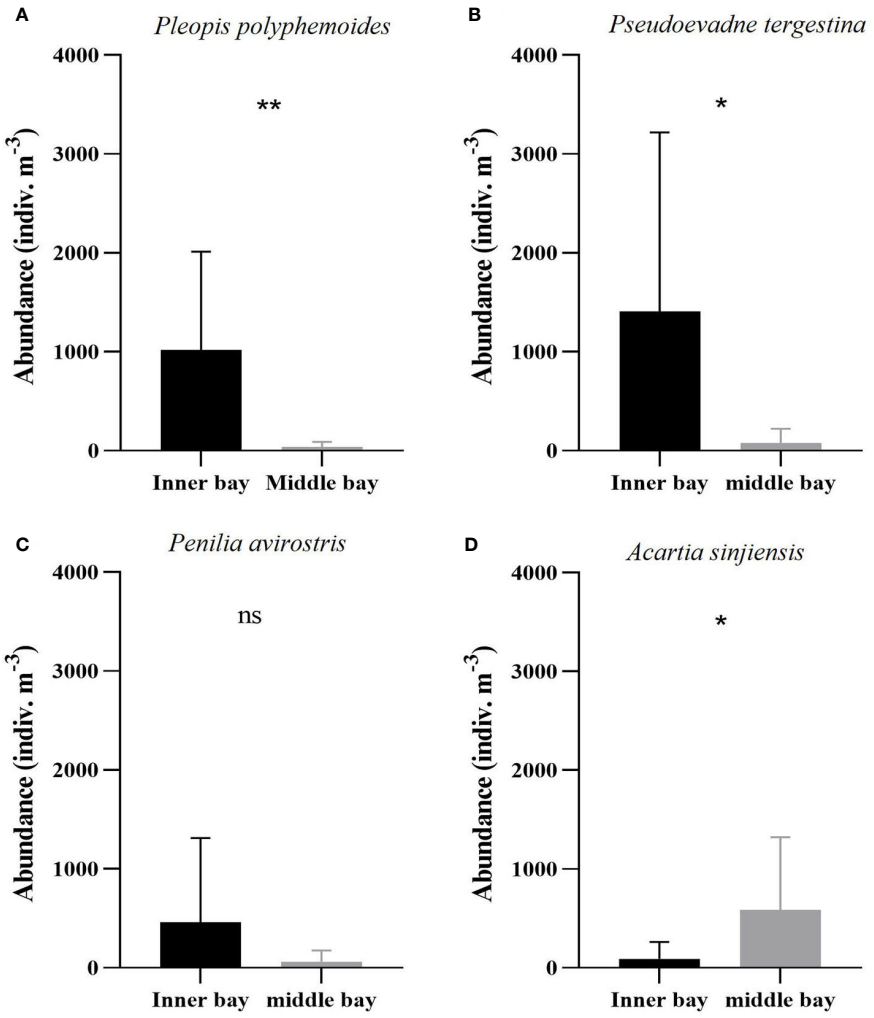


FIGURE 6
Mean dominant species abundance including **(A)** *Pleopis polyphemoides*, **(B)** *Pseudoevadne tergestina*, **(C)** *Penilia avirostris*, and **(D)** *Acartia sinjiensis* in the inner bay and the middle bay of Gamak Bay during the hypoxic period (from June to September). Spatial differences in dominant species abundance were tested with Man-Whitney U-tests. Asterisks stand for significant-difference levels between inner and middle bay: *$p < 0.05$; **$p < 0.01$; ns, not significant.

statistically significant according to Monte Carlo permutations. Temperature, salinity, bottom DO concentration, total Chl-*a* concentration, and the 3–20 μm and < 3 μm categories of Chl-*a* concentration were the most important parameters affecting the variation of certain dominant species ($p < 0.05$). *P. polyphemoides* showed a positive correlation with water temperature and the < 3 μm categories of Chl-*a* concentration, and a negative correlation with bottom DO concentration. *P. tergestina*, *P. avirostris* and *A. sinjiensis* showed a positive correlation with temperature, total and 3–20 μm categories of Chl-*a* concentration, and a negative correlation with salinity (Figure 8A).

In the middle bay, the model explained 56.6% of the variance of dominant species and environmental data on the first two axes (Table 3). Furthermore, the species-environment correlations of axes 1 (0.95) and 2 (0.71) were relatively high. The environmental variables in axes 1 and 2 explained 90% of the variance in dominant species. The eigenvalues of the RDA were statistically significant according to Monte Carlo permutations. Temperature, salinity, surface, bottom DO concentration, and the < 3 μm categories of Chl-*a* concentration were the most important parameters affecting the variation of certain dominant species ($p < 0.05$). The three cladoceran species showed a positive correlation with temperature, coupled with a negative correlation with salinity and surface and bottom DO concentration. *A. sinjiensis* showed a positive correlation with temperature and the < 3 μm categories of Chl-*a* concentration (Figure 8B).

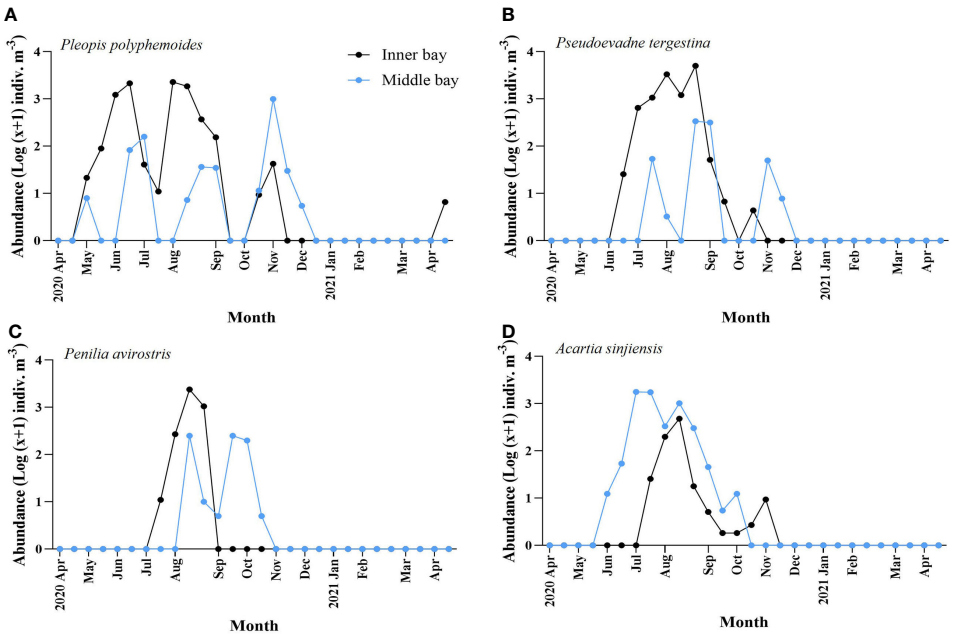


FIGURE 7
Temporal variation of abundance of dominant species including **(A)** *Pleopis polyphemoides*, **(B)** *Pseudoevadne tergestina*, **(C)** *Penilia avirostris*, and **(D)** *Acartia sinjiensis* in the inner bay and middle bay of Gamak Bay from April 2020 to April 2021.

Discussion

The unique marine environment of Gamak Bay caused a decrease in DO concentration in summer and, particularly, an oxygen deficiency in the bottom of the inner Gamak Bay, which affected the mesozooplankton community structure. Previous studies have shown that zooplankton exhibits multiple responses when exposed to hypoxia (Marcus et al., 2004; Ekau et al., 2010; Kimmel et al., 2010; Elliott et al., 2013; Keister et al., 2020; He et al., 2021). Hypoxia not only causes the direct mortality of mesozooplankton but also negatively affects metabolism, productivity, growth, vertical migration, and distribution (Auel and Verheye, 2007). However, previous studies have demonstrated that many zooplankton prefer hypoxia as a refuge to tolerate hypoxia or avoid predators, either through vertical or seasonal migration (Ludsin et al., 2009).

Although many approaches to zooplankton collection *in situ* have been performed with respect to hypoxia, none have been completely satisfactory and their uncritical use may confound the interpretation of the results (Roman et al., 1993; Moon et al., 2006; Jang et al., 2015). In this study, the vertical hauls sampling of mesozooplankton from the bottom to the surface using a conical net without a closing device has methodological problems (avoidance or depth of distribution of mesozooplankton) in understanding the effect of hypoxia (Roman et al., 1993; Jang et al.,2015). Nevertheless, this method can directly and conveniently collect mesozooplankton in coastal waters. Also, direct death under hypoxic conditions

TABLE 2 Summary of the results of the redundancy analysis (RDA) between environmental variables and dominant species in the inner bay.

Axes	1	2	3	4	Total variance
Eigenvalues	0.667	0.087	0.017	0.006	1
Species-environment correlations	0.92	0.809	0.542	0.549	
Cumulative percentage variance:					
- of species data	66.7	75.4	77.2	77.8	
- of species-environment relation	85.8	97	99.2	100	
Sum of all eigenvalues					1
Sum of all canonical eigenvalues					0.778

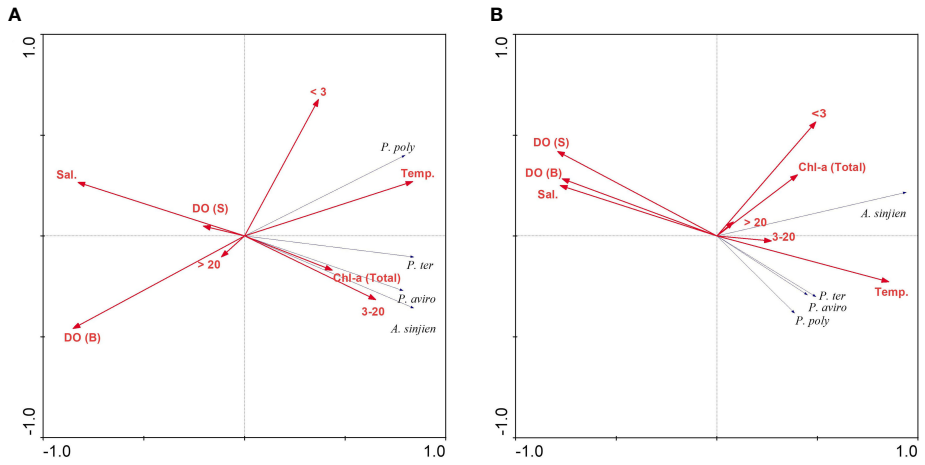


FIGURE 8
Results of the redundancy analysis (RDA) biplot of dominant species and environmental variables in the **(A)** inner bay and **(B)** middle bay. Dominant species are abbreviated as: *P. poly*, *Pleopis polyphemoides*; *P. ter*, *Pseudoevadne tergestina*; *P. aviro*, *Penilia avirostris*; *A. sinjien*, *Acartia sinjiensis*. Environmental variables are abbreviated as: Temp., Temperature; Sal., Salinity; DO (S), Dissolved oxygen (surface) concentration; DO **(B)**, Dissolved oxygen (bottom) concentration; Chl-*a* (Total), total Chl-*a* concentration; > 20, > 20 μm categories of Chl-*a* concentration; 3–20, 3–20 μm categories of Chl-*a* concentration; < 3, < 3 μm categories of Chl-*a* concentration.

will only occur if the organism is unable to move. The apparent avoidance behavior of zooplankton in hypoxic conditions may also respond differently depending on region and population. In the laboratory, the *Acartia tonsa* population from the Chesapeake Bay exhibited hypoxia avoidance behavior (Stalder and Marcus, 1997), and the *A. tonsa* population from the Gulf of Mexico did not avoid hypoxia at low 0.1 mg L^{-1} (Decker et al., 2003).

In this study, mesozooplankton abundance was higher in the inner bay than in the middle bay during the hypoxic period. This may be due to the high primary production in the inner bay, which increases the grazing and productivity of the zooplankton (Shi et al., 2019). During the hypoxic period in Gamak Bay, phytoplankton is largely generated by abundant nutrients under the thermocline and sufficient solar radiation (Kim et al., 2006). In this study, Chl-*a* concentration peaked in the inner bay during the hypoxic period. According to previous studies, the response of the zooplankton population was expected to increase with functional grazing and reproductive capacity as primary production increased (Blaxter et al., 1998; Tan et al., 2004). Therefore, the influx of nutrients causing hypoxia can indirectly improve mesozooplankton abundance through an increase in food supply (Shi et al., 2019).

In this study, a total of 45 and 52 taxa were identified in the inner and middle bay, respectively. Water temperature and salinity are important factors that determine the spatial and temporal distribution of zooplankton (Froneman, 2004; Shin et al., 2022). In the inner bay, most of the population was due to the active reproductive ability of cladocerans in summer when the water temperature was high, and copepods dominated in winter. In spring and autumn, copepods, planktonic larvae, and other zooplankton appeared to form the mesozooplankton community. In the middle bay, a higher proportion of copepods appeared compared to the inner bay. During the hypoxic period, cladocerans showed a high composition in July and August in the inner bay, whereas they were higher

TABLE 3 Summary of the results of the redundancy analysis (RDA) between environmental variables and dominant specie in the middle bay.

Axes	1	2	3	4	Total variance
Eigenvalues	0.48	0.086	0.053	0.01	1
Species-environment correlations	0.954	0.711	0.597	0.25	
Cumulative percentage variance:					
- of species data	48	56.6	61.9	62.9	
- of species-environment relation	76.3	90	98.5	100	
Sum of all eigenvalues					1
Sum of all canonical eigenvalues					0.629

after September in the middle bay. Our data confirmed that the composition of mesozooplankton species, abundance, and spatiotemporal distribution was different due to differences in the tolerance of taxa in the hypoxic period. Cladocerans may exhibit preferential growth compared to copepods at the inner station of Gamak Bay, where hypoxia frequently occurs in summer. When dissolved oxygen levels are between the minimum and critical levels, copepod growth, development, physiology, and behavior change with dissolved oxygen levels (Brett, 1979; Dinh et al., 2020). Copepod survival and egg production are significantly lower at lower DO concentrations (Lutz et al., 1992; Roman et al., 1993; Keister et al., 2000: Marcus et al., 2004; Sedlacek and Marcus, 2005). The ability of cladocerans to synthesize hemoglobin is common, and this ability has been suggested as an adaptation to an unpredictable environment in which oxygen concentrations may abruptly drop to fatally low levels (Heisey and Porter, 1977; Weider and Lampert, 1985).

Copepods and cladocerans that generally form their populations through dormant eggs, but they have different life history strategies. Most cladocerans can reproduce rapidly through parthenogenesis during periods of favorable conditions (Egloff et al., 1997; Uye et al., 2000). On the other hand, copepods exhibit sexual reproduction, and must undergo a series of developmental stages to reach the adult stage (Dussart and Defaye, 1995). The temporal difference in the life history of these two taxa is an important factor in maintaining adaption and population under favorable or unfavorable conditions.

One of the major characteristics of the seasonal dynamics of zooplankton in temperate waters is their dormancy during their life cycle. Particularly, copepods and cladocerans produce dormant eggs to survive in adverse environmental conditions (Onbé et al., 1996; Marcus, 1996). These dormant eggs go through a refractory period and when favorable conditions are established, they hatch temporarily and join the population. That is, repeated generation maintenance strategies are taken (Marazzo and Valentin, 2004; Choi et al., 2021). In this study, the rapidly increased mesozooplankton abundance in the inner bay in summer and autumn was likely due to the hatching of dormant eggs and provide an environment for temporary mass reproduction. However, dormant eggs in the field were not investigated, so it cannot be predicted easily. Nevertheless, the dormant eggs of copepods and cladocerans clearly hatched at the inner bay, which have been hypoxic for a considerable time, making significant contributions to the food web of the Gamak Bay ecosystem.

In this study, the total mesozooplankton abundance in the inner bay was mainly contributed by cladocerans during the hypoxic period. In the inner bay, cladocerans appeared from May, when the water temperature gradually increased, and the number of more than 5,000 indiv. m^{-3} continued to appear throughout August when the average water temperature was 25.6–26.5 °C and the average salinity was 29.3–31. After that, the water temperature gradually decreased and the salinity increased, so they did not appear. In this study, three species of cladocerans dominated at different times (coexisting and separating), and the order of appearance was *P. polyphemoides*, *P. tergestina*, and *P. avirostris*. The optimal environmental conditions for cladocerans are known to vary by region, and this separation is often explained by the optimal temperature and salinity conditions for each species (Egloff et al., 1997). *P. polyphemoides* appeared in a wider water temperature and salinity range than the other two species. Although *P. tergestina* and *P. avirostris* had similar preferred salinity ranges, *P. tergestina* had a wider range of water temperature than *P. avirostris*. Therefore, we concluded that the three species of cladocerans were able to maintain a high population by separating or coexisting in the inner bay because each species had different ranges of preferred water temperature and salinity according to their physiological characteristics.

Cladocerans responded to low oxygen conditions depending on their size. Karpowicz et al. (2020) found that small freshwater rotifers and small freshwater cladocerans were more resistant to hypoxia than larger freshwater cladocerans, and that this oxygen stress is one of the most important factors to alter the structure of zooplankton in lakes. In this study, cladocerans were far more dominant than copepods through their rapid reproductive capacity during the hypoxic period in the inner bay. The order of appearance was *P. polyphemoides*, *P. tergestina*, and *P. avirostris*, and the earlier the species appeared, the longer it appeared. *P. polyphemoides* appeared when the bottom DO concentration was 5.2 mg L^{-1}, and peaked when a low bottom DO concentration of 1.2 to 1.5 mg L^{-1} was formed. When the hypoxia had temporarily disappeared, they did not appear. Even after hypoxia had completely disappeared, they also appeared at a DO concentration of 6 mg L^{-1}. *P. tergestina* began to appear at the end of June when hypoxia first occurred, and the abundance increased even when hypoxia had temporarily disappeared. After that, the maximum abundance was shown in the hypoxic condition of 1.9 mg L^{-1}, and when the hypoxia had disappeared, and decreased rapidly and appeared in small numbers until October. *P. avirostris* appeared in mid-July, when the hypoxia had temporarily disappeared, and the maximum abundance was in mid-August, when the bottom DO concentration was very low at 0.7 mg L^{-1}. After that, they did not appear even though the hypoxia was not over. In this study, the average body length of the three species was approximately 0.65 mm for *P. polyphemoides*, 1.3 mm for *P. tergestina*, and 1.4 mm for *P. avirostris*, and the later appearance period, the larger the species appeared. Therefore, it is believed that *P. polyphemoides*, which are the smallest in size, tolerated the hypoxic period for the longest time, and the *P. avirostris*, which are relatively large in size, are not likely to survive the hypoxic period for long.

Copepods, cladocerans and planktonic larvae are the most important mesozooplankton taxa in Gamak Bay (Soh et al., 2002; Choi, 2020). Katechakis et al. (2004) suggested that

copepods, crustaceans, and dolioida could coexist in summer due to different food selectivity and ingestion and assimilation rates. *Acartia clausi* reached the highest grazing coefficient for large algae over 70 μm, and *P. avirostris* covered nanoflagellates and ciliates ranging from 2.5–100 μm. It is a known fact that cladocerans are mostly filter feeders with strong feeding preferences for bacteria, microzooplankton and certain phytoplankton species. The feeding pattern of Podonidae (*P. polyphemoides* and *P. tergestina*), which appeared dominant in this study, is known as a raptorial feeder (Jagger et al., 1988), they prey largely on diatoms (Jagger et al., 1988; Kim et al., 1989) and potentially on flagellates, including heterotrophs and autotrophs (Turner et al., 1988). *P. avirostris* is also known as a filter feeder, feeding on bacteria and nanoflagellates (Paffenhöfer and Orcutt, 1986; Turner et al., 1988) and larger diatoms (Kim et al., 1989). In this study, the reason cladocerans can dominate the mesozooplankton community in Gamak Bay may be due to their broader feeding efficiency. However, only three sizes of phytoplankton were considered in this study, and this may not be sufficient to explain the observed variability.

The RDA results indicated that the dominant species showed a significant correlation with water temperature, salinity, DO concentration, total Chl-*a* concentration, and size-fractionated Chl-*a* concentration among environmental variables. In the inner bay, *P. polyphemoides* showed a positive correlation with water temperature and the < 3 μm categories of Chl-*a* concentration, and a negative correlation with bottom DO concentration. *P. tergestina*, *P. avirostris*, and *A. sinjiensis* showed a positive correlation with water temperature and the 3–20 μm categories of Chl-*a* concentration and a negative correlation with salinity. In the middle bay, cladocerans showed a positive correlation with water temperature and a negative correlation with surface and bottom DO concentration, *A. sinjiensis* showed a positive correlation with water temperature and the < 3 μm categories of Chl-*a* concentration. In general, in temperate waters with distinct seasonal changes, mesozooplankton is more affected by water temperature and salinity. Therefore, the results of this study are considered valid. Furthermore, hypoxic environments may play a role in reducing zooplankton abundance in eutrophic systems (Park and Marshall, 2000). However, several studies have also shown that zooplankton can exhibit high abundance in hypoxic environments (Roman et al., 2019; Karpowicz et al., 2020). As a result, the environmental factors (non-oxygen) that affect the dominant species in the two regions are different, but considering the characteristics of the sea area where seawater flow was low and high phytoplankton proliferated, our findings indicated that an appropriate habitat for dominant species had been created.

Conclusion

The fluctuations of zooplankton communities in coastal areas where hypoxia occurs frequently depend on the tolerance of taxa and seasonal fluctuations. In this study, we observed the effect of hypoxia on zooplankton community distribution. During the hypoxic period, cladocerans were found to be more tolerant than copepods in the inner bay where hypoxia is formed. Most of them experience a strong hypoxic state rather than an anaerobic state over the years, eventually changing the structure and function of the ecosystem. However, we did not find clear evidence that cladocerans and copepods could advance their appearance according to space in the hypoxia period. These results provide important information for understanding the response of mesozooplankton under hypoxic conditions as hypoxia gradually intensifies due to climate change or environmental pollution in the future.

Data availability statement

The raw data supporting the conclusions of this article will be made available by the authors, without undue reservation.

Author contributions

EHL conceived and designed the experiments, performed the experiments, analyzed the data, prepared figures and/or tables, authored or reviewed drafts of the paper, and approved the final draft. SYC conceived and designed the experiments, performed the experiments, analyzed the data, authored or reviewed drafts of the paper, and approved the final draft. MHS conceived and performed the experiments, analyzed the data, prepared figures and/or tables, authored or reviewed drafts of the paper, and approved the final draft. HYS contributed to funding acquisition, conceptualization of the experiments, data interpretation and discussion, authored or reviewed drafts of the paper, and approved the final draft. All authors contributed to the article and approved the submitted version.

Funding

This research was part of a project titled “Research center for fishery resource management based on the information and communication technology” (2022, grant number 20180384), funded by the Ministry of Oceans and Fisheries, Korea, and by the National Marine Biodiversity Institute of Korea (grant number 2022M01100).

Acknowledgments

We thank the reviewers for their valuable comments and suggestions on the manuscript.

Conflict of interest

The authors declare that the research was conducted in the absence of any commercial or financial relationships that could be construed as a potential conflict of interest.

Publisher's note

All claims expressed in this article are solely those of the authors and do not necessarily represent those of their affiliated organizations, or those of the publisher, the editors and the reviewers. Any product that may be evaluated in this article, or claim that may be made by its manufacturer, is not guaranteed or endorsed by the publisher.

Supplementary material

The Supplementary Material for this article can be found online at: https://www.frontiersin.org/articles/10.3389/fmars.2022.1005442/full#supplementary-material

References

Altieri, A. H., and Gedan, K. B. (2015). Climate change and dead zones. *Glob. Change Biol.* 21, 1395–1406. doi: 10.1111/gcb.12754

Atienza, D., Saiz, E., Skovgaard, A., Trepat, I., and Calbet, A. (2008). Life history and population dynamics of the marine cladoceran *Penilia avirostris* (Branchiopoda: Cladocera) in the Catalan Sea (NW Mediterranean). *J. Plankton Res.* 30, 345–357. doi: 10.1093/plankt/fbm109

Auel, H., and Verheye, H. M. (2007). Hypoxia tolerance in the copepod *Calanoides carinatus* and the effect of an intermediate oxygen minimum layer on copepod vertical distribution in the northern benguela current upwelling system and the Angola–benguela front. *J. Exp. Mar. Biol. Ecol.* 352, 234–243. doi: 10.1016/j.jembe.2007.07.020

Bendtsen, J., and Hansen, J. L. S. (2013). Effects of global warming on hypoxia in the Baltic Sea – north Sea transition zone. *Ecol. Model.* 264, 17–26. doi: 10.1016/j.ecolmodel.2012.06.018

Blaxter, J. H. S., Douglas, B., Tyler, P. A., and Mauchline, J. (1998). *The biology of calanoid copepods* Vol. 33 (San Diego: Academic Press).

Breitburg, D., Levin, L. A., Oschlies, A., Grégoire, M., Chavez, F. P., Conley, D. J., et al. (2018). Declining oxygen in the global ocean and coastal waters. *Science* 359, eaam7240. doi: 10.1126/science.aam7240

Brett, J. R. (1979). "Environmental factors and growth," in *Fish physiology*, vol. VIII . Eds. W. S. Hoar, D. J. Randall and J. R. Brett (New York: Academic Press), 599–675.

Carstensen, J., Andersen, J. H., Gustafsson, B. G., and Conley, D. J. (2014). Deoxygenation of the Baltic Sea during the last century. *Proc. Natl. Acad. Sci.* 111, 5628–5633. doi: 10.1073/pnas.1323156111

Choi, S. Y. (2020). *Spatial and temporal distribution of acartia (Crustacea, copepoda, calanoida) species in the southern coastal waters of Korea and the physio-ecological characteristics of acartia erythraea* (Yeosu, Korea: Chonnam National University).

Choi, S. Y., Jang, M. C., Youn, S. H., Seo, M. H., and Soh, H. Y. (2021). Egg production and hatching patterns of *Acartia erythraea* (Copepoda, calanoida), with a note on its two egg types, in a eutrophic bay in Korea. *J. Plankton Res.* 43, 428. doi: 10.1093/plankt/fbab030

Conley, D. J., Bjoürck, S., Bonsdorff, E., Carstensen, J., Destouni, G., Gustafsson, B. G., et al. (2009). Hypoxia-related processes in the Baltic Sea. *Environ. Sci. Technol.* 43, 3412–3420. doi: 10.1021/es802762a

Decker, M. B., Breitburg, D. L., and Marcus, N. H. (2003). Geographical differences in behavioral responses to hypoxia: local adaptation to an anthropogenic stressor? *Ecol. Appl.* 13, 1104–1109. doi: 10.1890/1051-0761(2003)13[1104:GDIBRT]2.0.CO;2

Diaz, R. J. (2001). Overview of hypoxia around the world. *J. Environ. Qual.* 30, 275–281. doi: 10.2134/jeq2001.302275x

Diaz, R. J., and Rosenberg, R. (2008). Spreading dead zones and consequences for marine ecosystems. *Science* 321, 926–929. doi: 10.1126/science.1156401

Dinh, K. V., Cuevas-Sanchez, A. Y., Buhl, K. S., Moeser, E. A., and Dowd, W. (2020). Heat tolerance and thermal preference of the copepod *Tigriopus californicus* are insensitive to ecologically relevant dissolved oxygen levels. *Sci. Rep.* 10, 1–10. doi: 10.1038/s41598-020-75635-z

Dussart, B. H., and Defaye, D. (1995). *Copepoda: Introduction to the copepoda* (Amsterdam: SPB Academic Publishing), 277.

Egloff, D. A., Fofonoff, P. W., and Onbé, T. (1997). Reproductive biology of marine cladocerans. *Adv. Mar. Biol.* 31, 79–168. doi: 10.1016/S0065-2881(08)60222-9

Ekau, W., Auel, H., Pörtner, H. O., and Gilbert, D. (2010). Impacts of hypoxia on the structure and processes in pelagic communities (zooplankton, macro-invertebrates and fish). *Biogeosciences* 7, 1669–1699. doi: 10.5194/bg-7-1669-2010

Elliott, D. T., Pierson, J. J., and Roman, M. R. (2012). Relationship between environmental conditions and zooplankton community structure during summer hypoxia in the northern gulf of Mexico. *J. Plankton Res.* 34, 602–613. doi: 10.1093/plankt/fbs029

Elliott, D. T., Pierson, J. J., and Roman, M. R. (2013). Predicting the effects of coastal hypoxia on vital rates of the planktonic copepod *Acartia tonsa* Dana. *PloS One* 8, e63987. doi: 10.1371/journal.pone.0063987

Froneman, P. W. (2004). Zooplankton community structure and biomass in a southern African temporarily open/closed estuary. *Estuar. Coast. Shelf Sci.* 60, 125–132. doi: 10.1016/j.ecss.2003.12.002

Grodzins, M. A., Ruz, P. M., and Keister, J. E. (2016). Effects of oxygen depletion on field distributions and laboratory survival of the marine copepod *Calanus pacificus*. *J. Plankton Res.* 38, 1412–1419. doi: 10.1093/plankt/fbw063

Hansen, F. C., Möllmann, C., Schütz, U., and Neumann, T. (2006). Spatio-temporal distribution and production of calanoid copepods in the central Baltic Sea. *J. Plankton Res.* 28, 39–54. doi: 10.1093/plankt/fbi097

Heisey, D., and Porter, K. G. (1977). The effect of ambient oxygen concentration on filtering and respiration rates of *Daphnia galeata mendotae* and *Daphnia magna*. *Limnol. Oceanogr.* 22, 839–845. doi: 10.4319/lo.1977.22.5.0839

He, X., Pan, Z., Zhang, L., and Han, D. (2021). Physiological and behavioral responses of the copepod *Temora turbinata* to hypoxia. *Mar. pollut. Bull.* 171, 112692. doi: 10.1016/j.marpolbul.2021.112692

IPCC (2013). *Climate change 2013: the physical science basis: Working group I contribution to the fifth assessment report of the intergovernmental panel on climate change*. Eds. T. F. Stocker, D. Qin, G.-K. Plattner, M. Tignor, S. K. Allen, J. Boschung, A. Nauels, Y. Xia, V. Bex and P. M. Midgley (Cambridge: Cambridge Univ. Press).

Isinibilir, M. (2009). Annual crustacean zooplankton succession (Copepoda and cladocera) in the upper layer of ahirkapi coastal waters (northeastern Sea of marmara). *Crustaceana* 82, 669–678. doi: 10.1163/156854008X380273

Isinibilir, M., Kideys, A. E., Tarkan, A. N., and Yilmaz, I. N. (2008). Annual cycle of zooplankton abundance and species composition in izmit bay (the northeastern marmara Sea). *Estuar. Coast. Shelf Sci.* 78, 739–747. doi: 10.1016/j.ecss.2008.02.013

Jagger, R. A., Kimmerer, W. J., and Jenkins, G. P. (1988). Food of the cladoceran *Podon intermedius* in a marine embayment. *Mar. Ecol. Prog. Ser.* 43, 245–250. doi: 10.3354/meps043245

Jang, M. C., Shin, K., Jang, P. G., Lee, W. J., and Choi, K. H. (2015). Mesozooplankton community in a seasonally hypoxic and highly eutrophic bay. *Mar. Freshw. Res.* 66, 719–729. doi: 10.1071/MF14036

Jenny, J., Arnaud, F., Alric, B., Dorioz, J., Sabatier, P., Meybeck, M., et al. (2014). Global biogeochemical cycles lakes under global warming. *Glob. Biogeochem. Cycles* 28, 1413–1423. doi: 10.1002/2014GB004932

Karpowicz, M., Ejsmont-Karabin, J., Kozłowska, J., Feniova, I., and Dzialowski, A. R. (2020). Zooplankton community responses to oxygen stress. *Water* 12, 706. doi: 10.3390/w12030706

Katechakis, A., Stibor, H., Sommer, U., and Hansen, T. (2004). Feeding selectivities and food niche separation of *Acartia clausi*, *Penilia avirostris* (Crustacea) and *Doliolum denticulatum* (Thaliacea) in blanes bay (Catalan Sea, NW Mediterranean). *J. Plankton Res.* 26, 589–603. doi: 10.1093/plankt/fbh062

Keeling, R. F., Körtzinger, A. K., and Gruber, N. (2010). Ocean deoxygenation in a warming world. *Ann. Rev. Mar. Sci.* 2, 199–229. doi: 10.1146/annurev.marine.010908.163855

Keister, J. E., Houde, E. D., and Breitburg, D. L. (2000). Effects of bottom-layer hypoxia on abundances and depth distributions of organisms in patuxent river, Chesapeake bay. *Mar. Ecol. Prog. Ser.* 205, 43–59. doi: 10.3354/meps205043

Keister, J. E., Winans, A. K., and Herrmann, B. (2020). Zooplankton community response to seasonal hypoxia: a test of three hypotheses. *Diversity* 12, 21. doi: 10.3390/d12010021

Kemp, W. M., Boynton, W. R., Adolf, J. E., Boesch, D. F., Boicourt, W. C., and Brush, G. (2005). Eutrophication of Chesapeake bay: historical trends and ecological interactions. *Mar. Ecol. Prog. Ser.* 303, 1–29. doi: 10.3354/meps303001

Kim, S. Y., Jun, S. H., Lee, Y. S., Lee, Y. H., and Kim, B. M. (2011). Characteristics of phosphate flux at the sediment-water interface in gamak bay during the hypoxic water mass. *J. Environ. Sci. Int.* d20, 1069–1078. doi: 10.5322/JES.2011.20.9.1069

Kim, J., Lee, S. Y., Yu, J., Choi, Y. H., Jung, C., and Lee, P. (2006). The characteristics of oxygen deficient water mass in gamak bay. *J. Korean Soc Mar. Environ. Energy* 9, 216–224.

Kimmel, D. G., Boicourt, W. C., Pierson, J. J., Roman, M. R., and Zhang, X. (2010). The vertical distribution and diel variability of mesozooplankton biomass, abundance and size in response to hypoxia in the northern gulf of Mexico USA. *J. Plankton Res.* 32, 1185–1202. doi: 10.1093/plankt/fbp136

Kim, S. W., Onbé, T., and Yoon, Y. H. (1989). Feeding habits of marine cladocerans in the inland Sea of Japan. *Mar. Biol.* 100, 313–318. doi: 10.1007/BF00391145

Kim, J. B., Park, J. I., Jung, C. G., Choi, W. J., Lee, W. C., and Lee, Y. H. (2010). Physicochemical characteristics of seawater in gamak bay for a period of hypoxic water mass disappearance. *J. Korean Soc Mar.* 16, 241–248.

Klais, R., Lehtiniemi, M., Rubene, G., Semenova, A., Margonski, P., Ikauniece, A., et al. (2016). Spatial and temporal variability of zooplankton in a temperate semi-enclosed sea: implications for monitoring design and long-term studies. *J. Plankton Res.* 38, 652–661. doi: 10.1093/plankt/fbw022

Lee, T. (2015). Sediment oxygen consumption rate and hydrogen sulfide release by dissolved oxygen depletion in hypoxic area of the gamak bay, Korea. *J. Wet. Res.* 17, 293–302. doi: 10.17663/JWR.2015.17.3.293

Lee, K. H., and Cho, K. D. (1990). Distributions of the temperature and salinity in kamak bay. *Korean J. Fish. Aquat. Sci.* 23, 25–39.

Lee, Y. G., Jeong, D. U., Lee, J. S., Choi, Y. H., and Lee, M. O. (2016). Effects of hypoxia caused by mussel farming on benthic foraminifera in semi-closed gamak bay, south Korea. *Mar. pollut. Bull.* 109, 566–581. doi: 10.1016/j.marpolbul.2016.01.024

Lee, T., Kim, H. C., and Son, Y. B. (2019). Sediment oxygen consumption and hydrogen sulfide release in hypoxic areas of gamak bay, Korea. *Appl. Ecol. Environ. Res.* 17, 3199–3214. doi: 10.15666/aeer/1702_31993214

Li, D., Wen, Y., Zhang, G., Zhang, G., Xu, W., and Sun, J. (2022). Effects of terrestrial inputs on mesozooplankton community structure in bohai bay, China. *Diversity* 14, 410. doi: 10.3390/d14050410

Ludsin, S. A., Zhang, X., Brandt, S. B., Roman, M. R., Boicourt, W. C., Mason, D. M., et al. (2009). Hypoxia-avoidance by planktivorous fish in Chesapeake bay: implications for food web interactions and fish recruitment. *J. Exp. Mar. Biol. Ecol.* 381, S121–S131. doi: 10.1016/j.jembe.2009.07.016

Lutz, R. V., Marcus, N. H., and Chanton, J. P. (1992). Effects of low oxygen concentrations on the hatching and viability of eggs of marine calanoid copepods. *Mar. Biol.* 114, 241–247. doi: 10.1007/BF00349525

Marazzo, A., and Valentin, J. L. (2004). Reproductive aspects of marine cladocerans *Penilia avirostris* and *Pseudevadne tergestina* (Crustacea, branchiopoda) in the outer part of guanabara bay, Brazil. *Braz. J. Biol.* 64, 543–549. doi: 10.1590/S1519-69842004000300017

Marcus, N. H. (1996). Ecological and evolutionary significance of resting eggs in marine copepods: past, present, and future studies. *Hydrobiologia* 320, 141–152. doi: 10.1007/BF00016815

Marcus, N. H. (2001). "Zooplankton: responses to and consequences of hypoxia," in *Coastal hypoxia: Consequences for living resources and ecosystems*. Eds. N. N. Rabalais and R. E. Turner (Washington, DC: American Geophysical Union).

Marcus, N. H., Richmond, C., Sedlacek, C., Miller, G. A., and Oppert, C. (2004). Impact of hypoxia on the survival, egg production and population dynamics of *Acartia tonsa* Dana. *J. Exp. Mar. Biol. Ecol.* 301, 111–128. doi: 10.1016/j.jembe.2003.09.016

Moon, S. Y., Soh, H. Y., Choi, S. D., Jung, C. S., Kim, S. Y., and Lee, Y. S. (2006). Effect of a low-oxygen layer on the vertical distribution of zooplankton in gamak bay. *Korean J. Environ. Biol.* 24, 240–247.

Mullin, M. M., and Onbé, T. (1992). Diel reproduction and vertical distributions of the marine cladocerans, *Evadne tergestina* and *Penilia avirostris*, in contrasting coastal environments. *J. Plankton Res.* 14, 41–59. doi: 10.1093/plankt/14.1.41

NIFS (2010). *A survey on the actual conditions of fishery farming environment* (Yeosu: Chonnam National University), 109–150.

Noh, I. H. (2003). *The distribution of organic matter and its origin in core sediment in gamak bay, southern Korea* (Yeosu, Korea: Yeosu National University).

Omorii, M., and Ikeda, T. (1984). *Methods in marine zooplankton ecology* (New York: John Wiley and Sons. Inc), 25.

Onbé, T., Terazaki, M., and Nagasawa, S. (1996). Summer distribution of marine cladocerans in otsuchi bay, northeastern Honshu, Japan. *Bull. Plankton Soc Japan* 43, 121–131.

Paffenh¨ofer, G.-A., and Orcutt, J. D. (1986). Feeding, growth and food conversion of the marine cladoceran *Penilia avirostris*. *J. Plankton Res.* 8, 741–754. doi: 10.1093/plankt/8.4.741

Pan, J., Cheng, F., and Yu, F. (2018). The diel vertical migration of zooplankton in the hypoxia area observed by video plankton recorder. *Indian J. Mar. Sci.* 47, 1353–1363.

Park, G. S., and Marshall, H. G. (2000). The trophic contributions of rotifers in tidal freshwater and estuarine habitats. *Estuar. Coast. Shelf Sci.* 51, 729–742. doi: 10.1006/ecss.2000.0723

Parsons, T. R., Maita, Y., and Lalli, C. M. (1984). *A manual of chemical and biological methods for seawater analysis* (New York: Pergamon Press), 173.

Rabalais, N. N., Díaz, R. J., Levin, L. A., Turner, R. E., Gilbert, D., and Zhang, J. (2010). Dynamics and distribution of natural and human-caused hypoxia. *Biogeosciences* 7, 585–619. doi: 10.5194/bg-7-585-2010

Rakhesh, M., Raman, A. V., Ganesh, T., Chandramohan, P., and Dehairs, F. (2013). Small copepods structuring mesozooplankton community dynamics in a tropical estuary-coastal system. *Estuar. Coast. Shelf Sci.* 126, 7–22. doi: 10.1016/j.ecss.2013.03.025

Richmond, C., Marcus, N. H., Sedlacek, C., Miller, G. A., and Oppert, C. (2006). Hypoxia and seasonal temperature: Short-term effects and long-term implications for *Acartia tonsa* dana. *J. Exp. Mar. Biol. Ecol.* 328, 177–196. doi: 10.1016/j.jembe.2005.07.004

Roman, M. R., Brandt, S. B., Houde, E. D., and Pierson, J. J. (2019). Interactive effects of hypoxia and temperature on coastal pelagic zooplankton and fish. *Front. Mar. Sci.* 6. doi: 10.3389/fmars.2019.00139

Roman, M. R., Gauzens, A. L., Rhinehart, W. K., and White, J. R. (1993). Effects of low oxygen waters on Chesapeake bay zooplankton. *Limnol. Oceanogr.* 38, 1603–1614. doi: 10.4319/lo.1993.38.8.1603

Roman, M. R., Pierson, J. J., Kimmel, D. G., Boicourt, W. C., and Zhang, X. (2012). Impacts of hypoxia on zooplankton spatial distributions in the northern gulf of Mexico. *Estuaries coasts* 35, 1261–1269. doi: 10.1007/s12237-012-9531-x

Sedlacek, C., and Marcus, N. H. (2005). Egg production of the copepod *Acartia tonsa*: the influence of hypoxia and food concentration. *J. Exp. Mar. Biol. Ecol.* 318, 183–190. doi: 10.1016/j.jembe.2004.12.012

Seo, J. Y., Park, S. H., Lee, J. H., and Choi, J. W. (2012). Structural changes in macrozoobenthic communities due to summer hypoxia in gamak bay, Korea. *Ocean Sci. J.* 47, 27–40. doi: 10.1007/s12601-012-0003-9

Shi, Z., Liu, K., Zhang, S., Xu, H., and Liu, H. (2019). Spatial distributions of mesozooplankton biomass, community composition and grazing impact in association with hypoxia in the pearl river estuary. *Estuar. Coast. Shelf Sci.* 225, 106237. doi: 10.1016/j.ecss.2019.05.019

Shin, S. S., Choi, S. Y., Seo, M. H., Lee, S. J., Soh, H. Y., and Youn, S. H. (2022). Spatiotemporal distribution characteristics of copepods in the water masses of the northeastern East China Sea. *J. Mar. Sci. Eng.* 10, 754. doi: 10.3390/jmse10060754

Shin, H. H., Jung, S. W., Jang, M. C., and Kim, Y. O. (2013). Effect of pH on the morphology and viability of *Scrippsiella trochoidea* cysts in the hypoxic zone of a eutrophied area. *Harmful Algae* 28, 37–45. doi: 10.1016/j.hal.2013.05.011

Slater, W. L., Pierson, J. J., Decker, M. B., Houde, E. D., Lozano, C., and Seuberling, J. (2020). Fewer copepods, fewer anchovies, and more jellyfish: how does hypoxia impact the Chesapeake bay zooplankton community? *Diversity* 12, 35. doi: 10.3390/d12010035

Soh, H. Y., Lee, I. T., Yoon, Y. H., Choi, S. D., Lee, S. N., Han, M. I., et al. (2002). Species composition and occurrence patterns of zooplankton in gamag bay. *Korean J. Environ. Biol.* 20, 118–129.

Stalder, L. C., and Marcus, N. H. (1997). Zooplankton responses to hypoxia: behavioral patterns and survival of three species of calanoid copepods. *Mar. Biol.* 127, 599–607. doi: 10.1007/s002270050050

Tan, Y., Huang, L., Chen, Q., and Huang, X. (2004). Seasonal variation in zooplankton composition and grazing impact on phytoplankton standing stock in the pearl river estuary, China. *Cont. Shelf Res.* 24, 1949–1968. doi: 10.1016/j.csr.2004.06.018

Ter Braack, C. J. F., and Šmilauer, P. (2002). "CANOCO reference manual and user's guide to canoco for windows," in *Software for canonical community ordination (version 4.5)* (Ithaca, NY, USA: Microcomputer Power).

Turner, J. T., Tester, P. A., and Ferguson, R. L. (1988). The marine cladoceran *Penilia avirostris* and the "microbial loop" of pelagic food webs. *Limnol. Oceanogr.* 33, 245–255. doi: 10.4319/lo.1988.33.2.0245

Uye, S., Shimazu, T., Yamamuro, M., Ishitobi, Y., and Kamiya, H. (2000). Geographic and seasonal variations in mesozooplankton abundance and biomass in relation to environmental parameters in lake shinji-ohashi river- lake nakaumi brackish-water system, Japan. *J. Mar. Sys.* 26, 193–207. doi: 10.1016/S0924-7963(00)00054-3

Vaquer-Sunyer, R., and Duarte, C. M. (2008). Thresholds of hypoxia for marine biodiversity. *Proc. Natl. Acad. Sci.* 105, 15452–15457. doi: 10.1073/pnas.0803833105

Weider, L. J., and Lampert, W. (1985). Differential response of *Daphnia* genotypes to oxygen stress: respiration rates, hemoglobin content and low-oxygen tolerance. *Oecologia* 65, 487–491. doi: 10.1007/BF00379661

frontiers | Frontiers in Marine Science

TYPE Original Research
PUBLISHED 26 October 2022
DOI 10.3389/fmars.2022.986493

Check for updates

OPEN ACCESS

EDITED BY
Meilin Wu,
South China Sea Institute of Oceanology, (CAS), China

REVIEWED BY
Rajamanickam Krishnamurthy, Arignar Anna Government Arts and Science College Chennai, India
Thilagam Harikrishnan, Pachaiyappa's College for Men, India
Sudarshan Singh Rathore, Central Institute of Mining and Fuel Research, India

*CORRESPONDENCE
Gajendra Joshi
gajendrajoshi4@gmail.com

†PRESENT ADDRESS
Prasun Goswami,
Indian Institute of Science Education and Research, Kolkata, India

SPECIALTY SECTION
This article was submitted to Marine Pollution, a section of the journal Frontiers in Marine Science

RECEIVED 05 July 2022
ACCEPTED 06 September 2022
PUBLISHED 26 October 2022

CITATION
Joshi G, Verma P, Meena B, Goswami P, Peter DM, Jha DK, Vinithkumar NV and Dharani G (2022) Unraveling the potential of bacteria isolated from the equatorial region of Indian Ocean in mercury detoxification. *Front. Mar. Sci.* 9:986493. doi: 10.3389/fmars.2022.986493

COPYRIGHT
© 2022 Joshi, Verma, Meena, Goswami, Peter, Jha, Vinithkumar and Dharani. This is an open-access article distributed under the terms of the Creative Commons Attribution License (CC BY). The use, distribution or reproduction in other forums is permitted, provided the original author(s) and the copyright owner(s) are credited and that the original publication in this journal is cited, in accordance with accepted academic practice. No use, distribution or reproduction is permitted which does not comply with these terms.

Unraveling the potential of bacteria isolated from the equatorial region of Indian Ocean in mercury detoxification

Gajendra Joshi[1]*, Pankaj Verma[2], Balakrishnan Meena[1], Prasun Goswami[1†], D Magesh Peter[2], Dilip Kumar Jha[2], Nambali Valsalan Vinithkumar[1] and Gopal Dharani[2]

[1]Atal Centre for Ocean Science and Technology for Islands, National Institute of Ocean Technology, Ministry of Earth Sciences, Government of India, Port Blair, India, [2]Ocean Science and Technology for Islands, National Institute of Ocean Technology, Ministry of Earth Sciences, Government of India, Chennai, India

The marine environment is most vital and flexible with continual variations in salinity, temperature, and pressure. As a result, bacteria living in such an environment maintain the adaption mechanisms that are inherent in unstable environmental conditions. The harboring of metal-resistant genes in marine bacteria contributes to their effectiveness in metal remediation relative to their terrestrial counterparts. A total of four mercury-resistant bacteria (MRB) i.e. NIOT-EQR_J7 (*Alcanivorax xenomutans*); NIOT-EQR_J248 and NIOT-EQR_J251 (*Halomonas* sp.); and NIOT-EQR_J258 (*Marinobacter hydrocarbonoclasticus*) were isolated from the equatorial region of the Indian Ocean (ERIO) and identified by analyzing the 16S rDNA sequence. The MRBs can reduce up to 70% of Hg(II). The mercuric reductase (merA) gene was amplified and the mercury (Hg) volatilization was confirmed by the X-ray film method. The outcomes obtained from ICP-MS validated that the *Halomonas* sp. NIOT-EQR_J251 was more proficient in removing the Hg from culture media than other isolates. Fourier transform infrared (FT-IR) spectroscopy results revealed alteration in several functional groups attributing to the Hg tolerance and reduction. The Gas Chromatography-Mass Spectrometry (GC-MS) analysis confirmed that strain *Halomonas* sp. (NIOT-EQR_J248 and NIOT-EQR_J251) released Isooctyl thioglycolate (IOTG) compound under mercury stress. The molecular docking results suggested that IOTG can efficiently bind with the glutathione S-transferase (GST) enzyme. A pathway has been hypothesized based on the GC-MS metabolic profile and molecular docking results, suggesting that the compound IOTG may mediate mercuric reduction *via* merA-GST related detoxification pathway.

KEYWORDS

Mercury resistant bacteria, merA gene, FT-IR, GST enzyme, Metabolic pathway, Molecular docking

Introduction

Mercury (Hg) pollution poses a global threat to human and environmental health due to its noxiousness, mobility, and lengthy residence duration in the atmosphere (Raphael et al., 2011). Toxic metals rapidly accumulate in the food chain, impacting higher trophic levels, hence these are of principal concern nowadays (Raphael et al., 2011). According to recent research, oceanic release and biomass burning (organic compounds) account for the majority of worldwide Hg emissions, with anthropogenic activities accounting for the remaining significant percentage (Pirrone et al., 2010; Nelson et al., 2012; Serrano et al., 2013). Hg exists in elemental, inorganic, and organic forms in both land and water systems, depending on oxidation-reduction conditions. In the atmosphere, Hg with valence +2 is more extensively spread (Wang et al., 2004). In the biogeochemical cycle, a considerable part of Hg accumulates in seas and oceans by its atmospheric deposition (Bindler, 2003; Wang et al., 2004). The effects of human-induced sources on the Hg contents and its forms are extensively larger in the photic layers of oceans (Strode et al., 2007).

Numerous physico-chemical and biological methodologies have been implemented by industries and regulatory agencies to remediate Hg from polluted sites (Mahbub et al., 2017). Many studies suggested the use of marine bacteria for the bioremediation of harmful metals as they have an immense ability to conquer the continuous fluctuating pattern of pH, temperature, salinity, and other variable factors (Chikere et al., 2012; Naik et al., 2012; Dash et al., 2013). The population of Mercury-resistant bacteria (MRB) belongs to gram-positive as well as gram-negative groups that can easily grow in the toxic environment containing Hg and can convert the toxic form to a relatively nontoxic form (Dash and Das, 2012). The most commonly reported mechanism to develop resistance towards Hg in bacteria is mer operon mediated. It consists of various functional genes like merT, merP, merD, merA, merB, merG, merC along with the promoter and operator (Giri et al., 2014). Many MRB were previously isolated from Indian coastal areas which can thrive at 25 mg/L or greater levels of Hg (Dash and Das, 2014; De et al., 2014). These bacteria eliminate Hg through reductive volatilization, which means Hg^{2+} gets reduced to elemental Hg (Hg^0) through the catalytic activity of mercuric reductase enzyme encoded by merA gene and successfully detoxifies Hg polluted waters (De and Ramaiah, 2007; De et al., 2008).

In our recent study (Joshi et al., 2021), we isolated and characterized several MRBs from the deeper depth of the Central Indian Ocean and evaluated their ability to remove Hg from the culture media. However, no bacterial strain was observed from the surface seawater samples that were resistant to Hg up to 100 mg/L. Though various bacterial strains have been isolated from the coastal and oceanic region, so far. MRB from the equatorial region of the Indian Ocean (ERIO) is not studied. It is hypothesized that the marine bacteria from ERIO could be a potential resource for the reduction of Hg^{2+} as ERIO is highly dynamic in nature due to high current and intense climatological precipitation (Annamalai, 2010).

The present study was carried out to isolate the culturable MRBs (resistant up to 100 mg/L of Hg) from the surface seawater of the ERIO. To understand the effect of Hg ions on microbes and their mechanism to transform Hg^{2+} to Hg^0, various techniques such as PCR, ICP-MS, FT-IR, SEM, GC-MS, molecular docking etc. were used. The Hg tolerance, genotyping of merA gene, Hg reduction potential, Hg(II) depletion, alteration in functional groups, metabolites formed during Hg^{2+} reduction were determined for the isolates. This study explores the bacteria from the ERIO for Hg bioremediation potential which may be used in environmental pollution management.

Materials and methods

Study area, sample collection, and their analysis

The two sites of ERIO were selected for seawater samples collection. The GPS locations of selected sites were 00° 00′ 559″ N & 80° 37′ 919″ E and 00° 28′ 649″ N & 87° 50′ 546″ E. The samples were collected from the euphotic zone (5m depth) in sterile 100 mL glass bottles with the help of a Niskin water sampler fitted with a CTD rosette sampling device (Seabird Electronics), onboard ORV Sagar Nidhi (Cruise No. SN134) in October, 2018. Seawater samples were analyzed for temperature and salinity using a CTD profiler (Model 911 plus) and were processed immediately for microbial analysis. The CTD profiler was calibrated before use. The details of water sampling sites are given in supplementary information (SI) Table S1 and Figure 1.

Isolation and screening of total culturable bacteria (TCB) and CMRB

To isolate and enumerate total culturable bacteria (TCB) and culturable mercury-resistant bacteria (CMRB) under aerobic conditions, the previously described serial dilution method was adopted (Joshi et al., 2021). In brief, the stock solution (1 g/L) of mercuric chloride ($HgCl_2$, Merck) was prepared and the stability of the Hg stock solution was ensured by reducing the pH level below 2.0 using Suprapur elemental grade nitric acid (HNO_3, Merck, India). The detailed procedure is elaborated in the SI. TCB and CMRB were counted using the standard formula (CFU/mL). The percentage (%) of CMRB was calculated using the equation (1) as under:

$$\%\ of\ CMRB = (CMRB\ counts / TCB\ counts)\ x\ 100 \quad (1)$$

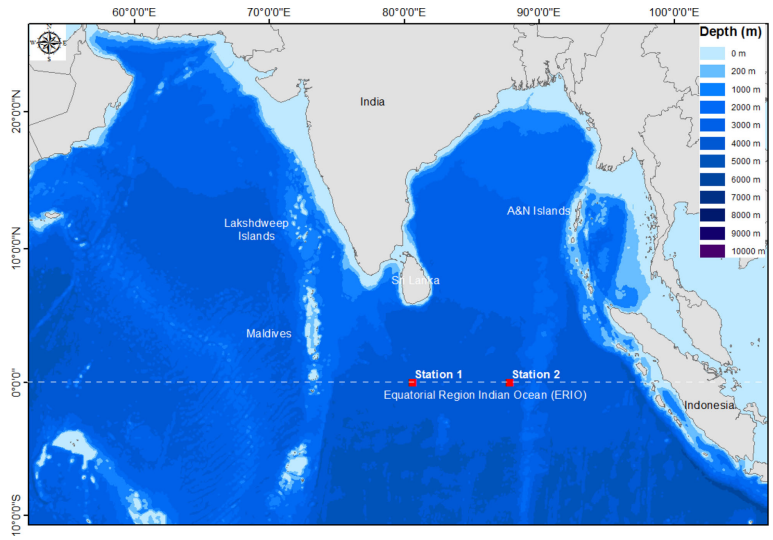


FIGURE 1
Study area map showing selected sites of ERIO for sample collection. The map was prepared using the Arc GIS software (Version 10.7.1).

Hg^{2+} tolerance by bacterial isolates

Hg tolerance of CMRBs was calculated by the broth dilution method (Konopka and Zakharova, 1999; Santos-Gandelman et al., 2014) with some modifications. CMRB cultures grown in Zobell Marine Broth medium (ZMB, Himedia, Mumbai) without Hg supplementation were used as a positive control, whereas ZMB treated with Hg (without bacteria) was used as a negative control in this study. To ensure the uniform bioavailability of Hg to the bacteria, uniform culture conditions were maintained across different experimental treatments. Based on the growth behavior of cultures in the presence of a higher concentration of $HgCl_2$, the selected isolates were classified into two different categories i.e. MRB and moderate MRB (MMRB). The detailed procedure is elaborated in the SI. To understand the effects of different Hg concentrations on bacterial growth, two qualitative analyses were carried out, i.e. monitoring the optical density (OD) at 600 nm and dry biomass.

16S rDNA based identification

The selected isolates were further analyzed by subjecting them to 16S rDNA sequencing. In brief, DNA was isolated and the polymerase chain reaction (PCR) amplification was executed with the universal 16S rDNA primers of 27F (5'-AGAGTTTGATCMTGGCTCAG-3') and 1495R (5'-GGHTACCTTGTTACGACTT-3') as described by Dash and Das (2014). The amplified PCR products were sequenced and submitted to NCBI, as described by Kumar et al. (2018). The detailed procedure is elaborated in the SI.

Genotyping of merA gene

A conserved region of merA gene encoding bacterial mercuric reductase enzyme was detected using the above isolated genomic DNA (Joshi et al., 2021). The PCR reactions were carried out using the primer set F1merA (5'-TCGTGATGTTCGACCGCT-3') and F2merA (5'-TACTCCCGCCGTTTCCAAT-3') containing 1 U/µl Taq polymerase (Sigma-Aldrich), 1 × Enzyme buffer, 200 µM of each dNTP (Sigma-Aldrich), 1.25 mM $MgCl_2$, and 0.5 µM of each primer and 50 ng template DNA in a thermal cycler (Applied Biosystems). PCR reaction was carried out under the following amplification conditions: pre-denaturation step at 94°C for 2 min followed by 30 cycles of 94°C for 1 min, 52°C for 1 min and an extension step at 72°C for 1 min and final extension at 72°C for 7 min as described by Dash and Das, (2014). For the isolates that showed negative PCR reactions with F1merA and F2merA primer set, a re-attempt has been made for amplifying the merA gene by gradient PCR method (annealing at 54 ± 5°C) and by using another set of primer A1F (5′-ACCATCGGCGGCACCTGCGT-3') and A5R (5′-ACCATCGTCAGGTAGGGGACCAA3-′) as described by De et al. (2008). Amplification of the merA gene was confirmed by visualizing it under the Gel Doc system (BioRad).

Confirmation of Hg^{2+} to Hg^0 reduction by the isolates

A simplified X-ray film method was adopted to look into the Hg reduction by bacterial volatilization in the presence of 50 and 100 mg/L of Hg as $HgCl_2$ (Nakamura and Nakahara, 1988; Joshi et al., 2021).

Briefly, the bacterial cells were collected by centrifugation at 5,000 rpm for 10 min. and washed with 0.07 M phosphate buffer (0.5 mM EDTA, 0.2 mM magnesium acetate, 5 mM sodium thioglycolate; pH 7.0) and transferred to the microplate. The cells were suspended into 50 µL of 0.07 M phosphate buffer containing 50 and 100 mg/L of Hg as $HgCl_2$ in a microplate. The phosphate buffers (pH 7.0) with 50 and 100 mg/L of $HgCl_2$ (without bacterial cells) were used as a negative control. The plate was covered with X-ray film and incubated in the dark for 2 h at 35°C.

Determination of Hg(II) depletion potential by isolates

The cultures were grown in a ZMB medium supplemented with 50 mg/L of $HgCl_2$ at 30°C and 150 rpm for 48 h. To collect the Hg associated with the bacterial cells, the cultures were centrifuged at 12,000 rpm for 10 min. To analyse the Hg concentration, the samples were processed as described by (Joshi et al. 2021). The detailed procedure for Hg estimation is elaborated in the SI. The concentration of Hg was analyzed by inductively coupled plasma mass spectrometry (ICP-MS, Agilent -7500) as described in the U.S. EPA (1994). The % of Hg elimination was calculated using equation (2).

$$\text{Percentage removal} = \frac{\text{Initial Hg concentration} - \text{Final Hg concentration}}{\text{Initial Hg Concentration}} \times 100 \quad (2)$$

To check the accuracy and precision of analysis, the nominal Hg concentration was compared with the replicates of analytical blank, working solution of $HgCl_2$, and control samples (without bacteria) which were analyzed by ICP-MS. The details of Hg recovery are shown in SI Table S2.

Alterations of functional groups

The modification in functional groups present in the culture pellets was identified by measuring the spectra in the range of 400 to 4000 cm^{-1} using Fourier transform infrared (FT-IR) spectroscopy (IR Affinity-I spectrometer, Shimadzu, Japan), as described by Joshi et al. (2021). In brief, 48 h grown cultures in ZMB medium without Hg supplementation were used as a control, whereas cultures with 50 mg/L of Hg supplementation were used as Hg treated. The mixtures (lyophilized cells and 2% KBr) were fixed in the FT-IR spectrometer after compressing them into translucent sample discs, followed by analyzing in ATR-FT-IR mode by following the manufacturer's protocol.

Scanning Electron Microscopy (SEM) analysis of MRB

To inspect the consequence of Hg^{2+} concentration on the morphology, the bacterial cells were freshly grown in the presence (50 and 100 mg/L - test samples) and absence (control) of Hg^{2+} as $HgCl_2$; and cell pellets were harvested by centrifugation (5000 rpm at 4°C for 5 min) after 48 h. SEM analysis has been carried out, as reported by Joshi et al. (2021). In brief, the bacterial cells were fixed with 2.5% glutaraldehyde followed by the post-fixing in 1% osmium tetroxide and dehydration of the cells with graded ethanol series (25%, 50%, 80%, 90%, and absolute). The processed samples were scanned using SEM (JEOL-JSM-IT500).

Extraction of metabolites and Gas Chromatography-Mass Spectrometry (GC-MS) analysis

GC-MS analysis was performed to characterize the bacterial response and the metabolomic changes leading to Hg tolerance. The solvent extraction method was used to extract the bacterial metabolites. In brief, the freshly inoculated and exponentially grown MRB and MMRB bacterial cells in ZMB medium (non-exposed and exposed to 50 mg/L of Hg) were freeze-dried using BENCHTOP lyophilizer (VIRTIS Instrument, Gardiner, NY). For extraction of compounds, 50 mg of lyophilized bacterial cells were suspended in ethyl acetate and chloroform (1:1; v/v) and homogenized. After homogenization, the solution (crude extract) containing the metabolites was transferred to the clean glass vial by pipetting. These steps were repeated two-three times to obtain a pure and ample amount of sample. The separated organic fractions (crude extract) were treated with anhydrous $NaSO_4$ (Sigma-Aldrich) to remove moisture, which was again concentrated on the rotary evaporator (BUCHI Rotavapor R-215/V advanced, Switzerland) at RT and stored at -80°C until further analysis. The concentrated crude extract was re-suspended in 1 mL of Dichloromethane (DCM) and 5 µL of the sample was injected into the GC-MS analyzer (Agilent Technologies Instrument 7890A GC System, 240 Ion Trap GC/MS, USA). The GC-MS analysis was carried out under external ionization mode using a fused silica column HP 5 MS column (30 m × 0.320 mm × 0.25 µm). High purity helium was used as a carrier gas at a constant flow rate of 1 mL/min. For analysis, the chromatographic conditions i.e. initial injector and detector temperature, were set at 250°C and 330°C, respectively. The temperature of the column was programmed from 50°C (hold for 2 min) to 320°C (2 min hold), with a constant 5°C increment per minute and 1 min hold at 330°C. A metabolic library of all the separated compounds found *via* GC-MS analysis of bacterial extract was created and identified using NIST mass spectral library match. The PubChem CID, structures, names, and molecular weight of those bioactive compounds were obtained from the PubChem database.

In-silico analysis

The compounds obtained in GC-MS analysis were evaluated for bioactivity using the Swiss-ADME server, as described by Daina et al. (2017). The compounds, which target the proteins/enzymes/molecules possessing the detoxification property were selected for molecular docking studies. The 3D structure of normalized GST and IOTG compound (in PDB file format) was used for further docking studies. Molecular docking was performed using AutoDock Vina (ADV) software as described by Trott and Olson (2010) and BIOVA Discovery Studio Visualizer Tool 21.1.0.0 was used to perceive the interactions between receptor and ligand. The detailed procedure is elaborated in the SI.

Using molecular docking results, reference pathways derived from the Kyoto Encyclopedia of Genes and Genomes (KEGG) website (http://www.kegg.jp/or http://www.genome.jp/kegg/) and based on the prior reports, a metabolomic pathway was hypothesized for detoxification of Hg in marine isolates.

Statistical analysis

Three experimental replicates were determined for each analysis and the statistical significance of the results was analyzed by one way ANOVA test. All Statistical analyses were carried out using SPSS (version 17) and GraphPad Prism 7 software. Differences were considered significant at $p< 0.05$ and values are reported as mean ± standard deviation (SD).

Results and discussion

Some microbes hold a vital role in the process of bio-remediation and bioprospecting in which halophilic or halotolerant microbes are the key players (Ventosa et al., 1998; Fukushima et al., 2005). Culture that can grow in heavy metals, organic solvents and produced antibiotics may be used for bioremediation process (De Souza et al., 2006). In the present study, four bacteria of three different species, *Alcanivorax xenomutans, Halomonas* sp., and *Marinobacter hydrocarbonoclasticus* were isolated from the ERIO and shown to be resistant to Hg. The physico-chemical characteristics of seawater samples at both sites of the ERIO are presented in SI Table S1.

TCB and MRB counts

The total bacterial colonies that appeared on the ZMA medium were counted and documented. The statistical analysis found no significant difference ($p > 0.05$) between the TCB of both sites. The TCB count at Site 1 and Site 2 was 176.66 ± 47.71 and 131 ± 37.04 (× 10^2 CFU/mL), respectively (Table S1). De and Ramaiah (2006) reported that the mean total viable count (TVC) on the surface in coastal and oceanic water of the Bay of Bengal (BOB) was 632.38 ± 551.31 and 61.90 ± 80.32 CFU/mL, respectively. The diversity of culturable bacterial counts at the photic zone of the New Britain Trench was 10^2 to 10^4 bacterial cells/mL (Liu et al., 2018). The total retrievable bacterial count in the water samples collected from the two different sites of the central region of the Indian Ocean (CRIO) was 286 ± 39.58 and 177 ± 30.51 (× 10^2 CFU/mL) (Joshi et al., 2021). Our results suggested that the TCB counts observed from different sites of the ERIO in this study are similar to those reported from the CRIO and New Britain Trench, whereas much higher than BOB. In the water column, the distribution of bacteria depends on the availability of utilizable organic carbon (Calleja et al., 2019). Consequently, a relatively large bacterial population is found in the euphotic layer.

The total mercury (THg) concentrations in marine waters in the different parts of the world are in the range of 0.5 – 27,060 ng/L (Gworek et al., 2016). As a consequence of the excessive use of Hg for industrial and agriculture activities and the ultimate disposal of this heavy metal effluent into marine zones, the Hg concentration in the marine environment, including the Indian Ocean is continuously increasing (Sarin, 1991). The Hg vapor released by resistant biota in an open system like the ocean might be the possible reason for re-polluting the environment which had become a part of the local Hg cycle (Lacerda and Pfeiffer, 1992). Among the total aerobic heterotrophic bacteria, the existence of 1-10% of MRB is quite normal in a particular environment (Muller et al., 2001). The MRB population ratio increases with the increasing level of Hg contamination. However, higher MRB had also existed in a comparatively Hg-free environment (Ramaiah and De, 2003). In the current study, the % of CMRB counts was found 16.20% (26.66 ± 10.21 × 10^2 CFU/mL) at Site 1 whereas 6.84% (9 ± 4 × 10^2 CFU/mL) at Site 2 (Table S1). There was a significant difference ($p< 0.05$) among the TCB and CMRB counts on both the sites, as a limited number of bacterial populations can survive in 10 mg/L of Hg as $HgCl_2$. The % frequency of MRB found in this work is lower than that of the other natural environment. In coastal and oceanic water of the BOB, around 97% of MRB were resistant to 10 mg/L of Hg. The authors concluded that MRB contributed to over 20% of the TVC in surface (1-10 m) samples. In the case of oceanic water, the % of MRB at two different sites of the BOB was 92% and 53% of total CFU (Ramaiah and De, 2003; De and Ramaiah, 2006). In our previous study, we reported the occurrence of 17.95% and 27.58% retrievable MRB at two different sites of CRIO (Joshi et al., 2021). Though so far, there are no reports about Hg pollution at the ERIO, the detection of bacterial population resistance to Hg in this study and other related studies suggest that marine bacteria resistant to Hg are widely distributed in the biosphere. Since there are many natural and anthropogenic sources of Hg in the biosphere that makes Hg a global pollutant.

Effect of Hg^{2+} on isolates

Based on phenotype characteristics, a total of 162 bacterial colonies grown on the ZMA media supplemented with 10 mg/L of Hg as $HgCl_2$ were selected for further analysis. In the presence of 25 mg/L of Hg^{2+}, only 63 isolates out of 162 showed resistance. Further, these 63 isolates were characterized based on their growth pattern in the presence of more than 25 mg/L i.e. 50, 75, and 100 mg/L of Hg^{2+} concentration. Among the 63 isolates, 21 isolates grew in the presence of 50 mg/L, followed by 9 and 4 isolates at 75 and 100 mg/L of $HgCl_2$, respectively. The growth pattern of 4 isolates in the presence of $HgCl_2$ is shown in Figure S1.

In terms of mean OD, all the 4 isolates i.e. NIOT-EQR_J7, NIOT-EQR_J248, NIOT-EQR_J251, and NIOT-EQR_J258 showed equivalent growth (OD_{600nm}) i.e. 1.77, 1.657, 1.752, and 1.342 in the presence of 50 mg/L of Hg^{2+} compared to the positive control 1.827, 1.717, 1.82 and 1.396, respectively. Out of 4 isolates, 3 isolates (NIOT-EQR_J7, NIOT-EQR_J248, and NIOT-EQR_J251) showed more than 60% of growth in the presence of 100 mg/L Hg^{2+} i.e. 1.273, 1.169, and 1.125 as compared to the positive control and were considered as MRB whereas NIOT-EQR_J258 growth was found to be less than 50% in the presence of 100 mg/L of Hg^{2+} (OD positive control-1.396 and OD with 100 mg/L of Hg^{2+} - 0.628) considered as MMRB. The statistical analysis revealed a non-significant difference ($p > 0.05$) among the four isolates in the presence of 25 and 50 mg/L of Hg^{2+}, whereas a significant difference ($p< 0.05$) in the presence of 75 and 100 mg/L of Hg as $HgCl_2$ when compared to positive control. Hence, we maintained the same Hg concentration (i.e. 50 mg/L) for all analyses. All the isolates showed less than 50% of mean dry biomass in the presence of 100 mg/L Hg^{2+} compared to the positive control which was outstandingly higher ($p< 0.05$). The isolate NIOT-EQR_J258 and NIOT-EQR_J251 showed dry biomass of 0.33 g/L and 0.36 g/L, respectively in the presence of 100 mg/L Hg^{2+}. The isolates showed good growth in the presence of 25 and 50 mg/L $HgCl_2$; however, low growth in higher concentrations of Hg^{2+} (100 mg/L) was observed. The qualitative analysis showed that the positive controls attained an exponential growth phase quickly as compared to the Hg-treated cultures.

Many strains of genera such as *Halomonas, Haloferax, Halobacterium, Halococcus, Alcanivorax* and *Marinobacter* could tolerate high concentrations of $HgCl_2$ i.e. from 15 to 400 mg/L (Sorkhoh et al., 2010; Al-Mailem et al., 2011; Dziewit et al., 2013; Abdel-Razik et al., 2020). Several scientific reports are available, suggesting Hg resistant bacterium like *Bacillus* sp. (100, 62.5, 12.8, 20, and 50 mg/L), *P. putida* (56 mg/L), *Citrobacter* (0.2 mg/L), *Corynebacterium* (6.4 mg/L), *Proteus* (0.2 mg/L), *Pseudomonas* (0.2 mg/L), *Staphylococcus* (12.8 mg/L) and *E.Coli* (55 mg/L) from different environmental conditions (Zeyaullah et al., 2010; Keramati et al., 2011; Zhang et al., 2012; De et al., 2014; Giri et al., 2014; Santos-Gandelman et al., 2014). Though a small amount of Hg is toxic to the bacterial cells, in this study, Hg tolerance is observed in reported isolates beyond the toxic level. The Hg resistance Gram-positive and Gram-negative isolates may probably be used to detoxify Hg species (Zeyaullah et al., 2010; Dash et al., 2013). This suggests that the isolates from the present study might be potential candidates for effective Hg bioremediation from contaminated sites.

Amplification of 16S rDNA

In the current study, the 16S rDNA was successfully amplified (Figure S2). The NIOT-EQR_J7 and NIOT-EQR_J258 were identified as *Alcanivorax xenomutans* and *Marinobacter hydrocarbonoclasticus*, whereas NIOT-EQR_J248 and NIOT-EQR_J251 belong to the *Halomonas* sp. The obtained 16S rDNA sequences were submitted to NCBI under accession numbers MT825200, MT825208, MT825209, and MT825210. The point of divergence and evolutionary closeness is showed by the formation of numerous external nodes and the presence of some clusters (Figure 2). A similar mechanism of Hg tolerance and its remediation may be possessed by evolutionarily related bacteria. Two organisms i.e. NIOT-EQR_J248 and NIOT-EQR_J251, are included in the domain Bacteria, Phylum Proteobacteria, Class Gammaproteobacteria, order Oceanospirillales, and family of Halomonadaceae. One isolates i.e. NIOT-EQR_J7 belongs to the family of Alcanivoracaceae, whereas NIOT-EQR_J258 is a member of the Alteromonadales order and Alteromonadaceae family.

Genus *Halomonas* is reported from most of the saline environments regardless of their geographical location, including the marine environment, salterns, saline lakes, and soil (Llamas et al., 2006). The MRB isolated from the coastal areas of Kuwait were identified as *Alcanivorax borkumensis, Marinobacter hydrocarbonoclasticus,* and *Halomonas taeheungii* (Sorkhoh et al., 2010). The 16S rDNA analysis and phenotypic characteristics revealed that the heavy metal-resistant halophilic bacteria WQL9 belong to the genus *Halomonas* sp (Abdel-Razik et al., 2020). The *Marinobacter* genus is comprised of widespread marine bacteria found exceptionally in marine or terrestrial environments rich in sodium salts, in the deep sea, coastal seawater, sediment, oceanic basalt, etc. (Handley and Lloyd, 2013). *Alcanivorax xenomutans* are also rich in the saline environment as they are halophilic and favorable to living in the marine environment. A comparative analysis of the partial sequence of the 16S rDNA of the four strains revealed a high level of similarity to the corresponding sequence of environmental isolates.

Detection of mercury reductase gene

In the present study, the presence of a distinct 431-bp size band (using F1merA and F2merA primer set) in two MRB isolates (NIOT-EQR_J248 and NIOT-EQR_J251) confirms that

these two isolates harbor the merA gene, which codes for mercuric ion reductase for the detoxification of inorganic Hg (Figure 3). The other isolates NIOT-EQR_J7 and NIOT-EQR_J258 did not showed any amplification, although both the primer sets were used and a gradient method was attempted. However, phenotypically they all were resistant to inorganic Hg and reduced Hg^{2+} to Hg^{0}. This may suggest the presence of other non-mer mediated Hg resistance mechanisms in NIOT-EQR_J7 and NIOT-EQR_J258 or the presence of a diverse merA gene, which could not be detected by the employed PCR primer sets.

Many studies suggest that mer operon is located on any one of either location such as mobile elements like plasmids, transposons, genomic or chromosomal DNA (Liebert et al., 1999; Schelert et al., 2004; Zeng et al., 2010). The mer operon contains many functional genes along with the operator, promoter, and regulatory elements. All functional genes encrypt for the diverse proteins that contribute to the detection, transportation, and reduction of Hg ions (Barkay et al., 2003; Dash and Das, 2012; Naguib et al., 2018). An extremely noteworthy positive correlation was found among the harboring of mer gene with the phenotypic resistance to Hg and concentration of the Hg in the source environment (Osborn et al., 1997). In this study, we did not find any Hg from the ecosystem (detectable limit - 0.73 µg/L), but the amplification of mer genes and available literature suggested that these are extensively dispersed in a non-highly contaminated or contamination-free environment such as an open ocean, Antarctic sea-ice, high Arctic snow, sea ice brine etc. and plays a key role in the biogeochemical cycle of Hg (Christakis et al., 2021). Thus, the Hg adaptation by these isolates is reasonably accepted.

Confirmation of Hg^{2+} reduction by the isolates

To confirm the mer gene function in the isolates, a bacterial Hg volatilization study was executed upon the higher concentration of Hg, i.e. 50 and 100 mg/L. It was confirmed after the incubation period of the microtiter plate for 2 h in the dark by developing foggy areas on the X-ray film in the wells region of the microplate where the isolates were present. The results revealed that NIOT-EQR_J7 and NIOT-EQR_J248 showed high fog development on X-ray film in the presence of 50 and 100 mg/L of Hg as compared to other isolates. However, NIOT-EQR_J258 showed a negligible amount of fog in the presence of 50 mg/L and failed to develop the foggy area in the presence of 100 mg/L of Hg. In the case of NIOT-EQR_J251, the development of foggy areas was higher in the presence of 50 mg/L of Hg as compared to 100 mg/L and equivalent to that of NIOT-EQR_J7 (Figure 4A). The un-inoculated phosphate buffers failed to develop any foggy areas confirming the sensitivity pattern for Hg. The bioremediation of Hg is allied with the mer operon, wherein the environmental and genetic factors influence its bioremediation efficiency. These outcomes are in agreement with the results obtained by De et al. (2008) and Joshi et al. (2021). The presence of foggy areas after 2 h on the

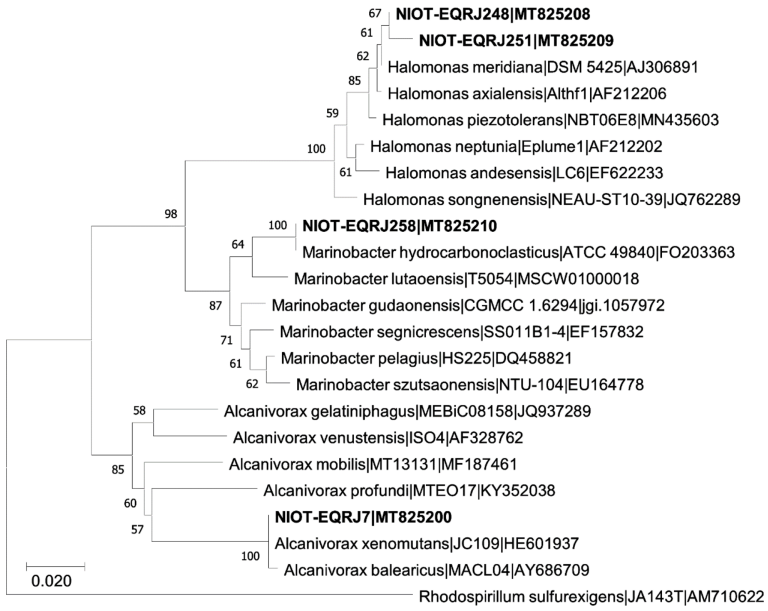


FIGURE 2
Phylogenetic analysis of *Alcanivorax xenomutans* strain NIOT-EQR_J7, *Halomonas* sp. NIOT-EQRJ_248 and NIOT-EQRJ_251; and *Marinobacter hydrocarbonoclasticus* strain NIOT-EQRJ_258.

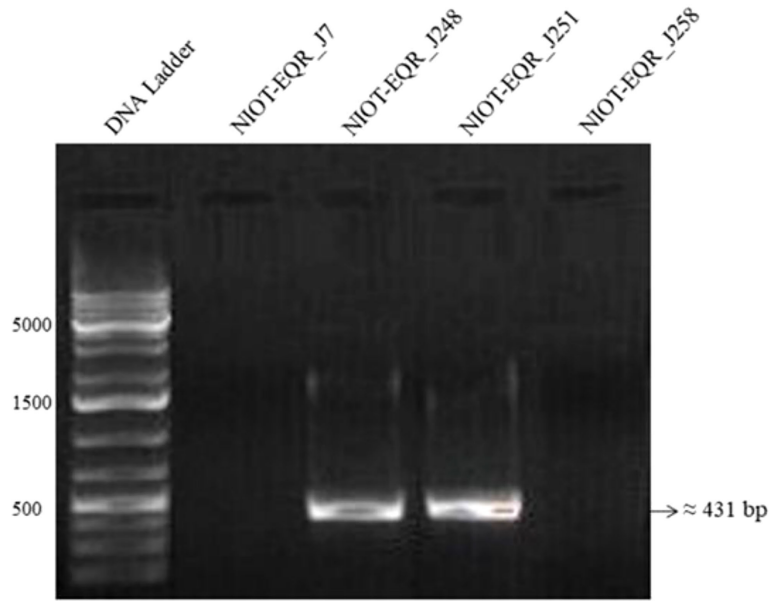


FIGURE 3
Gel electrophoresis of merA gene amplicons of MRB and MMRB strains using F1 merA and F2 merA primer set. Lane 1: Gene Ruler 1 kb Plus DNA Ladder, Lane 2 and 5: Negative PCR reaction, and Lane 3 and 4: amplified products.

silver (Ag) contained X-ray film assured Ag reduction by the Hg vapor released by isolates. However, in the negative control, no such signal was detected.

Based on the results obtained by the x-ray film method, ICP-MS analysis has been carried out to confirm the Hg removal potential of the isolates in the presence of 50 mg/L of Hg^{2+}. The ICP-MS outcomes showed significant changes in the level of Hg depletion. Among all, the marine culture NIOT-EQR_J251 possessed the highest potential (70.62%) to volatilize Hg. NIOT-EQR_J258 showed the least removal of Hg (17.48%), whereas NIOT-EQR_J7 and NIOT-EQR_J248 were capable to volatilize 29.18% and 52.17% of Hg^{2+} under similar conditions, respectively. (Figure 4B). NIOT-EQR_J251 could volatilize 32.54 mg of the initial inoculum of 46.07 mg of $HgCl_2$, whereas NIOT-EQR_J258 removes 8.03 mg of the initial supplement of 45.74 mg of Hg^{2+}. In presence of 50 mg/L of Hg^{2+}, NIOT-EQR_J7 and NIOT-EQR_J248 dominantly developed the fog on the x-ray film, whereas, in the ICP-MS analysis, NIOT-EQR_J251 showed the highest Hg removal as compared to the other isolates. This suggests that volatilization was not solely responsible for removing the Hg^{2+} from the culture media and the contribution of different processes like bioaccumulation and bio-adsorption may be involved.

The statistical analysis of Hg removal potential among the different species i.e., *Alcanivorax xenomutans, Halomonas* sp., *Marinobacter hydrocarbonoclasticus* and within the *Halomonas* spp. revealed that the Hg removal by NIOT-EQR_J251 was significantly higher ($p< 0.01$) than NIOT-EQR_J7 and NIOT-EQR_J258. There was a significant difference ($p< 0.05$) in the removal of Hg between NIOT-EQR_J248 vs. NIOT-EQR_J258 and NIOT-EQR_J248 vs. NIOT-EQR_J251. Al-Mailem et al. (2011) reported *Haloferax* sp. (HA1 and HA2), *Halobacterium* sp. HA3, and *Halococcus* sp. HA4 effectively volatilized (from 40 to 65%) the available 100 mg/L of Hg after 8 days. Many other isolates such as *Bacillus* sp., *Pseudomonas stutzeri, Pseudomonas putida, Vibrio fluvialis* could volatilize 60%-95%, 94%, 100%, 60% of Hg^{2+}, respectively, from culture (Zhang et al., 2012; Dash et al., 2013; Giri et al., 2014; Saranya et al., 2017; Zheng et al., 2018).

Hg volatilization by bacteria involves the reduction of Hg^{2+} *via* the mer system to Hg^0, which is less toxic. It is appealing from the essential and practical viewpoints that halophilic bacteria can also grow in the presence of a higher amount of Hg and volatilized Hg efficiently similar to the non-halophilic bacteria. The ICP-MS analysis did not detect significant Hg loss in the control sample (without bacteria), which confirms the volatility of Hg being biotic (Table S2). Thus, our results suggested that halophilic bacteria can also remove the Hg from the growth media, indicating that it may be potentially applied in contaminated environments. The Hg comes into the ocean either through atmospheric deposition or other several natural and active or passive processes. The results of this study imply that the two marine strains of *Halomonas* sp., isolated from ERIO may have the ability to remove Hg^{2+} from the growth medium.

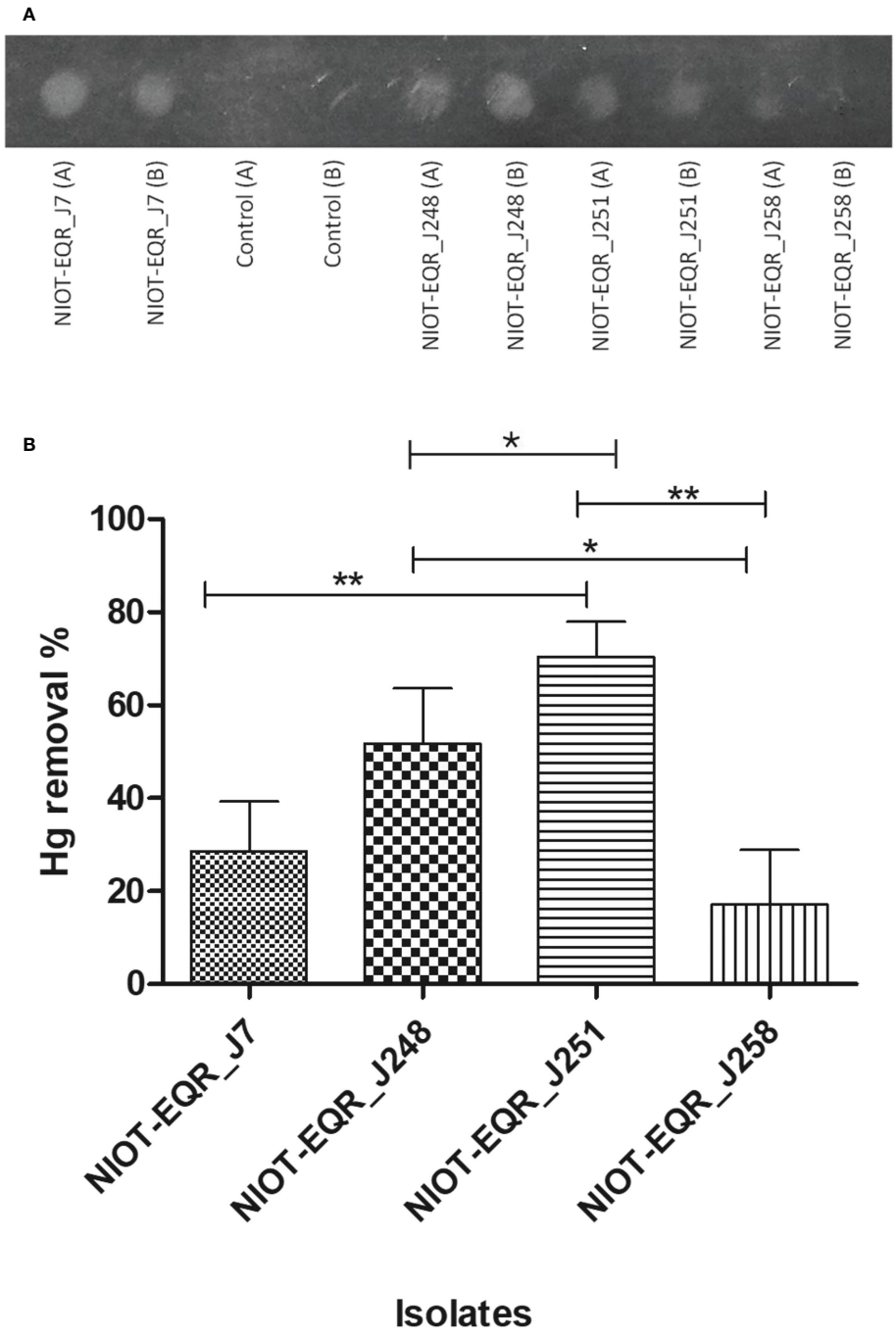


FIGURE 4
(A) Bacterial volatilization of $HgCl_2$ was confirmed by the X-ray film method. **(A)** Represents the Hg volatilization in the presence of 50 mg/L whereas **(B)** corresponds to the 100 mg/L of Hg as $HgCl_2$. **(B)** Hg depletion potential of the marine cultures in the presence of 50 mg/L of Hg as $HgCl_2$. Bars with an asterisk (* and **) indicate noteworthy differences among the cultures in the level of $p< 0.05$ and $p< 0.01$, respectively. Results are represented as mean $\pm$ SD (n=3).

Identification of functional groups changed during Hg(II) reduction

The cultures isolated in this study have shown significant fog development in the presence of 50 mg/L of Hg. Hence, we maintained the same Hg concentration for further studies. The binding of Hg ions to the bacteria depends mainly on the functional groups present on the active sites of bacterial cells and the physicochemical conditions of the solution. In the current study, ATR-FT-IR spectroscopic analysis of the MRB strains was carried out to understand the functional groups involved in the binding process. The IR spectra showed several peaks originating in the 3234.15, 2800.07-3017.95, 2246.72-2383.09, 1618.15-1736.53, 1358.84-1602.80, 1206.39-1273.25, 918.48-1209.93, and 721.47-864.95 cm^{-1} regions, that belong to OH (alcohol), alkane C-H, S-H stretch, Amide C=O, N-O, C–N, P=O stretch and alkyl halide groups, respectively. As clearly seen from Figures 5A–D and Table S4, in the presence of Hg^{2+}, there was a reduction in the intensity of the IR peaks bands in the S-H Stretch (NIOT-EQR_J7, NIOT-EQR_J248, and NIOT-EQR_J251), Amide C=O stretch (NIOT-EQR_J7), Amine (C-N) (NIOT-EQR_J7, NIOT-EQR_J251), N-O group (NIOT-EQR_J248), and the phosphate group (NIOT-EQR_J7, NIOT-EQR_J251) regions as compared to the control grown without Hg.

When the isolate NIOT-EQR_J7 was grown in the presence of Hg^{2+} supplementation, a slight reduction in the peak intensity attributed to the thiol group (S-H stretch) at 2383.09 cm^{-1} was observed as compared to the control along with the wavelength that shifted to 2442.42 cm^{-1}. In contrast, the peak intensity corresponding to the thiol group of NIOT-EQR_J248 at 2304.55 cm^{-1} increased compared to without Hg^{2+} supplementation and the shift in wavelength to 2246.72 cm^{-1} was observed. In the case of NIOT-EQR_J251, the peaks corresponding to the S-H group appeared at 2341.34 cm^{-1} in the presence of Hg^{2+} whereas, in the absence of Hg^{2+}, the peak was negligible. The peak was absent in both the presence and absence of Hg^{2+} in the case of isolate NIOT-EQR_J258 (Figures 5A–D). In accord with our findings, previous studies had also reported similar results (Dash and Das, 2014; De et al., 2014; Joshi et al., 2021) and suggested significant changes in the FT-IR spectrum such as a shift in wavenumber in the region of O-H groups, –S-H group, amide C=O, Nitrile C–N stretch, phosphate groups, etc. The changes in peak height and area have also been observed when isolates were grown in the presence of Hg^{2+} ions compared to the controlled ones. The transmittance of the infrared (IR) in the presence of Hg^{2+} was lower than in the absence of Hg^{2+}. The changes suggested that the presence of metal leads to a lesser degree of bond stretching, consequently reducing the IR transmittance. The contribution of functional groups in metal binding was legitimized undeniably by the formation of varying spectral bands with and without Hg (Oves et al., 2013).

In context to these four isolates, the shift in wavenumbers, changes in peak height, and the appearance/disappearance of new peaks in the presence of Hg^{2+}; suggest alterations in functional groups (especially -SH group), which might play an important role in the Hg detoxification.

SEM analysis of Hg treated and untreated isolates

All the isolates were grown in three different concentrations of Hg (0, 50, and 100 mg/L) and were scanned under SEM. The SEM analysis showed that the isolates are small or large rod-shaped (Figure 6). In the presence of the medium concentration of Hg^{2+} i.e. 50 mg/L, the selected strains were capable to survive and no significant morphological changes were observed. However, the foremost changes like shrinkage or enlargement in bacterial cells, pores formations in the cell wall, and destructions of some of the bacterial cells were noticed in the presence of 100 mg/L of $HgCl_2$.

It can be observed that high Hg concentration causes structural deformities which may be due to its toxic nature. In our previous study, we reported that cultures accustomed to grow in the presence of $HgCl_2$ manifested major morphological abnormalities (Joshi et al., 2021). We also suggested several structural asymmetries allied with the cell wall and cytoplasmic membrane, significantly affecting the cellular mechanism. Resultantly, there is a substantial delay at the beginning of growth and cell division in a higher concentration of Hg^{2+}.

Metabolites formed during Hg (II) reduction

The GC-MS study was included to get insight into the metabolic changes in the MRB isolates under Hg stress. It revealed that the metabolic profiles of MRB isolates are diverse with different biological properties. GC-MS metabolic profiles revealed that the number of compounds increased in the presence of Hg compared to the control isolates, where some compounds were found to be different in Hg-treated samples. A total of 50 metabolites were identified in the absence of Hg, whereas with 50 mg/L of Hg, 64 compounds were identified. The minimum metabolites (6) were identified in NIOT-EQR_J258 without Hg, whereas the maximum metabolites (22) was identified in NIOT-EQR_J251 with Hg^{2+}. The NIOT-EQR_J7 metabolic profile was almost the same in both control and Hg-treated samples. A total of 14 metabolites were present in the control sample, whereas 15 metabolites were identified with Hg. In the case of NIOT-EQR_J248, NIOT-EQR_J251, and NIOT-EQR_J258, a total of 10, 20, and 6 compounds were identified in

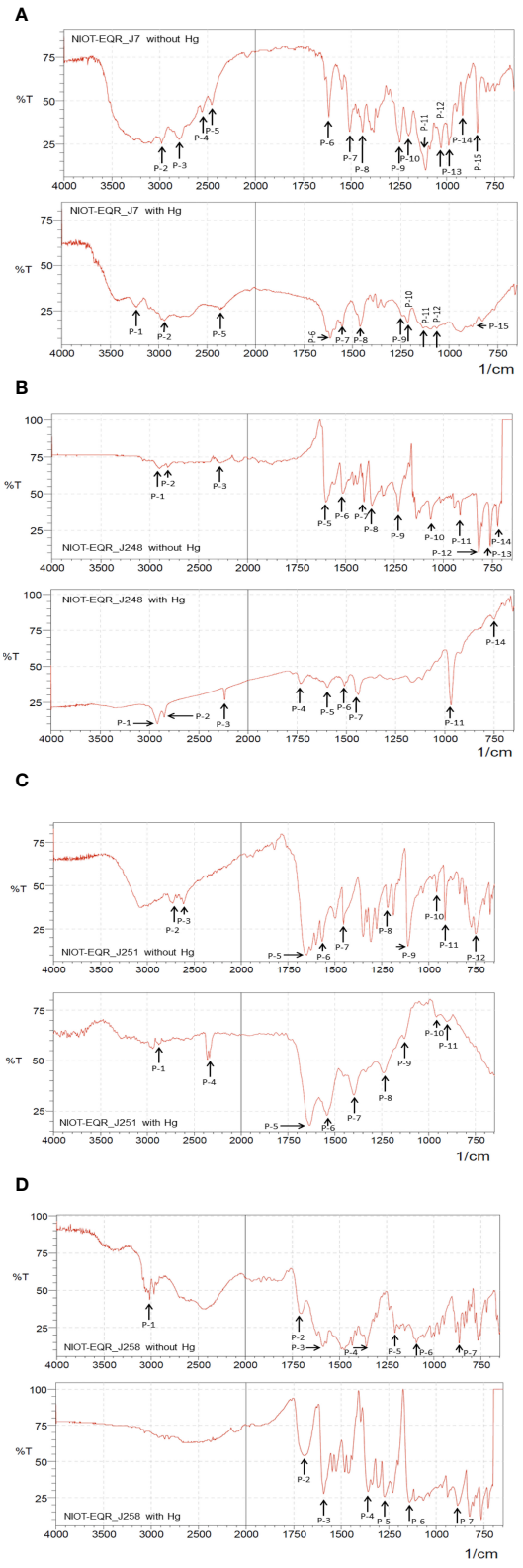


FIGURE 5
ATR-FT-IR spectra of four isolates in absence and presence of 50 mg/L Hg as $HgCl_2$ **(A)** NIOT-EQR_J7 **(B)** NIOT-EQR_J248 **(C)** NIOT-EQR_J251 and **(D)** NIOT-EQR_J258.

the control sample, whereas 16, 22, and 11 metabolites were present with Hg, correspondingly.

The GC-MS chromatograms suggested that in the presence of Hg^{2+}, a total of 30 different compounds were detected (3, 8, 13, and 6 nos. in NIOT-EQR_J7, NIOT-EQR_J248, NIOT-EQR_J251, and NIOT-EQR_J258, respectively) compared to control (Table 1 and Figure S3). However, 19 different compounds were observed in the absence of Hg^{2+} (2, 6, 9, and 2 nos. in NIOT-EQR_J7, NIOT-EQR_J248, NIOT-EQR_J251, and NIOT-EQR_J258, respectively). The new metabolites might be formed due to the bioremediation of Hg by marine strains. An organic compound, Isooctyl thioglycolate (IOTG, molecular formula $C_{10}H_{20}O_2S$ and the molecular weight 204.33 g/mol), was obtained from NIOT-EQR_J248 and NIOT-EQR_J251. The compound is also known as Mercaptoacetic acid or thioglycolic acid (http://pubchem.ncbi.nlm.nih.gov/compound/isooctyl-thioglycolate and http://pubchem.ncbi.nlm.nih.gov/compound/Thioglycolic-acid). It contains both thiol and carboxylic acid functional groups. In the marine environment, sulfur-containing amino acids contribute to the range of thiols, the environmental transformation of 3-mercaptopropionic acid as a metabolite of methionine, and the transformation of mercaptopyruvate to mercaptoethanol and mercaptoacetate (Dash and Das, 2014). The higher amount of sulfur-containing amino acids in marine microorganisms bind with Hg ions efficiently and diminishes its noxious effect, resultantly enhancing the bioremediation capability of that organism (Joyner et al., 2003; Dash and Das, 2014). Thus, IOTG may be considered a chemical lead for Hg^{2+} volatilization by bacteria as sulfhydryl compounds are required to pass off the Hg^{2+} in a vapor form (Nakamura and Nakahara, 1988). FT-IR analysis also revealed that the Hg reacts with the thiol (-SH) or amine ($-NH_{(1,2,3)}$) group of proteins before undergoing bioremediation (Deng and Wang, 2012). One of the reasons for the greater expression of the merA gene under similar experimental conditions is the higher existence of sulfur-containing amino acids in marine bacteria, as compared to terrestrial bacteria (Dash and Das, 2014). Based on GC-MS analysis, we report for the first time that in the presence of Hg^{2+}, a compound IOTG is released by MRB strains of *Halomonas* sp. that may play a key role in Hg bioremediation process. These findings open interesting perspectives on the possibility of using bacterial isolates and/or their derivatives to develop an eco-friendly technique for clean-up of Hg contaminated environment. Secondary metabolites play a vital role in Hg resistance as well as in bioremediation. The link between secondary metabolites and bioremediation needs further exploration.

In silico study

Based on Swiss-ADME server, among the 30 compounds which can target the number of proteins, one compound i.e.

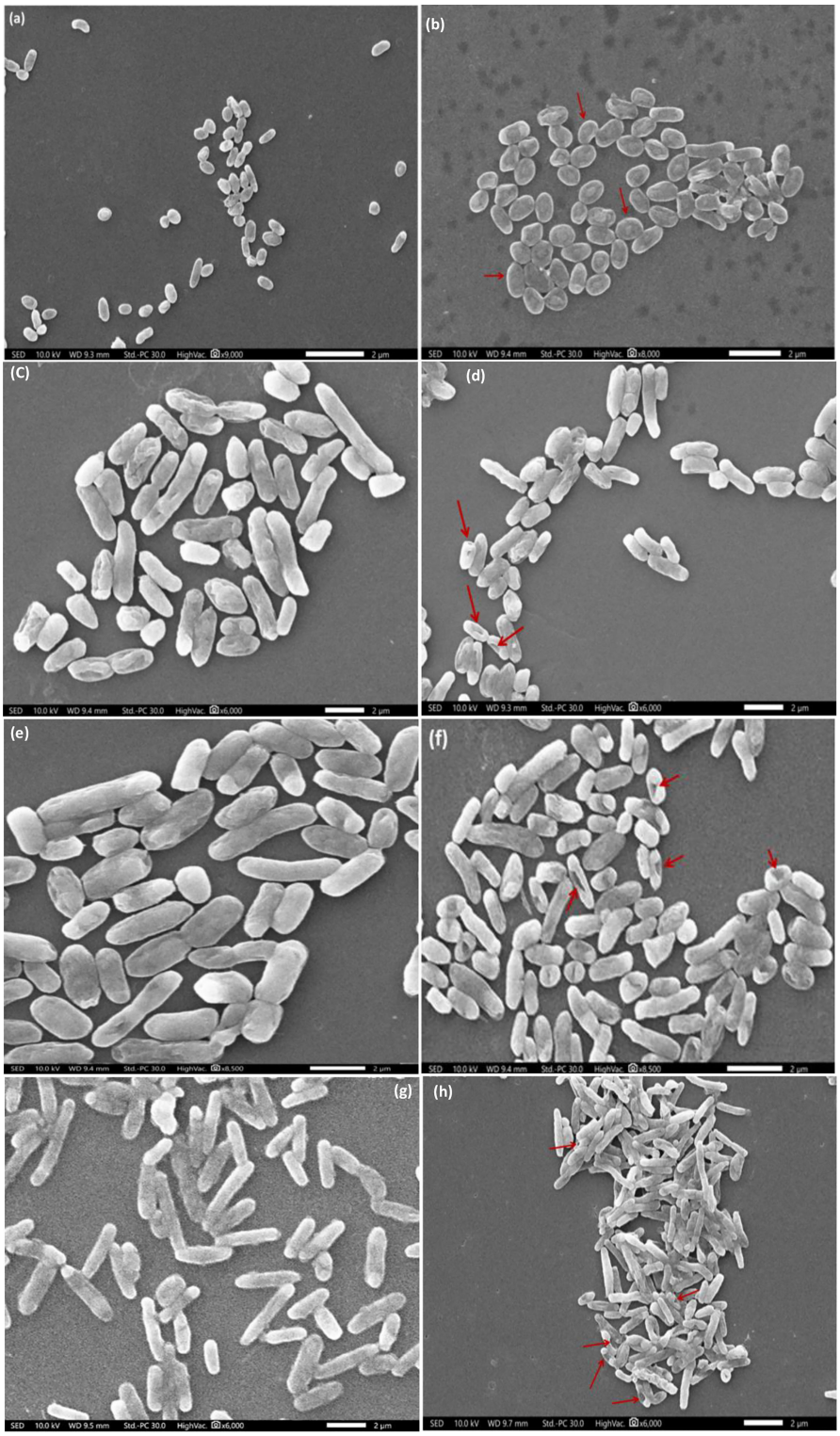


FIGURE 6
SEM analysis showing Hg effect on bacterial cells: **(A, B)** NIOT-EQR_J7, **(C, D)** NIOT-EQR_J248, **(E, F)** NIOT-EQR_J251 and **(G, H)** NIOT-EQR_J258. Images were taken in the presence of different concentrations of Hg^{2+}: (**A, C, E, G** - Control; **B, D, F, H** - 100 mg/L). The red arrow shows the structural deformities.

IOTG satisfied all the criteria and showed detoxification properties. The detailed physicochemical properties of ligand (IOTG) are mentioned in SI (Table S5). The SwissTargetPrediction server revealed that various proteins and enzymes may be targeted as receptors including the GST enzyme by the compound IOTG (Figure S4). Its probability to target the GST enzyme was quite higher compared to other GC metabolites. Hence, the compound IOTG was selected for further docking studies to broaden the understanding and obtain insight into the biomolecular interaction with the GST (Figure S5). In docking studies, the highest binding affinity of -15.89 kJ/Mol was observed at the 3rd position. The highest binding affinity of a ligand to a macromolecule refers to the lowest binding energy (Rahman et al., 2021). The molecular interaction results obtained in this study between ligand and protein are found interesting with respect to the GST-GSH interaction. Das et al. (2011) reported that GSH binds with GST dimers and monomers at D2 and M1 (G-site) nominal sites with an energy consumption rate of -39.3 and -32.12 kJ/Mol, respectively. The amino acids such as Glu, Ser, Asn, Thr, Asp, Ile, and Tyr are important for dimer stabilization and identification of GSH binding sites using GST dimer or monomer (Das et al., 2011). In this study, IOTG revealed four hydrogen bonds, four hydrophobic bonds, and five van der Waals interactions along with a best binding affinity with the lowest energy of protein-ligand complexes (Figure S5). The detailed results are mentioned in the SI file. The formation of hydrogen bonds between macromolecule and ligand indicates one of the important interactions and is the result of bioactivity. Therefore, the present docking study suggests that the compound IOTG showed energy-efficient interaction with GST, which may play a significant role in Hg^{2+} detoxification. The role and importance of specific interacting residues with ligands in the GST active sites could further be analyzed using site-directed mutagenesis.

In prior studies, many pathways have been reported for Hg^{2+} detoxification in microbes using various tools and technologies (Chang et al., 2020; Cursino et al., 2000; Chang et al., 2021). In the present study, a metabolic pathway is hypothesized based on the GC-MS metabolites and protein-ligand interaction (Figure S6) and an attempt has been made to correlate the proposed pathway with the different components of the already existing pathways. In this preliminary study, we found that general resistance/detoxification mechanisms of NIOT-EQR_J248 and NIOT-EQR_J251 in response to inorganic mercury (Hg^{2+}) exposure were a multisystem combined process.

GST is the major detoxifying enzyme catalyzing the conjugation of reduced GSH to different cytotoxic substrates, which is induced when exposed to heavy metals (Goswami et al., 2014; Huang et al., 2019; Chang et al., 2020). The GSH conjugation reaction is the first step of the mercapturic acid pathway, which is one of the most important detoxification processes. Hg^{2+} has a high affinity for the thiol group, which could reduce and sequester Hg^{2+} (Zagorchev et al., 2013; Norambuena et al., 2018). Low molecular weight (LMW) thiol compounds act as cellular antioxidants and could contribute toward defending the cells from reactive oxygen species (ROS) produced due to heavy metals, free radicals, lipid peroxides, and peroxides (Forman et al., 2009). The results obtained in this study are in the agreement with previous findings, which suggested that thiol compounds are playing a crucial role in heavy metal resistance (Zagorchev et al., 2013; Norambuena et al., 2018; Chang et al., 2021). In this study, thiol compound namely IOTG was obtained when isolates were grown in presence of Hg^{2+}. Based on the related reactions and literature, the GST enzyme may also catalyse the conjugation of the reduced form of IOTG to xenobiotic substrates for detoxification in *Halomonas* sp. NIOT-EQR_J248 and NIOT-EQR_J251.

Our preliminary study suggests that the detoxification of Hg^{2+} is the immediate result of the GST and merA function as shown in Figure S6. The existence of the glutathione reductase gene in some bacterial mer operons also supports the role of LMW thiols in Hg^{2+} detoxification (Norambuena et al., 2018). The *E. coli*, together with the integrated merA - GST gene, was able to survive in the high Hg stress environment and transform Hg^{2+} to Hg^{0} (Cursino et al., 2000). It is correlated that IOTG may act as Hg(II)-buffering agents and subsequently, Hg^{2+} is reduced by merA. In the case of merA, mercuric ion was uptaken by the active process i.e. mer mediated transport (merP and merT) and converted to Hg^{0} form by mercuric reductase. On the other hand, the Hg^{2+} that was uptaken through the passive process could subsequently be inactivated by GST or conjugated to merA. Thus, an alternative method is proposed via which Hg resistance level may be augmented in bacteria: the sequestering of Hg given a protein-ligand interaction may lead to an improved way for the volatilization process.

Conclusions

The overall results of this study revealed that bacterial isolates *Alcanivorax xenomutans*, *Halomonas* sp., and *Marinobacter hydrocarbonoclasticus* isolated from the ERIO possessed significant tolerance ability to Hg. In presence of 50 mg/L Hg^{2+}, the potent strains *Halomonas* sp. (NIOT-EQR_J248 and NIOT-EQR_J251) efficiently (upto 70%) convert the Hg^{2+} to Hg^{0} (elementary form) under laboratory conditions. These strains could be used in *in-situ* conditions to significantly avert the adverse environmental conditions arising from the inorganic Hg contamination. Due to metabolic changes taking place under Hg stress conditions, the two *Halomonas* strains i.e. NIOT-EQR_J248 and NIOT-EQR_J251, released a compound, namely IOTG. Further, the role of IOTG is reported in the bacterial-based Hg detoxification mechanism. In this study, amplification of merA gene and GC-MS-based metabolic profile suggests that

TABLE 1 Biochemical compounds identified in ethyl acetate and chloroform (1:1; v/v) extract of isolates in the absence and presence of 50 mg/L Hg as $HgCl_2$ by GC-MS.

Isolate	Without Hg		With Hg	
	Compound	RT (min)	Compound	RT (min)
NIOT-EQR_J7	Isophthalic acid, propyl tridec -2-ynyl ester	25.055	Isophthalic acid, propyl tridec-2-ynyl ester	25.058
	Oleyl alcohol, trifluoroacetate	27.421	Oleyl alcohol, trifluoroacetate	27.452
	17-Pentatriacontene	27.580	17-Pentatriacontene	27.599
	Oleyl alcohol, trifluoroacetate	32.814	Cyclooctasiloxane, hexadecamethyl-	29.567
	Tetracontane, 3,5,24-trimethyl-	32.966	Oleyl alcohol, trifluoroacetate	32.824
	Cyclononasiloxane, octadecamethyl-	33.777	Oxalic acid, cyclobutyl pentadecyl ester	32.972
	Phthalic acid, heptyl hex-2-yn-4-yl ester	34.788	Phthalic acid, heptyl hex-2-yn-4-yl ester	34.792
	4-[4-(1,1,3,3-Tetramethylbutyl)phenoxy]- 2,3,5,6-te	35.440	4-[4-(1,1,3,3-Tetramethylbutyl)phenoxy]-2,3,5,6-te	35.443
	Oleyl alcohol, trifluoroacetate	37.709	Oleyl alcohol, trifluoroacetate	37.712
	Tetracontane, 3,5,24-trimethyl-	37.843	Octatriacontyl pentafluoropropionate	37.848
	Oleyl alcohol, trifluoroacetate	42.233	Oleyl alcohol, trifluoroacetate	42.229
	Octatriacontyl pentafluoropropionate	42.337	Octatriacontyl pentafluoropropionate	42.341
	2-Octadecyl-propane-1,3-diol	46.396	1,3-Dioxolane, 4-ethyl-5-octyl-2,2-bis(trifluoromethyl)-, trans-	46.394
	Phthalic acid, octyl 2-pentyl ester	49.417	Hexadecane, 1-(ethenyloxy)-	46.493
			Phthalic acid, bis(2-pentyl) ester	49.427
NIOT-EQR_J248	Isophthalic acid, propyl tridec-2-ynyl ester	10.986	Isophthalic acid, propyl tridec-2-ynyl ester	25.056
	Oleyl alcohol, trifluoroacetate	11.634	Isooctyl Thioglycolate	27.438
	Oleyl alcohol, trifluoroacetate	13.092	17-Pentatriacontene	27.591
	1,2-Benzenedicarboxylic acid, butyl octyl ester	13.688	Cyclooctasiloxane, hexadecamethyl-	29.565
	4-[4-(1,1,3,3-Tetramethylbutyl)phenoxy] -2,3,5,6-te	13.898	Oleyl alcohol, trifluoroacetate	32.804
	1,2-Benzenedicarboxylic acid, butyl cyclohexyl ester	14.325	Tritetracontane	32.963
	cis-13-Octadecenoic acid	14.436	Phthalic acid, hexyl tridec-2-yn-1-yl ester	34.764
	1-Heptacosanol	15.676	4-[4-(1,1,3,3-Tetramethylbutyl)phenoxy]-2,3,5,6-te	35.426
	Valine, N-methyl-N-allyloxycarbonyl-, heptadecyl ester	15.814	Oleyl alcohol, trifluoroacetate	37.705
	1-(Hexahydropyrrolizin-3-ylidene)-3,3-dimethyl-butan-2-one	17.713	Octatriacontyl pentafluoropropionate	37.842
			Oleyl alcohol, trifluoroacetate	42.234
			Octatriacontyl pentafluoropropionate	42.341
			trans-13-Octadecenoic acid	44.470
			1,3-Dioxolane, 4-ethyl-5-octyl-2,2-bis(trifluoromethyl)-, trans-	46.398
			Hexadecane, 1-(ethenyloxy)-	46.497
			Phthalic acid, octyl 2-pentyl ester	49.394
NIOT-EQR_J251	Cycloheptasiloxane, tetradecamethyl-	10.803	Cycloheptasiloxane, tetradecamethyl-	10.802
	Isophthalic acid, propyl tridec-2-ynyl ester	10.978	Isophthalic acid, propyl tridec-2-ynyl ester	10.981
	Oleyl alcohol, trifluoroacetate	11.601	Isooctyl Thioglycolate	11.607
	Oleyl alcohol, trifluoroacetate	13.086	Oleyl alcohol, trifluoroacetate	13.087
	Phthalic acid, butyl hexyl ester	13.682	Phthalic acid, butyl hexyl ester	13.689
	Benzo[b]dihydropyran, 6-hydroxy-4,4,5,7,8-pentamethyl-	14.048	7,9-Di-tert-butyl-1-oxaspiro(4,5)deca-6,9-diene-2,8-dione	14.049
	Phthalic acid, heptyl undecyl ester	14.310	n-Hexadecanoic acid	14.310
	1-Heptacosanol	14.431	Oleyl alcohol, trifluoroacetate	14.434
	Ambucetamide	14.929	L-Proline, N-(2,5-ditrifluoromethylbenzoyl)-, heptadecyl ester	15.562
	Oleic acid, eicosyl ester	15.548	Pentacyclo[19.3.1.1(3,7).1(9,13).1(15,19)]octacosa	15.670
	Oleyl alcohol, trifluoroacetate	15.671	9-Desoxy-9x-chloroingol 3,7,8,12-tetraacetate	16.191

(Continued)

TABLE 1 Continued

Isolate	Without Hg		With Hg	
	Compound	RT (min)	Compound	RT (min)
	Docosanoic anhydride	16.298	Butyl 9-tetradecenoate	16.296
	3-(Pyrrol[1,1,3,3-tetramethyl-3-(undecyloxy)disilo	16.674	Benzo[1,2-c:4,5-c']dipyrrole-1,3,5,7(2H,6H)-tetrone,	16.673
	1,3-Dioxolane, 4-ethyl-5-octyl-2,2-bis(trifluoromethyl)-, trans-	16.809	Oleyl alcohol, trifluoroacetate	16.813
	9,12,15-Octadecatrienoic acid, 2-phenyl-1,3-dioxan-5-yl ester	17.341	Allopregnane-7.alpha.,11.alpha.-diol-3,20-dione	17.346
	Phthalic acid, octyl 2-pentyl ester	17.701	Dipyridamole	17.589
	17-Octadecen-1-ol acetate	17.904	Phthalic acid, octyl 2-pentyl ester	17.701
	2-Butenoic acid, 2-methyl-, 1,1a,1b,4,4a, 5,7a,7b,8	18.374	17-Octadecen-1-ol acetate	17.903
	17-Octadecen-1-ol acetate	19.265	Norcodeine di-TMS derivative	18.374
	psi.,.psi.-Carotene, 7,7',8,8',11,11',12,12',15,15'-decahydro-	19.610	9-Octadecene, 1-[2-(octadecyloxy)ethoxy]	19.264
			.psi.,.psi.-Carotene, 7,7',8,8',11,11',12,12',15,15'-decahydro-	19.612
			Octadecanoic acid, 2-(hexadecyloxy)ethyl ester	21.186
NIOT-EQR_J258	Phthalic acid, octyl 2-pentyl ester	17.713	Isophthalic acid, propyl tridec-2-ynyl ester	10.979
	Hexacosanol, acetate	17.915	Cyclopentane, 1-pentyl-2-propyl-	11.603
	Prost-13-en-1-oic acid, 9-(methoxyimino)	18.385	Oleyl alcohol, trifluoroacetate	13.088
	9-Hexadecenoic acid, 9-octadecenyl ester	19.274	Oleyl alcohol, trifluoroacetate	14.436
	2-Butenoic acid, 2-methyl-, 1,1a,1b,4,4a, 5,7a,7b,8	19.618	1,3-Dioxolane, 4-ethyl-5-octyl-2,2-bis(trifluoromethyl)-, trans-	15.672
	9-Octadecene, 1-[2-(octadecyloxy)ethoxy]	21.184	Phthalic acid, octyl 2-pentyl ester	17.704
			Hexacosanol, acetate	17.909
			Prost-13-en-1-oic acid, 9-(methoxyimino)	18.555
			17-Octadecen-1-ol acetate	19.277
			9-Hexadecenoic acid, 9-octadecenyl ester	20.157
			Octadecanoic acid, 2-(hexadecyloxy)ethyl ester	21.207

Hg detoxification is the result of a simultaneous process of GST and Mer mechanism. Based on the results obtained in this study IOTG may play a crucial role in strains NIOT-EQR_J248 and NIOT-EQR_J251 to reduce the Hg^{2+} concentration and establish a comparatively steady cellular environment for survival under Hg stress. Further studies are required at the molecular level using gene inactivation or knockouts to reveal the contribution made by different pathways in bacterial Hg reduction. This study will be useful to design effective environmentally friendly technology for bioremediation of Hg.

Data availability statement

The datasets presented in this study can be found in online repositories. The names of the repository/repositories and accession number(s) can be found in the article/Supplementary Material.

Author contributions

GJ: Conceptualization, Methodology, Formal analysis, Investigation, Writing-original draft, Writing-review & editing. PV: Investigation, Formal analysis, Writing-review & editing. BM: Investigation. PG: Formal analysis. DMP: Investigation. DKJ: Writing-review & editing. NVV: Supervision, Project administration, Writing-review & editing. GD: Supervision, Project administration, Writing-review & editing. All authors contributed to the article and approved the submitted version.

Funding

The authors thank the Ministry of Earth Sciences, Govt. of India, for the funding support.

Acknowledgments

The authors gratefully acknowledge the Ministry of Earth Sciences (MoES), Government of India, for the financial support and providing the necessary laboratory facilities to conduct this research. We are thankful to the Director, Dr. G. A. Ramadass and former director Dr. M.A. Atmanand, the National Institute of Ocean Technology (NIOT), for their continuous support and encouragement during this study. The authors are also indebted grateful to Mr. Karuppasamy Mookan of OSTI, NIOT, for his technical assistance in SEM analysis. Authors also wish to put a special word of thanks to Dr. Lawrance Anburajan, Scientist-D, Atal Centre for Ocean Science and Technology for Islands (ACOSTI), NIOT, Port Blair for his valuable suggestions and co-operation. We thank all the scientific staff of ACOSTI-NIOT and OSTI-MBT along with the cruise staff for their support in the onboard and laboratory analysis.

Conflict of interest

The authors declare that the research was conducted in the absence of any commercial or financial relationships that could be construed as a potential conflict of interest.

Publisher's note

All claims expressed in this article are solely those of the authors and do not necessarily represent those of their affiliated organizations, or those of the publisher, the editors and the reviewers. Any product that may be evaluated in this article, or claim that may be made by its manufacturer, is not guaranteed or endorsed by the publisher.

Supplementary material

The Supplementary Material for this article can be found online at: https://www.frontiersin.org/articles/10.3389/fmars.2022.986493/full#supplementary-material

References

Abdel-Razik, M. A., Azmy, A. F., Khairalla, A. S., and AbdelGhani, S. (2020). Metal bioremediation potential of the halophilic bacterium, *Halomonas sp.* strain WQL9 isolated from lake qarun, Egypt. *Egypt. J. Aquat. Res.* 46 (1), 19–25. doi: 10.1016/j.ejar.2019.11.009

Al-Mailem, D. M., Al-Awadhi, H., Sorkhoh, N. A., Eliyas, M., and Radwan, S. S. (2011). Mercury resistance and volatilization by oil utilizing Haloarchaea under hypersaline conditions. *Extremophiles* 15, 39–44. doi: 10.1007/s00792-010-0335-2

Annamalai, H. (2010). Moist dynamical linkage between the equatorial Indian ocean and the south Asian monsoon trough. *J. Atmos. Sci.* 67 (3), 589–610. doi: 10.1175/2009JAS2991.1

Barkay, T., Miller, S. M., and Summers, A. O. (2003). Bacterial mercury resistance from atoms to ecosystems. *FEMS Microbiol. Rev.* 27, 355–384. doi: 10.1016/S0168-6445(03)00046-9

Bindler, G. R. (2003). Estimating the natural background atmospheric deposition rate of mercury utilizing ombrotrophic bogs in southern Sweden. *Environ. Sci. Technol.* 37, 40–46. doi: 10.1021/es020065x

Calleja, M. L., Al-Otaibi, N., and Morán, X. (2019). Dissolved organic carbon contribution to oxygen respiration in the central red Sea. *Sci. Rep.* 9 (1), 4690. doi: 10.1038/s41598-019-40753-w

Chang, J., Shi, Y., Si, G., Yang, Q., Dong, J., and Chen, J. (2020). The bioremediation potentials and mercury(II)-resistant mechanisms of a novel fungus penicillium spp. DC-F11 isolated from contaminated soil. *J. Hazard. Mater.* 396, 122638. doi: 10.1016/j.jhazmat.2020.122638

Chang, J., Si, G., Dong, J., Yang, Q., Shi, Y., Chen, Y., et al. (2021). Transcriptomic analyses reveal the pathways associated with the volatilization and resistance of mercury(II) in the fungus lecythophora sp. DC-F1. *Sci. Total. Environ.* 752, 142172. doi: 10.1016/j.scitotenv.2020.142172

Chikere, C. B., Chikere, B. O., and Okpokwasili, G. C. (2012). Bioreactor-based bioremediation of hydrocarbon-polluted Niger delta marine sediment, Nigeria. *3. Biotech.* 2, 53–66. doi: 10.1007/s13205-011-0030-8

Christakis, C. A., Barkay, T., and Boyd, E. S. (2021). Expanded diversity and phylogeny of mer genes broadens mercury resistance paradigms and reveals an origin for MerA among thermophilic archaea. *Front. Microbiol.* 12. doi: 10.3389/fmicb.2021.682605

Cursino, L., Mattos, S. V., Azevedo, V., Galarza, F., Bucker, D. H., Chartone-Souza, E., et al. (2000). Capacity of mercury volatilization by mer (from escherichia coli) and glutathione s-transferase (from schistosoma mansoni) genes cloned in escherichia coli. *Sci. Total. Environ.* 261, 109–113. doi: 10.1016/S0048-9697(00)00629-X

Daina, A., Michielin, O., and Zoete, V. (2017). SwissADME: a free web tool to evaluate pharmacokinetics, drug-likeness and medicinal chemistry friendliness of small molecules. *Sci. Rep.* 7, 42717. doi: 10.1038/srep42717

Das, A., Chalil, S., Nigam, P., Magee, P., Janneh, O., and Owusu-Apenten, R. (2011). Glutathione transferase-P1-1 binding with naturally occurring ligands: Assessment by docking simulations. *J. Biophys. Chem.* 2, 401–407. doi: 10.4236/jbpc.2011.24046

Dash, H. R., and Das, S. (2012). Bioremediation of mercury and the importance of bacterial mer genes. *Int. Biodeter. Biodegr.* 75, 207–213. doi: 10.1016/j.ibiod.2012.07.023

Dash, H. R., and Das, S. (2014). Bioremediation potential of mercury by bacillus species isolated from marine environment and wastes of steel industry. *Bioremediat. J.* 3, 204–212. doi: 10.1080/10889868.2014.899555

Dash, H. R., Mangwani, N., Chakraborty, J., Kumari, S., and Das, S. (2013). Marine bacteria: Potential candidates for enhanced bioremediation. *Appl. Microbiol. Biotechnol.* 97, 561–571. doi: 10.1007/s00253-012-4584-0

De, J., Dash, H. R., and Das, S. (2014). *Mercury pollution and bioremediation - a case study on biosorption by a mercury-resistant marine bacterium. in: Das s (ed) microbial biodegradation and bioremediation* (London: Elsevier), 137–166. doi: 10.1016/B978-0-12-800021-2.00006-6

Deng, X., and Wang, P. (2012). Isolation of marine bacteria highly resistant to mercury and their bioaccumulation process. *Bioresour.Technol.* 121, 342–347. doi: 10.1016/j.biortech.2012.07.017

De, J., and Ramaiah, N. (2006). Occurrence of large fractions of mercury-resistant bacteria in the bay of Bengal. *Curr. Sci.* 91 (3), 368–372.

De, J., and Ramaiah, N. (2007). Characterization of marine bacteria highly resistant to mercury exhibiting multiple resistances to toxic chemicals. *Ecol. Ind.* 7, 511–520. doi: 10.1016/j.ecolind.2006.05.002

De, J., Ramaiah, N., and Vardanyan, L. (2008). Detoxification of toxic heavy metals by marine bacteria highly resistant to mercury. *Mar. Biotechnol.* 10, 471–477. doi: 10.1007/s10126-008-9083-z

De Souza, M. J., Nair, S., Bharathi, P. L., and Chandramohan, D. (2006). Metal and antibiotic resistance in psychrotrophic bacteria from Antarctic marine waters. *Ecotoxicol.* 15 (4), 379–3384. doi: 10.1007/s10646-006-0068-2

Dziewit, L., Pyzik, A., Matlakowska, R., Baj, J., Szuplewska, M., and Bartosik, D. (2013). Characterization of *Halomonas sp.* ZM3 isolated from the zelazny most post-flotation waste reservoir, with a special focus on its mobile DNA. *BMC Microbiol.* 13, 59. doi: 10.1186/1471-2180-13-59

Forman, H. J., Zhang, H., and Rinna, A. (2009). Glutathione: Overview of its protective roles, measurement, and biosynthesis. *Mol. Asp. Med.* 30, 1–12. doi: 10.1016/j.mam.2008.08.006

Fukushima, T., Mizuki, T., Echigo, A., Inoue, A., and Usami, R. (2005). Organic solvent tolerance of halophilic α-amylase from a haloarchaeon, haloarcula sp. strain s-1. *Extremophiles* 9, 85–89. doi: 10.1007/s00792-004-0423-2

Giri, S., Dash, H. R., and Das, S. (2014). Mercury resistant bacterial population and characterization of bacillus sp. isolated from sediment of solid waste discharged point of steel industry. *Natl. Acad. Sci. Lett.* 37 (3), 237–243. doi: 10.1007/s40009-014-0229-4

Goswami, P., Hariharan, G., Godhantaraman, N., and Munuswamy, N. (2014). An integrated use of multiple biomarkers to investigate the individual and combined effect of copper and cadmium on the marine green mussel (Perna viridis). *J. Environ. Sci. Health A. Tox. Hazard. Subst. Environ. Eng.* 49 (13), 1564–1577. doi: 10.1080/10934529.2014.938534

Gworek, B., Bemowska-Kałabun, O., Kije´nska, M., and Wrzosek-Jakubowska, J. (2016). Mercury in marine and oceanic waters–a review. *Water Air. Soil pollut.* 227 (10), 371. doi: 10.1007/s11270-016-3060-3

Handley, K. M., and Lloyd, J. R. (2013). Biogeochemical implications of the ubiquitous colonization of marine habitats and redox gradients by marinobacter species. *Front. Microbiol.* 4 (136). doi: 10.3389/fmicb.2013.00136

Huang, N., Mao, J., Zhao, Y., Hu, M., and Wang, X. (2019). Multiple transcriptional mechanisms collectively mediate copper resistance in cupriavidus gilardii CR3. *Environ. Sci. Technol.* 53, 4609–4618. doi: 10.1021/acs.est.8b06787

Joshi, G., Meena, B., Verma, P., Nayak, J., Vinithkumar, N. V., and Dharani, G. (2021). Deep-sea mercury resistant bacteria from the central Indian ocean: A potential candidate for mercury bioremediation. *Mar. Pollut. Bull.* 169, 112549. doi: 10.1016/j.marpolbul.2021.112549

Joyner, J. L., Peyer, S. M., and Lee, R. W. (2003). Possible roles of sulphur containing amino acids in a chemoautotrophic bacterium-mollusc symbiosis. *Biol. Bull.* 205, 331–338. doi: 10.2307/1543296

Keramati, P., Hoodaji, M., and Tahmourespour, A. (2011). Multi-metal resistance study of bacteria highly resistant to mercury isolated from dental clinic effluent. *Afr. J. Microbiol. Res.* 5, 831–837. doi: 10.5897/AJMR10.860

Konopka, A., and Zakharova, T. (1999). Quantification of bacterial lead resistance *via* activity assays. *J. Microbiol. Methods* 37, 17–22. doi: 10.1016/S0167-7012(99)00032-9

Kumar, S., Stecher, G., Li, M., Knyaz, C., and Tamura, K. (2018). MEGA X: Molecular evolutionary genetics analysis across computing platforms. *Mol. Biol. Evol.* 35, 1547–1549. doi: 10.1093/molbev/msy096

Kyoto Encyclopedia of Genes and Genomes (KEGG). Available at: http://www.genome.jp/kegg/.

Lacerda, L. D., and Pfeiffer, W. C. (1992). Mercury from gold mining in Amazon environment - an overview. *Quim. Nova.* 55, 238–294.

Liebert, C. A., Hall, R. M., and Summers, A. O. (1999). Transposon Tn21, flagship of the floating genome. *Microbiol. Mol. Biol. Rev.* 63, 507–522. doi: 10.1128/MMBR.63.3.507-522.1999

Liu, Q., Fang, J., Li, J., Zhang, L., Xie, B.-B., Chen, X.-L., et al. (2018). Depth-resolved variations of cultivable bacteria and their extracellular enzymes in the water column of the new Britain trench. *Front. Microbiol.* 9. doi: 10.3389/fmicb.2018.00135

Llamas, I., del Moral, A., Martínez-Checa, F., Arco, Y., Arias, S., and Quesada, E. (2006). Halomonas maura is a physiologically versatile bacterium of both ecological and biotechnological interest. *Antonie. Van. Leeuwenhoek.* 89, 395–403. doi: 10.1007/s10482-005-9043-9

Mahbub, K. R., Bahar, M. M., Labbate, M., Krishnan, K., Andrews, S., Naidu, R., et al. (2017). Bioremediation of mercury: Not properly exploited in contaminated soils! *Appl. Microbiol. Biotechnol.* 101, 963–976. doi: 10.1007/s00253-016-8079-2

Muller, A., Rasmussen, L., and Sorenson, S. (2001). Adaptation of the bacterial community to mercury contamination, FEMS microbial. *Lett.* 16, 49–53. doi: 10.1111/j.1574-6968.2001.tb10861.x

Naguib, M. M., El-Gendy, A. O., and Khairalla, A. S. (2018). Microbial diversity of mer operon genes and their potential rules in mercury bioremediation and resistance. *Open Biotechnol. J.* 12, 56–77. doi: 10.2174/1874070701812010056

Naik, M. M., Pandey, A., and Dubey, S. K. (2012). "Bioremediation of metals mediated by marine bacteria," in *Microorganisms in environmental management*. Eds. T. Satyanarayana, B. Johri and A. Prakash (Dordrecht: Springer), 665–682. doi: 10.1007/978-94-007-2229-3_29

Nakamura, K., and Nakahara, H. (1988). Simplified X-ray film method for detection of bacterial volatilization of mercury chloride by escherichia coli. *Appl. Environ. Microbiol.* 54, 2871–2873. doi: 10.1128/aem.54.11.2871-2873.1988

National Library of Medicine *Compound summary - isooctyl thioglycolate*. Available at: http://pubchem.ncbi.nlm.nih.gov/compound/isooctyl-thioglycolate.

National Library of Medicine *Compound summary - thioglycolic acid*. Available at: http://pubchem.ncbi.nlm.nih.gov/compound/Thioglycolic-acid.

Nelson, P. F., Morrison, A. L., Malfroy, H. J., Cope, M., Lee, S., Hibberd, M. L., et al. (2012). Atmospheric mercury emissions in Australia from anthropogenic, natural and recycled sources. *Atmos. Environ.* 62, 291–302. doi: 10.1016/j.atmosenv.2012.07.067

Norambuena, J., Wang, Y., Hanson, T., Boyd, J. M., and Barkay, T. (2018). Low-molecular-weight thiols and thioredoxins are important players in Hg(II) resistance in thermus thermophilus HB27. *Appl. Environ. Microbiol.* 84, e01931–e01917. doi: 10.1128/AEM.01931-17

Osborn, A. M., Bruce, K. D., Strike, P., and Ritchie, D. A. (1997). Distribution, diversity and evolution of the bacterial mercury resistance (mer) operon. *FEMS Microbiol. Rev.* 19, 239–262. doi: 10.1111/j.1574-6976.1997.tb00300.x

Oves, M., Khan, M. S., and Zaidi, A. (2013). Biosorption of heavy metals by bacillus thuringiensis strain OSM29 originating from industrial effluent contaminated north Indian soil. *Saudi. J. Biol. Sci.* 20 (2), 121–129. doi: 10.1016/j.sjbs.2012.11.006

Pirrone, N., Cinnirella, S., Feng, X., Finkelman, R. B., Friedli, H. R., Leaner, J., et al. (2010). Global mercury emissions to the atmosphere from anthropogenic and natural sources. *Atmos. Chem. Phys.* 10, 5951–5964. doi: 10.5194/acp-10-5951-2010

Rahman, M. S., Zilani, M. N. H., Islam, M. A., Hasan, M. M., Islam, M. M., Yasmin, F., et al. (2021). *In vivo* neuropharmacological potential of gomphandra tetrandra (Wall.) sleumer and *in-silico* study against ß-amyloid precursor protein. *Processes* 9, 1449. doi: 10.3390/pr9081449

Ramaiah, N., and De, J. (2003). Unusual rise in mercury resistant bacteria in coastal environments. *Microb. Ecol.* 45, 444–454. doi: 10.1007/s00248-001-1068-7

Raphael, E. C., Augustina, O. C., and Frank, E. O. (2011). Trace metals distribution in fish tissues, bottom sediments and water from okumeshi river in delta state, Nigeria. *Environ. Res. J.* 5, 6–10. doi: 10.3923/erj.2011.6.10

Santos-Gandelman, J. F., Cruz, K., Crane, S., Muricy, G., Giambiagi-deMarval, M., Barkay, T., et al. (2014). Potential application in mercury bioremediation of a marine sponge-isolated bacillus cereus strain Pj1. *Curr. Microbiol.* 69, 374–380. doi: 10.1007/s00284-014-0597-5

Saranya, K., Sundaramanickam, A., Shekhar, S., Swaminathan, S., and Balasubramanian, T. (2017). Bioremediation of mercury by vibrio fluvialis screened from industrial effluents. *BioMed. Res. Int.* 6509648, 6. doi: 10.1155/2017/6509648

Sarin, R. (1991). *In proceeding of the third indo-Dutch workshop on aquatic toxicology* (Chennai: Centre for Environment Studies, Anna University), 1–29.

Schelert, J., Dixit V Hoang, V., Simbahan, J., Drozda, M., and Blum, P. (2004). Occurrence and characterization of mercury resistance in the hyperthermophilic archaeon sulfolobus solfataricus by use of gene disruption. *J. Bacteriol.* 186, 427–437. doi: 10.1128/JB.186.2.427-437.2004

Serrano, O., Martínez-Cortizas, A., Mateo, M., Biester, H., and Bindler, R. (2013). Millennial scale impact on the marine biogeochemical cycle of mercury from early mining on the Iberian peninsula. *Global Biogeochem. Cy.* 27, 21–30. doi: 10.1029/2012GB004296

Sorkhoh, N. A., Ali, N., Dashti, N., Al-Mailem, D. M., Al-Awadhi, H., Eliyas, M., et al. (2010). Soil bacteria with the combined potential for oil utilization, nitrogen fixation, and mercury resistance. *Int. Biodeterior. Biodegr.* 64, 226–231. doi: 10.1016/j.ibiod.2009.10.011

Strode, S., Jaegle, L., Selin, N., Jacob, D., Park, R., Yantosca, R., et al. (2007). Air-sea exchange in the global mercury cycle. *Global Biogeochem. Cy.* 21, GB1017. doi: 10.1029/2006GB002766

Trott, O., and Olson, A. J. (2010). AutoDock vina: improving the speed and accuracy of docking with a new scoring function, efficient optimization, and multithreading. *J. Comput. Chem.* 31 (2), 455–461. doi: 10.1002/jcc.21334

U.S. EPA (1994). *Method 200.8: Determination of trace elements in waters and wastes by inductively coupled plasma-mass spectrometry," revision 5.4* (U.S. Environmental Protection Agency: Cincinnati, OH).

Ventosa, A., Nieto, J. J., and Oren, A. (1998). Biology of moderately halophilic aerobic bacteria. *Microbiol. Mol. Biol. Rev.* 62, 504–544. doi: 10.1128/MMBR.62.2.504-544.1998

Wang, Q., Kim, D., Dionysiou, D. D., Soriala, G. A., and Timberlake, D. (2004). Sources and remediation for mercury contamination in aquatic systems - a literature review. *Environ. pollut.* 131, 323–336. doi: 10.1016/j.envpol.2004.01.010

Zagorchev, L., Seal, C. E., Kranner, I., and Odjakova, M. (2013). A central role for thiols in plant tolerance to abiotic stress. *Int. J. Mol. Sci.* 14, 7405–7432. doi: 10.3390/ijms14047405

Zeng, X., Tagn, J., Jiang, P., Liu, H., Dai, Z., and Liu, X. (2010). Isolation, characterization and extraction of mer gene of Hg^{2+} resisting strain D2. *Trans. Nonferr. Met. Soc China* 20, 507–512. doi: 10.1016/S1003-6326(09)60170-9

Zeyaullah, M., Islam, B., and Ali, A. (2010). Isolation, identification and PCR amplification of merA gene from highly mercury polluted yamuna river. *Afr. J. Biotechnol.* 9, 3510–3514. Available at: https://www.ajol.info/index.php/ajb/article/view/82390.

Zhang, W., Chen, L., and Liu, D. (2012). Characterization of a marine-isolated mercury-resistant pseudomonas putida strain SP1 and its potential application in marine mercury reduction. *Appl. Microbiol. Biotechnol.* 93, 1305–1314. doi: 10.1007/s00253-011-3454-5

Zheng, R., Wu, S., Ma, N., and Sun, C. (2018). Genetic and physiological adaptations of marine bacterium pseudomonas stutzeri 273 to mercury stress. *Front. Microbiol.* 9. doi: 10.3389/fmicb.2018.00682

frontiers | Frontiers in Marine Science

TYPE Data Report
PUBLISHED 15 November 2022
DOI 10.3389/fmars.2022.1006689

Check for updates

OPEN ACCESS

EDITED BY
Pablo Muniz,
Universidad de la República, Uruguay

REVIEWED BY
Rajamanickam Krishnamurthy,
Arignar Anna Government Arts and Science College Chennai, India
Thilagam Harikrishnan,
Pachaiyappa's College for Men, India
Helio Checon,
State University of Campinas, Brazil

*CORRESPONDENCE
Vikas Pandey
vicky2555@gmail.com
Gopal Dharani
dhara@niot.res.in

SPECIALTY SECTION
This article was submitted to Marine Pollution, a section of the journal Frontiers in Marine Science

RECEIVED 29 July 2022
ACCEPTED 17 October 2022
PUBLISHED 15 November 2022

CITATION
Pandey V, Jha DK, Ratnam K, Venkatnarayanan S, Sathish Kumar P, Verma P and Dharani G (2022) Seasonal variability and its impact on the sub-tidal macrobenthic fauna of Diu Island, north-eastern Arabian Sea: A multivariate approach. *Front. Mar. Sci.* 9:1006689. doi: 10.3389/fmars.2022.1006689

COPYRIGHT
© 2022 Pandey, Jha, Ratnam, Venkatnarayanan, Sathish Kumar, Verma and Dharani. This is an open-access article distributed under the terms of the Creative Commons Attribution License (CC BY). The use, distribution or reproduction in other forums is permitted, provided the original author(s) and the copyright owner(s) are credited and that the original publication in this journal is cited, in accordance with accepted academic practice. No use, distribution or reproduction is permitted which does not comply with these terms.

Seasonal variability and its impact on the sub-tidal macrobenthic fauna of Diu Island, north-eastern Arabian Sea: A multivariate approach

Vikas Pandey*, Dilip Kumar Jha, Krupa Ratnam, Srinivas Venkatnarayanan, Ponnusamy Sathish Kumar, Pankaj Verma and Gopal Dharani*

Ocean Science and Technology for Islands, National Institute of Ocean Technology, Ministry of Earth Sciences (Govt. of India), Chennai, India

KEYWORDS

macrofauna, temporal variation, Diu Island, nutrients, environmental relationship

Introduction

The productivity and sustainability of coastal, marine, and estuarine ecosystems are heavily reliant on the quality of coastal waters (Jha et al., 2013; Jha et al., 2015; Dheenan et al., 2016). These locations are thought to have greater biodiversity than open ocean zones (Gray, 1997). Among the biological components of soft bottom sediments, macrobenthic organisms are essential for ecosystem functioning (Pandey et al., 2022). They play a vital role in secondary production and nutrient exchange between the pelagic and benthic realms and therefore constitute essential elements of estuarine and coastal habitats (Snelgrove, 1998) and are a reliable indicator for assessing the biotic integrity of the coastal ecosystem (Ryu et al., 2011; Pandey et al., 2021). Due to their sedentary lifestyle, long life cycle, and differential response against the perturbation, they also serve as useful bio-indicator (Gesteira-Gomez et al., 2003) for health monitoring and assessment of coastal ecosystems (Ganesh et al., 2014) and evaluating the success of conservation efforts (Winberg et al., 2007).

Identification of factors responsible for spatiotemporal patterns in macrofaunal assemblages is the primary goal amongst many marine benthic ecological studies (Bolam et al., 2008; Dutertre et al., 2013; Pandey and Ganesh, 2019b). However, such pattern in the benthic community is often hard to predict due to the complex interplay between environmental parameters and biological interactions (Ellis et al., 2006). The relationship between natural environmental factors and macrobenthos is reported to help delineate faunal distribution patterns, characterising benthic habitats, establish baseline

knowledge, and enabling the detection of spatial and temporal variations (Bolam et al., 2008; Shumchenia and King, 2010; Dutertre et al., 2013). Numerous studies (Van Hoey et al., 2004; Hily et al., 2008; Dutertre et al., 2013; Pandey and Ganesh, 2019b) have identified sediment properties as a significant factor for the distribution of macrofauna. However, hydrodynamic conditions and physicochemical properties are also reported to influence the presence and abundance of benthic species (Ysebaert and Herman, 2002) as these factors control the food supply, larval dispersion, and metabolism (Pearson and Rosenberg, 1987; Shanks et al., 2003). At short temporal scale, such as seasonal, monthly, or fortnightly, the physicochemical properties of the water column can vary significantly while sediment properties remain relatively stable (Dutertre et al., 2013), therefore, in addition to sediment properties, evaluation of physicochemical properties of the water column is equally important for elucidating the distribution of benthic fauna.

Studies relating the environmental parameters and macrobenthos has received global (Bolam et al., 2008; Shumchenia and King, 2010; Cisneros et al., 2011; Dutertre et al., 2013) as well as regional attention in India (Sivadas et al., 2012; Equbal et al., 2018; Pandey and Ganesh, 2019a; Pandey and Ganesh, 2019b; Rehitha et al., 2019). However, the sub-tidal macrobenthic community dynamics concerning environmental drivers are limited, particularly for Diu Island. The island receives the majority of rainfall between June to September due to the southwest monsoon. There are no industries but tourist, domestic discharge, fishing, and port activities are the major source of disturbances to the natural environment. The lack of knowledge about temporal variability makes it difficult to distinguish between natural and man-induced changes (Hewitt and Thrush 2007; Sivadas et al., 2011). The present study was undertaken to understand the temporal variability of macrofaunal community composition and diversity, effects of monsoon-mediated variability in the physicochemical parameters of the water column as well as sediment and their impacts on the macrofauna community.

Materials and methods

Diu (20.71°N and 70.98°E), a union territory of India, is a small island with a geographical area of 40 Km^2, situated in the northeastern Arabian Sea. The average annual rainfall is recorded 550 millimeters (https://diu.gov.in/about-diu.php), while the average annual ambient atmospheric temperature ranged between 15°C and 42°C (Jha et al., 2021; Kumar et al., 2022). The benthic sampling was carried out at seven predetermined stations (S-1,2,3,4,5,6, and 7) of Diu island in February, September, and November during the year 2018 covering pre-monsoon (PRM), monsoon (MON), and post-monsoon (POM) periods, respectively (Figure 1A). Each season, triplicate samples were collected from all the stations to estimate the physiochemical properties of seawater and sediments. Seawater samples were collected in polypropylene bottles for nutrient estimation using a Niskin's water sampler from a boat. Samples for Dissolved Oxygen (DO) and Biochemical Oxygen Demand (BOD) were analyzed by Winkler's titration method (Grasshoff et al., 1999). For BOD estimation, before titration, samples were stored in a dark chamber for 5 days at 20 ± 1°C (APHA 5210B). Salinity, pH, and temperature were analyzed with a pre-calibrated handheld water quality probe (Hanna HI9829). The nutrient parameters namely nitrite, nitrate, inorganic phosphate (IP), silicate, total nitrogen (TN), ammonia, and total phosphorus (TP) were estimated by following the standard spectrophotometric methods of Grasshoff et al. (1999). At each station, sediment samples were taken for the analysis of organic matter (OM). The sediment samples were dried at 60°C in a hot air oven for the estimation of OM. The total organic carbon (TOC) was estimated by following the modified Walkley Black wet oxidation method (Gaudette et al., 1974) and multiplied with a Van Bemmelen factor of 1.724 (Trask, 1939) and expressed as OM in percentage (%).

Macrofaunal samples were collected in triplicates with a van Veen grab (0.02 m^2) at each station. To prevent movement and distortion of the macrofauna during sieving, the collected sediment samples were mixed with relaxant (magnesium chloride solution, 73 g of $MgCl_2$ in 1000 ml of filtered seawater) before sieving. A test sieve with a mesh size of 0.5 mm was used to sieve the samples and retained content was transferred to a sample container with 5% buffered formalin mixed with Rose Bengal stain. In the laboratory, the samples were again washed and macrofauna was picked up from the residue, labelled, and stored in 70% ethanol (v/v). All taxa were first segregated into different groups and then identified up to the lowest possible taxonomic level followed by the count of individuals. The species' taxonomic information was validated and authenticated by the WoRMS Editorial Board (2021) and the density of the macrofauna was represented as individuals per 0.02 square meter area (ind/0.02m^2).

Data analysis

The analysis of variance (ANOVA-one way) and Tukey's Honest Significant Difference (HSD) *post hoc* test were carried out to find out the significance of spatial and temporal variation for the univariate measures of macrofauna and environmental parameters. The data were examined for normality with Shapiro-Wilk's W test before being subjected to ANOVA. In case of data normality violation, non-parametric ANOVA (Kruskal–Wallis H test) was used followed by pairwise Wilcoxon tests with multiple testing corrections. The univariate indices such as the number of taxa (S), abundance (N, ind/0.02m^2), Margalef's species richness (d), Shannon-

Wiener diversity index (H′, $\log_e$), and Pielou's evenness (J′) were estimated. Principal Component Analysis (PCA) after the normalization of data was performed to identify the dominant environmental factors responsible for sample segregation. To examine how macrofauna and environmental variables were related, BIOENV (Clarke and Ainsworth, 1993) and BVSTEP (Clarke and Warwick, 1998) analyses were used. These analyses helped to find out the best set of environmental variables and taxa by examining all the possible subsets of variables showing the maximum correlation with community dissimilarities. Similarity matrices for taxonomic and environmental data were computed based on Bray-Curtis similarity and Spearman rank correlation coefficients between the two matrices. The Spearman rank ρ values indicate the rank correlation between the matrix; the macrofauna community composition and similarity matrices from the environmental variables. The best subset of taxa was identified by Mantel tests performed by the BVSTEP and subjected to a permutation test to determine significance. The vectors of the best correlated environmental variables and macrofauna were overlaid on the NMDS plot. All the statistical analyses were carried out in open-source software R version 3.6.3 (R Core Team, 2020). Packages used for the analyses were "vegan" (Oksanen et al., 2020), "tidyverse" (Wickham, 2017), and "ggplot2" (Wickham et al., 2019).

Results and discussion

Environmental parameters

The overall seasonal variability of the physicochemical parameters is given in Figure 1B. Salinity ranged between 30.05 and 35.16 PSU with maximum mean salinity of 34.99 ± 0.32 PSU in PRM and a minimum of 30.15 ± 0.06 PSU in MON. The lowering of salinity values during the MON may be attributed to the influx of freshwater due to the high rainfall associated with this season (Kumar et al., 2022). A Kruskal-Wallis H test showed that there was a statistically significant difference in salinity between different seasons, $\chi^2 = 17.853$, $p = 0.0001$. The pairwise comparison revealed that the salinity was significantly different in each season. Similarly, dissolved oxygen, water temperature, and pH also followed the same trend, showing higher values during the PRM and lower values during the MON. The record of high DO (5.83 ± 0.05 mg/L) values during the PRM is associated with the photosynthetic activities of phytoplankton increasing the DO concentration of seawater (Kumar et al., 2022). In contrast, BOD was higher during the MON (1.12 ± 0.45 mg/L) and lower values were observed during the PRM (0.86 ± 0.06 mg/L). Similarly, nutrients (nitrite, nitrate, ammonia, TN, IP, TP, and silicate) in seawater also showed higher values in MON (Figure 1B) whereas organic matter in sediment also showed higher levels in MON (1.58 ± 0.86%) followed by POM (0.95 ± 0.55%) and PRM (0.53 ± 0.3%). The higher level of BOD, nutrients, and OM during the MON appropriately showed a decreasing trend from MON to the PRM. The rainfall is known to impact the physicochemical properties of seawater in tropical regions (Ratnam et al., 2022). The increased OM during the MON was possibly due the land runoff resulting from heavy rainfall that occur during this period (Pandey and Ganesh, 2019b). The one-way parametric and non-parametric ANOVA test showed that, except for BOD and IP ($p > 0.05$), all the physicochemical parameters were significantly different ($p < 0.05$) between seasons. The *post hoc* pairwise comparison revealed that the significant difference in ammonia was due to lower concentration (0.11 ± 0.05 µL/L) during the PRM, whereas the variation in nitrite, nitrate, TN, TP, and OM was due to their significantly high concentration during the MON. In contrast, pH, salinity, silicate, and water temperature were significantly different for each season.

The eigenvalues (>1) showed three significant components and explained 78.7% of the variance in the PCA plot (Figure 1C). However, only the first two components were taken for the result interpretation as they explained 68% of variations. Liu et al. (2003) criteria were followed for factor loadings classification as strong (> 0.75), moderate (0.75-0.50), and weak (0.50-0.30). The first principal component (PC1) explained 56.1% variance and showed strong negative loadings of salinity (-0.95), DO (-0.91), and pH (-0.92) which prevailed during PRM. The second principal component (PC2) explained 11.8% of the variance and showed strong positive loading of water temperature (0.79) and weak negative loadings for BOD (-0.14) and ammonia (-0.34). Overall, the PCA showed a strong temporal variability of physicochemical parameters during the study period. The factor loading matrix, eigenvalues, total & cumulative variance values, and variable loadings (communality) are presented in Table S1 (Supplemental Material).

Macrobenthos structure

Thirty-seven taxa were recorded from the sampling stations covered during the present study at the Diu coast. The majority of taxa belonged to two major faunal groups namely Polychaeta (24 taxa) and Amphipoda (8 taxa), whereas one representative taxa of Tanaidacea, Nemertea, Ophiuroidea, Sipuncula, and Scaphopoda were also observed. Overall, 1083 individuals were recorded during the study, of which 66.94% of the total abundance belonged to Polychaeta and 22.06% to Amphipoda. Numerically, Cirratulidae (12.83%) dominated the community followed by Spionidae (10.24%), Maldanidae (7.66%), Tanaissuidae (7.47%), and Urothoidae (5.63%). The detail on the mean abundance of all the taxa recorded during the study is given in Table S2. The overall abundance of macrofauna ranged between 18 and 100 ind/0.02m^2 with maximum mean abundance recorded during the MON (59 ± 27 ind/0.02m^2) and the minimum was recorded during the POM (40.71 ± 5.64 ind/0.02m^2). However, the difference in the abundance was

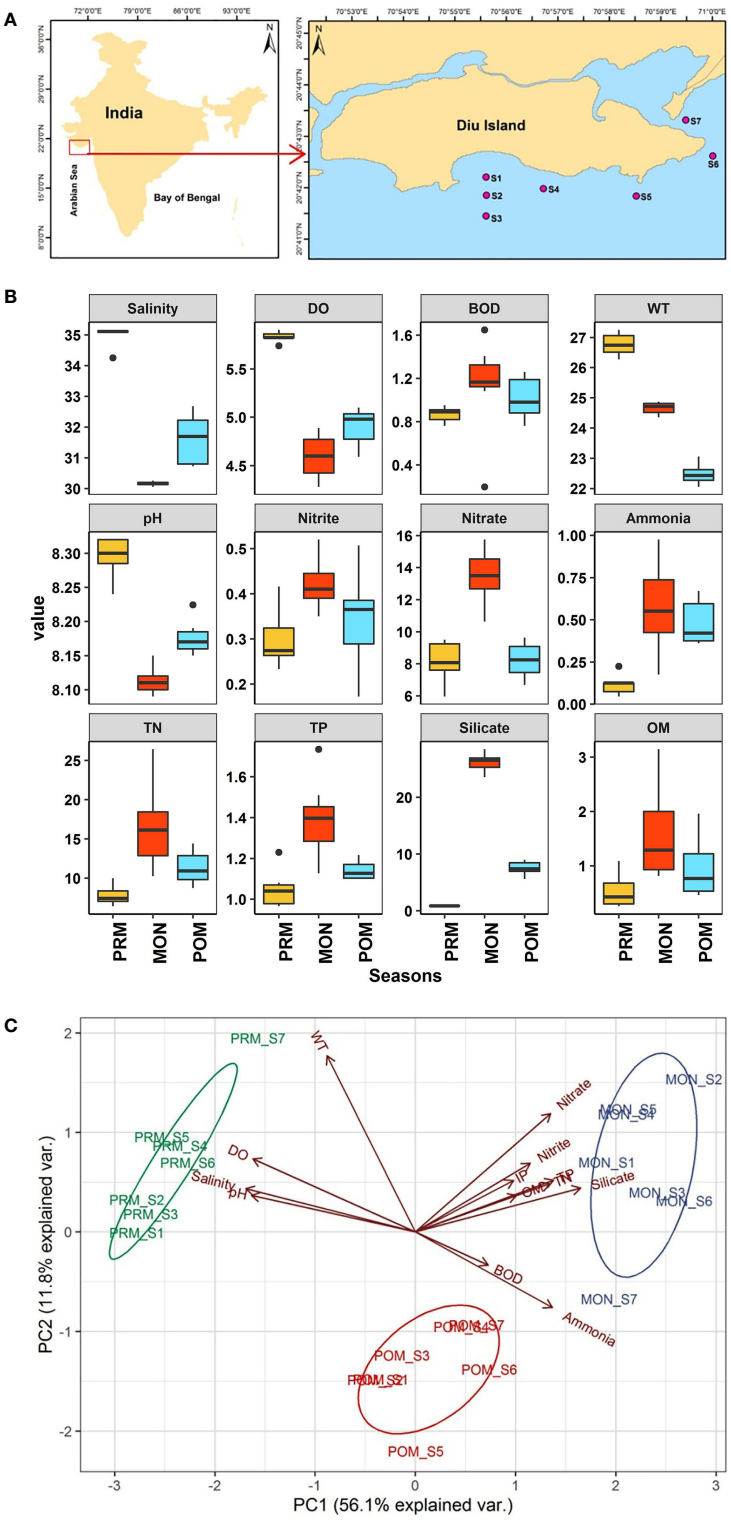


FIGURE 1
(A) Study area map, red points in enlarged map show the sampling stations along the coastal region of Diu island, **(B)** Box plots showing the variations in physicochemical parameters during different seasons. The central line of each boxes represents the median, the rectangle gives the interval between 25% and 75% percentiles, whiskers indicate the range and black dots represent outliers. Y- axis represents the value of each parameter namely DO and BOD are in mg/L, Salinity (PSU), WT (°C) and OM in %, whereas Ammonia, IP, Nitrate, Nitrite, Silicate, TN and TP are in µL/L. X-axis represents different seasons, **(C)** PCA biplot illustrating the variability in the environmental parameters between three seasons.

insignificant between all the seasons (ANOVA; F = 1.663, p = 0.21).

The number of macrofaunal taxa (S) ranged between 13 and 29, species richness (Margalef's d) (3.03 to 7.53), and evenness (J') (0.84 to 0.97), Shannon-Wiener diversity index (H′ $\log_e$) (2.36 to 3.26). All the indices showed higher values during the PRM (Figure 2A). Except for the evenness ($\chi^2 = 2.278$, p = 0.32), all the indices showed a significant difference ($p < 0.05$) between the seasons. The Tukey pairwise HSD *post hoc* test revealed that the significant difference was due to lower values during the MON, whereas, there was no significant difference between PRM and POM (Table S3). The results of ANOVA and pairwise seasonal comparison of environmental as well as univariate measures of macrofauna is summarised in Table S3. Taken together, the results indicate that the PRM and POM period harbored a rather diverse and stable macrobenthic faunal community compared to that of MON. Generally, in tropical conditions, the abundance of macrofauna tends to decrease during the monsoon due to the variation in the environmental parameters (Alongi, 1990; Sivadas et al., 2011; Sivadas et al., 2012). However, in the island ecosystem, this general pattern varies as our results did not show significant variation in the abundance between seasons which is in agreement with the macrofaunal community pattern in the Andaman Islands (Pandey and Ganesh, 2019b). Since, all macrofauna are not equally adapted to withstand the salinity fluctuation and organic matter influx that happens during the monsoon (Gray et al., 2002), therefore, as the monsoon progresses, sensitive species that are susceptible to such disturbances start to diminish in abundance and are replaced by tolerant species in greater numbers. As a result, overall abundance increases while diversity begins to decrease. Further, heavy metals are also known to impact the benthic fauna and may limit the species composition or defaunate the sediment (Pandey et al., 2021). A comparatively higher concentration of cadmium metal was reported from the same region in the MON (Jha et al., 2021). Under such a scenario, sensitive taxa get eliminated which paves the way for tolerant and opportunistic fauna to proliferate. However, in present study, the abundance of macrofauna was not different from a random pattern but the relative abundance of tolerance and opportunistic taxa such as *Cirriformia filigera, C. tentaculata, Dodecaceria* sp., *Paraprionospio cordifolia, P. patiens, Cossura coasta, Maldanella capensis*, and *Notomastus aberans* was higher during the MON (Table S2). These opportunistic faunas have remarkable tolerance to organic enrichment and other pollutants (Levin et al., 1996; Chandler et al., 1997; Holmer et al., 1997) and proliferate in a reduced environment which was evident from their higher numbers during the MON. As the monsoon passes and the environment progresses towards stability, the abundance of tolerant species declines due to competition for food and space leading to increased evenness, higher diversity, and a stable benthic environment during the post-monsoon condition (Parulekar et al., 1980; Harkantra and Rodrigues, 2003). The post-monsoon period in the present study also showed significant improvement in terms of richness and diversity indicating the faster recovery of the macrobenthic faunal community during the stable POM and PRM.

The NMDS ordination revealed temporal variability in the macrobenthic assemblage pattern. However, the major differences in the assemblage were observed between the MON and the non-monsoon periods including PRM and POM. A distinct assemblage composition was not observed between PRM and POM. BIOENV analysis showed a relatively weak correlation between the environmental parameters and macrofauna. However, the best subset of environmental parameters with the highest rank correlation was obtained with a combination of salinity, temperature, nitrite, total nitrogen, total phosphate, silicate, and OM ($\rho = 0.42$). Environmental parameters namely nitrite, total nitrogen, total phosphate, silicate, and OM were important variables associated with differences in macrofaunal community structure between monsoon (MON) and non-monsoon (PRM and POM) seasons (Figure 2B). The best subset of taxa identified by BVSTEP routine were *Cossura coasta, Sigambra robusta, Goniada emerita, Notomastus aberans, Armandia intermedia, Ophelina acuminata, Paraprinospio patiens, Sabella fusca, Urothoe marina*, and *Aoroides* sp., with a rank correlation of 0.89. Among the identified fauna, except *S. robusta*, *O. acuminata*, and *Aoroides* sp., all were significantly correlated with community dissimilarity (Table S4). Macrobenthic community is structured by a combination of different parameters rather than being controlled by any single parameter alone (Snelgrove and Butman, 1994). This was also reflected in the marofaunal community pattern of the Diu coast which was supported by the integrated NMDS and BIOENV results which revealed a combination of parameters plays different roles in different seasons. The different assemblage pattern during the MON was governed by the increased concentration of nitrite, total nitrogen, total phosphate, silicate, and OM. In contrast, increased salinity and temperature were responsible for the assemblage pattern during PRM and POM. Likewise, taxa that showed significant association with the corresponding seasons were identified by BVSTEP. The analysis revealed three species, namely *Cossura coasta, Notomastus aberans*, and *Paraprinospio patiens* showing significant association with the MON (Figure 2B). These species may be indicators given their prevalence in the MON with increased organic concentration. The significant association of these taxa with the MON justified the prevailing notion of disturbance caused by monsoon turbulence along the west coast of the Indian Peninsula. The current assessment is a preliminary investigation that will be useful to assess the health of the local benthic and associated aquatic fauna, which in turn will help in coastal conservation and fisheries management (Murugan et al., 2005; Kumar et al., 2009; Jha et al., 2017).

Conclusion

The environmental perturbation during the monsoon season in Diu Island brings significant changes in physicochemical and

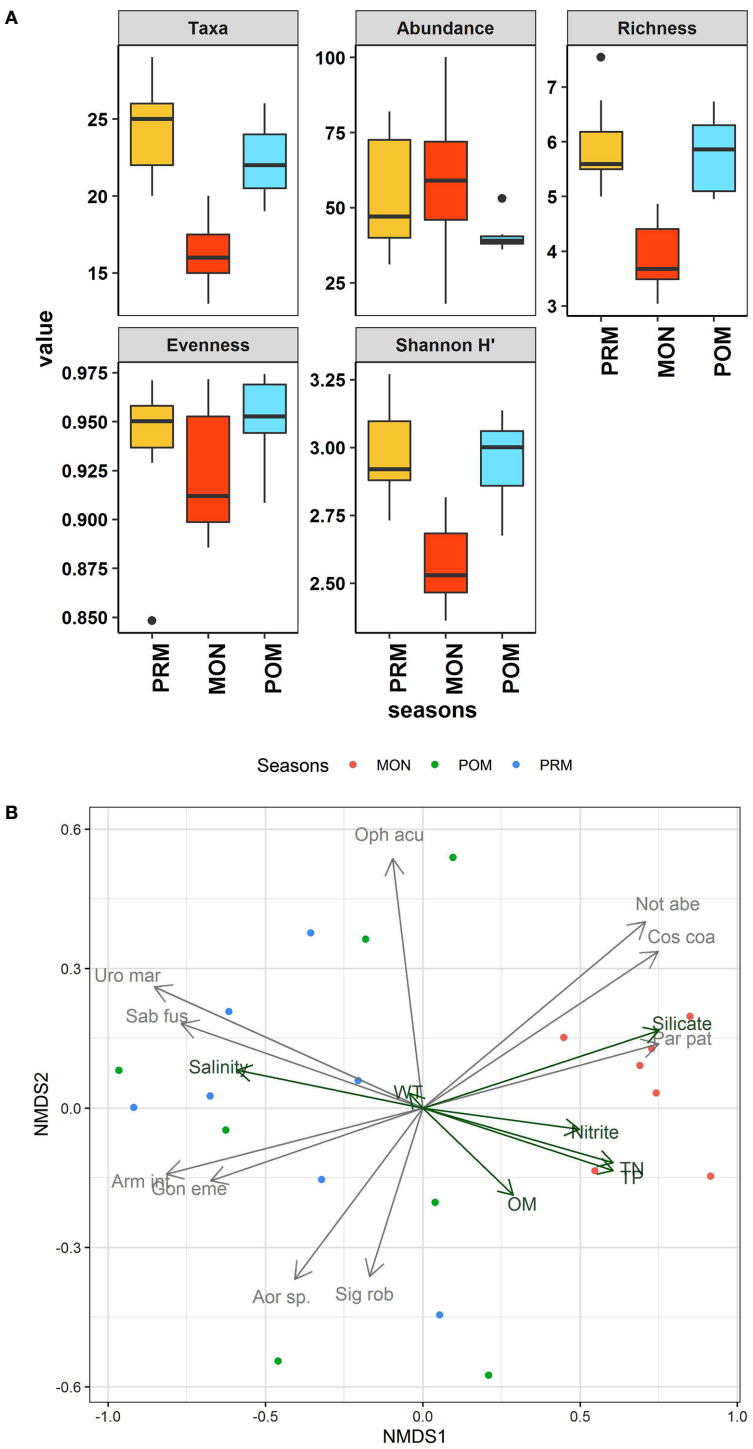


FIGURE 2
(A) Box plots showing the variations in community characteristics of macrobenthic fauna during different season. In each boxplot, the central line represents the median, the rectangle gives the interval between 25% and 75% percentiles, whiskers indicate the range and black dots represent outliers. Abundance is represented as ind/0.02m^2. **(B)** NMDS ordination of the correlation between the macrofaunal community composition and the best subset of environmental variables and taxa with maximum correlation with community dissimilarities plotted as vectors. The vectors represented in green correspond to environmental variable whereas grey vectors represent taxa (abbreviation as per Table S4).

biological characteristics. The study revealed that nutrient and organic enrichment during the monsoon season were the main drivers of the community pattern observed along the Diu coast. These community drivers were stable and did not show significant variation during the post and pre-monsoon periods thereby justifying the healthy benthic environment. The influence of these variables was evidenced on the macrofaunal community during the monsoon which resulted in lower diversity and higher relative abundance of tolerant and opportunistic taxa which is consistent with the community pattern of other tropical islands. This could also be attributed to organic enrichment and nutrient influx resulting from land runoff and natural upwelling incidents on the west coast of India. The result will be significant for comparing benthic diversity and its impact on the ecosystem to other tropical coastal environments.

Data availability statement

The original contributions presented in the study are included in the article/Supplementary Material, further inquiries can be directed to the corresponding author/s.

Author contributions

VP: Conceptualization, sample collection, laboratory analysis, data processing, and writing-original draft. DJ: Sampling design, data validation, and manuscript review. KR: Sample collection and manuscript review. SV: Field investigation. PSK: Field investigation. PV: Data validation and review. GD: Reviewing the manuscript, suggestion, and project administration. All authors contributed to the article and approved the submitted version.

Acknowledgments

The authors are grateful for the support provided by the Earth System Sciences Organization (ESSO), Ministry of Earth Sciences (MoES), Govt. of India, in carrying out the present research study. We are thankful to Dr. G.A. Ramadass, Director, NIOT, Chennai, for his constant encouragement, guidance, and support in completing this research work. We are also thankful to all the supporting staff for their help during the sampling.

Conflict of interest

The authors declare that the research was conducted in the absence of any commercial or financial relationships that could be construed as a potential conflict of interest.

Publisher's note

All claims expressed in this article are solely those of the authors and do not necessarily represent those of their affiliated organizations, or those of the publisher, the editors and the reviewers. Any product that may be evaluated in this article, or claim that may be made by its manufacturer, is not guaranteed or endorsed by the publisher.

Supplementary material

The Supplementary Material for this article can be found online at: https://www.frontiersin.org/articles/10.3389/fmars.2022.1006689/full#supplementary-material

References

Alongi, D. (1990). The ecology of tropical soft-bottom benthic ecosystems. *Oceanogr. Mar. Biol. an Annu. Rev.* 28, 381–496.

Bolam, S. G., Eggleton, J., Smith, R., Mason, C., Vanstaen, K., and Rees, H. L. (2008). Spatial distribution of macrofaunal assemblages along the English channel. *J. Mar. Biol. Assoc. U. K.* 88, 675–687. doi: 10.1017/S0025315408001276

Chandler, G. T., Shipp, M. R., and Donelan, T. L. (1997). Bioaccumulation, growth and larval settlement effects of sediment-associated polynuclear aromatic hydrocarbons on the estuarine polychaete, *Streblospio benedicti* (Webster). *J. Exp. Mar. Biol. Ecol.* 213, 95–110. doi: 10.1016/S0022-0981(97)00011-7

Cisneros, K. O., Smit, A. J., Laudie, J., and Schoeman, D. S. (2011). Complex dynamic combination of physical, chemical and nutritional variables controls spatio-temporal variation of sandy beach community structure. *PLosOne* 6 (8), e23724. doi: 10.1371/journal.pone.0023724

Clarke, K. R., and Ainsworth, M. (1993). A method of linking multivariate community structure to environmental variables. *Mar. Ecol. Prog. Ser.* 92, 205–219. doi: 10.3354/meps092205

Clarke, K. R., and Warwick, R. M. (1998). Quantifying structural redundancy in ecological communities. *Oecologia* 113, 278–289. doi: 10.1007/s004420050379

Dheenan, P. S., Jha, D. K., Das, A. K., Vinithkumar, N. V., Prashanthi Devi, M., and Kirubagaran, R. (2016). Geographic information systems and multivariate analysis to evaluate fecal bacterial pollution in coastal waters of Andaman, India. *Environmental Pollution* 214, 45–53. doi: 10.1016/j.envpol.2016.03.065

Dutertre, M., Hamon, D., Chevalier, C., and Ehrhold, A. (2013). The use of the relationships between environmental factors and benthic macrofaunal distribution in the establishment of a baseline for coastal management. *ICES (Int. Counc. Explor. Sea) J. Mar. Sci.* 70 (2), 294–308. doi: 10.1093/icesjms/fss170

Ellis, J. T., Ysebaert, T., Hume, A., Norkko, T., Bult, P., Herman, S., et al. (2006). Predicting macrofaunal species distributions in estuarine gradients using logistic regression and classification systems. *Mar. Ecol. Prog. Ser.* 316, 69–83. doi: 10.3354/meps316069

Equbal, J., Lakra, R., Savurirajan, M., Satyam, K., and Ganesh, T. (2018). Testing performances of marine benthic biotic indices under the strong seasonality in the tropical intertidal habitats, south Andaman, India. *Mar. pollut. Bull.* 135, 266–282. doi: 10.1016/j.marpolbul.2018.07.034

Ganesh, T., Rakhesh, M., Raman, A. V., Sateesh, N., Moore, S., and Rajanna, B. (2014). Macrobenthos response to sewage pollution in a tropical inshore area. *Environ. Monit. Assess.* 186, 3553–3566. doi: 10.1007/s10661-014-3638-4

Gaudette, H. E., Wilson, R. F., Toner, L., and Folger, D. W. (1974). An inexpensive titration method for determination of organic carbon in recent sediments. *J. Sediment. Petrol.* 44, 249–253. doi: 10.1306/74D729D7-2B21-11D7-8648000102C1865D

Gesteira-Gomez, J. L., Dauvin, J. C., and Salvande Fraga, M. (2003). Taxonomic level for assessing oil spill effects on soft-bottom sublittoral benthic communities. *Mar. Poll. Bull.* 46, 562–572. doi: 10.1016/S0025-326X(03)00034-1

Grasshoff, K., Kremling, K., and Ehrhardt, M. (1999). *Methods of Seawater Analysis*, *Third Ed* (Weinheim, Germany: Verlag Chemie), 159–228.

Gray, J. S., Wu, R. S. S., and Ying, Y. O. (2002). Effects of hypoxia and organic enrichment on the coastal marine environment. *Mar. Ecol. Prog. Ser.* 238, 249–279. doi: 10.3354/meps238249

Gray, J. S. (1997). Marine biodiversity: Patterns, threats and conservation needs. *Biodiversity and Conservation* 6, 153–175. doi: 10.1023/A:1018335901847

Harkantra, S. N., and Rodrigues, N. R. (2003). Pattern of species succession of soft-bottom macrofauna in the estuaries of goa, west coast of India. *Curr. Sci.* 85 (10), 1458–1474.

Hewitt, J.E., and Thrush, S.F. (2007). Effective Long-term Ecological Monitoring Using Spatially and Temporally Nested Sampling. *Environ Monit Assess* 133, 295–307. doi: 10.1007/s10661-006-9584-z

Hily, C., Le Loc'h, F., Grall, J., and Glemarec, M. (2008). Soft bottom macrobenthic communities of north Biscay revisited: Long-term evolution under fisheries-climate forcing. *Estuar. Coast. Shelf Sci.* 78, 413–425. doi: 10.1016/j.ecss.2008.01.004

Holmer, M., Forbes, V. E., and Forbes, T. L. (1997). Impact of the polychaete capitella sp. on microbial activity in organic-rich marine sediment contaminated with the polycyclic aromatic hydrocarbon fluoranthene. *Mar. Biol.* 128, 679–688. doi: 10.1007/s002270050135

Jha, D. K., Dharani, G., Verma, P., Ratnam, K., Sendhil Kumar, R., and Rajaguru, S. (2021). Evaluation of factors influencing the trace metals in puducherry and diu coasts of India through multivariate techniques. *Mar. pollut. Bull.* 167, 112342. doi: 10.1016/j.marpolbul.2021.112342

Jha, D. K., Rajaprabhu, G., Kirubagaran, R., Sendhil Kumar, R., Dharani, G., Das, A. K., et al. (2017). Estimation of potential zones for offshore mariculture in the Indian Sea using geographical information system as a management tool. *J. Coast. Conserv.* 21, 893–902. doi: 10.1007/s11852-017-0556-y

Jha, D. K., Vinithkumar, N. V., Sahu, B. K., Dheenan, P. S., Das, A. K., Mehmuna, B., et al. (2015). Multivariate and geo-spatial approach for seawater quality of chidiyatappu bay, south Andaman islands, India. *Marine Pollution Bulletin* 96, 1–2, 463–470. doi: 10.1016/j.marpolbul.2015.05.004

Jha, D. K., PrashanthiDevi, M., Vinithkumar, N.V., Das, A.K., Kumar, A., Dheenan, P. S., et al. (2013). Comparative investigation of water quality parameters of aerial & rangat bay, Andaman islands using In-situ measurements and spatial modelling techniques. *Water Qual. Expo. Health* 5, 57–67. doi: 10.1007/s12403-013-0086-2

Kumar, P. S., Venkatnarayanan, S., Pandey, V., Ratnam, K., Jha, D. K., Rajaguru, S., et al. (2022). Multivariate approach to evaluate the factors controlling the phytoplankton abundance and diversity along the coastal waters of diu, northeastern Arabian Sea. *Oceanologia* 64, 2, 267–275. doi: 10.1016/j.oceano.2021.11.005

Kumar, T. S., Vijayakumaran, M., Murugan, T. S., Jha, D. K., Sreeraj, G., and S., M. (2009). Captive breeding and larval development of the scyllarine lobster petrarctusrugosus. *New Z. J. Mar. Freshw. Res.* 43:1, 101–112. doi: 10.1080/00288330909509985

Levin, L., Caswell, H., Bridges, T., Di Bacco, C., Cabrera, D., and Plaia, G. (1996). Demographic responses of estuarine polychaetes to pollutants: Life table response experiments. *Ecol. Appl.* 6, 1295–1313. doi: 10.2307/2269608

Liu, C.W., Lin, K.H0., and Kuo, Y.M.. (2003). Application of factor analysis in the assessment of groundwater quality in a blackfoot disease area in Taiwan. *Sci. Total Environ.* 313, 77–89. doi: 10.1016/S0048-9697(02)00683-6

Murugan, T. S., Remany, M. C., Mary Leema, T., Jha, D. K., Santhanakumar, J., Vijayakumaran, M., et al. (2005). Growth, repetitive breeding, and aquaculture potential of the spiny lobster, panulirus ornatus. *New Z. J. Mar. Freshw.* 39:2, 311–315. doi: 10.1080/00288330.2005.9517311

Oksanen, J., Blanchet, F. G., Friendly, M., Kindt, R., Legendre, P., McGlinn, D., et al. (2020). Vegan: Community ecology package. *R Package version* 2, 5–7.

Pandey, V., and Ganesh, T. (2019a). Spatial and temporal variability in the vertical distribution of gastropods on the rocky shores along the east coast of south Andaman island, India. *Mar. Biodivers.* 49, 633–645. doi: 10.1007/s12526-017-0838-5

Pandey, V., and Ganesh, T. (2019b). Spatial and temporal variability of sandy intertidal macrobenthic communities and their relationship with environmental factors in a tropical island. *Estuar. Coast. Shelf Sci.* 224, 73–83. doi: 10.1016/j.ecss.2019.04.045

Pandey, V., Jha, D. K., Sathish Kumar, P., Santhanakumar, J., Venkatnaraynan, S., Prince Prakash Jebakumar, J., et al. (2022). Effect of multiple stressors on the functional traits of sub-tidal macrobenthic fauna: a case study of the southeast coast of India. *Mar. pollut. Bull.* 175, 113355. doi: 10.1016/j.marpolbul.2022.113355

Pandey, V., Venkatnarayanan, S., Kumar, P. S., Ratnam, K., Jha, D. K., Rajaguru, S., et al. (2021). Assessment of ecological health of swarnamukhi river estuary, southeast coast of India, through AMBI indices and multivariate tools. *Mar. pollut. Bull.* 164, 112031 doi: 10.1016/j.marpolbul.2021.112031

Parulekar, A. H., Dhargalkar, V. K., and Singbal, S. Y. S. (1980). Benthic studies in goa estuaries: Part III- annual cycle of macrofaunal distribution, production and trophic relations. *Indian J. Mar. Sci.* 9, 189–200.

Pearson, T. H., and Rosenberg, R. (1987). "Feast and famine: Structuring factors in marine benthic communities," in *Organization of communities past and present*. Eds. J. H. R. Gee and P.S.G. Wiley-Blackwell (Oxford), 373–395.

Ratnam, K., Jha, D. K., Prashanthi Devi, M., and Dharani, G. (2022). Evaluation of physicochemical characteristics of coastal waters of nellore, southeast coast of India, by a multivariate statistical approach. *Front. Mar. Sci.* 9. doi: 10.3389/fmars.2022.857957

R Core Team (2020). R: A language and environment for statistical computing. *RFoundation for Statistical Computing*, Vienna, Austria. Available at: https://www.R-project.org/.

Rehitha, T. V., Madhu, N. V., Vineetha, G., Vipindas, P. V., Resmi, P., and Revichandran, C. (2019). Spatio-temporal variability in macrobenthic communities and trophic structure of a tropical estuary and its adjacent coastal waters. *Environ. Monit. Assess.* 191, 341. doi: 10.1007/s10661-019-7460-x

Ryu, J., Khim, J.S., Kang, S.G., Kang, D., Lee, C., and Koh, C. (2011). The impact of heavy metal pollution gradients in sediments on benthic macrofauna at population and community levels. *Environ. Pollut.* 159 (10), 2622–2629. doi: 10.1016/j.envpol.2011.05.034

Shanks, A. L., Grantham, B. A., and Carr, M. H. (2003). Propagule dispersal distance and the size and spacing of marine reserves. *Ecol. Appl.* 13, S159–S169. doi: 10.1890/1051-0761(2003)013[0159:PDDATS]2.0.CO;2

Shumchenia, E. J., and King, J. W. (2010). Comparison of methods for integrating biological and physical data for marine habitat mapping and classification. *Cont. Shelf Res.* 30, 1717–1729. doi: 10.1016/j.csr.2010.07.007

Sivadas, S. K., Ingole, B., Ganesan, P., Sautya, S., and Nanajkar, M. (2012). Role of environmental heterogeneity in structuring the macrobenthic community in a tropical sandy beach, west coast of India. *J. Oceanogr* 68, 295–305. doi: 10.1007/s10872-011-0099-z

Sivadas, S., Ingole, B., and Nanajkar, M. (2011). Temporal variability of macrofauna from a disturbed habitat of zuari estuary, west coast of India. *Environ. Monit. Assess.* 173, 65–78. doi: 10.1007/s10661-010-1371-1

Snelgrove, P. V. R. (1998). The biodiversity of macrofaunal organisms in marine sediments. *Biodiver. Conserv.* 7, 1123–1132. doi: 10.1023/A:1008867313340

Snelgrove, P. V. R., and Butman, C. A. (1994). Animal-sediment relationships revisited: cause versus effect. *Oceanogr. Mar. Biol. Annu. Rev.* 32, 111–117.

Trask, P. D. (1939). Recent marine sediments. *Am. Assoc. Pet. Geol. Publ. Tulsa OK*, 736.

Van Hoey, G., Degraer, S., and Vinx, M. (2004). Macrobenthic community structure of soft-bottom sediments at the Belgian continental shelf. estuarine. *Coast. Shelf Sci.* 59, 599–613. doi: 10.1016/j.ecss.2003.11.005

Wickham, H. (2016). *ggplot2: Elegant graphics for data analysis* (New York, NY: Springer-Verlag).

Wickham, H., Averick, M., Bryan, J., Chang, W., McGowan, L.D., François, R., Grolemund, G., Hayes, A., et al (2019). Welcome to the tidyverse. *J. Open Source Softw.* 4 (43), 1686. doi: 10.21105/joss.01686.

Winberg, P. C., Lynch, T. P., Murray, A., Jones, A. R., and Davis, A. R. (2007). The importance of spatial scale for the conservation of tidal flat macrobenthos: An example from new south Wales, Australia. *Biol. Conserv.* 134, 310–320. doi: 10.1016/j.biocon.2006.07.019

WoRMS Editorial Board (2021) *World register of marine species*. Available at: https://www.marinespecies.org.

Ysebaert, T., and Herman, P. M. J. (2002). Spatial and temporal variation in benthic macrofauna and relationships with environmental variables in an estuarine, intertidal soft-sediment environment. *Mar. Ecol. Prog. Ser.* 244, 105–124. doi: 10.3354/meps244105

frontiers | Frontiers in Marine Science

TYPE Original Research
PUBLISHED 21 November 2022
DOI 10.3389/fmars.2022.1011564

Check for updates

OPEN ACCESS

EDITED BY
Meilin Wu,
South China Sea Institute of Oceanology (CAS), China

REVIEWED BY
Liancong Luo,
Yunnan University, China
Lijie Duan,
Sun Yat-sen University, China
Qiao Yongmin,
Jinan University, China

*CORRESPONDENCE
Yutao Lei
leiyutao@scies.org

SPECIALTY SECTION
This article was submitted to Marine Pollution, a section of the journal Frontiers in Marine Science

RECEIVED 04 August 2022
ACCEPTED 28 October 2022
PUBLISHED 21 November 2022

CITATION
Zhou W, Cao Q, Hong M, Lei Y, Wen D and Zhang D (2022) Spatial distribution and risk assessment of heavy metals in seawater and sediments in Jieshi Bay, Shanwei, China.
Front. Mar. Sci. 9:1011564.
doi: 10.3389/fmars.2022.1011564

COPYRIGHT
© 2022 Zhou, Cao, Hong, Lei, Wen and Zhang. This is an open-access article distributed under the terms of the Creative Commons Attribution License (CC BY). The use, distribution or reproduction in other forums is permitted, provided the original author(s) and the copyright owner(s) are credited and that the original publication in this journal is cited, in accordance with accepted academic practice. No use, distribution or reproduction is permitted which does not comply with these terms.

Spatial distribution and risk assessment of heavy metals in seawater and sediments in Jieshi Bay, Shanwei, China

Wen Zhou[1], Qian Cao[1], Man Hong[1], Yutao Lei[1]*, Ding Wen[1] and Dengfeng Zhang[2]

[1]South China Institute of Environment Sciences, Ministry of Environment Protection of People's Republic of China (PRC), Guangzhou, China, [2]College of Resource and Environment, Huazhong Agricultural University, Wuhan, China

The contamination of heavy metals due to human activities has attracted great attention and may lead to serious environmental problems. This research was performed on seawater, sediments, and organisms in Jieshi Bay, China. The level of Cu, Pb, Zn, Cd, Hg, and As, respectively, was measured in each environment to acquire a comprehensive understanding of their sources and distribution and to accomplish a risk assessment. The results showed that the concentration of heavy metals in autumn was higher than those in spring, and surface water has a higher heavy metal content than bottom water. The main sources of these heavy metals could be surface runoff and industrial wastewater discharge in the said bay. Hg was the main pollutant in the seawater. Hg, Cu, Zn, and Cd could easily accumulate in organisms than other heavy metal contents. In addition, even though the concentration of Pb did not exceed the Seawater Quality Standard, decision-makers should still be attentive to the Pb content in fish because of bioaccumulation from seafood product consumption.

KEYWORDS

risk assessment, heavy metal, coastal contamination, bay, marine environment quality

1 Introduction

Heavy metal is one of the many global concerns, and the increasing quantity of heavy metals in seafood has threatened human health. Heavy metals (HMs) are characterized by high toxicity, difficult degradation, and easy biological enrichment. Some heavy metals are also important components of environmental endocrine disruptors, which are considered as one of the main characteristic pollutants harmful to water organisms and are typical marine priority control pollutants (Jiang et al., 2012; Wang et al., 2020). Once a heavy metal enters the ocean, it bioaccumulates and bio-amplifies in food webs,

thereby harming ecosystems and human health (Jiang et al., 2012; Wang et al., 2018). Heavy metals may come from the natural weathering and erosion of rocks, many dispersed pollution sources, polluted rivers, domestic wastewater, industrial and agricultural sewage discharge, *etc*. (Birch et al., 1996; Matthiessen et al., 1999). The discharge of heavy metals into seawater environments may lead to bioaccumulation and bio-amplification in predators and, eventually, harm human health through the food chain (Bosch et al., 2016; Baltas et al., 2017; Liu et al., 2021; Liu et al., 2022).

Since the industrial revolution, the industrial construction and population boom in a bay's watershed has caused a sharp rise in heavy metal pollution. This dramatic increase in heavy metals flowing into the bays has overburdened the waterbody (Zhen et al., 2016; Zhixin et al., 2016). Some bays in China were severely polluted by heavy metals—for example, Cd and Hg pollution in Bohai Bay (Wei et al., 2008; Hu et al., 2013a), Liaodong Bay (Hu et al., 2013b; Zhang A. et al., 2017), and Hangzhou Bay (Pang et al., 2015; Fang et al., 2016) and Cu and Zn pollution in Xiangshan Bay and Quanzhou Bay (Sun et al., 2014; Liu et al., 2019; Yan et al., 2020; Zhang M. et al., 2020). The Jieshi Fishing Port is one of the top 10fishing ports in Guangdong, with vast fishing grounds and rich resources, and the protection of its ecological environment is particularly important. Although in the recent years there has been abundant research on the geochemical characteristics of heavy metals in the sediments of the South China Sea, investigations on heavy metals in Jieshi Bay are quite limited; most scholars have focused on the distribution characteristics of heavy metals and have only considered the water quality or sediment without studying the ecological risks of heavy metals from the perspective of the ecosystem. This paper investigated the spatial distribution of heavy metals in Jieshi Bay in spring and autumn, identified the degree of pollution of heavy metals, analyzed the possible sources and correlations of various heavy metals, and evaluated the ecological risks and potential threats to human health from heavy metals in this area. We hope that these studies will contribute to a comprehensive understanding of the distribution, source, accumulation, transport, and ecological risks of heavy metals in the various media of marine ecosystems and help the government to scientifically supervise the protection of coastal and marine ecosystems and public health.

2 Materials and methods

2.1 Study area

Jieshi Bay, located in the south of Shanwei City, Guangdong Province (22°39′–22°52′ N, 115°31′–115°49′ E), is a bay that connects to the South China Sea. The bay covers an area of 890 km^2, with an average depth of 5–18 m and a maximum depth of 20.5 m. The mouth of the bay faces south, having a width of 27 km and a depth of 18 km. It gradually becomes shallow from the mouth to the inside of the bay. The climate in Jieshi Bay is a typical South Asian tropical oceanic monsoon climate, with an annual average temperature of 22.8°C and an annual average precipitation of 2,019.8 mm. The irregular diurnal tide has affected the hydrodynamic condition of Jieshi Bay, making it special to study. The rising tide in the bay flows to the north-northwest, while the falling tide flows to the southeast. The large waves generated by northeast gales and tropical cyclones can reach 3 m in height. There are many harbors along the coast of Jieshi Bay, which has an average coastline of length 23.3 km. There are many excellent breeding harbors along the coast, with vast breeding areas and rich marine fishery resources, and it has a long history of seawater aquaculture.

The region is rich in seawater, port, and fishery resources and has significant ecological and economic value. In recent years, industry, mariculture, and tourism in this region have developed rapidly, and human activities have had a certain impact on the marine environment. To comprehend the spatial distribution and evaluate the ecological risks of HMs in the bay's semi-closed estuary and marine ecosystem, the presence of Cu, Pb, Cd, Hg, As, and Zn in seawater, sediments, and organisms was investigated. The results of the present research may contribute to scientifically regulating enterprises and managing government policies.

2.2 Sample collection and analysis

In April 2021 (spring) and August 2021 (summer), 20 seawater sampling sites, 10 sediment sites, and 12 ecological sites were selected in Jieshi Bay, China (Figure 1). All the samples were collected and preserved according to the *Specification for Marine Monitoring* (GB17378.3-2007) (Ma et al., 2008). Since the near-shore seawater depth ranged from 0 to 20.5 m, the bottom seawater sample was collected from both 0.5 m below the water surface and 2 m above the bottom for a water depth range of 10 to 20.5 m.

Seawater sample (500 ml) was collected and stored at 4°C. The sediment sample was taken using a grab sampler (China Qingdao Juchuang Environmental Protection Group Co., Ltd., JC8000S) from 0 to 5 cm above the bottom and stored in a polyethylene bag at 0–4°C. A 1.5-kg biological sample was grabbed from the selected site and then washed with seawater and cryopreserved. A 5-L acrylic sampler was used for surface water sampling. The surface seawater was filtered immediately once received and stored at 4°C. All sampling methods were performed in accordance with GB17378.3-2007. The seawater sample was filtered with a 0.45-μm filter and then acidified to pH<2 with sulfuric acid. The sediment sample was stored in a dry and ventilated environment, ground with an agate mortar, and then sifted through 160-mesh sieves. The biological samples

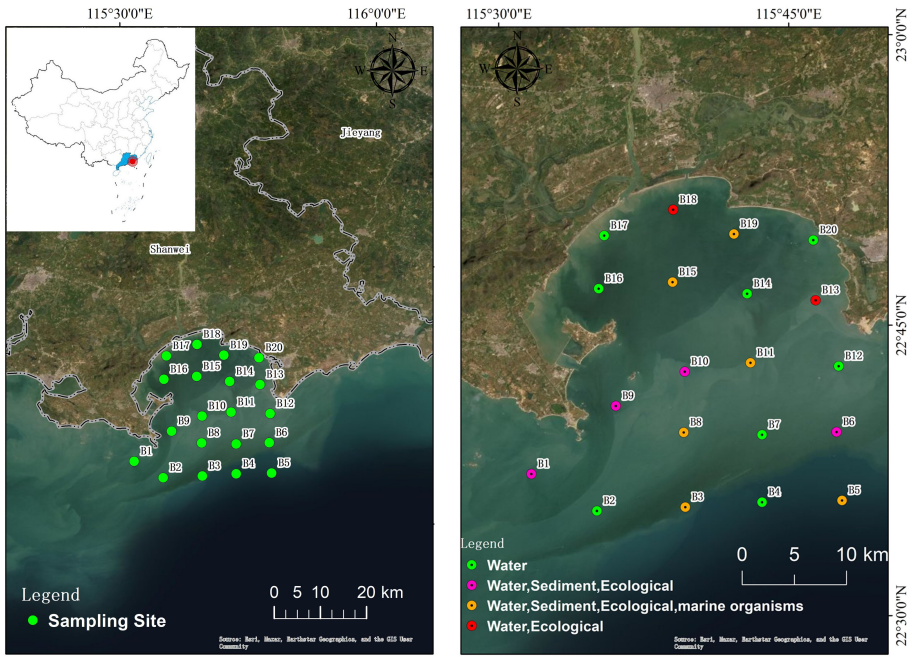


FIGURE 1
Location of sampling sites in Jieshi Bay, China.

were dissected and freeze-dried for 24 h. A 200-mg muscle tissue sample was extracted and then acidified with HNO_3–H_2O_2 (4:2) solution and heated to 120–140°C. Hg and As were tested with atomic fluorescence spectroscopy (Beijing Titan Instruments Co., Ltd, AFS-930). Cu, Pb, Zn, and Cd were measured with atomic absorption spectroscopy 10 times and measured with UV–visible spectrophotometry (The PinAAcle series of atomic absorption spectrometers, 900Z). The samples were analyzed using the national standard (GBW07309). The quality control of the standards was performed by using the national standard (GBW07309), the error of the parallel samples was less than 5%, and the recoveries of the standards were between 95% and 110%.

The species of biological samples from which muscle tissues were extracted were fish, crab, and other invertebrates. The study involving animals was reviewed and approved by the Ethics Committee of South China Institute of Environment Sciences.

2.3 Analytical assessment method

2.3.1 Pollution assessment

Three methods to evaluate the degree of pollution in the study area were applied, and they were water quality index assessment, coefficient of variation method, and principal component analysis.

As an indicator of water quality, the Water Quality Index (WQI) is widely applied in water quality assessments (Tyagi et al., 2013; Kükrer and Mutlu, 2019), turning complex water quality data into information that is understandable and useable to the public. It provides a single number that expresses the overall water quality at a certain location and time based on several water quality parameters. The calculation formula is as follows:

$$\mathrm{WQI} = \frac{1}{n}\sum_{i=1}^{n}\frac{C_i}{C_{i0}} \quad (1)$$

where C_i is the measured concentration of HM, C_{i0} is the first-class standard concentration of HM in the *Seawater Quality Standard* (GB3097-1997), and n is the number of water quality elements that were considered. In this assessment, Cu, Pb, Zn, Cd, Hg, and As were the HMs involved. WQI< 1 means that the pollution in seawater was slight and could be ignored, 1 ≤ WQI< 2 means that the seawater pollution is small, 2 ≤ WQI< 3 means that the seawater pollution is medium, 3 ≤ WQI< 5 means that the seawater pollution is strong, and WQI ≥ 5 means that the seawater is seriously polluted.

To reflect the volatility of the analytical chemistry data, coefficient variation (CV) (Brown, 1998; Bedeian and Mossholder, 2000) was used, which is a standardized measurement of the dispersion of a probability distribution or frequency distribution. The calculation formula is as follows:

$$CV = \frac{\sigma}{\mu} \quad (2)$$

where σ is the standard deviation of the measured concentration of the elements, and μ is the mean of the measured concentration of the elements.

Principal component analysis (PCA) (Shin and Lam, 2001; Li et al., 2006) is one of the most popular multivariate statistical techniques, describing chemical compound properties in order to extract and express information from the data.

2.3.2 Risk assessment

In this paper, the potential ecological hazard index method established by Swedish scholar Hankanson was used to evaluate the pollution level of heavy metals in sediments (Hakanson, 1980). Compared with the single-factor pollution index method, the potential ecological hazard index method more comprehensively considers the synergism between different heavy metals and the difference in pollution level and toxicity (Rezaee Ebrahim Saraee et al., 2011; Liu et al., 2021) as calculated in Equation (3):

$$E_f^i = T_f^i \times C_f^i = T_f^i \times \frac{C^i}{C_n^i} \tag{3}$$

where E_f^i is the potential ecological hazard coefficient of the metal, T_f^i is heavy metal toxicity response coefficient, C_f^i is the pollution coefficient of the metal, C^i is the measured concentration of the heavy metal, and C_n^i is the evaluation standard for the metal (this paper adopts the national standard for class I sediments).

The comprehensive potential ecological hazard index of heavy metals in a single location is the sum of the potential ecological hazard indexes:

$$E_{RI} = \sum_{1}^{n} E_r^i \tag{4}$$

The potential ecological hazard index of a single metal can be divided into five levels from low to high, and the comprehensive potential ecological hazard index can be divided into four levels. The pollution degree of single or multiple pollutants at a certain point can be evaluated through the evaluation standard of the potential ecological hazard index. The specific evaluation standard is shown in Table 1 (Hakanson, 1980; Yi et al., 2016).

TABLE 1 Potential ecological harm index evaluation criteria.

	Degree	E_{RI}	Degree
<40	Low	<150	Low
40–80	Medium	150–300	Medium
80–160	Heavier	300–600	Heavier
160–320	Heavy	≥600	Serious
≥320	Serious		

Target hazard quotients (THQs) are a method used to evaluate the risk of pollutants to human health (Gu et al., 2018), calculated as Equation (5):

$$\mathrm{THQ} = \frac{\mathrm{EF} \times \mathrm{ED} \times \mathrm{FIR} \times \mathrm{c} \times 10^{-3}}{\mathrm{RFD} \times \mathrm{WAB} \times \mathrm{TA}} \tag{5}$$

where EF is contaminant exposure frequency (365 days/year), ED is the exposure years of the pollutants (the average lifespan of man is 70 years), and FIR is the food intake rate of the human body. The statistical data of the Food and Agriculture Organization of the United Nations (FAO) were used, in which the intake of fish is 36 g/day, and the intake of crustaceans is 5.42 g/day. C is heavy metal content in seafood (mg/kg), RFD is the daily reference dose of pollutants [Hg = 0.0005 mg/(kg·day), Cd = 0.001 mg/(kg·day), Pb = 0.004 mg/(kg·day), As = 0.0003 mg/(kg·day)],WAB is the average human body weight (60 kg), TA is the mean exposure time (365 days/year × ED) to non-carcinogenic sources (Storelli, 2008), and TTHQ is the sum of the hazard quotients of various heavy metals in seafood. If the hazard quotient is less than 1, it means that the seafood does not pose a health risk to human beings. On the contrary, when the hazard quotient is greater than 1, it indicates that there is a potential risk in consumption.

To evaluate the risk of heavy metal intake to human health, it is necessary not only to evaluate the hazard quotient of seafood but also to determine the dietary intake. The World Health Organization (WHO) formulated the provisional allowable weekly intake (PTWI) scale for heavy metals. The allowable weekly intakes of Hg, Cd, Pb, and As are 5, 7, 25, and 15 μg/(kg·body weight), respectively (Agusa et al., 2007). The formula for the weekly assessed intake of heavy metals (EWI) is as follows:

$$\mathrm{EWI} = \frac{\mathrm{c} \times \mathrm{FIR} \times 7}{\mathrm{WAB}} \tag{6}$$

2.3.3 Partitioning and bioaccumulation

For the evaluation of sediments, biota-sediment and bio-accumulation factors are commonly applied to evaluate the ecological risk of sediments (Hao et al., 2013; Hao et al., 2019). The bio-accumulation factor (BAF) is used to describe the ability of marine organisms to accumulate trace metals from the surrounding medium and is calculated *via* Equation (7):

$$\mathrm{BAF} = \frac{C_{\mathrm{organisms}}}{C_{\mathrm{sediments}} \text{ or } C_{\mathrm{seawater}}} \tag{7}$$

where $C_{\mathrm{sediments}}$ is the measured concentration in sediments, C_{seawater} is the measured concentration in seawater, and $C_{\mathrm{organisms}}$ is the measured concentration in organisms.

Since a marine organism and its food are exposed to similar environments, the ratio of a substance's lipid-normalized concentration in the tissue of an aquatic organism to its organic carbon-normalized concentration in surface sediment does not

change substantially over time. Thus, a BAF< 100 or a biota-sediment accumulation factor< 1 indicated no significant accumulating effect between organisms and the surrounding environment.

2.3.4 Data analysis tools

Software and statistical tools were utilized to accomplish the spatial distribution, data analysis, and correlation exploration procedures. The Kriging interpolation was completed by ArcGIS (ESRI, v10.2) to draw the spatial distribution of the study area. SSD curves were generated by Buzzlioz 2.0 in the R software. The correlation analysis figures were drawn with Origin and Excel.

3 Results and discussion

3.1 Distribution and pollution assessment of HMs in seawater

The concentration variation ranges of Cu, Pb, Cd, Hg, As, and Zn are shown in Table 2. Zn was the element with the highest concentration, while the concentration of Cd was relatively low. From highest to lowest, the mean concentrations of all the heavy metal elements in the seawater were Zn (3.84μg/L) > As (2.29μg/L) > Cu (2.04μg/L) > Pb (0.93μg/L) > Hg (0.06μg/L)> Cd (0.02μg/L), and the same rule applies to spring and autumn and the bottom layer. The dissolution of trace metals in the surface water and bottom water followed the same time change law for Cu, Pb, Cd, and As; the mean was greater than in spring. The average concentrations of Hg and Zn in autumn were greater than those in spring; this is due to differences in water temperature in different seasons. Temperature is a factor that influences the existing speciation of Hg and Zn, which, in very warm autumn weather, are released more frequently. More Cu, Pb, Cd, and As were released in spring when the water temperature was low (Gerringa et al., 2001; Gundersen and Steinnes, 2003; Nystroem et al., 2005).

According to the horizontal distribution of heavy metal content in the surface and bottom seawater of each site (Figure 2), the concentration of Hg in seawater in spring was higher than in autumn, and the concentration of pollutants in the coastal area was higher than in the offshore area, mainly because the coastal area is more affected by the discharge of industrial and domestic sewage. The water quality of the bottom seawater of Jieshi Bay is significantly better than that of the upper seawater, mainly because the upper seawater is greatly affected by aquaculture, industrial pollutant discharge, and other activities. In Jieshi Bay, heavy metal concentrations in seawater have an obvious seasonal trend, with autumn surface waters containing higher concentrations of Cu, Pb, Cd, Hg, and As than those of spring. These results could be associated with seasonal river flow changes in Guangdong. The distribution of Guangdong's rainy seasons is due to high-pressure recessions; studies show that the monsoon rainfall increases in summer but decreases in spring. The rainy season in Shanwei starts in late March, and the flood season spans from April to September

TABLE 2 Heavy metal concentrations in seawater.

Season		Index	Concentration: μg/L					
			Cu	Pb	Cd	Hg	As	Zn
Spring	Surface	Range	0.30–4.60	0.015–0.87	0.005–0.02	0.03–0.182	2.0–2.5	1.55–29.60
		Average	1.90	0.316	0.008	0.07	2.25	5.72
		Standard deviation	1.39	0.29	0.01	0.03	0.14	7.43
		Variable coefficient	72.98%	90.83%	69.60%	48.96%	6.38%	129.87%
	Bottom	Range	0.4–3.9	0.015–0.460	0.005–0.050	0.035–0.114	1.9–2.6	1.55–18.30
		Average	2.07	0.112	0.008	0.062	2.24	3.72
		Standard deviation	1.14	0.17	0.01	0.02	0.21	4.57
		Variable coefficient	55.11%	152.70%	138.29%	30.80%	9.36%	122.95%
Autumn	Surface	Range	0.9–5.0	0.43–4.62	0.005–0.260	0.017–0.141	2.1–3.0	1.55–8.60
		Average	1.99	1.71	0.040	0.055	2.38	2.46
		Standard deviation	1.07	1.19	0.08	0.03	0.20	1.97
		Variable coefficient	54.00%	69.36%	191.24%	54.79%	8.60%	91.45%
	Bottom	Range	0.6–4.1	0.46–3.15	0.005–0.450	0.016–0.114	2.0–2.6	1.55–18.30
		Average	2.19	1.571	0.040	0.048	2.29	3.45
		Standard deviation	0.94	0.85	0.11	0.03	0.15	4.62
		Variable coefficient	42.65%	54.30%	276.02%	61.61%	6.46%	133.84%
		Average	2.04	0.927	0.024	0.059	2.29	3.84
Marine Water Quality Standards (I)			≤5	≤1	≤1	≤0.05	≤20	≤20

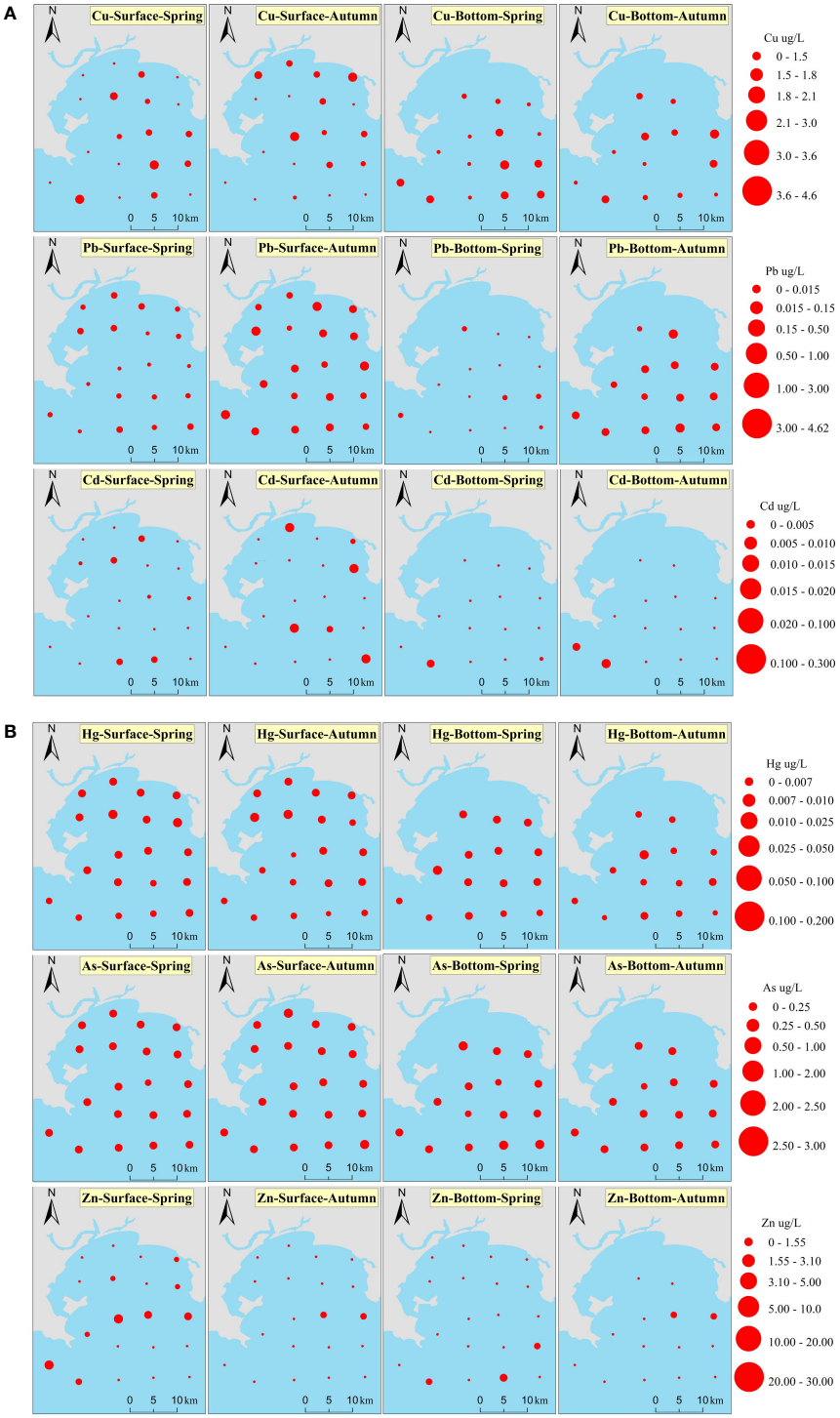


FIGURE 2
(A) The concentrations of HMs in seawater for Cu, Pb, Cd. **(B)** The concentrations of HMs in seawater for Hg, As, Zn.

(Zhang G. et al., 2017; Liu et al., 2018). There is more rain in spring, and the concentration of heavy metals in seawater decreases due to rainfall dilution.

To compare the variability between disparate groups and characteristics, the coefficient of variation was calculated (Table 2) to learn how much the data varied relatively. The result of the coefficient variation showed a relatively high variation in HMs, except As, indicating a diverse distribution of HMs in the study area, which might be from other different sources.

The comprehensive pollution index of HMs in the seawater of Jieshi Bay is shown in Figure 3. It shows that, regarding the bottom and surface seawaters of Jieshi Bay, the comprehensive pollution index of the heavy metals Cu, Pb, Hg, Cd, As, and Zn was less than an average of 1; thus, the pollution in the bottom seawater of Jieshi Bay is slight and could be ignored. The bottom seawater is clean. The mean of the comprehensive pollution index measured at two meteorological stations was greater than 1 only for the surface seawater in autumn, while the pollution comprehensive index for all other timepoints was less than 1. It can be seen that, in autumn, the respective stations on the west side of the bay and the east side of the bay's mouth were slightly affected by pollution. According to the annual wind speed variation statistics from Lufeng Meteorological Station, warm and cold air masses are active and cyclones are frequent. According to a study on the hydrodynamic characteristics of the sea area, the waves of Jieshi Bay are strong: their current

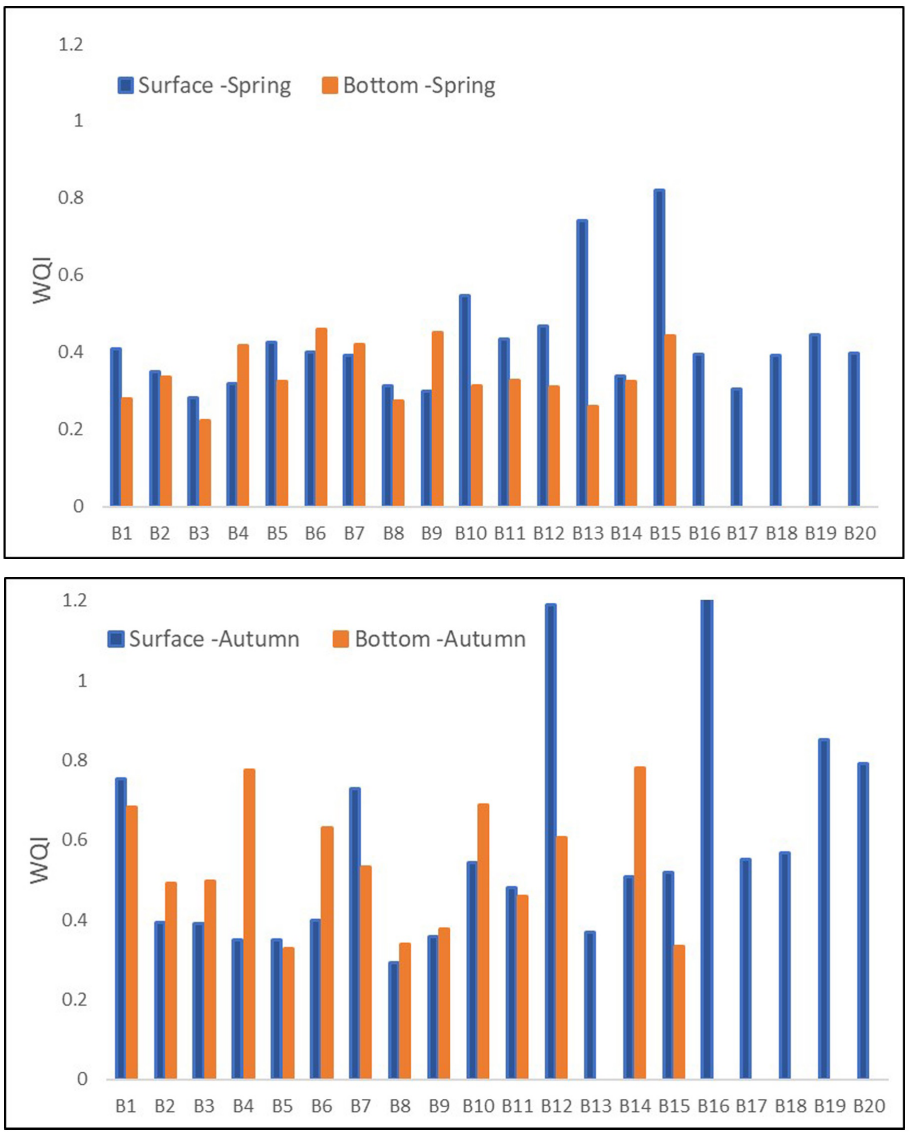


FIGURE 3
WQI of HMs in seawater.

velocity is large, their reflow was dominant in the past, their flow direction is perpendicular to the shoreline, strong waves are mainly in the E direction, and their occurrence frequency is about 27.3%. It can be speculated that the high comprehensive index of seawater pollution recorded in autumn at the stations on the west side of the Bay and the northeast side of the bay's mouth was mainly due to a seasonal phenomenon caused by the diffusion of high concentrations of heavy metals in the near-shore surface caused by high wind speeds and tidal current. The west and east sides of the bay's mouth appear to have larger pollution indices. In the new Shanwei port area and the west side of the Wukan waterway, particularly the mouth on the east side of the channel, the combined Pb and Hg ion concentration was higher, and it may be that the meteorological station was affected by the port wastewater, such as emissions from ships (Zhan et al., 2010).

Based on the water quality monitoring results taken over the years, it can be seen that Pb in Jieshi Bay has experienced an obvious upward trend, while other elements have experienced a steady downward trend (Gao and Chen, 2012; Pan et al., 2014; Gu, 2018; Zhao et al., 2018). Compared with other studies on heavy metals in seawater, the content of toxic metals, such as Cu, Pb, Cd, As, and Zn, in the seawater of Jieshi Bay was low, but Hg was slightly higher than in other research areas (Gu et al., 2012; Xiao et al., 2013; Li et al., 2017; Tang et al., 2018; Zhao et al., 2018; Lao et al., 2019; Nour, 2019; Zhang C. et al., 2020). On the whole, the seawater of Jieshi Bay is not polluted by heavy metals at present, but it should be noted that, with the expansion of the port, potential heavy metal pollution may be brought on by improvements in ship throughput and the rapid development of industry.

3.2 Distribution and risk assessment of HMs in sediment

The content of heavy metals in sediments can reflect the degree of heavy metal pollution in an area, which can provide a relevant basis to further understand the migration and transformation of various heavy metals in sediments as well as their possible sources. It can be seen from Table 3 that the sediment quality in the study area was good. From highest to lowest, the mean concentrations of all the heavy metal elements in the sediment were Zn (96.10mg/kg) > Pb (18.55mg/kg) > Cu (12.45mg/k.mg/kg) > As (6.13mg/k.mg/kg) > Hg (0.06mg/k.mg/kg) > Cd (0.02mg/kg). The coefficient of variation for Hg and As in spring, as well as for Cd in autumn, was greater than 50%, which is highly variable (CV > 36%). It can be inferred that Hg, As, and Cd in the sediments of Jieshi Bay may have been influenced by man-made sources, resulting in a high coefficient of variation (Wilding, 1985; Ma and Zhao, 2010; Liu et al., 2016). The anthropogenic source of Cd in sediments is mainly from industrial and agricultural activities, the anthropogenic source of Hg is mainly atmospheric deposition from human activities (Li et al., 2006), and the anthropogenic source of As in sediments is mainly from industrial activities (Mohammadi et al., 2015; Huang et al., 2018). This conclusion is also consistent with the large spatial dispersion of heavy metals in seawater found in this study.

It can be seen from the survey data on sediment heavy metals taken in this area for the last 15 years that heavy metal pollution in Jieshi Bay generally presents a downward trend (Qiu et al., 2011; Ye et al., 2018; Zhang L. et al., 2020), with Pb and As significantly declining, Cu and Zn remaining basically stable, and Hg and Cd slightly increasing. Combined with the coefficient of variation, it can be inferred that human activities have a great influence on the presence of Pb, As, Hg, and Cd in the sediments of this sea area.

The potential ecological hazard index method was used to evaluate the content of heavy metals in the sediments in the study area. The results in Table 4 showed that the potential ecological hazard index of six heavy metals, in descending order, was Hg > As > Pb > Cu > Cd > Zn, all of which are less than 40 and belong to the low hazard degree, among which, Hg, As, and Pb have a relatively high hazard degree. Hg and As were affected

TABLE 3 Heavy metal concentrations in sediments.

Season	Index	Concentration: mg/kg					
		Cu	Pb	Cd	Hg	As	Zn
Spring	Range	8.3–15.6	17.5–29.3	0.02	0.014–0.184	0.37–8.89	65.4–110.7
	Average	12.0	22.4	0.02	0.059	5.41	92.5
	Standard deviation	2.72	4.30	0.00	0.05	2.76	17.79
	Variable coefficient	22.68%	19.23%	0.00%	79.36%	51.15%	19.23%
Autumn	Range	9.1–16.0	5.8–22.8	0.04–0.19	0.055–0.118	5.32–11.80	77.0–116.7
	Average	12.9	14.7	0.02	0.069	6.84	99.7
	Standard deviation	2.44	4.55	0.05	0.02	1.82	13.20
	Variable coefficient	18.82%	30.92%	229.73%	26.14%	26.55%	13.24%
	Average	12.45	18.55	0.02	0.064	6.13	96.10

10.3389/fmars.2022.1011564

TABLE 4 Potential hazard index of heavy metals in sediments.

Season	Index	E_f^i						E_{RI}
		Cu	Pb	Cd	Hg	As	Zn	
Spring	Range	0.83–1.56	1.25–2.09	0.60	2.24–29.44	0.25–5.93	0.37–0.63	5.54–39.65
	Average	1.20	1.60	0.60	9.44	3.61	0.53	16.98
Autumn	Range	0.91–1.60	0.41–1.63	1.20–5.70	8.80–18.88	3.55–7.87	0.44–0.67	15.31–36.34
	Average	1.29	1.05	0.60	11.04	4.56	0.57	19.11
	Average	1.25	1.33	0.60	10.24	4.08	0.55	18.04

by man-made sources in the coefficient of variation. Therefore, the potential ecological hazard index of sediments in the study area was mainly affected by coastal industrial and agricultural activities and anthropogenic emissions. The comprehensive potential ecological hazard index was higher in autumn, but the overall hazard degree was low.

Compared with the coastal waters of the surrounding South China Sea, the overall quality of Jieshi Bay sea sediment is good (Liu et al., 2012; Wang et al., 2013; Zhang et al., 2015; Zhang et al., 2016; Wang et al., 2022; Zhang et al., 2022). We found that most of the heavy metal contents in the surface sediment was at the medium level, though the Hg and Zn contents were comparatively high in some sea areas. Although there was no obvious heavy metal pollution, we should still pay attention to human activities, which can, in part, lead to potential heavy metal pollution.

3.3 Concentrations and human health risk of HMs in organisms

The concentrations of Cu, Zn, As, Pb, Cd, and Hg in fish and crustaceans in summer and autumn are shown in Table 5. No shellfish were collected at the survey station; only fish and crustaceans were collected. The average contents of various metals in crustaceans captured in spring and autumn were Cu—13.8 and 12.6 mg/kg, Pb—0.20 and 0.59 mg/kg, Cd—0.140 and 0.212 mg/kg, Hg—0.017 and 0.009 mg/kg, As—1.50 and 1.20 mg/kg, and Zn—8.50 and 18.50 mg/kg, respectively. The average heavy metal contents in spring and autumn were Cu—1.3 and 0.8mg/kg, Pb—1.12 and 0.05mg/kg, Cd—0.044 and 0.005 mg/kg, Hg—0.022 and 0.007 mg/kg, As—0.40 and 0.40 mg/kg, and Zn—3.55 and 12.6 mg/kg, respectively. The differences between the same elements in different species may be related to the living habits, physiological characteristics, and specific physiological methods of metal accumulation in various marine organisms (Wenxiong and Jinfen, 2004). Crustaceans generally live in an environment close to the bottom of the sea, with polychaetes and other zooplanktons in the sediment serving as their main feeding source, causing them to absorb more heavy metals. The HM content in fish was low, which is closely related to their water layer habitat and feeding habits (Yi et al., 2014).

In spring, the average content of each pollutant in organisms was (in specific order) Cu > Zn > As > Pb > Cd > Hg, and in autumn, the average content of each pollutant in organisms was Zn > Cu > As > Pb > Cd > Hg. Cu and Zn are essential trace elements in living organisms, so their content in living organisms was higher than other metals. Pb and Hg are inimical to living organisms, so their contents were relatively low. Only in spring did the presence of Pb in fish exceed the relevant standards. As Pb ions in organisms may cause protein inactivation (Pourrut et al., 2008), higher Pb content in environmental media may affect the biological production of testosterone and estrogen; therefore, it can cause reproductive toxicity in human beings (Yang et al.,

TABLE 5 Biological quality monitoring results for Jieshi Bay.

Season	Species	Value	Concentration: mg/kg					
			Cu	Pb	Cd	Hg	As	Zn
Spring	Crustaceans	Range	9.4–22.2	0.02–0.51	0.041–0.298	0.009–0.023	0.50–2.80	0.20–18.8
		Average	13.8	0.20	0.140	0.017	1.50	8.50
	Fish	Range	1.0–2.2	0.02–3.92	0.003–0.061	0.008–0.055	0.30–0.50	0.2–7.2
		Average	**1.3**	**1.12**	**0.044**	**0.022**	**0.40**	**3.55**
Autumn	Crustaceans	Range	6.8–20.7	0.20–1.86	0.050–0.416	0.006–0.012	0.70–1.80	10.6–24.5
		Average	12.6	0.59	0.212	0.009	1.20	18.5
	Fish	Range	0.7–0.9	0.05–0.07	0.004–0.006	0.006–0.010	0.37–0.45	11.0–13.2
		Average	**0.8**	**0.05**	**0.005**	**0.007**	**0.40**	**12.6**

2019; Liu et al., 2022). Given the above-mentioned phenomenon of excessive Pb in seawater in autumn, in the future, the control of Pb emissions should be prioritized with respect to water pollution control in this region.

As can be seen from Table 6, the weekly assessed intake (EWI) of heavy metals in seafood in this region was lower than the PTWI for human beings as established by WHO. The harm quotient values of Pb, Cd, Hg, and As in crustaceans were all less than 1, indicating that there was no potential risk from Pb, Cd, Hg, and As to human health when eating this kind of seafood. The harm quotient values of the heavy metals Cd and Hg in fish were less than 1, indicating that there is no potential risk from Cd and Hg to human health when eating this kind of seafood. However, the hazard quotients of Pb and As in fish were greater than 1, indicating that there is a certain health risk in eating fish. The anthropogenic sources of Pb are mainly lead mining, metallurgy, and waste gas. Lead is a toxic heavy metal that can cause great harm to the human body. Lead and its compounds can cause harm to the nervous system, hematopoietic system, digestive system, kidney system, cardiovascular system, and endocrine system after entering the body. If the content is too high, lead poisoning will occur. As exists widely in the natural environment, and its anthropogenic sources are mainly smelting activities and chemical synthesis agents. As is divided into two forms: an organic form without toxicity and an inorganic form with high toxicity. The total amount of As was measured in laboratory tests and analyses, and the organic form of As was about 90%. As poisoning can cause abdominal pain, vomiting, and muscle weakness and can persist in the body for a long time.

3.4 Interrelationship and source analysis of HMs

In this study, the coefficient of variation was selected to quantitatively reflect the difference in heavy metal fluctuation degrees on a spatial scale among the monitoring stations. Excel statistical software was used to conduct a statistical analysis of the survey data, and the results are shown in Table 2. Except for As, the coefficient of variation for the elements was relatively large. This indicates that the spatial dispersion of heavy metal content in the water between the survey stations was large; thus, the heavy metal pollutants in the study sea area may have come from different pollution sources.

Since the HMs were hardly absorbed in the seawater, they were not stable. They were easily affected and transferred by hydrodynamic and environmental conditions. Thus, the sources of HMs in seawater were difficult to distinguish. The coefficient of variation for the HMs presented strong correlations, which means that they may originate from the same source; thus, the homology of the source must be determined by correlating the HMs (Li et al., 2009). Pearson's correlation coefficient was used to measure the statistical association between the continuous variables of interest. The results of Pearson's correlation coefficient matrix for the HMs in Jieshi Bay (Figure 4) showed a moderate degree of correlation between Cd and As in the surface water. For the bottom water, the HMs had weak correlations. In conclusion, Cd and As in surface water may share common sources, and the other HMs might not have a strong relationship.

PCA is a mathematical tool that represents variations present in a dataset using a small number of factors (Granato et al., 2018). For visual analysis, a two- or three-dimensional projection of samples is usually constructed with axes (principal components, PCs) as factors. PCA was applied to explore similarities and hidden patterns among the HMs to find potential sources for the principal components (Table 7). PC1, accounting for 30.36% of the total data variance, had high positive loading for Cd and As. PC2, accounting for 19.97% of the total data variance, had negative loading for Pb and Zn. PC3, accounting for 17.22% of the total data variance, had negative loading for Cu and Hg. The accumulated percentage of variance in the three PCs was 67.54%, which means that these three PCs could represent the principal component of the samples. The characteristic performance factor variable of principal component 1 had a high load of Cd and As elements, indicating that Cd and As may have the same source (Figure 5). The results of the principal component analysis are similar to the Pearson correlation analysis. The waters around Jieshi Bay are surrounded by several Shanwei towns (Lufeng City, Jieshi Town, Taihu Town, Jinxiang Town, and Jiesheng Town). The industrial park is distributed around the continental area of Jieshi Bay, and it is reasonable to assume that a large amount of Cd and

TABLE 6 Weekly assessed intake and hazard quotients of heavy metals in marine organisms.

Season	Species	TTHQ	THQ				EWI			
			Pb	Cd	Hg	As	Pb	Cd	Hg	As
Spring	Crustaceans	0.47	0.005	0.013	0.003	0.452	0.126	0.089	0.011	0.949
	Fish	1.02	0.168	0.026	0.026	0.8	4.704	0.185	0.092	1.68
Autumn	Crustaceans	0.40	0.013	0.019	0.002	0.361	0.373	0.134	0.006	0.759
	Fish	0.82	0.008	0.003	0.008	0.8	0.21	0.021	0.029	1.68

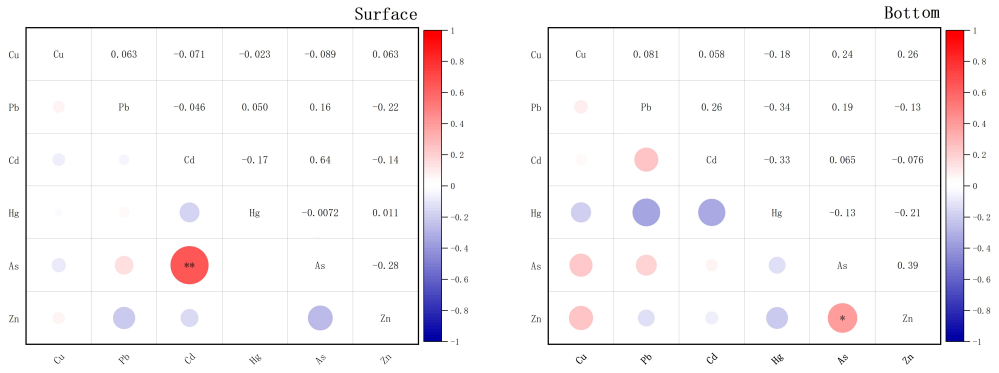


FIGURE 4
The correlation analysis of HMs in the seawater of Jieshi bay, respectively (P<0.05, P<0.1).

TABLE 7 Principal component analysis results for heavy metals in the seawater of Jieshi Bay.

Principal component	Initial eigenvalue			HMs	Load of each item		
	Eigenvalue	Percentage of variance (%)	Cumulative (%)		PC1	PC2	PC3
PC1	1.821	30.358	30.358	Cu	-0.136	0.162	0.798
PC2	1.198	19.973	50.331	Pb	0.173	0.701	0.206
PC3	1.033	17.216	67.547	Cd	0.605	-0.334	0.065
PC4	0.911	15.188	82.735	Hg	-0.125	0.427	-0.560
PC5	0.731	12.186	94.921	As	0.651	-0.015	-0.038
PC6	0.305	5.079	100.000	Zn	-0.382	-0.434	0.031

As in this area comes from surface runoff and industrial wastewater discharge. The characteristic performance factor variable of principal component 2 had a high load of Pb and Zn elements, but the Zn load in principal component 2 was negative, so it is difficult to judge whether the source is the same. The results of the principal component analysis are similar to the Pearson correlation analysis. The characteristic performance factor variables of principal component 3 had a high load of Cu and Hg elements, but the Hg load on principal component 3 was negative, so it is difficult to judge whether the source is the same. The results of the principal component analysis are similar to the Pearson correlation analysis. Based on the analysis of the correlation coefficient relationship matrix of heavy metals in seawater, except for Cd and As, elements such as Cu, Pb, Zn, and Hg had little correlation with each other, and the probability of a common source is low, which is consistent with the conclusion of the Pearson correlation analysis.

The ability of marine organisms to accumulate heavy metals was quantified with BAF: $BAF_{sediment} > 1$ indicates that the organism can accumulate heavy metals. $BAF_{seawater} > 1$ indicates that the organism has a strong enrichment capacity for heavy metals (enrichment capacity is proportional to the value), and $BAF_{seawater} > 100$ indicates that the organism has a strong enrichment capacity for heavy metals. The data in Table 8 show that, in addition to the Pb data from different stations, the $BAF_{seawater}$ of Cu, Cd, Hg, As, and Zn was greater than 100, indicating that the organisms in this sea area have an enrichment capacity for these six heavy metals, especially Cu, Cd, and Zn, which had the highest $BAF_{seawater}$ values. However, as essential elements for biological growth, Cu and Zn levels are relatively high in fish and crustaceans, indicating that the organisms in this sea area have a stronger enrichment capacity for Cd. There were excessive Zn and Hg levels in the seawater of the study area, and the organisms also showed a strong enrichment ability, especially for Zn. In the spring sample data, it was found that the $BAF_{sediment}$ value of Cd for organisms was greater than 1, and the $BAF_{sediment}$ values of Cu and Hg in some sites were within the critical value. In the autumn sample data, it was found that the $BAF_{sediment}$ value of Cd for organisms in most sites was greater than 1. The $BAF_{sediment}$ value of Cu at some sites was within the critical value, and the $BAF_{sediment}$ value of other heavy metals was low.

$BAF_{seawater}$ and $BAF_{sediment}$ were used to evaluate the accumulation of heavy metals in the medium. Cd was the most accumulated element. According to relevant studies,

10.3389/fmars.2022.1011564

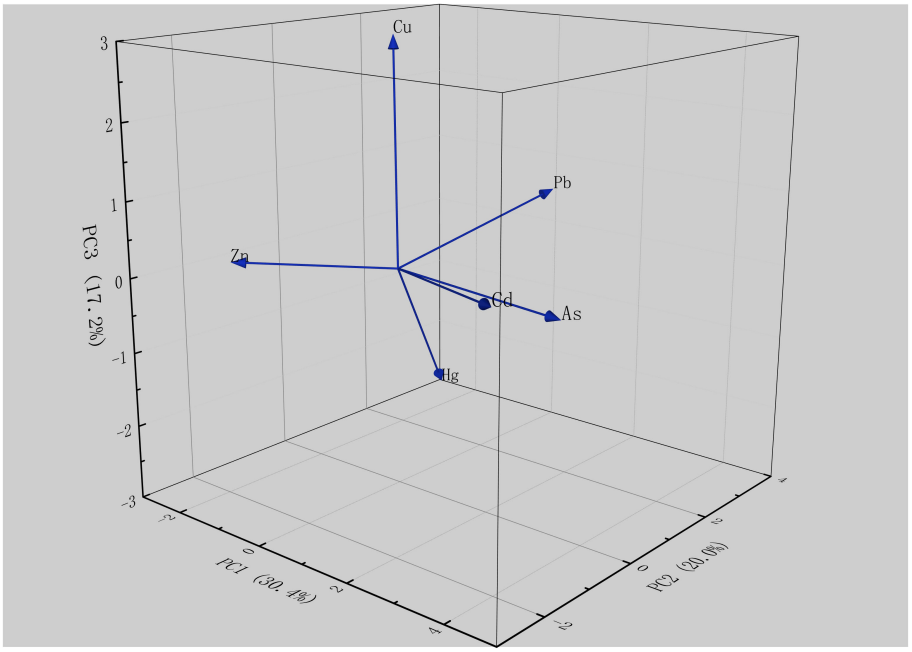


FIGURE 5
PCA analysis of HMs in seawater.

TABLE 8 Biological enrichment index of heavy metals in each phase of Jieshi Bay.

Parameter	Time	Spring						Autumn					
	location	Cu	Pb	Cd	Hg	As	Zn	Cu	Cu	Cu	Cu	Cu	Cu
$BAF_{sediment}$	3	0.77	0.01	2.38	0.24	0.1	0.09	0.88	0.88	0.88	0.88	0.88	0.88
	5	0.06	0	2.7	1.2	0.09	0	0.05	0.05	0.05	0.05	0.05	0.05
	8	1.04	0.01	8.8	0.19	0.24	0.11	0.9	0.9	0.9	0.9	0.9	0.9
	11	0.17	0	2.43	1.34	0.44	0.03	1.32	1.32	1.32	1.32	1.32	1.32
	15	1.22	0.1	2.88	0.68	0.06	0.04	1.06	1.06	1.06	1.06	1.06	1.06
	19	1.4	0.08	2.98	0.18	0.05	0.04	0.98	0.98	0.98	0.98	0.98	0.98
$BAF_{seawater}$	3	24,750	425	2,375	375	282.61	5,838.71	8,843.75	8,843.75	8,843.75	8,843.75	8,843.75	8,843.75
	5	3,333.33	22.99	10,800	763.89	227.27	129.03	500	500	500	500	500	500
	8	21,500	428.57	35,200	185.48	750	5,806.45	15,166.67	15,166.67	15,166.67	15,166.67	15,166.67	15,166.67
	11	592.59	3,000	4,850	515.38	375	176.92	6,125	6,125	6,125	6,125	6,125	6,125
	15	4,528.57	2,736.11	2,875	199.37	180	902.44	8,233.33	8,233.33	8,233.33	8,233.33	8,233.33	8,233.33
	19	7,000	3,362.9	2,975	146.15	173.91	2,387.1	4,540	4,540	4,540	4,540	4,540	4,540

the metabolic period of Cd in organisms is longer than that of other metals, which is also the reason why the Cd content in organisms exceeds that of other metals (Lin et al., 2017). Moreover, Cd and Ca have similar geochemical properties (Zhang, 1991), which also makes it easier for Cd to accumulate in organisms. The chemical form of heavy metals is also an important factor affecting the content of heavy metals in marine organisms. Cd in the sediments of East Guangdong Sea, where Jieshi Bay is located, mainly exists in an acid-soluble state, which is easier to absorb by organisms. On the whole, organisms in this sea area have a stronger ability to enrich heavy metals in seawater, and the quality of seawater is more important for people who mainly eat seafood.

4 Conclusion

In summary, this study analyzed the distribution characteristics of six heavy metals in the seawater, sediments, and organisms in Jieshi Bay. Generally, the level of heavy metal content was relatively low, and the main sources for these heavy metals could be surface runoff and industrial wastewater discharge in the bay. For seawater, the concentration of the heavy metals in autumn was higher than those in spring, and the surface water has higher heavy metal content than the bottom water. Hg is the main limiting factor according to the statistics. For sediments, the potential ecological risks of Hg, As, and Pb in sediments were relatively high compared with the rest of the contents. For the organisms, the content of heavy metals in fish was much lower than that in crustaceans, and lead in fish had exceeded the standard in spring. The seawater contributes more to bioaccumulation in fish and crustaceans than sediments, indicating that it is important to protect the seawater quality because of the bioaccumulation from seafood product consumption. Even if the heavy metals have not threatened the environment in the bay, it remains necessary to enhance pollutant management while especially developing the discharge of wastewater.

Data availability statement

The original contributions presented in the study are included in the article/supplementary material. Further inquiries can be directed to the corresponding author.

Ethics statement

The study involving animals was reviewed and approved by the Ethics Committee of South China Institute of Environment Sciences.

Author contributions

WZ: main contributor to conception, design of the work, and result analysis. QC: drafting of the article, revising it critically for important intellectual content, and ensuring the discussions related to the work. MH: data analysis and interpretation. YL: data collection and contributes to conception design. DW: data collection. DZ: using PCA analysis to determine the correlationship of heavy metals. All authors contributed to the article and approved the submitted version.

Funding

This study is supported by the Major Science and Technology Program for Water Pollution Control and Treatment, Ministry of Ecology and Environment (2018ZX07601-002-05).

Conflict of interest

The authors declare that the research was conducted in the absence of any commercial or financial relationships that could be construed as a potential conflict of interest.

Publisher's note

All claims expressed in this article are solely those of the authors and do not necessarily represent those of their affiliated organizations, or those of the publisher, the editors and the reviewers. Any product that may be evaluated in this article, or claim that may be made by its manufacturer, is not guaranteed or endorsed by the publisher.

References

Agusa, T., Kunito, T., Sudaryanto, A., Monirith, I., Kan-Atireklap, S., Iwata, H., et al. (2007). Exposure assessment for trace elements from consumption of marine fish in southeast Asia. *Environ. pollut.* 145, 766–777. doi: 10.1016/j.envpol.2006.04.034

Baltas, H., Sirin, M., Dalgic, G., Bayrak, E. Y., and Akdeniz, A. (2017). Assessment of metal concentrations (Cu, zn, and Pb) in seawater, sediment and biota samples in the coastal area of Eastern black Sea, Turkey. *Mar. pollut. Bull.* 122, 475–482. doi: 10.1016/j.marpolbul.2017.06.059

Bedeian, A. G., and Mossholder, K. W. (2000). On the use of the coefficient of variation as a measure of diversity. *Organizational Res. Methods* 3, 285–297. doi: 10.1177/109442810033005

Birch, G., Evenden, D., and Teutsch, M. (1996). Dominance of point source in heavy metal distributions in sediments of a major Sydney estuary (Australia). *Environ. Geology* 28, 169–174. doi: 10.1007/s002540050090

Bosch, A. C., O'neill, B., Sigge, G. O., Kerwath, S. E., and Hoffman, L. C. (2016). Heavy metals in marine fish meat and consumer health: A review. *J. Sci. Food Agric.* 96, 32–48. doi: 10.1002/jsfa.7360

Brown, C. E. (1998). *Coefficient of Variation*. In: Applied Multivariate Statistics in Geohydrology and Related Sciences. (Berlin, Heidelberg: Springer). doi: 10.1007/978-3-642-80328-4_13

Fang, H., Huang, L., Wang, J., He, G., and Reible, D. (2016). Environmental assessment of heavy metal transport and transformation in the hangzhou bay, China. *J. hazardous materials* 302, 447–457. doi: 10.1016/j.jhazmat.2015.09.060

Gao, X., and Chen, C.-T. A. (2012). Heavy metal pollution status in surface sediments of the coastal bohai bay. *Water Res.* 46, 1901–1911. doi: 10.1016/j.watres.2012.01.007

Gerringa, L. J., De Baar, H. J., Nolting, R., and Paucot, H. (2001). The influence of salinity on the solubility of zn and cd sulphides in the scheldt estuary. *J. Sea Res.* 46, 201–211. doi: 10.1016/S1385-1101(01)00081-8

Granato, D., Santos, J. S., Escher, G. B., Ferreira, B. L., and Maggio, R. M. (2018). Use of principal component analysis (PCA) and hierarchical cluster analysis (HCA) for multivariate association between bioactive compounds and functional properties in foods: A critical perspective. *Trends Food Sci. Technol.* 72, 83–90. doi: 10.1016/j.tifs.2017.12.006

Gu, Y.-G. (2018). Heavy metal fractionation and ecological risk implications in the intertidal surface sediments of zhelin bay, south China. *Mar. pollut. Bull.* 129, 905–912. doi: 10.1016/j.marpolbul.2017.10.047

Gundersen, P., and Steinnes, E. (2003). Influence of pH and TOC concentration on Cu, zn, cd, and Al speciation in rivers. *Water Res.* 37, 307–318. doi: 10.1016/S0043-1354(02)00284-1

Gu, Y.-G., Ning, J.-J., Ke, C.-L., and Huang, H.-H. (2018). Bioaccessibility and human health implications of heavy metals in different trophic level marine organisms: a case study of the south China Sea. *Ecotoxicology Environ. Saf.* 163, 551–557. doi: 10.1016/j.ecoenv.2018.07.114

Gu, L., Song, B., Tong, Z. Q., and Ma, J. H. (2012). Spatial distribution and potential ecological risk assessment of heavy metals in roadside soils on different operated times along the lianyungang-horgas highway. *Advanced Materials Res.*, 356–360, 630–635. Trans Tech Publ. doi: 10.4028/www.scientific.net/AMR.356-360.630

Hakanson, L. (1980). An ecological risk index for aquatic pollution control. A sedimentological approach. *Water Res.* 14, 975–1001. doi: 10.1016/0043-1354(80)90143-8

Hao, Z., Chen, L., Wang, C., Zou, X., Zheng, F., Feng, W., et al. (2019). Heavy metal distribution and bioaccumulation ability in marine organisms from coastal regions of hainan and zhoushan, China. *Chemosphere* 226, 340–350. doi: 10.1016/j.chemosphere.2019.03.132

Hao, Y., Chen, L., Zhang, X., Zhang, D., Zhang, X., Yu, Y., et al. (2013). Trace elements in fish from taihu lake, China: Levels, associated risks, and trophic transfer. *Ecotoxicology Environ. Saf.* 90, 89–97. doi: 10.1016/j.ecoenv.2012.12.012

Huang, Y., Deng, M., Wu, S., Japenga, J., Li, T., Yang, X., et al. (2018). A modified receptor model for source apportionment of heavy metal pollution in soil. *J. hazardous materials* 354, 161–169. doi: 10.1016/j.jhazmat.2018.05.006

Hu, B., Li, G., Li, J., Bi, J., Zhao, J., and Bu, R. (2013a). Spatial distribution and ecotoxicological risk assessment of heavy metals in surface sediments of the southern bohai bay, China. *Environ. Sci. pollut. Res.* 20, 4099–4110. doi: 10.1007/s11356-012-1332-z

Hu, B., Li, J., Zhao, J., Yang, J., Bai, F., and Dou, Y. (2013b). Heavy metal in surface sediments of the liaodong bay, bohai Sea: Distribution, contamination, and sources. *Environ. Monit. Assess.* 185, 5071–5083. doi: 10.1007/s10661-012-2926-0

Jiang, X., Wang, W., Wang, S., Zhang, B., and Hu, J. (2012). Initial identification of heavy metals contamination in taihu lake, a eutrophic lake in China. *J. Environ. Sci.* 24, 1539–1548. doi: 10.1016/S1001-0742(11)60986-8

Kükrer, S., and Mutlu, E. (2019). Assessment of surface water quality using water quality index and multivariate statistical analyses in saraydüzü dam lake, Turkey. *Environ. Monit. Assess.* 191, 1–16. doi: 10.1007/s10661-019-7197-6

Lao, Q., Su, Q., Liu, G., Shen, Y., Chen, F., Lei, X., et al. (2019). Spatial distribution of and historical changes in heavy metals in the surface seawater and sediments of the beibu gulf, China. *Mar. pollut. Bull.* 146, 427–434. doi: 10.1016/j.marpolbul.2019.06.080

Li, F., Fan, Z., Xiao, P., Oh, K., Ma, X., and Hou, W. (2009). Contamination, chemical speciation and vertical distribution of heavy metals in soils of an old and large industrial zone in northeast China. *Environ. geology* 57, 1815–1823. doi: 10.1007/s00254-008-1469-8

Li, H., Kang, X., Li, X., Li, Q., Song, J., Jiao, N., et al. (2017). Heavy metals in surface sediments along the weihai coast, China: Distribution, sources and contamination assessment. *Mar. pollut. Bull.* 115, 551–558. doi: 10.1016/j.marpolbul.2016.12.039

Lin, L., Wei, H., and Huang, H. (2017). Contamination status and bioaccumulation of the heavy metals in the surface sediments and benthos in daya bay. *Ecol. Sci.* 36, 173–181. doi: 10.14108/j.cnki.1008-8873.2017.06.024

Liu, R., Jiang, W., Li, F., Pan, Y., Wang, C., and Tian, H. (2021). Occurrence, partition, and risk of seven heavy metals in sediments, seawater, and organisms from the eastern sea area of Shandong peninsula, yellow Sea, China. *J. Environ. Manage.* 279, 111771. doi: 10.1016/j.jenvman.2020.111771

Liu, Y., Kuang, W., Xu, J., Chen, J., Sun, X., Lin, C., et al. (2022). Distribution, source and risk assessment of heavy metals in the seawater, sediments, and organisms of the daya bay, China. *Mar. pollut. Bull.* 174, 113297. doi: 10.1016/j.marpolbul.2021.113297

Liu, Y., Ma, Z., Lv, J., and Bi, J. (2016). Identifying sources and hazardous risks of heavy metals in topsoils of rapidly urbanizing East China. *J. Geographical Sci.* 26, 735–749. doi: 10.1007/s11442-016-1296-x

Liu, Q., Wang, F., Meng, F., Jiang, L., Li, G., and Zhou, R. (2018). Assessment of metal contamination in estuarine surface sediments from dongying city, China: use of a modified ecological risk index. *Mar. pollut. Bull.* 126, 293–303. doi: 10.1016/j.marpolbul.2017.11.017

Liu, Q., Xu, X., Zeng, J., Shi, X., Liao, Y., Du, P., et al. (2019). Heavy metal concentrations in commercial marine organisms from xiangshan bay, China, and the potential health risks. *Mar. pollut. Bull.* 141, 215–226. doi: 10.1016/j.marpolbul.2019.02.058

Liu, J., Yan, W., Chen, Z., and Lu, J. (2012). Sediment sources and their contribution along northern coast of the south China Sea: Evidence from clay minerals of surface sediments. *Continental Shelf Res.* 47, 156–164. doi: 10.1016/j.csr.2012.07.013

Li, Y., Yu, Z.-M., and Song, X.-X. (2006). Application of principal component analysis (PCA) for the estimation of source of heavy metal contamination in marine sediments. *Huan Jing ke Xue= Huanjing Kexue* 27, 137–141. doi: 10.13227/j.hjkx.2006.01.026

Matthiessen, P., Reed, J., and Johnson, M. (1999). Sources and potential effects of copper and zinc concentrations in the estuarine waters of Essex and Suffolk, united kingdom. *Mar. pollut. Bull.* 38, 908–920. doi: 10.1016/S0025-326X(99)00090-9

Ma, Y., Xu, H., Yu, T., He, G., Zhao, Y., and Fu, Y. (2008). *The specification for marine monitoring-part 5: Sediment analysis* (Beijing: China Standardization Press).

Ma, Q., and Zhao, G. (2010). Effects of different land use types on soil nutrients in intensive agricultural region. *J. Natural Resour.* 25, 1834–1844.

Mohammadi, R. M., Sobhan, A. S., Karimi, H., and Sorooshnia, R. (2015). Natural and anthropogenic source of heavy metals pollution in the soil samples of an industrial complex; a case study. *Iran. J. Toxicol.*. 9, 29.

Nour, H. E. S. (2019). Distribution, ecological risk, and source analysis of heavy metals in recent beach sediments of sharm El-sheikh, Egypt. *Environ. Monit. Assess.* 191, 1–12. doi: 10.1007/s10661-019-7728-1

Nystroem, G. M., Ottosen, L. M., and Villumsen, A. (2005). Electrodialytic removal of Cu, zn, Pb, and cd from harbor sediment: Influence of changing experimental conditions. *Environ. Sci. Technol.* 39, 2906–2911. doi: 10.1021/es048930w

Pang, H.-J., Lou, Z.-H., Jin, A.-M., Yan, K.-K., Jiang, Y., Yang, X.-H., et al. (2015). Contamination, distribution, and sources of heavy metals in the sediments of andong tidal flat, hangzhou bay, China. *Continental Shelf Res.* 110, 72–84. doi: 10.1016/j.csr.2015.10.002

Pan, J., Pan, J.-F., and Wang, M. (2014). Trace elements distribution and ecological risk assessment of seawater and sediments from dingzi bay, Shandong peninsula, north China. *Mar. pollut. Bull.* 89, 427–434. doi: 10.1016/j.marpolbul.2014.10.022

Pourrut, B., Perchet, G., Silvestre, J., Cecchi, M., Guiresse, M., and Pinelli, E. (2008). Potential role of NADPH-oxidase in early steps of lead-induced oxidative burst in vicia faba roots. *J. Plant Physiol.* 165, 571–579. doi: 10.1016/j.jplph.2007.07.016

Qiu, Y.-W., Lin, D., Liu, J.-Q., and Zeng, E. Y. (2011). Bioaccumulation of trace metals in farmed fish from south China and potential risk assessment. *Ecotoxicology Environ. Saf.* 74, 284–293. doi: 10.1016/j.ecoenv.2010.10.008

Rezaee Ebrahim Saraee, K., Abdi, M. R., Naghavi, K., Saion, E., Shafaei, M. A., and Soltani, N. (2011). Distribution of heavy metals in surface sediments from the south China Sea ecosystem, Malaysia. *Environ. Monit. Assess.* 183, 545–554. doi: 10.1007/s10661-011-1939-4

Shin, P., and Lam, W. (2001). Development of a marine sediment pollution index. *Environ. pollut.* 113, 281–291. doi: 10.1016/S0269-7491(00)00192-5

Storelli, M. (2008). Potential human health risks from metals (Hg, cd, and Pb) and polychlorinated biphenyls (PCBs) *via* seafood consumption: estimation of target hazard quotients (THQs) and toxic equivalents (TEQs). *Food Chem. Toxicol.* 46, 2782–2788. doi: 10.1016/j.fct.2008.05.011

Sun, W., Yu, J., Xu, X., Zhang, W., Liu, R., and Pan, J. (2014). Distribution and sources of heavy metals in the sediment of xiangshan bay. *Acta Oceanologica Sin.* 33, 101–107. doi: 10.1007/s13131-014-0456-z

Tang, H., Ke, Z., Yan, M., Wang, W., Nie, H., Li, B., et al. (2018). Concentrations, distribution, and ecological risk assessment of heavy metals in daya bay, China. *Water* 10, 780. doi: 10.3390/w10060780

Tyagi, S., Sharma, B., Singh, P., and Dobhal, R. (2013). Water quality assessment in terms of water quality index. *Am. J. Water Resour.* 1, 34–38. doi: 10.12691/ajwr-1-3-3

Wang, X., Fu, R., Li, H., Zhang, Y., Lu, M., Xiao, K., et al. (2020). Heavy metal contamination in surface sediments: A comprehensive, large-scale evaluation for the bohai Sea, China. *Environ. pollut.* 260, 113986. doi: 10.1016/j.envpol.2020.113986

Wang, Y., Wang, Y., Chen, X., and Zhang, L. (2022). Source-to-sink process and risk assessment of heavy metals for the surface sediment in the northern South China Sea. *Environmental Science and Pollution Research* doi: 10.21203/rs.3.rs-1593522/v1

Wang, S.-L., Xu, X.-R., Sun, Y.-X., Liu, J.-L., and Li, H.-B. (2013). Heavy metal pollution in coastal areas of south China: a review. *Mar. pollut. Bull.* 76, 7–15. doi: 10.1016/j.marpolbul.2013.08.025

Wang, X., Zhao, L., Xu, H., and Zhang, X. (2018). Spatial and seasonal characteristics of dissolved heavy metals in the surface seawater of the yellow river estuary, China. *Mar. pollut. Bull.* 137, 465–473. doi: 10.1016/j.marpolbul.2018.10.052

Wei, M., Yanwen, Q., Zheng, B., and Zhang, L. (2008). Heavy metal pollution in tianjin bohai bay, China. *J. Environ. Sci.* 20, 814–819. doi: 10.1016/S1001-0742(08)62131-2

Wenxiong, W., and Jinfen, P. (2004). The transfer of metals in marine food chains: A review. *Acta Ecologica Sin.* 24, 599–604.

Wilding, L. (1985). "Spatial variability: its documentation, accomodation and implication to soil surveys," in *Soil spatial variability*(Netherlands, Pudoc, Wageningen), 166–194.

Xiao, R., Bai, J., Huang, L., Zhang, H., Cui, B., and Liu, X. (2013). Distribution and pollution, toxicity and risk assessment of heavy metals in sediments from urban and rural rivers of the pearl river delta in southern China. *Ecotoxicology* 22, 1564–1575. doi: 10.1007/s10646-013-1142-1

Yang, W., Huang, D., Chen, J., Chen, X., Liu, W., and Wang, Y. (2019). Research on ecological environment quality in the sea area near the second petrochemical sewage pipeline discharge outlet in daya bay. *J. Mar. Sci.* 37, 85–91.

Yan, Y., Han, L., Yu, R.-L., Hu, G.-R., Zhang, W.-F., Cui, J.-Y., et al. (2020). Background determination, pollution assessment and source analysis of heavy metals in estuarine sediments from quanzhou bay, southeast China. *Catena* 187, 104322. doi: 10.1016/j.catena.2019.104322

Ye, L., Huang, M., Zhong, B., Wang, X., Tu, Q., Sun, H., et al. (2018). Wet and dry deposition fluxes of heavy metals in pearl river delta region (China): Characteristics, ecological risk assessment, and source apportionment. *J. Environ. Sci.* 70, 106–123. doi: 10.1016/j.jes.2017.11.019

Yi, Y.-J., Sun, J., Tang, C.-H., and Zhang, S.-H. (2016). Ecological risk assessment of heavy metals in sediment in the upper reach of the Yangtze river. *Environ. Sci. pollut. Res.* 23, 11002–11013. doi: 10.1007/s11356-016-6296-y

Yi, B., Zhou, P., Zhou, J., Li, H., Zhang, H., Wu, L., et al. (2014). Distribution and quality assessment of Hg, Pb, cd and as in marine organisms from daya bay during 2007–2010. *Mar. Environ. Sci.* 33, 226–231.

Zhang, Y. (1991). A background value study on heavy metal elements in the sediments of daya bay. *Tropic oceanology/Redai Haiyang. Guangzhou* 10, 76–80.

Zhang, G., Bai, J., Xiao, R., Zhao, Q., Jia, J., Cui, B., et al. (2017). Heavy metal fractions and ecological risk assessment in sediments from urban, rural and reclamation-affected rivers of the pearl river estuary, China. *Chemosphere* 184, 278–288. doi: 10.1016/j.chemosphere.2017.05.155

Zhang, Z., Jin, J., Zhang, J., Zhao, D., Li, H., Yang, C., et al. (2022). Contamination of heavy metals in sediments from an estuarine bay, south China: Comparison with previous data and ecological risk assessment. *Processes* 10, 837. doi: 10.3390/pr10050837

Zhang, L., Shi, Z., Zhang, J., Jiang, Z., Wang, F., and Huang, X. (2015). Spatial and seasonal characteristics of dissolved heavy metals in the east and west guangdong coastal waters, south China. *Mar. pollut. Bull.* 95, 419–426. doi: 10.1016/j.marpolbul.2015.03.035

Zhang, L., Shi, Z., Zhang, J., Jiang, Z., Wang, F., and Huang, X. (2016). Toxic heavy metals in sediments, seawater, and molluscs in the eastern and western coastal waters of guangdong province, south China. *Environ. Monit. Assess.* 188, 1–14. doi: 10.1007/s10661-015-4999-z

Zhang, M., Sun, X., and Xu, J. (2020). Heavy metal pollution in the East China Sea: A review. *Mar. pollut. Bull.* 159, 111473. doi: 10.1016/j.marpolbul.2020.111473

Zhang, A., Wang, L., Zhao, S., Yang, X., Zhao, Q., Zhang, X., et al. (2017). Heavy metals in seawater and sediments from the northern liaodong bay of China: Levels, distribution and potential risks. *Regional Stud. Mar. Sci.* 11, 32–42. doi: 10.1016/j.chemosphere.2017.05.155

Zhang, L., Yan, W., Xie, Z., Cai, G., Mi, W., and Xu, W. (2020). Bioaccumulation and changes of trace metals over the last two decades in marine organisms from guangdong coastal regions, south China. *J. Environ. Sci.* 98, 103–108. doi: 10.1016/j.jes.2020.05.007

Zhang, C., Zheng, Z., Yao, S., Jia, H., Xian, X., and Wang, L. (2020). Ecological risk of heavy metals in sediment around techeng island special marine reserves in zhanjiang bay. *J. Ocean Univ. China* 19, 561–568. doi: 10.1007/s11802-020-4042-z

Zhan, S., Peng, S., Liu, C., Chang, Q., and Xu, J. (2010). Spatial and temporal variations of heavy metals in surface sediments in bohai bay, north China. *Bull. Environ. contamination Toxicol.* 84, 482–487. doi: 10.1007/s00128-010-9971-6

Zhao, B., Wang, X., Jin, H., Feng, H., Shen, G., Cao, Y., et al. (2018). Spatiotemporal variation and potential risks of seven heavy metals in seawater, sediment, and seafood in xiangshan bay, China, (2011–2016). *Chemosphere* 212, 1163–1171. doi: 10.1016/j.chemosphere.2018.09.020

Zhen, G., Li, Y., Tong, Y., Yang, L., Zhu, Y., and Zhang, W. (2016). Temporal variation and regional transfer of heavy metals in the pearl (Zhujiang) river, China. *Environ. Sci. pollut. Res.* 23, 8410–8420. doi: 10.1007/s11356-016-6077-7

Zhixin, N., Xia, Z., Weixu, C., Jingqin, L., and Xiaoping, H. (2016). Distribution, speciation and risk assessment of trace metals in surface sediment of the zhujiang estuary. *Mar. Environ. Sci.* 35, 321–328. doi: 10.13634/j.cnki.mes.2016.03.001

frontiers | Frontiers in Marine Science

TYPE Original Research
PUBLISHED 09 January 2023
DOI 10.3389/fmars.2022.1012260

Check for updates

OPEN ACCESS

EDITED BY
Dilip Kumar Jha,
National Institute of Ocean Technology, India

REVIEWED BY
Wentao Ma,
Shanghai Jiao Tong University, China
Qiyan Ji,
Zhejiang Ocean University, China
Heng Zhang,
School of Marine Sciences,
Sun Yat-sen University, China

*CORRESPONDENCE
Wen Zhou
zhouwen@scies.org
Lingyan Lu
936501365@qq.com

SPECIALTY SECTION
This article was submitted to Marine Pollution, a section of the journal Frontiers in Marine Science

RECEIVED 05 August 2022
ACCEPTED 19 December 2022
PUBLISHED 09 January 2023

CITATION
Geng B, Lu L, Cao Q, Zhou W, Li S, Wen D and Hong M (2023) Three-dimensional numerical study of cooling water discharge of Daya Bay Nuclear Power Plant in southern coast of China during summer. *Front. Mar. Sci.* 9:1012260. doi: 10.3389/fmars.2022.1012260

COPYRIGHT
© 2023 Geng, Lu, Cao, Zhou, Li, Wen and Hong. This is an open-access article distributed under the terms of the Creative Commons Attribution License (CC BY). The use, distribution or reproduction in other forums is permitted, provided the original author(s) and the copyright owner(s) are credited and that the original publication in this journal is cited, in accordance with accepted academic practice. No use, distribution or reproduction is permitted which does not comply with these terms.

Three-dimensional numerical study of cooling water discharge of Daya Bay Nuclear Power Plant in southern coast of China during summer

Bingxu Geng[1], Lingyan Lu[2]*, Qian Cao[3], Wen Zhou[3]*, Shiyu Li[4], Ding Wen[3] and Man Hong[3]

[1]Marine Environment Engineering Center, South China Sea Institute of Oceanology, Chinese Academy of Sciences, Guangzhou, China, [2]Guangdong Center for Marine Development Research, Guangzhou, China, [3]South China Institute of Environmental Sciences, Ministry of Ecology and Environment of the People's Republic of China, Guangzhou, China, [4]School of Environmental Science and Engineering, Sun Yat-Sen University, Guangzhou, China

The impact of thermal pollution caused by cooling water discharge of power plant on the surrounding marine ecology has been a hot issue in oceanographic research. To reveal the distribution pattern of cooling water discharge of Daya Bay Nuclear Power Plant in summer and the impact on the surrounding marine environment, this research established a high-resolution three-dimensional (3D) numerical model based on ECOMSED in the Daya Bay. The model results are consistent with the observations on the distribution of tide level and temperature. The simulated horizontal distribution of temperature rise is consistent with the distribution trend of remote sensing images. The study showed that the stratification of the Daya Bay water is stronger in summer. The cooling water mainly spreads in the surface layer, and the temperature rise in the bottom layer is not apparent. Quantitative analysis showed that around 18.8-21.6 km^2 of the area has 1°C surface temperature rises. The area of temperature rises that exceeds 2 °C is between 6.2 and 8.1 km^2. The area of temperature rises that exceeds 4 °C is between no more than 1.2 km^2. The area with a bottom temperature rises of 1 °C does not exceed 2.2 km^2, and there is no area that has a bottom temperature rise over 1 °C. The tidal dynamics process influences on the dispersion of cooling water discharge from Daya Bay Nuclear Power Plant, where the influence is more significant in the spring tide period than in the neap tide period. Our findings are consistent with previous researches.

KEYWORDS

Nuclear power plant, cooling water discharge, 3D numerical model, tidal dynamics, monsoon

1 Introduction

The impact of cooling water discharge on the environment from nuclear power plants has attracted increased attention, especially after the accident at Fukushima Daiichi Nuclear Power Plant in Japan and agreement on carbon neutrality. The nuclear power plants contribute to the reduction of fossil fuel consumption, helping the earth's atmospheric temperature to reduce somehow (Hassan et al., 2020; Mahmood et al., 2020). However, the serious concerns on long-term radioactive and environmental impact had always been a popular topic (Musyoka and Field, 2018; Wu et al., 2013; Kaviani et al., 2021). Not only the radionuclide release from cooling water could have ecological consequences, but also the heat carried (Liu et al., 2022). Daya Bay is a large semi-closed drowned valley-type bay along the coast of Guangdong Province, China, surrounded by the Dapeng Peninsula, the southern coast of Huiyang, and the Pinghai Peninsula of Huidong (Figure 1). It is located on the east side of the Pearl River Estuary, adjacent to Hong Kong in the southwest, connected to Honghai Bay in the east and the continental shelf of the South China Sea in the south, covering an area of about 600 km^2. Daya Bay Nuclear Power Plant (DBNPP) is located in the west coast of Daya Bay on the north shore of Dapeng'ao with a total installed capacity of 6 million kilowatts (Figure 1). The environmental impact of the cooling water discharge from the DBNPP has received great attention from society (Wang et al., 2008; Hao et al., 2016; Ye et al., 2018). Many scholars have conducted a lot of research work on the impact of the cooling water discharge from the plant on the marine environment and marine ecosystem dynamics of Daya Bay (Yue et al., 2018; Jiang and Wang, 2020; Mao et al., 2021).

Various research methods are applied to predict the extent and impact of power plant cooling water discharge (George, 2017; Lin et al., 2021), including field observation, remote sensing observations (Lima and Wethey, 2012; Liu et al., 2020), physical models, and numerical simulations (George, 2017). With the continuous development of computer technology and numerical calculation methods, the computing speed of mathematical models is getting higher and higher, and the application of the method is more and more extensive (Lin et al., 2021).

In bays with deep water depths, the diffusion of cooling water discharge is a three-dimensional process. Baroclinic effect caused by temperature gradient has certain influence on the surrounding hydrodynamic process and cooling water diffusion. Therefore, three-dimensional baroclinic model for cooling water discharge has been gradually promoted recently.

Previous research had been conducted on the three-dimensional numerical stimulation of cooling water discharge from power plant and discussed on the diffusion and effect of warm water discharge from Daya Bay (Zhang and Zhou, 2004; Zhou, 2007; Wei et al., 2013). In these researches, the heat transfer coefficient of the sea surface was directly introduced to characterize the heat exchange process at the air-sea interface. These methods did not consider the dynamic exchange processes of latent heat flux due to evaporation, sensible heat flux due to air-sea temperature difference at the interface, and the forcing processes of solar short-wave and long-wave radiation. As a result, the cooling water discharge model might not simulate the spatial and temporal distribution of the background temperature field well, which in turn affects the simulation of the temperature rise and diffusion process of cooling water discharge. In this paper, we construct a three-dimensional (3D) baroclinic model of Daya Bay based on the ECOMSED model (Blumberg and Mellor, 1987), using real-time sea surface momentum and heat forcing to simulate the spatio-temporal distributions of hydrodynamic, thermal dynamic processes and diffusion of cooling water discharge in Daya Bay in summer.

2 Methodology

2.1 Cooling water discharge model of Daya Bay

This paper carried out three-dimensional (3D) baroclinic stimulation for Daya Bay using the ECOMSED model. The

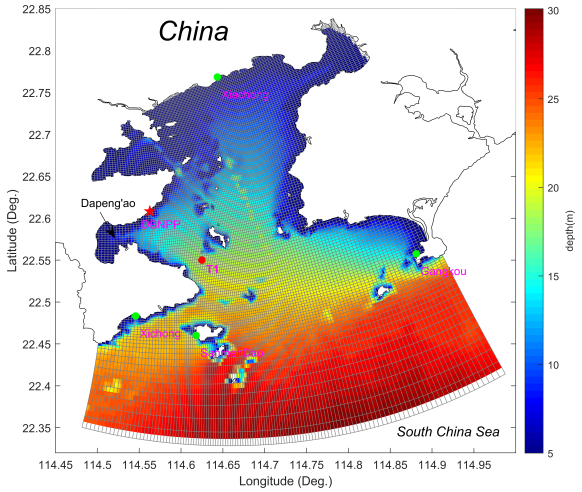


FIGURE 1
Horizontal curvilinear orthogonal grid (curves) and bottom bathymetry (shaded) of the three-dimensional numerical model of Daya Bay. The bathymetry was interpolated from nautical charts. Red star indicates the position of the Daya Bay Nuclear Power Plant (DBNPP). Green dots demonstrate the four tidal gauge stations (i.e., Gangkou, SanmenDao, Xiachong, and Xichong). Red dot illustrates the T1 station with temperature observations conducted.

vertical turbulent mixing coefficient was calculated using the Mellor-Yamada level 2.5 turbulent closure scheme (Mellor and Yamada, 1974). The model consists of nonlinear momentum equations that consider upwelling and downwelling flows and horizontal convection of fluids due to differences in fluid density caused by temperature and salt. It simulates several state variables, including sea surface elevation, 2D and 3D flow velocity, temperature, salinity, turbulent kinetic energy, and turbulent mixing length. The model is solved by a mode splitting technique, where the horizontal movement of the fluid volume and the vertical shear flow rate are solved separately and independently. Thus, the model can take a more extensive computational time step to improve computational efficiency (Ahsan and Blumberg, 1999). This model has been widely used to study the coastal circulation dynamics, hypoxia and eutrophication processes in rivers, estuary, and continental shelf regions around the world (Hellweger et al., 2004; Hu and Li, 2009; Zhang and Li, 2010).

2.2 Model grid and bathymetry

The shoreline and topographic data required for the model was obtained from the nautical chart released by the Guangdong Provincial Maritime Bureau. Figure 1 shows the model domain, including the whole Daya Bay and the regions within the 30-meter isobath outside the bay. It maintains a high resolution around the DBNPP and keeps the inner area of the bay away from the open boundary of the model to reduce the influence of the open boundary on the inner computational area. A curvilinear orthogonal grid is used in the horizontal (Figure 1). The number of grids in the x and y directions is 266×292, and the minimum horizontal resolution of the grid is about 75 m, while the grid resolution in the outer sea is lower (about 500 m).

The bathymetry of the Daya Bay model is interpolated from nautical charts (Figure 1). The model uses sigma coordinates in the vertical and there are 5 sigma levels in the vertical. As the bathymetry is shallow in the coastal regions of DBNPP with the maximum water depth less than 10 m. And previous model studies always used vertical levels less than 5 (Wu et al., 2007; Zhou, 2007). So, it is meaningful for our model to use 5 sigma levels in the vertical. The external mode time step of the model is taken 2 seconds, and the inner mode time step is taken 30 seconds.

2.3 Setup of the numerical model

In the model, the initial water level and horizontal flow velocity is taken as 0. Thus, the model is calculated from the stationary state. Except some small rivers, there are no big rivers with large freshwater discharged into the Daya Bay. Furthermore, the Pearl River plume with low salinity water detaches offshore with the Yuedong coastal current and has little influence on the salinity distribution in Daya Bay during summer (Gan et al., 2009). As a result, the seasonal variability of salinity in the Daya Bay is not significant. Thus, the model only calculates the convective diffusion process of temperature, salinity is kept constant during the simulation, and the effect of salinity change on the density gradient is not considered.

The time-series of tidal elevation on the lateral open boundary are calculated using eight primary harmonic constituents (M_2, S_2, N_2, K_2, K_1, O_1, P_1, and Q_1). The above harmonic constituents are interpolated from the global tidal inversion model (TPXO version 7.2) developed by Oregon State University (USA). The temperature lateral boundary condition is given by the field observed data.

The heat fluxes (solar short-wave radiation, long-wave radiation, latent heat flux, and sensible heat flux) at the air-sea interface are mainly governed by the solar altitude angle, the air temperature at 2m above the sea surface, the atmospheric pressure at the sea surface, the relative humidity at 2m above the sea surface, the cloud, and the wind speed at 10m above the sea surface. In this paper, the dynamic processes of the above meteorological parameters related to heat fluxes are considered. Sea surface momentum forcing uses summer mean wind field. The meteorological parameters are derived from the National Oceanic and Atmospheric Administration's (NOAA) NCAR/NCEP reanalysis data, which has a temporal resolution every 6 hours.

Firstly, the model ran for 30 days forced with summer mean surface meteorological parameters and wind. After the spin-up, we carried out prognostic simulations from August 5, 2008 to September 30, 2008 forced with summer mean wind forcing and real-time surface meteorological parameters. Model simulated hourly results were used to do model verifications and thermal influence analysis.

2.4 Cooling water discharge sources

Based on the above 3D numerical model of Daya Bay, we simulated the diffusion process of the cooling water discharge from the DBNPP in summer. The source strength of the cooling water discharge is taken as 190 m^3/s, and the temperature rise at the discharge point is 8°C. The model results are compared with the field observational data to verify the performance of the model. Then the model results are used to analyze the dispersion pattern of the DBNPP's cooling water.

3 Results and discussion

3.1 Model validation

The time series of modeled tidal elevations were compared with the measured data at four stations: Gangkou, SanmenDao, Xiachong, and Xichong (with positions shown in Figure 1). The results showed that the model reasonably reproduced the trend of tidal rise and fall in Daya Bay, and the amplitude and phase of

tide levels calculated by the model were generally consistent with the measured results (Figure 2). As our model did not consider M_4 and M_6 tide, the model could not simulate the double peak structure well during spring and neap tide which mainly attributed to the interaction of bottom topography and shallow water tidal constituents (Song et al., 2016). The model predictive capability for temperature was tested by comparing model results with the measured temperatures at the surface, middle, and bottom of the T1 station (Figure 3). The result indicated that the model could reproduced the temporal variations of temperature in different layers of the water column. Even though, there was some discrepancy between the model results and observations because of the low spatial resolution (about 2.5 degree) of the NCAR/NCEP reanalysis data used in our model.

Figures 4 and 5 compared the temperature rise calculated by the model with the remote sensing results for the corresponding periods. Both remote sensing data and numerical model results show that the temperature rise intensity due to the cooling water discharge from the DBNPP gradually decreases from the center of the discharge point. The 4°C temperature rise area is mainly confined to the area near the outfall, and generally the simulation results are similar to the remote sensing observations.

3.2 Horizontal tidal currents

Figures 6 and 7 show the distribution of flood and ebb tidal currents calculated by the model. Constrained by the shoreline and bottom topography, the tidal flow in Daya Bay is basically

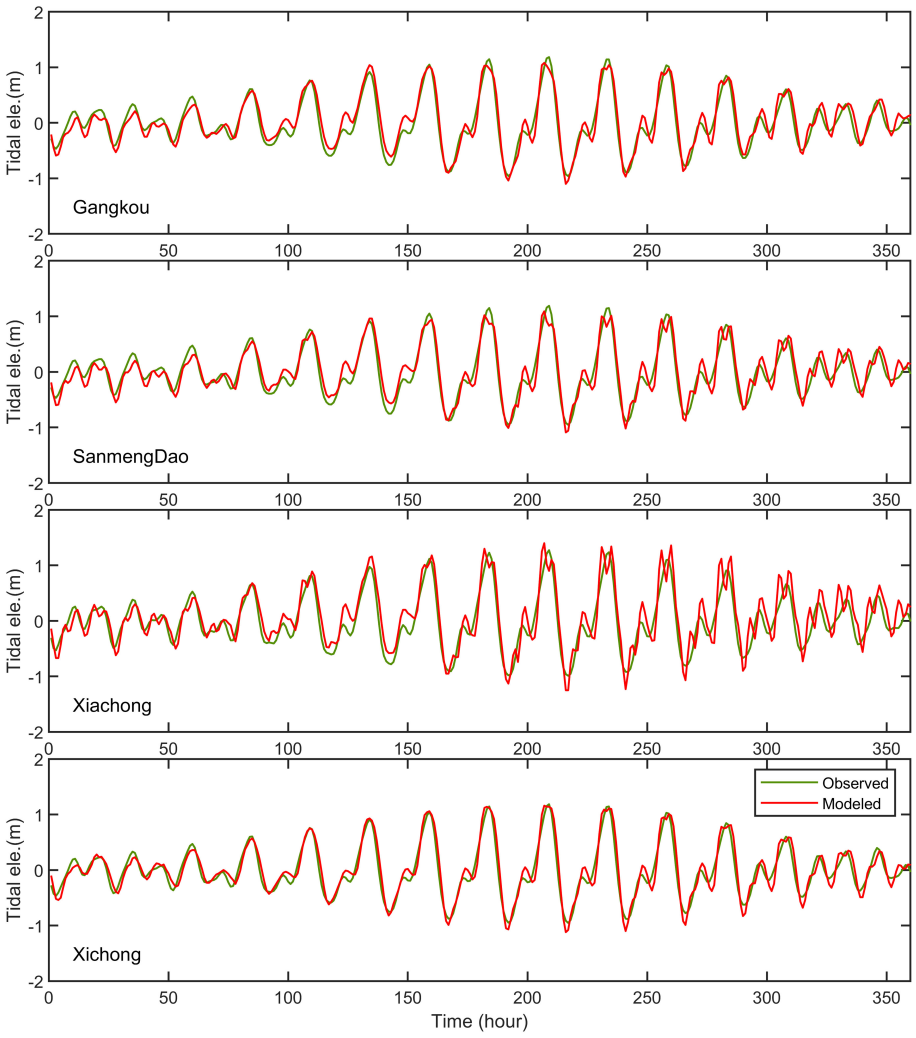


FIGURE 2
Comparisons of modeled hourly tidal level (red curves) with field observations (green curves) at four stations (i.e., Gangkou, SanmenDao, Xiayong, and Xichong) with the positions shown in Figure 1.

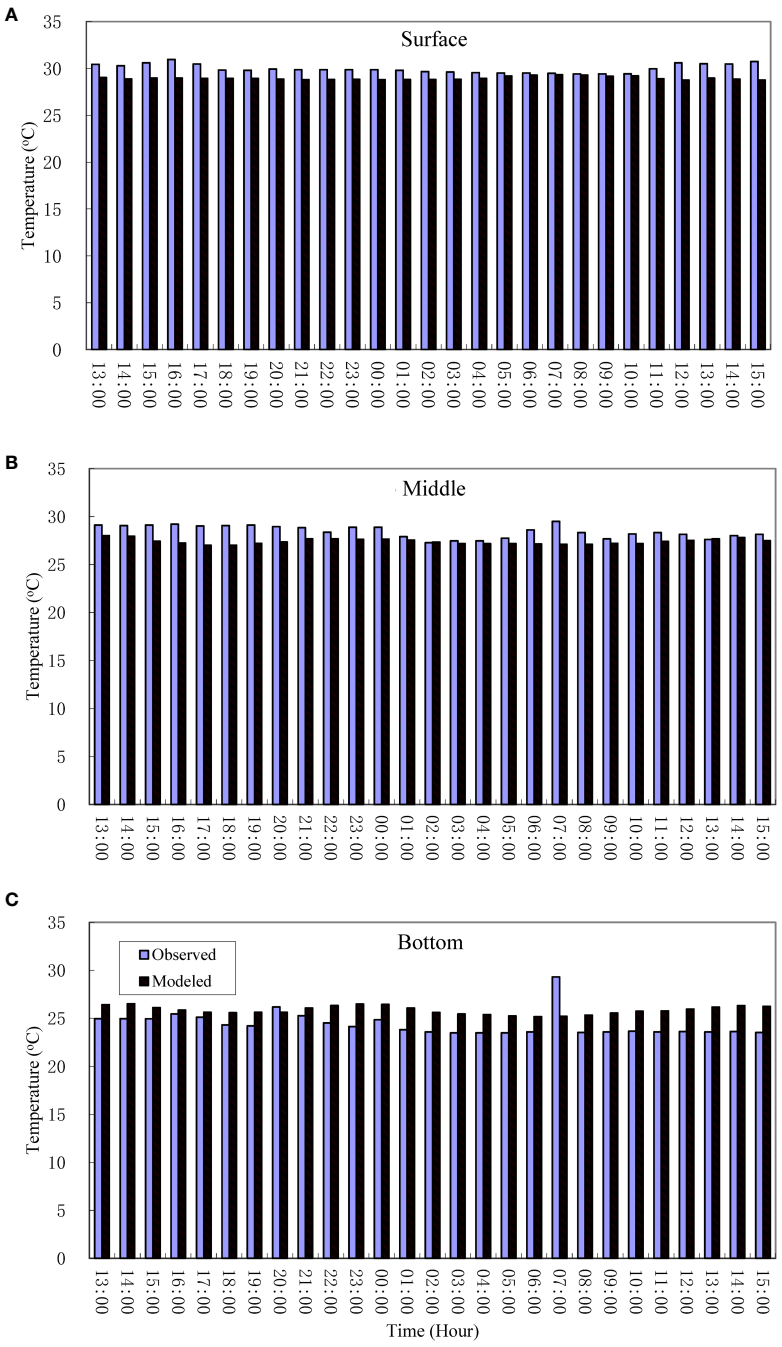


FIGURE 3
Comparisons of modeled temperature with field observations at stations T1: **(A)** Surface; **(B)** Middle layer; and **(C)** Bottom layer. The field observations conducted at September 12 and 13, 2008.

reciprocal. Flooding tidal currents at Daya Bay basically flows from south to north. The direction of ebb tide is generally opposite to that of the flood tide, but its flow velocity is stronger than that of the flood tide. The island in the middle of Daya Bay roughly divides the sea into two halves, with the eastern side having a wide area and a deeper water depth, which is the main channel for tidal currents. The water bodies at the top of Daya Bay exchange with the outer sea mainly through the eastern part, while the water bodies in Yaling Bay and Dapeng'ao flow out of Daya Bay mainly through the western channel. The tidal currents distributions were consistent with the results of Wu et al. (2007) and Zhou (2007).

10.3389/fmars.2022.1012260

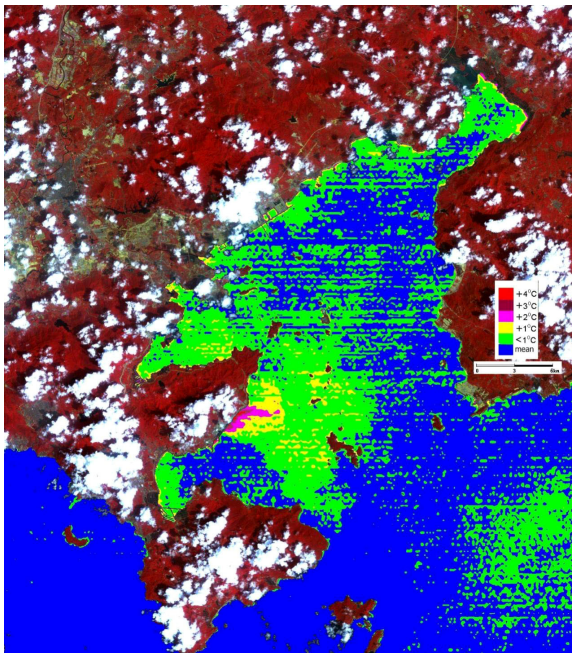


FIGURE 4
Distributions of temperature rise intensity of Daya Bay nuclear power cooling water discharge on September 21, 2008 (TM data) derived from satellite observations.

3.3 Sea surface temperature

Away from the open ocean, the water depth in Daya Bay is shallow (Figure 1). The spatio-temporal variations in temperature field is mainly controlled by the heat flux at the air-sea interface in addition to the influence of hydrodynamic processes in Daya Bay.

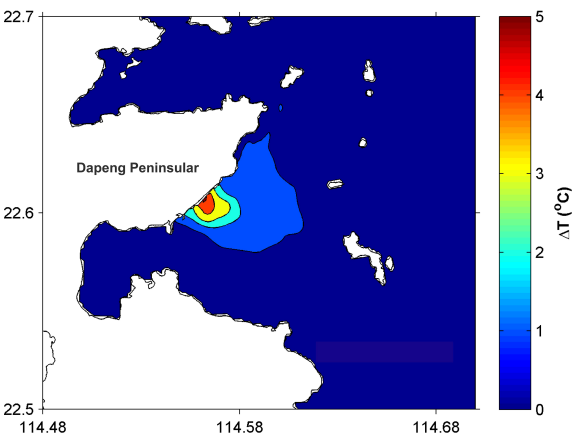


FIGURE 5
Distribution of daily mean surface temperature rise on September 21, 2008 calculated by the model of Daya Bay.

In this section, we analyzed the spatial distributions of the surface and bottom temperature in summer based on the model results.

In summer, the solar radiation in Daya Bay is strong, which results to strong water column stratification. The sea surface temperature (SST) of the whole area is above 28°C. The temperature distributions in the surface and bottom layer in the mouth of the bay and the outer sea are obviously different (Figures 8, 9). In the top of the bay and near-shore area, due to the shallow water depth, the temperature difference between the surface and bottom layers is not significant and the stratification is weak. In summer, the eastern coast of Guangdong in the northern South China Sea produces a more significant upwelling process under the influence of the southwest monsoon (Gan et al., 2009). The results also show that very strong outer seawater invasion with lower temperature occurred at the bottom in the entrance of the bay during summer, and its influence can reach to the area near Gangkou (Figure 9).

The results also show that the temperature distribution in summer is significantly influenced by the cooling water discharge from the nuclear power plant (Figure 8). Under the influence of southwest monsoon, the cooling water discharge from nuclear power plant spreads to the northeast, which has less influence on the temperature distribution in Dapeng'ao.

3.4 Temperature rise area distribution

Figures 10 and 11 illustrate the model simulated surface and bottom temperature rise during spring and neap tide period, respectively. Model results show that the cooling water discharge from the DBNPP first expands in a fan shape far out to sea near the outfall, and then spreads mainly to the northeast under the influence of the southwest monsoon. In summer, the water column stratification in Daya Bay is strong, and the cooling water discharge mainly tend to diffuse in the surface layer, and the temperature rise in the bottom layer is not significant (Figures 10B, D, 11B, D). Statistical analysis showed that the total area for summer cooling water discharge led to 1 °C surface temperature rise area near the power plant of about 18.8 to 21.6 km^2. The area with temperature rises of 2 °C is between 6.2 and 8.1 km^2. The area with temperature rises of 4 °C is no more than 1.2 km^2. In the bottom layer, the area within 1°C temperature rise near the power plant is no more than 2.2 km^2. There is no area with temperature rise above 1°C (Table 1).

Further comparison of the temperature rise area near the outfall of the DBNPP during spring tide and neap tide shows that the tide also has effect on the diffusion of warm discharge water, with a more significant influence during spring tide (Table 1). According to the tidal dynamics in Daya Bay calculated by the model (Figures 6, 7), the flood tidal current in the sea near the power plant outfall basically flows in the northeast direction along the shoreline, while the direction of the ebb tidal current is opposite. Under the action of such tidal dynamics, the cooling

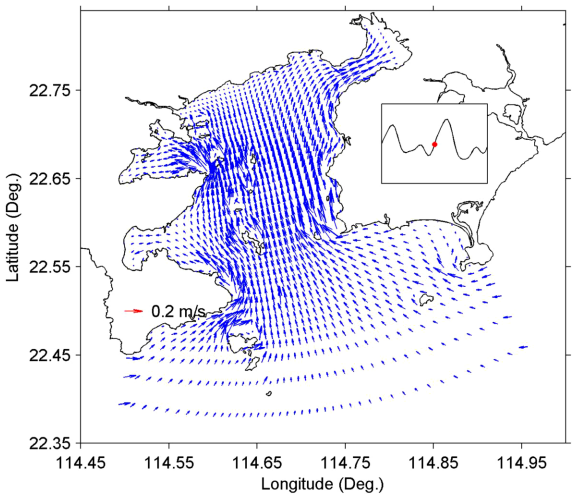


FIGURE 6
Simulated surface tidal currents during flood tide period in the Daya Bay.

water discharge will expand to the northeast during the flood tide period, which is basically in the same direction as the action of the monsoon, thus extending the temperature rise envelope farther to the northeast (Figure 10A). At ebb tide period, the surface warm water is influenced by the southwestward ebbing tide, and the temperature rise envelope is deflected clockwise. Under the joint influences of summer wind and ebbing tide, the cooling water spreads east-northeastward (Figure 10C). During the period of neap tide, the difference between the expansion pattern of warm water at the time of flood and neap tide is small, indicating that the

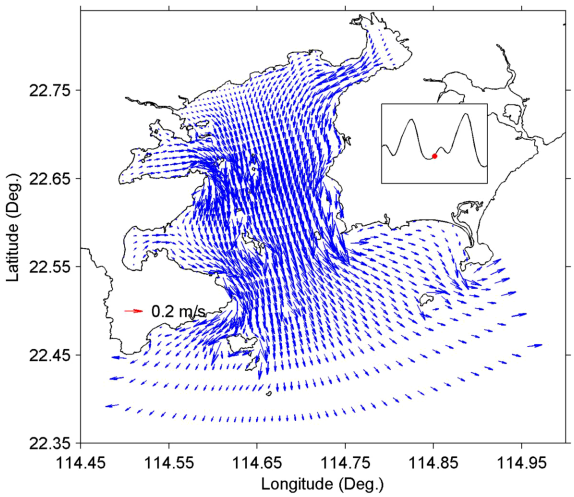


FIGURE 7
Same as Figure 7, but for the tidal currents during ebb tide period.

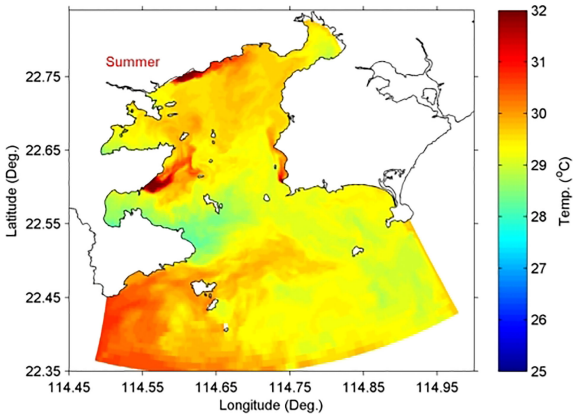


FIGURE 8
Model simulated summer mean surface temperature distribution in the Daya Bay.

diffusion of cooling water at this time is mainly controlled by the monsoon (Figure 11).

Modeled hourly time-series of surface 1°C and 4°C temperature rises area, surface tidal current speed and direction, and tidal elevation during spring and neap tide periods are shown in Figures 12. The temperature rise area illustrates obvious flood and ebb tide variations. And the distribution pattern has significant difference during spring and neap tide periods (Figures 12A, B). It demonstrates that the flooding and ebbing tides play important roles on the offshore spreading of cooling water discharge from the DBNPP. The influence is more significant during spring tide, especially for the 4°C temperature rise area with the maximum value occurred during the end of flooding and ebbing tide. The results further support our previous findings. And our findings

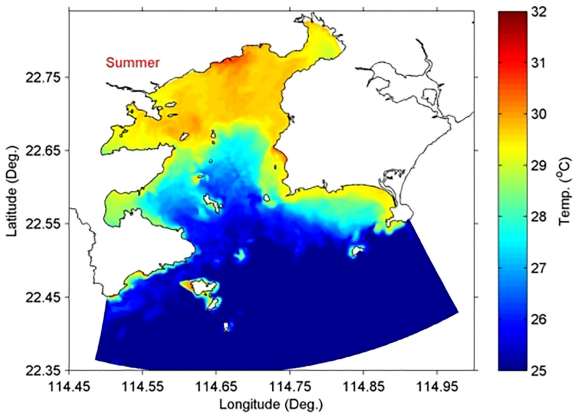


FIGURE 9
Model simulated summer mean bottom temperature distribution in the Daya Bay.

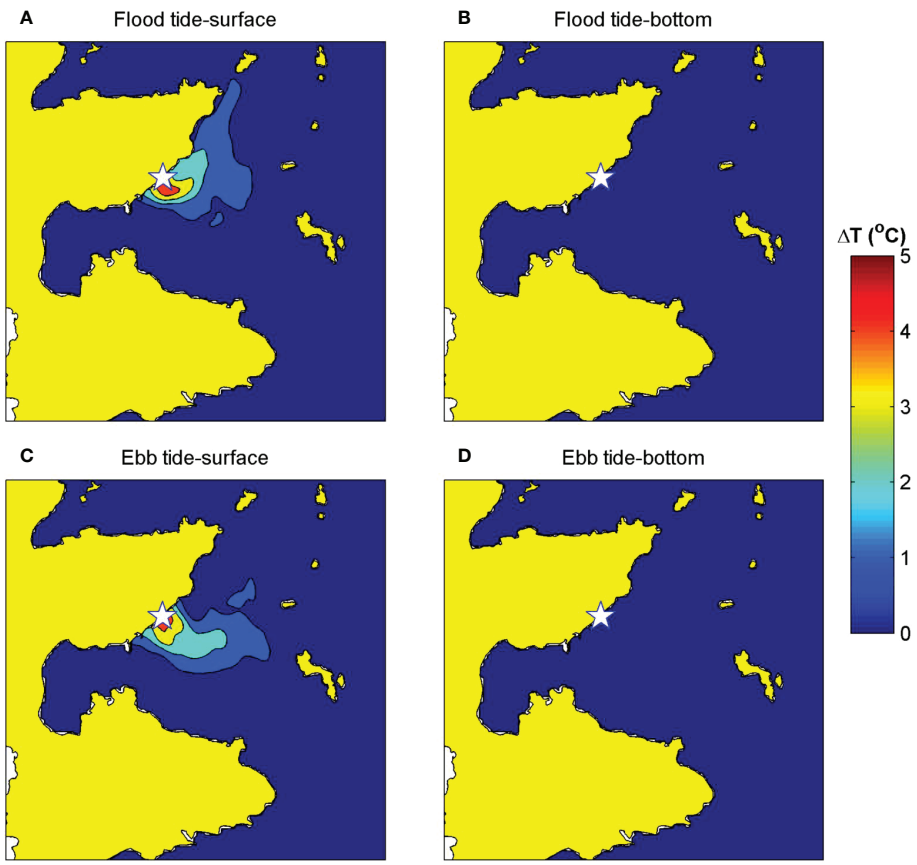


FIGURE 10
Model simulated temperature rise: **(A)** surface and flood tide period; **(B)** bottom and flood tide period; **(C)** surface and ebb tide period; and **(D)** bottom and ebb tide period, near the Daya Bay Nuclear Power Plant (DBNPP) during spring tide in summer.

are consistent with the results of Jiang and Wang (2020) who also had reported the different distributions of temperature rise area during spring and neap tide periods.

In order to quantitatively estimate the tidal influence on the diffusion of cooling water discharge from the DBNPP. We calculated the correlation coefficients between the surface temperature rise area with the tidal elevation and tidal current (tidal current speed and direction) shown in Table 2. Generally, negative correlation relationships were found between the tides (i.e., tidal elevation, tidal current speed and direction and temperature rise area). And significant correlations were found between the 4°C temperature rise area and tidal elevation, tidal current speed and direction during spring tide period. Among them, the largest absolute value of correlation coefficient (with R=-0.72) was occurred between the 4°C temperature rise area and tidal elevation. The negative correlation coefficient between the 4°C temperature rise area and tidal current speed indicates that the strong tidal current induced significantly vertical mixing inhibited the horizontal diffusion of cooling water discharge to offshore (Figures 12C, E). Jiang and Wang (2020) also found that the weaker current in neap tide than in spring tide period affected the mixing of cooling water less. Besides the cooling water discharge, the spring-neap tide can also influence the nutrient supply and the primary production of the phytoplankton (Sharples, 2008).

Our findings imply that tidal effects should not be neglected in the numerical simulation of cooling water discharge in coastal regions. Clearly understanding of the driving mechanisms of tidal influence on the cooling water discharge can improve the capability of the numerical model to precict the dispersion of cooling water discharge. It can also help us to better understand the effects of cooling water discharge on marine environment and ecosystem dynamics.

4 Conclusions

Thermal pollution caused by cooling water discharge from power plants is a severe marine ecological problem of great concern. To reveal the diffusion of cooling water discharge from Daya Bay Nuclear Power Plant (DBNPP) and its impact on the

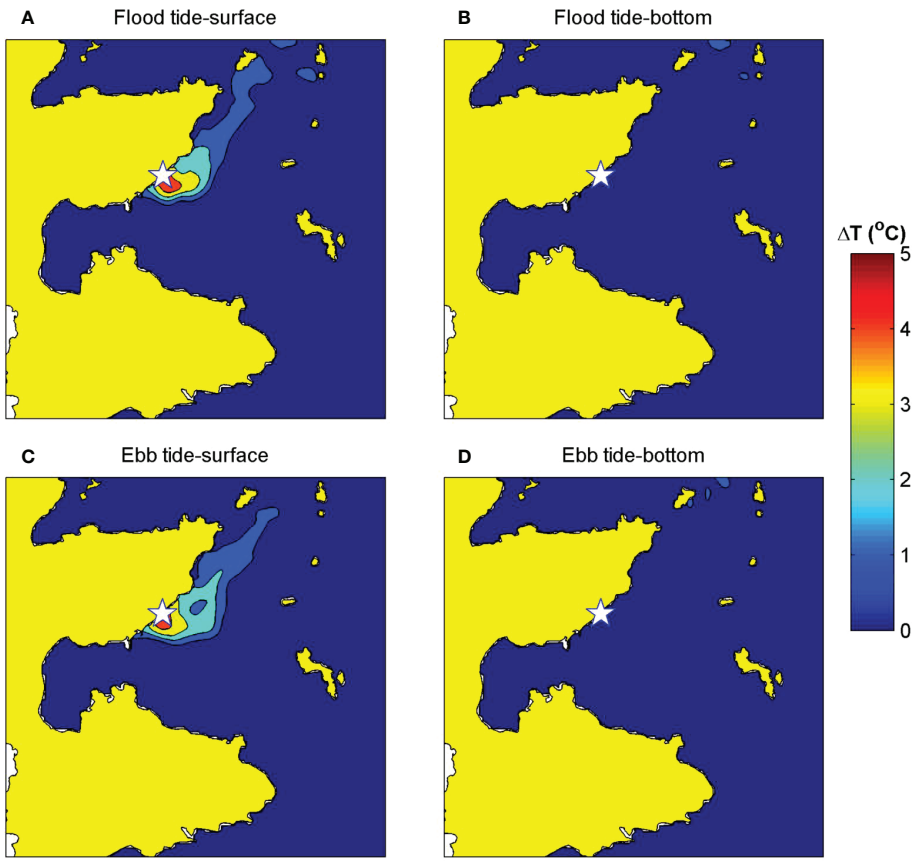


FIGURE 11
Same as Figure 11, but during neap tide.

surrounding marine environment, this paper establishes a high-resolution three-dimension (3D) baroclinic model in Daya Bay. The main conclusions are:

(1) The model results are consistent with the observations. The simulated temperature rise distribution and the remote sensing results both show that the intensity of temperature rise gradually decreases from the center of the outfall to the outer sea. 4°C temperature rise area is mainly confined to the area near the outfall. It shows that the model can better reproduce the hydrodynamic and thermodynamic processes in Daya Bay.

(2) The results show that the horizontal tidal currents in Daya Bay is basically reciprocal due to the shoreline and bottom topography constraints. At flood tide, the tide in Daya Bay basically flows from south to north, from the

TABLE 1 Statistics of model simulated surface and bottom temperature rise area (Unit: km^2) during spring and neap tide periods due to the cooling water discharge from the Daya Bay Nuclear Power Plant (DBNPP) in summer.

Temperature rises(℃)	Surface				Bottom			
	spring tide		neap tides		spring tide		neap tides	
	flood	ebb	flood	ebb	flood	ebb	flood	ebb
≥1.0	21.55	20.28	18.81	18.91	0.13	0.0	2.22	2.20
≥2.0	6.20	7.41	6.71	8.06	0.0	0.0	0.0	0.0
≥3.0	2.42	2.28	3.20	2.59	0.0	0.0	0.0	0.0
≥4.0	1.08	0.81	1.15	0.79	0.0	0.0	0.0	0.0

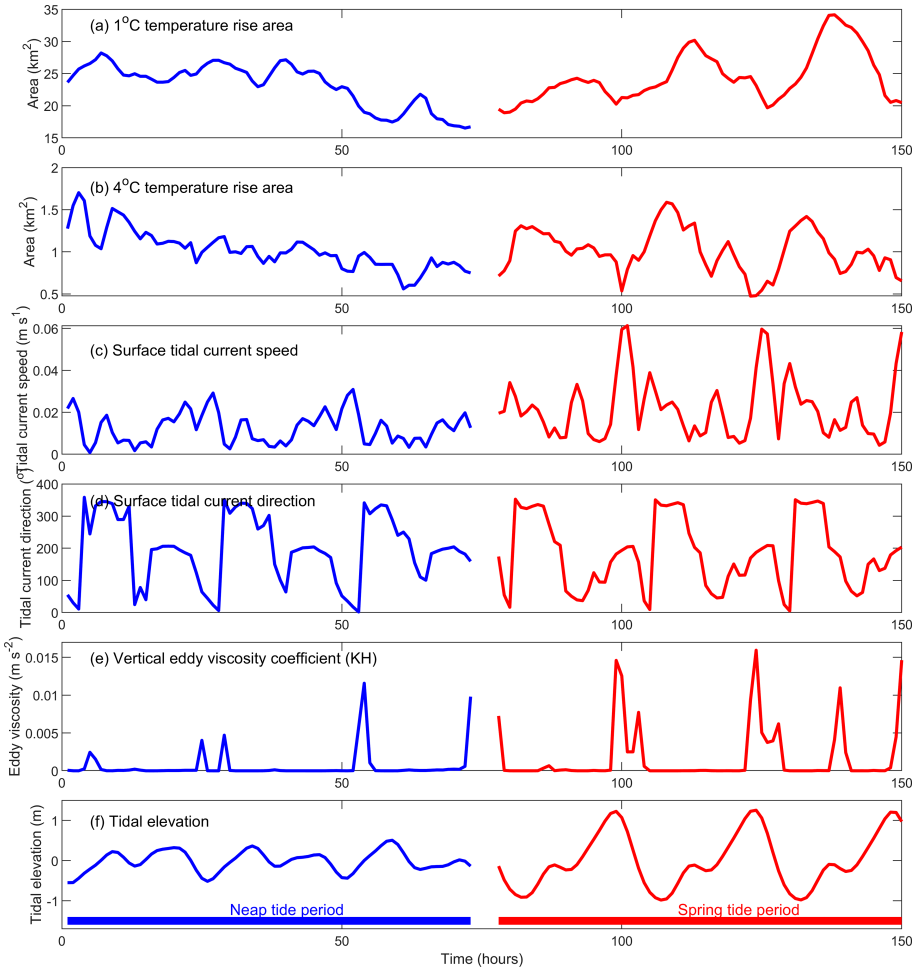


FIGURE 12
Modeled time-series of: **(A)** 1℃ temperature rise area; **(B)** 4℃ temperature rise area; **(C)** Surface tidal current speed; **(D)** Surface tidal current direction; **(E)** Vertical eddy viscosity coefficient and **(F)** Tidal elevation during spring and neap tide periods.

mouth of the bay to the top of the bay, and the ebb tide is roughly opposite to the flood tide, but its strength is stronger than that of the flood tide.

(3) In summer, the surface and bottom temperatures in Daya Bay are high, especially at the top of the bay and near-shore waters, and the bottom water temperature at the mouth of the bay and in the outer sea is low. The warm water discharge led to 1°C surface temperature rise in the sea near the power plant envelope area of about 18.8 to 21.6 km^2. The area where the rising temperature over 2 °C is between 6.2 and 8.1 km^2. The area with rising temperature over 4 °C is no more than 1.2 km^2. The area with 1°C temperature rise near the power plant is no more than 2.2 km^2 at the bottom layer.

TABLE 2 Correlation coefficients between the temperature rise (1°C and 4°C) envelope area and tidal elevation, tidal current during spring and neap tide periods.

Temperature rise area (km^2)	Tidal period	Tidal elevation	Tidal current speed	Tidal current direction
1°C temperature rise	Spring tide	-0.15	-0.38	-0.001
	Neap tide	-0.19	-0.02	-0.06
4°C temperature rise	Spring tide	-0.72	-0.25	-0.53
	Neap tide	-0.12	-0.03	-0.04

(4) The tidal process also has certain influence on the diffusion of cooling water diffusion in the DBNPP. The diffusion trend in different tidal processes will have some differences, among which the influence of the spring tide period is more significant than that of the neap tide period.

Data availability statement

The original contributions presented in the study are included in the article/Supplementary Material. Further inquiries can be directed to the corresponding authors.

Author contributions

BG: main contributor to conception, design of the work and result analysis LL: revise the article and ensure the discussions related to the work QC: Drafting the article, revising it critically for important intellectual content WZ : Data analysis and interpretation, check for content, and approval of publications SL: Validation of model DW: Data collection and analysis MH: Data collection and analysis. All authors contributed to the article and approved the submitted version.

Funding

This study is supported by the Guangdong Basic and Applied Basic Research Foundation (No. 2019A1515012108), the National Natural Science Foundation of China (U20A20103, 42230402), and the research fund from the State Key Laboratory of Tropical Oceanography (LTOZZ2101).

Conflict of interest

The authors declare that the research was conducted in the absence of any commercial or financial relationships that could be construed as a potential conflict of interest.

Publisher's note

All claims expressed in this article are solely those of the authors and do not necessarily represent those of their affiliated organizations, or those of the publisher, the editors and the reviewers. Any product that may be evaluated in this article, or claim that may be made by its manufacturer, is not guaranteed or endorsed by the publisher.

References

Ahsan, A. Q., and Blumberg, A. F. (1999). Three-dimensional hydrothermal model of Onondaga lake, new York. *J. Hydraulic Eng.* 125, 912–923. doi: 10.1061/(ASCE)0733-9429(1999)125:9(912)

Blumberg, A. F., and Mellor, G. L. (1987). A description of a three-dimensional coastal ocean circulation model. *Three-dimensional Coast. Ocean Models* 4, 1–16. doi: 10.1029/CO004p0001.

Gan, J. P., Li, L., Wang, D. X., and Guo, X. Y. (2009). Interaction of a river plume with coastal upwelling in the northern south China Sea. *Continental Shelf Res.* 29, 728–740. doi: 10.1016/j.csr.2008.12.002

George, A. M. (2017). *Numerical simulation of warm discharge in cold fresh water* (Loughborough University). Thesis. Available at: https://hdl.handle.net/2134/27376

Hao, Y., Tang, D., Boicenco, L., and Wang, S. (2016). Environmental ecological response to increasing water temperature in the daya bay, southern China in 1982-2012. *Natural Resour.* 7, 184. doi: 10.4236/nr.2016.74017

Hassan, S. T., Baloch, M. A., and Tarar, Z. H. (2020). Is nuclear energy a better alternative for mitigating CO2 emissions in BRICS countries? an empirical analysis. *Nucl. Eng. Technol.* 52, 2969–2974. doi: 10.1016/j.net.2020.05.016

Hellweger, F. L., Blumberg, A. F., Schlosser, P., Ho, D. T., Caplow, T., Lall, U., et al. (2004). Transport in the Hudson estuary: a modeling study of estuarine circulation and tidal trapping. *Estuaries* 27 (3), 527–538. doi: 10.1007/BF02803544

Hu, J. T., and Li, S. Y. (2009). Modeling the mass fluxes and transformations of nutrients in the pearl river delta, China. *J. Mar. Syst.* 78, 146–167. doi: 10.1016/j.jmarsys.2009.05.001

Jiang, R., and Wang, Y.-S. (2020). Modeling the ecosystem response of the semi-closed daya bay to the thermal discharge from two nearby nuclear power plants. *Ecotoxicology* 29, 736–750. doi: 10.1007/s10646-020-02229-w

Kaviani, F., Memarian, M. H., and Eslami-Kalantari, M. (2021). Radioactive impact on Iran and the world from a postulated accident at bushehr nuclear power plant. *Prog. Nucl. Energy* 142, 103991. doi: 10.1016/j.pnucene.2021.103991

Lima, F. P., and Wethey, D. S. (2012). Three decades of high-resolution coastal sea surface temperatures reveal more than warming. *Nat. Commun.* 3, 1–13. doi: 10.1038/ncomms1713

Lin, J., Zou, X., and Huang, F. (2021). Quantitative analysis of the factors influencing the dispersion of thermal pollution caused by coastal power plants. *Water Res.* 188, 116558. doi: 10.1016/j.watres.2020.116558

Liu, M., Yin, X., Xu, Q., Chen, Y., and Wang, B. (2020). Monitoring of fine-scale warm drain-off water from nuclear power stations in the daya bay based on landsat 8 data. *Remote Sens.* 12, 627. doi: 10.3390/rs12040627

Liu, Q., Zhou, L., Zhang, W., Zhang, L., Tan, Y., Han, T., et al. (2022). Rising temperature contributed to the outbreak of a macrozooplankton creseis acicula by enhancing its feeding and assimilation for algal food nearby the coastal daya bay nuclear power plant. *Ecotoxicology Environ. Saf.* 238, 113606. doi: 10.1016/j.ecoenv.2022.113606

Mahmood, N., Wang, Z., and Zhang, B. (2020). The role of nuclear energy in the correction of environmental pollution: Evidence from Pakistan. *Nucl. Eng. Technol.* 52, 1327–1333. doi: 10.1016/j.net.2019.11.027

Mao, H., Qi, Y., Qiu, C., Luan, Z., Wang, X., Cen, X., et al. (2021). High-resolution observations of upwelling and front in daya bay, south China Sea. *J. Mar. Sci. Eng.* 9, 657. doi: 10.3390/jmse9060657

Mellor, G., and Yamada, T. (1974). Development of a turbulence closure model of geophysical layers. *J. Atmospheric Sci.* 33, 1791–1896. doi: 10.1175/1520-0469(1974)031<1791:AHOTCM>2.0.CO;2

Musyoka, D., and Field, R. M. (2018). Review of the environmental oversight framework in Kenya, in light of a nuclear power programme. *Prog. Nucl. Energy* 108, 89–98. doi: 10.1016/j.pnucene.2018.05.005

Sharples, J. (2008). Potential impacts of the spring-neap tidal cycle on shelf sea primary production. *J. Plankton Res.* 30 (2), 183–197. doi: 10.1093/plankt/fbm088

Song, D. H., Yan, Y. H., Wu, W., Diao, X. L., Ding, P., and And Bao, X. W. (2016). Tidal distortion caused by the resonance of sexta-diurnal tides in a micromesotidal embayment. *J. Geophysical Rsearch: Oceans* 121, 7599–7618. doi: 10.1002/2016JC012039

Wang, Y.-S., Lou, Z.-P., Sun, C.-C., and Sun, S. (2008). Ecological environment changes in daya bay, China, from 1982 to 2004. *Mar. Pollut. Bull.* 56, 1871–1879. doi: 10.1016/j.marpolbul.2008.07.017

Wei, X., Ni, P., and Zhan, H. (2013). Monitoring cooling water discharge using Lagrangian coherent structures: A case study in daya bay, China. *Mar. Pollut. Bull.* 75, 105–113. doi: 10.1016/j.marpolbul.2013.07.056

Wu, R. H., Cai, S. Q., Wang, S. A., and Zhang, W. J. (2007). Three-dimensional numerical simulation of tidal current and residual current at daya bay. *J. Trop. Oceanography* 26 (3), 18–23.

Wu, J. W., Zhou, K. B., and Dai, M. H. (2013). Impacts of the Fukushima nuclear accident on the China Seas: Evaluation based on anthropogenic radionuclide 137Cs. *Chinese Science Bulletin* 58 (4-5), 552–558. doi: 10.1007/s11434-012-5426-2

Ye, Y., Chen, K., Zhou, Q., Xiang, P., Huo, Y., and Lin, M. (2018). Impacts of thermal discharge on phytoplankton in Daya Bay. *J. Coast. Res.*, 83 (10083), 135–147. doi: https://doi.org/10.2112/SI83-022.1

Yue, W.-Z., Sun, C.-C., Shi, P., Engel, A., Wang, Y.-S., and He, W.-H. (2018). Effect of temperature on the accumulation of marine biogenic gels in the surface microlayer near the outlet of nuclear power plants and adjacent areas in the daya bay, China. *PloS One* 13, e0198735. doi: 10.1371/journal.pone.0198735

Zhang, H., and Li, S. Y. (2010). Effects of physical and biochemical processes on the dissolved oxygen budget for the pearl river estuary during summer. *J. Mar. Syst.* 79, 65–88. doi: 10.1016/j.jmarsys.2009.07.002

Zhang, W., and Zhou, R. (2004). Thermal impact analysis of discharge of circulating cooling water at daya bay nuclear power station (GNPS) and ling'ao nuclear power station (LNPS). *Radiat. Prot. (Taiyuan)* 24, 257–262.

Zhou, Q. J. (2007). A three-dimensional numerical simulation of thermal discharge in daya bay. *Trans. Oceanology Limnology* 4, 37–46.

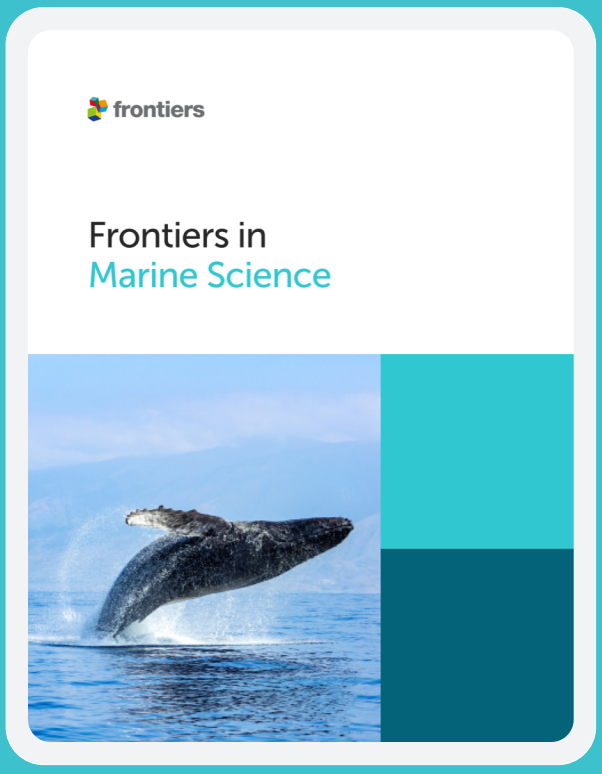
Frontiers in Marine Science

Explores ocean-based solutions for emerging global challenges

The third most-cited marine and freshwater biology journal, advancing our understanding of marine systems and addressing global challenges including overfishing, pollution, and climate change.

Discover the latest Research Topics

See more →



Frontiers

Avenue du Tribunal-Fédéral 34
1005 Lausanne, Switzerland
frontiersin.org

Contact us

+41 (0)21 510 17 00
frontiersin.org/about/contact